

# University of St Andrews



Full metadata for this thesis is available in  
St Andrews Research Repository  
at:

<http://research-repository.st-andrews.ac.uk/>

This thesis is protected by original copyright

**RHODIUM CATALYSED**  
**HYDROFORMYLATION OF ALLYL ALCOHOL**  
**WITH DIPHOSPHINE LIGANDS.**



A thesis presented by

**Daniel Ferrier Sinclair White**

to the

**University of St. Andrews**

in application for

**THE DEGREE OF DOCTOR OF PHILOSOPHY**

St. Andrews

July 2001

**DECLARATION.**

I, Daniel Ferrier Sinclair White, hereby certify that this thesis, which is approximately 65,000 words in length, has been written by me, that it is the record of work carried out by me and that it has not been submitted in any previous application for a higher degree.

date 2/10/01 signature of candidate

I was admitted as a research student in May, 1998 and as a candidate for the degree of Doctor of Philosophy in May, 1999 the higher study for which this is a record was carried out in the University of St Andrews between 1998 and 2001.

date 2/10/01 signature of candidate

I hereby certify that the candidate has fulfilled the conditions of the Resolution and Regulations appropriate for the degree of Doctor of Philosophy in the University of St Andrews and that the candidate is qualified to submit this thesis in application for that degree.

date ..... signature of supervisor .....

## DECLARATION

In submitting this thesis to the University of St Andrews I wish access to it to be subject to the following conditions: for a period of 5 years from the date of submission, the thesis shall be withheld from use;

I understand, however, that the title and abstract of the thesis will be published during this period of restricted access; and that after the expiry of this period the thesis will be made available for use in accordance with the regulations of the University Library for the time being in force, subject to any copyright in the work not being affected thereby, and a copy of the work may be made and supplied to any bona fide library or research worker.

date 2/10/01...

signature of candidate .

## ACKNOWLEDGEMENTS.

I would like to thank my supervisor Professor Cole-Hamilton for his invaluable help, encouragement and advice over the past three years, I am indebted to him. I would also like to thank my industrial supervisor, Doctor Wilfred Shum for all of his help and support, and indeed for beginning instrumental in the starting of this work.

I would like to thank the CATS service, here at St Andrews and give a special thanks to Doug Foster the service co-ordinator for all of his efforts over the last six months with the new ligands.

I would also like to give my thanks to all those I have had the pleasure to share a lab and my work with during my time in St. Andrews. There are too many to name them all but I would like to mention a few who have been exceptionally helpful; Peter Pogorzelec, Andrew Marr, Gary Schwarz, Ruth Robertson, and especially Ann McConnell whose help and encouragement over the last two years has been invaluable.

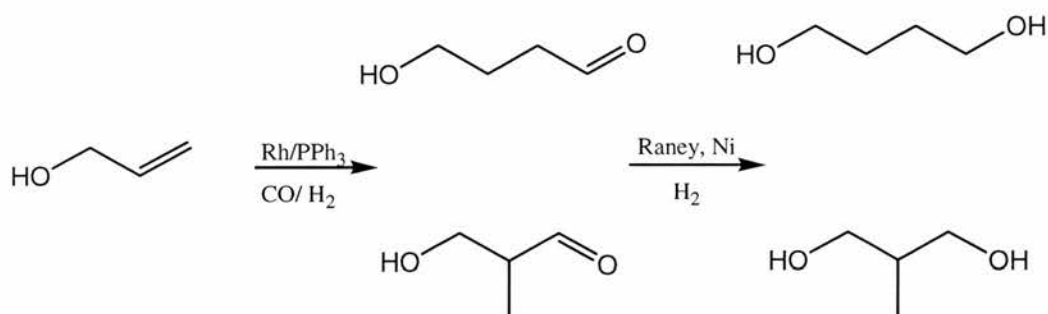
My thanks must also go to the technical staff in the department; Melanja Smith for all the help on the NMR, Colin Miller for all the glassware, Marge Parker from stores, Jim Bews for his work with the computers, and finally Bobby Cathcart and Jim Rennie for all their work in the workshop. I also thank Dr. Alex Slawin for the excellent X-ray crystallography service she supplies.

My thanks also to the Lyondell Chemical Company who have provided the funding for my research.

And finally a big thanks to all of my family and friends who have supported me whilst completing this work. To my mother and father for putting up with a student in the family a little longer. To my friends from Nottingham and Leeds who provided an escape from St. Andrews whenever required. To all the good friends I have made in St. Andrews, some have been mentioned already many have not. And lastly my thanks to Kate.

## ABSTRACT.

1,4-Butanediol is a commodity chemical produced in industry by a variety of methods. One such method involves the rhodium catalysed hydroformylation of allyl alcohol to 4-hydroxybutanal and 3-hydroxy-2-methylpropanal, which are further hydrogenated to 1,4-butanediol and 2-methyl-1,3-propanediol. The industrial method currently employs a catalyst generated from rhodium and triphenylphosphine. One method of making the reaction more desirable is to increase the amount of the linear product, 4-hydroxybutanal, over that of the branched product, 3-hydroxy-2-methylpropanal. It has been observed that use of a catalyst generated from rhodium and the diphosphine ligand (-)-2,3-O-Isopropylidene-2,3-dihydroxy-1,4-bis(diphenyl-phosphino)butane (DIOP) achieves this.

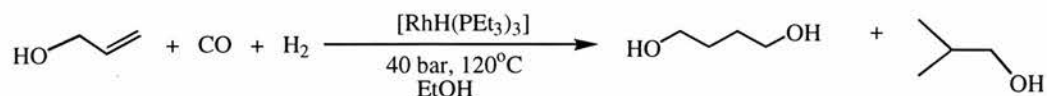


This thesis investigates the reason why DIOP as ligand instead of triphenylphosphine improves the reaction so. It details the rhodium DIOP complex species which were formed *in situ* from [Rh(CO)<sub>2</sub>(acac)] and DIOP under an inert atmosphere, and under an atmosphere of CO and H<sub>2</sub>. The thesis also details extensive studies of the complex species present under catalytic conditions of 20 bar CO and H<sub>2</sub> and temperatures up to 80 °C. This was achieved by using a high pressure NMR and high-pressure IR cell. The hydroformylation reaction itself was also studied *in situ* with these techniques and in a kinetic autoclave. The results allowed us to speculate how the mechanism of the reaction might be changed by the presence of the complex species we observed.

The third chapter of the thesis details the study of catalyst poisoning with oxygen and iron. It compares the stability of the rhodium DIOP catalytic system with other catalytic systems containing rhodium and dppb and triphenylphosphine. It compares how the systems react in aerobic and anaerobic conditions, and compares how different complex species react. The studies identify the complex [HRh(CO)(diphosphine)<sub>2</sub>], where one

diphosphine molecule is bound bidentate and one molecule is bound unidentatae, as possible catalyst for the oxidation of the diphosphine.

It is possible, when using highly electron donating alkyl phosphines such as triethylphosphine, to hydroformylate alkenes directly to the alcohol products of reaction.



The fourth chapter of the thesis details the synthesis of several alkyl diphosphines, and their performance as ligands of rhodium in the hydroformylation of allyl alcohol and 1-octene, and compares their performance to the aryl diphosphines DIOP and Xantphos.

The fifth chapter explores some possible further work, based on the conclusions come to in chapters two to four.

Chapter six details the experimental work involved in this thesis.

## ABBREVIATIONS.

This list contains abbreviations which may be used in this thesis without definition.

$\beta_n$	Natural bite angle.
$\delta$	Chemical shift.
$\Omega$	Solid angle.
$\chi$	Electronic Parameter.
Acac	$\eta^2$ -acetylacetonone.
Ar	Aryl.
b	Branched
BD	Butadiene.
BDO	1,4-Butanediol.
BDPP	(2S,4S)-bis(diphenylphosphino)pentane.
BINAP	2,2'-Bis(diphenylphosphino)-1,1'-binaphthyl.
BISBI	<i>trans</i> -2,2'-Bis[(diphenylphosphino)methyl]-1,1-biphenyl.
<sup>t</sup> Bu	<i>tert</i> -Butyl.
Bz	Benzyl.
CATS	Catalytic Evaluation and Optimisation Services.
CHIRAPHOS	(2R,3R)-bis(diphenylphosphino)butane.
CIR	Cylindrical internal reflectance.
DBPphos	1,8-bis(diphenylphosphino) dibenzofuran.
DIMAMP	(R,R)-1,2-bis(phenyl- <i>ortho</i> -anisoylphosphino)ethane.
1,8-Dinap	1,8-bis(diphenylphosphinomethyl) naphthalene.
DIOP	(-)-2,3-O-Isopropylidene-2,3-dihydroxy-1,4-bis(diphenylphosphino)butane.
<i>trans</i> -Dmecb	<i>trans</i> -1,2-bis(diphenylphosphinomethyl)-3-ethoxy-4,4-dimethylcyclobutane
<i>trans</i> -Dmcb	<i>trans</i> -1,2-bis(diphenylphosphinomethyl)-3,3-dimethylcyclobutane.
DPEphos	Bis(2-(diphenylphosphino)phenyl)phenyl ether.
Dppb	Bis(diphenylphosphino)butane.
Dppe	Bis(diphenylphosphino)ethane.
Dppf	1,1'-Bis(diphenylphosphino)ferrocene.

Dppm	Bis(diphenylphosphino)methane.
<i>trans</i> -Dpnr	<i>trans</i> -2,3-Bis(diphenylphosphinomethyl) [2-2-1] bicycloheptane.
Dppp	Bis(diphenylphosphino)propane.
Ea	Equatorial axial.
Ee	Equatorial equatorial.
FTIR	Fourier transform infrared.
GBL	$\gamma$ -Butyrolactone.
GC	Gas chromatography.
GCMS	Gas chromatography mass spectroscopy.
HBA	4-Hydroxybutanal.
HMPA	3-Hydroxy-2-methylpropanal.
HP IR	High pressure infrared.
HP NMR	High pressure nuclear magnetic resonance.
ID	Inner diameter.
l	Linear.
MA	Maleic anhydride.
MPD	2-methyl-1,3-propanediol
NMP	N-methyl-2-pyrrolidone.
NMR	Nuclear magnetic resonance.
OD	Outer diameter.
PBT	Polybutylene terephthalate.
PBu <sub>3</sub>	Tributyl phosphine.
PEt <sub>3</sub>	Triethyl phosphine.
ppm	Parts per million.
<sup>i</sup> Pr	<i>iso</i> -Propyl.
<sup>31</sup> P{ <sup>1</sup> H}	Phosphorus, proton decoupled.
PO	Propylene oxide.
Sixantphos	4,6-Bis(diphenylphosphino)-10,10-dimethylphenoxasilin.
TBP	Trigonal bi-pyramid.
Thixantphos	2,8-dimethyl-4,6-bis(diphenylphosphino) phenoxathiin.
TosOH	<i>para</i> -Toluene sulfonic acid.
TPP	Triphenylphosphine.
Tppts	Tri(meta-sulfonyl)triphenylphosphine.

Xantphos

9,9-dimethyl-4,6-bis(diphenylphosphino) xanthene.

## TABLE OF CONTENTS

<b>1</b>	<b>CHAPTER ONE: INTRODUCTION.....</b>	<b>1</b>
1.1	Hydroformylation .....	2
1.1.1	History of Hydroformylation.....	2
1.1.2	Steric and Electronic Effects.....	9
1.1.3	Rhodium Catalysed Hydroformylation with Diphosphine Ligands.....	14
1.1.3.1	First Examples of Diphosphine Modified Rhodium Catalysed Hydroformylation.....	14
1.1.3.2	1,1'-Bis(diphenylphosphino)ferrocene and Related Ligands.....	18
1.1.3.3	2,2'-Bis(phosphinomethyl)-1,1'-biphenyl and the Natural Bite Angle..	20
1.1.3.4	Xanthene Based Diphosphines.....	33
1.1.4	Rhodium Catalysed Hydroformylation with Alkyl-Phosphine Ligands.....	41
1.2	1,4-Butanediol .....	44
1.2.1	BDO A Commodity Chemical.....	44
1.2.2	The Production of 1,4-Butanediol From Acetylene and Formaldehyde "The Reppe Process".....	45
1.2.3	1,4-Butanediol From Butadiene.....	46
1.2.4	1,4-Butanediol From n-Butane and Maleic Anhydride.....	46
1.2.5	1,4-Butanediol From Propylene Oxide and the Hydroformylation of Allyl Alcohol.....	49
1.3	References for Chapter One.....	55
<b>2</b>	<b>CHAPTER TWO: THE RHODIUM / DIOP CATALYTIC SYSTEM. ....</b>	<b>59</b>
2.1	(-)-2,3-O-Isopropylidene-2,3-dihydroxy-1,4-bis(diphenylphosphino)butane, a New Chiral Diphosphine.....	60
2.2	HP NMR and HP FTIR Experimental Techniques.....	63
2.2.1	HP NMR Experiments.....	63
2.2.2	HP FTIR Experiments.....	65
2.2.3	Kinetic Measurement Experiments.....	67
2.3	Rhodium DIOP Species at 1 Bar and 25 °C.....	69
2.3.1	Rhodium DIOP Species Present Under an Argon Atmosphere.....	69

TABLE OF CONTENTS.

2.3.2	Rhodium DIOP Species Under Synthesis Gas. ....	82
2.3.2.1	Rhodium to DIOP ratio of 1:1. ....	86
2.3.2.2	Rhodium to DIOP ratio of 1:1.5 & 1:2. ....	89
2.3.3	Addition of Hydrogen Gas.....	93
2.4	Rhodium DIOP Species Present Under High Pressures. ....	94
2.4.1	Rhodium DIOP Ratio of 1:1.5. ....	94
2.4.1.1	High Pressure NMR Studies. ....	94
2.4.1.2	High Pressure IR Studies. ....	102
2.4.2	Rhodium to DIOP Ratio 1:1. ....	108
2.4.2.1	High Pressure NMR Studies. ....	108
2.4.2.2	High Pressure IR Studies. ....	110
2.4.3	Changing the CO and H <sub>2</sub> Partial Pressures. ....	111
2.4.4	Changing the Total Pressure. ....	113
2.5	<i>In-Situ</i> High Pressure Studies of the Hydroformylation of Allyl Alcohol. ....	115
2.5.1	HP NMR Studies of the Hydroformylation of Allyl Alcohol.....	115
2.5.2	Increasing the HP NMR Cell Size. ....	123
2.5.3	HP IR Studied of the Hydroformylation of Allyl Alcohol. ....	128
2.5.4	Kinetic Studies of the Hydroformylation of Allyl Alcohol. ....	132
2.5.4.1	CO to H <sub>2</sub> Ratio 1:1.....	132
2.5.4.2	CO to H <sub>2</sub> Ratio 2:3.....	133
2.5.4.3	CO to H <sub>2</sub> Ratio 3:2.....	133
2.5.4.4	Conclusions.....	133
2.6	<i>In-Situ</i> High Pressure Studies of the Hydroformylation of 1-Hexene. ....	134
2.6.1	HP NMR Studies of the Hydroformylation of 1-Hexene. ....	134
2.6.2	HP IR Studies of the Hydroformylation of 1-Hexene. ....	139
2.6.3	Kinetic Studies of the Hydroformylation of 1-Hexene.....	142
2.7	References for Chapter Two. ....	144
<b>3</b>	<b>CHAPTER THREE: CATALYST POISONING. ....</b>	<b>148</b>
3.1	A Study of The Oxidation Properties of DIOP and DPPB. ....	149
3.1.1	Experiment One: Results For the Rhodium DIOP Ratio 1:1.5 Catalytic Solution.....	151

3.1.2	Experiment Two: Results For the Rhodium DIOP TPP Ratio 1:2:3 Catalytic Solution. ....	155
3.1.3	Experiment Three: Results For the Rhodium dppb TPP Ratio 1:2:3 Catalytic Solution. ....	159
3.1.4	Experiment Four: Results For the Rhodium DIOP Ratio 1:1 Catalytic Solution. ....	164
3.1.5	Experiment Five: Results For the Rhodium dppb Ratio 1:1 Catalytic Solution. ....	164
3.1.6	Experiment Six: Results For the Rhodium DIOP Ratio 1:1 Catalytic Solution in the Presence of Allyl Alcohol. ....	167
3.1.7	Experiment Seven: Results For the Rhodium dppb Ratio 1:1 Catalytic Solution in the Presence of Allyl Alcohol. ....	170
3.1.8	Conclusions. ....	177
3.2	Effect of $\text{Fe}(\text{CO})_5$ on the Oxidation Properties of DIOP. ....	180
3.2.1	Experiment One: $\text{Fe}(\text{CO})_5$ / DIOP. ....	180
3.2.2	Experiment Two: $\text{Fe}(\text{CO})_5$ / DIOP under Synthesis gas 20 bar. ....	182
3.2.3	Experiment Three: $\text{Fe}(\text{CO})_5$ / DIOP / Allyl Alcohol Under Synthesis Gas 20 bar. ....	186
3.2.4	Experiment Four: $\text{Rh}(\text{CO})_2(\text{acac})$ / $\text{Fe}(\text{CO})_5$ / DIOP / Allyl Alcohol Under 98 % Synthesis Gas & 2 % Air at 20 bar. ....	189
3.2.5	Conclusions. ....	194
3.3	References for Chapter Three. ....	196
<b>4</b>	<b>CHAPTER FOUR: NEW LIGANDS FOR THE HYDROFORMYLATION REACTION..</b>	<b>197</b>
4.1	9,9-Dimethyl-4,6-bis(diethylphosphino)xanthene [Et-Xantphos]. ....	199
4.1.1	Synthesis. ....	200
4.1.2	Rhodium Et-Xantphos complexes. ....	203
4.1.3	Catalytic Results. ....	212
4.1.3.1	Hydroformylation of Allyl Alcohol with the Rh/ Et-Xantphos Catalytic System in Toluene. ....	221
4.1.3.2	Hydroformylation of Allyl Alcohol with the Rh/ Et-Xantphos Catalytic System in Ethanol. ....	225

4.1.3.3 Hydroformylation of Allyl Alcohol with the Rh/ Et-Xantphos Catalytic System in THF. ....	228
4.1.3.4 Hydroformylation of Allyl Alcohol with the Rh/ Et-Xantphos Catalytic System in MTBE. ....	230
4.1.3.5 Hydroformylation of Allyl Alcohol with the Rh/ Et-Xantphos Catalytic System in Amyl Alcohol. ....	231
4.1.3.6 Hydroformylation of Allyl Alcohol with the Rh/ Et-Xantphos Catalytic System in THF/H <sub>2</sub> O. ....	233
4.1.3.7 Hydroformylation of Allyl Alcohol with the Rh/ Et-Xantphos Catalytic System in Toluene/ Acetic Acid. ....	233
4.1.3.8 Hydroformylation of Allyl Alcohol with the Rh/ Et-Xantphos Catalytic System in MTBE / EtOH. ....	234
4.1.3.9 Hydroformylation of 1-Octene with the Rh/ Et-Xantphos Catalytic System in Toluene. ....	235
4.1.3.10 Hydroformylation of 1-Octene with the Rh/ Et-Xantphos Catalytic System in Ethanol. ....	237
4.1.3.11 Iridium Et-Xantphos Hydrogenation Catalysts?.....	239
4.1.3.12 Comparison of the Results of the Hydroformylation of Allyl Alcohol in Different Solvents. ....	244
4.2 9,9-Dimethyl-4,6-bis(di- <i>tert</i> -butylphosphino)xanthene [ <sup>t</sup> Bu-Xantphos].....	245
4.2.1 Synthesis. ....	245
4.2.2 Catalytic Results. ....	246
4.2.2.1 Hydroformylation of Allyl Alcohol with the Rh/ <sup>t</sup> Bu-Xantphos Catalytic System in Toluene. ....	246
4.2.2.2 Hydroformylation of Allyl Alcohol with the Rh/ <sup>t</sup> Bu-Xantphos Catalytic System in Ethanol. ....	246
4.3 9,9-Dimethyl-2,7-di- <i>t</i> -butyl--4,5-bis(diethylphosphino)xanthene [Et- <sup>t</sup> BuXantphos]. ....	248
4.3.1 Synthesis. ....	248
4.3.2 Catalytic Results. ....	249
4.3.2.1 Hydroformylation of Allyl Alcohol with the Rh/ Et- <sup>t</sup> BuXantphos Catalytic System in Ethanol.....	252
4.3.2.2 Hydroformylation of 1-Octene with the Rh/ Et- <sup>t</sup> BuXantphos Catalytic System in Ethanol.....	254

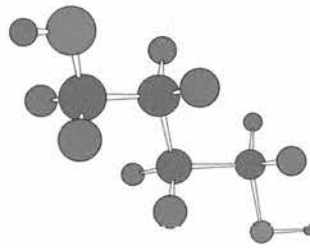
TABLE OF CONTENTS.

4.4	2,2'-Bis di- <i>iso</i> -propylphosphanyl biphenyl [ <sup>i</sup> Pr-Bisbite].	256
4.4.1	Synthesis.	256
4.4.2	Catalytic Results.	256
4.4.2.1	Hydroformylation of Allyl Alcohol with the Rh/ <sup>i</sup> Pr-Bisbite Catalytic System in Toluene.	258
4.4.2.2	Hydroformylation of Allyl Alcohol with the Rh/ <sup>i</sup> Pr-Bisbite Catalytic System in Ethanol.	258
4.5	DIOP.	259
4.5.1	Catalytic Results.	259
4.5.1.1	Hydroformylation of Allyl Alcohol with the Rh/DIOP Catalytic System in Toluene.	261
4.5.1.2	Hydroformylation of 1-Octene with the Rh/DIOP Catalytic System in Toluene.	261
4.6	Xantphos.	262
4.6.1	Catalytic Results.	262
4.6.1.1	Hydroformylation of Allyl Alcohol with the Rh/Xantphos Catalytic System in Toluene.	265
4.6.1.2	Hydroformylation of Allyl Alcohol with the Rh/Xantphos Catalytic System in Ethanol.	266
4.6.1.3	Hydroformylation of 1-Octene with the Rh/Xantphos Catalytic System in Toluene.	266
4.7	Comparison of the Ligands.	269
4.7.1	Hydroformylation of Allyl alcohol.	269
4.7.2	Hydroformylation of 1-Octene.	271
4.8	References for Chapter Four	273
<b>5</b>	<b>CHAPTER FIVE: FURTHER WORK.</b>	<b>275</b>
5.1	References for Chapter Five	282
<b>6</b>	<b>CHAPTER SIX: EXPERIMENTAL.</b>	<b>283</b>
6.1	General Procedure	284
6.1.1	Laboratory Reagents.	284
6.1.2	Analytical Techniques.	285

## TABLE OF CONTENTS.

6.2	Synthesis.....	285
6.2.1	(Acetylacetonato) (dicarbonyl) rhodium(I) $[\text{Rh}(\text{CO})_2(\text{acac})]^{1,2}$ .....	285
6.2.2	$[\text{Rh}(\text{acac})(\text{DIOP})]$ .....	286
6.2.3	$[\text{Rh}_2(\text{CO})_4(\text{DIOP})_2]$ .....	286
6.2.4	$[\text{HRh}(\text{CO})_2(\text{DIOP})]$ .....	287
6.2.5	$[\text{Rh}(\text{COCH}_2\text{CH}_2\text{CH}_2\text{OH})(\text{CO})_2(\text{DIOP})]$ & $[\text{Rh}(\text{COCHCH}_3\text{CH}_2\text{OH})(\text{CO})(\text{DIOP})]$ , Complex Species 49 and 50.....	288
6.2.6	9,9-Dimethyl-4,6-bis(diethylphosphino)xanthene, [Et-Xantphos].....	289
6.2.7	$[\text{Rh}_2(\text{CO})_4(\text{Et-Xantphos})_2]$ .....	289
6.2.8	9,9-Dimethyl-4,6-bis(di- <i>tert</i> -butylphosphino)xanthene [ <sup>1</sup> Bu-Xantphos]..	290
6.2.9	2,7-Di- <i>tert</i> -butyl-9,9-dimethyl-4,6-bis(diethylphosphino)xanthene, [Et- <sup>1</sup> BuXantphos].....	291
6.2.10	2,2'-Bis di-iso-propylphosphanyl biphenyl, [ <sup>1</sup> Pr-Bisbite].....	291
6.2.11	Chlorodibenzylphosphine, $[\text{Bz}_2\text{PCl}]$ .....	292
6.2.12	$[\text{Bz}_2\text{P}(\text{COH})(\text{CH}_3)\text{CH}_2\text{C}(\text{CH}_3)_2\text{O}]\text{Cl}$ .....	293
6.3	High Pressure Nuclear Magnetic Resonance Studies.....	296
6.3.1	Apparatus.....	296
6.3.2	General Procedure.....	297
6.3.3	High Pressure NMR Conditions.....	298
6.4	High Pressure Infrared Experiments.....	298
6.4.1	General Procedure.....	299
6.4.2	High Pressure IR Experiments.....	299
6.5	Hydroformylation with the CATS Catalyst Testing Unit.....	300
6.5.1	Apparatus.....	300
6.5.2	General Procedure.....	302
6.5.3	Reaction Conditions.....	302
6.6	References for Chapter Six.....	303

*CHAPTER ONE: INTRODUCTION*



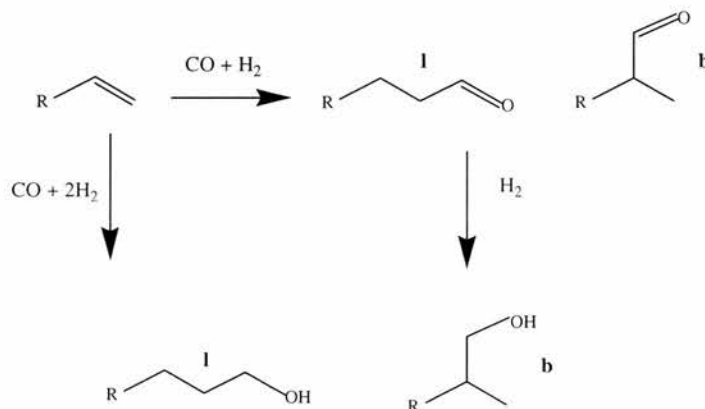
# 1 CHAPTER ONE: INTRODUCTION

## 1.1 Hydroformylation

The hydroformylation reaction is one of the most important homogeneous catalytic reactions used in industry today.<sup>1</sup> The process introduces carbon monoxide and hydrogen to the double bond of an alkene to form an aldehyde or alcohol. The alcohol is usually the desired product so aldehyde products are usually converted to alcohols.<sup>2</sup> There are also two possible geometric products of reaction, the linear, **1**, and the branched, **b**, see Scheme 1.1. Because of its industrial importance, the subject is one of great interest and much study; for most substrates this has been aimed at maximising the production of the linear product over the branched.

### Scheme 1.1

*The l and b isomers of the aldehyde and alcohol products available from the hydroformylation reaction.*



### 1.1.1 History of Hydroformylation.

The first hydroformylation catalysts were discovered by Otto Roelen in 1938.<sup>3, 4</sup> They are unmodified cobalt carbonyl compounds, such as dicobalt octacarbonyl [Co<sub>2</sub>(CO)<sub>8</sub>], which generates [HCo(CO)<sub>4</sub>]<sup>1</sup> as the catalyst precursor. The mechanism of reaction was elucidated by Heck and Breslow<sup>5</sup> and can be seen in scheme 1.2. The process relies on relatively vigorous conditions (200-400 bar and 150-200 °C) as the reactivity and



The breakthrough came when Wilkinson discovered that triarylphosphine modified rhodium complexes were extremely active hydroformylation catalysts<sup>11</sup>. The most famous catalyst precursor is  $[\text{RhH}(\text{PPh}_3)_3\text{CO}]$  which forms  $[\text{RhH}(\text{PPh}_3)_2(\text{CO})_2]$ , species **1** in scheme 1.3, under carbon monoxide and hydrogen, and  $[\text{RhH}(\text{PPh}_3)_2\text{CO}]$ , species **2** in Scheme 1.3 during hydroformylation. A high triphenylphosphine (**TPP**) to rhodium ratio is required to prevent the formation of a monophosphine complex such as  $[\text{RhH}(\text{PPh}_3)(\text{CO})_2]$  during hydroformylation. The regioselectivity of the catalyst system can be up to 92 %<sup>6</sup> for the linear product. The reaction produces aldehydes, so the desired alcohols are obtained *via* a subsequent hydrogenation step.

A further development has involved the use of biphasic systems. This is addressing the problems encountered with product separation in homogeneous catalytic reactions. Usually, reaction products are separated in one of two ways, either by gas phase separation via distillation, or by keeping the reactants and products in the gas phase though out the reaction by controlling the reaction conditions.<sup>6</sup> These approaches are only appropriate if the reaction products can be distilled at temperatures below the decomposition temperature of the catalyst ( $[\text{RhH}(\text{CO})(\text{PPh}_3)_3]$  decomposes at  $\sim 110^\circ\text{C}$ ). For this reason only  $\text{C}_3\text{-C}_5$  aldehydes can be distilled directly from the reaction solution; for the production of longer chain aldehydes, the separation of the products becomes a serious problem. One way to overcome this problem is to use a heterogeneous solid catalyst by fixing rhodium to a support. However, in almost all cases, leaching of the catalyst occurs from the support, and the activity, therefore, reduces with time.

Liquid biphasic systems allow easy separation of products and catalyst as they are in different phases, but they retain a high efficacy and selectivity. An example of such is the extremely successful Ruhrchemie-RhonePoulenc process<sup>12</sup> for hydroformylation. The process has been commercialised for the hydroformylation of propene (operated by Celanese since 1984) and butene (operated since 1995). The catalyst in this process is a tri(*m*-sulfonyl)triphenylphosphine (Tppts), see Figure 1.1, modified rhodium complex which is highly soluble in water. The process is carried out in the presence of an aqueous phase containing the catalyst, an organic solvent, and the alkene to be hydroformylated. Under hydroformylation conditions the phases are mixed, and after hydroformylation the phases separate and the organic phase containing the products of reaction can be decanted from the aqueous phase containing the catalyst.

## Scheme 1.3

The Wilkinson mechanism for the rhodium catalysed hydroformylation of alkenes.

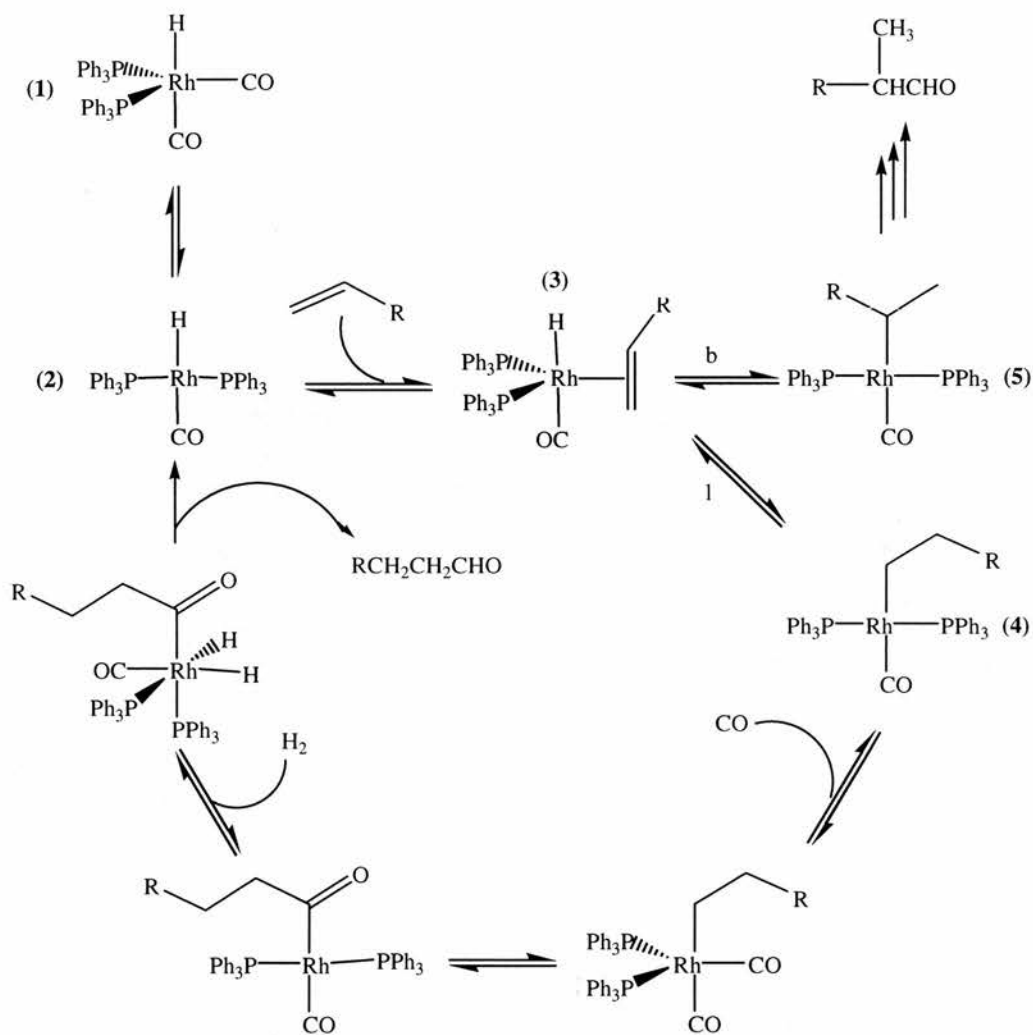
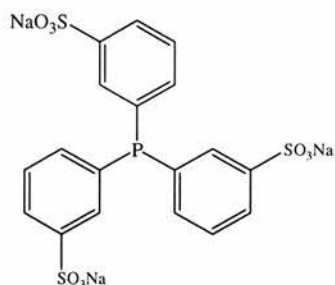


Figure 1.1

*Tri(m-sulfonyl)triphenylphosphine (Tppts), ligand in the biphasic Ruhrchemie-RhonePoulenc hydroformylation process.*

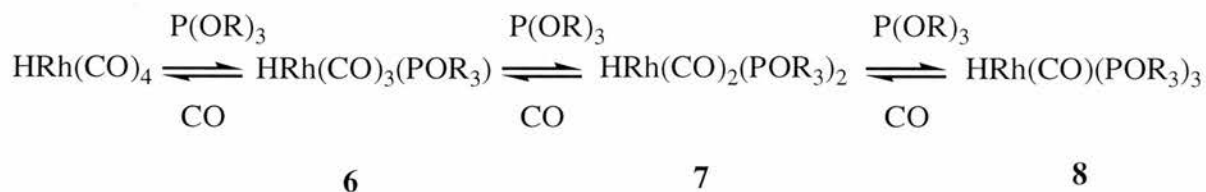


In 1969, shortly after Wilkinson's discovery of rhodium triarylphosphine catalysts, Pruett and Smith reported that phosphite ligands, both aryl and alkyl, were effective ligands for rhodium catalysed hydroformylation of 1-octene and methylacrylate.<sup>13</sup> From their results they postulated that the rates of reaction and the l:b selectivity were governed by three possible active catalytic species in solution, 6, 7 & 8 in Figure 1.2. This proposal arose from the effect on the rate and selectivity when changing the carbon monoxide partial pressure, the ligand concentration, the electronic character of the ligand, and the steric character of the ligand. Increasing the total pressure of a gas with a 1:1 CO to H<sub>2</sub> composition increased the reaction rate and decreased the l:b ratio; similarly, increasing the CO:H<sub>2</sub> ratio had the same effect. A higher ligand to rhodium ratio, however, had the opposite effect, giving a slower rate of reaction and a higher l:b ratio.

Phosphorus ligands which are stronger  $\sigma$ -donors and weaker  $\pi$ -acceptors than CO cause the remaining CO ligands to be more strongly bound to the metal centre, thus slowing alkene co-ordination and the rate of reaction. Steric crowding around the rhodium centre also decreased the rate of reaction but favoured the formation of the linear product. Increased CO partial pressure favoured the less crowded species 6, and increased ligand to rhodium ratio would favour the more sterically crowded species 8.

**Figure 1.2**

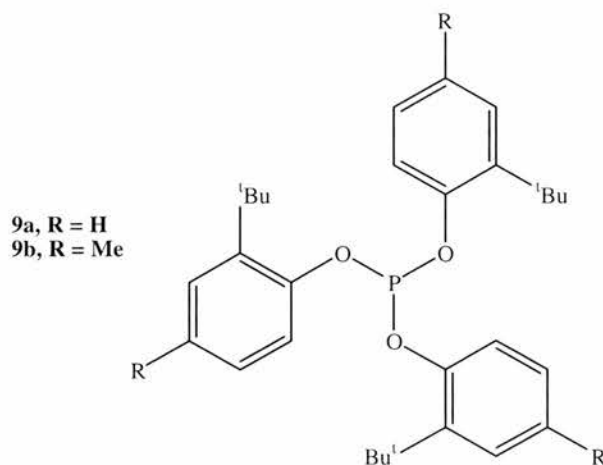
*Active rhodium phosphite catalytic species.*



Interest in phosphites was renewed recently with van Leeuwen and coworker's discovery<sup>14,15</sup> that bulky monophosphites, see **9** in Figure 1.3 used as ligands in the rhodium catalysed hydroformylation can give high rates of reaction for the hydroformylation of both terminal and internal alkenes.

**Figure 1.3**

An example of van Leeuwen's "Bulky Mono-phosphites".

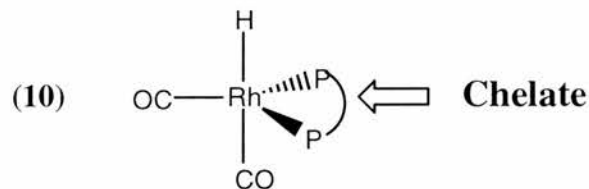


A rhodium complex containing tris(ortho *tert*-butylphenyl)phosphite **9a** was used in the hydroformylation of 2-methyl-1-hexene,<sup>14</sup> and gave rates up to  $1600 \text{ mol mol}^{-1} \text{ Rh}^{-1} \text{ h}^{-1}$  with almost 100 % selectivity to the linear product 3-methyl-heptaldehyde (the branched product would have a quaternary carbon and is therefore sterically unfavoured). Similar results were reported for the hydroformylation of limonene.

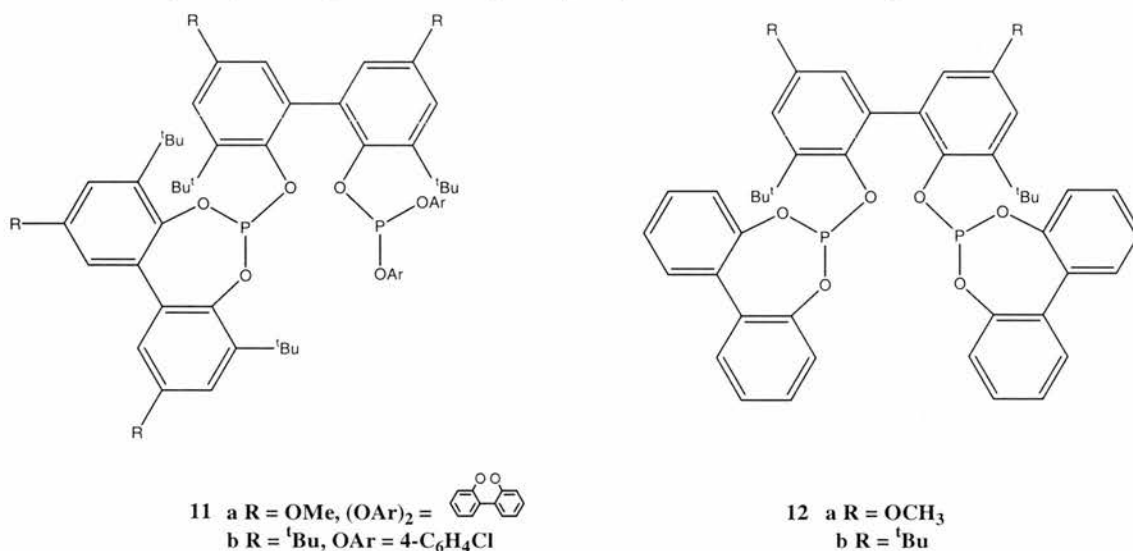
Another bulky mono-phosphite ligand, tris(ortho *tert*-butyl-4-methylphenyl)phosphite **9b**, was used in the rhodium catalysed hydroformylation of 1-octene.<sup>6</sup> This gave exceptionally high rates of up to  $161000 \text{ mol.mol}^{-1} \text{ Rh}^{-1} \text{ h}^{-1}$ , but suffered from a poor l:b ratio (1.9) and high levels of isomerisation products (13 %).

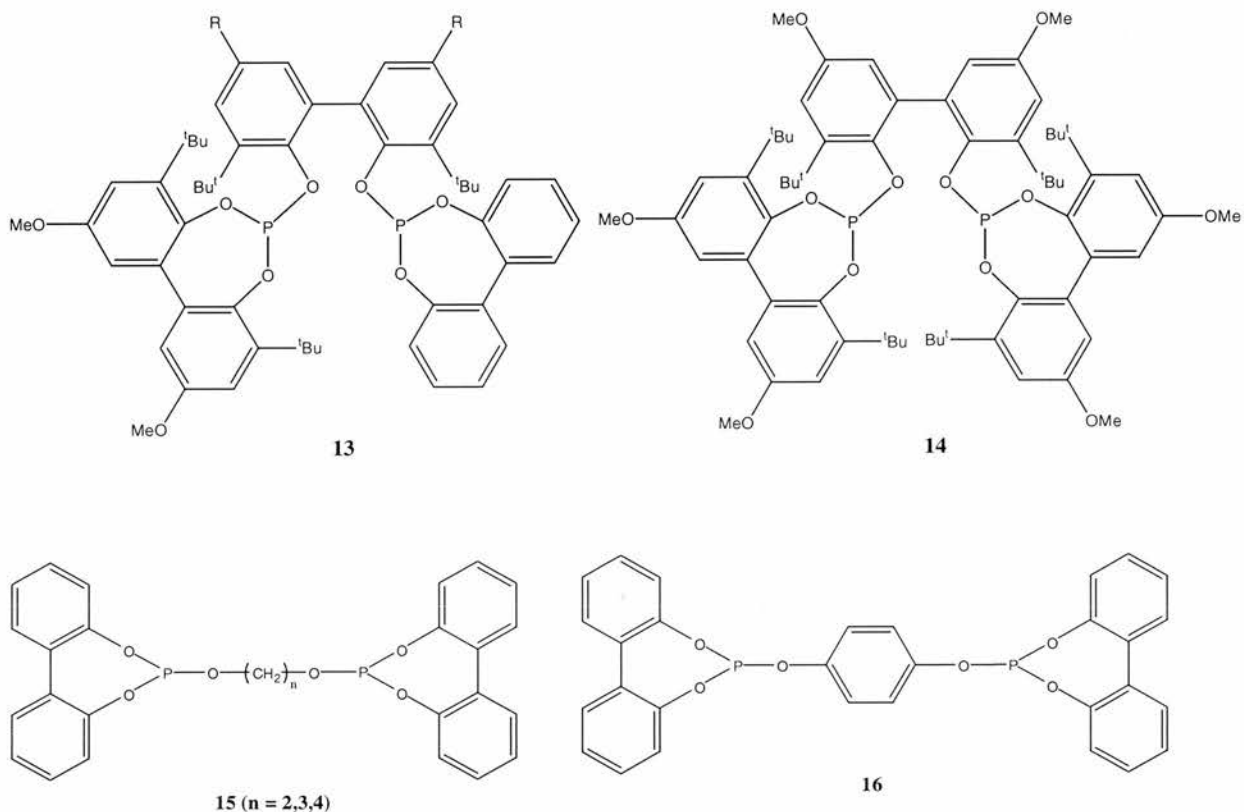
Soon after this, it was reported by Bryant and co-workers that increased selectivity could be achieved by using diphosphites as ligands. The rates of reaction were reduced, however, although they were still faster than the analogous triphenylphosphine reactions.

Because of their large cone angles,<sup>16, 17</sup> see section 1.1.2, bulky mono-phosphites form mono-phosphite complexes with rhodium, such as **6** in Figure 1.2, which favour higher reaction rates and lower selectivities, see above. For diphosphite ligands, the chelate effect means that they do not form mono-phosphite complexes but are di-phosphite complexes, see **10** in Figure 1.4; thus, they have a lower reactivity but higher selectivity when used as ligands in the rhodium catalysed hydroformylation. It is also observed that diphosphite ligands do not have as high reactivities for the hydroformylation of internal alkenes as observed for bulky mono-phosphites.

**Figure 1.4***Chelate effect influencing rhodium complex structure.*

An important factor in the diphosphite modified rhodium system is that the exact structures of the diphosphite ligands have a strong influence on the selectivities observed. The following ligands are some examples of diphosphite ligands developed by Bryant and co-workers for Union Carbide Corporation,<sup>18-20</sup> see Figure 1.5. Ligands **11** and **12** gave high selectivities with linear to branched of ratios up to 50:1 for the rhodium catalysed hydroformylation of 1-butene and propene respectively. However, the structurally similar ligands **13** and **14** gave poor selectivities with linear to branched ratios of 2-6 for the rhodium catalysed hydroformylation of 1-butene and propene. Whilst ligands with aryl backbones such as **15** do not generally give as high selectivities as ligands with the biphenol backbone such as **11** and **12**, the ligand with the propane linkage ( $n=3$ ) gave a higher l:b ratio of 3.8:1 than the ligands with the ethane or butane linkage ( $n=2$  and 4). Ligands such as **16**, which cannot form chelates, behave as bulky-mono-phosphite ligands with faster rates but low selectivities; they also produce high rates for the hydroformylation of internal alkenes.

**Figure 1.5***Diphosphite ligands developed by Bryant and co-workers for UCC.*



Further work on diphosphite modified rhodium catalysts for the hydroformylation of 1-octene and styrene has been carried out by van Leeuwen and co-workers.<sup>21, 22</sup> They have studied the influence of the ligand structure, both the bridge length and the steric bulk, on the l:b ratio.

As with phosphite ligands, there has been a lot of interest in the use of diphosphines to improve selectivities in the hydroformylation reaction. This work is discussed in some detail in section 1.1.3 “Rhodium Catalysed Hydroformylation with Diphosphine Ligands”. Before we do this, it is important to discuss some ligand parameters which are important when rationalising the benefit of diphosphine ligands.

### 1.1.2 Steric and Electronic Effects.

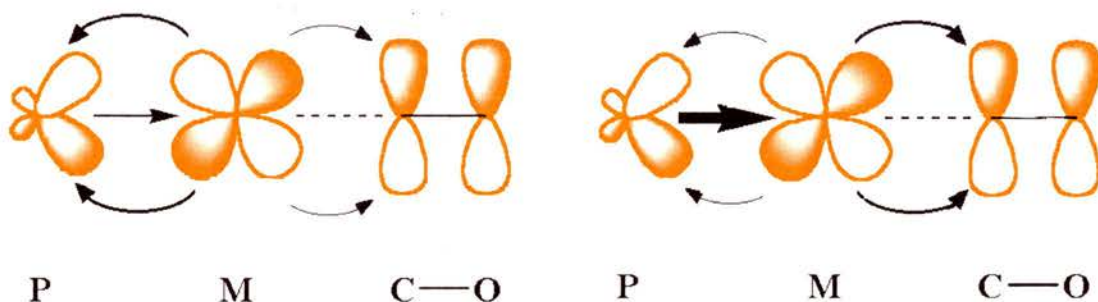
In the 1970's, Tolman proposed a rationalisation on how changing the substituents on phosphorus ligands can dramatically change the properties of their transition metal complexes. Previously there were a number of attempts to do this considering only electronic effects.<sup>23,24</sup> Tolman developed quantitative measurements of both the electronic effect<sup>25</sup> and also the steric effect<sup>26</sup>. Tolman suggested that steric effects

would generally be as important as electronic ones, and in some circumstances more so.<sup>17</sup>

The electron parameter was defined as the overall effect of the electron donating and electron accepting properties of the phosphorus ligand. It is termed as  $\chi$ , and is derived from the symmetric ( $A_1$ ) carbonyl stretching frequency of the nickel complex  $[\text{Ni}(\text{CO})_3\text{L}]$ , where L is the phosphorus ligand. Since backbonding to the CO  $\pi^*$  molecular orbital is a measure of the electron density on the metal, an electron rich metal centre will result in a higher degree of backbonding. As backbonding strengthens the M-C bond but weakens the C-O bond, it leads to lowering of the C-O stretching frequencies. Thus, if a phosphorus ligand is a strong  $\sigma$ -donor and weak  $\pi$ -acceptor, it will have a low  $\chi$  value, and if a phosphorus ligand is a weak  $\sigma$ -donor and strong  $\pi$ -acceptor, it will have a high  $\chi$  value, see Figure 1.1.

**Figure 1.1**

*Tolman's electronic parameter,  $\chi$ , based on backbonding between the phosphorus ligand, the metal centre and the carbonyl ligand.*



**High  $\chi$  value – strong phosphorus  $\pi$ -acceptor.**

**weak phosphorus  $\sigma$ -donnor**

**Low  $\chi$  value – weak phosphorus  $\pi$ -acceptor.**

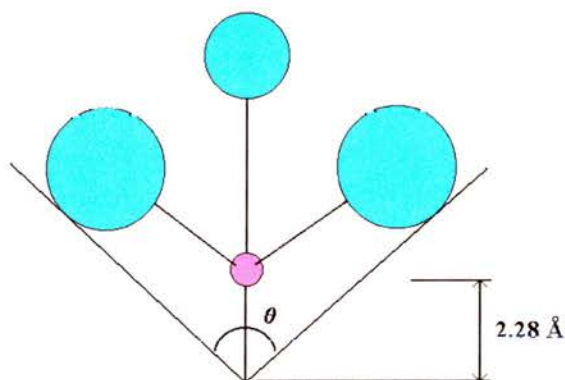
**strong phosphorus  $\sigma$ -donnor**

Tolman's steric parameter is known as the ligand cone angle, and is measured as  $\theta$ . The cone angle for a symmetrical phosphine ligand (one with all three substituents the same), is measured as the apex angle of a cylindrical cone centred 2.28 Å from the centre of the P atom which just touches the van der Waals radii of the outermost atoms of the ligand, see Figure 1.2. If there are degrees of freedom in the phosphorus ligand, the ligand is folded back to form the minimum cone angle. For unsymmetrical

phosphines, the cone angle is measure as an average of the differing substituents, and for cone angles above  $180^\circ$  trigonometry is used.

**Figure 1.2**

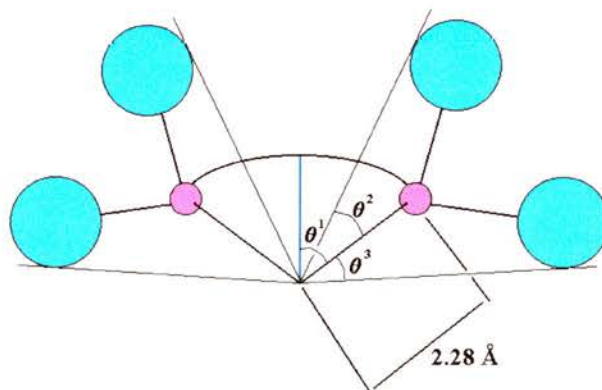
*Tolman's ligand cone angle.*



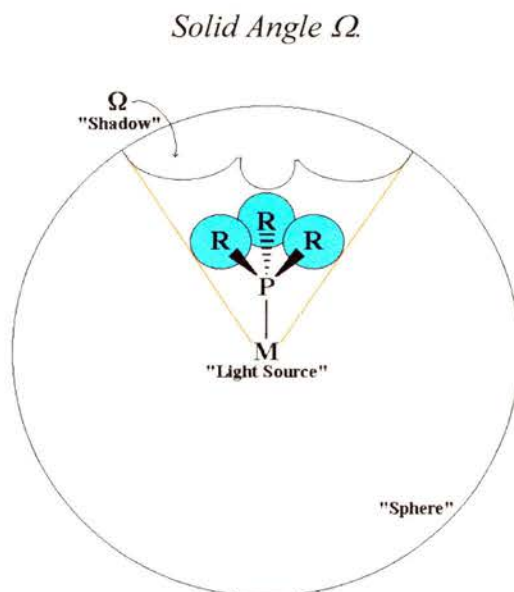
The cone angle theory has been extended to diphosphines and defined as the average cone angle as measured for the two substituents ( $\theta^2$  and  $\theta^3$ ) and the angle between the M-P bond and the bisector of the P-M-P angle ( $\theta^1$ ), see Figure 1.3.

**Figure 1.3**

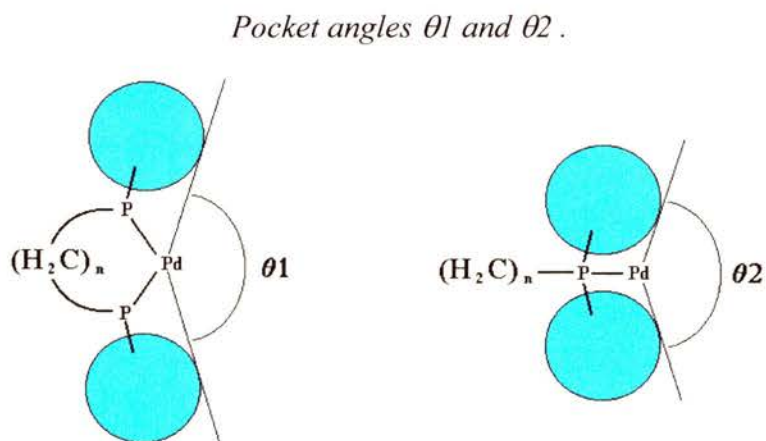
*Tolmans ligand cone angle for diphosphines.*



There have been many other attempts to define a parameter which will describe the effect of steric size in molecules, including that of bidentate ligands. These include the solid angle  $\Omega$  which is defined as the integral of the scalar products of the vector  $r$  with a vector element of surface divided by the cube of the magnitude of  $r$ .<sup>27, 28</sup> In more simple terms this is a measure of the “shadow” cast by an atom or group of atoms on a sphere when placed next to a light source, at the centre of that sphere, see Figure 1.4.

**Figure 1.4**

The pocket angle has also been used as a measure of ligand steric parameters.<sup>29</sup> Using the solid state structures of a complex as a model, and assuming free rotation of the substituents around the phosphorus atom, the pocket angle is measured both parallel to the plane of co-ordination and perpendicular to it. The parallel pocket angle is defined as the angle between two planes perpendicular to the plane of co-ordination and intersecting at the metal, that can exclude the van der Waals surface of all the ligands over all rotational orientations about the C-P bonds  $\theta_1$ . Similarly, the perpendicular pocket angle is defined as the angle between two planes parallel with the plane of co-ordination, and intersecting at the metal, that can exclude the van der Waals surface of all the ligands over all rotational orientations about the C-P bonds  $\theta_2$ , see Figure 1.5.

**Figure 1.5**

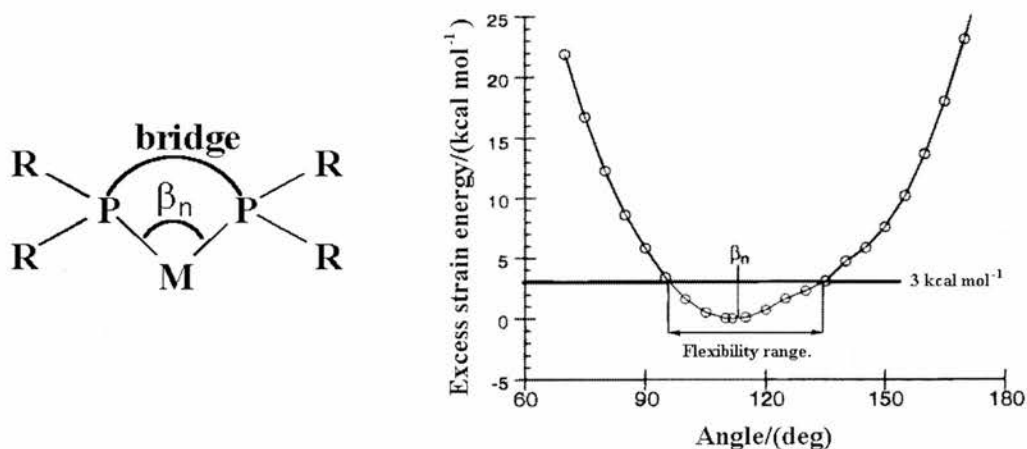
Molecular mechanics have also been employed by T. L. Brown<sup>30</sup> to compute a measure of the ligand steric effect. The energy minimised structures of complexes are calculated from molecular mechanics, then the exponential form of the van der Waals potential employed in the calculations is replaced by a purely repulsive form. The result is an energy quantity  $E_R$  which can be interpreted as the energy required to move the ligand a distance  $r_e$  against a constant force it experiences at the equilibrium distance,  $r_e$ .

Recently, a simpler method of determining the steric effect of bidentate phosphine ligands complexed to a metal centre has been developed, first by Casey<sup>31</sup> and co-workers, and then by van Leeuwen<sup>32</sup> and co-workers. In this model, the steric properties of diphosphines can be determined by the four substituents of the two phosphorus atoms, and the length of the bridge between them. The principle is based on the idea that a diphosphine ligand will prefer a particular geometry in a complex because of its sterics. For example, for a square planar complex, or apical-equatorial co-ordination in a trigonal bipyramidal structure, a diphosphine with a bite angle of  $90^\circ$  would be preferred. For a tetrahedral complex, a bite angle of  $109^\circ$ , and for bisequatorial co-ordination in the trigonal bipyramidal structure,  $120^\circ$  would be preferred. The bisequatorial co-ordination in the trigonal bipyramidal structure played an important role in the development of the ligand preferred bite angle's history, as will be seen later in section 1.1.3. For now, it is sufficient to say that it was desirable to study ligands which would be predisposed to have this geometry; thus, it was desirable to calculate a ligand's preferred bite angle. To do this, Casey and co-workers developed the "natural bite angle"  $\beta_n$ , and the ligand flexibility range. These parameters are determined by the ligand backbone and the phosphorus substituents only, not by metal valences. They are therefore independent of any electronic preferences of the metal and are a reflection solely of the ligand steric demand. The natural bite angle itself is determined by molecular mechanics, it is obtained by minimising the strain energy of the M(diphosphine) fragment with a P-M-P bending force constant of  $0 \text{ kcal mol}^{-1} \text{ rad}^{-2}$ . A potential energy diagram can then be drawn by fixing the bite angle at various values by applying a large bending force constant and calculating the strain energy at those values, such a potential energy diagram can be seen in Figure 1.11. The flexibility range is determined from the potential energy diagram by taking the available bite angles within a  $3 \text{ kcal mol}^{-1}$  excess strain energy range. Casey and co-workers worked out the natural bite angle and flexibility range of several diphosphines and

compared them to the known P-M-P angles available through x-ray crystallography data and found the correlation to be good.

**Figure 1.11**

*The bite angle  $\beta_n$  of bidentate phosphorus ligands, and an example of a potential energy diagram used to work out the flexibility range.*



### 1.1.3 Rhodium Catalysed Hydroformylation with Diphosphine Ligands.

#### 1.1.3.1 First Examples of Diphosphine Modified Rhodium Catalysed Hydroformylation.

The use of diphosphines as ligands in the hydroformylation reaction has recently become a topic of much interest. This has been due to reports of greatly improved l:b ratios over those obtained when using monophosphines as ligands. The idea is not a new one; in their investigations of the cobalt catalysed hydroformylation reaction Heck and Breslow reported that dppe reacts with acetyl cobalt carbonyl to form a complex which only has one phosphorus atom attached to the cobalt.<sup>33</sup> The other then reacts, presumably intramolecularly, which leads to an unstable product which was unidentified. This result was surprising as it is noted that generally, bis-phosphines form more stable complexes than mono-phosphines.

Later, Slaugh and co-workers reported the use of dppe in the phosphine modified cobalt catalysed hydroformylation of 1-hexene. The results, however, showed that compared

to the [PBU<sub>3</sub>] phosphine modified cobalt catalyst, there was little effect on the rates and selectivity of the reaction.<sup>34</sup>

Pittmann suggested, in 1978, that the use of *cis*-chelating diphosphines as ligands in the rhodium catalysed hydroformylation could lead to higher l:b ratios.<sup>35</sup> The reasoning behind this hypothesis was that by using chelating ligands the equilibrium between [RhH(CO)<sub>2</sub>(PR<sub>3</sub>)<sub>2</sub>] and [RhH(CO)<sub>2</sub>(PR<sub>3</sub>)] could be influenced in favour of the former complex, and it was known that this gives better selectivity towards the linear isomer.<sup>35</sup> Pittmann studied the hydroformylation of 1-pentene with dppe modified rhodium catalysts at temperatures of 60-120 °C and at pressures of 7-55 bar. At 60 °C and 7 bar CO/ H<sub>2</sub>, the l:b ratio was 2.0. On increasing the temperature to 80 °C the l:b ratio was 1.9, and at 100 °C the l:b ratio was 1.7 and at 120 °C the l:b ratio was 1.0. At higher pressures, 28 bar and 55 bar, the effect was not so pronounced, with an l:b ratio of about 1.9 at 28 bar at all temperatures and 1.8 at 55 bar at all temperatures. The results were surprising as the l:b ratio was lower than when using a TPP modified rhodium catalyst system; under the same conditions the l:b ratio using this system was 3.0 to 3.5. The use of the dppe modified rhodium catalyst system also promotes the isomerisation of 1-pentene to 2-pentene in significant quantities where no isomerisation is observed using the TPP modified rhodium catalyst system.

The dppe system is more reactive than the TPP system for cyclic alkenes, as cyclohexene is hydroformylated to cyclohexanecarboxaldehyde at 85 °C, 400 bar CO/ H<sub>2</sub> 1:1 in 20 hrs using dppe, but no aldehyde is observed using TPP.

It is well known that increasing the P/Rh ratio in the TPP rhodium catalysed hydroformylation reaction causes an increase in the l:b ratio,<sup>35</sup> the l:b ratio increases from 3.0 to 7.6 on increasing the P/Rh ratio from 5:1 to 50:1 in the hydroformylation of 1-pentene at 80 °C and at 7 bar. However, with the dppe rhodium catalysed hydroformylation reaction, an increase in the dppe/ Rh ratio from 1 to 9 the l:b ratio decreased under all the temperatures and pressures studied, for example from 2.0 to 1.2 at 60 °C and 7 bar and from 1.8 to 1.0 at 120 °C and 55 bar. It must be noted, however, that the catalyst was made in situ from [RhH(CO)(PPh<sub>3</sub>)<sub>3</sub>]. Therefore, when the dppe/ Rh ratio was 1:1, the P/ Rh ratio was 5/ 1 as the dppe/ PPh<sub>3</sub>/ Rh ratio was 1:3:1. Increasing the dppe ratio could, therefore, shift an equilibrium between the dppe and TPP catalyst system towards the less selective dppe catalyst system.

In an attempt to see whether other diphosphine ligands gave similar results to dppe, Pittmann also studied the hydroformylation of 1-pentene with

bis(diphenylphosphino)propane (dppp) and bis(diphenylphosphino)butane (dppb). At 80 °C, 7 bar CO/ H<sub>2</sub> 1:1, and P/Rh 21 (diphosphine/ PPh<sub>3</sub>/ Rh 9:3:1) the l:b ratio for the dppp modified catalytic system was 0.9 and for the dppb modified catalytic system was 1.2, both similar to that obtained for the dppe modified catalytic system, 1.1, and lower than for the TPP catalytic system, 6.7.

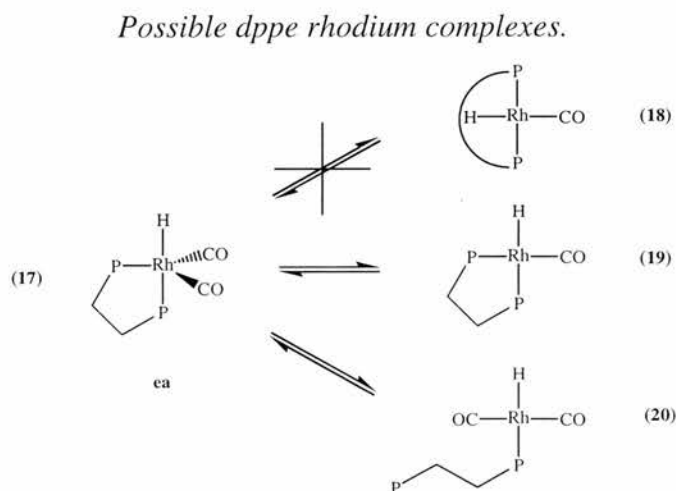
The low reactivity of dppe modified rhodium catalysts for the hydrogenation of styrene is attributed to the strong chelation effect of the ligand, as it forms a five membered ring when bidentate. It is therefore believed that this leads to the formation of stable complexes instead of the reactive catalytic ones. Thorn and Hoffman suggested that a diphosphine such as dppe would be co-ordinated equatorial-axial in the trigonal bipyramidal structure (TBP),<sup>36</sup> see Figure 1.12. For insertion of the coordinated alkene into the rhodium hydride to occur, a rearrangement to a four co-ordinate complex is required, see species **3** and **4** in Wilkinson's mechanism of hydroformylation in Scheme 1.3. This will involve a widening of the already strained P-M-P bond angle making the reaction unfavourable.

In a recent publication, van Leeuwen and co-workers<sup>6</sup> suggested two alternative explanations for the low selectivities in the dppe modified rhodium catalysed hydroformylation reaction. The first is that dppe occupies an equatorial-axial orientation in the TBP resting state of the catalyst, see **17** in Figure 1.12, and that with the dissociation of CO, this will form a complex with *cis* orientated phosphines, as dppe cannot accommodate *trans* orientated phosphines in the four co-ordinate structure, see **18** in Figure 1.12. It is therefore postulated that either a catalyst of this geometry will lead to a low regioselectivity in the hydroformylation reaction, or that after the complex adds to an alkene, the resulting 5-coordinate complex will also have an equatorial-axial bound dppe ligand geometry in the TBP structure and this will lead to the low regioselectivity observed. The second possibility is that the complex species, **17**, can undergo phosphine dissociation to form complex **20** in Figure 1.12 with only one rhodium bound phosphorus and that this will also lead to low regioselectivity.

The only beneficial use of dppe as a ligand in the rhodium catalysed hydroformylation reaction was reported by van Leeuwen and Roobeek for the hydroformylation of 1,3-butene. Hydroformylation of 1,3-butadiene to pentaldehyde with a TPP modified rhodium catalyst gives rise to rates of less than 6 (mol aldehyde) (molRh)<sup>-1</sup> h<sup>-1</sup> which are only slightly better than the use of unmodified rhodium as catalyst. They report that because of the low rates they detected no products over their reaction period. However,

use of dppe modified rhodium catalysts at 120 °C and 12 bar CO/ H<sub>2</sub> 1:2, P/ Rh 4:1 gives rates of 200 (mol aldehyde) (molRh)<sup>-1</sup> h<sup>-1</sup>. The selectivity to saturated aldehydes was 90 %, of which 99 % were the linear isomer 1,6-hexanedial, the other product of reaction was the unsaturated C<sub>5</sub> aldehyde.

**Figure 1.12**



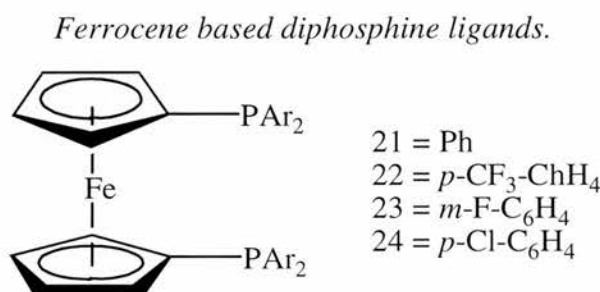
In 1973, Consiglio reported the use of DIOP in the asymmetric catalysed hydroformylation of terminal and internal alkenes. They were interested in inducing enantiomeric excesses in the branched product of reaction, and they reported optical purity ranging from 1.4 % for 2-methylhexanal from the hydroformylation of *trans*-2-hexene to 27 % optical purity in 2-methylbutanal from the hydroformylation of *cis*-but-2-ene.

They also reported the linear to branched ratios of 1-butene as 12.6, 1-pentene as 13.5, and 1-octene as 8.8, “under normal hydroformylation conditions” with a Rh/ DIOP ratio of 1:4. For a comparison Wilkinson, reported the linear to branched ratios from the hydroformylation of 1-pentene as 2.8, and of 1-butene 2.7, at 80 °C and 7 bar CO/H<sub>2</sub> 1:1; however, this was using [RhCOH(PPh<sub>3</sub>)<sub>2</sub>] as the catalyst precursor so the P/ Rh ratio was only 2:1.<sup>11</sup> van Leeuwen and co-workers reported the hydroformylation of 1-pentene<sup>37</sup> with [(Rh(COD)OAc)<sub>2</sub>] and TPP 1:10 at 90 °C and 20 bar CO/ H<sub>2</sub> 1:1 to give a l:b ratio of 3.6. They also reported the hydroformylation of 1-octene<sup>38</sup> with [Rh(CO)<sub>2</sub>(dipivaloylmethanoate)] and TPP 1:10 at 80 °C and 20 bar CO/H<sub>2</sub> 1:1 which gives an l:b ratio of 3.1. Consiglio’s results, therefore, represent the first example of using diphosphine ligands in the rhodium catalysed hydroformylation reaction to give improved l:b ratios.

### 1.1.3.2 1,1'-Bis(diphenylphosphino)ferrocene and Related Ligands.

In 1982 Unruh, developed the work further by using several ferrocene based diphosphine modified rhodium catalysts, see Figure 1.13; the diphosphines were based on 1,1'-bis(diphenylphosphino)ferrocene (dppf) or ligand 21.<sup>39</sup> A later review<sup>6</sup> described ferrocene as a flexible ligand with known P-M-P angle of 92-120 °C, but preferring  $\sim 97 \pm 2^\circ$ . It is also expected that rotation of the cyclopentadienyl ligands anti to each other will allow the ligand to accommodate a variety of bridging structures.

**Figure 1.13**

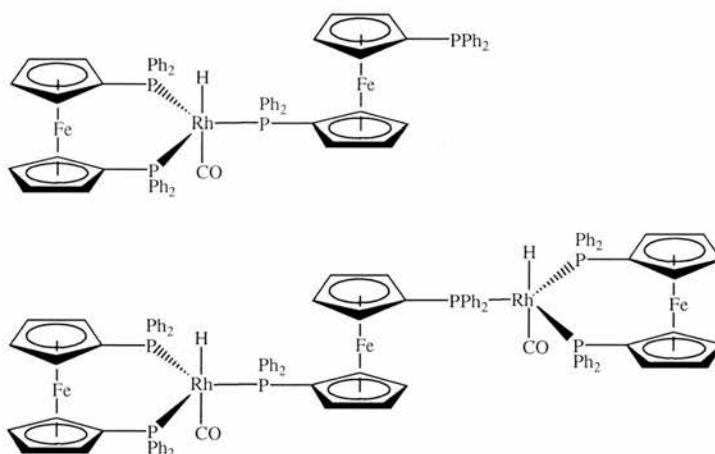


A study of the effect of dppf: Rh ratio on the product selectivity (l:b) was undertaken to see whether exploiting the chelate effect of bidentate ligands allowed regioselective hydroformylation to occur with lower P/ Rh ratios. The results of the hydroformylation of 1-hexene at 110 °C, and 7.9 bar CO/ H<sub>2</sub> 1:1, are given in Table 1.1. In summary, they show that there is a large increase in the l:b ratio and in the heptanal selectivity as the dppf:Rh ratio increased to 1.5, but there is very little effect after this. This led Unruh and coworkers to speculate that there are three phosphorus atoms bound to each rhodium atom, where one dppf ligand chelates to each rhodium, and another bridges two rhodium atoms, see Figure 1.14, and that this catalytic species is more selective to the linear product.

**Table 1.1***Effect of dppf:Rh ratio on the selectivity in the hydroformylation of 1-hexene.*

dppf: Rh ratio	L:b ratio	Heptanal selectivity	2-methyl hexanal selectivity.	2-hexene selectivity.	Hexane selectivity
1.0	2.1	54.2	25.6	19.2	1.0
1.25	2.8	57.5	20.8	20.8	0.9
1.5	5.1	82.5	16.1	0.5	0.9
2.0	5.2	83.0	15.8	0.5	0.7
3.0	5.2	82.6	15.9	0.6	0.9

Indeed, there is NMR evidence for this type of complex<sup>40</sup> in solution at varied dppf/ Rh ratios where all three phosphines occupy equatorial sites. It should be noted however, that these experiments were carried out at a rhodium concentration two or three times the magnitude of the actual catalytic situation.

**Figure 1.14***Possible Rh-P<sub>3</sub> complexes.*

A re-examination of the dppf-Rh system by van Leeuwen and coworkers has shown that the only in situ species are, in fact,  $[\text{RhH}(\text{dppf})(\text{CO})_2]$  existing with ee and ea coordination in rapid equilibrium.<sup>6</sup>

Unruh and coworkers also studied the effect of decreasing basicity of the ferrocene catalyst on the l:b ratio. To do this, they synthesised the ligands 22 to 24 in Figure 1.13; the basicity of these ligands was altered by adding electron withdrawing substituents to the meta or para positions of the phenyl groups of the phosphine in ligand 21. It was believed that such alteration would decrease the basicity of the phosphine without altering the steric environment of the chelated complex. Although this is true, we shall see in the next section that the mode of chelation is changed when altering the

electronics of a ligand, as the less basic phosphine will have a greater preference for an equatorial site. The  $\chi$  value of the phosphines, and the results of the hydroformylation of 1-hexene at 110 °C and 7.9 bar CO/ H<sub>2</sub> 1:1, can be seen in Table 1.2. As the electron withdrawing capacity of the modified phenyl rings is increased, the basicity of the ligand decreases and there is an increase in both the rate and l:b ratio of the reaction. However, it is important to look at the selectivity of the reaction to each product. It is observed that there is an increase in the selectivity for the linear aldehyde, heptanal, the isomerisation product 2-hexene, and a slight increase in the hydrogenation product hexane. There is a concurrent decrease in the selectivity to the branched aldehyde, 2-methyl hexanal. Apparently there are two factors contributing to the increased l:b ratio with decreasing basicity. First, there is an increased preference for the terminal alkyl intermediates of reaction, as indicated by the greater selectivity for heptanal observed. Secondly, there is an increase in the amount of  $\beta$ -hydrogen abstraction for the branched alkyl-rhodium species which reforms the alkene-rhodium species and can result in either 1-hexene or 2-hexene being reformed or formed. This is discussed in more detail in the next section. The increased amounts of 2-hexene in the reaction solution signify that this does occur and that this contributes to the decrease in 2-methylhexanal selectivity and increased l:b ratio.

**Table 1.2**

*Effect of ligand basicity on the selectivity in the hydroformylation of 1-hexene.*

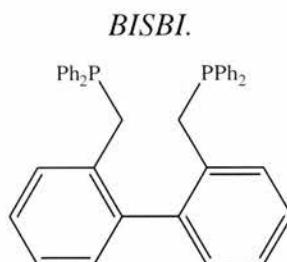
Ligand	$\chi$ -value	L:b ratio	Relative rate	Heptanal Selectivity	2-methyl hexanal selectivity	2-hexene selectivity	Hexane selectivity
<b>21</b> (dppf)	4.3	5.4	7.2	80.8	15.0	3.7	0.5
<b>22</b>	5.6	6.8	9.3	82.3	12.1	5.0	0.6
<b>23</b>	6.0	8.0	13.7	83.9	10.4	5.0	0.7
<b>24</b>	6.4	11.4	13.8	85.3	7.5	6.4	0.8

### **1.1.3.3 2,2'-Bis(phosphinomethyl)-1,1'-biphenyl and the Natural Bite Angle.**

In 1987, a new class of diphosphine ligand, the 2,2'-bis(phosphinomethyl)-1,1'-biphenyls was developed by Deven and co-workers<sup>41</sup> at the Eastman Kodak Company. Of this class of ligands, the diphosphine 2,2'-bis(diphenylphosphinomethyl)-1,1'-biphenyl or BISBI ligand was the most preferred, see Figure 1.15. The ligands were

developed for the diphosphine modified rhodium catalysed hydroformylation of terminal alkenes at pressures of 3.5-55 bar and at temperatures of 20-250 °C.

**Figure 1.15**



The hydroformylation of propene using rhodium complexes of BISBI and several other diphosphines was reported and compared with the results of using rhodium TPP complexes. The reaction was carried out in a vapour stripped reactor, synthesis gas and propene were fed into the reactor continuously to sustain constant pressure and constant molar ratios of CO, H<sub>2</sub> and propene. The reaction conditions were 16 bar CO/ H<sub>2</sub> 1:1, 125 °C, 5 bar propene, [Rh] = 1.5 mmol dm<sup>-3</sup>, and the solvent used was 2,2,4-trimethyl pentane-1,3-diolmonoisobutyrate (Texanol). The results are summarised in Table 1.3, and it is clear that the use of the diphosphine can greatly improve the regioselectivity in the reaction, BISBI being the most selective with an l:b ratio of 25.1:1 compared to an l:b ratio of only 2.43:1 when using TPP in much larger excess.

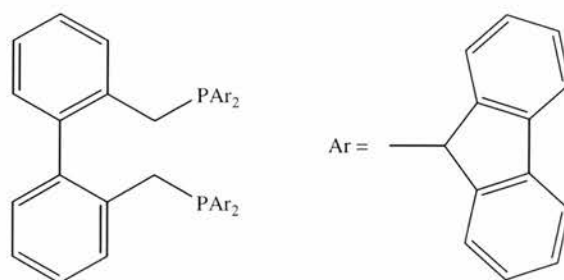
The same paper reported the effect of temperature on the hydroformylation of propene with the BISBI modified rhodium catalyst system. As the temperature is lowered the rate of reaction decreased and the l:b ratio increased, see Table 1.4. The ligand to rhodium ratio is 2.4 in all cases and the conditions are as above.

In a later patent, Deven and co-workers improved on these results with the 2,2'-bis(dibenzophosphinomethyl)-1,1'-biphenyl, see Figure 1.16.<sup>42</sup> This catalyst system was also studied in much detail, the best reported result having an l:b ratio of 288:1 when the reaction conditions were 110 °C, partial pressures of hydrogen 9.1 bar, carbon monoxide 1.72 bar, nitrogen 2 bar, and propene 6.07 bar, and a ligand to Rh ratio of 2.

**Table 1.3***Hydroformylation of propene using several ligand modifiers including BISBI.*

Ligand/ L	Ligand: Rh ratio	Rate/ mol mol <sup>-1</sup> h <sup>-1</sup>	l:b ratio
BISBI	2.4:1	3650	25.1
<i>trans</i> -dmcb	2.4:1	3200	4.4
<i>trans</i> -dmecb	2.4:1	2780	4.2
<i>trans</i> -dpnor	2.4:1	2560	4.3
<i>cis</i> -dpnor	2.4:1	1540	2.7
1,8-dinap	2.4:1	530	1.0
Dppf	2.4:1	3800	3.6
DIOP	2.4:1	3250	4.0
1,4-dppb	2.4:1	790	2.5
1,3-prop	2.4:1	610	0.8
1,5-pent	2.4:1	1460	2.3
1,6-hex	2.4:1	2520	1.5
TPP	124:1	5930	2.4

*trans*-dmcb = *trans*-1,2-bis(diphenylphosphinomethyl)-3,3-dimethylcyclobutane; *trans*-dmecb = *trans*-1,2-bis(diphenylphosphinomethyl)-3-ethoxy-4,4-dimethyl cyclobutane; *trans*-dpnor = *trans*-2,3-bis(diphenylphosphinomethyl) [2-2-1] bicycloheptane; 1,8-dinap = 1,8-bis(diphenylphosphinomethyl) naphthalene; dppf = 1,1-bis(diphenylphosphinomethyl) ferrocene; DIOP = 2,3-O-isopropylidene-2,3-dihydroxy-1,4-bis(diphenylphosphino) butane; 1,4-dppb = 1,4-bis(diphenylphosphino) butane; 1,5-pent = 1,5-bis(diphenylphosphino) pentane; 1,6-hex = 1,6-bis(diphenylphosphino) hexane.

**Figure 1.16***2,2'-bis(dbenzophosphinomethyl)-1,1'-biphenyl.*

In 1992, Casey and coworkers published a paper which would revolutionise the way in which we thought about diphosphine modified catalysts.<sup>31</sup> The paper recognised two important points from previous publications. The first was that in solution the five coordinate complex  $[\text{RhH}(\text{PPh}_3)_2(\text{CO})_2]$  with a TBP structure exists as a mixture of two geometric isomers with the phosphine co-ordinated equatorial-equatorial (ee) or equatorial-axial (ea) in a ratio of 85:15,<sup>43</sup> see complexes, **24** and **25**, in Figure 1.17.

The second was that the BISBI modified rhodium catalysts gave very high regioselectivity for the hydroformylation of propene.

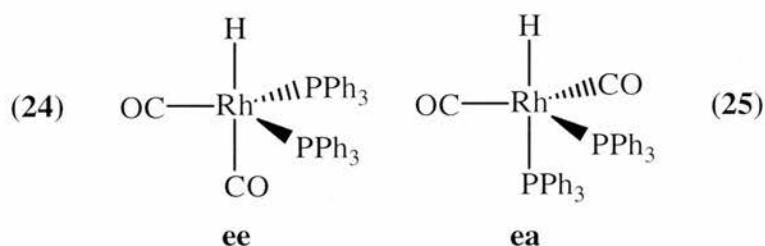
**Table 1.4**

*Temperature effect on the hydroformylation of propene with Rh/ BISBI catalysts.*

Temperature/ °C	Rate/ mol mol <sup>-1</sup> h <sup>-1</sup>	l:b ratio
125	3650	25.1
115	2160	27.2
105	1390	28.7
95	540	32.2

**Figure 1.17**

*Rhodium diphosphine complex [RhH(PPh<sub>3</sub>)<sub>2</sub>(CO)<sub>2</sub>] with ee and ea diphosphine coordination.*



The regioselectivity of the hydroformylation reaction is determined by the conversion of the five co-ordinate complex species **3** [RhH(CO)(PPh<sub>3</sub>)<sub>2</sub>(alkene)] with a TBP structure to the four coordinate complex species **4** and **5** [Rh(CO)(PPh<sub>3</sub>)<sub>2</sub>(alkyl)], formally the addition of a rhodium hydride species to the coordinated alkene, see Scheme 1.3. As the phosphines may occupy several different coordination sites in species **3** [RhH(CO)(PPh<sub>3</sub>)<sub>2</sub>(alkene)] as they do in [RhH(PPh<sub>3</sub>)<sub>2</sub>(CO)<sub>2</sub>] see Figure 1.17, Casey and coworkers suggested that to understand the effect of the exact structure of the TBP intermediates on the regioselectivity of the catalyst, investigation of diphosphine chelates which are designed for an enhanced preference for a specific coordination should be carried out. For example, the diphosphine ligand dppe is known to prefer a P-M-P bite angle of about 90° from X-ray structure determinations, and therefore, it was theorised that it would prefer ea coordination in the TBP structure. Casey and coworkers also wanted to study diphosphines with a preferred bite angle of 120° that would prefer ee coordination in the TBP structure. It was theorised that diphosphines with bite angles of 90° and ea coordination would have a different regioselectivity than diphosphines with bite angles of 120° and ee coordination

Examination of molecular models of [Rh(BISBI)] complexes indicated that the chelate bite angle of BISBI was much greater than  $90^\circ$ , suggesting that the wide bite angle may be important in controlling the regioselectivity. To test this theory it was necessary to work out the bite angles of diphosphine ligands. To do this Casey and coworkers defined the “natural bite angle” and the ligand flexibility as described earlier.

The natural bite angle and the flexibility of several diphosphine ligands were calculated using this method and are listed in Table 1.5. The diphosphine modified hydroformylation of 1-hexene was carried out at  $34^\circ\text{C}$ , 6 bar CO/  $\text{H}_2$  1:1 with a diphosphine/ rhodium ratio of 1:1 and the results are also shown in Table 1.5.

**Figure 1.18**

*Various diphosphine ligands used for hydroformylation.*

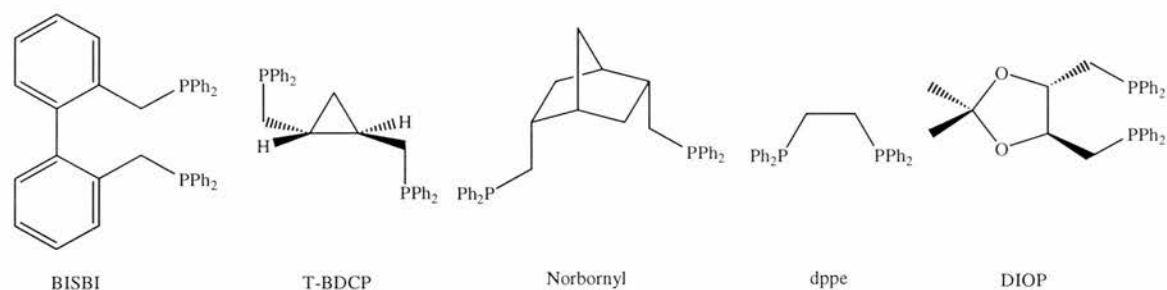


**Table 1.5**

*Results of the hydroformylation of 1-hexene with various diphosphine ligands.*

Diphosphine Ligand	Natural Bite Angle/ $\beta_n$	Ligand Flexibility	l:b Ratio	ee:ea
Norbornyl	$123^\circ$	$110\text{-}145^\circ$	2.9	-
BISBI	$113^\circ$	$92\text{-}155^\circ$	66.5	100:0
T-BDCP	$107^\circ$	$93\text{-}131^\circ$	12.1	37:63
DIOP	$85^\circ$	$70\text{-}95^\circ$	8.5	-
Dppe	$102^\circ$	$90\text{-}120^\circ$	2.1	0:100

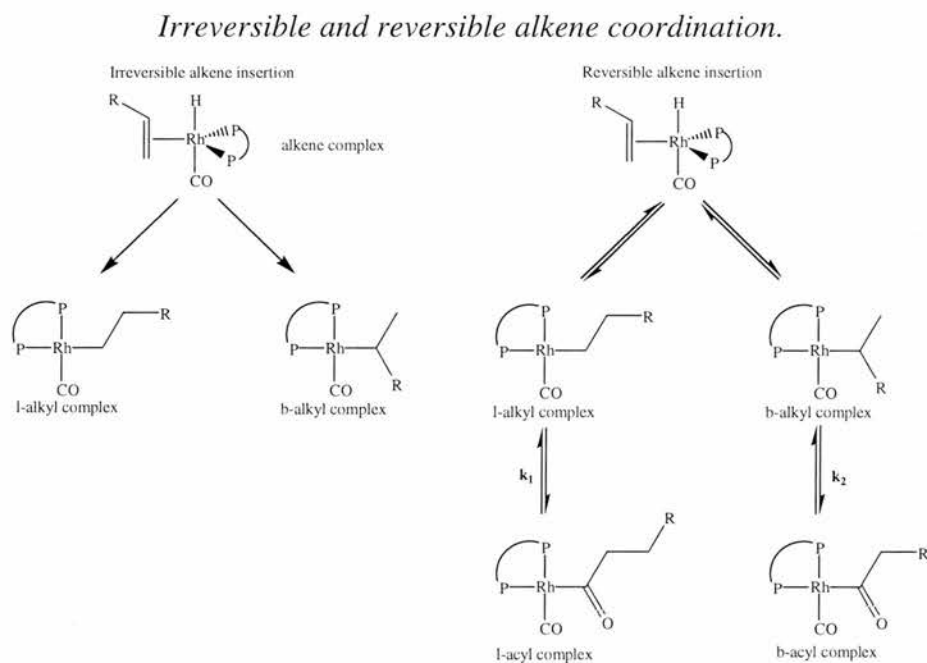
It can be seen that with the exception of norbornyl there is a clear correlation between the widening bite angle and the increasing l:b ratio. It was postulated that norbornyl was unable to form stable complexes with rhodium, as no monomeric complexes of norbornyl were identified, so it actually behaved as a monophosphine and gave the results expected for that.

It was also postulated that the increasing l:b ratio with widening the bite angle for dppe/ DIOP/ T-BDCP and BISBI was due to the greater preference of the wider bite angle

diphosphine to occupy ee coordination in the TBP structure, and that intermediates in the catalytic reaction with such a structure have a higher selectivity for the formation of the linear aldehyde than intermediates with ea coordinated diphosphine ligands. In a later paper, the ee:ea ratio of the chelates of  $[(\text{diphosphine})\text{Ir}(\text{CO})_2\text{H}]$  at room temperature was used as an indication of the coordination preference of the ligands.<sup>44</sup>

It has been assumed that addition of the rhodium hydride complex to a coordinated alkene is irreversible. The regioselectivity is therefore determined by the ratio of two alkyl intermediates formed as they are committed to hydroformylation. An alternative is that this step is in fact fast and reversible, *via*  $\beta$ -hydrogen abstraction. It is well documented that if so the linear and branched alkyl complex species will be in equilibrium with one another. The regioselectivity will then be determined by the relative rates ( $k_1$  and  $k_2$ ) of carbonylation of the linear and branched alkyl complexes, see Scheme 1.4.<sup>45</sup>

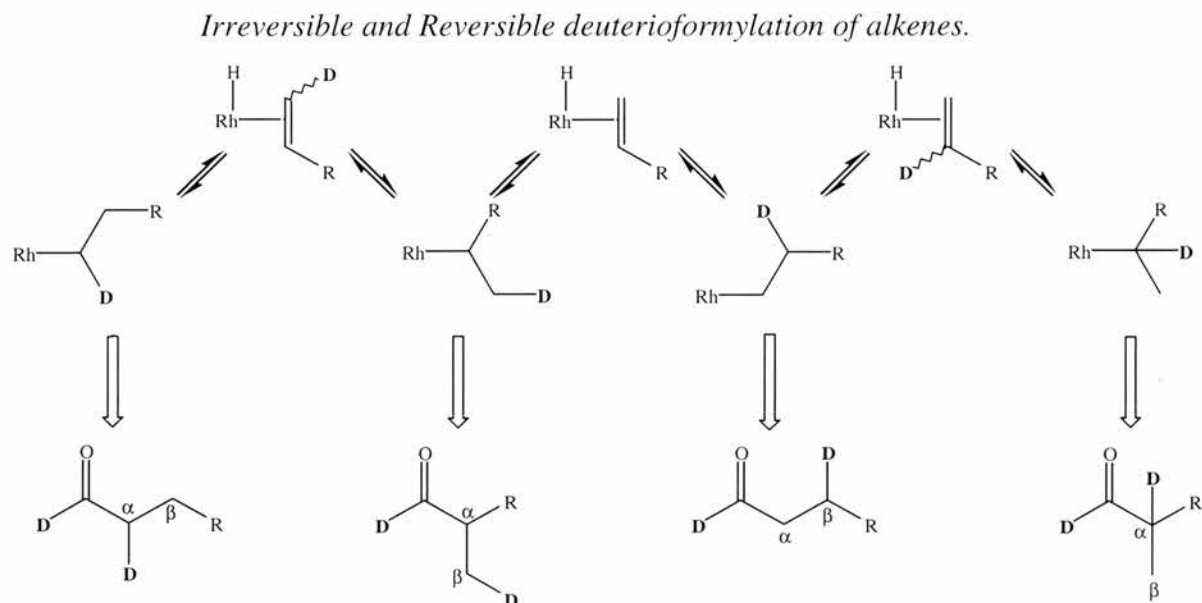
#### Scheme 1.4



To test where regioselectivity is determined Casey carried out the deuterioformylation of 1-hexene with various phosphines, TPP, dppe, T-BDCP, and BISBI.<sup>45</sup> If the formation of the four coordinate complex is irreversible, and the ratio of l and b-alkyl complex formation determines the regioselectivity, then the products of deuterioformylation will only have D atoms on the acyl carbon and on the carbon  $\beta$  to the acyl carbon. If this step is reversible, however, and it is the relative rates of

carbonylation that determine the regioselectivity then there is a mechanism for the D atom to be on the carbon  $\alpha$  to the acyl carbon, see Scheme 1.5.

**Scheme 1.5**



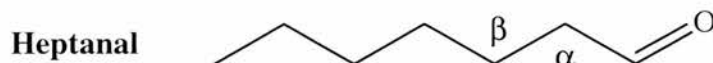
Deuterioformylation of 1-hexene was carried out at 32 °C, 6 bar CO/ D<sub>2</sub> with a P/ Rh ratio of 2:1 to a conversion of 40-50 % or 300 turnovers. Table 1.6 shows the level of deuterium incorporation, and its position in the products of the reaction, heptanal and 2-methylhexanal; the analysis was carried out using <sup>2</sup>H NMR.

If the alkene becomes dissociated from the rhodium, deuterium should be incorporated in the unreacted 1-hexene. The deuterium content of the unreacted 1-hexene was therefore also determined by <sup>2</sup>H NMR analysis of the reaction solution. The level is indicated as a multiple of the natural deuterium abundance expected and as the percentage in the hexene, see Table 1.7.

In all the examples deuterium is incorporated almost exclusively in the  $\beta$  position of heptanal and 3-methyl hexanal. Only for the BISBI modified catalyst was there any appreciable amount of D incorporated in the  $\alpha$  position of the two aldehydes. Similarly there is very little D incorporated in the recovered 1-hexene, again only when the BISBI modified catalyst was used was there an appreciable amount.

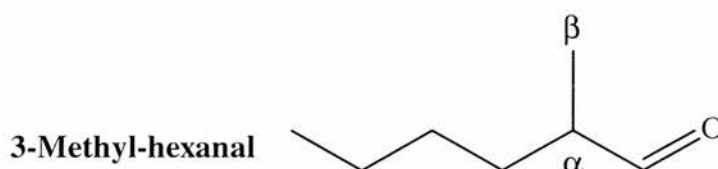
**Table 1.6**

*Deuterium content of heptanal and 2-methylhexanal from rhodium catalysed deuterioformylation of 1-hexene.*



Ligand	$\beta$ Carbon	$\alpha$ Carbon	Acyl-Carbon
BISBI	0.98	0.02	1.00 <sup>a</sup>
T-BDCP	1.00	-	1.00
Dppe	0.99	-	1.00
TPP	1.00	-	1.00

<sup>a</sup>The integration value is set as 1.00 deuterium.



Ligand	$\beta$ Carbon	$\alpha$ Carbon	Acyl-Carbon
BISBI	0.97	0.02	1.00
T-BDCP	0.98	-	1.00
Dppe	0.95	-	1.00
TPP	0.98	-	1.00

**Table 1.7**

*Deuterium levels in 1-hexene as a multiple of the natural deuterium abundance and (% D in hexene solution).*

Ligand	$\text{CH}_2=\text{CHD}(\text{CH}_2)_3\text{CH}_3$	$\text{CHD}=\text{CH}_2(\text{CH}_2)_3\text{CH}_3$
BISBI	133 (2.0)	128 (1.9)
T-BDCP	4.5 (0.07)	4.4 (0.07)
Dppe	6.5 (0.10)	5.5 (0.08)
TPP	12.4 (0.19)	3.6 (0.05)

Therefore, for T-BDCP, dppe, and TPP modified rhodium catalysts the regioselectivity is set by the irreversible rhodium hydride addition to the alkene. But for the BISBI modified catalyst the situation must be more complicated. Detailed analysis of the results by Casey and coworkers showed that the initial ratio of the l-alkyl and b-alkyl intermediates is 17:1. The l-alkyl complex then partitions between hydroformylation and reversal to the rhodium alkene complex in a ratio of 38:1, in other words, the insertion of CO into the Rh-C bond is much favoured over  $\beta$ -hydrogen abstraction, but

not completely. The b-alkyl intermediate is also partitioned between hydroformylation and reversal to the rhodium alkene complex in a ratio of 1:3, in other words, 75 % of the b-alkyl complex formed from rhodium hydride addition to the complex is reversible. Thus, the observed l:b ratio of 66:1 which exceeds the initial 17:1 ratio of l to b-alkyl intermediates is due to the l-alkyl intermediate mainly being converted to the linear aldehyde but the b-alkyl intermediate mainly reverting back to 2-hexene.

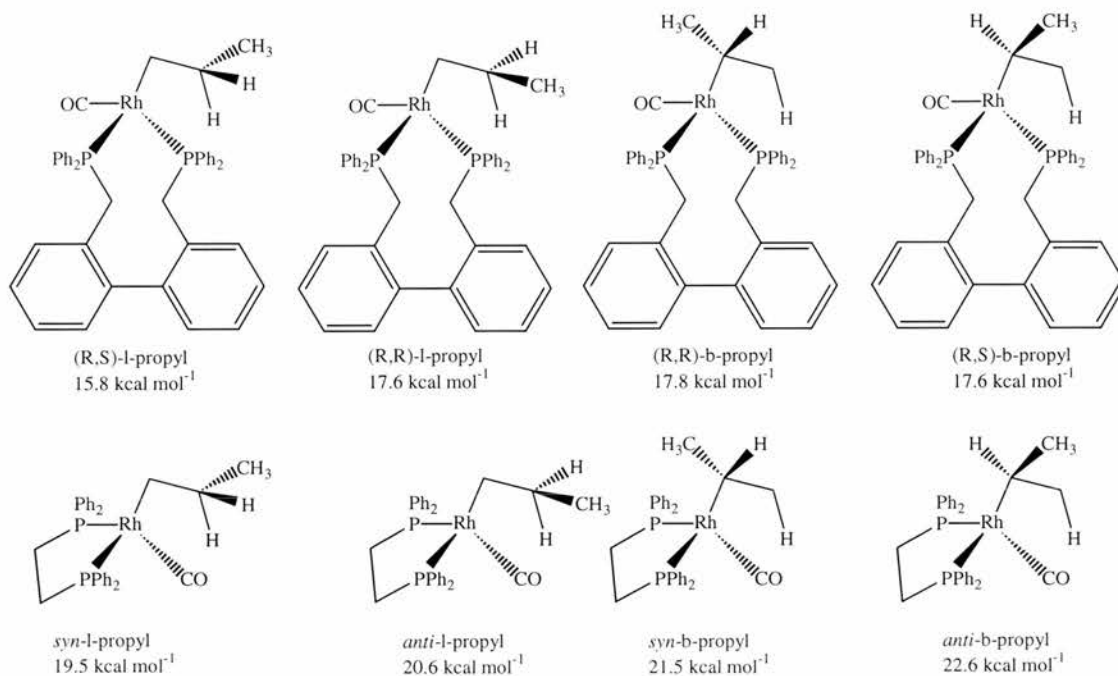
It is proven, therefore, that the regioselectivity is largely determined by the migration of the hydride to the coordinated alkene, and the change from a TBP structure to a square planar one. It is theorised that the increased l:b ratio with BISBI as ligand of rhodium in the hydroformylation reaction is due either to steric or electronic effects of ee coordination as the wide bite angle could provide a mechanism to increase the steric bulk of the ligand, and as the ee and ea sites would be electronically different.

To determine whether steric effects could explain the difference in the observed l:b ratio, molecular mechanics calculations were carried out to measure the energies of rhodium complexes of BISBI and dppe with ee and ea diphosphine coordination respectively.<sup>45</sup> The relative energies of transition state intermediates in the conversion of the TBP [(diphosphine)Rh(propene)(CO)H] complex to the square planar [(diphosphine)Rh(l-propyl)(CO)] and [(diphosphine)Rh(b-propyl)(CO)] complexes were considered, see Figure 1.19.

The energy difference between the lowest energy [(BISBI)Rh(l-propyl)(CO)] complex and the lowest energy [(BISBI)Rh(b-propyl)(CO)] complex is 1.9 kcal mol<sup>-1</sup>. This value is very close to the value required for the 17:1 partition between the l and b alkyl intermediates in the catalytic cycle, which is 1.7 kcal mol<sup>-1</sup>. However, the energy difference between the lowest energy [(dppe)Rh(l-propyl)(CO)] complex and the lowest energy [(dppe)Rh(b-propyl)(CO)] complex is 2.1 kcal mol<sup>-1</sup>. This value is much larger than the value required for the observed l:b ratio in the hydroformylation reaction with dppe which is 0.5 kcal mol<sup>-1</sup>. In fact, the value is larger than that calculated for the BISBI complexes, such that the calculations suggest dppe should be more selective for the linear aldehyde than BISBI. The molecular mechanics calculations of other transition states along the reaction coordinate were considered, but none supported steric reasons for the increased l:b ratio with ee diphosphine coordination.

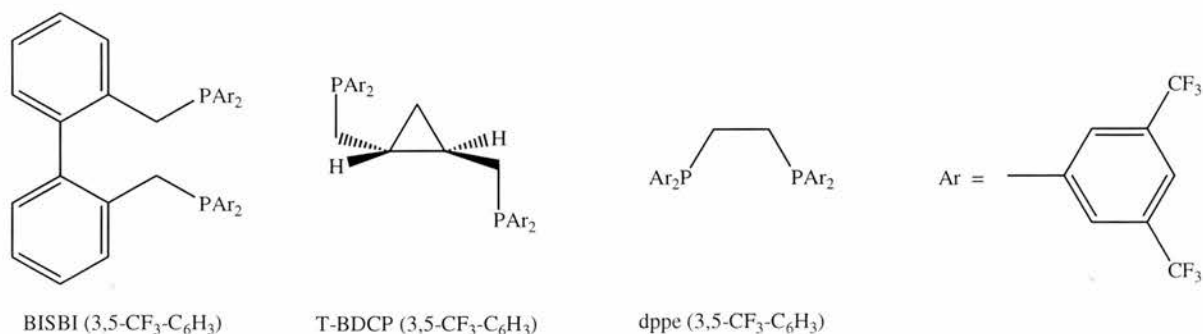
**Figure 1.19**

*Calculated energies of Rh-BISBI & Rh-dppe propene transition state models.*



Electronic differences between the ee and ea chelates were considered as the interaction between two equatorial phosphorus atoms is stronger than the interaction between an equatorial and an axial phosphorus.<sup>44</sup> Casey and co-workers therefore synthesised analogues of the diphosphines previously used for hydroformylation of 1-hexene. These new ligands were electronically modified with trifluoromethyl substituents on the aryl rings of the phosphine, see Figure 1.20. They also measured the ratio of ee:ea diphosphine coordination in the TBP structure at room temperature in related iridium complexes. The hydroformylation reaction was carried out at 36 °C, 6 bar CO/ H<sub>2</sub> 1:1, with a diphosphine rhodium ratio of 1:1.

The iridium complexes suggested that BISBI and its more electron withdrawing analogue BISBI(3,5-CF<sub>3</sub>-C<sub>6</sub>H<sub>4</sub>) are both coordinated one hundred percent ee. The rhodium catalysed hydroformylation of 1-hexene with BISBI(3,5-CF<sub>3</sub>-C<sub>6</sub>H<sub>4</sub>) as ligand gave an l:b ratio of 123:1, almost double that when using BISBI as ligand l:b 66:1. This suggests the increased electron withdrawing ability of the phosphine in the equatorial position increases the linear selectivity of the catalyst.

**Figure 1.20***Electronically modified diphosphine catalysts.*

The iridium complexes suggested that T-BDCP is coordinated both ee and ea in a ratio of 37:63 but its more electron withdrawing analogue T-BDCP (3,5-CF<sub>3</sub>-C<sub>6</sub>H<sub>4</sub>) is coordinated ee and ea in a ratio of 90:10. The rhodium catalysed hydroformylation of 1-hexene with T-BDCP (3,5-CF<sub>3</sub>-C<sub>6</sub>H<sub>4</sub>) as ligand gave an l:b ratio of 17.7:1, where using T-BDCP as ligand gave a l:b ratio of 12.1:1. The increased ratio for the more electron withdrawing phosphine can be ascribed to two effects. Firstly, the proportion of ee diphosphine coordination is greater for the T-BDCP (3,5-CF<sub>3</sub>-C<sub>6</sub>H<sub>4</sub>) complex than for the T-BDCP complex and this complex is more selective for the linear aldehyde. Molecular mechanics calculations have shown that weaker  $\sigma$ -donors ligands have a greater preference for equatorial coordination in the TBP structure than stronger  $\sigma$ -donors ligands.<sup>46</sup> The second is that the increased electron withdrawing ability of the phosphine in the equatorial position increases the linear selectivity of the catalyst as for BISBI.

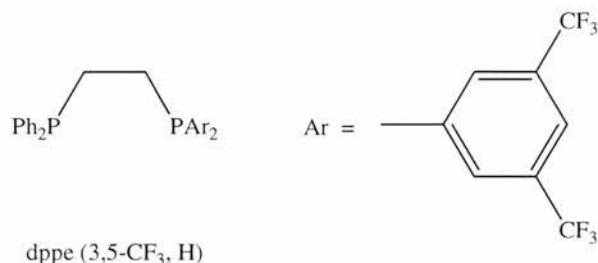
The iridium complexes of dppe and dppe (3,5-CF<sub>3</sub>-C<sub>6</sub>H<sub>4</sub>) suggested that they are both coordinated one hundred percent ea. When the electronically modified ligand dppe (3,5-CF<sub>3</sub>-C<sub>6</sub>H<sub>4</sub>) was used as ligand in the rhodium catalysed hydroformylation of 1-hexene the l:b ratio was 1.3:1 with respect to 2.6:1 when dppe was used as ligand. We have already seen that increased electron withdrawing ability of the phosphine in the equatorial position increases the linear selectivity of the catalyst for the BISBI ligand. Therefore, as the l:b ratio when using dppe (3,5-CF<sub>3</sub>-C<sub>6</sub>H<sub>4</sub>) as ligand is lower than when using dppe, an increased electron withdrawing ability of the phosphine in the axial position must decrease the linear selectivity of the catalyst, and this effect must be greater than that in the equatorial position.

Casey and coworkers hypothesised that electron withdrawing substituents on the aryl groups of a phosphine in the equatorial position increase the regioselectivity towards the linear aldehyde, but in the axial position they decrease the regioselectivity towards the linear aldehyde.<sup>47</sup>

To test this hypothesis, the disymmetric dppe derivative [PPh<sub>2</sub>CH<sub>2</sub>CH<sub>2</sub>P(3,5-CF<sub>3</sub>-C<sub>6</sub>H<sub>3</sub>)] or dppe (3,5-CF<sub>3</sub>, H) was synthesised. This ligand was designed to have the electron withdrawing phosphorus atom in the equatorial position, and an electron donating phosphorus ligand in the axial position, see Figure 1.21. The iridium analogues, [(diphosphine)Ir(CO)<sub>2</sub>H], of the catalytic rhodium complexes were synthesised to determine the diphosphine chelate geometry.

**Figure 1.21**

*The disymmetric dppe derivative dppe (3,5-CF<sub>3</sub>, H)*

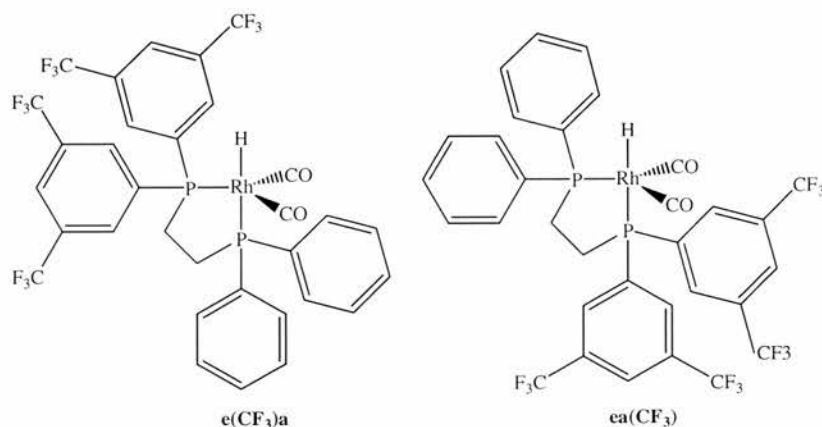


There are three possible isomers of diphosphine coordination, one ee and two ea isomers. It has already been demonstrated that dppe ligands have a strong preference for ea coordination, with dppe and dppe (3,5-CF<sub>3</sub>-C<sub>6</sub>H<sub>3</sub>) coordinated fully in the ea geometry. Dppe (3,5-CF<sub>3</sub>, H) does also. The two ea isomers of dppe (3,5-CF<sub>3</sub>, H) undergo rapid interconversion on the NMR time scale *via* Berry pseudorotations giving averaged chemical shifts and coupling constants at room temperature. However, by low temperature NMR, the interconversion is slowed down and the individual isomers can be observed. The P(3,5-CF<sub>3</sub>-C<sub>6</sub>H<sub>3</sub>)<sub>2</sub> phosphorus atom and the PPh<sub>2</sub> phosphorus atoms can be distinguished by comparing their chemical shifts with the chemical shifts of dppe and dppe (3,5-CF<sub>3</sub>-C<sub>6</sub>H<sub>3</sub>). By selectively coupling the hydride hydrogen in the <sup>31</sup>P{<sup>1</sup>H} NMR spectrum it was possible to determine the site of the phosphorus atom. The <sup>2</sup>J<sub>HP</sub> coupling constant for a phosphorus in the axial position will be in the range of 90-110 Hz but only 15 Hz for a phosphorus in the equatorial position.

At -94 °C the **e**(CF<sub>3</sub>)**a** and **ea**(CF<sub>3</sub>) ratio is 94:6 in favour of the geometry expected. By analysis of the averaged chemical shifts and coupling constants it was shown that at room temperature the two isomers exist in a **e**(CF<sub>3</sub>)**a** to **ea**(CF<sub>3</sub>) ratio of 83:1.

**Figure 1.22**

*The two ea isomers of  $[(dppe(3,5-CF_3, H))Rh(CO)_2H]$ .*



The rhodium catalysed hydroformylation of 1-hexene with  $dppe(3,5-CF_3, H)$  as ligand at 36 °C and 6 bar CO/ H<sub>2</sub> 1:1 gives a l:b ratio of 4.2. Under the same conditions using  $dppe$  as ligand the l:b ratio is 2.6 and using  $dppe(3,5-CF_3-C_6H_3)$  as ligand the l:b ratio is 1.3. It is, therefore, observed that introducing a more electron withdrawing phosphorus in the equatorial position, or going from using  $dppe$  as ligand to  $dppe(3,5-CF_3, H)$  as ligand, increases the l:b ratio. It is also observed that introducing a more electron withdrawing phosphorus in the axial position, or going from using  $dppe(3,5-CF_3, H)$  as ligand to  $dppe(3,5-CF_3-C_6H_3)$  as ligand, decreases the l:b ratio.

Some doubt was expressed on consideration of the macroscopic effect of going from the BISBI to  $dppe$  ligand.<sup>44</sup> In effect, this involves the exchange of an electron-donating phosphine ligand with a strongly electron accepting CO ligand in the equatorial position, and in turn exchanging a CO ligand with an electron donating phosphine ligand in the apical position. From the conclusions discussed already, it is suggested that an increase in the linear regioselectivity should therefore be observed when changing from a BISBI to a  $dppe$  complex rather than the actual marked decrease.

This showed that the effect on the regioselectivity of equatorial electron withdrawing phosphines and  $\pi$ -acceptor CO ligands is not identical,<sup>6</sup> and that the regioselectivity is in fact governed by a complex mix of steric and electronic effects.

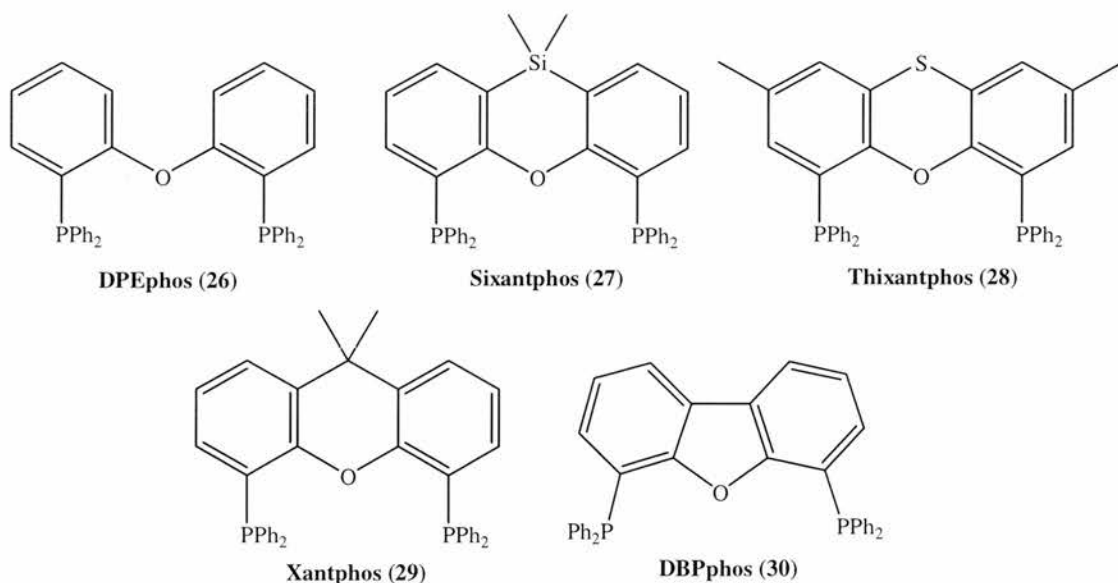
### 1.1.3.4 Xanthene Based Diphosphines.

After the studies by Casey and co-workers, which indicated that a large bite angle does lead to an increased l:b ratio in the rhodium catalysed hydroformylation reaction, van Leeuwen also published results of a study relating selectivity to bite angle.<sup>48</sup> In this study, van Leeuwen and co-workers synthesised a series of diphosphine ligands based on the xanthene backbone. They used molecular mechanics calculations to define the bite angles and flexibilities of their ligands as defined by Casey and co-workers. Finally, they studied the rhodium catalysed hydroformylation of 1-octene to see what effect the different ligands had on the resulting l:b ratio.

In their first publication they reported the diphosphine modified rhodium catalysed hydroformylation with the ligands 26-30 depicted in Figure 1.23. They are bis(2-(diphenylphosphino)phenyl) ether (DPEphos), 4,6-bis(diphenylphosphino)-10-10-dimethylphenoxasilin (Sixantphos), 2,8-dimethyl-4,6-bis(diphenylphosphino) phenoxathiin (Thixantphos), 9,9-dimethyl-4,6-bis(diphenylphosphino) xanthene (Xantphos), and 1,8-bis(diphenylphosphino) dibenzofuran (DBPphos).

**Figure 1.23**

*Diphosphine ligands based on the xanthene backbone.*



To study the effect of the ligand to rhodium ratio on the hydroformylation of 1-octene, Thixantphos was used as an example ligand at ratios of 1.1 to 10 at 40 °C and 10 bar CO/H<sub>2</sub> 1:1, and the results can be seen in Table 1.8. An optimum was found at 2.2:1,

with no improvement in the l:b ratio found after this. The percentage of the isomerisation product 2-octene was less than 1 % and no hydrogenation product octane was observed in any of the reactions.

**Table 1.8**

*Results of the rhodium catalysed hydroformylation of 1-octene with thixantphos as ligand at varying ligand to rhodium ratios.*

<b>L : Rh ratio</b>	<b>l : b ratio</b>	<b>% l-aldehyde</b>
1.1	5.7	85.1
2.0	40.5	97.6
2.2	47.6	97.9
5.0	45.1	97.8
10.0	45.4	97.8

Binuclear species of the type suggested by Hughes and Unruh were discounted because of the rigid nature of the ligands and as a third phosphine was readily displaced under an atmosphere of CO. The observed optimum ligand to rhodium ratio was therefore attributed to the result of a dissociation equilibrium between Rh-P complex species and Rh-P<sub>2</sub> complex species which is dependent on the overall concentration of P in solution. The rhodium catalysed hydroformylation of 1-octene modified with the ligands 26-30 was also studied at 40 °C 10 bar CO/ H<sub>2</sub> 1:1, ligand/ Rh 2.2, and BISBI, was also used as ligand for comparison. The results are summarised in Table 1.9.

**Table 1.9**

*Hydroformylation of 1-octene at 40 °C*

<b>Ligand</b>	<b>Bite angle/ βn</b>	<b>Flexibility range/ °</b>	<b>l : b</b>	<b>% l-aldehyde</b>	<b>% isomerisation</b>	<b>tof</b>
DPEphos	102.2	86-120	10.5	91.3	0	5
Sixantphos	108.7	93-132	35.0	96.3		4.4
Thixantphos	109.4	94-130	47.6	97.0	1.0	13.2
Xantphos	111.7	97-135	57.1	98.3	0	10
DBFphos	131.1	117-147	3.4	76.1	1.6	1.9
BISBI	122.6	101-148	58.2	95.5	2.9	30

NB: The calculated natural bite angle for BISBI is 122.6 ° compared to 113 ° as stated by Casey. This is due to the different molecular modelling packages used by van Leeuwen and Casey.

DBEphos gave an enhanced selectivity over TPP (3.1) see section 1.1.3.1, but the ligands which have a second bridging atom between the two aryl rings gave much

higher l:b ratios. Such ligands all have bite angle near  $110^\circ$  and showed a very high regioselectivity and very low isomerisation activity.

DBFphos, with a very large bite angle of  $131.1^\circ$ , had the lowest selectivity, close to that observed for monophosphines. It is probable that DBFphos behaves like norbornyl in Casey's studies and does not form chelates with rhodium because of the excess strain energy required. It therefore behaves as a monophosphine or a bridging phosphine. It is interesting to note that in the X-ray crystal structures of the TBP complex [(diphosphine)RhH(CO)(PPh<sub>3</sub>)] of the xanthene type diphosphine ligands, the P-M-P bond angle was always about  $110^\circ$ , outside the flexibility range of DBFphos. Attempts to synthesis [(DBFphos)RhH(CO)(PPh<sub>3</sub>)] resulted in a mixture of unknown complexes.

As stated above, the ligands **26-30** show very high regioselectivities, and l:b ratios that increase with the calculated bite angle. BISBI which has an even larger bite angle, has an even higher l:b ratio under the same conditions. When considering the linear aldehyde selectivity instead of the l:b ratio the xanthene type diphosphine ligands are in fact more regioselective. This is because of the low level of isomerisation in the xanthene based systems (0-1 %) compared with the BISBI system (2.9 %).

When the temperature of reaction was raised to  $80^\circ\text{C}$ , there was an important change in the product distribution. The l:b ratio for the ligands **27-29** was slightly lower than at  $40^\circ\text{C}$ , the percentage of isomerisation products was slightly increased, and there was still no hydrogenation product. The overall effect was a slight decrease in the linear aldehyde selectivity.

**Table 1.10**

*Hydroformylation of 1-octene at  $80^\circ\text{C}$*

Ligand	Bite angle/ $\beta\text{n}$	Flexibility range/ $^\circ$	l : b	% l-aldehyde	% isomerisation	Tof
DPEphos	102.2	86-120	6.7	87.0	0	250
Sixantphos	108.7	93-132	34	94.2	3	168
Thixantphos	109.4	94-130	41	93.0	4.7	445
Xantphos	111.7	97-135	53.5	97.7	0.5	800
DBFphos	131.1	117-147	3	71	5.5	125
BISBI	122.6	101-148	80.5	89.6	9.3	850

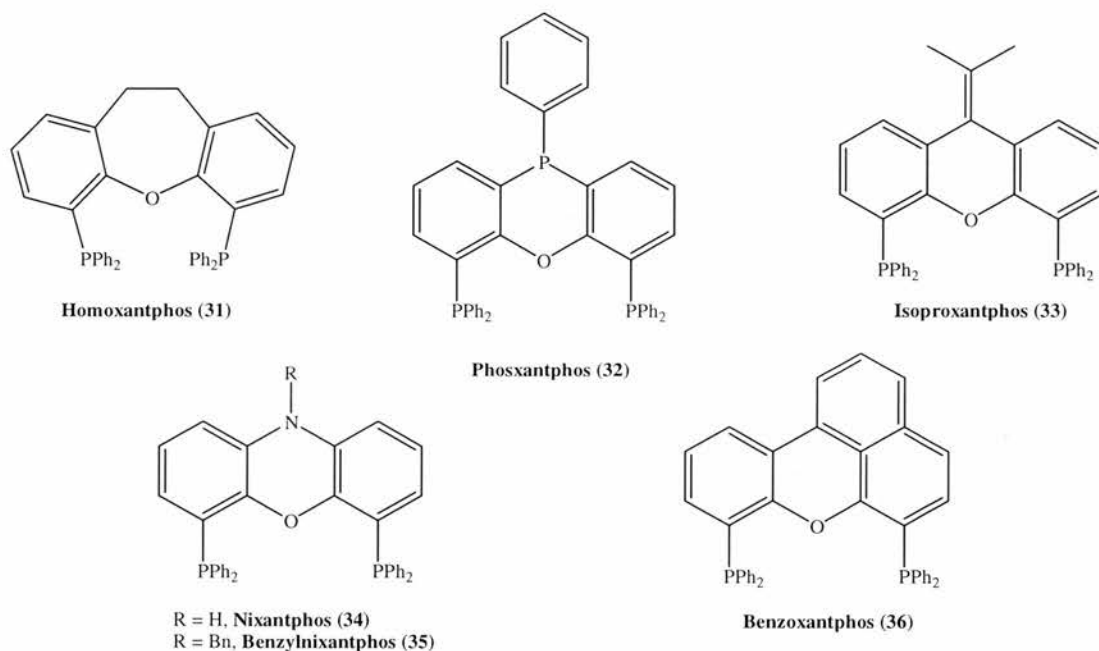
For BISBI, there was a large increase in the l:b ratio, a large increase in the percentage of isomerisation product and no hydrogenation product. This means there is a large decrease in the resulting linear selectivity, which is now much lower than that observed

in the xanthene based systems. Since BISBI has a larger flexibility range than the xanthene type ligands, it is believed that this means its rhodium complexes will be less rigid and that this gives a lower selectivity for linear alkyl intermediates. However, it also means that the branched alkyl intermediate is more likely to undergo  $\beta$ -hydrogen abstraction, or reversible rhodium hydride addition to the coordinated alkene which is a mechanism for isomerisation. This will lead to a greater proportion of the branched alkyl intermediate being reverted to 1-octene and 2-octene which will increase the 1:b ratio but not the linear aldehyde selectivity.

As an extension of this work, the ligands 31-36 shown in Figure 1.24 were synthesised and, along with the ligands 27-29 in Figure 1.23, they were used as ligands in the rhodium catalysed hydroformylation of 1-octene, at 80 °C, 20 bar CO/ H<sub>2</sub> 1:1, ligand/ Rh 5:1. The results can be seen in Table 1.11.

**Figure 1.24**

*Diphosphine ligands based on the xanthene backbone.*



There is a clear correlation between both the selectivity of the reaction and the rate of reaction with the increasing bite angle. For ligand 31 with a natural bite angle of 102 ° in the rhodium catalysed hydroformylation of 1-octene the percentage selectivity for the linear aldehyde is 88 %. For ligand 36 with a natural bite angle of 120.6 ° the percentage selectivity for the linear aldehyde is 96.5 %, and the rate increases from 36.9 to 343 (mol aldehyde)(mol of Rh)<sup>-1</sup> h<sup>-1</sup>. The low rates associated with ligands 34 and 35 are explained by the electron donating capacity of the N moiety in both backbones.

However, there is apparently no correlation between the bite angle and the ee/ ea ligand coordination ratio.

**Table 1.11**

*Results of the hydroformylation of 1-octene at 80 °C.*

Ligand	Bite angle/ $\beta$ n	l : b Ratio	% linear aldehyde	% isomerisation	Tof/ (mol aldehyde) (mol of Rh) <sup>-1</sup> h <sup>-1</sup>
31	102.0	8.50	88.2	1.4	36.9
32	107.9	14.6	89.7	4.2	74.2
27	108.5	34.3	94.4	2.9	76.5
28	109.6	56.6	93.7	4.7	94.1
29	111.4	52.2	94.5	3.7	187
33	113.2	49.8	94.3	3.8	162
35	114.1	50.6	94.3	3.9	154
34	114.2	69.4	94.9	3.7	160
36	120.6	50.2	96.5	1.6	343

The [(diphosphine)RhH(CO)<sub>2</sub>] complexes were prepared and studied under hydroformylation conditions by <sup>31</sup>P {<sup>1</sup>H} and <sup>1</sup>H NMR spectroscopy. The <sup>31</sup>P {<sup>1</sup>H} NMR spectra show a characteristic doublet at 19-25 ppm for all the ligands **27-29** & **31-35**, and two doublet of doublets for ligand **36** which has in equivalent phosphorus atoms. The <sup>1</sup>H NMR spectra for ligands **27-29** & **31-35** show a triplet of doublets and the <sup>1</sup>H NMR spectrum for ligand **36** shows a double doublets for the hydride proton.

It has been shown that such complexes exist in solution as a mixture of geometric isomers of ee and ea diphosphine coordination, and that these isomers are in dynamic equilibrium with each other *via* pseudo Berry rotations. This interchange of the phosphorus atoms is faster than the NMR time scale thus averaged chemical shifts and coupling constants for the two isomers are observed in the NMR spectra. It has been demonstrated by Yagupsky and Wilkinson, and more recently by Casey, that knowing the <sup>2</sup>J<sub>PH</sub> coupling constants of the individual isomers it is possible to work out the ee:ea ratio from the averaged <sup>2</sup>J<sub>PH</sub> coupling constant. In this case it proved impossible to freeze out the two isomers even at 163 K. However, estimates of the ee:ea ratio were calculated assuming the *cis* <sup>2</sup>J<sub>PH</sub> coupling constant in the ee isomer was ±2 Hz and the *trans* <sup>2</sup>J<sub>PH</sub> coupling constant in the ea isomer was 106 Hz.

The subsequent ee:ea values showed no correlation with the natural bite angle. The complexes of ligands **28** and **32** had high ee:ea ratios, possibly because the electron

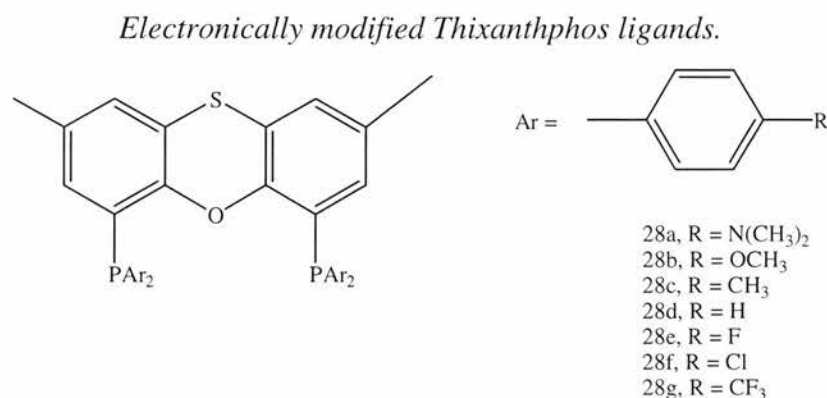
withdrawing ability of the S and P moieties in the diphosphine. It has already been shown that less basic phosphines prefer equatorial coordination. The low ee:ea ratio for the complex of **36** could be due to the highly rigid nature of the ligand, and the inequivalence of the phosphine could also affect the coordination. It is surprising as the P-M-P angle of the diphosphine in ea coordination sites of a perfect TBP geometry will be  $90^\circ$ , outside the calculated  $3 \text{ kcal mol}^{-1}$  flexibility range of the ligand,  $102\text{-}146^\circ$ .

It is also interesting that in the [(diphosphine)RhH(CO)(PPh<sub>3</sub>)] complexes ligand **34** with a calculated natural bite angle of  $114.2^\circ$  has a P-M-P angle of  $114.2^\circ$ , but the ligand **28** with a larger calculated natural bite angle of  $120.6^\circ$  has a smaller P-M-P angle of  $109.16^\circ$ .

This is described as unambiguous evidence that the ee:ea ratio of the catalyst precursor is not a key parameter of the regioselectivity and the bite angle effect must manifest itself in some other manner. It is speculated that it is the effective increasing steric bulk of the ligand with increasing bite angle that causes steric congestion about the rhodium centre which causes the increase in the regioselectivity by favouring the linear alkyl intermediate because it is less sterically demanding.

To study further the electronic effect of the ligand on the l:b ratio of rhodium catalysed hydroformylation, van Leeuwen and coworkers synthesised a series of the thixantphos ligands with varying basicity. The modification was accomplished by adding electronic modifying substituents in the para position of the phenyl groups on the phosphorus atoms, see **28a-28g** in Figure 1.25. The ee:ea ratios were calculated from the averaged  $^2J_{\text{PH}}$  coupling constant in the  $^1\text{H}$  NMR spectrum of [(diphosphine)RhH(CO)<sub>2</sub>]. As the basicity of the ligand was reduced, (from **28a** to **28g**), the ee:ea ratio increased. For the strongly electron withdrawing CF<sub>3</sub> substituent the amount of ee coordination was almost 100 %.

**Figure 1.25**



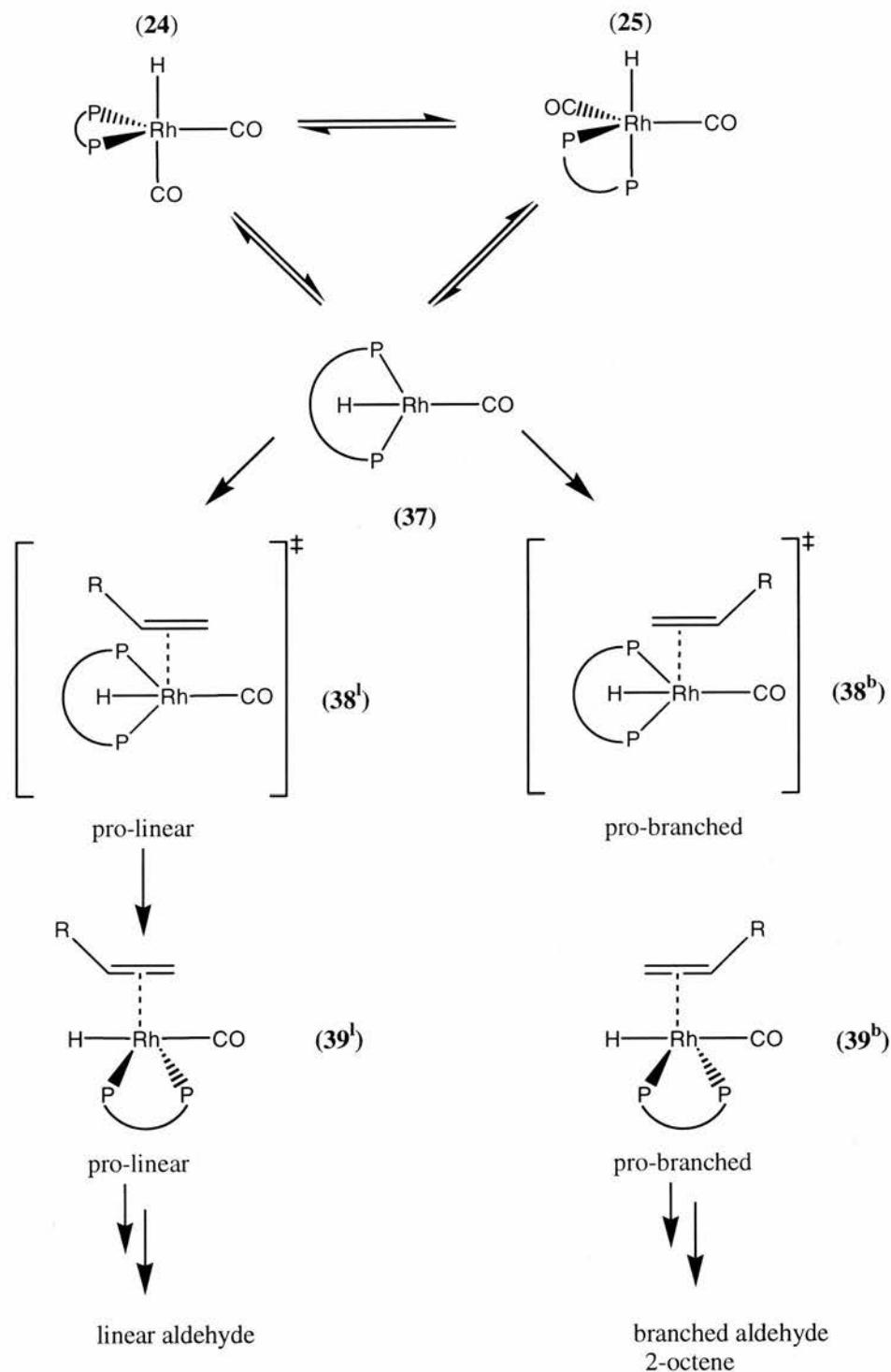
For the hydroformylation of 1-octene there was an increase in the l:b ratio with decreasing basicity (from **28a** to **28g**), with the exception of ligand **28b**. However, the linear aldehyde selectivity was constant for all ligands used at 92-93 %. The increase in the l:b ratio for hydroformylation with ligands **28a-28g** is attributed to the increase in the amount of the isomerisation product 2-octene produced with decreasing basicity. This is because the more electrophilic rhodium centre leads to the branched alkyl species having a greater reactivity for  $\beta$ -hydrogen elimination.

Although the actual [(diphosphine)RhH(CO)(alkene)] complex cannot be observed, the fact that the ee:ea ratio of [(diphosphine)RhH(CO)<sub>2</sub>] shows no correlation with the linear aldehyde selectivity led van Leeuwen and coworkers to suggest that CO dissociation from the two ee and ea isomers results in the formation of the same reactive four coordinate complex **37** in Scheme 1.6, and that the interchange between the two geometric isomers ee and ea is very fast. The regioselectivity is then determined by the next two steps of alkene coordination then hydride migration. It is suggested that the regioselectivity is controlled by the alkene attack on the four coordinate complex, **37**, via a square pyramidal transition state, **38** in Scheme 1.6, and that increasing the bite angle of the diphosphine in the four coordinate complex **37**, results in an increased embracing of the rhodium centre by the ligand and a greater steric hindrance for the approaching alkene. The steric hindrance will therefore be greater for the pro-branched transition state **38<sup>b</sup>**, than for the pro-linear transition state **38<sup>l</sup>**, of the approaching alkene, see Scheme 1.6. Increasing the bite angle will therefore favour the less sterically hindered pro-linear transition state **38<sup>l</sup>** and thus favour the linear product of reaction.

The preference for the formation of the pro-linear or pro-branched transition state cannot be determined by the angle between the two phosphine substituents in intermediate **37** though as TPP is able to occupy a larger P-M-P angle than diphosphines like thixantphos. Inspection of molecular models show that the backbones of the diphosphines play an important role in the relative stabilities of the linear and branched intermediate species **39<sup>l</sup>** & **39<sup>b</sup>**. The backbone will constrain the phenyl substituents on the phosphorus in such a way that the formation of the pro-linear complex **39<sup>l</sup>** is favoured over that of the pro-branched complex **39<sup>b</sup>**.

**Scheme 1.6**

*Proposed mechanism for the control of regioselectivity.*



### 1.1.4 Rhodium Catalysed Hydroformylation with Alkyl-Phosphine Ligands.

One method for the production of an important industrial chemical 1,4-butanediol involves the hydroformylation of prop-2-en-1-ol (allyl alcohol). In this process allyl alcohol is hydroformylated to its respective linear and branched hydroxyaldehydes with a homogeneous rhodium catalyst,<sup>49-51</sup> and sequentially hydrogenated to the diols with a heterogeneous hydrogenation catalyst,<sup>52</sup> see section 1.2.2.

Earlier we saw how the hydroformylation process can give both aldehydes or alcohols as the products of reaction depending on the catalytic system, see section 1.1. As it is the di-alcohol products of reaction that are required it would be desirable to hydroformylate allyl alcohol directly to diols rather than to hydroxyaldehydes, which require to be hydrogenated.

The hydroformylation of allyl alcohol to give alcohol products has been reported using a rhodium cluster compound  $[\text{Rh}_6(\text{CO})_{16}]$ , in the presence of tributylphosphine ( $\text{Bu}_3\text{P}$ ) in benzene under a  $\text{H}_2/\text{CO}$  2:1 atmosphere. The reaction produces 1,4-butanediol (41 %), propanol (39%), 2-methylpropane-1,3-diol (9%), and 2-methylpropan-1-ol (6%).<sup>53</sup> It is possible by using  $[\text{RhH}(\text{CO})(\text{PR}_3)_3]$ , where  $\text{R}=\text{Bu}$ , or  $\text{C}_6\text{H}_{11}$  to reduce the amounts of the hydrogenation product propanol but the main products are then the hydroxyaldehydes not the diols.<sup>54</sup> By using a catalyst system generated from  $[\text{Rh}(\text{CO})_2(\text{acac})]$  and trialkylphosphines in a carbonitrile solvent it has been possible to improve the selectivity towards 1,4-butanediol to 69%.<sup>55, 56</sup>

In the presence of amines the  $[\text{Rh}_6(\text{CO})_{16}]$  can catalyse the hydroformylation of allyl alcohol to the di-alcohol products, using CO and water instead of CO and  $\text{H}_2$  by promoting the water gas shift reaction.<sup>57</sup>

It has been shown by Cole-Hamilton and coworkers that it is possible to hydrocarbonylate alkenes to alcohols directly under mild conditions by using electron donating trialkylphosphine ligands with rhodium catalysts in protic solvents.<sup>58</sup>

With toluene as solvent 1-hexene was hydroformylated with  $[\text{RhH}(\text{PEt}_3)_3]$  at 40 bar  $\text{CO}/\text{H}_2$  1:1 and 120 °C, minor amounts of alcohol products were detected, however, most of the products were aldehydes. Even after 16 hours only 4 % of the reaction products were alcohols.

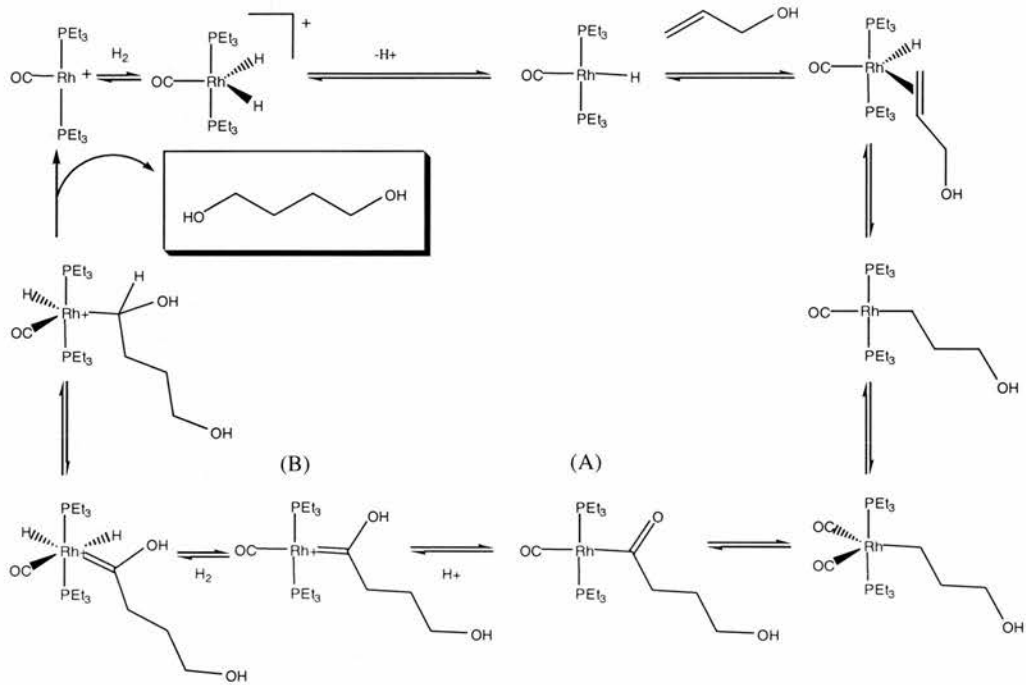
In THF the reaction showed higher selectivity to alcohols. After 2 hours the majority of the products were aldehydes but alcohols predominate after 16 hours. Improved

conversion to alcohols was achieved by adding a small amount of water to the THF, and after 2 hours 50 % of the 1-hexene was been hydroformylated to alcohols, and 46 % was been hydroformylated to aldehydes. In alcohol solvents, (primary, secondary and tertiary alcohol solvents) alcohols were the only products after 2 hours of reaction, i.e. no aldehydes were observed. Similar results were reported for the hydroformylation of ethene and propene, and soon after the hydroformylation of allyl alcohol to alcohol products was reported also.<sup>59</sup> In these systems the alcohol products were proven to be the primary products of reaction, rather than being formed via the aldehydes.

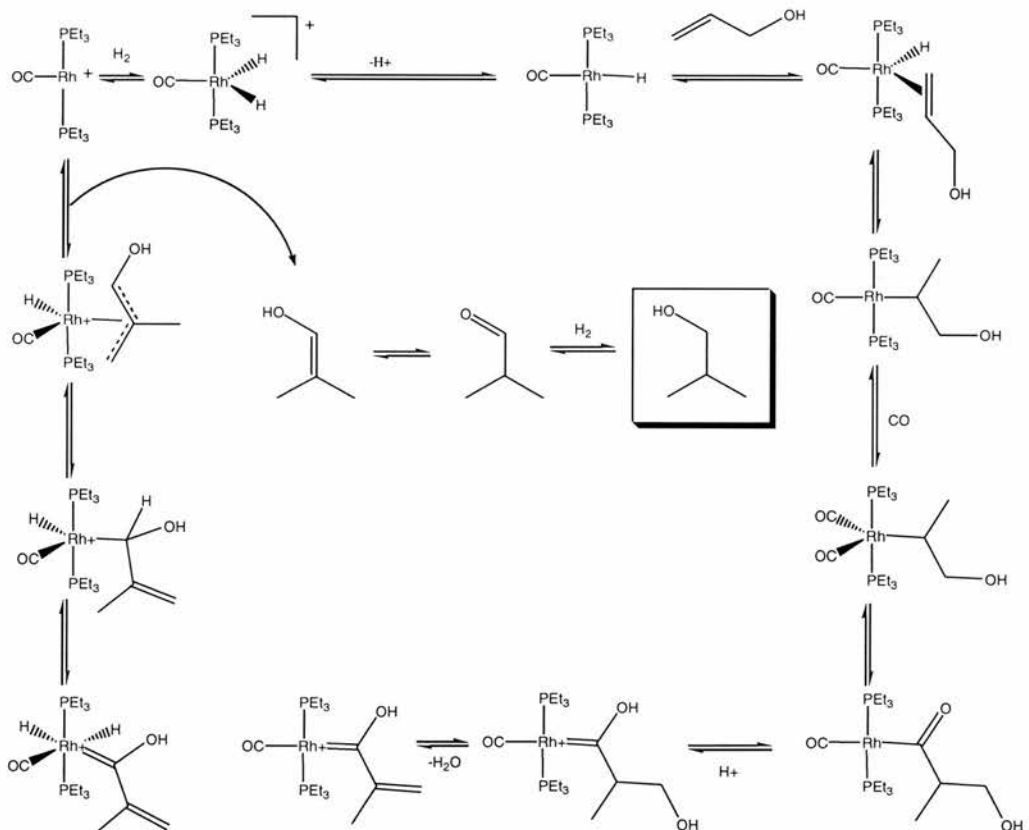
In the hydroformylation of allyl alcohol using rhodium triethylphosphine complexes in ethanol, the alcohol products formed were 1,4-butanediol and 2-methylpropan-1-ol. The process relies upon the electron donating trialkylphosphines increasing the electron density on the metal and therefore on the acyl oxygen formed by the insertion of CO into the rhodium-alkyl intermediate, species A in Scheme 1.7. This is then protonated by the protic solvent (ethanol) or by the allyl alcohol itself, species B in Scheme 1.7. Subsequent hydrogen transfer then leads to the alcohol (butanediol in the linear case) as the primary product of reaction, therefore 4-hydroxybutanal is not an intermediate of the reaction. The branched product of reaction requires further explanation however. Following the same mechanism as for the production of 1,4-butanediol the branched product of reaction would be 2-methyl-1,3-propanediol rather than 2-methylpropan-1-ol. Formally the later product arises from the addition of methane across the carbon-carbon double bond. The production of 2-methylpropan-1-ol must therefore involve dehydration at some point, and it is possible that this could occur in several ways. Analysis of the products showed that 2-methylpropan-1-ol was not the primary product of reaction but that it is formed *via* 2-methylpropanal, which is hydrogenated to 2-methylpropan-1-ol by the catalytic system. The mechanism for the production of 2-methylpropan-1-ol was postulated to be as in Scheme 1.7.

## Scheme 1.7

*Proposed mechanism for the direct formation of 1,4-butandiol in the rhodium triethylphosphine catalysed hydroformylation of allyl alcohol.*



*Proposed mechanism for the formation of 2-methylpropan-1-ol via 2-methylpropan in the rhodium triethylphosphine catalysed hydroformylation of allyl alcohol.*

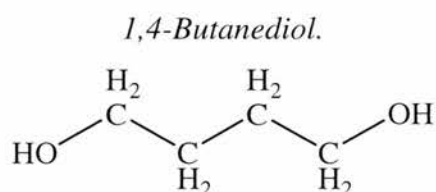


## 1.2 1,4-Butanediol

### 1.2.1 BDO A Commodity Chemical.

The aim of this research is to investigate improved methods of producing the bifunctional alcohol, 1,4-butanediol or BDO, see Figure 1.26. The reason for this is that the demand for BDO is growing. In the 1980's the world BDO capacity was about 235,000 tpa, by the mid 1990's this had risen to 500,000 tpa, by 1997 740,00 tpa and the current global capacity is reported to be about 980,000 tpa. This is not the end, however, as BDO demand is expected to grow by 5-7 % p.a. in the near future.<sup>60</sup>

**Figure 1.26**



The main use of BDO is as a precursor for the production of other chemicals.<sup>61</sup> Traditionally THF production was its main use although this is changing as the demand for other chemicals made from BDO increase and new technology enables THF to be made from other sources such as *n*-butane, see section 1.2.4.<sup>62</sup> THF itself is used in manufacture of polytetramethylene ether glycol or poly-THF. The demand for poly-THF is growing because of its use in the production of spandex fibres such as lycra. THF is also used as a solvent, for example in the synthesis of Grignard reagents, as a carrier of alkali metal alumino-hydrides and for polyvinyl chloride cements and glues.<sup>62</sup>

BDO is also used for the production of polybutylene terephthalate (PBT) resins and  $\gamma$ -butyrolactone (GBL).<sup>62</sup> PBT is a thermoplastic polymer produced by the polycondensation of BDO with terephthalic acid or dimethylterephthalate. Since its introduction in 1970, the PBT market has undergone rapid growth, due PBT's attractive properties, as it shows an inherent heat resistance, low water absorption, good electrical properties dimensional stability, satisfactory impact strength and the retention of these properties on exposure to humidity and other chemicals. GBT is produced from the dehydration of BDO. It has several solvent uses but its main use is as an intermediate in

the production of N-methyl-2-pyrrolidone (NMP) and 2-pyrrolidone through reaction with methyl amine and ammonia respectively.

Other uses include the production of polyurethanes, use as a solvent, as a coating of resins and in pharmaceutical production.<sup>61</sup>

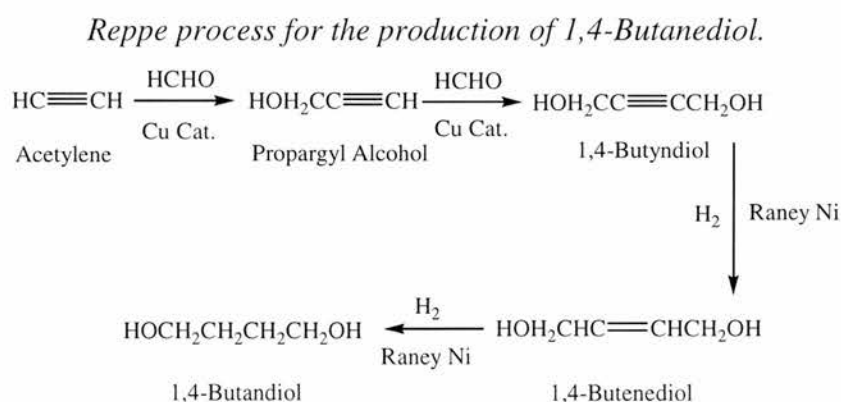
There are several technologies available for the production of BDO. The next section gives a review of the main five techniques used for the production of BDO from acetylene and formaldehyde, butadiene (BD), maleate anhydride (MA), n-butane and propylene oxide (PO).

### 1.2.2 The Production of 1,4-Butanediol From Acetylene and Formaldehyde: “The Reppe Process”.

The technology for the production of BDO production is based largely on the available feedstock. The Reppe process for the production of BDO, which was developed by Walter Reppe in the 1930's and was first commercialised at Ludwigshafen in Germany in 1940, still accounts for about 70 % of the worlds production capacity.<sup>60</sup> The Reppe Process uses acetylene and formaldehyde as the feedstock. Both can be obtained from coal or natural gas. Condensation is carried out using a cuprous acetylide catalyst supported on magnesium silicate. The resulting products are propargyl alcohol and 1,4-butynediol which are hydrogenated over Raney nickel to produce 1,4-butanediol with an overall yield of 41 %, see Scheme 1.8.

One of the major drawbacks in employing the Reppe Process is in the handling of acetylene. Even in an inert atmosphere under moderate pressures acetylene has a tendency to spontaneously decompose. For this reason, special reactors and handling systems have be employed .

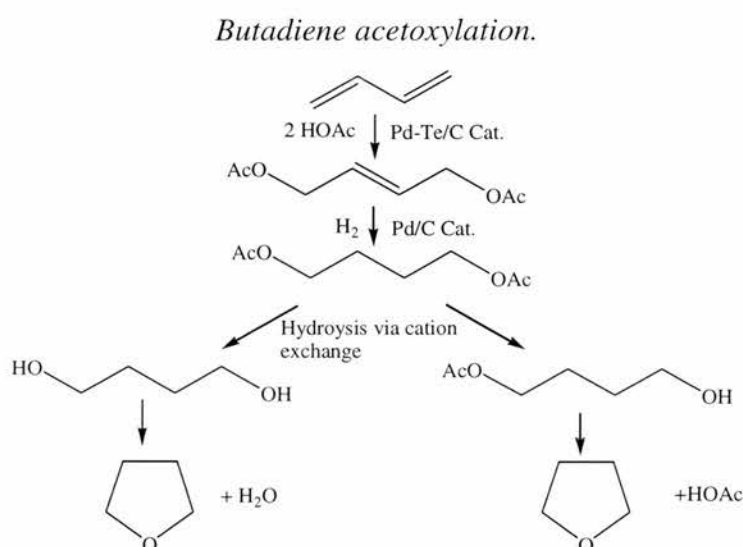
#### Scheme 1.8



### 1.2.3 1,4-Butanediol From Butadiene.

In the 1970's Mitsubishi chemicals developed the technology of BDO production from butadiene.<sup>61</sup> The process can be used to produce BDO or THF directly and proceeds via the acetoxylation of butadiene with acetic acid catalysed by a heterogeneous catalyst consisting of palladium and tellurium on a carbon support. Subsequent hydrogenation to the diacetate, followed by hydrolysis leads either BDO or to monoacetate. THF can then either be made from the dehydration of BDO or from the spontaneous deacetylation of the monoacetate, see Scheme 1.9.

**Scheme 1.9**



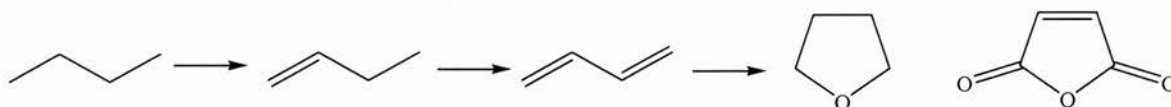
### 1.2.4 1,4-Butanediol From n-Butane and Maleic Anhydride.

The production of BDO from maleic anhydride was originally developed by Davey McKee in the 1980's in collaboration with CONSER and SISAS. The Davey McKee process involves the esterification and hydrogenation of maleic anhydride or maleic acid to produce BDO. Production of BDO from maleic anhydride was desirable as it could be obtained through the oxidation of n-butane or benzene precursors over transition metal catalysts such as vanadium phosphorus oxide. This involves the abstraction of eight hydrogen atoms and the insertion of 3 oxygen atoms and is recognised as one of the most complex selective oxidation reactions used in industry today.<sup>63</sup> It has been proposed that the reaction follows one of two routes, the alkoxide route or the alkene route. The alkene route is shown in Scheme 1.10. As no intermediate species have been identified (the intermediates of the reaction being more

reactive towards oxidation than n-butane), the evidence for the alkene route is based on kinetic studies and observations of butenes, butadiene, and furans in the reaction mixture.<sup>64</sup>

### Scheme 1.10

*Olefin route for the oxidation of n-butane to maleic anhydride.*



Maleic anhydride, maleic acid or a mixture of both are then converted to the dialkyl maleate via esterification. This can either be done in a two step process via the mono-alkyl maleate or in a one step process directly to the dialkyl maleate. The Davey McKee process proceeds via the two step process, the mono-esterification step is carried out non-catalytically by heating the maleic anhydride and an alkyl alcohol such as ethanol. For the second esterification step, it is necessary for the product of the first step to be dried to below 1 % water content, this improves the selectivity. The first esterification step is therefore carried out by passing the maleic anhydride down a reactor against the flow of a vaporous stream of ethanol, this then carries away the water by-product.<sup>65,66</sup>

The mono-alkyl maleate is then converted to the dialkyl maleate by reaction with ethanol in the presence of an esterification catalyst which comprises of an immobilised ion exchange resin containing sulfonic acid and carboxylic acid groups. The di-esterification is a reversible reaction in the presence of the catalyst such that the reaction yields an equilibrium mixture of the dialkyl maleate and the mono-alkyl maleate. Dialkyl maleate of low concentration for the next stage of reaction is obtained by feeding the reaction products to a primary distillation zone, where the thermal decomposition of the mono-alkyl maleate to maleic anhydride and ethanol occurs. The products of the primary distillation are: 1) a bottom fraction which contains mono-alkyl maleate and dialkyl maleate; 2) a vaporous phase comprising of the ethanol; and 3) an intermediate phase comprising of the majority of the di-alkyl maleate and a small amount of maleic anhydride. The intermediate fraction, 2, is then transferred into for a

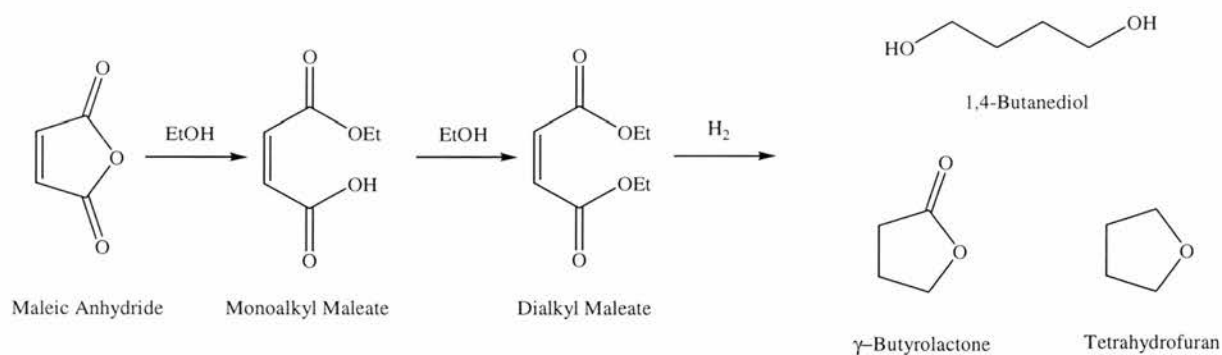
second distillation. This yields a vaporous fraction of maleic anhydride and a bottom fraction of substantially pure dialkyl maleate.

The next stage in the process is the hydrogenation of the dialkyl maleate to BDO. The hydrogenation is carried out in the vapour phase at a temperature of 150 °C to 240 °C, and at pressures of 25 bar to 75 bar in the presence of a reduced copper chromate catalyst, the catalyst containing about 25-45 % copper and 20-35 % chromium before reduction. The reaction results in the production of BDO, THF, GBA and n-butanol.

In practice the process is done in two steps, the first step being at slightly higher temperature than the second. The temperature in the first step is selected to maximise the production of BDO and GBA over THF. Temperatures above 190 °C result in an increase in THF production. In the second step of hydrogenation the temperature is selected to convert as much of the GBA to BDO as possible.<sup>67-69</sup>

### Scheme 1.11

#### *BDO production from maleic anhydride.*



BP Chemicals Inc. in collaboration with Lurgi Öl-Gas-Chemie has developed its own process for the production of BDO from n-butane via maleic anhydride. The process uses a fluidised-bed reactor with a catalyst like the VPO system described earlier. The fluidised-bed reactor design also has a uniform temperature profile that prevents hot spots in the reactor, which results in a higher selectivity but has the disadvantage of intense mixing of the products.

The products of this reaction are water, maleic anhydride and fumaric acid.<sup>70</sup> Part of the maleic anhydride is removed in the liquid or solid form but part must also be washed out of the gas stream with water to produce a concentrated aqueous solution of maleic acid and fumaric acid. The fumaric acid is then separated from a stream of the molten maleic anhydride and the two can be isolated separately.

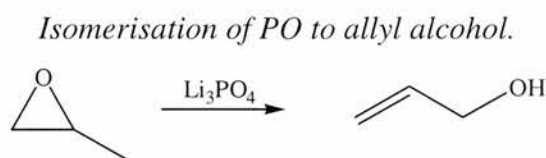
The maleic anhydride is then hydrogenated to give a high percentage of 1,4-butanediol along with smaller quantities of THF and GBA. The technology is very new but it builds on technology developed by The Standard Oil Company. This technology outlines the production of THF in a one stage process though the hydrogenation of a mixture of maleic anhydride and an alcohol. The hydrogenation catalyst in this case is comprised of mixed oxides of copper, zinc and aluminium.<sup>71</sup> The catalyst can be changed to favour 1,4-butanediol if it comprises palladium, silver, rhenium, and at least one or mixtures of iron, aluminium, and cobalt, on a carbon support.

### 1.2.5 1,4-Butanediol From Propylene Oxide and the Hydroformylation of Allyl Alcohol.

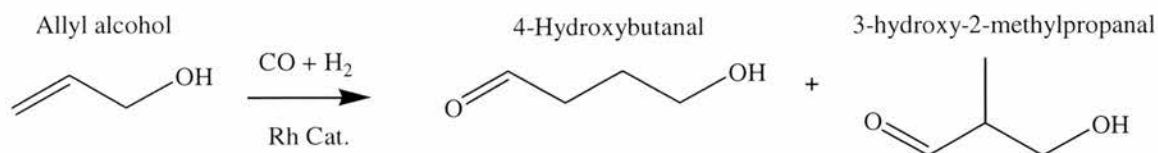
The last process for the production of BDO reviewed is from propene oxide. The process is in operation by the Lyondell Company in Channelview in the USA, and a second plant is planned in the Netherlands.

The first step of the process is the isomerisation of propene oxide (PO) to allyl alcohol. This is achieved using technology developed for glycerol manufacture by FMC. It takes place at temperatures of 250-300 °C and under a pressure of 10 bar, catalysed by  $[\text{Li}_3\text{PO}_4]$ , see Scheme 1.12.<sup>62</sup>

#### Scheme 1.12



The next step in the process is the hydroformylation of allyl alcohol to 4-hydroxybutanal. The hydroformylation reaction has been reviewed already in section 1.1 and much emphasis was placed on the linear to branched ratio, l:b. Again this is important as it is the linear product which is the desirable one, not the branched product, 3-hydroxy-2-methylpropanal, see Scheme 1.13.

**Scheme 1.13***Hydroformylation products of allyl alcohol.*

Lyondell use technology developed by Kuraray Company Ltd. and Daicel Chemical Industries Ltd.<sup>6,51,52,72,73</sup> The process uses a triphenylphosphine rhodium catalyst with a small amount of the diphosphine, bis(diphenylphosphino)butane (dppb), added; Rh/TPP/DPPB ratio 1:150:0.2. High TPP ratios are used to ensure the rhodium catalyst species is of the form  $[\text{RhP}_2]$  which is accepted to be the rhodium phosphine complex which can produce high l:b ratios, see section 1.1. The small quantities of dppb are reported to prevent deactivation of the catalyst by poisoning, either from acyl intermediates, or from methacrolein, (formed by the dehydration of the branched product of reaction), or from ligand oxidation.

Because of the higher activity of allyl alcohol compared with non-functionalised alkenes the operating conditions can be kept very mild, from 60-65 °C and 2-2.5 bar. This also has the effect of suppressing the formation of the high boiling point by-products (acetals) often associated with the reaction.

The reaction is carried out in toluene as a solvent. The solution is continuously removed from the reactor and the products are extracted by washing with water. The hydrophilic products can then be recovered from the aqueous phase and the catalyst recycled in the organic phase. Some bleed of the catalyst solution is required to remove heavy boiling point by-products and triphenylphosphine oxide, which are not soluble in the aqueous layer and so remain in the organic phase with the catalyst.

The reaction is also very sensitive to the CO pressure, if it is too low, low selectivities are observed though the production of the isomerisation product propanal and the hydrogenation product propanol, and catalyst deactivation can also occur. Yet if the CO pressure is too high the l:b ratio is low.

The hydroformylation of allyl alcohol with the rhodium triphenylphosphine catalytic system has also been investigated by Pittmann and Honnick.<sup>49</sup> They studied the effect of temperature (40-129 °C), pressure (50-800 psi) and  $\text{H}_2/\text{CO}$  ratios of 0.1 to 10. They

also studied the effect of changing the phosphine ligand to triphenylphosphite ( $\text{P}(\text{OPh})_3$ ), tris(*p*-chlorophenyl) phosphite ( $\text{P}(\text{p-Cl-PhO})_3$ ), tributylphosphine ( $\text{PBu}_3$ ), 1,2-bis(diphenylphosphino)ethane (diphos), bis(2-phenylphosphinoethyl)phenyl phosphine (triphos), and 1,1'-bis(diphenylphosphino) ferrocene (dppf)

Using triphenylphosphine as ligand at 7 bar,  $\text{CO}/\text{H}_2$  1:1, and 60 °C with a P/Rh ratio of 3 gave an **l** to **b** ratio of 1.7, increasing the P/Rh ratio to 40 only gave a slight improvement in the l:b ratio to 2.5, the l:b ratio at P/Rh ratios below 3 are not reported however.

A slight negative relationship was found with increasing the total pressure; as it was increased from 3.5-55 bar  $\text{CO} / \text{H}_2$  1:1, at 60 °C and with a P / Rh ratio of 3 the l:b ratio decreased from 2.05 to 1.73.

In the temperature range of 40-60 °C the linear and branched aldehyde products were the only products of reaction, but at higher temperature the product distribution was more complex. At 7 bar  $\text{CO} / \text{H}_2$  1:1, and 60 °C, P/Rh = 3, the amount of the isomerisation product propanal was less than 1 % and the combined percentage of the linear and branched aldehyde products was over 99 % with a l:b ratio of 1.7. On increasing the temperature to 120 °C the l:b ratio increased to 3.1 but the amount of the isomerisation product increased to 34.1 %, along with 29.2 % of unidentified products and 0.7 % of the hydrogenation product propanol. This means the combined percentage of the linear and branched aldehyde products was only 36 %. This is not as pronounced at 28 bar where the l:b ratio was 1.9, the combined percentage of the linear and branched aldehyde products was 56.7 %, and the by-products were 27.1 % propanol, 16.1 % unidentified and 0.1 % propanol.

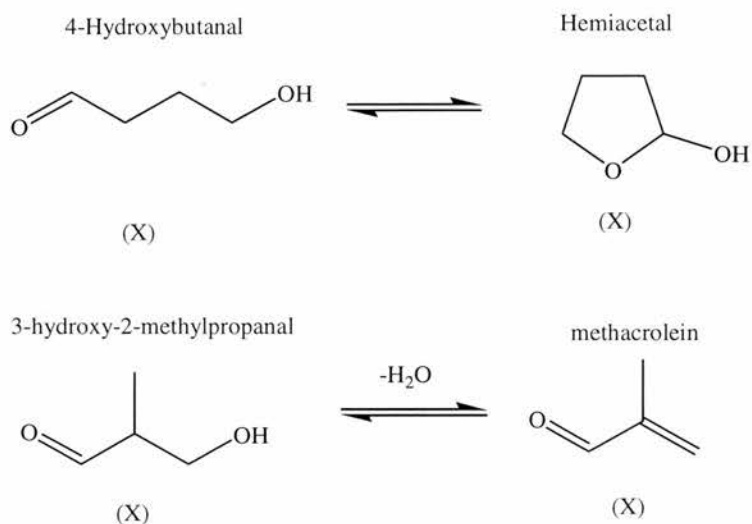
The unknown products of reaction are reported to be due to the decomposition of the linear and branched aldehyde products. The branched aldehyde product, 3-hydroxy-2-methylpropanol can be dehydrated at higher temperatures to give methacrolein which can oligomerise or polymerise. The linear aldehyde product, 4-hydroxybutanal, can undergo ring closure to form the hemiacetal, 2-hydroxytetrahydrofuran, which was found to be thermally unstable and degraded to new products with higher boiling points, see Scheme 1.14.

The degradation of the linear and branched aldehyde products is important when considering the l:b ratios. If we consider the last two examples, at 7 bar the l:b ratio was 3.1 compared with 1.9 at 28 bar, but the yield of the linear and branched aldehyde products at 7 bar was only 36 % and the amount of unidentified products was 29.2 %

compared with 56.7 % and 16.1 % at the higher pressure, 28 bar. Therefore, the true l:b ratio is distorted by the destruction of the linear and branched aldehyde products at higher temperatures, as it is probable that the branched product is destroyed quicker at higher temperatures than the linear aldehyde product.

### Scheme 1.14

*The degradation products of 4-hydroxybutanal and 3-hydroxy-2-methylpropanol.*



By changing the CO/H<sub>2</sub> ratio from 1 to 0.1 there was a substantial increase in the l:b ratio, at 7 bar, 60 °C and P/Rh = 3, the l:b ratio increased from 1.70 to 6.54 when the CO/H<sub>2</sub> ratio was changed from 1 to 0.1. However, this was accompanied by a large increase in the hydrogenation product propanol, 33.7 % yield, and when P/Rh = 20, at 7 bar, and 60 °C the l:b ratio increased from 2.02 to 8.33 as the CO/H<sub>2</sub> ratio was changed from 1 to 0.1, the amount of propanol in this case was again high at 25.5 %.

By using triphenylphosphite [P(OPh)<sub>3</sub>] instead of triphenylphosphine as ligand the l:b ratio was slightly lower, 1.57 compared to 2.04, at 7 bar, 60 °C and P/Rh = 20. There was a small amount of propanal formed, 0.2 %, but no high boiling point by-products.

Tris(p-chlorophenyl)phosphite [P(OC<sub>6</sub>H<sub>4</sub>Cl)<sub>3</sub>] as ligand gives a high proportion of the higher boiling point products either in benzene where phase separation occurs, 78.3 %, or in THF, 36.0 % with l:b ratios of 0.6 and 1.52 respectively. Although the use tributylphosphine [P(Bu)<sub>3</sub>] as ligand leads to a very large l:b ratio, 27.95, the combined l and b selectivity was only 41.2 %, with 12.4 % of the product propanal and 46.4 % the higher boiling point products.

A *cis*-chelating diphosphine ligand, dppe, was also used at 28 bar CO/ H<sub>2</sub> = 1, 60 °C, P/Rh = 3, the l:b ratio was 0.29 where use of TPP gave 1.70,. It also gave 74 % of the higher boiling products where TPP gave none. Increasing the temperature to 100 °C resulted in 50.4 % of propanal being produced, compared with 3.1 % when using TPP under the same conditions.

When the triphosphine ligand bis(2-diphenylphosphinoethyl)phenylphosphine (triphos) was used in the reaction at 7 bar CO/H<sub>2</sub> =1:1, 60 °C, P/Rh = 20, no hydroformylation of by-products was observed even after 47 hours.

The highest l:b ratios were achieved by using dppf, at 7 bar CO/H<sub>2</sub> 1:1, 60 °C, P/Rh 20,<sup>†</sup> an l:b ratio of 3.26 was achieved with 99.3 % conversion after 22.6 hours and only 0.6 % propanal and 1.9 % propanol being formed. The l:b ratio increased as the pressure was increased. When the pressure was increased to 28 bar under the same conditions as before the l:b ratio was 7.07 with 90.4 % conversion after 23 hours and 1.3 % propanal and 1.2 % propanol, and at 55 bar the l:b ratio was 7.88, but the conversion was only 70.2 % after 23 hours with no propanal and 1.5 % propanol. This trend is opposite to that observed when using TPP as ligand, at 7, 28, and 55 bar CO/H<sub>2</sub> 1:1, 60 °C, P/Rh 20, with the TPP catalytic system the l:b ratios were 2.04, 1.75, and 1.68 respectively.

Increasing the H<sub>2</sub> partial pressure resulted in an increase in the by-product formation as it did in the TPP catalytic system. At 7 bar CO/H<sub>2</sub> 0.1, 60 °C, P/Rh 20 using BDPF as ligand the percentage of the linear and branched aldehyde products was 11.3 % with 15.8 % propanol and 72.9 % propanal produced.

High P/Rh ratio also led to higher l:b ratios, as in the TPP system. At 55 bar CO/H<sub>2</sub> 1:1, 60 °C the l:b ratio increased from 3.85 to 7.88 as the dppf/Rh ratio was increased from 1 to 8.5.<sup>‡</sup>

As mentioned earlier, the linear and branched hydroxyaldehyde products are extracted from the organic catalyst phase with water. This aqueous solution containing 4-hydroxybutanal and 2-methyl-3-hydroxypropanal is then hydrogenated in the presence of a Raney nickel catalyst and hydrogen,<sup>52</sup> see Scheme 1.15. The product is an aqueous

---

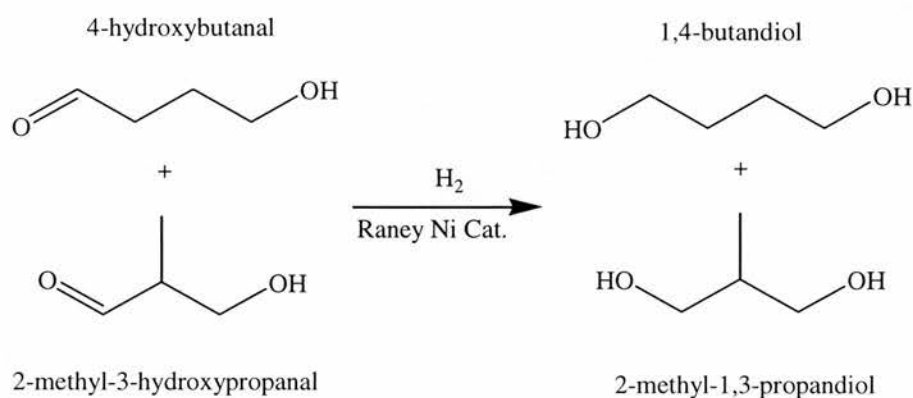
<sup>†</sup> The catalyst is made from [ClRh(PPh<sub>3</sub>)<sub>3</sub>] and dppf, a mono-phosphine and a diphosphine, both of which are taken into account in the P/Rh ratio. For a P/Rh ratio of 20, therefore, the dppf/PPh<sub>3</sub>/Rh ratio is 8.5:3:1.

<sup>‡</sup> For a dppf/Rh ratio of 1:1, the P/Rh ratio is 5:1 and the dppf/PPh<sub>3</sub>/Rh ratio is 1:3:1.

solution of 1,4-butandiol and 2-methyl-1,3-propanediol, as well as small amounts of nickel, 4-hydroxybutanal, and unidentified products of high boiling point products. Alkali is then added to the aqueous solution to adjust the pH to 8.5 or above, which causes nickel to precipitate, thus reducing the nickel content of the solution. The solution is then distilled at 100 °C to remove the water and 4-hydroxybutanal fractions. Further distillation at 180 °C removes the 1,4-butandiol and 2-methyl-1,3-propanediol fraction. The two diols are subsequently separated.

### Scheme 1.15

*Hydrogenation products of 4-hydroxybutanal and 2-methyl-3-hydroxypropanal.*



### 1.3 References for Chapter One.

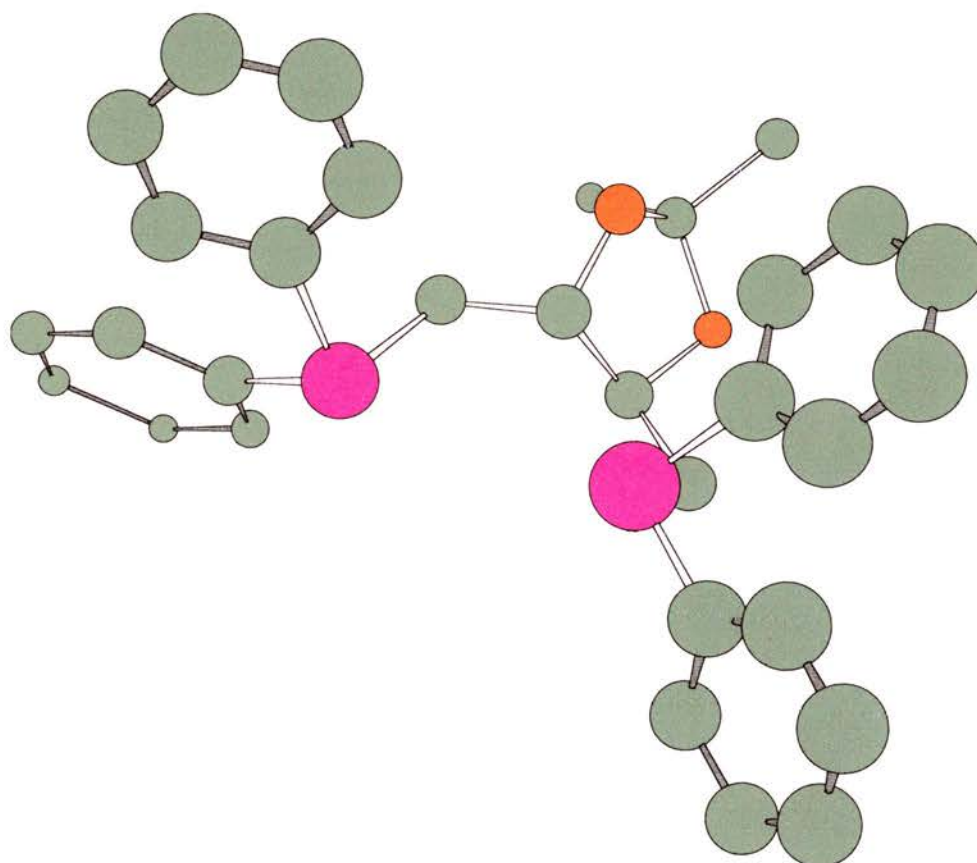
- 1 H. M. Colquhoun, D. J. Thompson, and M. V. Twigg, 'Carbonylation-Direct Synthesis of Carbonyl Compounds', Plenum, New York, 1991.
- 2 <http://www.britannica.com/bcom/eb/article/9/0,5716,118749+3,00.html>
- 3 O. Rolelen, *Ger. Pat.*, 849,548, 1938, .
- 4 O. Rolelen, *Ger. Pat.*, 2,317,066, 1943, .
- 5 R. F. Heck and D. S. Breslow, *J. Am. Chem. Soc.*, 1962, **83**, 4023.
- 6 P. W. N. M. v. Leeuwen and C. Claver, in 'Rhodium Catalysed Hydroformylation', ed. B. R. James and R. Ugo, Rhodium Catalysed Hydroformylation, Kluwer Academic Publishers, Dordrecht, 2000.
- 7 L. H. Slaugh and R. D. Mullineaux, *J. Organomet. Chem.*, 1968, **13**, 469.
- 8 L. H. Slaugh and D. Mullineaux, *Chem. Abstr.*, 1966, **64**, 15745.
- 9 L. H. Slaugh and R. D. Mullineaux, US Pat., 3,239,570, 1966, Shell Oil Company.
- 10 J. L. Vidal and W. E. Walker, *Inorg. Chem.*, 1981, **20**, 249.
- 11 G. Wilkinson, D. Evans, and J. A. Osborn, *J. Chem. Soc. A*, 1968, 3133.
- 12 E. Kuntz, US Pat., RE31,812, 1985, Rhone-Poulenc Industries.
- 13 R. L. Pruett and R. L. Smith, *J. Org. Chem.*, 1969, **34**, 327.
- 14 P. W. N. M. van Leeuwen and C. Roobeek, *J. Organomet. Chem.*, 1983, **258**, 343.
- 15 P. W. N. M. van Leeuwen and C. F. Roobeek, US Pat., 4,467,116, 1984, Shell Oil Company.
- 16 P. W. N. M. van Leeuwen, P. C. J. Kamer, J. N. H. Reek, and P. Dierkes, *Chem. Rev.*, 2000, **100**, 2741.
- 17 C. Tolman, *Chem. Rev.*, 1977, **77**, 313.
- 18 E. Billig, A. G. Abatjoglou, D. R. Bryant, R. E. Murray, and J. M. Mather, US Pat., 4,885,401, 1986, Union Carbide Corporation.
- 19 E. Billig, A. G. Abatjoglou, and D. R. Bryant, *Chem. Abstr.*, 1987, **107**, 7392.

- 20 E. Billig, A. G. Abatjoglou, and D. R. Bryant, US Pat., 4,769,498, 1988, Union Carbide Corporation.
- 21 G. J. H. Buisman, L. A. van der Veen, P. C. J. Kamer, and P. W. N. M. van Leeuwen, *Organometallics*, 1997, **16**, 5681.
- 22 P. W. N. M. van Leeuwen, G. J. H. Buisman, E. J. Vos, and P. C. J. Kamer, *J. Chem. Soc., Dalton Trans.*, 1995, 409.
- 23 W. Stroheier and F. J. Muller, *Chem. Ber.*, 1967, **100**, 2812.
- 24 J. Horrocks, W. D. and R. C. Taylor, *Inorg. Chem.*, 1963, **2**, 723.
- 25 C. A. Tolman, *J. Am. Chem. Soc.*, 1970, 2953.
- 26 C. A. Tolman, *J. Am. Chem. Soc.*, 1970, 2956.
- 27 D. White, B. C. Taverner, N. J. Coville, and P. W. Wade, *J. Organomet. Chem.*, 1995, **495**, 41.
- 28 D. White, B. C. Taverner, P. G. L. Leach, and N. J. Coville, *J. Organomet. Chem.*, 1994, **478**, 205.
- 29 Y. Koide, S. G. Bott, and A. R. Barron, *Organometallics*, 1996, **15**, 2213.
- 30 T. L. Brown, *Inorg. Chem.*, 1992, **31**, 1286.
- 31 C. P. Casey, G. T. Whiteker, M. G. Melville, L. M. Petrovich, J. A. G. Jr., and D. R. Powell, *J. Am. Chem. Soc.*, 1992, **114**, 5535.
- 32 P. W. N. M. van Leeuwen, G. J. Busman, and P. C. J. Kamer, *Tetrahedron: Asymmetry*, 1993, **4**, 1625.
- 33 R. F. Heck and D. S. Breslow, *J. Am. Chem. Soc.*, 1962, **84**, 2499.
- 34 L. G. Cannel, L. H. Slauch, and R. D. Mullineaux, *Chem. Abstr.*, 1965, **62**, 16054.
- 35 G. Wilkinson, G. Yagupsky, and C. K. Brown, *J. Chem. Soc. A*, 1970, 1392.
- 36 D. L. Thorn and R. Hoffmann, *J. Am. Chem. Soc.*, 1978, **100**, 2079.
- 37 A. van Rooy, J. N. H. de Bruijn, K. F. Roobeek, P. C. J. Kamer, and P. W. N. M. van Leeuwen, *J. Organomet. Chem.*, 1996, **507**, 69.
- 38 L. A. van der Veen, P. C. J. Kamer, and P. W. N. M. van Leeuwen, *Angew. Chem. Int. Ed.*, 1999, **38**, 336.
- 39 J. D. Unruh and J. R. Christenson, *J. Mol. Catal.*, 1982, **14**, 19.
- 40 O. R. Hughes and D. A. Young, *J. Am. Chem. Soc.*, 1981, 6636.

- 41 T. J. Devon, G. W. Phillips, T. A. Puckette, J. L. Stavinoha, and J. J. Vanderbilt, US Pat, 4,694,109, 1987, Eastman Kodak Company.
- 42 T. J. Devon, G. W. Phillips, T. A. Puckette, J. L. Stavinoha, and J. J. Vanderbilt, US Pat, 5,332,846, 1994, Eastman Kodak Company.
- 43 J. M. Brown and A. G. Kent, *J. Chem. Soc., Perkin Trans II*, 1987, 1597.
- 44 C. P. Casey, E. L. Paulsen, E. W. Beuttenmueller, B. R. Proft, L. M. Petrovich, B. A. Matter, and D. R. Powell, *J. Am. Chem. Soc.*, 1997, **119**, 11817.
- 45 C. P. Casey and L. M. Petrovich, *J. Am. Chem. Soc.*, 1995, **117**, 6007.
- 46 A. R. Rossi and R. Hoffmann, *Inorg. Chem.*, 1975, **14**, 365.
- 47 C. P. Casey, E. L. Paulsen, E. W. Beuttenmueller, B. R. Proft, B. A. Matter, and D. R. Powell, *J. Am. Chem. Soc.*, 1999, **121**, 63.
- 48 P. W. N. M. van Leeuwen, M. Kranenburg, Y. E. M. van der Burgt, and P. C. J. Kamer, *Organometallics*, 1995, **14**, 3081.
- 49 C. U. Pittman and W. D. Honnick, *J. Org. Chem.*, 1980, **45**, 2132.
- 50 M. Matsumoto and M. Tamura, US Pat., 4,215,077, 1980, Kuraray Co., Ltd.
- 51 M. Matsumoto, K. Shinichi, K. Kikuchi, M. Tamura, H. Kojima, K. Koga, and S. Yamashita, US Pat., 4,567,305, 1986, Daicel Chemical Industries, Ltd.; Kuraray Company, Ltd.
- 52 Y. Harano, US Pat., 4,465,873, 1984, Daicel Chemical Industried, Ltd.; Kuraray Co., Ltd.
- 53 W. E. Smith, *Chem. Abstr.*, 1978, **89**, 163050t.
- 54 T. Shimizu, *Chem. Abstr.*, 1976, **85**, 45962m.
- 55 E. Drent, *Chem. Abstr.*, 1986, **104**, 88112n.
- 56 E. Drent, US Pat, 4,590,311, 1986, Shell Oil Company.
- 57 K. Kameda, T. Imanaka, and S. Teranishi, *Chem. Lett.*, 1983, 1465.
- 58 D. J. Cole-Hamilton, J. K. MacDougall, M. C. Simpson, and M. J. Green, *J. Chem. Soc., Dalton Trans.*, 1996, 1161.
- 59 D. J. Cole-Hamilton, M. C. Simpson, A. W. S. Currie, and J. M. Anderson, *J. Chem. Soc. Dalton Trans*, 1996, 1793.
- 60 [www.chemicalweekly.com/current/Aug\\_08/spf01-I.htm](http://www.chemicalweekly.com/current/Aug_08/spf01-I.htm).
- 61 A. M. Brownstein, *Chemtech*, 1991, **21**, 506.

- 62 M. L. Morgan, *Chem. Ind.*, 1997, **5**, 166.
- 64 B. Chen and E. J. Munson, *J. Am. Chem. Soc.*, 1999, **121**, 11024.
- 65 B. Chen and E. J. Munson, *J. Am. Chem. Soc.*, 1999, **121**, 11024.
- 66 M. Sharif and K. Turner, US Pat., 4,584,419, 1986, Davy McKee Ltd.
- 67 A. G. Hiles and M. W. M. Tuck, US Pat., 5,254,758, 1993, Davy McKee Ltd.
- 68 N. Harris, C. Rathmell, K. Turner, and J. Scarlett, US Pat., 4,765,869, 1988, Davy McKee Ltd.
- 69 J. W. Kippax and C. Rathmell, US Pat., 4,795,824, 1989, Davy McKee Ltd.
- 70 K. Turner, M. Sharif, C. Rathmell, J. W. Kippax, A. B. Carter, J. Scarlett, A. J. Reason, and N. Harris, US Pat., 4,751,334, 1988, Davy McKee Ltd.
- 71 J. M. Forgac, US Pat., 5,929,255, 1999, BP Amoco Corporation.
- 72 J. R. Budge and S. E. Pedersen, US pat., 4,810,807, 1989, The Standard Oil Company.
- 73 H. Kojima, T. Horikawa, and M. Kagotani, US Pat, 4,537,997, 1985, Daicel Chemical Industries, Ltd.; Kuraray Co., Ltd.
- 74 M. Matsumoto and M. Tamura, US Pat., 4,238,419, 1980, Kuraray Co., Ltd.

*CHAPTER TWO: THE RHODIUM DIOP CATALYTIC SYSTEM.*



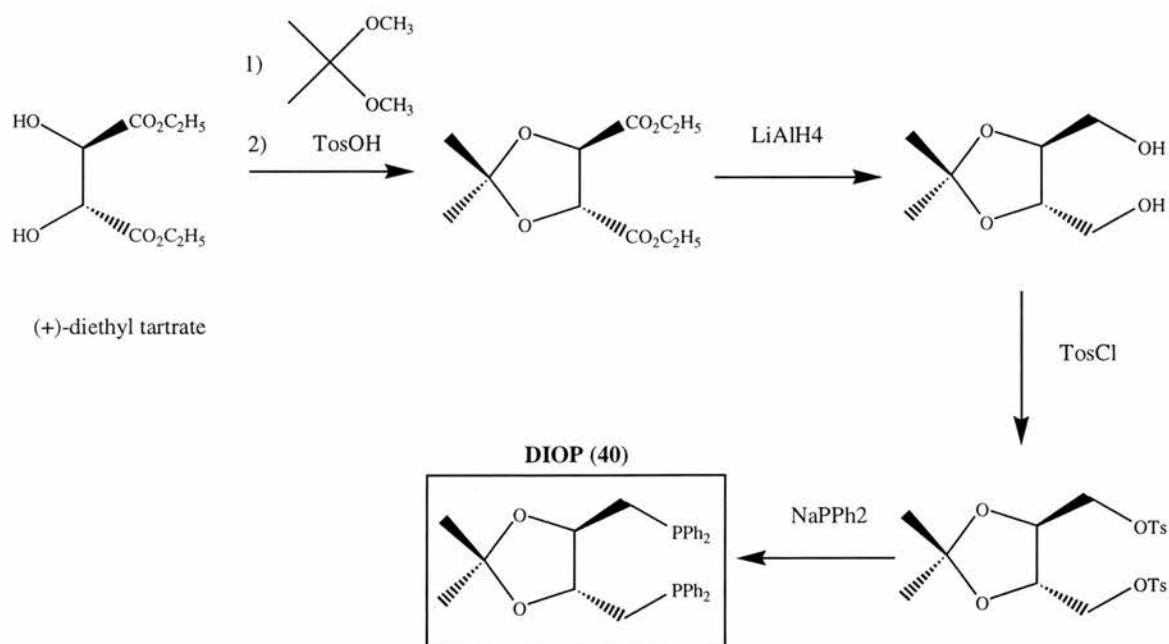
## 2 CHAPTER TWO: THE RHODIUM / DIOP CATALYTIC SYSTEM.

## 2.1 (-)-2,3-O-Isopropylidene-2,3-dihydroxy-1,4-bis(diphenylphosphino)butane.

In the early 1970's Henri B. Kagan and Tuan-Phat Dang reported the asymmetric reduction of alkenes catalysed by a new homogeneous catalytic system of rhodium modified with (-)-2,3-O-Isopropylidene-2,3-dihydroxy-1,4-bis(diphenylphosphino)butane (**DIOP**).<sup>1-3</sup> DIOP is a chiral diphosphine ligand prepared from (+)-diethyl tartrate as in Scheme 2.1. There have been several modifications of the synthesis since<sup>4-6</sup> in order to optimise the final stage which involves the reaction between a diphenylphosphide ion and a tosylate. The best route uses sodium-potassium alloy to form the potassium diphenylphosphide ion.

## Scheme 2.1

*The synthesis of DIOP as first proposed by Kagan & Dang.*

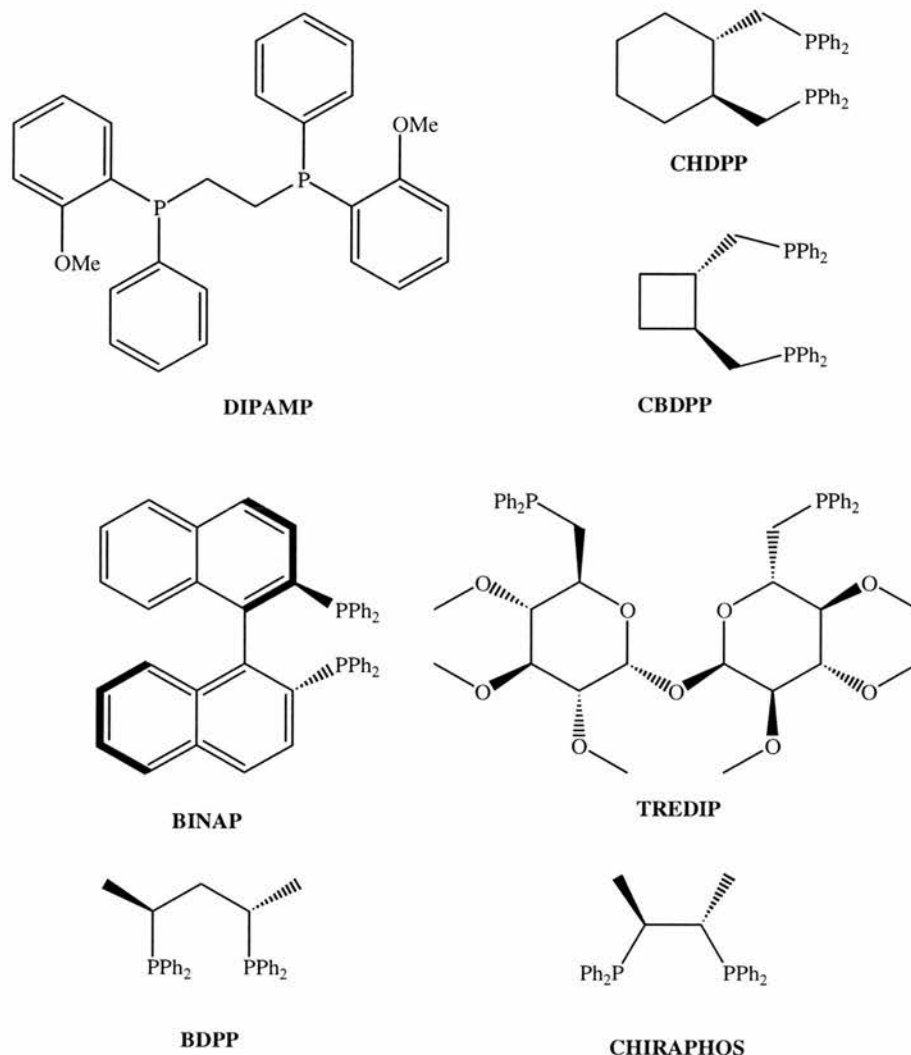


Kagan and Dang used DIOP as the ligand in the asymmetric hydrogenation of alkenes using homogeneous rhodium catalysts. Previously, there had been reports of the use of asymmetric heterogeneous catalysts<sup>7, 8</sup> for the reaction, but these suffered from low optical yields. Kagan and Dang proposed that a more rational approach to obtain higher selectivities would be to introduce an external element of symmetry into the extensively studied Wilkinson catalyst  $[\text{ClRh}(\text{PPh}_3)_3]$  for homogeneous catalytic reduction.<sup>9-11</sup> There had been several reports of using chiral monophosphines in the literature, either by using phosphines with three different substituents on the phosphorus<sup>12, 13</sup> or by attaching asymmetric substituents to the phosphorus.<sup>14</sup> The use of DIOP was the first case using a chiral diphosphine modified homogeneous catalyst system.

Soon after, Knowles and co-workers reported the synthesis of another chiral diphosphine, DIPAMP,<sup>15, 16</sup> which they also used as ligand in the rhodium catalysed asymmetric hydrogenation of alkenes.

Since Kagan and Dang's paper there have also been a plethora of reports using DIOP and other chiral diphosphines, such as CHDPP, CBDPP, BINAP, TREDIP, BDPP and CHIRAPHOS as ligands in asymmetric hydrogenation using rhodium,<sup>17</sup> palladium<sup>18</sup> and ruthenium<sup>19</sup> catalysts. The ligands have also been employed in the hydroformylation reaction of several substrates such as styrene,<sup>20</sup> 1-octene, 1-hexene, N-acetamidoacrylate,<sup>21</sup> and vinyl acetate,<sup>22, 23</sup> using platinum,<sup>24, 25</sup> and rhodium<sup>26</sup> catalytic systems.

DIOP has been the subject of much interest as a ligand with an intermediate bite angle and a relatively rigid backbone,<sup>27</sup> see section 1.1.3. As we discussed earlier, it is thought that both the bite angle and rigidity of a diphosphine<sup>28</sup> play a part in its effectiveness as a ligand in the rhodium catalysed hydroformylation reaction. While BISBI gave a higher l:b ratio as ligand in the rhodium catalysed hydroformylation of 1-octene, using DIOP gave fewer by-products such that the selectivity of the reaction towards the linear aldehyde was greater.

**Figure 2.1***Some chiral diphosphines.*

Maki, Fujita and Murumo first showed that rhodium-DIOP catalytic systems could be used for the hydroformylation of allyl alcohol to give 2-hydroxytetrahydrofuran and 3-hydroxy-2-methylpropanal.<sup>29</sup> Further studies by the Lyondell Chemical Company showed that the rhodium-DIOP system could hydroformylate allyl alcohol to 4-hydroxybutanal and 3-hydroxy-2-methylpropanal giving higher l:b ratios than more traditional catalysts,<sup>30, 31</sup> see section 2.4.4.

In this chapter we discuss studies in which we have attempted to understand why DIOP as ligand in the rhodium catalysed hydroformylation of alkenes, especially allyl alcohol gives better selectivities.

## 2.2 HP NMR and HP FTIR Experimental Techniques.

In order to try and understand how the ligand structure effects the regioselectivity of the reaction it is desirable to gain a greater understanding of the catalytic species present in solution during the hydroformylation reaction. We have already seen that there are a number of intermediates in the accepted Wilkinson mechanism, see section 1.1. We have also seen how there can be more than one geometric isomer of any given intermediate, i.e. the ee and ea geometric isomers of phosphine coordination in the TBP structure, see section 1.1.3.

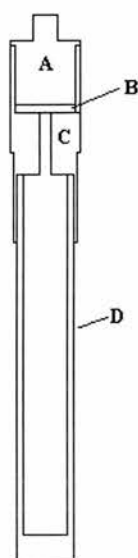
This chapter attempts to gain a greater understanding of the reaction by characterisation of the different complex species present in solution at different stages. This has been done by a number of common techniques, NMR, FTIR, GC, GCMS Chapter , and by some more specialised techniques that allow us to study the reaction *in situ*. These *in situ* techniques are high pressure NMR (HP NMR), high pressure FTIR (HP FTIR) and kinetic measurements, see sections 2.2.1, 2.2.2, and 2.2.3 respectively.

### 2.2.1 HP NMR Experiments.

The HP NMR experiments were carried out in two high pressure titanium-sapphire cells. The cells are constructed of a sapphire tube either 88 mm or 79 mm in length and 10 mm or 5 mm in diameter respectively, and titanium. The sapphire tubes were supplied by Saphikon. The cell was designed and built in the University of St. Andrews, School of Chemistry Workshop.

A schematic diagram of the HP cell can be seen in Figure 2.2. It consists of a titanium screw cap (A) with a PTFE seal which acts as a valve for pressurising the cell from a conventional cylinder via a specially designed spiral hose, see Chapter 6. The screw cap can be screwed into the top of a titanium holder for the sapphire tube. The sapphire tube (10 mm OD and 8 mm ID or 5 mm OD and 3 mm ID) is glued into the titanium holder with an epoxy resin. The other end of the sapphire tube is bought sealed.

A spinner has been designed so that the titanium head of the cell sits within it which gives the cell a low centre of gravity, this way it is possible to adjust the air flow in the spectrometer to spin the cell.

**Figure 2.2***Schematic of the HP NMR cell.*

The rhodium complex is made up under a nitrogen or argon atmosphere using Schlenk techniques. The phosphorus ligand is dissolved in toluene- $d_8$  ( $2.5 \text{ cm}^3$ ), the solution is then used to dissolve the rhodium precursor  $[\text{Rh}(\text{CO})_2(\text{acac})]$  ( $0.1 \text{ mmol}$ ), and allyl alcohol or 1-hexene is then added in the *in situ* experiments.

The solution ( $1.5 \text{ cm}^3$ ) is then transferred to the sapphire tube under a nitrogen or argon atmosphere using Schlenk techniques, and the tube is sealed and pressurised with  $\text{H}_2/\text{CO}$ . This process is done over several hours to ensure total conversion of the complex species present in solution as gas transport over the gas liquid interface can be very slow, see section 2.5. The HP cell is lowered into the NMR spectrometer with an extendable clamp, as the assembly is too heavy to be lowered on the spectrometer's air lift.

The internal volume of the 10 mm cell is  $4.7 \pm 0.1 \text{ cm}^3$  and  $0.53 \pm 0.01 \text{ cm}^3$  for the 5 mm cell. The maximum working pressure<sup>†</sup> is 144 bar for the 10 mm cell and 207 bar for the 5 mm cell, both cells have been pressure tested to 100 bar at  $25 \text{ }^\circ\text{C}$  and  $100 \text{ }^\circ\text{C}$ .

The advantage of using a HP NMR cell over other types of high pressure NMR techniques, e.g. HP NMR probes,<sup>32, 33</sup> is that they can be employed in a commercial

---

<sup>†</sup> Information supplied by Saphikon.

probe head. The disadvantage is that they provide less sensitivity<sup>34</sup> than HP NMR probes and the gas volume is limited.

**Figure 2.3**

*Photograph of the 10 mm HPNMR Cell and its spinner.*



**2.2.2 HP FTIR Experiments.**

The high pressure infrared studies have been carried out in a cylindrical internal reflectance Fourier transform infrared high pressure (HP CIR FTIR) autoclave.<sup>35, 36</sup> The autoclave has an internal volume of 35 cm<sup>3</sup>, it is fitted with an injection port for the substrate, a gas inlet / outlet for pressurising / depressurising, a pressure gauge, a mechanical stirrer, a thermocouple located in the reaction medium, and a cylindrical internal reflectance (CIR) crystal, see schematic in Figure 2.1. The CIR crystal was made of either silicon or zinc selenide and was obtained from Spectra-Tech.

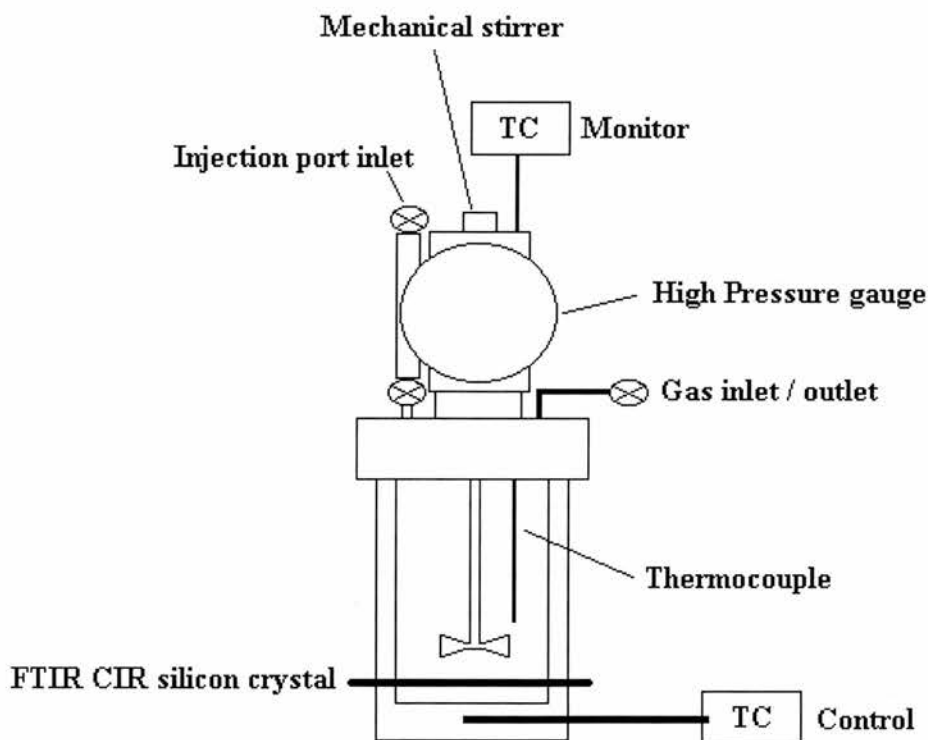
The CIR crystal is a polished cylinder with 45 ° conical ends. The HP CIR FTIR autoclave is placed on the optical bench of an FTIR spectrometer where the infrared beam is directed into a set of convex cone mirrors and a toroidal mirror where the energy is focused onto the 45 ° angle of the CIR crystal. As the beam passes through the crystal it undergoes internal reflection, approximately ten times, at the sample surface. At each point of reflection, the IR beam penetrates into the surrounding solution by

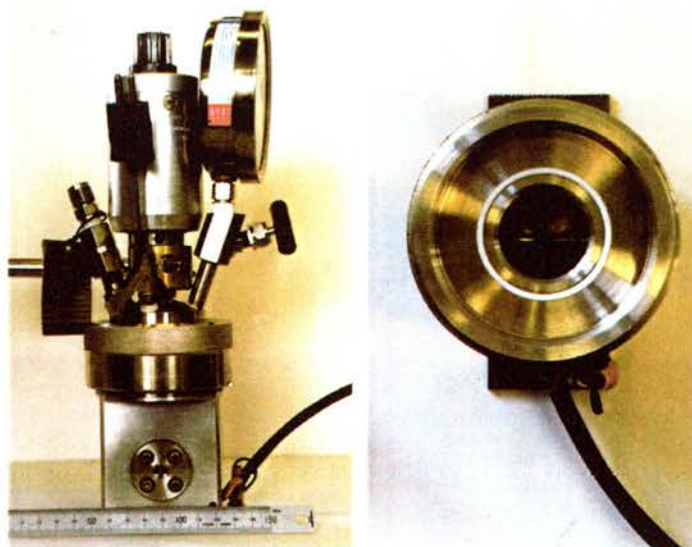
about 1.0 to 1.5  $\mu\text{m}$  giving a total path length of about 10-15  $\mu\text{m}$ . When the IR beam exits the CIR crystal it is directed through another set of toroidal and convex cone mirrors by the  $45^\circ$  angle. The IR beam is thus directed into the detector of the FTIR spectrometer.

In a typical reaction the rhodium complex is made up under a nitrogen or argon atmosphere using Schlenk techniques. The phosphorus ligand is dissolved in toluene (9  $\text{cm}^3$ ), the solution is then used to dissolve the rhodium precursor  $[\text{Rh}(\text{CO})_2(\text{acac})]$ . The solution is then transferred to the HP CIR FTIR autoclave under a nitrogen or argon atmosphere, and the autoclave is pressurised with  $\text{H}_2/\text{CO}$ . The autoclave is then placed on the optical bench of a Nicolet Protege 460 infrared spectrometer, where the heating elements and mechanical stirrer were fitted, and the CIR crystal aligned. The autoclave was then heated to the desired temperature and the FTIR spectrum recorded on an interfaced PC via the ONNIC operating system.

**Figure 2.4**

*Schematic of the HP CIR FTIR reactor cell.*



**Figure 2.5***Photograph of the HP CIR Cell.***2.2.3 Kinetic Measurement Experiments.**

The kinetic measurement hydroformylation experiments were done on a specially designed autoclave owned and operated by the CATS (Catalytic Evaluation and Optimisation Services) service.<sup>37</sup>

A schematic of the CATS kinetic autoclave can be seen in Figure 2.6. The set-up includes an autoclave (A), an injection arm (B), a pressure controller and transducer (C), a ballast vessel (D), and a control panel (E). Each section can be isolated from each other with valves. The autoclave parts were supplied by Baskerville and assembled by the University of St. Andrews, School of Chemistry Workshop.

The reaction takes place in the autoclave which is heated to reaction temperature and pressurised to just below reaction pressure. The substrate is then injected with a stream of synthesis gas which brings the autoclave to reaction pressure. As the reaction proceeds the synthesis gas is consumed. The pressure in the autoclave, however, is kept constant by the pressure controller, the gas stream is fed by the ballast vessel which is pressurised to a value such that when the reaction is over it will still be higher than the pressure of the reaction. There are gas inlets to the autoclave and ballast vessel which allow for them to be filled with gas independently of each other. The pressures of the autoclave, ballast vessel, and injection port are all monitored by pressure transducers which are in turn controlled from the control panel.



## 2.3 Rhodium DIOP Species at 1 Bar and 25 °C.

At first the rhodium-DIOP catalytic system was studied at pressures of 1 bar and at 25 °C. In these studies the catalyst was prepared in situ by adding a solution of DIOP usually in toluene or *d*<sub>8</sub>-toluene to acetylacetonatodicarbonylrhodium(I) [Rh(CO)<sub>2</sub>(acac)]. Generating the catalyst in this manner is a well documented<sup>27, 38-40</sup> way of avoiding the complications of having other phosphine species present in the catalytic system. Gases were added either by bubbling through the solution, or by pressurising the complex solutions.

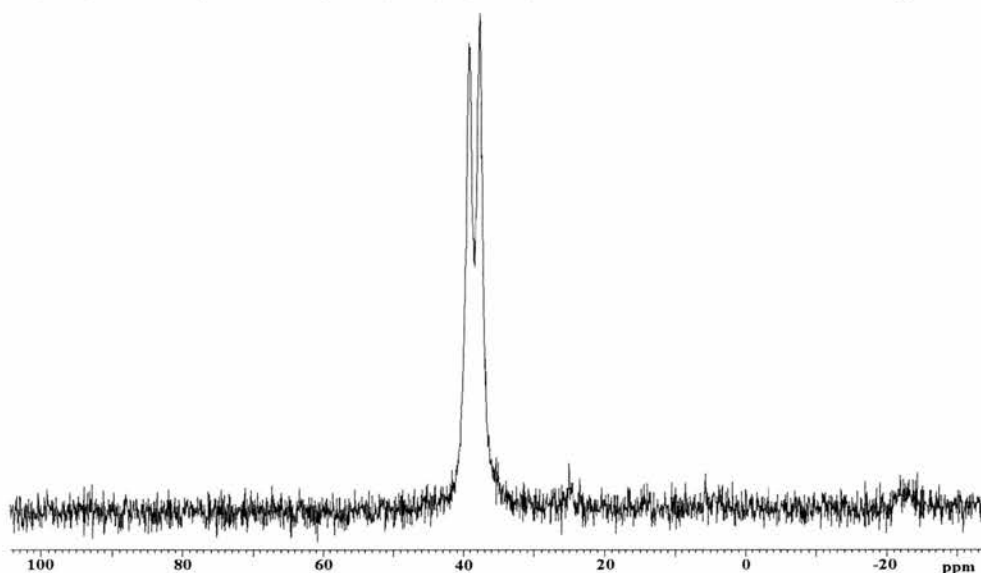
### 2.3.1 Rhodium DIOP Species Present Under an Argon Atmosphere.

The <sup>31</sup>P {<sup>1</sup>H} NMR spectra of the rhodium-DIOP complex species present in solution under an argon atmosphere, with varying rhodium to DIOP ratios can be seen in NMR 2.1 to NMR 2.5, and are summarised in Table 2.1.

The <sup>31</sup>P {<sup>1</sup>H} NMR spectrum of the rhodium-DIOP complex species present with a rhodium-DIOP ratio of 1:1 can be seen in NMR 2.1. The spectrum has a strong broad doublet at ~39 ppm, and a weak broad singlet at ~23 ppm.

#### NMR 2.1

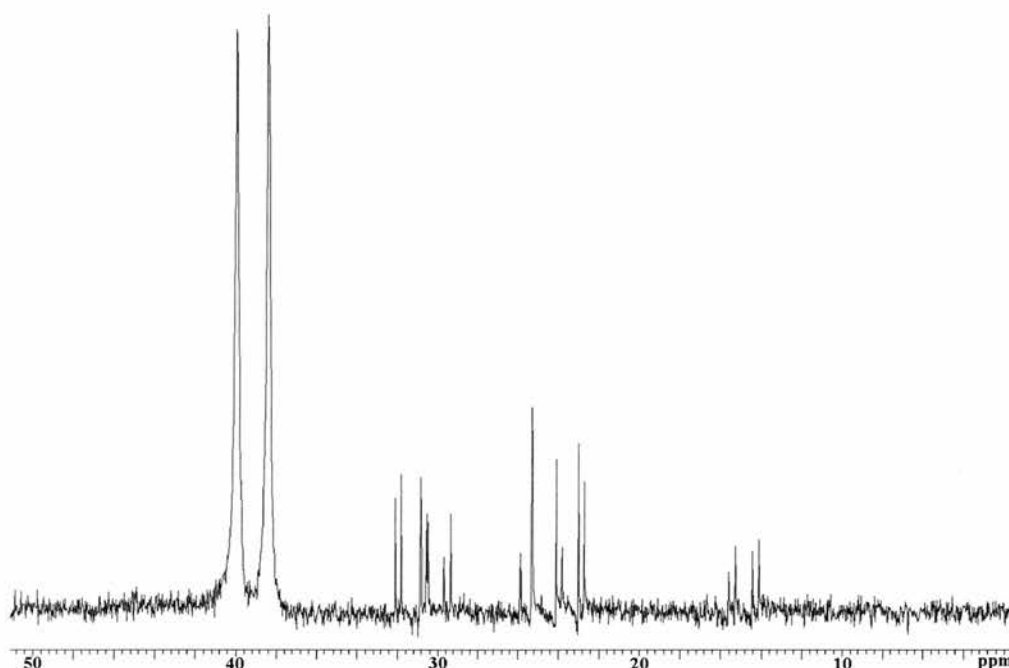
*The <sup>31</sup>P {<sup>1</sup>H} NMR Spectrum of Rh(CO)<sub>2</sub>(acac) / DIOP 1:1 under 1 bar argon at 25 °C.*



The  $^{31}\text{P}$   $\{^1\text{H}\}$  NMR spectrum of the rhodium-DIOP complex species present with a rhodium-DIOP ratio of 1:1.5 can be seen in NMR 2.2-2.4. The spectrum has the same doublet at  $\sim 39$  ppm, see NMR 2.2, four sets of double doublets from 32-14 ppm, and two singlets at 25 ppm and 26 ppm, see NMR 2.3. The solution was monitored over time and was observed that the four sets of double doublets decrease in intensity over time, see NMR 2.4.

## NMR 2.2

*The  $^{31}\text{P}$   $\{^1\text{H}\}$  NMR Spectrum of  $\text{Rh}(\text{CO})_2(\text{acac}) / \text{DIOP}$  1:1.5 under 1 bar argon at  $25^\circ\text{C}$ .*

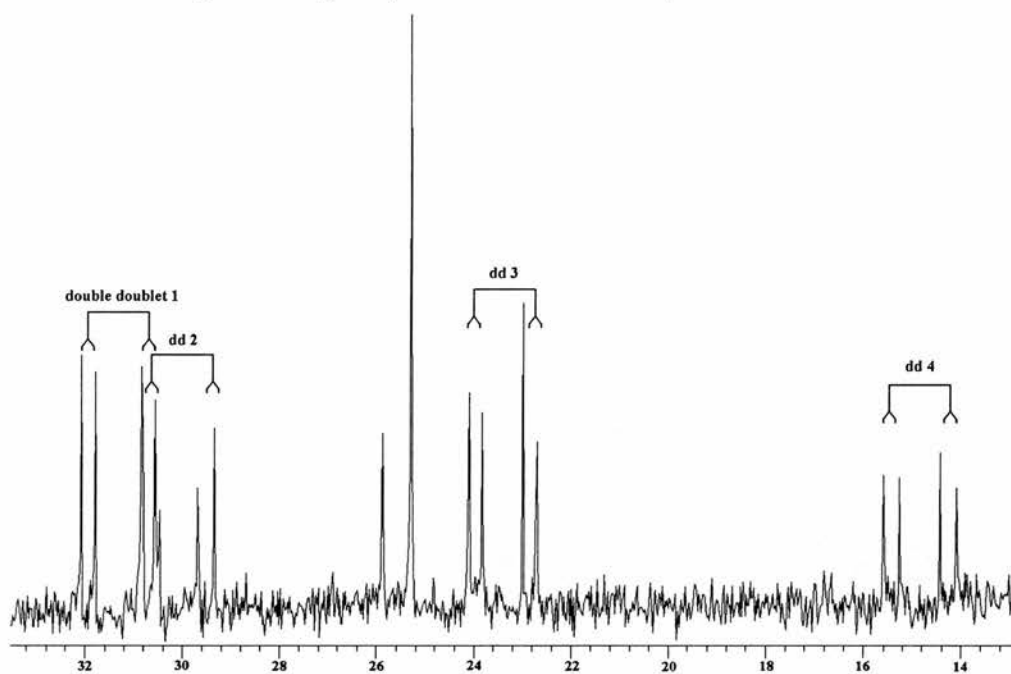


The  $^{31}\text{P}$   $\{^1\text{H}\}$  NMR spectrum of the rhodium-DIOP complex species present with a rhodium-DIOP ratio of 1:2 can be seen in NMR 2.5. The spectrum has the same doublet at  $\sim 39$  ppm, a singlet at 25 ppm, a doublet at  $\sim 5$  ppm and a singlet at  $-23$  ppm. The singlet at  $-23$  ppm is due to free DIOP. The doublet at  $\sim 5$  ppm in the rhodium-DIOP 1:2 ratio spectrum is a dimeric species which is characterised as the dimeric species  $[\text{Rh}_2(\text{CO})_4(\text{DIOP})_2]$  in section 2.2.2.

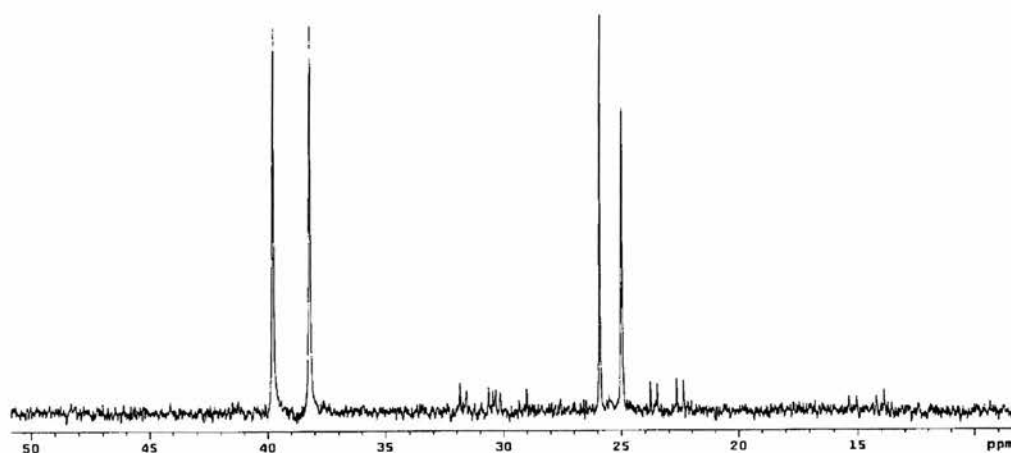
The singlets present in all three spectra at all three rhodium-DIOP ratios are not DIOP oxide species, as they are slightly downfield of the oxide peaks 27-26 ppm, see section 2.2.2.1. They also disappear with the addition of synthesis gas, see section 2.2.3. They may be resonances from a phosphorus of DIOP which is bound unidentate to rhodium through the other phosphorus atom. This could suggest evidence of fluxional species in which there is exchange between free DIOP and rhodium bound DIOP in solution.

**NMR 2.3**

*Expansion of the four double doublets from NMR 2.2.*

**NMR 2.4**

*The  $^{31}\text{P}$   $\{^1\text{H}\}$  NMR spectrum of  $\text{Rh}(\text{CO})_2(\text{acac})$  / DIOP 1:1.5 under 1 bar argon at 25 °C after 3 hours.*



## NMR 2.5

The  $^{31}\text{P}\{^1\text{H}\}$  NMR spectrum of  $\text{Rh}(\text{CO})_2(\text{acac}) / \text{DIOP}$  1:2 under 1 bar argon at 25 °C

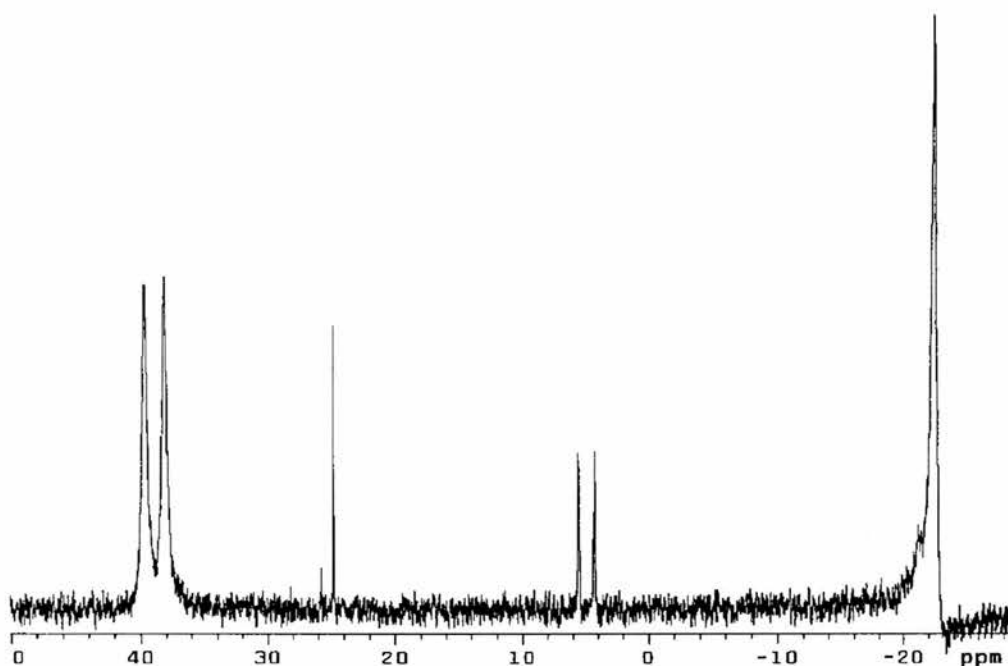


Table 2.1

$^{31}\text{P}\{^1\text{H}\}$  data for solutions of  $\text{Rh}(\text{CO})_2(\text{acac})$  & DIOP in various ratios under argon.

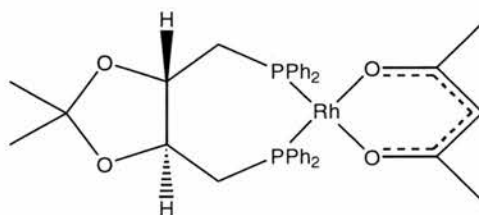
Solution.	Rh(CO) <sub>2</sub> (acac): DIOP ratio.	$^{31}\text{P}\{^1\text{H}\}$		
		$\delta(\text{ppm})$	$J_{\text{Rh-P}} (\text{Hz})$	$J_{\text{P-P}} (\text{Hz})$
(a)	1:1	38.67, d	188.4	-
		26.06, s	-	-
		25.48, s	-	-
(b)	1:1.5	39.00, d	188.4	-
		31.31, dd	149.7	34.1
		30.07, dd	136.4	40.0
		25.90, s	-	-
		25.00, s	-	-
		23.40, dd	136.4	34.1
		14.84, dd	142.3	40.0
(c)	1:2	38.94, d	190.1	-
		24.80, s	-	-
		4.90, d	159.4	-
		-22.50, s	-	-

The doublet at ~39 ppm has been identified as the rhodium complex species **41** in Figure 2.8. Crystals of [Rh(acac)(DIOP)] were grown from acetone at low temperature. A view of the X-ray molecular structure can be seen in Figure 2.9.

Selected bond lengths and angles can be seen in Table 2.2. The complex is almost square planar with one molecule of DIOP chelated to the rhodium centre and acac still bound to the rhodium through both oxygen atoms. The P(1)-Rh-P(6) bond angle is  $95.5^\circ$  (10), the P(1)-Rh-O(35) bond angle is  $88.7^\circ$  (2), and the O(35)-Rh-O(37) bond angle is  $88.1^\circ$  (3). The P(1)-Rh bond length is 2.181 Å (7) and the O(35)-Rh bond length is 2.051 Å (7). For the full set of crystallography data see Tables 1 to 5 in Appendix One.

**Figure 2.8**

*The rhodium-DIOP complex species 41, observed at ~39 ppm in the  $^{31}\text{P}$  NMR, under inert conditions.*



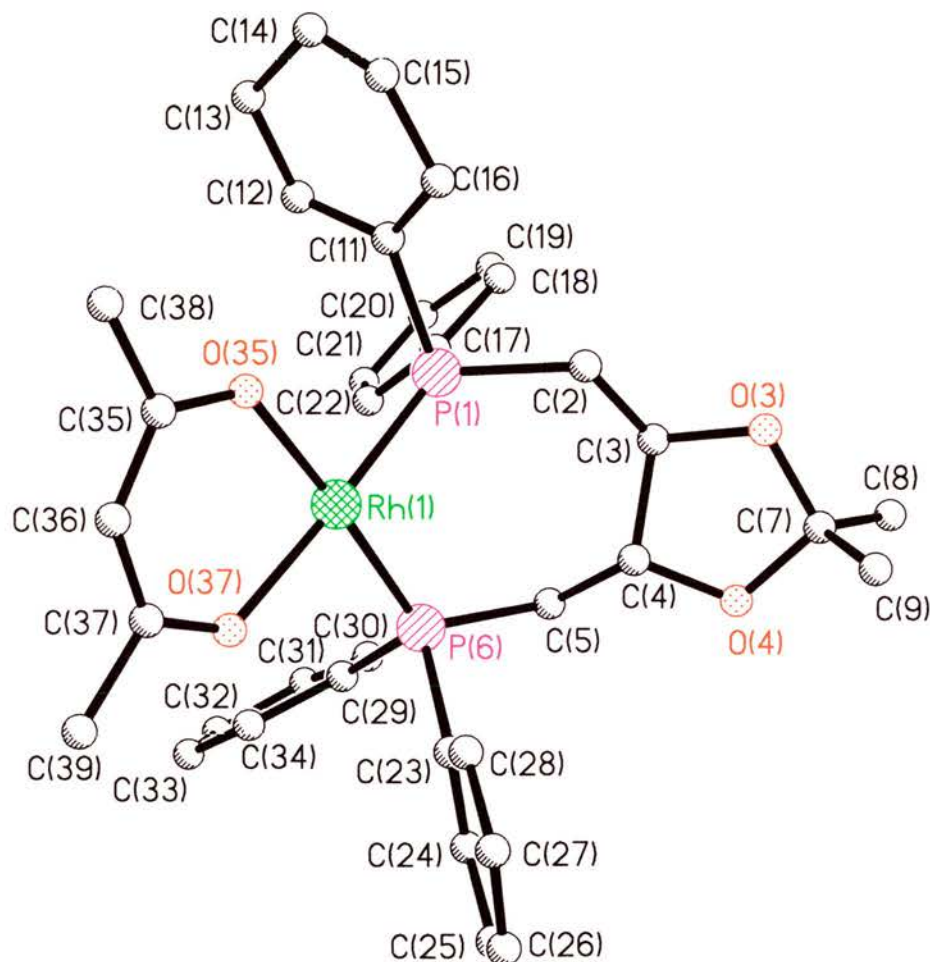
(41)

**Table 2.2**

*Selected crystallography data for the [Rh(acac)(DIOP)] complex.*

Selected bond lengths (Å) and angles ( $^\circ$ ) for the complex [Rh(acac)(DIOP)]			
Rh-P(1)	2.181 (3)	C(35)-C(36)	1.37 (2)
Rh-P(6)	2.195 (2)	C(35)-C(38)	1.483 (14)
Rh-O(35)	2.051 (7)	P(1)-C(17)	1.824 (13)
Rh-O(37)	2.090 (7)	P(1)-C(11)	1.847 (12)
O(35)-C(35)	1.298 (12)	P(1)-C(2)	1.855 (10)
O(37)-C(37)	1.266 (12)	P(6)-C(29)	1.847 (10)
C(39)-C(37)	1.51 (2)	P(6)-C(23)	1.827 (11)
C(37)-C(36)	1.36 (2)	P(6)-C(5)	1.826 (9)
P(1)-Rh-P(6)	95.50 (10)	O(37)-C(37)-C(39)	114.9 (11)
P(1)-Rh-O(35)	88.7 (2)	O(37)-C(37)-C(36)	125.7 (11)
P(1)-Rh-O(37)	176.8 (2)	C(39)-C(37)-C(36)	119.4 (11)
P(6)-Rh-O(37)	87.7 (2)	C(37)-C(36)-C(35)	128.5 (11)
P(6)-Rh-O(35)	175.6 (2)	C(36)-C(35)-C(38)	121.2 (11)
O(35)-Rh-O(37)	88.1 (3)	O(35)-C(35)-C(38)	114.4 (11)
Rh-O(37)-C(37)	126.2 (7)	O(35)-C(35)-C(36)	127.0 (11)

Figure 2.9

*X-Ray crystal structure of [Rh(acac)DIOP].*

It can be observed in the appendix that the empirical formula of the complex from the x-ray crystallography data is given as  $C_{37.5}H_{42}O_{4.5}P_2Rh$ , but the actual molecular formula of the given complex is  $C_{36}H_{39}O_4P_2Rh$ . The reason for this is that half a molecule of acetone co-crystallises with every molecule of  $[Rh(acac)(DIOP)]$ .

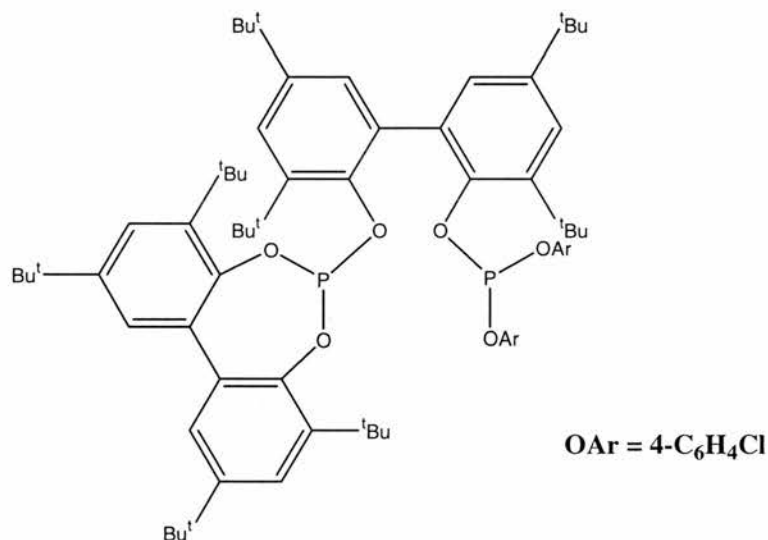
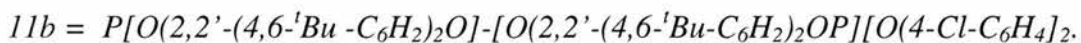
There are only a few examples of  $[Rh(acac)(PR_3)_2]$  complexes in the literature.<sup>40,41,42,43</sup> It has been reported that the reaction of  $[Rh(CO)_2(acac)]$  with  $PR_3$  to give  $[Rh(acac)(CO)(PR_3)]$  is favourable,<sup>41</sup> but the reaction  $[Rh(acac)(CO)(PR_3)]$  with  $PR_3$  and the displacement of the second CO is rather sluggish. It is reported that even with

the removal of free CO by purging with an inert gas, strong  $\pi$ -accepting ligands such as  $\text{PR}_3 = \text{P}(\text{OPh})_3$  or  $\text{P}(\text{NC}_4\text{H}_4)_3$  are required in order to obtain the di-substituted  $[\text{Rh}(\text{acac})(\text{PR}_3)_2]$ ,<sup>41</sup> and that weak  $\pi$ -accepting ligands, even when in large excess, afford only the mono-substituted  $[\text{Rh}(\text{acac})(\text{CO})(\text{PR}_3)]$ .

For this reason, most of the reported of  $[\text{Rh}(\text{acac})(\text{PR}_3)_2]$  complexes are in fact rhodium phosphite complexes, such as  $[\text{Rh}(\text{acac})(\text{P}(\text{OPh})_3)_2]$ <sup>42</sup> and  $[[\text{Rh}(\text{acac})(11b)]]$ <sup>40</sup> where 11b is the diphosphite  $\text{P}[\text{O}(2,2'-(4,6\text{-}^t\text{Bu-C}_6\text{H}_2)_2\text{O})-\text{O}(2,2'-(4,6\text{-}^t\text{Bu-C}_6\text{H}_2)_2\text{OP})][\text{O}(4\text{-Cl-C}_6\text{H}_4)_2]$ , see Figure 2.10. There are some phosphine  $[\text{Rh}(\text{acac})(\text{PR}_3)_2]$  complexes reported, however, such as  $[\text{Rh}(\text{acac})(\text{PCy}_3)_2]$ .<sup>43</sup>

There are, however, several reports of  $[(\text{P-P})\text{Rh}(\text{hfacac})]$  compounds, [ref] (hfacac = hexafluoroacetylacetonate, and P-P = dppe,  $\text{C}_2\text{P}(\text{CH}_2)_2\text{PCy}_2$ ,  $^i\text{Pr}_2\text{P}(\text{CH}_2)_2\text{P}^i\text{Pr}_2$ ,  $\text{Me}_2\text{P}(\text{CH}_2)_2\text{PMe}_2$ , dppp, dppb,  $\text{C}_2\text{P}(\text{CH}_2)_4\text{PCy}_2$ ).<sup>44, 45</sup> The compounds were synthesised as models for the investigation of the  $[(\text{P}_2)\text{Rh}]$  fragment. Their structures are not reviewed here however.

**Figure 2.10**



The acac complexes exhibited slightly distorted square planar coordination around the rhodium centre, as did our complex,  $[\text{Rh}(\text{acac})(\text{DIOP})]$ .

The P(1)-Rh-P(2) bond angle was  $93.8^\circ$  (7) for  $[\text{Rh}(\text{acac})(\text{P}(\text{OPh})_3)_2]$ ,  $97.5^\circ$  (1) for  $[\text{Rh}(\text{acac})(11b)]$ ,  $105.6^\circ$  (4) for  $[\text{Rh}(\text{acac})(\text{P}(\text{Cy})_3)_2]$ , and  $95.5^\circ$  (10) for the complex  $[\text{Rh}(\text{acac})(\text{DIOP})]$ . The large P(1)-Rh-P(2) angle of  $[\text{Rh}(\text{acac})(11b)]$  with respect to that in  $[\text{Rh}(\text{acac})(\text{P}(\text{OPh})_3)_2]$  is attributed to steric hindrance of the diphosphite, similar large P(1)-Rh-P(2) bond angles have been previously observed for diphosphites.<sup>46</sup> The large

P(1)-Rh-P(2) bond angle in  $[\text{Rh}(\text{acac})(\text{P}(\text{Cy})_3)_2]$  is also attributed to there being large steric hindrance between the tricyclohexylphosphine groups which have a large cone angle. The bond angle of  $95.5^\circ$  (10) for  $[\text{Rh}(\text{acac})(\text{DIOP})]$  suggests there is some steric hindrance attributed to the DIOP ligand compared with that of the monophosphite  $(\text{P}(\text{OPh})_3)_2$ , but it is slight compared to the monophosphine  $\text{PCy}_3$  or even the diphosphite **11b**.

The O(1)-Rh-O(2) bond angle for the complexes are all similar,  $88.8^\circ$  (2) for  $[\text{Rh}(\text{acac})(\text{P}(\text{OPh})_3)_2]$ ,  $87.2^\circ$  (3) for  $[\text{Rh}(\text{acac})(\text{11b})]$ , and  $85.9^\circ$  (2) for  $[\text{Rh}(\text{acac})(\text{P}(\text{Cy})_3)_2]$ . For the complex  $[\text{Rh}(\text{acac})(\text{DIOP})]$  the O(1)-P-O(2) angle is  $88.1^\circ$  (3).

The P(1)-Rh-O(1) bond angle was  $87.5^\circ$  (2) for  $[\text{Rh}(\text{acac})(\text{P}(\text{OPh})_3)_2]$ ,  $86.6^\circ$  (2) for  $[\text{Rh}(\text{acac})(\text{11b})]$ , and  $84.3^\circ$  (9) for  $[\text{Rh}(\text{acac})(\text{P}(\text{Cy})_3)_2]$ . The P(1)-Rh-O(35) bond angle for the complex  $[\text{Rh}(\text{acac})(\text{DIOP})]$  the P(1)-Rh-O(35) angle is  $88.7^\circ$  (2).

The Rh-P bond distances was  $2.15 \text{ \AA}$  (2) for  $[\text{Rh}(\text{acac})(\text{P}(\text{OPh})_3)_2]$ ,  $2.13 \text{ \AA}$  (3) for  $[\text{Rh}(\text{acac})(\text{11b})]$ , and  $2.25 \text{ \AA}$  (1) for  $[\text{Rh}(\text{acac})(\text{P}(\text{Cy})_3)_2]$ . For the complex  $[\text{Rh}(\text{acac})(\text{DIOP})]$ , the Rh-P bond distance is  $2.18 \text{ \AA}$  (3).

The Rh-O bond distances was  $2.07 \text{ \AA}$  (5) for  $[\text{Rh}(\text{acac})(\text{P}(\text{OPh})_3)_2]$ ,  $2.206 \text{ \AA}$  (8) for  $[\text{Rh}(\text{acac})(\text{11b})]$ , and  $2.09 \text{ \AA}$  (4) for  $[\text{Rh}(\text{acac})(\text{P}(\text{Cy})_3)_2]$ . For the complex  $[\text{Rh}(\text{acac})(\text{DIOP})]$ , the Rh-O(35) bond distance is  $2.05 \text{ \AA}$  (7).

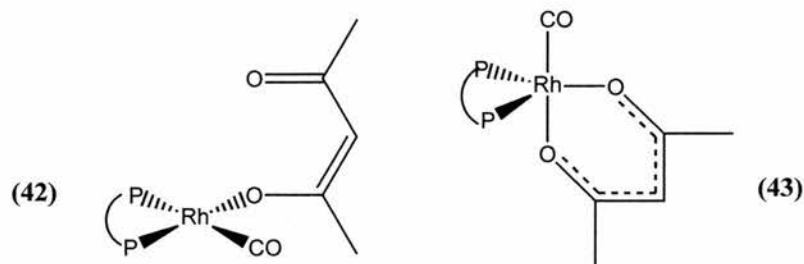
All the bond lengths are clearly in the range expected, and no further comment on them is therefore necessary.

At first, characterisation of the species present under an inert atmosphere was difficult because of conflicting evidence from the IR and  $^{13}\text{C}$  NMR.

The *in situ* FT IR spectrum of the rhodium DIOP (ratio = 1:1.5) complex species in solution under nitrogen or argon can be seen in IR 2.1. It shows a single absorption in the  $\nu_{\text{CO}}$  region ( $2100\text{-}1800 \text{ cm}^{-1}$ ).<sup>47</sup> This fits for a terminally bound rhodium carbonyl group, it was theorised that the complex species at  $\sim 39 \text{ ppm}$  could be  $[\text{Rh}(\text{DIOP})(\text{acac})(\text{CO})]$  were the DIOP chelate has displaced one acac carbonyl and one CO moiety see species **42** in Figure 2.11, or a five co-ordinate trigonal bipyramidal complex where both the acac and DIOP are chelated and one CO moiety is displaced and one is retained, see species **43** in Figure 2.11, although we now know this is not the case. If the species was **42** you should also observe a second  $\nu_{\text{CO}}$  band at a lower wavenumber from the acac carbonyl, it is noted that this is not the case.

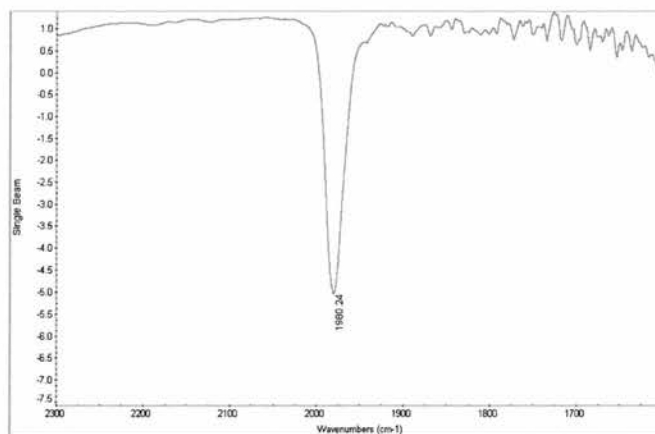
Figure 2.11

*Possible complex species present under an inert atmosphere.*



## IR 2.1

*The carbonyl region of the Infra-Red spectrum of the inert complex species.*



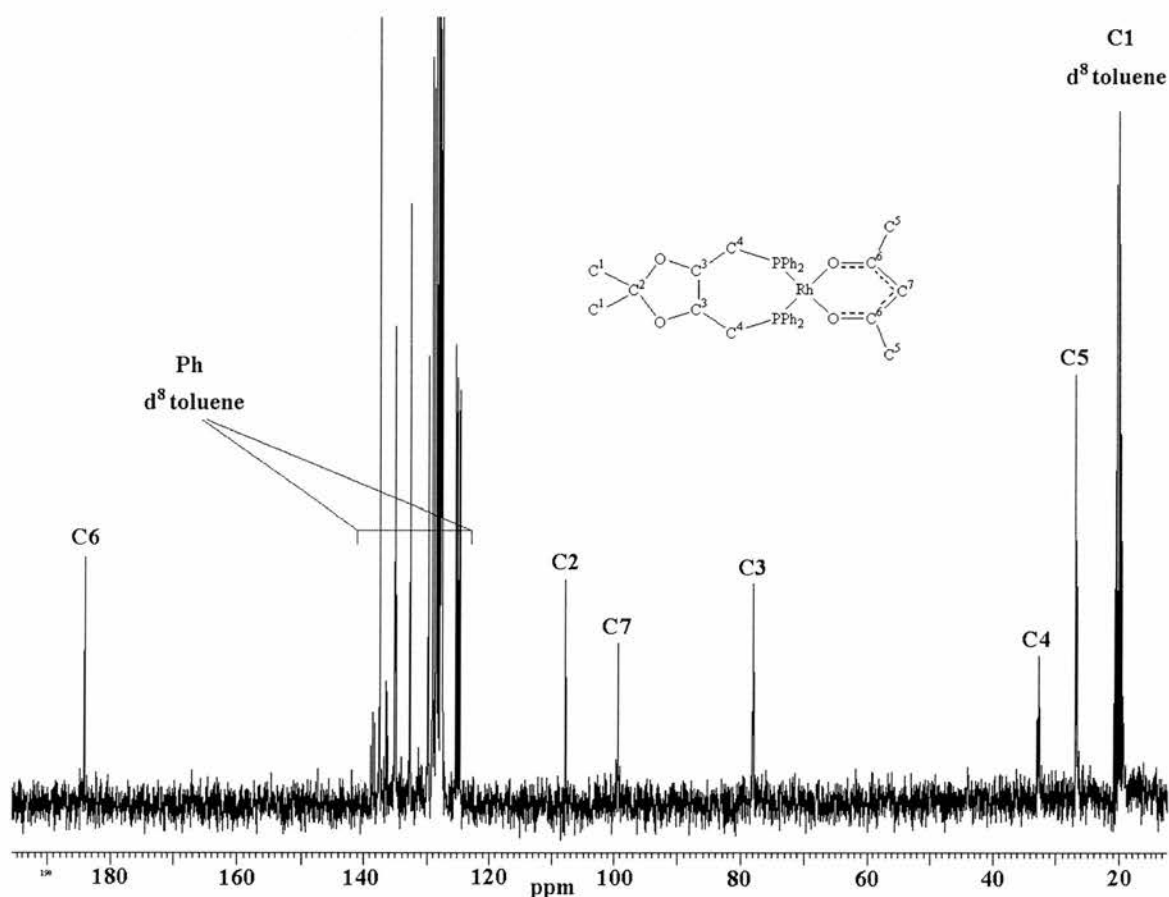
The  $^{13}\text{C}$  NMR spectrum (NMR 2.6), shows resonances at 184.14 ppm ( $\text{CH}_3\text{COCH}_2^-$ , s), 137.35-127.41 ppm ( $-\text{PPh}_2$ , m), 108.00 ppm ( $((\text{CH}_3)_2\text{C}(\text{O})_2$ , s), 99.38 ppm ( $-\text{COCH}_2\text{CO}-$ , s), 78.00 ppm ( $-\text{OCH}-$ , t), 32.91 ppm ( $-\text{CHCH}_2\text{P}-$ , t), 26.90 ppm ( $\text{CH}_3\text{C}-$ , s), 26.701 ( $-\text{COCH}_3$ , s) ppm. The spectrum also displays resonances from  $d^8$ -toluene at 137.85 ppm (s), 129.23 ppm (t), 128.32 ppm (t), 125 ppm (t), 20.40 ppm (hept). The spectrum does not show carbon resonances in the carbonyl region  $\sim 200$  ppm. This supports the structure observed though x-ray crystallography, but it does not explain why we see an adsorption at  $1980\text{ cm}^{-1}$  in the IR spectrum.

On addition of the diphosphine to  $[\text{Rh}(\text{acac})(\text{CO})_2]$  we see the liberation of CO, and the main complex formed is species **41**. Later, we will see that this is not instantaneous, and that there are intermediates in the formation of species **41**. It is suggested that such intermediates have a terminally bound CO moiety such as species **42** or **43**. And that

small amounts of such species are present in a solution of species **41**, and that the CO of such species gives rise to a very strong  $\nu_{\text{CO}}$  stretching vibration in the IR spectrum. The concentration is small, however, so the carbonyl resonance is not observed in the  $^{13}\text{C}$  NMR spectrum. The CO is quite strongly bound as it is still observed in the IR spectrum of the complex after the solution has been removed under vacuum and the complex re-dissolved.

## NMR 2.6

$^{13}\text{C}$  NMR spectrum of the inert complex species.



The four sets of double doublets in the rhodium-DIOP 1:1.5 ratio spectrum are evidence that the formation of the main complex species at  $\sim 39$  ppm is not instantaneous. It is proposed that the species could either be rival complex species, or intermediates in the formation of the complex species at  $\sim 39$  ppm. The patterns are interesting as it shows the complex must contain inequivalent phosphorus atoms. They could be intermediates in the formation of species **41**, with structures like that of species **42** or **43** in Figure 2.11.

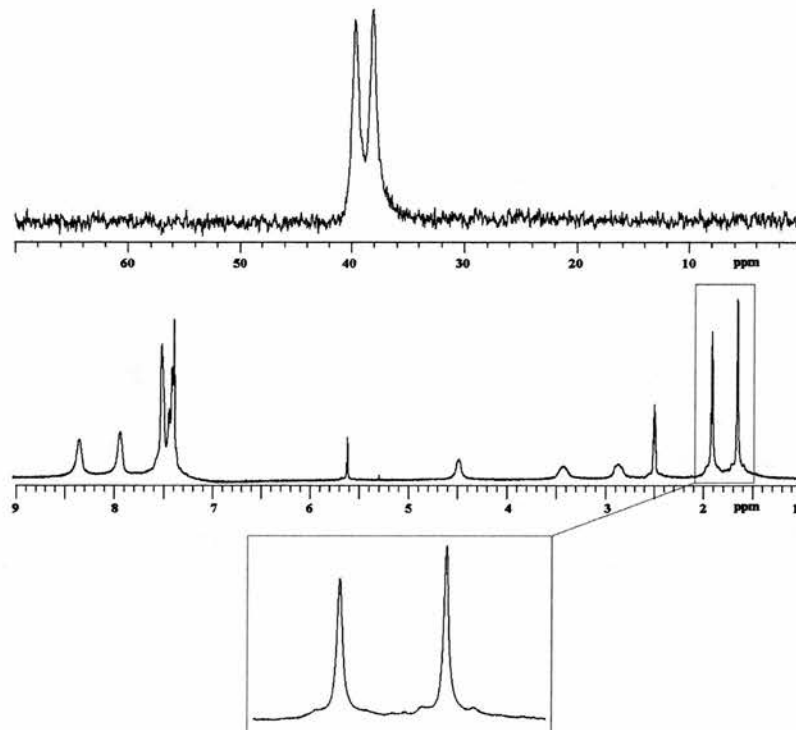
The low temperature  $^{31}\text{P}\{^1\text{H}\}$ NMR and  $^1\text{H}$  NMR spectrum of  $[\text{Rh}(\text{DIOP})(\text{acac})]$  can be seen in NMR 2.8 and can be compared to the spectrum at 25 °C in NMR 2.7. The spectra were taken to distinguish between structures **41** and **42** before the structure was identified by X-ray crystallography. The methyl groups of the acac ligand will be equivalent in species **41** but inequivalent in species **42**. At room temperature the methyls are equivalent but this could be due to fluxionality of the acac ligand.

On cooling the complex from 25 °C to -25 °C the methyl groups on the acac ligand do become inequivalent, however, so do the methyl groups of DIOP, see the expansion of the methyl resonances in NMR 2.8. However, it is known from the X-ray crystal structure that the complex species present is species **41** which has equivalent methyl acac groups. It is proposed that as the species is cooled the fluxionality of the complex becomes slower and more like the solid state. From the X-ray structure of species **41** in Figure 2.9 we see that the methyl groups of the DIOP ligand are indeed inequivalent in the solid state. Also because DIOP is a chiral ligand the orientation of the phenyl rings on the phosphorus with respect to the methyl groups of the acac ligand differ for each of the phosphorus atoms. The difference in the  $^1\text{H}$  chemical shifts of the hydrogens on the two methyl groups of the acac ligand can therefore be ascribed to the fact that hydrogens of one are orientated correctly to have  $\pi$ -H interactions[Sugimoto, 1995 #281] with the adjacent phenyl groups on one of the phosphorus atoms. The hydrogens of the other are not so orientated to have  $\pi$ -H interactions with the adjacent phenyl groups on the other phosphorus atom, see Figure 2.12.

We have to be careful however, as DIOP is a C2 chiral ligand, as is acac. Thus in solution there is no fundamental reason that the methyl groups are inequivalent.

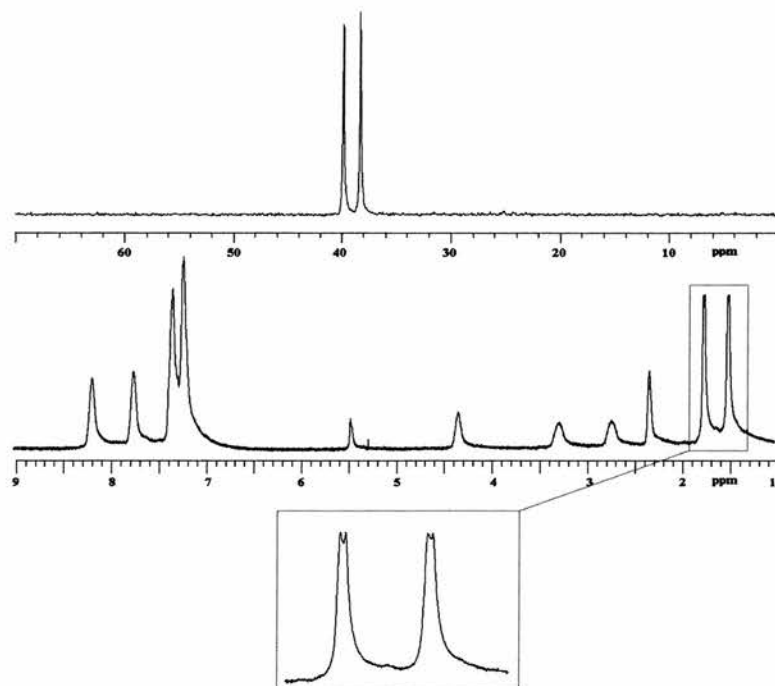
## NMR 2.7

$^{31}\text{P}\{^1\text{H}\}$  NMR and  $^1\text{H}$  NMR spectrum of  $[\text{Rh}(\text{DIOP})(\text{acac})]$  at  $25\text{ }^\circ\text{C}$ .



## NMR 2.8

$^{31}\text{P}\{^1\text{H}\}$  NMR and  $^1\text{H}$  NMR spectrum of  $[\text{Rh}(\text{DIOP})(\text{acac})]$  at  $-25\text{ }^\circ\text{C}$ .



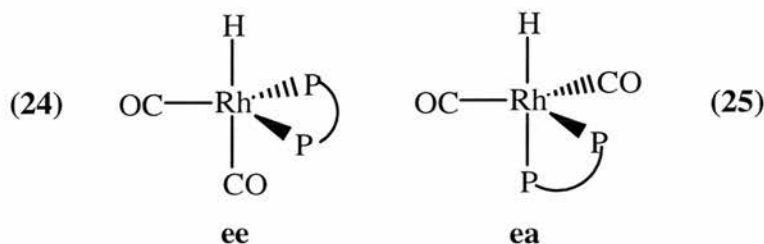


### 2.3.2 Rhodium DIOP Species Under Synthesis Gas.

Solutions prepared as in section 2.2.1 were reacted with synthesis gas, a mixture of carbon monoxide and hydrogen gas in a ratio of 1:1. We anticipated that the rhodium hydride complex species **24** and **25** in Figure 2.13 might be formed in this way. The complex species **24** and **25** are the equatorial-equatorial (**ee**) and equatorial-axial (**ea**) geometric isomers of  $[\text{RhH}(\text{CO})_2(\text{DIOP})]$ .

**Figure 2.13**

*The ee and ea geometric isomers of  $[\text{RhH}(\text{CO})_2(\text{DIOP})]$ .*



As in the case with the products of the reaction under inert gas,  $^{31}\text{P}\{^1\text{H}\}$  NMR spectra of the complex after reaction with synthesis gas raised as many questions as they answered. Aspects of the  $^{31}\text{P}\{^1\text{H}\}$  NMR spectrum of all three solutions are common, and can be seen in NMR 2.9. The data is also collected in Table 2.3.

#### NMR 2.9

*$^{31}\text{P}\{^1\text{H}\}$  NMR spectrum of  $\text{Rh}(\text{CO})_2(\text{acac})/\text{DIOP}$  1:1 under 1 bar synthesis gas at 25 °C for 3 hrs.*

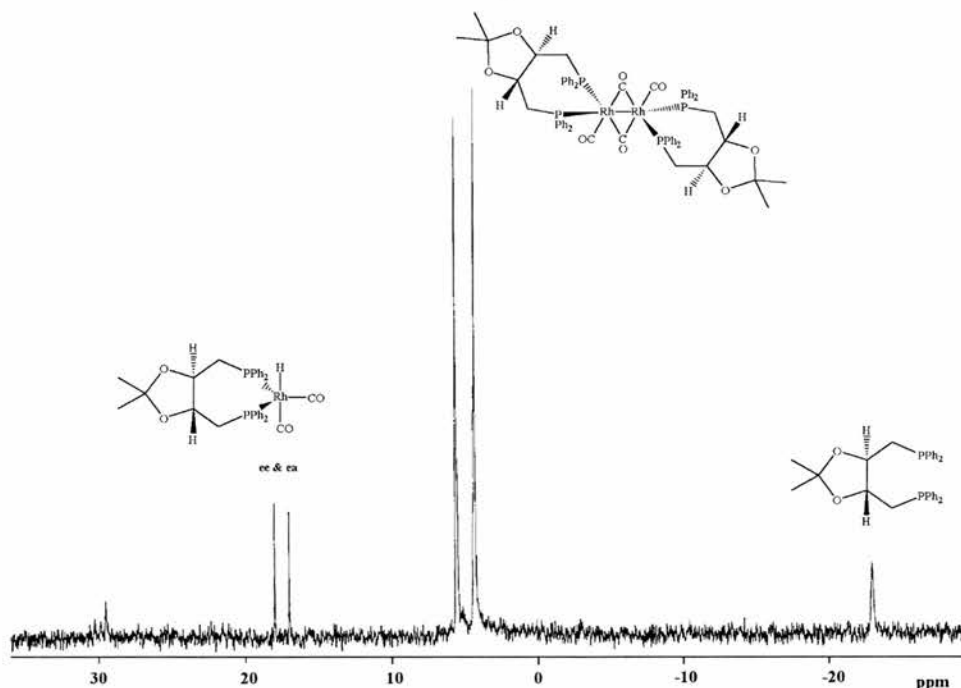


**Table 2.3**

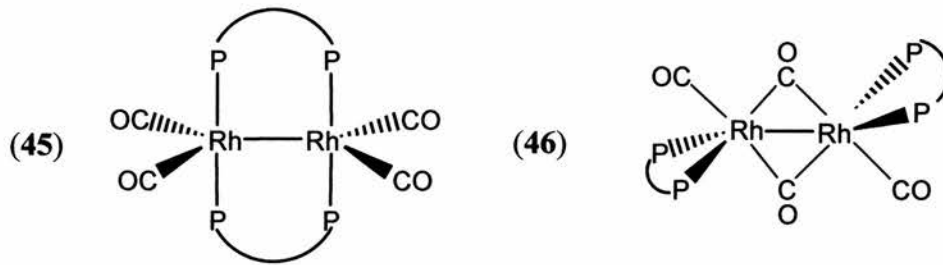
$^{31}\text{P} \{^1\text{H}\} \delta / \text{ppm}$	$J_{\text{Rh-P}} / \text{Hz}$
17.5 (d)	120
5 (d <sup>a</sup> )	160
-23 (s)	----

<sup>a</sup> Second order pattern.

It is observed that there is a signal due to excess DIOP at -23 ppm, a doublet of high intensity at 5.3 ppm and a doublet of low intensity at 17 ppm. The expansion of the signal at 5.3 ppm shows that it exhibits a complex second order pattern consistent with a AA'A"A'XX' spin system<sup>48, 49</sup> (see the expanded  $^{31}\text{P}\{^1\text{H}\}$  NMR spectrum in NMR 2.10). This is consistent with the complex being a dimer a Rh-Rh bond and two diphosphine ligands. The existence of only one doublet indicates that the four phosphorous atoms are chemically equivalent on the NMR time scale. It was theorised that the diphosphines could be bridging the rhodium atoms, as in structure **45** in Figure 2.14, or terminal to separate rhodium atoms, as in structure **46** in Figure 2.14. Studies of such dimeric species, which include X-ray crystallography of  $[\text{Rh}_2(\text{CO})_4(\text{dppb})]$  (dppb = 1,2-bis(diphenylphosphino)butane), the spectroscopic parameters of  $[\text{Rh}_2(\text{CO})_4(\text{DIOP})]$  (which has previously been synthesised from  $[\text{RhH}(\text{DIOP})_2]$  and CO gas),<sup>48</sup> and  $[\text{Rh}_2(\text{CO})_4(\text{BDPP})_2]$ <sup>49</sup> (BDPP = (2S,4S)-bis(diphenylphosphine)pentane), see Table 2.4, suggest **46** is the most probable structure. This is consistent with the IR spectrum of the solution, see IR 2.2 It shows strong absorptions at  $1985 \text{ cm}^{-1}$  in the terminal carbonyl region, and  $1764 \text{ cm}^{-1}$ ,  $1744 \text{ cm}^{-1}$ ,  $1716 \text{ cm}^{-1}$  in the bridging carbonyl region. The bands at  $1764 \text{ cm}^{-1}$  and  $1744 \text{ cm}^{-1}$  have been shown to be from 1,4-pentaendione, released during the synthesis of the complex. A 0.1 M solution of 1,4-pentaendione in toluene gives  $\nu_{\text{CO}}$  bands at  $1759 \text{ cm}^{-1}$  and  $1740 \text{ cm}^{-1}$  in the infrared spectrum.

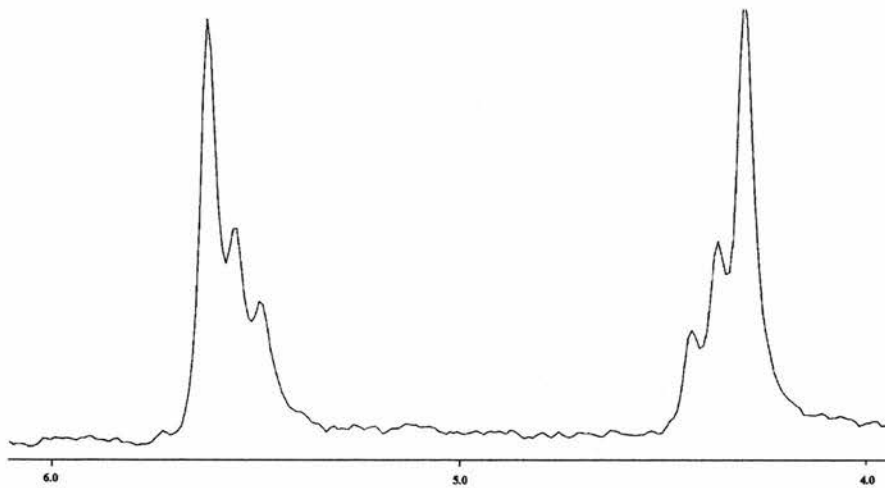
Figure 2.14

Possible rhodium dimers with  $AA'XX'X''X'''$



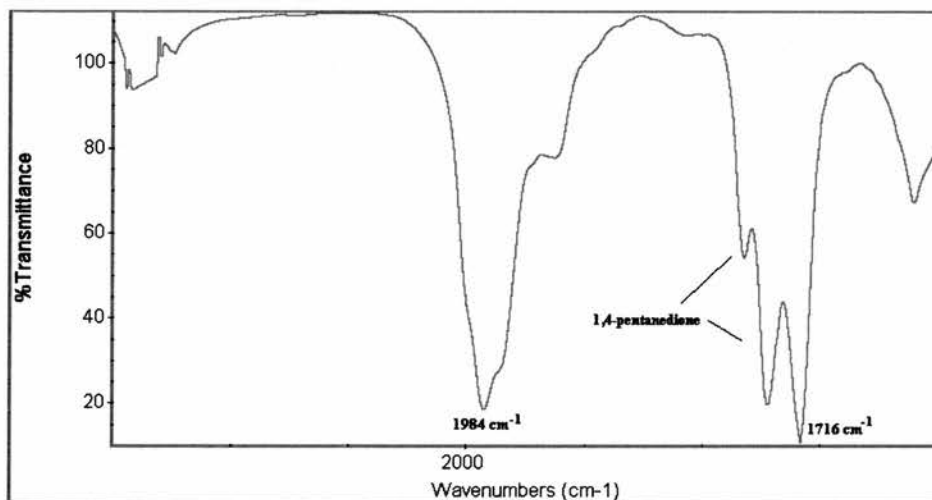
NMR 2.10

Expansion of the observed  $AA'XX'X''X'''$  spin system.



IR 2.2

IR spectrum of the dimer  $[Rh_2(CO)_4(DIOP)_2]$ .



The  $^{13}\text{C}$  NMR spectrum of the dimeric species **46** shows a single broad resonance in the carbonyl region at 222 ppm. This tells us that the four CO ligands are fluxional, exchanging between the terminal and bridging sites on the rhodiums on the NMR time scale, (see NMR 2.11).

Dimeric species similar to **46** under 20 bar CO / H<sub>2</sub> 1:1 have been reported to be in equilibrium with their mononuclear hydrides, such as **24** and **25**, the proposed pre-catalyst. Weak absorptions in the terminal  $\nu_{\text{CO}}$  region of the infrared spectrum and the doublet resonance at 17.5 ppm in the  $^{31}\text{P}\{^1\text{H}\}$  NMR spectra, see (NMR 2.9) have been assigned to these species. The  $^1\text{H}$  NMR in the hydride region showed no clear evidence of these complex species; the rhodium hydride gives a characteristic resonance at approximately -10 ppm with a triplet of doublets. Further studies at higher pressures were required, as is discussed later. It is noted that there is only one resonance in both the  $^{31}\text{P}\{^1\text{H}\}$  and  $^1\text{H}$  NMR spectra for the complex species **24** and **25**. This is because they undergo fluxional interchange with each other at a rate faster than the NMR time scale. Thus, a single resonance is observed with an averaged chemical shift and averaged coupling constants for the two isomers, as discussed in Chapter One and later in section 2.3.1.

## NMR 2.11

*$^{13}\text{C}$  NMR spectra in the CO region of the dimeric rhodium species.*

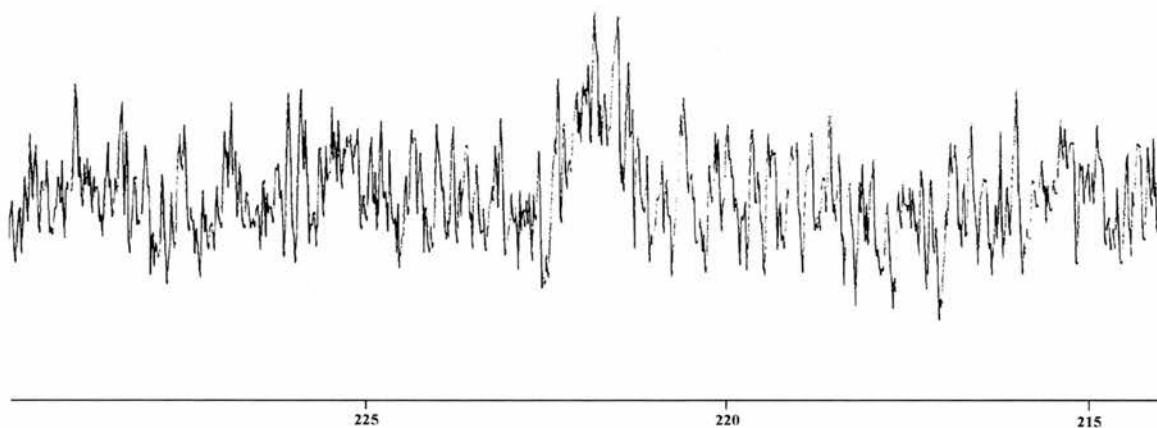


**Table 2.4***Spectroscopic data for  $[Rh_2(CO)_4(P-P)_2]$  complexes from the literature.*

	$\delta (^{31}P)$ / ppm	$^1J_{RH-P}$ / Hz	$^2J_{P,P}$ / Hz	$^3J_{P,P''}$ / Hz	$^2J_{P',Rh}$ / Hz	$\nu(CO)$ / $cm^{-1}$
<b>DIOP*</b>	3.7	160	—	—	—	1960 1740
<b>BDPP</b>	24.4	145.7	45.7	5	8	1965 1744 1718

P-P = diphosphine ligands.

\* Note the slightly different values for the DIOP complex than those observed, this is assumed to be due to the different spectrometers used.

### 2.3.2.1 Rhodium to DIOP ratio of 1:1.

NMR 2.12 shows the observed  $^{31}P\{^1H\}$  NMR spectrum of the complex species present in a solution of rhodium and DIOP, ratio 1:1 after synthesis gas has been bubbled through for 3 minutes. Again, the second order pattern at ~5 ppm and the doublet at ~17.5 ppm are observed. There is also a complex pattern of multiplets up-field of these, which are discussed later in section 2.2.2.2, but, it is important to note at this stage that they are intermediates in the formation of the dimeric species **46**  $[Rh_2(CO)_4(DIOP)_2]$ . Two double doublets at ~22 and ~32 ppm are also observed with values similar to those seen in the formation of species **40** (see NMR 2.3), which was speculated to be a unidentate acac complex of rhodium (cf **42** in Figure 2.11). It is possible, therefore, that this is also an intermediate in the formation of the dimeric species **46**.

It is noted from the presence of these complexes that the formation of the dimer and hydride complex species at 25 °C and under 1 atm synthesis gas is a relatively slow process. It is also noted that with the removal of synthesis gas, the equilibrium between the complex species present at that time is retained.

NMR 2.13 shows the observed spectrum of the same reaction mixture after 3.5 hrs of bubbling synthesis gas. Common features in the spectrum of the reaction mixture include the second order pattern characterised as species **46** and the doublet

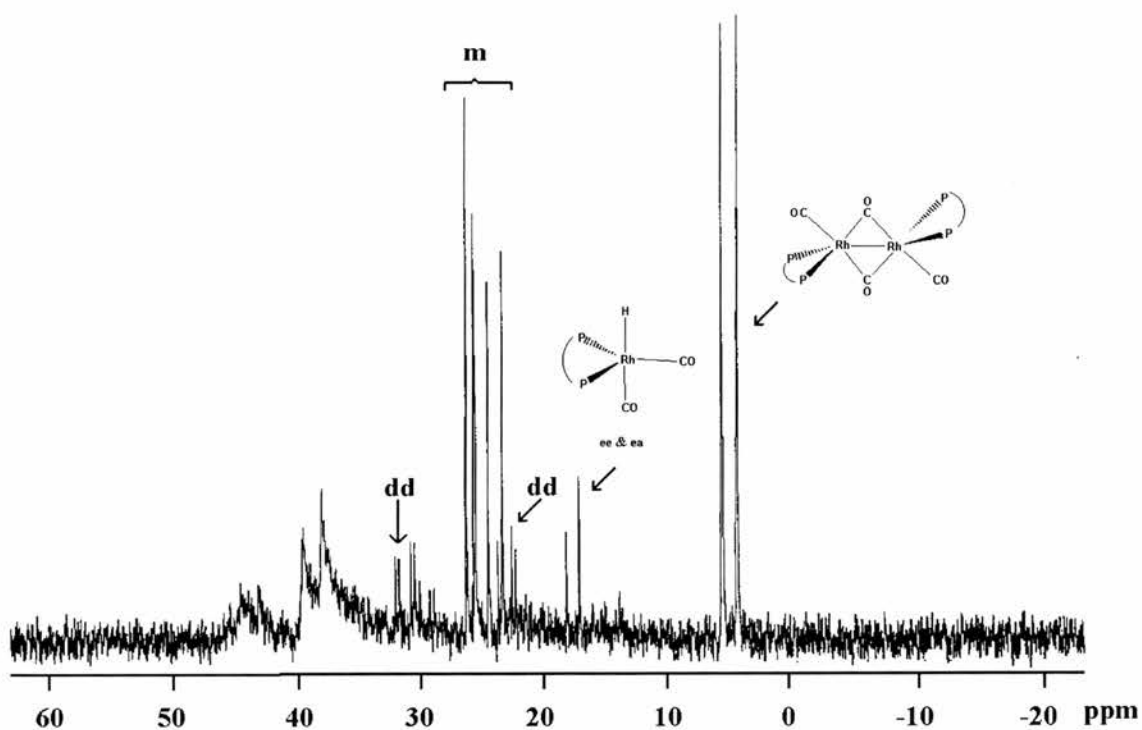
hypothesised to be the mononuclear complex species **24** and **25**. The spectrum also shows two unknown doublets at approximately 9 and 20 ppm, and three singlets in the ~26 ppm region.

The three singlets represent 3 types of oxidised DIOP phosphine, oxygen being introduced at some stage during the preparation of the sample. The one at 26.18 ppm represents the dioxide [DIOP(O)<sub>2</sub>] A in figure 2.4, and the other two singlet resonances at 25.61 ppm and 25.13 ppm represent the oxidised phosphorous of the monoxide [DIOP(O)] which are complexed to rhodium though the non-oxidised phosphorous atom, C in figure 2.4. Neither is the non-complexed monoxide [DIOP(O)] as this would have a corresponding resonance in the DIOP region at approximately -23 ppm.

The doublet at 8.48 ppm ( $^1J_{P-Rh} = 153$  Hz) is speculated to be a rhodium complex of the form [HRh(CO)<sub>3</sub>(DIOP)], where only one DIOP phosphorus is bonded to the metal. However, as there is no free DIOP phosphorus signal it is suggested that the other DIOP phosphorus is either oxidised or bridging like in Figure 2.16.

## NMR 2.12

*<sup>31</sup>P{<sup>1</sup>H} NMR spectrum of Rh(CO)<sub>2</sub>(acac) / DIOP 1:1 under 1 bar synthesis gas at 25 °C for 3 minutes.*



## NMR 2.13

$^{31}\text{P}\{^1\text{H}\}$  NMR Spectrum of  $\text{Rh}(\text{CO})_2(\text{acac}) / \text{DIOP}$  1:1 under 1 bar synthesis gas at 25 °C for 3.5 hours.

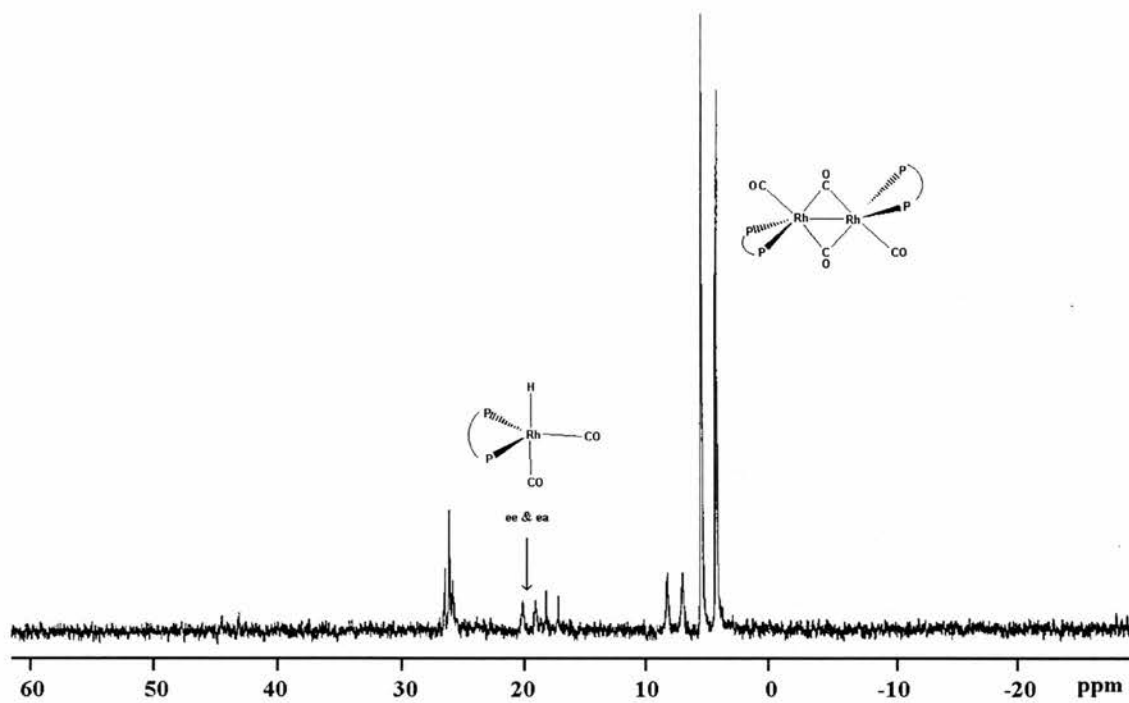


Figure 2.15

*DIOP and DIOP oxide compounds and complexes.*

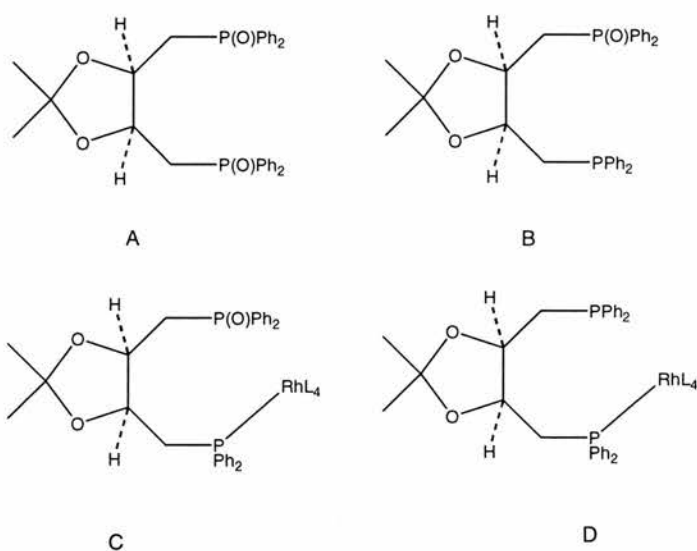
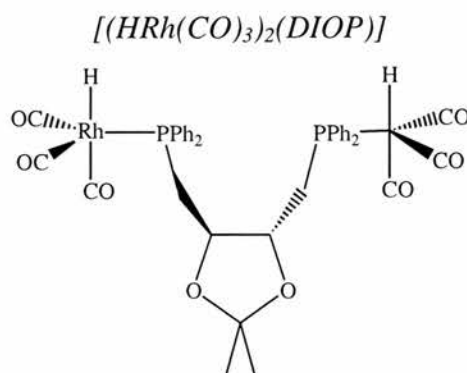


Figure 2.16

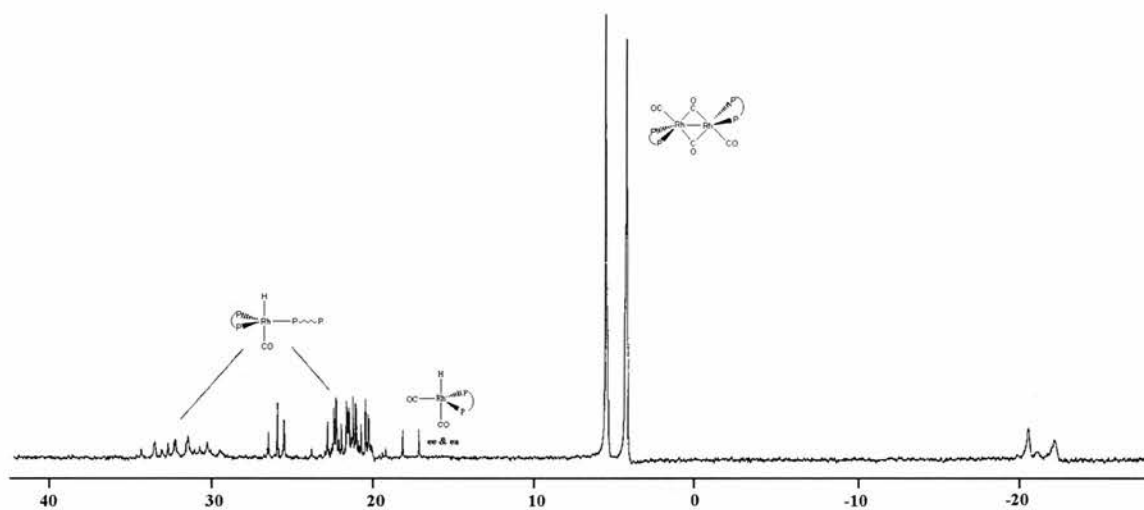


### 2.3.2.2 Rhodium to DIOP ratio of 1:1.5 & 1:2.

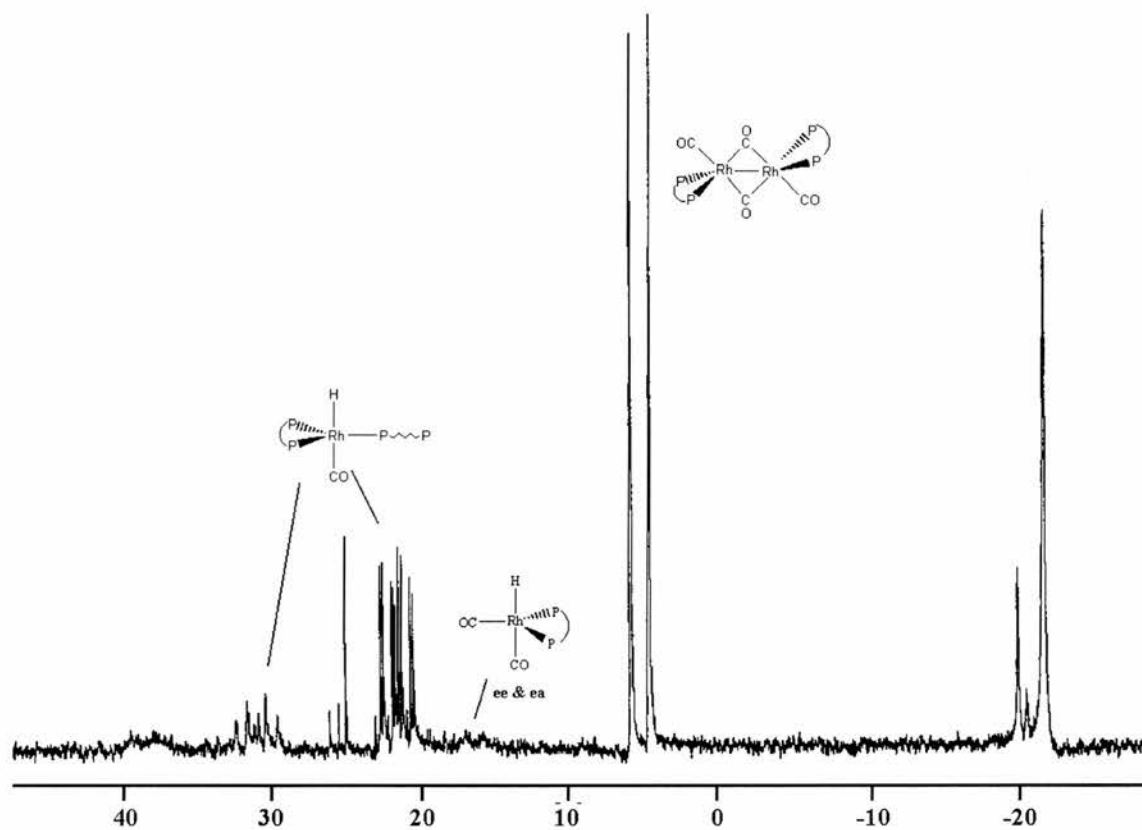
NMR 2.14 shows the  $^{31}\text{P}\{^1\text{H}\}$  NMR spectrum of the complex species present in a solution of rhodium / DIOP, ratio 1:1.5, and NMR 2.15 the  $^{31}\text{P}\{^1\text{H}\}$  NMR spectrum of the complex species present in a solution of rhodium / DIOP, ratio 1:2. Each of these have had synthesis gas bubbled through for 3 minutes. They both display the multiplets at ~21 ppm and ~32 ppm briefly mentioned earlier, which are expanded in NMR 2.15. There are also three singlet resonances at ~26 ppm and ~ -23 ppm in both spectra. The three singlet resonances at ~26 ppm represent 3 types of oxidised DIOP phosphine. One at 26.0 ppm represents the dioxide  $[\text{DIOP}(\text{O})_2]$  A in Figure 2.15, one at 25.5 ppm represents oxidised phosphorous of the monoxide  $[\text{DIOP}(\text{O})]$  B in Figure 2.15 and the singlet at 25.0 ppm represents the oxidised phosphorous of the monoxide B, complexed to rhodium though only the non-oxidised phosphorous atom, C in Figure 2.15. The three signals at ~ -23 ppm are in the DIOP region. One is DIOP, at -23.0 ppm, one at -21.0 ppm is the non-oxidised phosphorus atom from the mono-oxidised DIOP,  $[\text{DIOP}(\text{O})]$ , B in Figure 2.15. The other is the signal from a non-complexed phosphorus atom of DIOP where the other phosphorous atom is complexed to rhodium, D in Figure 2.15. The two sets of multiplets are a 16-line multiplet that originates from a four spin half system,<sup>49, 50</sup> similar to those observed for species such as **47** and **48** which have a  $\text{AB}_2\text{X}$  spin system see Figure 2.17. There is interest in such complexes as it is speculated by some that such triphosphine complexes may be important intermediates in the catalytic cycle.<sup>56</sup> This is cited as a possible reason why the diphosphine ratio is often required to be 1:1.5 or greater. Our work may also suggest the possibility that this species acts as a catalyst for phosphine oxidation, as discussed later in chapter 3.

**NMR 2.14**

$^{31}\text{P}\{^1\text{H}\}$  NMR spectrum of  $\text{Rh}(\text{CO})_2(\text{acac}) / \text{DIOP}$  1:1.5 under 1 bar synthesis gas at 25 °C for 3 minutes.

**NMR 2.15**

$^{31}\text{P}\{^1\text{H}\}$  NMR spectrum of  $\text{Rh}(\text{CO})_2(\text{acac}) / \text{DIOP}$  1:2 under 1 bar synthesis gas at 25 °C for 3 minutes.



## NMR 2.16

Expansion of NMR 2.15.

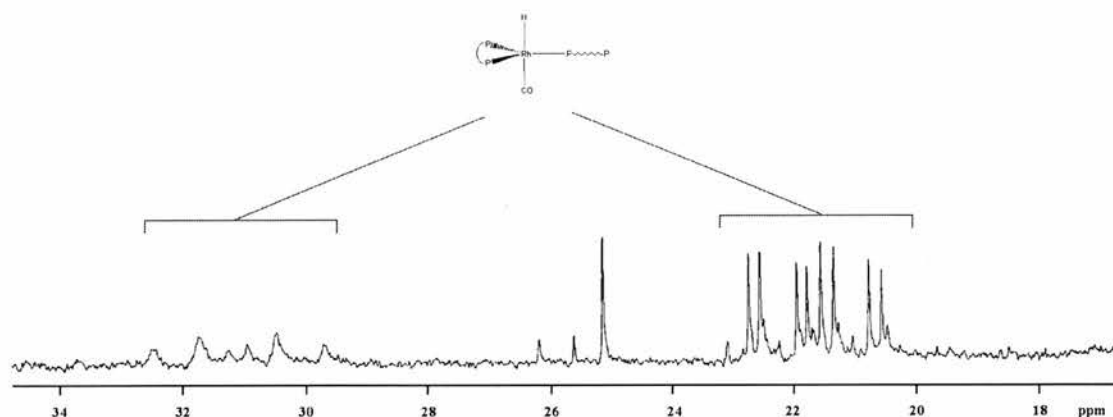
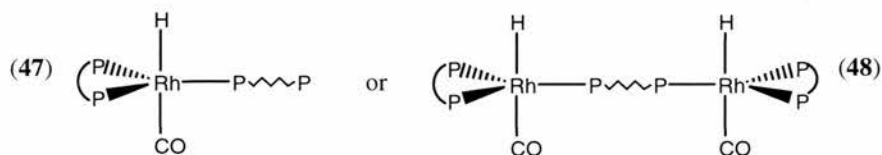


Figure 2.17

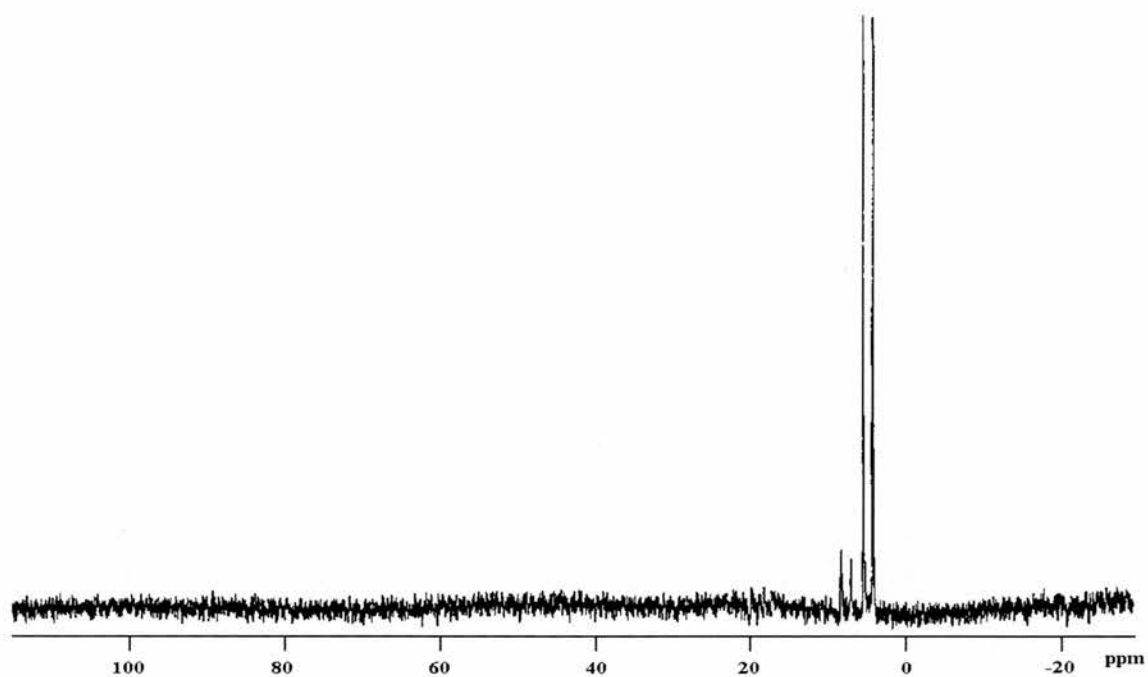
Rhodium triphosphine complexes exhibiting  $AB_2X$  spin systems.

Synthesis gas was bubbled through the solutions for another 3.5 hrs. The  $^{31}\text{P}\{^1\text{H}\}$  NMR spectrum of the complex species present in the solution of rhodium DIOP ratio 1:1.5 shows almost complete conversion to the dimeric species **46** at  $\sim 5$  ppm, characterised in section 2.3. Two sets of doublets, one at  $\sim 18$  ppm previously hypothesised to arise from the mononuclear complex species **24** or **25**, and one at  $\sim 8$  ppm from an unknown complex species are also observed (see NMR 18).

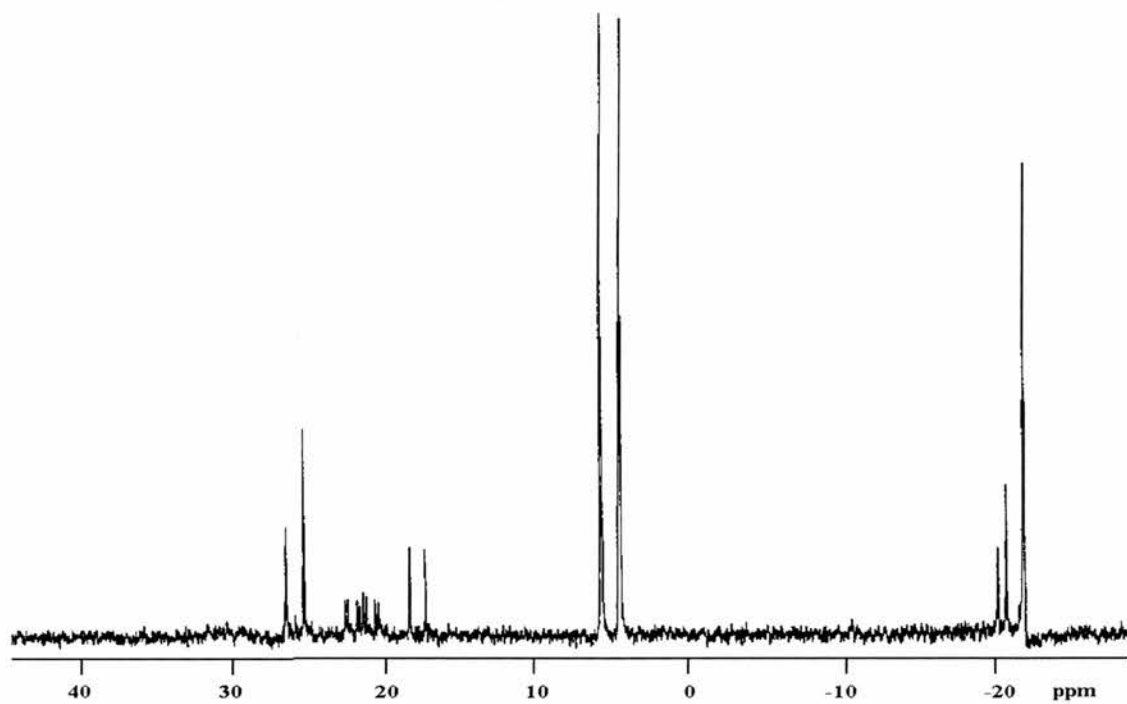
The  $^{31}\text{P}\{^1\text{H}\}$  NMR spectrum of the species present in the solution of rhodium DIOP ratio 1:2 shows the dimeric species **46** as the major component which is in equilibrium with the hydride complex species **24** and **25** at 18 ppm. It also still contains the triphosphine species **47** and **48** and unreacted DIOP ( $-22.4$  ppm, see NMR 2.18).

**NMR 2.17**

$^{31}\text{P}\{^1\text{H}\}$  NMR Spectra of  $\text{Rh}(\text{CO})_2(\text{acac}) / \text{DIOP}$  1:1.5 under 1 bar synthesis gas at 25 °C for 3.5 hours

**NMR 2.18**

$^{31}\text{P}\{^1\text{H}\}$  NMR Spectra of  $\text{Rh}(\text{CO})_2(\text{acac}) / \text{DIOP}$  1:2 under 1 bar synthesis gas at 25 °C for 3.5 hours.



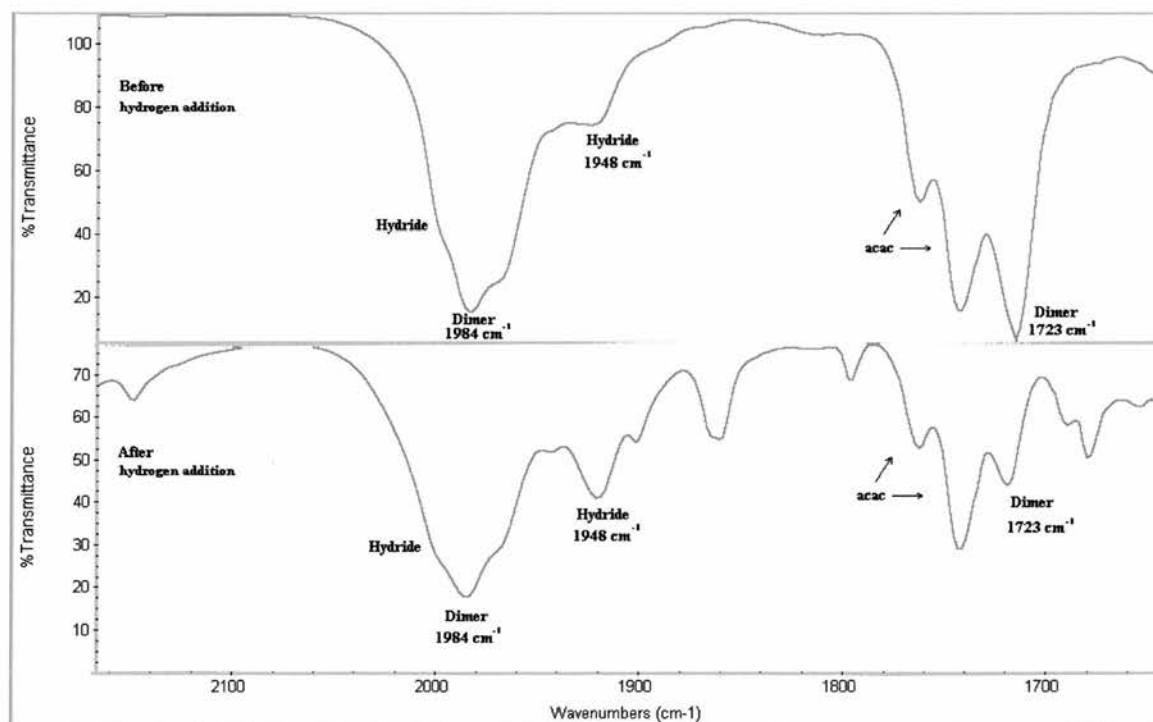
### 2.3.3 Addition of Hydrogen Gas.

It was mentioned in Chapter One that the CO partial pressure of the reaction is of importance to the formation of the active rhodium catalyst. It may be possible that the partial pressure of CO is too great for the formation of the mononuclear complex species **24** or **25** rather than the dimeric complex species, **46**. Hydrogen gas was bubbled through a solution of rhodium / DIOP, ratio 1:1 which had previously been reacted with synthesis gas as in section 2.2.2. The complex species present were studied by FT IR and  $^{31}\text{P}\{^1\text{H}\}$  NMR.

IR 2.3 shows the infrared spectra of the solution before and after hydrogen gas was bubbled through for one hour. They show distinct differences that may be due to the increase in concentration of the mononuclear hydride complex in solution.

#### IR 2.3

*Solution of rhodium DIOP ratio 1:1 before and after hydrogen gas was bubbled through.*



In the first IR spectrum, we see  $\nu_{\text{CO}}$  bands assigned to the dimeric complex **46**, at  $1984\text{ cm}^{-1}$  and  $1723\text{ cm}^{-1}$ , as well as a  $\nu_{\text{CO}}$  band at  $1948\text{ cm}^{-1}$  assigned to the hydride complex **24** and **25**. These are accompanied by several bands which appear as shoulders of the band at  $1984\text{ cm}^{-1}$ . The spectrum also contains two bands assigned to the acac ligand 1,4-pentanedione. In the second IR spectrum, we see an increase in the

intensity of the band at  $1948\text{ cm}^{-1}$  with respect to the band at  $1984\text{ cm}^{-1}$ . We also see a decrease in the intensity of the band at  $1723\text{ cm}^{-1}$  with respect to the acac bands. The  $^{31}\text{P}\{^1\text{H}\}$  NMR spectrum of the solution showed both the dimer and hydride species present but the change in concentration between the two was not quantifiable. It is therefore thought that by reacting a mixture of CO and  $\text{H}_2$  with a lower CO/  $\text{H}_2$  ratio or greater hydrogen partial pressure it may be possible to make the hydride complex at low temperatures

## 2.4 Rhodium DIOP Species Present Under High Pressures.

So far the studies that have been discussed are of the rhodium-DIOP complex species present in solution under argon, carbon monoxide and hydrogen atmospheres of 1 atm at  $25\text{ }^\circ\text{C}$ . The hydroformylation reaction, as described in Chapter One is carried out at higher pressures and temperatures than this. This system is typically carried out under 8 bar synthesis gas at  $60\text{-}70\text{ }^\circ\text{C}$ . It is, therefore, necessary to study the system under such conditions. To do this, high pressure NMR, high pressure IR and kinetic measurement techniques were employed, as described Chapter 6.

### 2.4.1 Rhodium DIOP Ratio of 1:1.5.

Initial high pressure studies of the complex species were carried out under the conditions, rhodium DIOP ratio 1:1.5, CO /  $\text{H}_2$  ratio 1:1, total pressure 20 bar, and at temperatures of  $25\text{-}80\text{ }^\circ\text{C}$ . The high pressure infrared spectra of the complex species under these conditions can be seen in IR 2.4-IR 2.5 in section 2.4.1.2, and the high pressure  $^{31}\text{P}\{^1\text{H}\}$  NMR spectra can be seen in NMR 2.19 to NMR 2.25 in section 2.4.1.1. The  $^{31}\text{P}\{^1\text{H}\}$  NMR spectroscopic data can also be seen in Table 2.5.

#### 2.4.1.1 High Pressure NMR Studies.

In NMR 2.19, the observed  $^{31}\text{P}\{^1\text{H}\}$  NMR spectrum of the complex species present at  $25\text{ }^\circ\text{C}$  can be seen. The same species are present here as under 1 bar CO/  $\text{H}_2$  1:1, with the rhodium dimer species, **46**, at 5 ppm being the major species and the proposed rhodium hydride species, **24** and **25**, at 18 ppm, the minor species. This was surprising

as the results from similar systems<sup>49</sup> suggest that these species are in equilibrium with each other and that, at high pressures, the hydride is the dominant species, there is also a broad resonance at 30 ppm which is unidentified. At 40 °C, we see an increase in the concentration of the hydride species and the emergence of a new species at 8 ppm, see NMR 2.20. This new species becomes more important later on and is discussed in section 2.3.2. On heating further to 60 °C and 80 °C we see this pattern continue with the concentration of the hydride and the unidentified species increasing in proportion with respect to the dimer. However, even at 80 °C, the operating temperature of the catalytic system, the dimer complex, **46**, is still a major species present, (NMR 2.21 & NMR 2.22), the unidentified resonance at 30 ppm is also present at higher temperatures. It is conceivable, however, that if an alkene were present, the hydride would react with it forming one of the species present in the catalytic cycle, thereby removing the hydride and shifting the equilibrium between the dimer and hydride towards the hydride, until there is neither left in solution.

NMR 2.23 shows the <sup>31</sup>P NMR spectrum which is partially hydrogen coupled in the hydride region of Rh(CO)<sub>2</sub>(acac) / DIOP 1:1.5 under 20 bar synthesis gas at 80 °C. It can be seen that the doublet of the proposed hydride splits into a double doublet as we would expect with phosphorous-hydrogen coupling of <sup>2</sup>J<sub>PH</sub> = 8 Hz (although with partially decoupled spectra you often do not get true coupling constants). NMR 2.24 shows the hydrogen NMR spectrum of the catalytic solution at 80 °C, with the expanded spectrum of the hydride region at -9.2 ppm. It show a triplet of doublet resonance with <sup>1</sup>J<sub>H-Rh</sub> = 8 Hz, and <sup>2</sup>J<sub>H-P</sub> = 35 Hz from the hydride hydrogen of the [HRh(CO)<sub>2</sub>(DIOP)] species.

**Table 2.5**

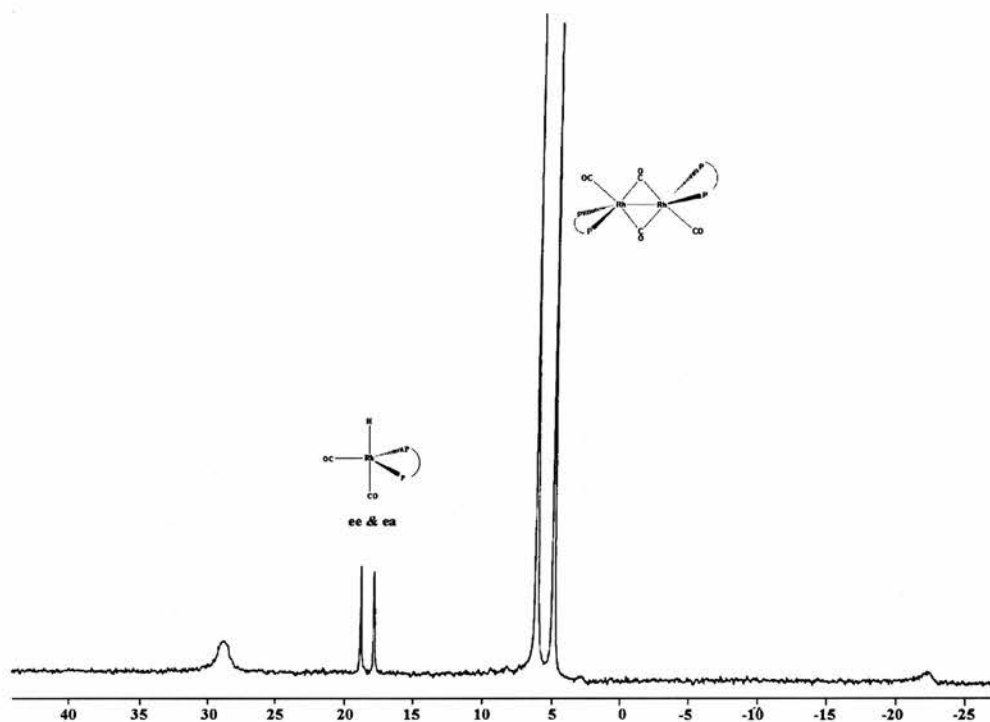
*High pressure <sup>31</sup>P{<sup>1</sup>H} NMR data for the complex species present at Rh(CO)<sub>2</sub>(acac) to DIOP ratio 1:1.5, total pressure 20 bar, CO to H<sub>2</sub> ratio 1:1 at 80 °C.*

$\delta$ (ppm)	$J_{\text{Rh-P}}$ (Hz)
17.76 (d)	120
8.38 (d)	150
5.40 (d <sup>a</sup> )	157

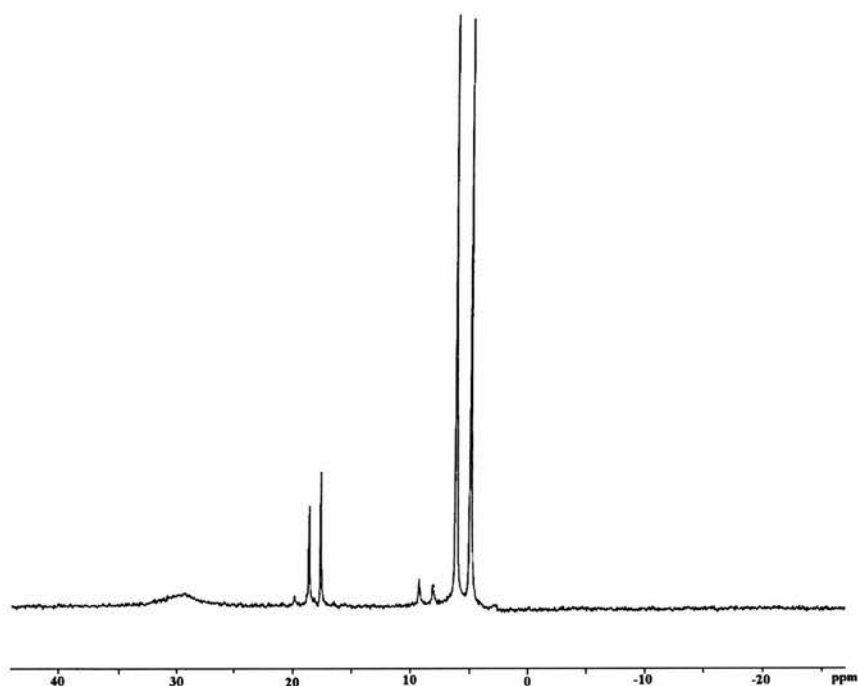
<sup>a</sup>Second order pattern.

**NMR 2.19**

$^{31}\text{P}\{^1\text{H}\}$  NMR spectrum of  $\text{Rh}(\text{CO})_2(\text{acac}) / \text{DIOP}$  1:1.5 under 20 bar synthesis gas at  $25^\circ\text{C}$ .

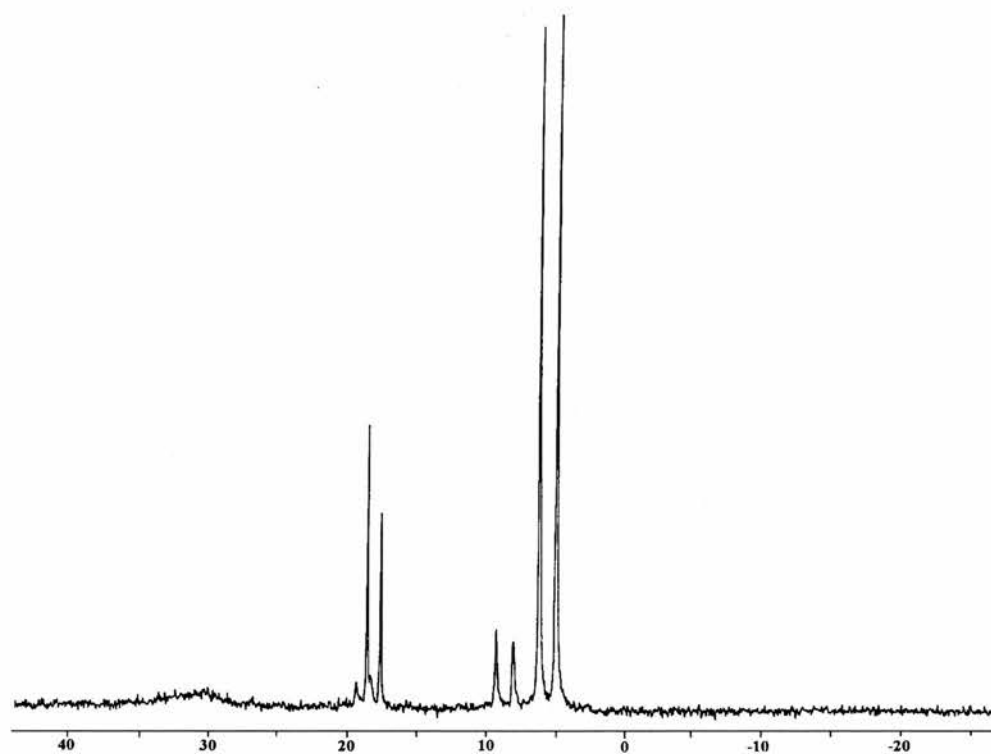
**NMR 2.20**

$^{31}\text{P}\{^1\text{H}\}$  NMR Spectra of  $\text{Rh}(\text{CO})_2(\text{acac}) / \text{DIOP}$  1:1.5 under 20 bar synthesis gas at  $40^\circ\text{C}$ .

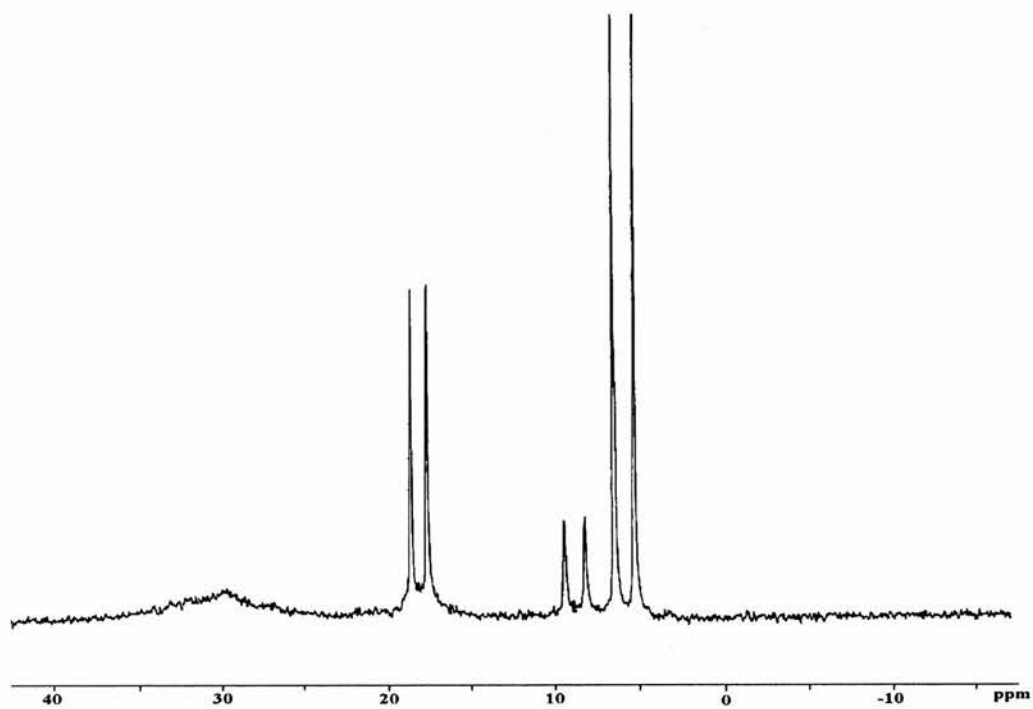


**NMR 2.21**

$^{31}\text{P}\{^1\text{H}\}$  NMR spectrum of  $\text{Rh}(\text{CO})_2(\text{acac}) / \text{DIOP}$  1:1.5 under 20 bar synthesis gas at  $60^\circ\text{C}$ .

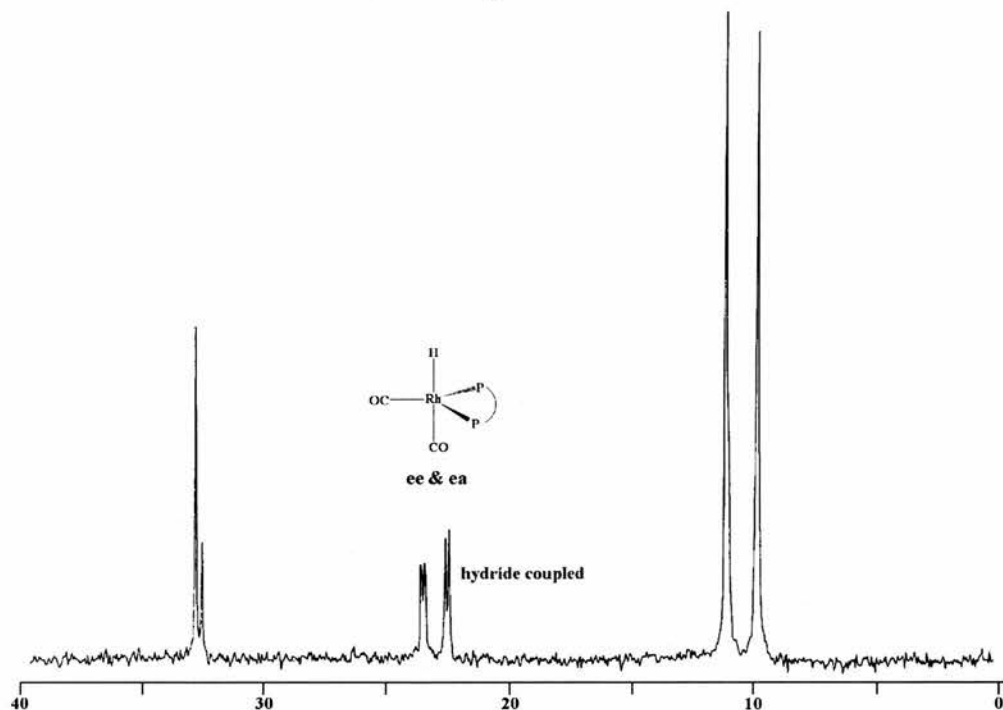
**NMR 2.22**

$^{31}\text{P}\{^1\text{H}\}$  NMR Spectrum of  $\text{Rh}(\text{CO})_2(\text{acac}) / \text{DIOP}$  1:1.5 under 20 bar synthesis gas at  $80^\circ\text{C}$ .

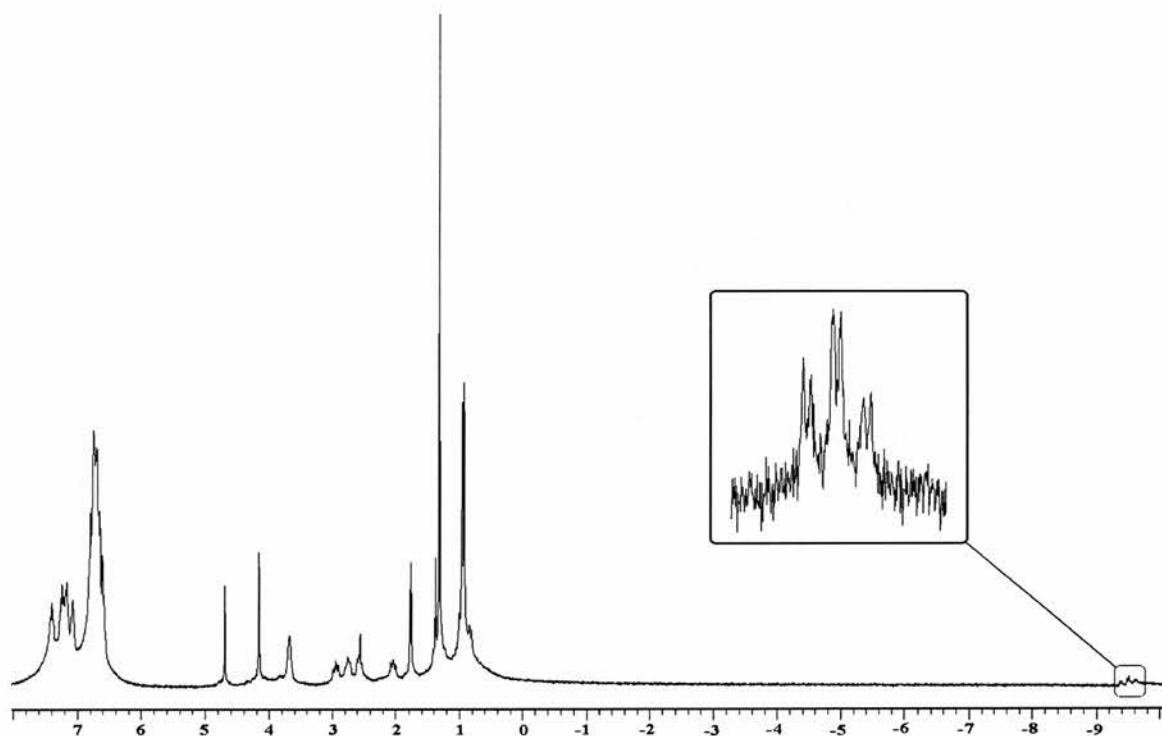


**NMR 2.23**

*Partially  $^1\text{H}$  coupled  $^{31}\text{P}$  NMR spectrum of  $\text{Rh}(\text{CO})_2(\text{acac}) / \text{DIOP}$  1:1.5 under 20 bar synthesis gas at  $80^\circ\text{C}$ .*

**NMR 2.24**

*$^1\text{H}$  NMR spectrum of  $\text{Rh}(\text{CO})_2(\text{acac}) / \text{DIOP}$  1:1.5 under 20 bar synthesis gas at  $80^\circ\text{C}$ .*



The  $^{31}\text{P}\{^1\text{H}\}$  NMR and the  $^1\text{H}$  NMR show one signal for the two geometric isomers **24** and **25** in solution. The reason we only see one signal in the  $^{31}\text{P}\{^1\text{H}\}$  NMR and  $^1\text{H}$  NMR spectra is because the interchange between the two geometric isomers<sup>51</sup> is faster than the NMR time scale, 1 to 10 seconds.<sup>47</sup> This results in the complex giving a single resonance in the  $^{31}\text{P}\{^1\text{H}\}$  and  $^1\text{H}$  NMR spectra with averaged chemical shifts and averaged coupling constants of the two isomers. It is, therefore, theorised that if the sample could be cooled down to a low enough temperature, the fluxional interchange would be slowed down sufficiently to observe the separate resonances, and, therefore, the separate coupling constants for the two geometric isomers. From this, it would be possible to work out the ee to ea ratio from the averaged coupling constants at higher temperatures, see section 1.3.4.

NMR 2.25 shows the  $^{31}\text{P}\{^1\text{H}\}$  NMR spectra of  $[\text{Rh}(\text{CO})_2(\text{acac})]$  at 25 °C, having been heated up to 70 °C, cooled down to -80 °C and heated back to 25 °C. The sample was heated prior to cooling to maximise the hydride dimer ratio. It can be seen that although we begin to see coalescence of the hydride signal we do not see separate resonances for the two geometric isomers. It has been stated by van Leeuwen and co-workers that the energy difference between the two geometric isomers is as low as 2 kcal mol<sup>-1</sup> such that even at very low temperature the interchange between them is faster than the NMR time scale.<sup>52</sup>

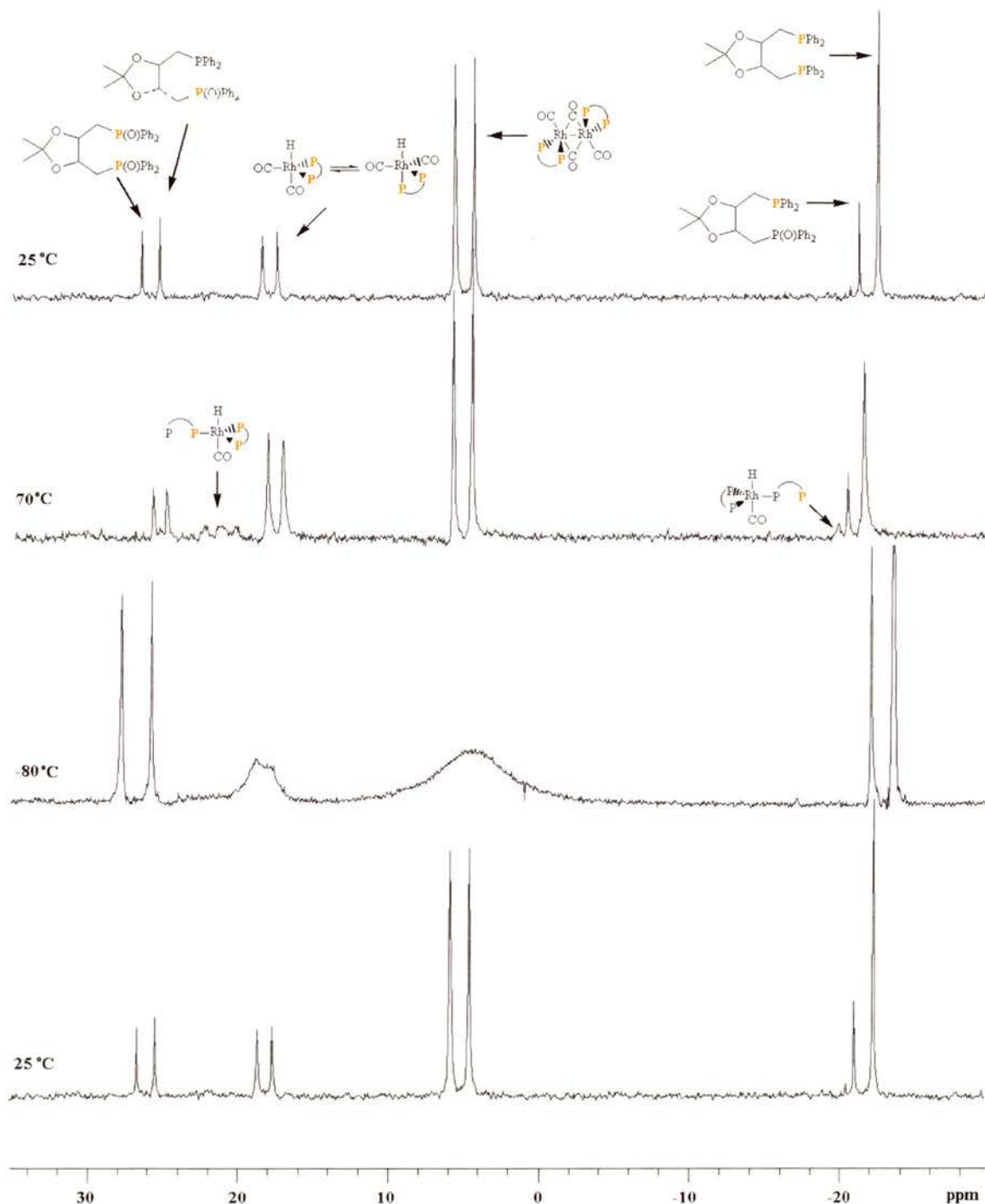
It is also observed that the dimer resonance at 5 ppm also becomes broad at -80 °C. It has already been observed in the  $^{13}\text{C}$  NMR spectrum of the dimer complex species, **46**, that there is only one resonance for the carbonyls because the terminal and bridging CO's are exchanging with each other, and that in the  $^{31}\text{P}\{^1\text{H}\}$  NMR spectrum there is only one second order doublet because the four phosphorus atoms are chemically equivalent. The broadness of the resonance at -80 °C therefore is accounted for by the slowing down of this fluxionality, see section 2.2.2. Therefore, if the sample is cooled further, it would be expected that the resonance would be split into two second order doublets.

It has already been described that it is possible to estimate the ee/ ea ratio from the  $^2J_{\text{av-P-H}}$  coupling constant, see section 1.1.3.4.<sup>52</sup> This assumes values for the *cis* and *trans* phosphorus hydride coupling constants of the two geometric isomers. The *cis*  $^2J_{\text{P-H}}$  phosphorus hydride coupling constant is assumed to be between -2 and +2 Hz and the *trans*  $^2J_{\text{P-H}}$  phosphorus hydride coupling constant is assumed to be 106 Hz, this value

is taken from the  $^1\text{H}$  NMR spectrum of the *ea* geometric isomer of  $[(\text{DPEphos})\text{Rh}(\text{CO})_2\text{H}]$  observed at 173 K.

### NMR 2.25

$^{31}\text{P}\{^1\text{H}\}$  NMR spectrum of  $\text{Rh}(\text{CO})_2(\text{acac}) / \text{DIOP}$  1:1.5 under 20 bar synthesis gas at  $-80$  to  $70^\circ\text{C}$



There is some doubt using these as the *cis* and *trans*  $^2J_{\text{P-H}}$  phosphorus hydride coupling constants as the electronic properties of DIOP and DPEphos are significantly different,

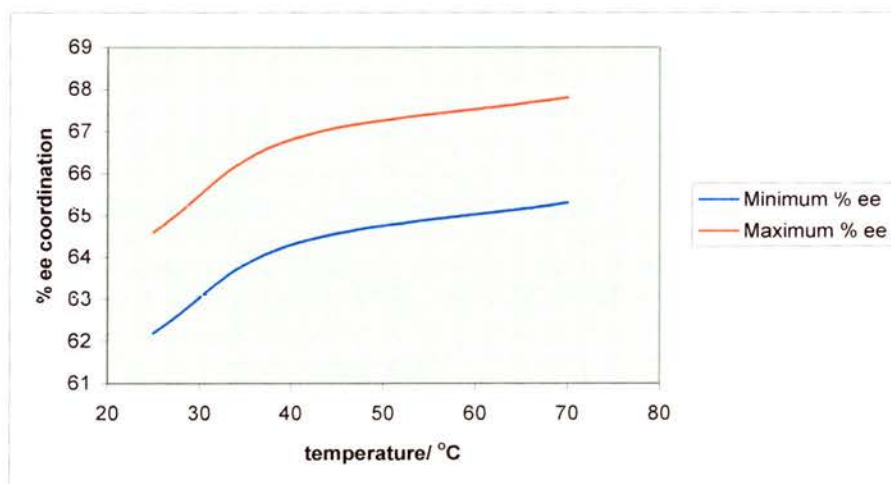
the  $^{31}\text{P}\{^1\text{H}\}$  NMR chemical shifts of DIOP and DPEphos are  $-23$  ppm and  $-16$  ppm respectively, and the  $^{31}\text{P}\{^1\text{H}\}$  NMR chemical shifts of  $[(\text{DIOP})\text{Rh}(\text{CO})_2\text{H}]$  and  $[(\text{DPEphos})\text{Rh}(\text{CO})_2\text{H}]$  are  $18.5$  ppm and  $25.5$  ppm respectively. This difference in the electronic nature of the ligand could effect the coupling constants of the ee and ea geometric isomers of  $[(\text{DIOP})\text{Rh}(\text{CO})_2\text{H}]$ .

A maximum and minimum ee / ea ratio can be defined by using  $-2$  and  $+2$  as the limits of the cis  $^2J_{\text{P-H}}$  phosphorus hydride coupling constant. The average of the max and min was worked out from the observed  $^2J_{\text{avP-H}}$  coupling constant and is given below. Graph 2.1 also plots the max and min values with temperature.

At  $25\text{ }^\circ\text{C}$ , the  $^2J_{\text{avP-H}}$  coupling constant was  $38.8$  Hz, at  $40\text{ }^\circ\text{C}$ , the  $^2J_{\text{avP-H}}$  coupling constant was  $36.5$  Hz, and at  $70\text{ }^\circ\text{C}$ , the  $^2J_{\text{avP-H}}$  coupling constant was  $35.5$  Hz. This gives ee:ea ratios of  $1.74$  at  $25\text{ }^\circ\text{C}$ ,  $1.90$  at  $40\text{ }^\circ\text{C}$ , and  $1.99$  at  $70\text{ }^\circ\text{C}$ .

### Graph 2.1

*Graph of percentage ee coordination of DIOP in  $[\text{RhH}(\text{CO})_2(\text{DIOP})]$  at various temperatures.*



### 2.4.1.2 High Pressure IR Studies.

From previous reports<sup>52, 53</sup> we assume that the hydridorhodium complex [(DIOP)Rh(CO)<sub>2</sub>H] exists as a mixture of the diequatorial complex **24** and the equatorial-axial complex **25**. It is proposed that this interchange between the geometric isomers is faster than the NMR time scale, see section 2.3.1.1, so averaged chemical shifts and coupling constants are observed for the two isomers.

However, the infrared time scale ( $10^{-8}$  s) is much faster than the NMR one. It is therefore possible to observe the separate IR spectra for the two isomers in solution. In practice this is done by observation of their separate CO stretching vibrations, each isomer should exhibit a symmetric and an antisymmetric stretching vibration.

IR 2.4 shows the infrared spectra of the complex species present in a solution with a rhodium DIOP ratio 1:1.5, under 20 bar synthesis gas, IR 2.4a is at 25 °C, IR 2.4b is at 40 °C, IR 2.4c is at 60 °C, and IR 2.4d is at 80 °C.

In IR 2.4a, at 25 °C, we see a mixture of the rhodium dimer and hydride as we would expect from the HP-NMR results. We can see a major terminal  $\nu_{\text{CO}}$  band from the dimer complex, **46**, at  $1984\text{ cm}^{-1}$  with several shoulders, a terminal  $\nu_{\text{CO}}$  band from the hydride complexes, **24** and **25**, at  $1948\text{ cm}^{-1}$ , a bridging  $\nu_{\text{CO}}$  band from the dimer complex at  $1723\text{ cm}^{-1}$ ; the two bands at  $1764$  and  $1742\text{ cm}^{-1}$  are due to 1,4-pentanedione or **acac**. With increasing temperature, we see a reduction in the relative intensities of the dimer  $\nu_{\text{CO}}$  bands at  $1984$  and  $1723\text{ cm}^{-1}$ . We see the growth of the  $\nu_{\text{CO}}$  band from one of the hydride complexes at  $1948\text{ cm}^{-1}$ , and are now able to assign three more  $\nu_{\text{CO}}$  bands to the hydride complexes at  $2030$ ,  $1990$ , and  $1980\text{ cm}^{-1}$  (the band at  $1980\text{ cm}^{-1}$  appears as a shoulder on the band at  $1990\text{ cm}^{-1}$ ). The four bands are the symmetric and antisymmetric  $\nu_{\text{CO}}$  vibrations of the ee and ea geometric isomers, species **24** and **25**.

Previously this has been seen as unambiguous evidence for the existence of a dynamic equilibrium between the ee and ea isomers of [HRh(CO)<sub>2</sub>(diphosphine)].<sup>52</sup> The spectra for the [HRh(CO)<sub>2</sub>(diphosphine)] complexes, where the diphosphine is ligand 28a to 28g in Figure 2.18 can be seen in Figure 2.19. All show four absorptions in the carbonyl region, the information is also summarised in Table 2.6, alongside selected NMR data and the data for [HRh(CO)<sub>2</sub>(DIOP)]. It is observed that the most similar  $\nu_{\text{CO}}$  frequencies are from ligands 28c and 28d, which also have the most similar % ee value.

Figure 2.18

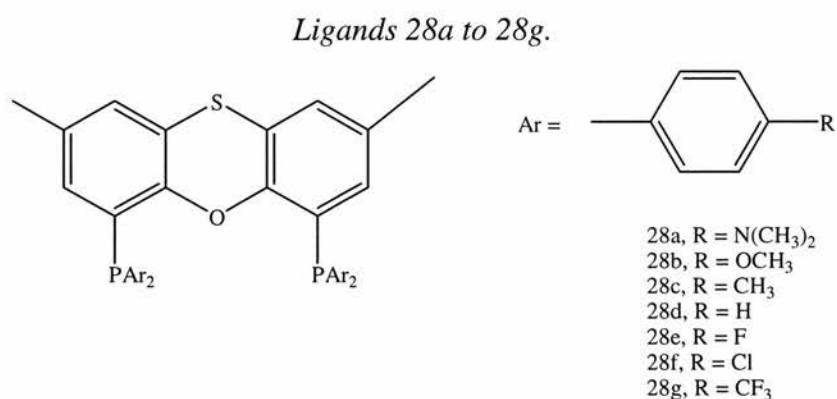
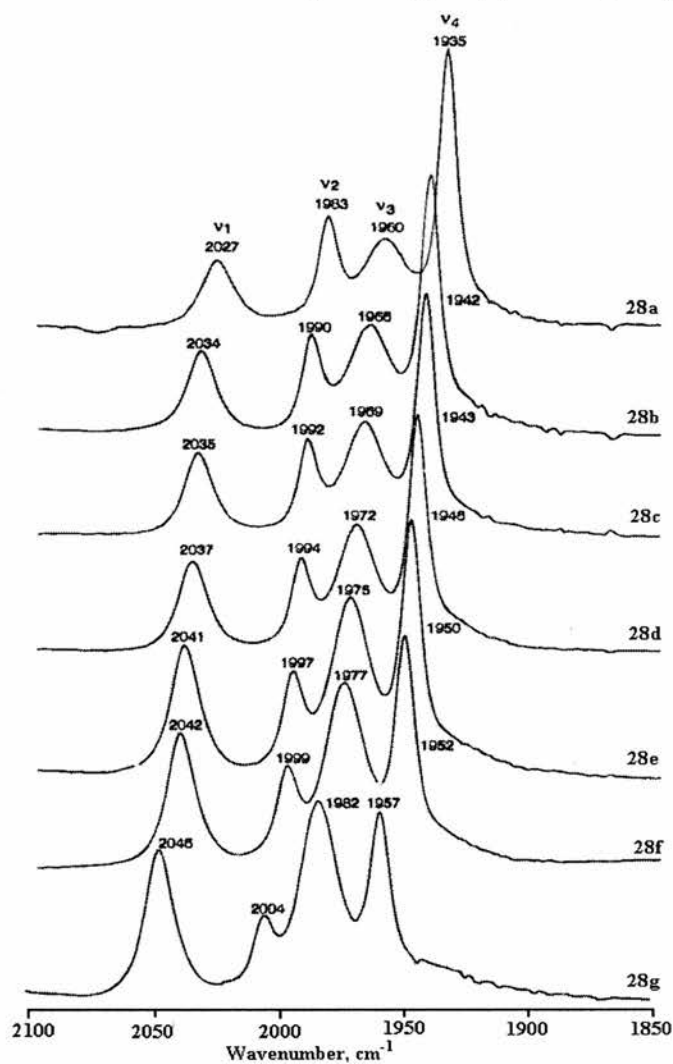


Figure 2.19

*HP-IR spectra for [HRh(CO)<sub>2</sub>(diphosphine)] complexes, diphosphine = 28a-28g, in 2-Me-THF at 80 °C and 20 bar of CO/H<sub>2</sub> (1:1) (carbonyl region).<sup>52</sup>*



**Table 2.6**

*Selected NMR and IR data for [HRh(CO)<sub>2</sub>(diphosphine)] complexes 28a-28g and DIOP.*

Ligand	<sup>1</sup> J <sub>RhH</sub> , Hz	<sup>1</sup> J <sub>RhP</sub> , Hz	ν <sub>CO</sub> frequency, cm <sup>-1</sup>	% ee
<b>28a</b>	8.7	121	2027, 1983, 1960, 1935.	44-50
<b>28b</b>	7.5	124	2034, 1990, 1966, 1942.	56-62
<b>28c</b>	7.2	126	2035, 1992, 1969, 1943.	63-69
<b>28d</b>	6.6	128	2037, 1994, 1972, 1946.	69-75
<b>28e</b>	6.3	130	2041, 1997, 1975, 1950.	76-83
<b>28f</b>	6.0	132	2042, 1999, 1977, 1952.	81-88
<b>28g</b>	4.5	134	2046, 1004, 1982, 1957.	89-96
<b>DIOP</b>	8.0	120	2030, 1990, 1980, 1948.	65-68

For comparison, the FT-IR spectrum was taken using CO / D<sub>2</sub> in place of CO / H<sub>2</sub>. This would simplify the results as bands due to ν<sub>Rh-H</sub> interaction would disappear (ν<sub>Rh-D</sub> bands appear shifted by a frequency 1/√2 to that of ν<sub>Rh-H</sub> bands). The position of ν<sub>CO</sub> bands attributed to the ee complex would be affected to a greater extent than bands attributed to the ea complex because of a *trans* relationship between the hydride and one of the CO ligands in the ee complex. The ν<sub>CO</sub> bands due to the rhodium dimer will not be affected by H / D exchange as it does not possess a hydrogen atom bound to the rhodium. This method of verifying ee and ea ν<sub>CO</sub> bands has been employed previously for [HRh(CO)<sub>2</sub>(thixantphos)],<sup>52</sup> where thixantphos is ligand 28d in Figure 2.18. Upon H/D exchange, only the bands at 2037 and 1972 cm<sup>-1</sup> shift to lower wavenumbers, by 18 and 14 cm<sup>-1</sup> respectively.

The theoretical IR spectra of [HRh(CO)<sub>2</sub>(PH<sub>3</sub>)<sub>2</sub>] and [DRh(CO)<sub>2</sub>(PH<sub>3</sub>)<sub>2</sub>] were also calculated by DFT methods (see Table 2.7). Comparison of the frequencies showed that H/D exchange only effects the carbonyl frequencies of the ee isomer of the complex. The calculated shift to lower frequencies was in perfect agreement with the observed spectra and confirms the peak assignment to the ee and ea isomers.

**Table 2.7**

*Calculated C-O stretching frequencies and assignments for the ee and ea isomers of the complexes [HRh(CO)<sub>2</sub>(PH<sub>3</sub>)<sub>2</sub>] and [DRh(CO)<sub>2</sub>(PH<sub>3</sub>)<sub>2</sub>].*

[HRh(CO) <sub>2</sub> (Ph <sub>3</sub> ) <sub>2</sub> ]	[DRh(CO) <sub>2</sub> (Ph <sub>3</sub> ) <sub>2</sub> ]
ee isomer 2041 (sym) 1983 (anti)	ee isomer 2006 (sym) 1963 (anti)
ea isomer 1985 (sym) 1948 (anti)	ea isomer 1985 (sym) 1948 (anti)

The HP FTIR spectrum of the rhodium DIOP catalytic system under CO/ D<sub>2</sub> 1:1, 20 bar can be seen in IR 2.5. For comparison, the HP FTIR spectrum of the rhodium DIOP catalytic system under CO/ H<sub>2</sub> 1:1, 20 bar, 80 °C can also be seen as 4d, or the blue spectrum, alongside the CO/ D<sub>2</sub> spectrum at 80 °C, IR 2.5d.

In IR 2.5a, at 25 °C, there is a shift in one of the shoulders on the major band previously at 1980 cm<sup>-1</sup> to a lower wavenumber of 1966 cm<sup>-1</sup>. We can also see the disappearance of a low intensity band at 1961 cm<sup>-1</sup> which we can now assign to a  $\nu_{\text{Rh-H}}$  vibration. What is surprising is that the main  $\nu_{\text{CO}}$  band attributed to the rhodium hydride at 1948 cm<sup>-1</sup> is unaffected by H/ D exchange. We believed this would be the ee complex as it is the most intense band and the ee isomer is the most abundant (see section 2.3.1.1). It is worth noting, however, that intensities do not necessarily reflect abundance.<sup>54</sup>

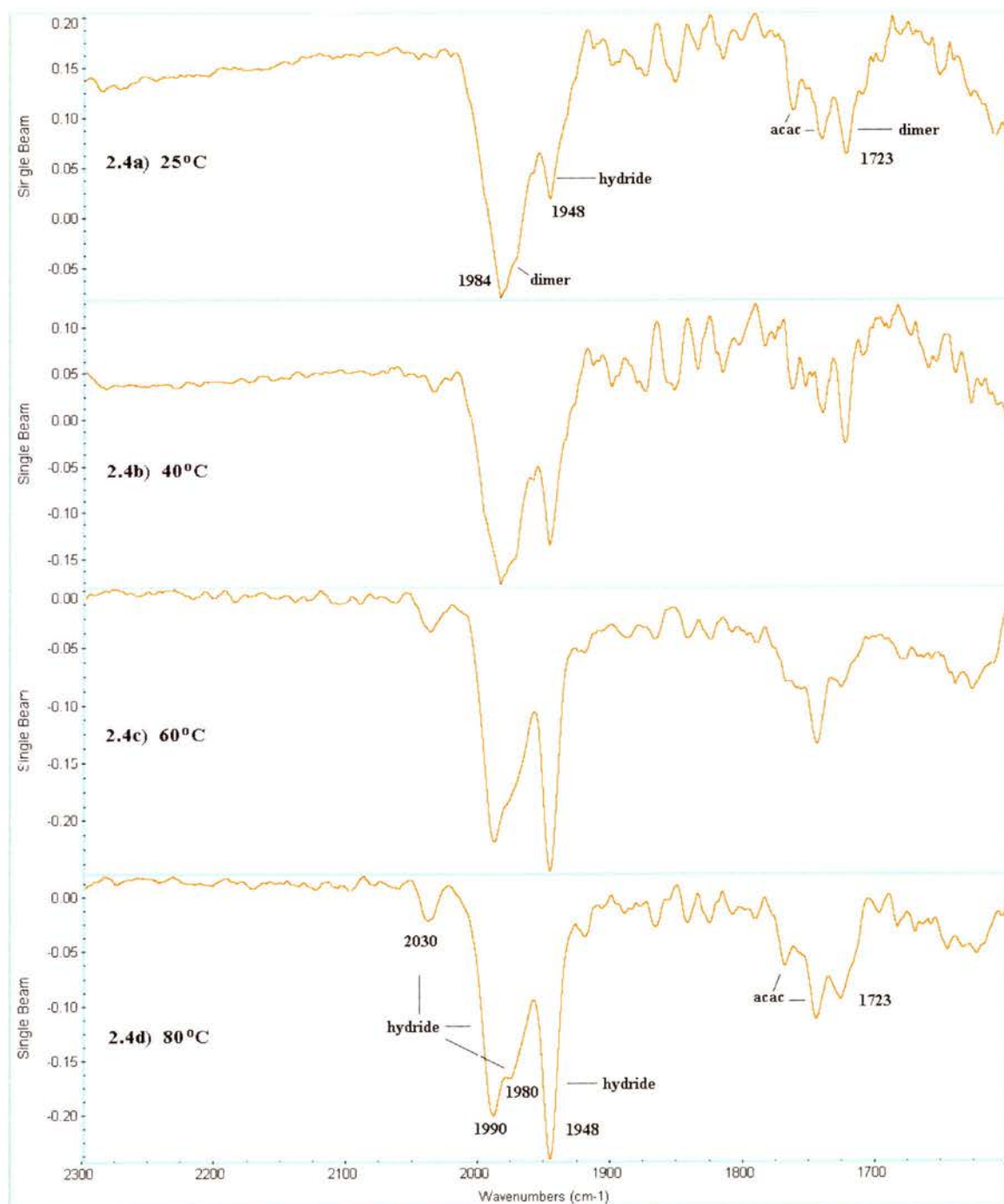
On heating to 40 °C and 60 °C, the hydride bands become stronger in intensity and the dimer bands become reduced in intensity. We can also see that two of the four hydride bands are shifted (see IR 2.5b and IR 2.5c).

At 80 °C, the concentration of the hydride is greatest (see section 2.3.1). The band which is at 1980 cm<sup>-1</sup> in IR 2.4d shifts to 1966 cm<sup>-1</sup> in IR 2.5d, and the band at 2030 cm<sup>-1</sup> in IR 2.4d also shifts to 2020 cm<sup>-1</sup> in IR 2.5d. These bands can therefore be assigned to the  $\nu_{\text{CO}}$  vibrations of the rhodium hydride of ee DIOP co-ordination, or species **24**.

We also observe that the bands at 1943 cm<sup>-1</sup> and 1990 in IR 2.4d are not shifted on H/D exchange in IR 2.5d. These bands are therefore assigned to the  $\nu_{\text{CO}}$  vibrations of the rhodium hydride of ea DIOP coordination, or species **25**.

## IR 2.4

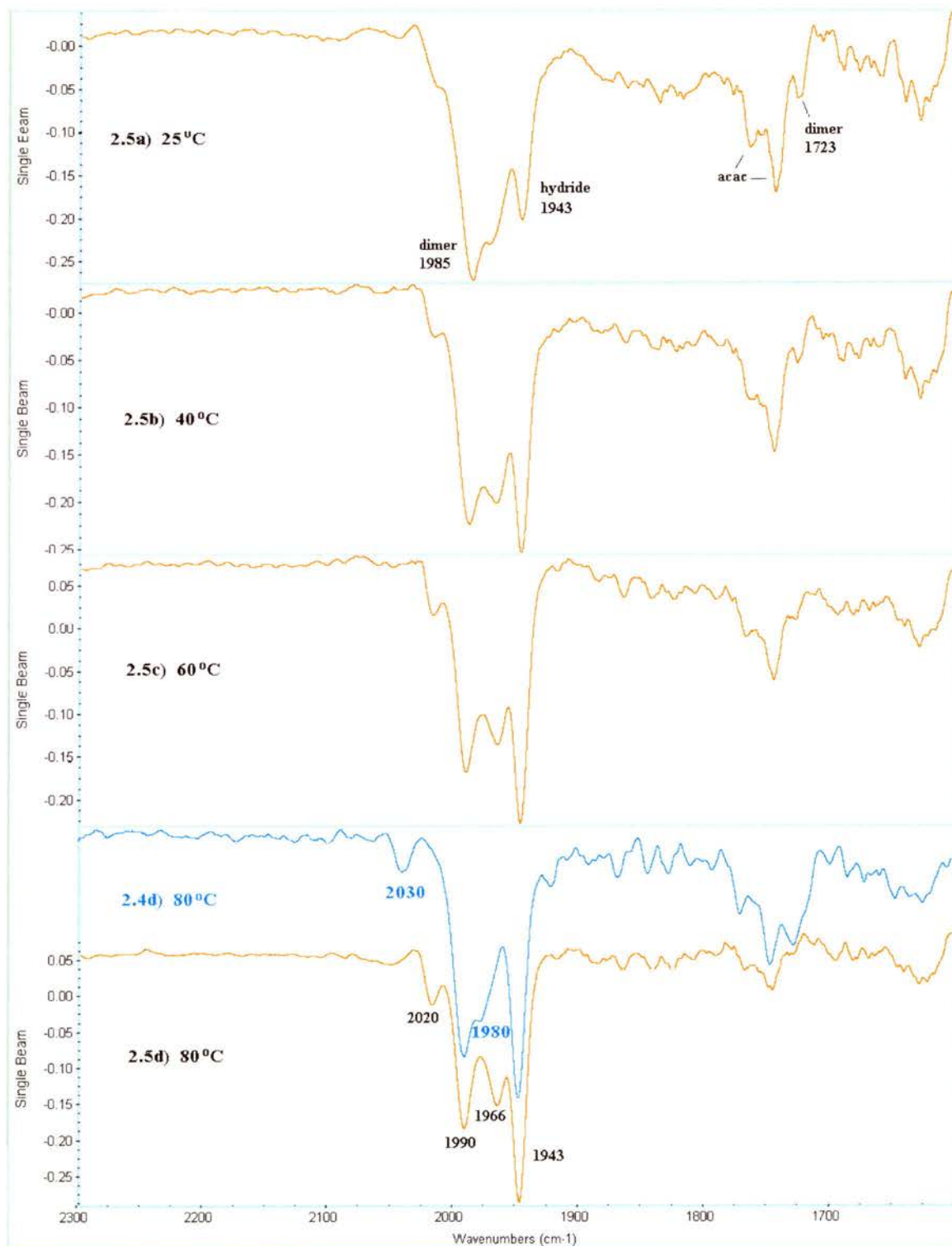
*Rh: DIOP = 1:1.5, total pressure 20 bar, CO: H<sub>2</sub> = 1:1, temperature 25-80 °C.*



## IR 2.5

*Rh: DIOP = 1:1.5, total pressure 20 bar, CO: D<sub>2</sub> = 1:1, temperature 25-80 °C.*

*(Note: IR 2.4d overlays 2.5d to compare the band shifts.)*



## 2.4.2 Rhodium to DIOP Ratio 1:1.

The hydroformylation of alkenes using rhodium phosphine catalysts exhibits a dependence on the rhodium to phosphine ratio, (the ratio often must be above three P atoms per Rh atom for the most selective results)<sup>31</sup> that has yet to be comprehensively explained. It is hypothesised that complexes with three phosphines attached may play an important role in the catalytic cycle or that there is an equilibrium set up between rhodium complexes with one P atom attached, two P atoms attached and three P atoms attached. At a phosphine to rhodium ratio of 3:1, this equilibrium is most favourable towards  $[P_2Rh(CO)_2H]$ , believed to be the selective catalyst precursor in the hydroformylation reaction.

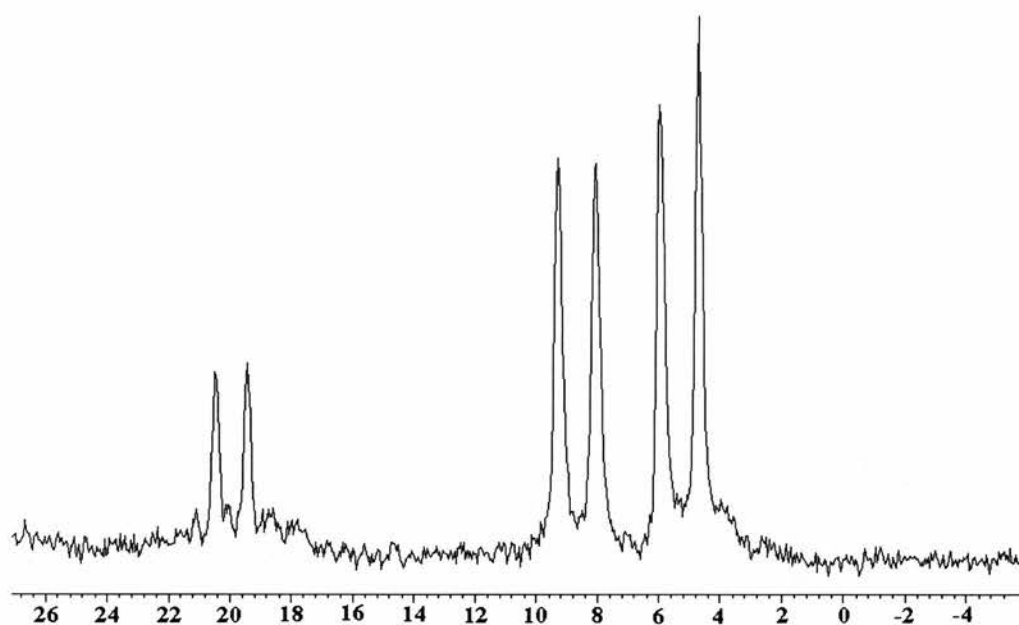
The rhodium DIOP catalysed hydroformylation of allyl alcohol also exhibits a dependence on the diphosphine to rhodium ratio. The best results are obtained when this ratio is 1:1.5, analogous to 1:3 for monophosphines. In an attempt to understand this relationship, the system was studied by HP IR and HP NMR with a diphosphine to rhodium ratio of 1:1. The results can be seen below in IR 12-15, and NMR 2.26-2.27, and the NMR data is given in Table 2.8.

### 2.4.2.1 High Pressure NMR Studies.

In NMR 2.26, the  $^{31}P \{^1H\}$  NMR spectrum of the species observed at 25 °C can be seen. A new species is observed ( $\delta = 8.51$  ppm,  $J_{Rh-P} = 153$  Hz) which could be a mono phosphine complexed rhodium species  $[HRh(CO)_3(DIOP)]$ , where only one DIOP phosphorus is bonded to the metal. However, as there is no free DIOP phosphorus signal, it is suggested that the other DIOP phosphorus is either oxidised or bound to another rhodium atom, as in Figure 2.16; this species has already been observed in section 2.2.3.1. On heating, the ratio between this new species and the rhodium dimer species **46** is not greatly affected, the rhodium hydride species **24** and **25** suffer a decrease in concentration to almost zero at 80 °C rather than the significant increase observed previously in NMR 2.22. This supports the theory that an equilibrium is set up between species with one or two bound phosphines.

**NMR 2.26**

$^{31}\text{P}\{^1\text{H}\}$  NMR spectrum of  $\text{Rh}(\text{CO})_2(\text{acac})$  / DIOP 1:1 under 20 bar synthesis gas at  $25^\circ\text{C}$ .

**NMR 2.27**

$^{31}\text{P}\{^1\text{H}\}$  NMR spectrum of  $\text{Rh}(\text{CO})_2(\text{acac})$  / DIOP 1:1 under 20 bar synthesis gas at  $80^\circ\text{C}$ .

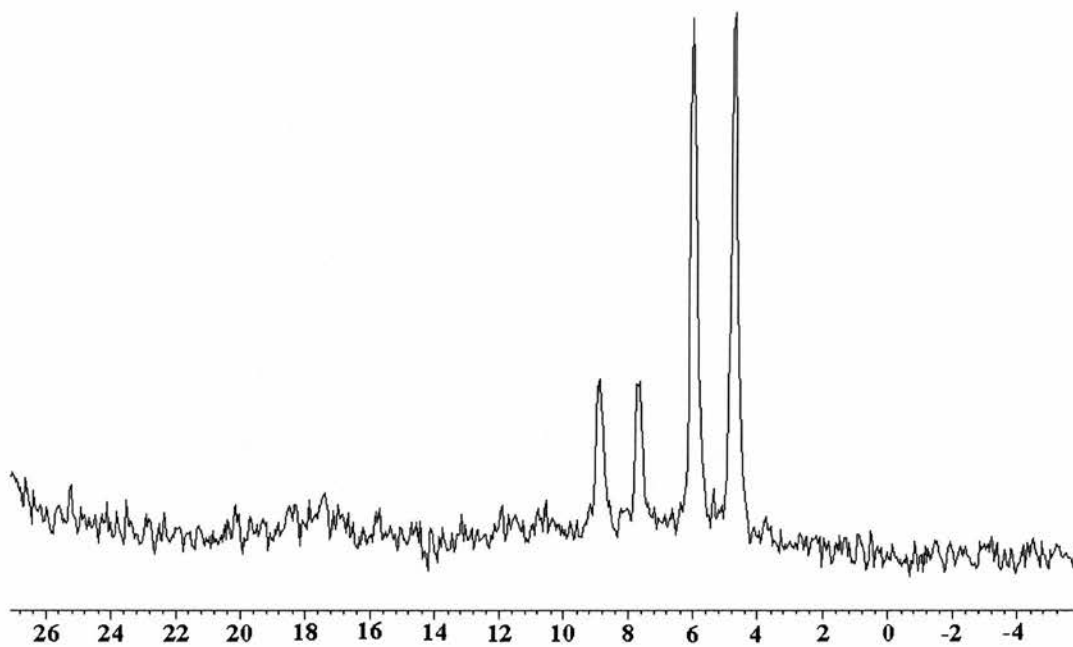


**Table 2.8**

*High pressure  $^{31}\text{P}\{^1\text{H}\}$  NMR data for the species present at  $\text{Rh}(\text{CO})_2(\text{acac})$  to DIOP  
Ratio 1:1, total pressure 20 bar, CO to  $\text{H}_2$  ratio 1:1, at 25 °C.*

$\delta$ (ppm)	$J_{\text{Rh-P}}$ (Hz)
19.78 (d)	126
8.51 (d)	150
5.18 (d <sup>a</sup> )	153

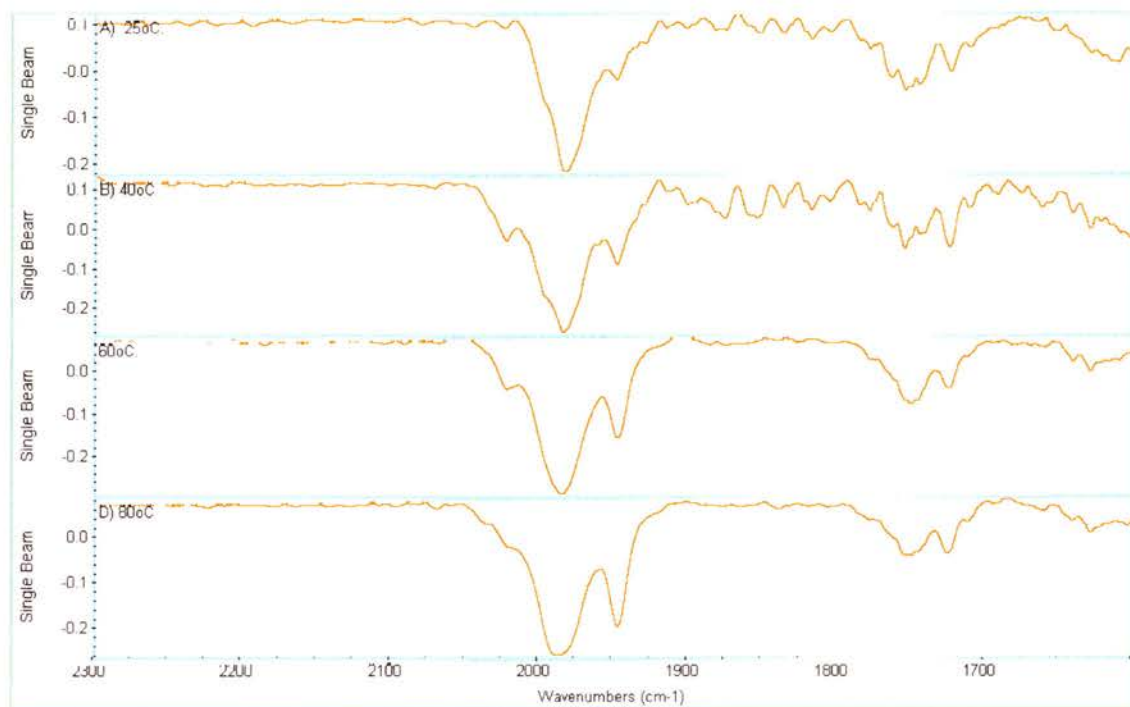
<sup>a</sup>Second order pattern.

#### 2.4.2.2 High Pressure IR Studies.

The results from the HP IR agree with the results observed from the  $^{31}\text{P}\{^1\text{H}\}$  NMR studies in section 2.3.2.1. The rhodium hydride  $\nu_{\text{CO}}$  bands are lower in intensity relative to those from the rhodium dimer when the rhodium DIOP ratio is 1:1.5, see IR 2.6. This agrees with the assumption that there are several species in the solution which compete with each other, and that a rhodium to diphosphine ratio of 1:1.5 is required to be favourable towards formation of the rhodium hydride  $[\text{RhH}(\text{CO})_2(\text{DIOP})]$  or species **24** and **25**. These competing species, particularly that observed at  $\delta = 8.51$  ppm, may be rhodium complexes with only one P atom attached, or species still containing the acac ligand, as there are literature reports of  $[\text{Rh}(\text{CO})_2(\text{acac})]$  not being completely converted at small diphosphine to rhodium ratios.<sup>41, 55</sup>

**IR 2.6**

*Rh(CO)<sub>2</sub>(acac) / DIOP ratio 1:1, total pressure 20 bar, CO to H<sub>2</sub> ratio 1:1*

**2.4.3 Changing the CO and H<sub>2</sub> Partial Pressures.**

Because of the surprising fact that even at high pressures the rhodium dimer is still the major species at 25 °C, the effect of changing the partial pressures of CO and H<sub>2</sub> on the complex species was studied by HP IR. The infrared spectra IR 2.7 and IR 2.8 show the results of changing the CO / H<sub>2</sub> ratios to 2:1 and 1:2 respectively; the rhodium / DIOP ratio is 1:1.5 in all cases.

IR 2.7 is the infrared spectrum when the carbon monoxide partial pressure is increased to a CO / H<sub>2</sub> ratio 2:1. The catalytic species present are the same with the position of the  $\nu_{\text{CO}}$  bands appearing at the same frequency in the spectrum. With the increased partial pressure of CO and the reduced partial pressure of H<sub>2</sub> the intensity of the main hydride band at 1947 cm<sup>-1</sup> in the 80 °C spectrum is very much reduced. It seems that the H<sub>2</sub> pressure is important for the formation of the hydride. What is interesting about these spectra is that at 80 °C we can clearly see the presence of both geometric isomers of the complex species **24** and **25**, and the rhodium dimer complex species **46** in the

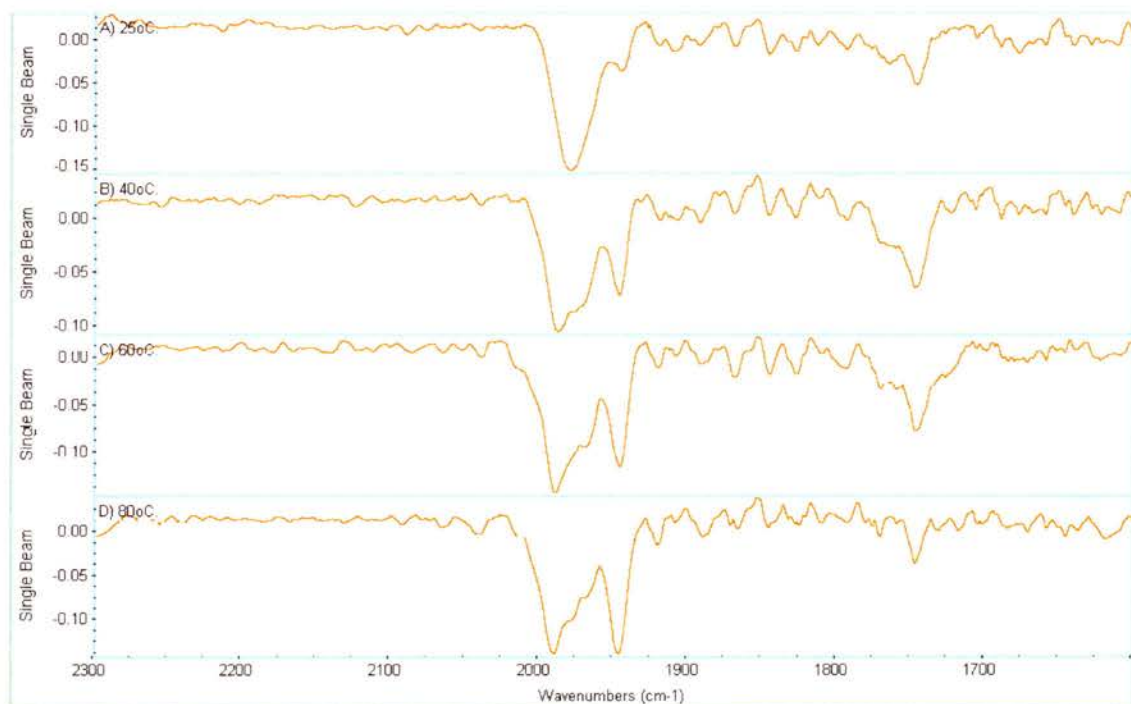
same spectrum. Usually the rhodium dimer  $\nu_{\text{CO}}$  band at  $1985 \text{ cm}^{-1}$  is obscured by the rhodium hydride  $\nu_{\text{CO}}$  bands at  $1990 \text{ cm}^{-1}$  and  $1980 \text{ cm}^{-1}$ .

IR 2.8 is the infrared spectrum when the hydrogen partial pressure is increased to a CO / H<sub>2</sub> ratio 1:2. Again, the  $\nu_{\text{CO}}$  bands appear at the same frequencies in the spectrum, however, at lower temperatures, the rhodium hydride  $\nu_{\text{CO}}$  bands are more intense.

It would seem that at this stage the CO and H<sub>2</sub> partial pressures are important for the formation of the rhodium hydride species. This agrees with observations made under conditions of 1 atm synthesis gas, described in section 2.3.3

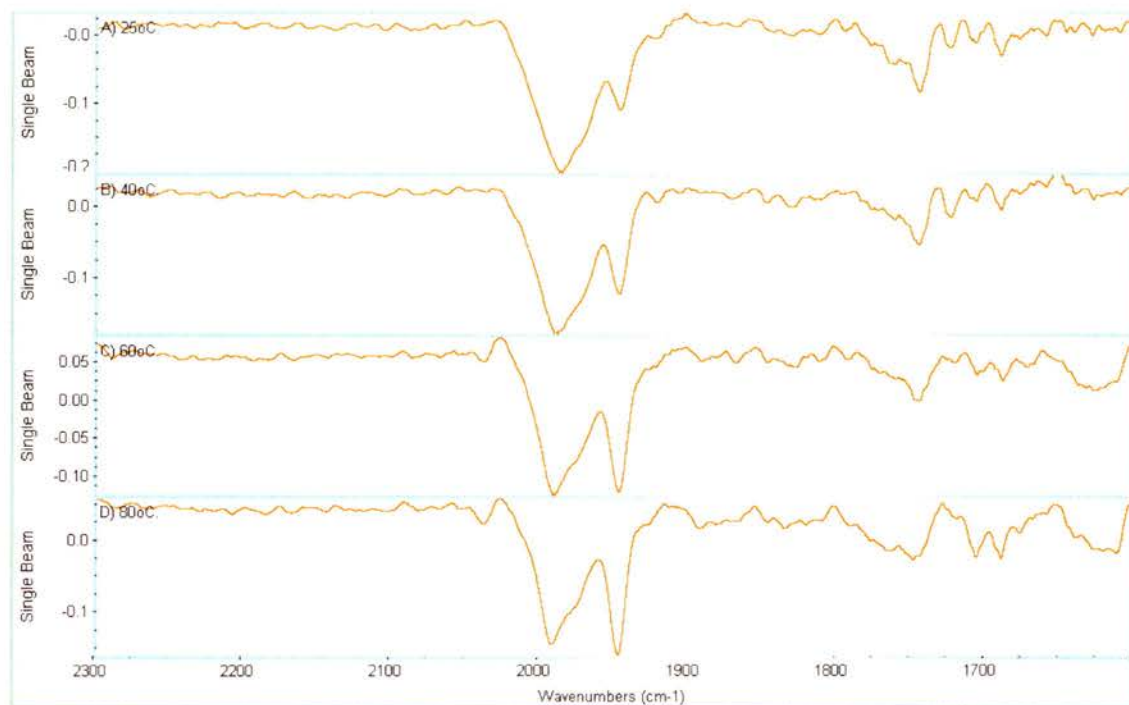
## IR 2.7

*Rh(CO)<sub>2</sub>(acac) / DIOP ratio 1:1.5, total pressure 20 bar, CO to H<sub>2</sub> ratio 2:1*



**IR 2.8**

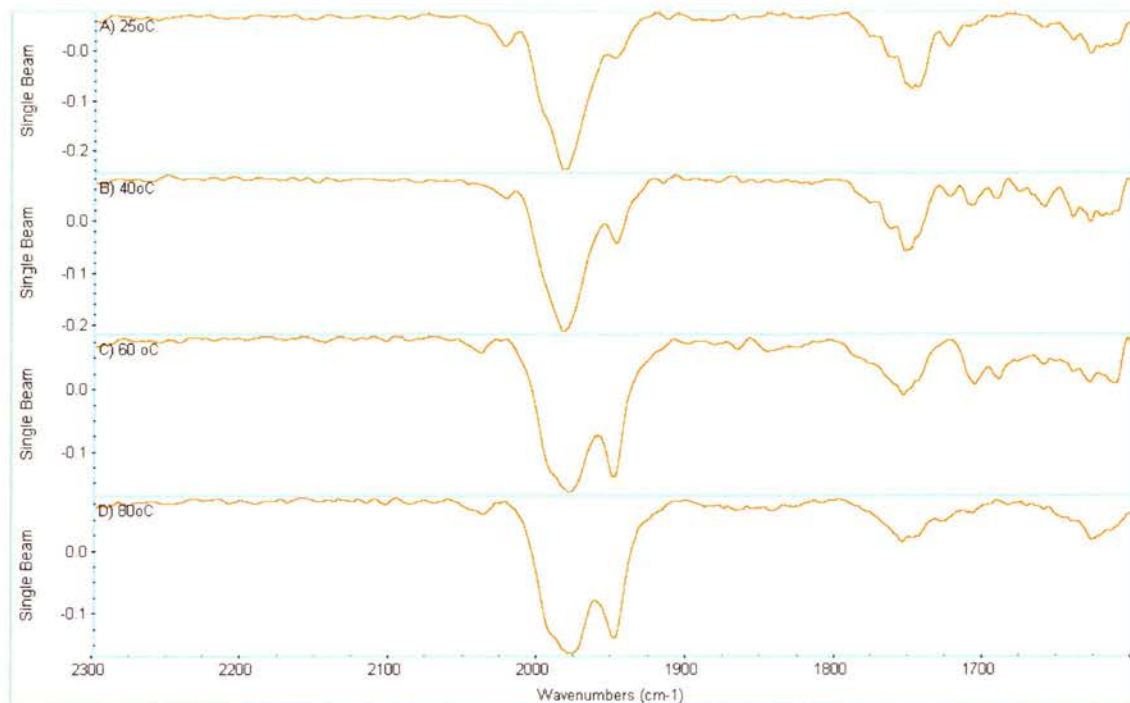
*Rh(CO)<sub>2</sub>(acac) / DIOP ratio 1:1.5, total pressure 20 bar, CO to H<sub>2</sub> Ratio 1:2.*

**2.4.4 Changing the Total Pressure.**

Since the working industrial process involving this catalytic system is run between 5 and 10 bar, the same systems already studied were investigated at 5 bar total pressure. The results can be seen in IR 2.9 to 2.11. The band frequencies are the same as those assigned in the previous studies. There is a slight reduction in the proportion of the hydride produced under 5 bar compared with 20 bar but the system is not greatly affected by the total pressure.

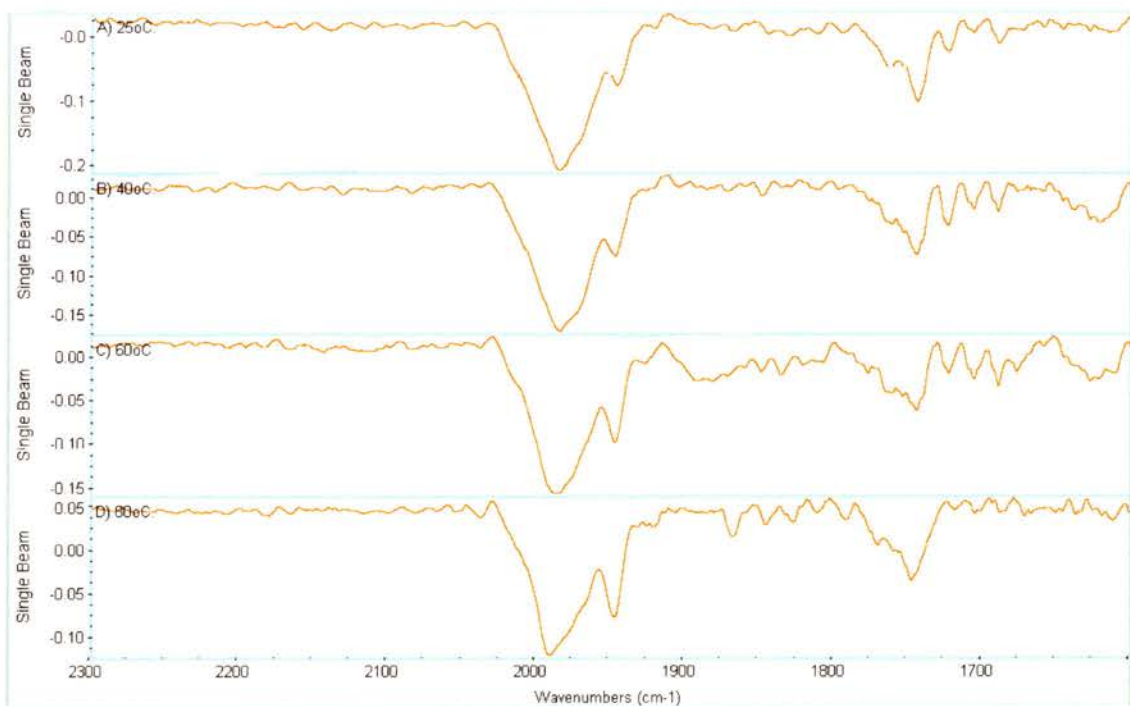
## IR 2.9

*Rh(CO)<sub>2</sub>(acac) / DIOP ratio 1:1.5, total pressure 5 bar, CO to H<sub>2</sub> ratio 1:1*



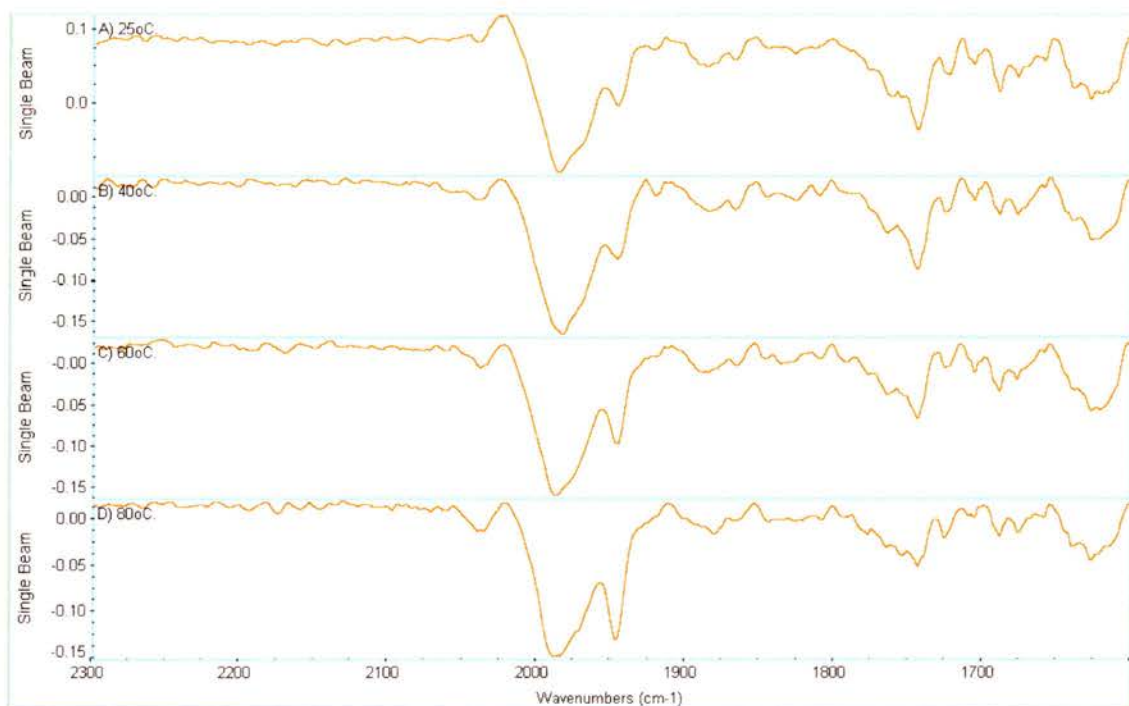
## IR 2.10

*Rh(CO)<sub>2</sub>(acac) / DIOP ratio 1:1.5, total pressure 5 bar, CO to H<sub>2</sub> ratio 2:1*



**IR 2.11**

*Rh(CO)<sub>2</sub>(acac) / DIOP ratio 1:1.5, total pressure 5 bar, CO to H<sub>2</sub> ratio 1:2*



## **2.5 *In-Situ* High Pressure Studies of the Hydroformylation of Allyl Alcohol.**

To understand the species formed under hydroformylation conditions, it was necessary to begin to look at the hydroformylation reaction as it was taking place. Several ways of doing this were chosen and are described here.

### **2.5.1 HP NMR Studies of the Hydroformylation of Allyl Alcohol.**

The high pressure  $^{31}\text{P}\{^1\text{H}\}$  spectra of the catalytic system in the presence of substrate, allyl alcohol, under 20 bar synthesis gas were taken at 25-80 °C. The spectra are shown in NMR 2.28-NMR 2.30 and the results from the spectra are listed in Table 2.9.

**Table 2.9**

*<sup>31</sup>P{<sup>1</sup>H} HP NMR data of the hydroformylation of allyl alcohol under 20 bar synthesis gas at varying temperature.*

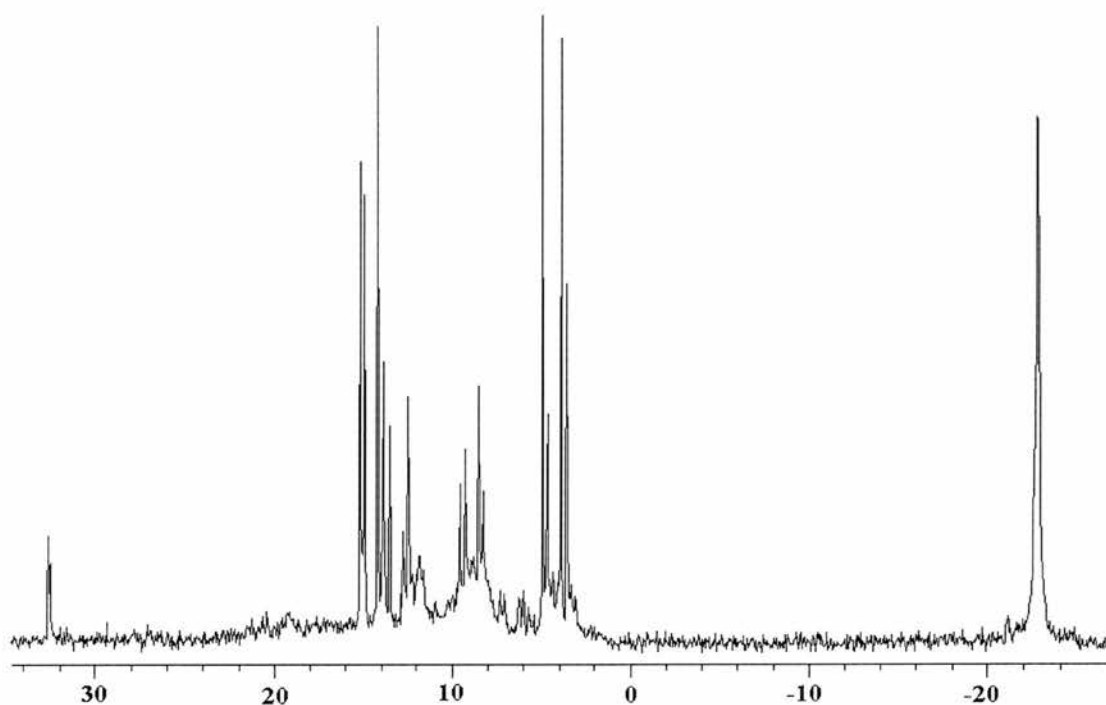
Temperature	$\delta$ (ppm)	$J_{\text{Rh-P}}$ (Hz)	$J_{\text{P-P}}$ (Hz)
25 °C NMR 29	14.49 (dd)	125	33
	13.08 (dd)	129	34
	8.81 (dd)	129	35
	4.19 (dd)	125	33
80 °C NMR 30	15.13 (dd)	125	33
	13.72 (dd)	129	33
	8.39 (d)	109	
	9.45 (dd)	128	34
	4.84 (dd)	124	33
25 °C (cooled down) NMR 31	14.49 (dd)	124	34
	13.08 (dd)	129	33
	—		
	8.81 (dd)	128	34
	4.25 (dd)	125	34

It can be seen in NMR 2.28 that at room temperature there are two major species present, each with two double doublet resonances at 14.49 and 4.19 ppm and 13.08 and 8.81 ppm. These originate from two rhodium complexes, both of which have chelating DIOP ligands in which their P atoms are inequivalent. These patterns are very similar to others observed in the literature<sup>53, 56</sup> for complexes of the form  $[\text{Rh}(\text{COR})(\text{CO})_2(\text{P})_2]$  (P=PPh<sub>3</sub>, R= styrene or octyl; P=PEt<sub>3</sub>, R=Me or Et. The compound  $[\text{Rh}(\text{COstyryl})(\text{CO})_2(\text{PPh}_3)_2]$  was identified by <sup>1</sup>H and <sup>13</sup>C NMR as a mixture of the branched and linear isomers. It was also observed that with time, the major branched acyl species depleted in concentration in favour of the initially minor linear acyl species. The octyl analogues were synthesised to carry out a more detailed examination of the structure of the acyls, as the linear isomer is kinetically favoured and skeletal isomerisation does not occur. At room temperature, the <sup>13</sup>C NMR spectrum shows that the acyl carbon resonance exhibits a fine structure consistent with coupling to two equivalent phosphorus nuclei. However at low temperatures, the acyl carbon resonance is coupled to two inequivalent nuclei ( $J=8, 75$  Hz), thus defining the structure at low temperature as ours with equatorial-axial phosphorus atoms. What is different, of course, is that at room temperature, the complex is in dynamic equilibrium between the ee and ea forms, and in our case, the ea form is still the only one present even at higher temperatures.



**NMR 2.28**

*<sup>31</sup>P{<sup>1</sup>H} NMR spectrum of [Rh(CO)<sub>2</sub>(acac)] / DIOP 1:1.5 & allyl alcohol under 20 bar synthesis gas at 25 °C.*



It is also possible that the major isomer is in fact the branched isomer which is more stable than the linear one because of the chelate effect described above. This could also explain the increased l:b ratio of the aldehyde products in this reaction as the linear isomer would be more reactive than the branched one. It has been observed that of the complex branched and linear [Rh(styryl)(CO)<sub>2</sub>(PPh<sub>3</sub>)<sub>2</sub>] complexes, the branched is at first the most abundant isomer, 85 % over 15 % of the linear isomer; however after 45 minutes, the linear isomer was the most abundant, 60 % over 40 % of the branched isomer. This is interesting as the branched isomer must be the kinetically favoured one in this case, but the linear the thermodynamically favoured one. The octyl rhodium acyl isomers were synthesised because the linear isomer was the only observed one, because it was both the kinetic and thermodynamic favoured product. Although functionalised allyl alcohol is a terminal alkene, it is conceivable, therefore, that it would behave as octene and favour the linear acyl rhodium complex kinetically and thermodynamically. If this were so we would expect to only see the linear isomer. This is not the case, however. It has also been shown, in the styrene case, that even if the branched isomer is kinetically favoured, we would expect the concentration of it to decrease over time as it

is thermodynamically less favoured. In our case, we do not see a change in the concentration of the complexes. This is seen as evidence that in the allyl alcohol case, there is an additional factor that is stabilising the branched acyl rhodium complex, and we propose this to be through the chelation of the OH from the allyl alcohol and the loss of CO. It is also noted that for the octyl case it was observed that at 278 K there was reversible CO loss from the complex to give the 4 coordinate complex species  $[\text{Rh}(\text{octyl})(\text{PPh}_2)_2(\text{CO})]$ .

The presence of these two isomers could also hold more clues to why the DIOP modified rhodium catalysts gives higher l:b ratios in the hydroformylation of allyl alcohol. The catalyst system fits so called type II kinetics as defined<sup>58</sup> by van Leeuwen and Claver (see Equation 2.1). For type II kinetics, the acylrhodium complex species is the resting state of the catalyst system, and its reaction with hydrogen is the rate-determining step. This type of kinetics is rare; most systems, e.g. TPP / rhodium catalyst systems, obey type I kinetics, see Equation 2.2. In such systems, the resting state of the catalyst is the hydride complex  $[\text{RhH}(\text{PPh}_3)_2(\text{CO})_2]$  and the rate determining step is the addition of the alkene to the 4-coordinate  $[\text{RhH}(\text{PPh}_3)_2(\text{CO})]$  or the migration of the rhodium hydride onto the coordinated alkene. Later kinetic studies of the hydroformylation of allyl alcohol with the DIOP rhodium catalytic system are described, in section Scheme 2.2. These show that the rate of reaction does increase with increasing hydrogen partial pressure and decrease with increasing carbon monoxide partial pressure. Further work would be required, however, to fully understand the rate equation and confirm the DIOP rhodium system obeys type II kinetics, but it seems probable.

### Equation 2.1

$$\text{Rate (typeII)} = \frac{A[\text{H}_2][\text{Rh}]}{B + [\text{CO}]}$$

### Equation 2.2

$$\text{Rate (typeI)} = \frac{C[\text{alkene}][\text{Rh}]}{D + [L]}$$

*A, B, C, and D are constants (they do not refer to any specific rate constant) and [L] is proportional to  $[\text{PPh}_3]$  and  $[\text{CO}]$ .*<sup>58</sup>

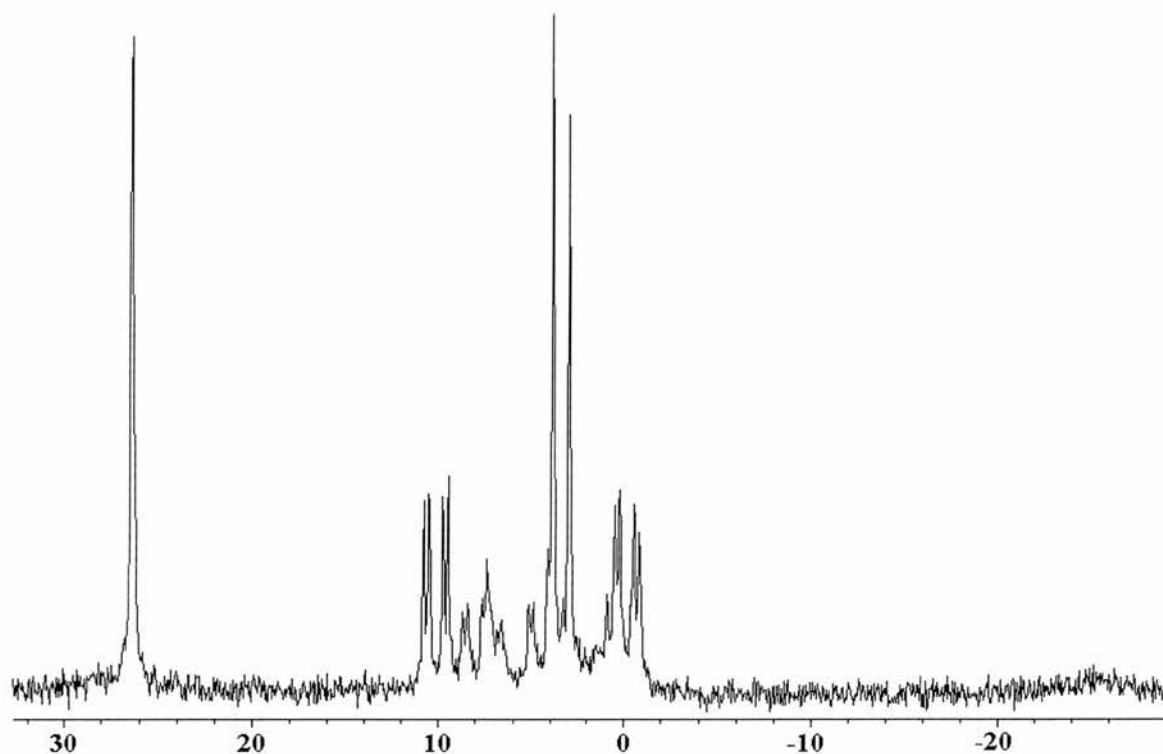
On heating to 80 °C, the working temperature of the system, these species are still observed (see NMR 2.29), but are no longer the major species present; a doublet at ~8.5 ppm becomes the dominant species present. Any excess DIOP in the system is also converted to (DIOP)O<sub>2</sub> by oxygen presumably introduced in the preparation.

On cooling to 25 °C, the doublet is reduced in intensity and the two sets of double doublets assigned to the acyl rhodium complex species **49** and **51** become dominant again, see NMR 2.30.

It is important to note at this stage that the gas volume in the HP NMR cell is very small (~0.5 cm<sup>3</sup>) in these studies, and that there are no detectable products from the hydroformylation reaction (by g.l.c. analysis). It is believed that the gas in the cell is quickly exhausted on heating as the temperature becomes favourable for the hydroformylation reaction to occur, and the reaction therefore runs out of CO and H<sub>2</sub> and becomes trapped somewhere in the cycle, see Scheme 2.2.

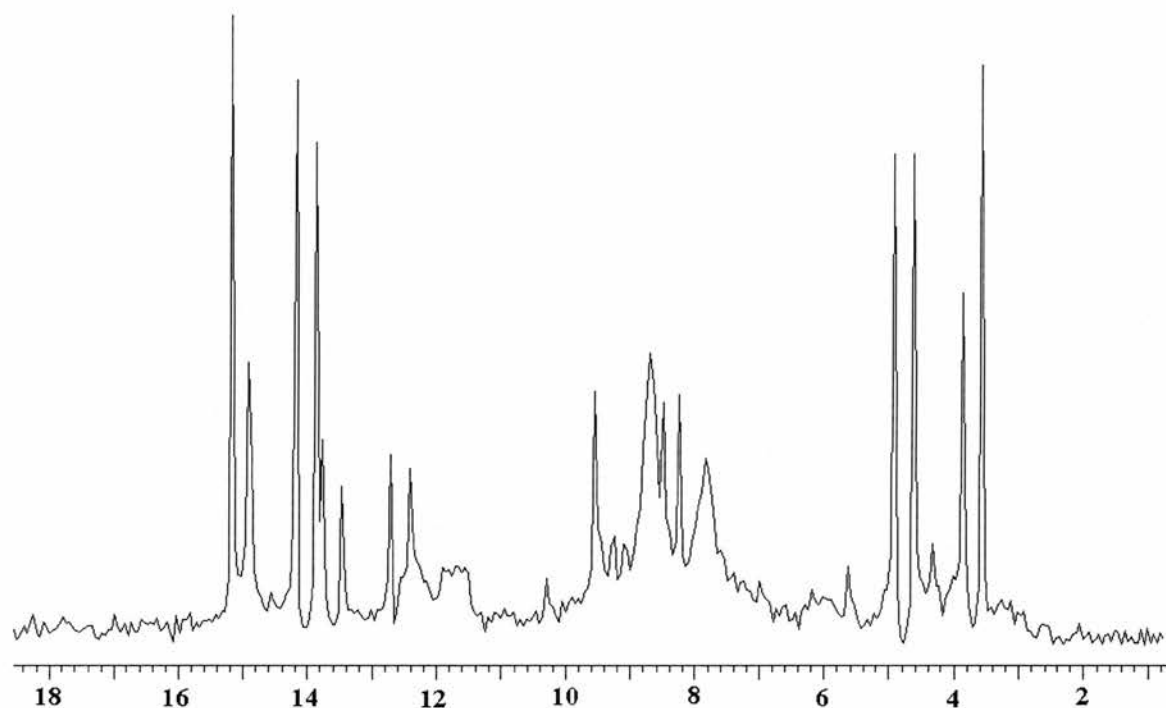
### NMR 2.29

*<sup>31</sup>P{<sup>1</sup>H} NMR spectrum of Rh(CO)<sub>2</sub>(acac) / DIOP 1:1.5 & allyl alcohol under 20 bar synthesis gas at 80 °C.*



**NMR 2.30**

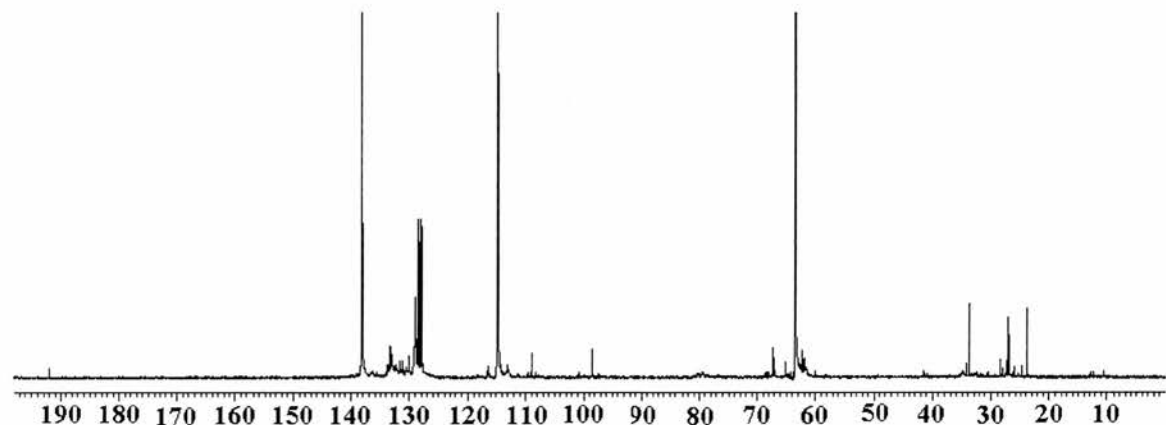
*<sup>31</sup>P{<sup>1</sup>H} NMR spectrum of Rh(CO)<sub>2</sub>(acac) / DIOP 1:1.5 & allyl alcohol under 20 bar synthesis gas cooled to 25 °C.*



The <sup>13</sup>C NMR spectrum of the complex species present at 25 °C before heating can be seen in NMR 2.31. The singlets at 137, 115 and 65 ppm are from allyl alcohol, the studies so far have used excess allyl alcohol. There are several resonances of weak intensity, one close to 190 ppm where carbonyl resonances would be expected.

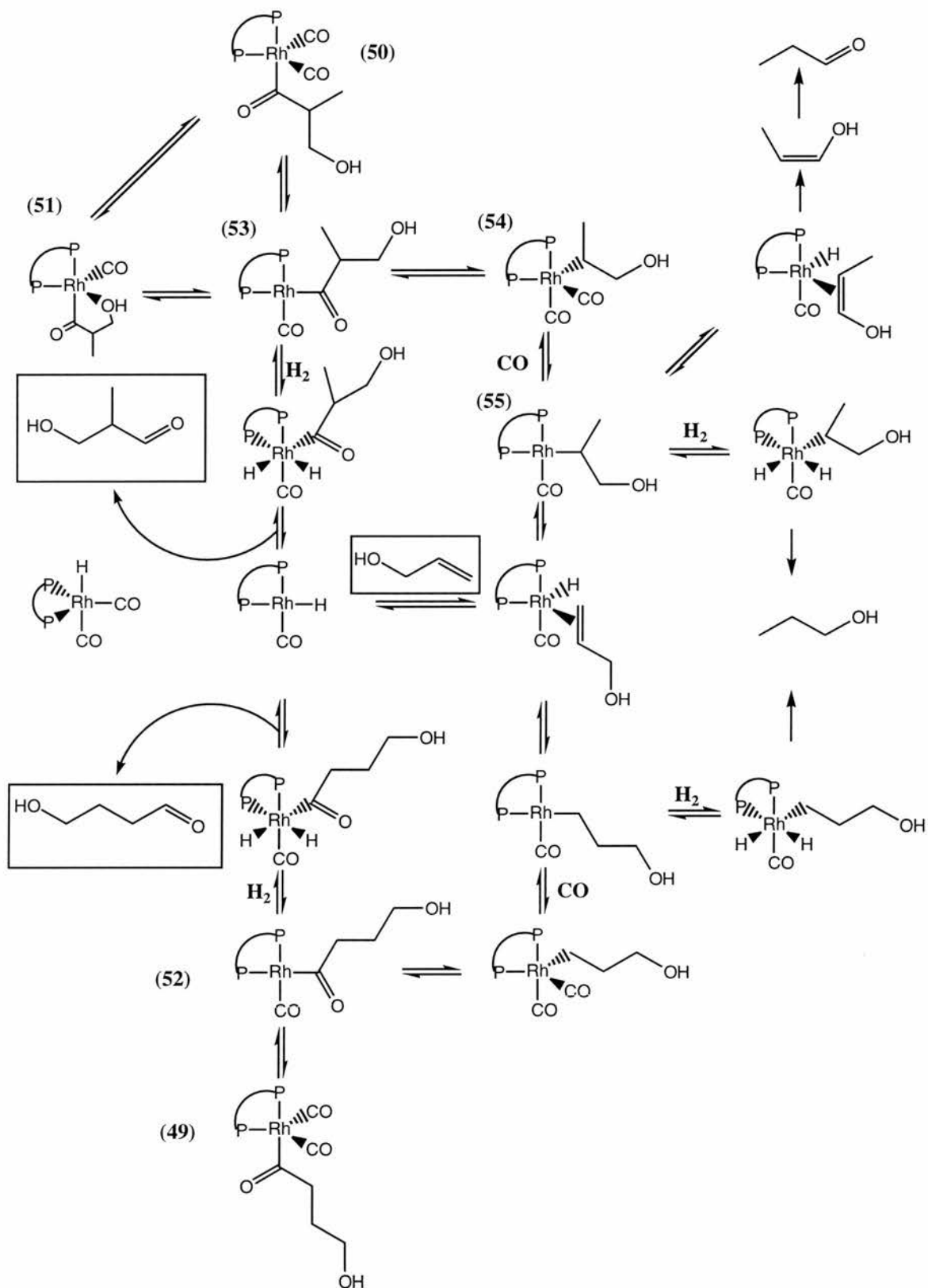
**NMR 2.31**

*<sup>13</sup>C spectra of Rh(CO)<sub>2</sub>(acac) / DIOP 1:1.5 & allyl alcohol under 20 bar synthesis gas at 25 °C.*



## Scheme 2.2

*Proposed Mechanism for the Hydroformylation of Allyl Alcohol with the Rhodium-DIOP Catalytic System*



### 2.5.2 Increasing the HP NMR Cell Size.

The gas volume and the area of the gas/ liquid interface are of concern when considering if a true picture of events is being observed in the NMR cell, or whether the results are distorted because of these limiting factors. In the kinetic measurement experiments (see later) the reaction is stirred to maximise the gas/ liquid interface, so gas diffusion into the liquid phase is not the rate determining step. The pressure of the autoclave is kept constant, so the gas supply never runs out and the reaction will run to completion, but this is not possible in the NMR cell, see section 6.3. By increasing the diameter (from 3 mm ID to 8 mm ID), and length of the cell (from 78 mm to 94 mm), we are able to increase the volume by  $4.2 \text{ cm}^3$  (increase in length times increase in inner area) and the gas/ liquid interface by 7.1 times (increase in internal area) Also, it has already been pointed out that one of the advantages of the 10 mm cell over the 5 mm cell is that the experiment is done with the same amount of catalyst (0.1 mmol) but in a greater volume of solution  $2 \text{ cm}^3$  with respect to  $0.25 \text{ cm}^3$ .

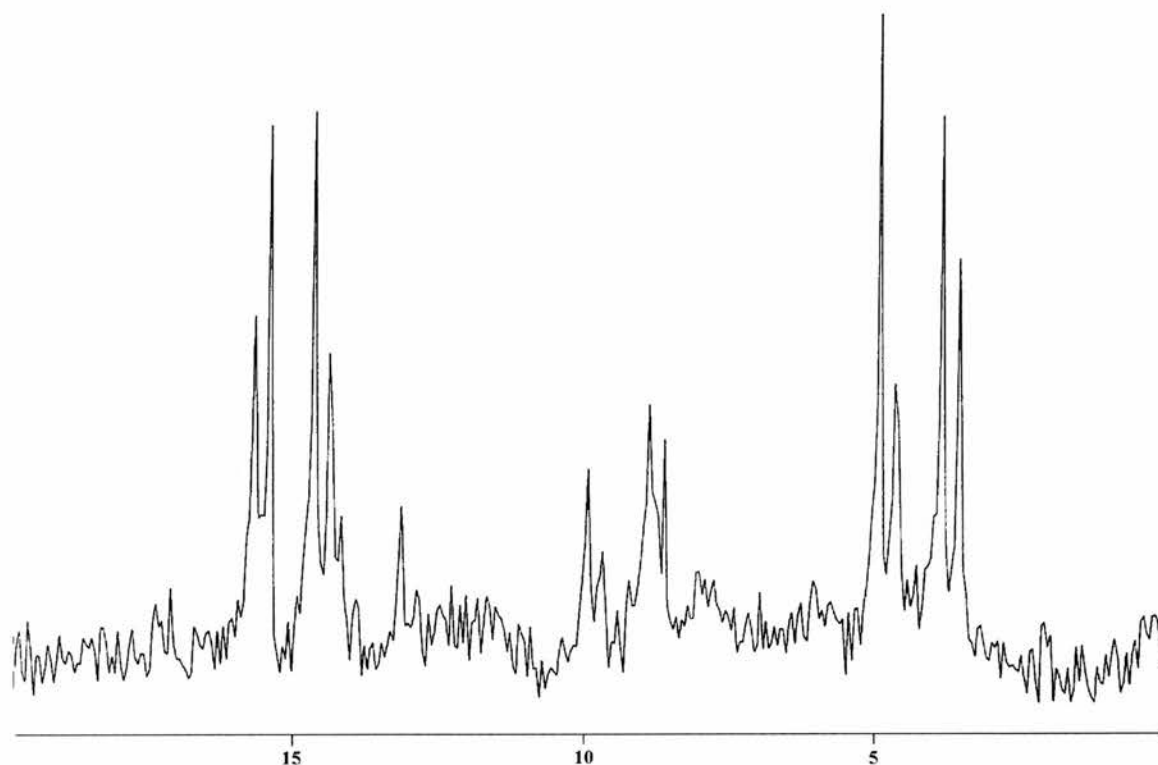
At  $25 \text{ }^\circ\text{C}$ , the  $^{31}\text{P}\{^1\text{H}\}$  NMR spectrum shows the two sets of double doublets at 15.25 ppm, 13.75 ppm and 9.5 ppm, 4.5 ppm corresponding to species **49** and **51**, see NMR 2.32. This is the same as observed in the smaller cell, see section 2.4.1.1. This is not surprising, as at  $25 \text{ }^\circ\text{C}$ , the solution is below the working temperature of the reaction ( $60\text{-}80 \text{ }^\circ\text{C}$ ) so the gas phase should not be reacting with the liquid phase, and you would expect both spectra to be the same.

The  $^{31}\text{P}\{^1\text{H}\}$  NMR spectra NMR 2.33- NMR 2.35, show the continuing development of the spectra with time at  $70 \text{ }^\circ\text{C}$ . NMR 2.33 shows the first recorded spectrum after 5 minutes at  $70 \text{ }^\circ\text{C}$ . It can be seen that the predominant species exhibits a doublet at 8.4 ppm with  $^1J_{\text{P-Rh}} = 110 \text{ Hz}$ . Species **49** and **51** are also present but in very low concentration. The dimer species **46** (5.3 ppm,  $^1J_{\text{P-Rh}} = 150 \text{ Hz}$ ) is also present at low concentrations.

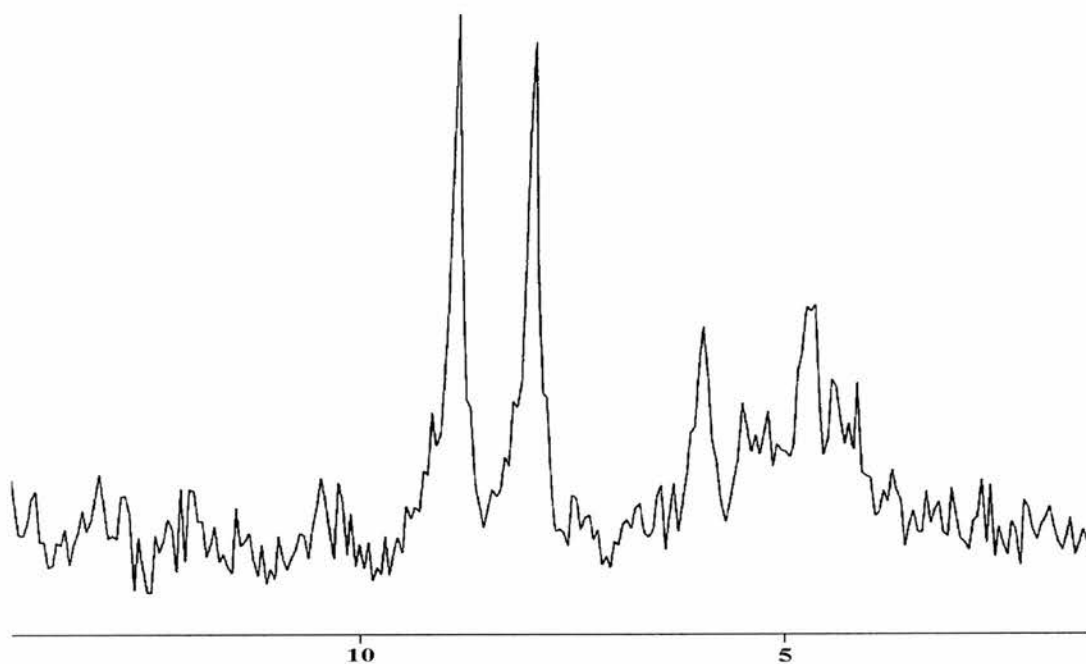
NMR 2.34 shows the second recorded spectrum after 10 minutes at  $70 \text{ }^\circ\text{C}$ . This shows a rise in the concentration of the species **49** and **51** with respect to the uncharacterised doublet and the dimer species **46**.

**NMR 2.32**

*$^{31}\text{P}\{^1\text{H}\}$  NMR spectrum of  $\text{Rh}(\text{CO})_2(\text{acac}) / \text{DIOP}$  1:1.5 & allyl alcohol under 20 bar synthesis gas at 25 °C, in the 10 mm cell.*

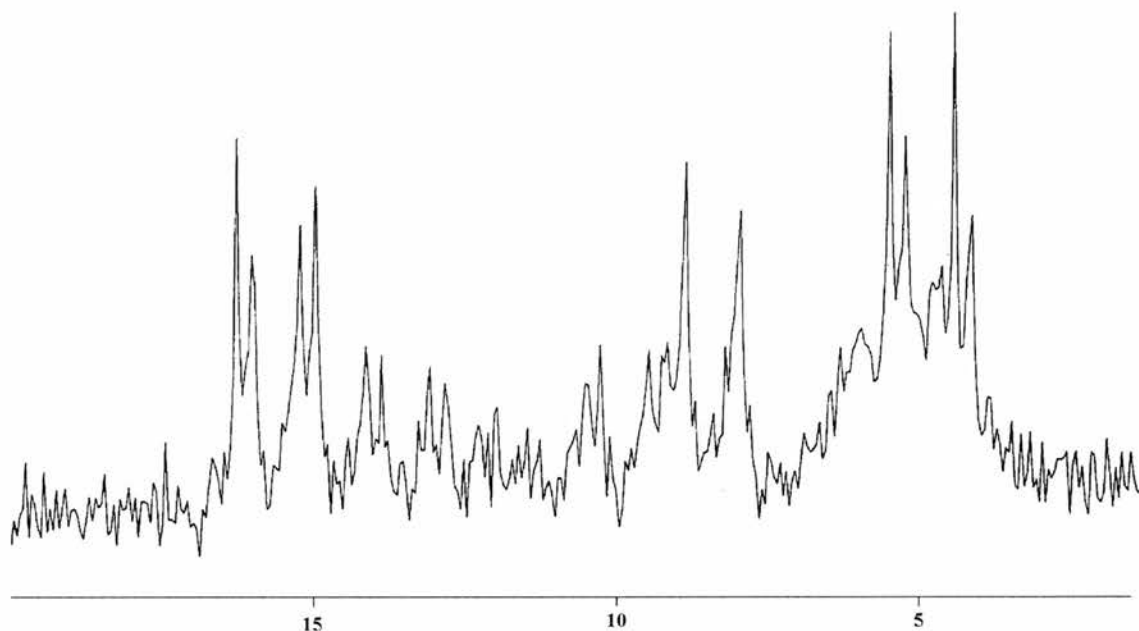
**NMR 2.33**

*$^{31}\text{P}\{^1\text{H}\}$  NMR spectrum of  $\text{Rh}(\text{CO})_2(\text{acac}) / \text{DIOP}$  1:1.5 & allyl alcohol under 20 bar synthesis gas at 70 °C after 5 minutes, in the 10 mm cell.*



**NMR 2.34**

*$^{31}\text{P}\{^1\text{H}\}$  NMR spectrum of  $\text{Rh}(\text{CO})_2(\text{acac}) / \text{DIOP}$  1:1.5 & allyl alcohol under 20 bar synthesis gas at 70 °C after 10 minutes, in the 10 mm cell.*

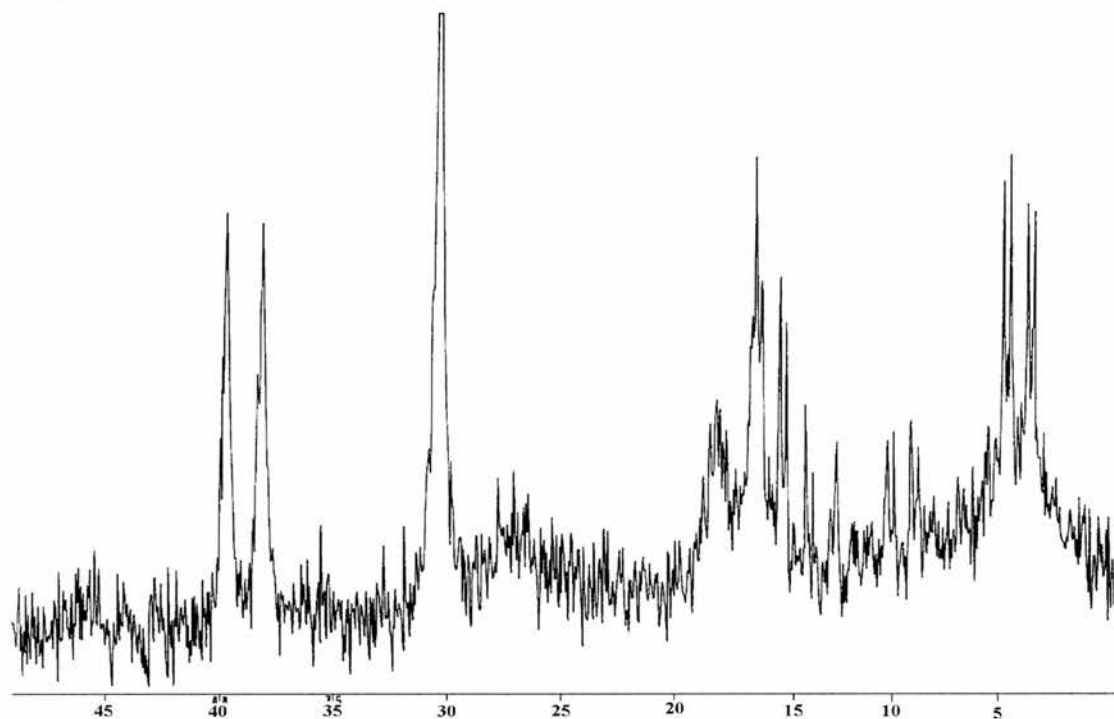


The spectra NMR 2.33 and NMR 2.34 represent the continuing development of an NMR acquisition with time. NMR 2.35 shows the third recorded spectrum at 70 °C, in this case the previous acquisition was stopped and a new one started. The spectrum is the same 30 minutes after the sample was heated to 70 °C as it was 15 minutes after the sample was heated to 70 °C. The reaction has therefore gone to completion at least 15 minutes after heating to 70 °C. In fact, it had probably gone to completion (the gas supply exhausted) before the first acquisition was stopped. The spectrum shows the presence of species **49** and **51**, the dimer species **46** and the species **41** found under an inert atmosphere (38.76 ppm,  $^1J_{\text{P-Rh}} = 190$  Hz), see section 2.2.1.

The  $^{31}\text{P}\{^1\text{H}\}$  NMR spectrum after the cell has been cooled back down to 25 °C shows the same species present as in NMR 2.35. Species **49** and **51**, species **41**, the dimer species **46** and a doublet in the region expected for  $[\text{RhH}(\text{CO})_2(\text{DIOP})]$  first thought to be the hydride **24** and **25**. However, it has a larger coupling constant of  $^1J_{\text{P-Rh}} = 180$  Hz not  $^1J_{\text{P-Rh}} = 120$  Hz as observed for the hydride complex species. The spectrum also has a large peak at 31 ppm which arises from the protonated DIOP oxide  $[(\text{DIOP}(\text{OH})_2)^{2+}]$ .

**NMR 2.35**

*<sup>31</sup>P{<sup>1</sup>H} NMR spectra of Rh(CO)<sub>2</sub>(acac) / DIOP 1:1.5 & allyl alcohol under 20 bar synthesis gas at 70 °C after 15 minutes, in the 10 mm cell.*



The <sup>31</sup>P{<sup>1</sup>H} NMR spectrum after the cell was opened shows that all the species present after cooling whilst still under pressure are still present.

GC analysis of the reaction solution showed products of the hydroformylation of allyl alcohol, both the linear 4-hydroxybutanal and the branched 3-hydroxy-2-methylpropanal. It also showed the reactant allyl alcohol is still present. In other words, the conversion of the hydroformylation reaction was gas limited as it was previously, and not substrate limited as the true case would be.

It was worked out using the ideal gas equation ( $pV = nRT$ ,  $R = 8.31451 \text{ pa m}^3 \text{ K}^{-1}$ ) that at 20 bar ( $2 \times 10^6 \text{ pa}$ ) of gas in a volume of  $3.2 \times 10^{-6} \text{ m}^3$  (volume of cell minus volume of catalyst solution), at 25 °C (298 K) there are  $2.58 \times 10^{-3}$  moles of gas present. This means there are  $1.29 \times 10^{-3}$  moles of CO and  $1.29 \times 10^{-3}$  moles of H<sub>2</sub> present. In the catalyst solution, there is  $0.3 \text{ cm}^3$  or  $4.41 \times 10^{-3}$  moles of allyl alcohol. This means there is a 3.4 fold excess of allyl alcohol to CO and H<sub>2</sub>.

The reaction was designed this way to have the longest window possible to look at the species present during the reaction itself, in an attempt to identify them. However, it is also important to look at what species are present at the end of reaction in the “true”

case when the reaction is substrate limited not gas limited. The experiment was, therefore, repeated with  $0.1 \text{ cm}^3$  or  $1.47 \times 10^{-3}$  moles of allyl alcohol, and 40 bar of gas or  $2.58 \times 10^{-3}$  moles of CO and  $2.58 \times 10^{-3}$  moles of  $\text{H}_2$ . This means you have a 1.8 fold excess of CO and  $\text{H}_2$  over allyl alcohol.

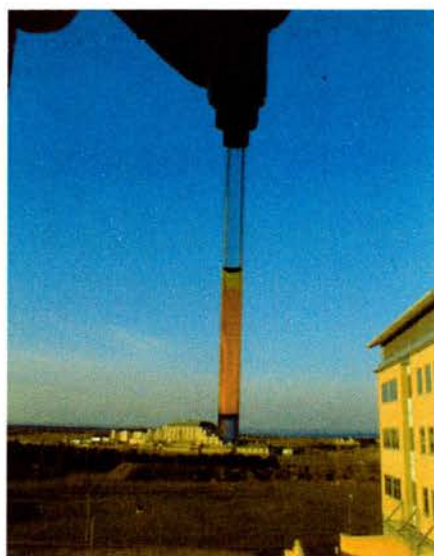
At  $25^\circ\text{C}$ , the  $^{31}\text{P}\{^1\text{H}\}$  NMR spectrum shows the two sets of double doublets at 15.25 ppm, 13.75 ppm and 9.5 ppm, 4.5 ppm corresponding to species **49** and species **51** ( $^1J_{\text{PRh}}=125 \text{ Hz}$ ,  $^2J_{\text{PP}}=33 \text{ Hz}$ , and  $^1J_{\text{PRh}}=129 \text{ Hz}$ ,  $^2J_{\text{PP}}=33 \text{ Hz}$ ). On heating, the disappearance of the double doublet resonances and the appearance of a short lived doublet resonance at 8.4 ppm ( $^1J_{\text{PRh}}=109 \text{ Hz}$ ) is observed. By the time the cell is at  $70^\circ\text{C}$ , the doublet has disappeared and the only species present are the rhodium hydride, **24** and **25**, at 17.8 ppm ( $^1J_{\text{PRh}}=120 \text{ Hz}$ ) and the rhodium dimer, **46**, at 5.3 ppm ( $^1J_{\text{PRh}}=160 \text{ Hz}$ ). When cooled to  $25^\circ\text{C}$ , the  $^{31}\text{P}\{^1\text{H}\}$  NMR spectrum shows the presence of rhodium hydride, **24** and **25**, and, **46**. The presence of  $[\text{Rh}(\text{DIOP})(\text{acac})]$ , and other intermediates, after the reaction is over, when substrate was present in excess suggests the high reactivity of the system which utilises as much gas as possible, even that which is ligand to rhodium.

From these results we can say that initially (in the first 5 minutes) during the hydroformylation reaction in the HP NMR cell a new uncharacterised species is formed with a doublet at 8.4 ppm  $^1J_{\text{P-Rh}}=109 \text{ Hz}$  in the  $^{31}\text{P}\{^1\text{H}\}$  NMR. By the time the next spectrum was taken the reaction has slowed down, see kinetic data in section 2.4.4, and other complex species, **49**, **51**, and **46** begin to form. Initially it is probable that the species corresponding to the doublet at 8.4 ppm is the only rhodium DIOP complex species present in solution, and that this is the predominant species present during the hydroformylation reaction when both substrate and gasses are readily available. It was noted that the resonance has a similar chemical shift to a complex species observed in section 2.3.2, speculated to be a mono phosphine rhodium complex where there are low concentrations of DIOP present. The  $^1J_{\text{P-Rh}}$  coupling constant for the hydroformylation intermediate is 110 Hz compared to 152 Hz in the complex observed previously in section 2.3.2.

These results give us a greater understanding of the species present during the different stages of the hydroformylation reaction than those obtained from the 5 mm cell. The gas / liquid interface is an important consideration when studying this type of system. Factors such as temperature, and pressure, alter the time it takes for gas diffusion over the gas / liquid interface. Figure 2.22 shows a rhodium diphosphine complex in

solution which was prepared under argon, and has been held open to synthesis gas at 20 bar for one hour in the 5 mm HP NMR cell. It clearly shows two layers, the lower layer is orange and represents the complex species present in the absence of CO and H<sub>2</sub>. The upper layer is yellow and represents the complex species present after reaction with synthesis gas. From this it is clear that gas diffusion into the solution is very slow.

**Figure 2.22**



### 2.5.3 HP IR Studies of the Hydroformylation of Allyl Alcohol.

The HP IR results are important as they show a truer picture of what is happening during the reaction. Conditions are such that the hydroformylation reaction can be studied over longer periods of time, and to completion without danger of gas starvation. The reaction mixture is also stirred with a mechanical stirrer.

The HP FTIR spectrum of the hydroformylation of allyl alcohol can be seen in IR 2.12. At 25 °C, the IR spectrum is very similar to when there is no substrate present, the dimer exhibits  $\nu_{\text{CO}}$  absorption bands at 1984  $\text{cm}^{-1}$  and 1744  $\text{cm}^{-1}$  and the hydride exhibits an absorption at 1948  $\text{cm}^{-1}$ . On heating to 40 °C, the dimer  $\nu_{\text{CO}}$  band at 1745  $\text{cm}^{-1}$  disappears, but the  $\nu_{\text{CO}}$  band at 1987  $\text{cm}^{-1}$  is still present in the spectrum. Also, the  $\nu_{\text{CO}}$  band at 1948  $\text{cm}^{-1}$  becomes very strong relative to the other  $\nu_{\text{CO}}$  bands, but we do not see the emergence of the  $\nu_{\text{CO}}$  bands at 2030, 1990, and 1980  $\text{cm}^{-1}$  which should accompany the  $\nu_{\text{CO}}$  band at 1948  $\text{cm}^{-1}$  if it belonged to the rhodium hydride species, **24** and **25**. It is therefore proposed that the  $\nu_{\text{CO}}$  bands at 1986  $\text{cm}^{-1}$  and

1948  $\text{cm}^{-1}$  in the spectrum at 40 °C are from two of the bands of the acyl rhodium complex species, **49** and **51**, and that these are the only complex species present at this temperature. It is also proposed that at 25 °C the dimer rhodium complex species, **46**, and the acyl rhodium complex species, **49** and **51** are present. It is noted that the acyl rhodium complex species, **49** and **51**, should have six  $\nu_{\text{CO}}$  bands between them. These are the four terminal rhodium carbonyl  $\nu_{\text{CO}}$  bands, the symmetric and antisymmetric  $\nu_{\text{CO}}$  bands of the two complexes, from the complexed CO, and the acyl  $\nu_{\text{CO}}$  bands from the two complexes. The band at 1642  $\text{cm}^{-1}$  is from the substrate allyl alcohol, which gave a band at 1646  $\text{cm}^{-1}$  in the IR spectrum of a 1:9 solution in toluene. Although we have reported the existence of only two of the terminal  $\nu_{\text{CO}}$  bands, it is clear from the spectrum that there are shoulders either side of the  $\nu_{\text{CO}}$  band at 1986  $\text{cm}^{-1}$  which could account for the other two.

On heating to 70 °C, the  $\nu_{\text{CO}}$  bands at 1986  $\text{cm}^{-1}$  and 191948  $\text{cm}^{-1}$  are still present as well as those possibly due to the acyl rhodium  $\nu_{\text{CO}}$  band at 1642  $\text{cm}^{-1}$  and 1630  $\text{cm}^{-1}$ . There are two interesting changes though. The shoulders on the  $\nu_{\text{CO}}$  band at 1986  $\text{cm}^{-1}$  are more visible and there is a new  $\nu_{\text{CO}}$  band at 1727  $\text{cm}^{-1}$ , which is from the products of the reaction. At 70 °C, the  $\nu_{\text{CO}}$  bands now assigned to the acyl rhodium complex species, **49** and **51** begin to disappear, and the spectrum in the 1900  $\text{cm}^{-1}$  to 2000  $\text{cm}^{-1}$  region is complicated due to many overlapping  $\nu_{\text{CO}}$  bands. At 80 °C, the spectrum shows none of the known  $\nu_{\text{CO}}$  bands assigned to previously observed complexes. It does show a broad  $\nu_{\text{CO}}$  band at 1980  $\text{cm}^{-1}$  and a band of low intensity at 1949  $\text{cm}^{-1}$ . It is possible to speculate that these bands could belong to the new complex species observed under hydroformylation conditions in the *in situ*  $^{31}\text{P}\{^1\text{H}\}$  NMR experiments under hydroformylation conditions, (8.4 ppm  $^1J_{\text{PRh}} = 109$  Hz).

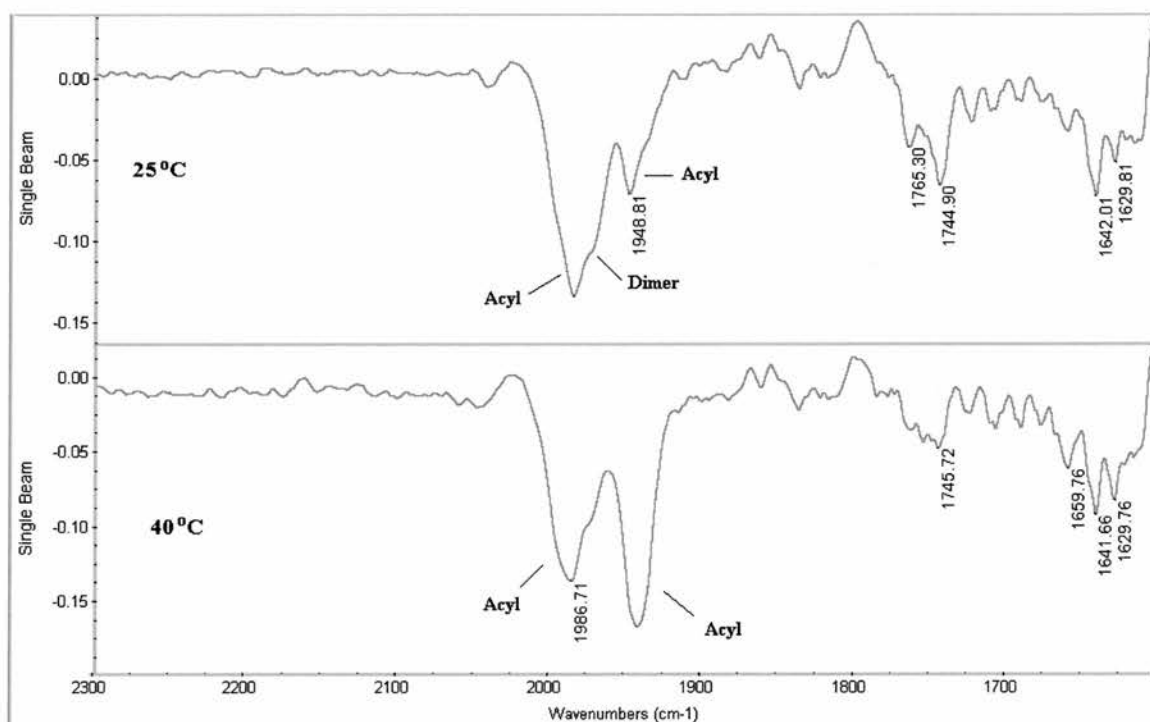
The band of low intensity at 1949  $\text{cm}^{-1}$  is possibly a  $\nu_{\text{RhH}}$  band from the complex. It would be interesting to observe the spectrum under a CO and D<sub>2</sub> atmosphere as the band at 1949  $\text{cm}^{-1}$  would shift to a frequency  $1/\sqrt{2}$  to that of  $\nu_{\text{Rh-H}}$  band. If it does we can speculate that the complex species contains both a rhodium carbon monoxide bond and a rhodium hydrogen bond.

After the reaction has been at 80 °C for two hours, the spectrum exhibits  $\nu_{\text{CO}}$  bands at 1985  $\text{cm}^{-1}$  and 1948  $\text{cm}^{-1}$ . The band at 1985  $\text{cm}^{-1}$  also has several shoulders. These look like the bands assigned to the rhodium dimer complex species, **46**, and the rhodium hydride complex species, **24** and **25**. It is noted that the relative intensity of the hydride

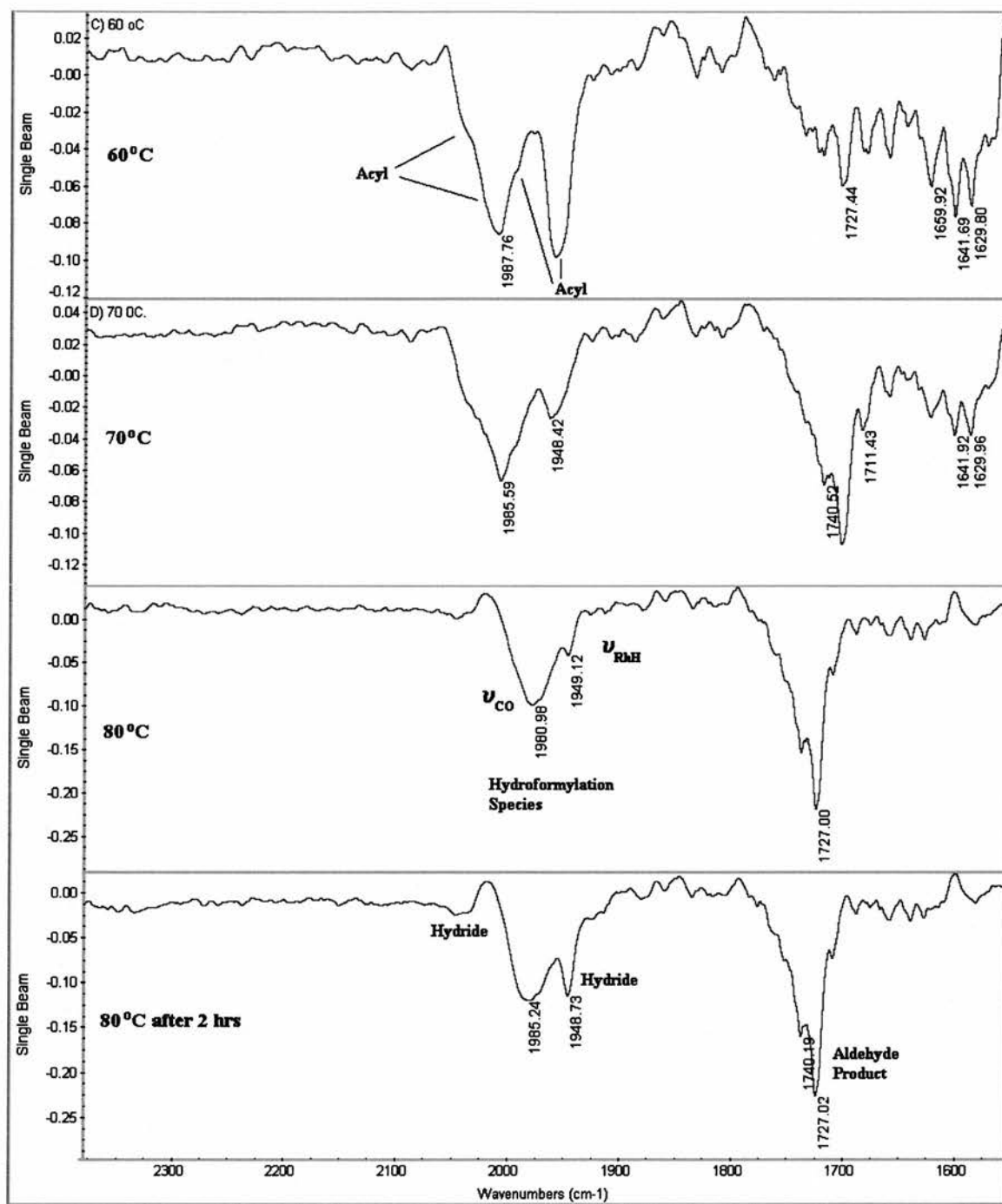
$\nu_{\text{CO}}$  bands with respect to the dimer  $\nu_{\text{CO}}$  bands is not as high as one might expect. The pressure in the HP CIR FTIR autoclave at the end of reaction was about 3 bar. It has already been observed in section 2.4.4 that there is a slight reduction in the proportion of the hydride produced under lower pressures. The conclusion, therefore, is that the reaction is finished and the complex species present at the end of reaction are the rhodium hydride, **24** and **25**, and the rhodium dimer, **46**. This is in agreement with the HP NMR results in section 2.5.2.

## IR 2.12

*In-situ infrared spectra of the hydroformylation of allyl alcohol.*



IR 2.12 continued.

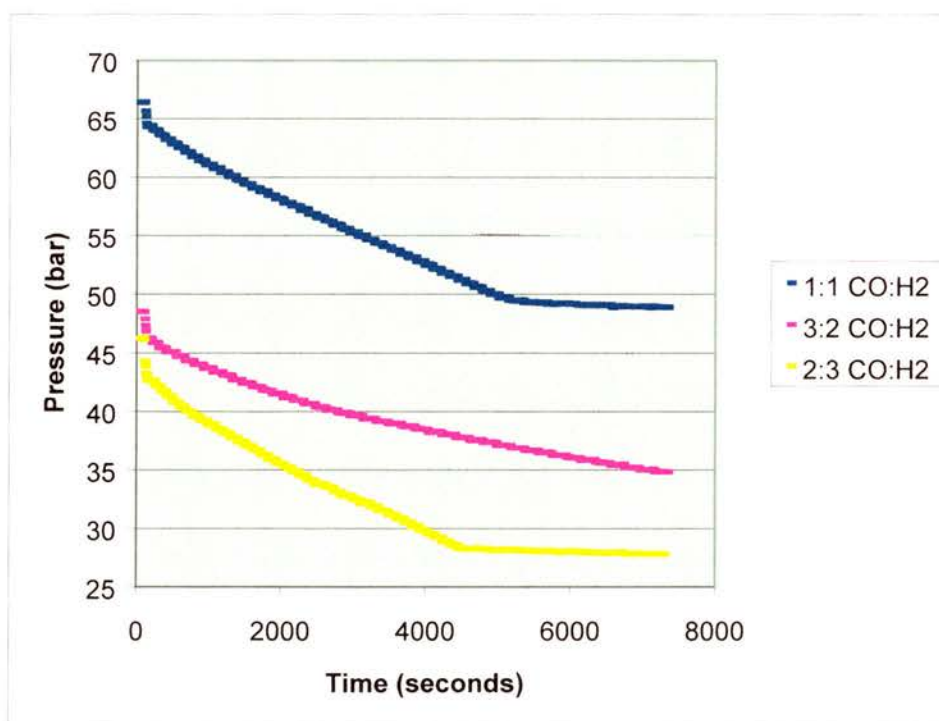


### 2.5.4 Kinetic Studies of the Hydroformylation of Allyl Alcohol.

The hydroformylation of allyl alcohol with the rhodium DIOP catalytic system was carried out at 70 °C, under a constant pressure of 8 bar CO and H<sub>2</sub>, with a rhodium concentration of 200 ppm and a rhodium: diphosphine ratio of 1:1.5. The reaction was kept at constant pressure by replenishing the reacted CO and H<sub>2</sub> from a ballast vessel. The reaction was monitored over the reaction period by measuring the gas uptake from the ballast vessel. The effect on the rate of reaction of the partial pressures of CO and H<sub>2</sub> was observed by using CO:H<sub>2</sub> gas ratios of 1:1, 3:2, and 2:3. The gas uptake from the ballast vessel, representing the gas uptake of the reaction can be seen in Graph 2.2.

#### Graph 2.2

*The Rate Profile of the Hydroformylation Reaction of Allyl Alcohol under Various CO to H<sub>2</sub> Ratios*



#### 2.5.4.1 CO to H<sub>2</sub> Ratio 1:1.

The rate profile for CO: H<sub>2</sub> = 1:1 shows zero order kinetics with respect to substrate over almost the whole reaction, although there is slight curvature over the first half of the profile. The reaction is shown to be complete after 90 minutes and g.l.c results show

a high selectivity towards the linear aldehyde, l:b ratio = 5.5:1, and low levels of by-products.

#### 2.5.4.2 CO to H<sub>2</sub> Ratio 2:3

The rate profile for CO:H<sub>2</sub> = 2:3 is very similar to the profile for CO:H<sub>2</sub> = 1:1. However, the rate is slightly faster, the reaction is finished after a shorter amount of time, 75 minutes, and there is a smaller overall pressure drop from the ballast vessel. The results from g.l.c. analysis still show a high l:b ratio, 5.4:1, however, in this case, there are significant levels of by-products (propanal and propanol) from the reaction.

#### 2.5.4.3 CO to H<sub>2</sub> Ratio 3:2.

The rate profile for CO:H<sub>2</sub> = 3:2 shows a much greater degree of curvature and a much slower rate of reaction. After two hours, the reaction is still incomplete. The g.l.c. results confirm the reaction is not complete, although the l:b ratio is still high, 5.6:1, and there are low levels of propanal and propanol produced.

#### 2.5.4.4 Conclusions.

The slight curvature in the rate profiles, over approximately the first 50 % of the reaction time scale, is an indication that the rate is > zero order over this period. It has also been observed in the hydroformylation reaction that the l:b ratio is better at lower allyl alcohol concentrations. This suggests that product built up may inhibit the reaction slightly and that this may favour the formation of the branched product.

It is also noted that an increase in the partial pressure of H<sub>2</sub> and therefore reducing that of CO, CO:H<sub>2</sub> = 2:3, increases the rate of reaction. This is to be expected as we have already suggested that the reaction follows type II kinetics where the oxidative addition of dihydrogen is the rate-determining step, see section 2.4.1. However, it is believed that this will also effect the positions of other equilibria in the proposed mechanistic cycle, especially those driven by CO addition, e.g. the equilibrium between [Rh(DIOP)(CO)(CHCH<sub>3</sub>CH<sub>2</sub>OH)] and [Rh(DIOP)(CO)(COCHCH<sub>3</sub>CH<sub>2</sub>OH)], complex species **54** and **53**, in Scheme 2.2 on page 122, and their linear analogues, [Rh(DIOP)(CO)(CH<sub>2</sub>CH<sub>2</sub>CH<sub>2</sub>OH)] and [Rh(DIOP)(CO)(COCH<sub>2</sub>CH<sub>2</sub>CH<sub>2</sub>OH)], complex species **55** and **52** respectively in Scheme 2.2.

If the equilibrium is shifted towards species **54** or **55** away from CO insertion, the complex species **54** will be more likely to undergo  $\beta$ -hydrogen elimination leading to greater amounts of the isomerisation product, propanal. Attack of dihydrogen on species **54** and **55** could lead to greater amounts of the hydrogenation product, propanol as observed in the reaction.

An increase in the partial pressure of CO and, therefore, a decrease in that of H<sub>2</sub> will decrease the rate of reaction, since dihydrogen addition is the rate determining step. However, there is also an observed greater rate order, of <1, with respect to allyl alcohol, demonstrated in the greater curvature of the kinetic plot. It is proposed that the equilibrium between [RhH(CO)<sub>2</sub>(DIOP)] and [RhH(CO)(allyl alcohol)(DIOP)] in Scheme 2.2, is shifted from being completely towards alkene co-ordination, required for zero order kinetics when excess CO is present, because the rhodium becomes tied up as the rhodium hydride complex species, **24** and **25**.

## 2.6 *In-Situ* High Pressure Studies of the Hydroformylation of 1-Hexene.

The rhodium DIOP catalytic system has been shown to give high l:b ratios<sup>59</sup> for the hydroformylation of allyl alcohol with respect to the l:b ratios obtained when using the rhodium triphenylphosphine catalytic system.<sup>31</sup> However, when the rhodium DIOP catalytic system was used to catalyse the hydroformylation of 1-hexene, the marked increased l:b ratio over the rhodium triphenylphosphine system was not observed.<sup>59</sup> A study of the hydroformylation of 1-hexene was, therefore, initiated to investigate why this was the case.

### 2.6.1 HP NMR Studies of the Hydroformylation of 1-Hexene.

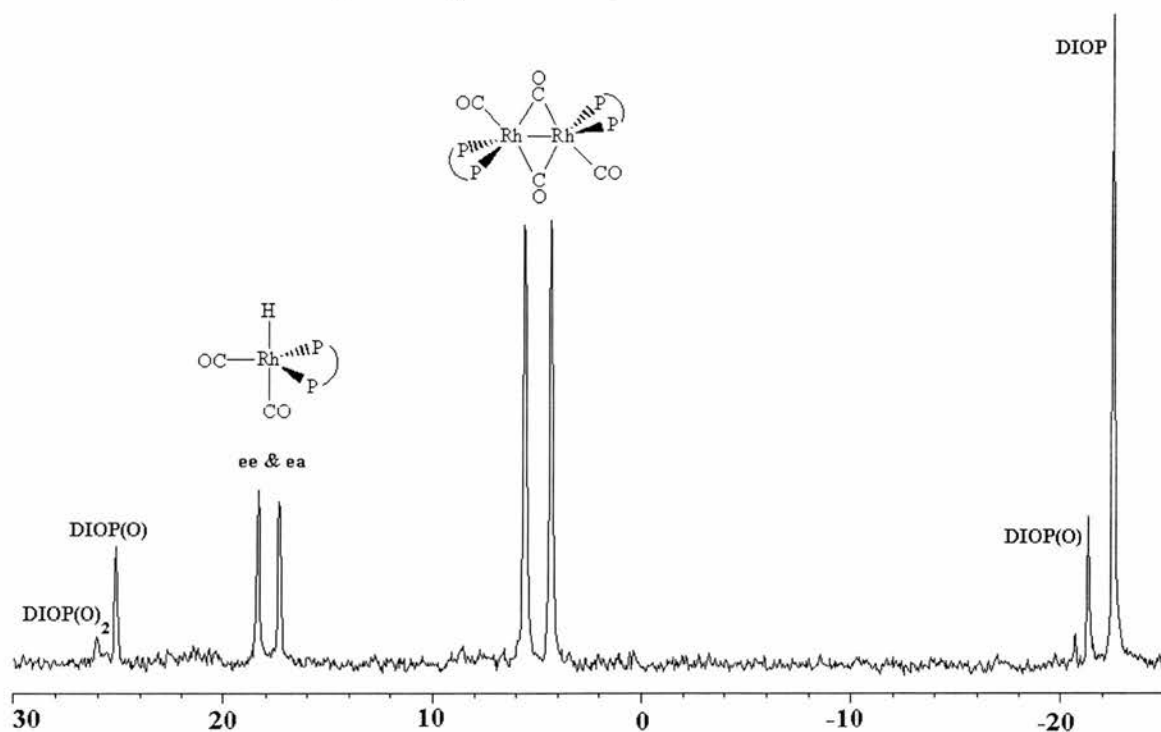
The results from the HP <sup>31</sup>P {<sup>1</sup>H} NMR study of the hydroformylation of 1-hexene can be seen in NMR 2.36-2.41. The studies were carried out in the 10 mm HP NMR cell. At 25 °C, see NMR 2.36, we see the presence of the dimeric complex **46** and the hydride complexes **24** and **25**. This is different from the allyl alcohol case, where the

acylrhodium species **49** and **51** are the only ones present at this stage. In fact, this is analogous to when there is no substrate present at all.

On heating to 40 °C, see NMR 2.37, the  $^{31}\text{P}\{^1\text{H}\}$  NMR spectrum shows a doublet at 8.25 ppm, with  $^1J_{\text{P-Rh}} = 110$  Hz. This is similar to a resonance observed in the HP NMR study of the hydroformylation of allyl alcohol with the DIOP-rhodium catalytic system where there is a doublet at 8.4 ppm with the same coupling constant of  $^1J_{\text{P-Rh}} = 110$  Hz. It could be that this is the same species, the different chemical shift being explained by what is effectively a different solvent system, toluene and hexene or toluene and allyl alcohol. If so, there would be no alkene (hexene or allyl alcohol) in the complex. Alternatively, the complexes could contain alkene and be analogous to each other, the identical coupling constants being a coincidence from the similarity of the complex species. However, unlike the allyl alcohol case, the dimer **46** and the hydride **49** and **51** are still present. This is important as in the allyl alcohol case it is believed the complex which has the doublet resonance in the  $^{31}\text{P}\{^1\text{H}\}$  NMR at  $\delta = 8.4$  ppm is the only present during the hydroformylation reaction, and this does not have to be the case here.

### NMR 2.36

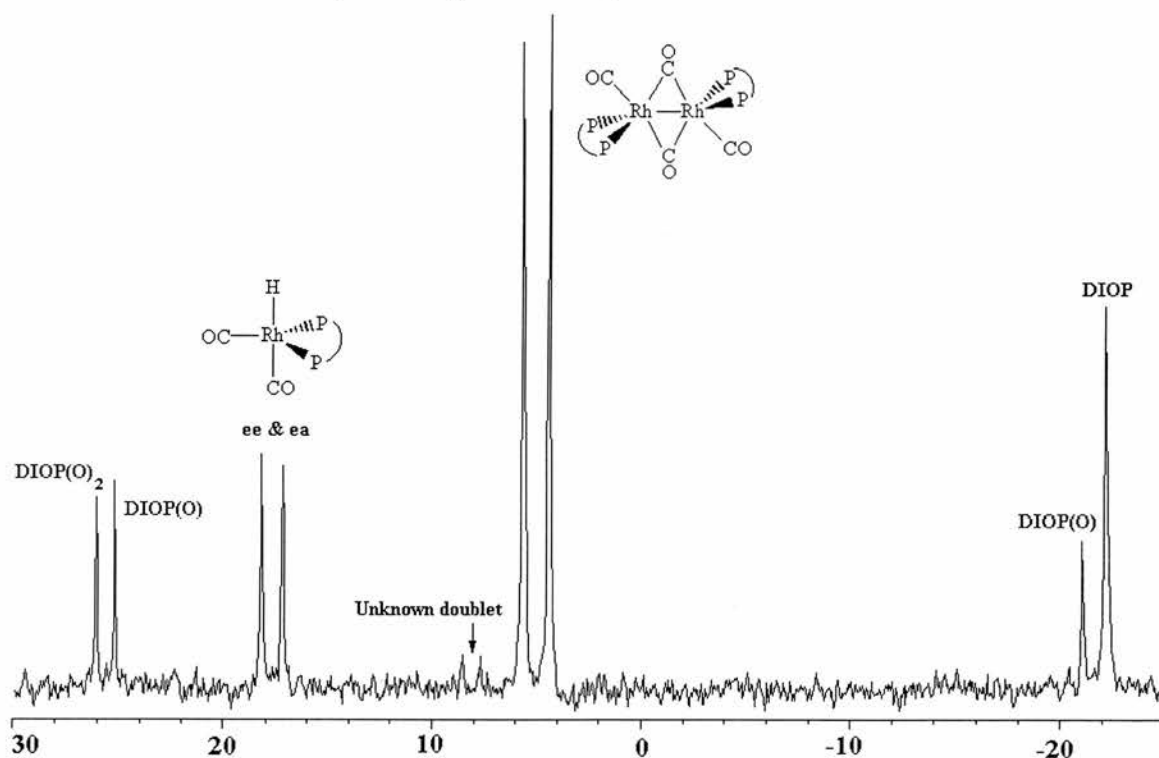
*$^{31}\text{P}\{^1\text{H}\}$  NMR spectrum of  $\text{Rh}(\text{CO})_2(\text{acac}) / \text{DIOP}$  1:1.5 & 1-hexene under 20 bar synthesis gas at 25 °C, in the 10 mm cell*



At 70 °C the hydride has completely disappeared leaving only the dimer and unknown species, see NMR 2.38. The two singlet resonances at -20 ppm are from DIOP and the non-oxidised phosphorus of DIOP mono-oxide, the two singlet resonances at 26 ppm are DIOP di-oxide and the oxidised phosphorus of DIOP mono-oxide. After 30 minutes at 70 °C, the spectrum is still the same; only the dimer and the unknown species are present. In the HP NMR study of the hydroformylation of allyl alcohol with the DIOP-rhodium catalytic system, the doublet resonance at 8.4 ppm was due to a short-lived species and was present only during the hydroformylation reaction itself. The kinetic study of the hydroformylation of 1-hexene with the rhodium DIOP catalytic system, see later in section 2.5.3, tells that as the reaction must have gone to completion, for the hydroformylation of 1-hexene the species is still present after hydroformylation has stopped.

### NMR 2.37

$^{31}\text{P}\{^1\text{H}\}$  NMR spectrum of  $\text{Rh}(\text{CO})_2(\text{acac}) / \text{DIOP}$  1:1.5 & 1-hexene under 20 bar synthesis gas at 40 °C, in the 10 mm cell.



On cooling, the unknown species disappears and the hydride species reappears, see NMR 2.39.

As in the HP NMR study of the hydroformylation of allyl alcohol with the DIOP-rhodium catalytic system, the substrate 1-hexene in this case was added in excess, there being  $1.29 \times 10^{-3}$  moles of CO and  $1.29 \times 10^{-3}$  moles of H<sub>2</sub> and 0.3 cm<sup>3</sup> or of 1-hexene. The reaction was designed this way to have the longest possible window possible to look at the species present during the reaction itself. However, as with allyl alcohol, it is important to look at the species that are present at the end of reaction in the “true” case when the reaction is substrate limited not gas limited. The experiment was therefore repeated with 0.1 cm<sup>-1</sup> or  $8.00 \times 10^{-4}$  moles of 1-hexene, and 40 bar of gas or  $2.58 \times 10^{-3}$  moles of CO and  $2.58 \times 10^{-3}$  moles of H<sub>2</sub>. This means there was a 3.2 fold excess of CO and H<sub>2</sub> over 1-hexene.

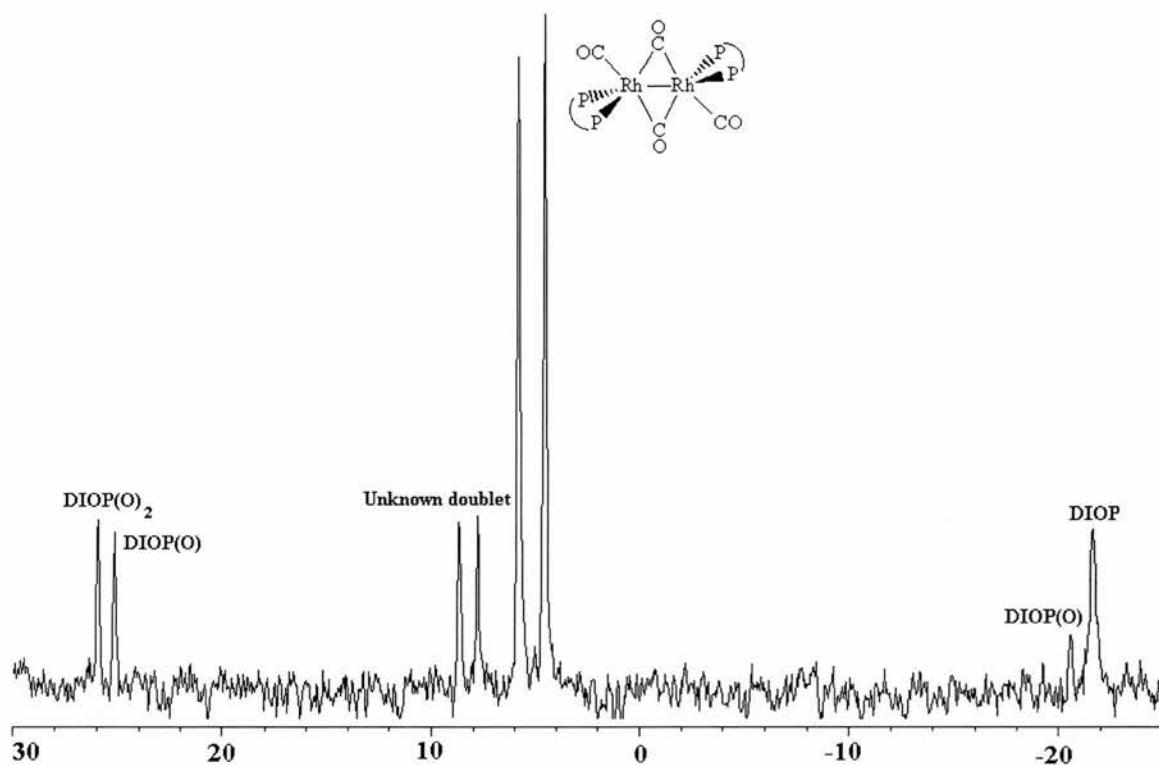
At 25 °C, we see the presence of the dimeric complex species, **46**, and the hydride complex species, **24** and **25**, the same complexes present with excess 1-hexene. Initially, at 70 °C, the hydride has completely disappeared leaving only the dimer and unknown species at 8.4 ppm with  $^1J_{PRh} = 110$  Hz; this is also the same as the case with excess 1-hexene. After 30 minutes, however, the unknown complex species at 8.4 ppm had disappeared and the hydride reappeared. On cooling, the dimer and the hydride were the only species present.

It is clear that there are similarities in the complexes present in the hydroformylation of 1-hexene and allyl alcohol, however there are a great many differences. It is necessary to identify the two complexes which give doublet resonances at 8.4 and 8.5 ppm in the  $^{31}P\{^1H\}$  HP NMR studies to see whether they are analogous to each other. It will also be necessary to fully characterise species **49** and **51**. These factors may give us an insight into where the two reactions differ.

From our conclusions so far, we believe species **49** and **51** to be the acylrhodium complexes of DIOP and allyl alcohol, and they are the resting state of the catalyst outside the catalytic cycle. However, for the hydroformylation of 1-hexene with the DIOP rhodium catalytic system, the resting states are the dimer and hydride complex species.

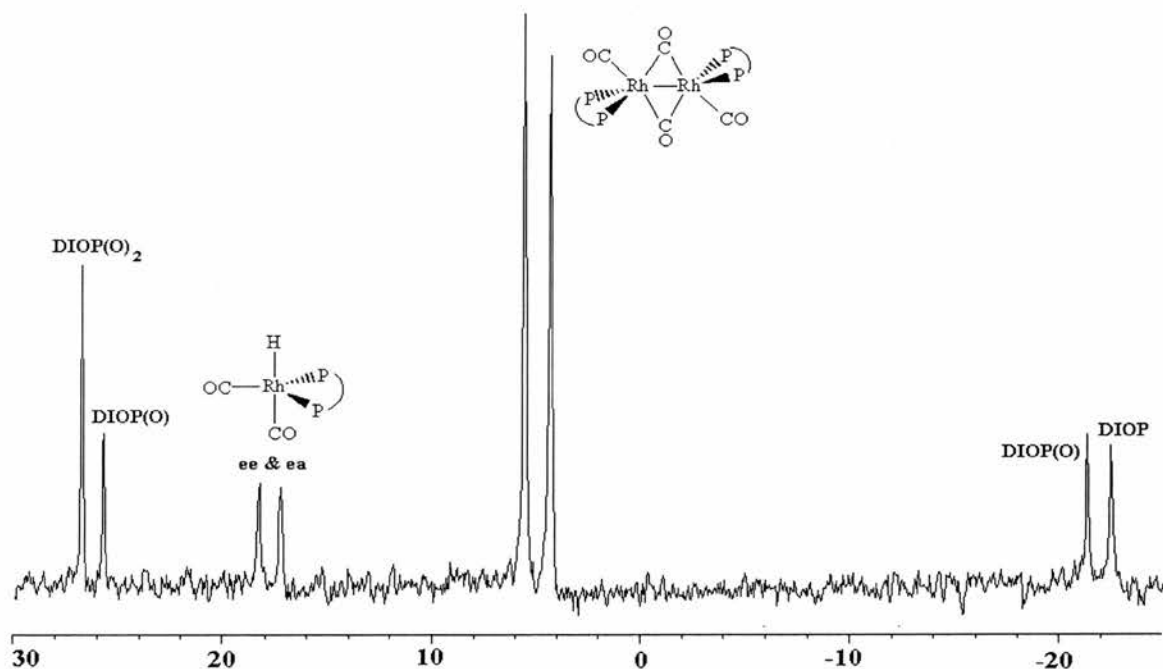
## NMR 2.38

$^{31}\text{P}\{^1\text{H}\}$  NMR spectrum of  $\text{Rh}(\text{CO})_2(\text{acac}) / \text{DIOP}$  1:1.5 & 1-hexene under 20 bar synthesis gas at 70 °C, in the 10 mm cell.



## NMR 2.39

$^{31}\text{P}\{^1\text{H}\}$  NMR spectrum of  $\text{Rh}(\text{CO})_2(\text{acac}) / \text{DIOP}$  1:1.5 & 1-hexene under 20 bar synthesis gas cooled to 25 °C, in the 10 mm cell.



This is obviously a big difference between two reactions which use the same catalyst system. It is hypothesised that the difference originates from the differing stabilities of the allyl alcohol or 1-hexene intermediates that make the acylrhodium complex species of DIOP and allyl alcohol more stable than the acylrhodium complex species of DIOP and 1-hexene. Such a difference may be due to an effect similar to the chelate effect suggested for the difference in the chemical shifts of the linear and branched acylrhodium species. It is important to characterise the complex species at 8.4 ppm, as if it is the active catalytic species observed during the reaction itself, it is the next step of reaction which is rate determining. Knowing this would be very important in fully understanding the reaction kinetics.

### 2.6.2 HP IR Studies of the Hydroformylation of 1-Hexene.

The *in-situ* infrared spectrum of the hydroformylation of 1-hexene with the rhodium DIOP catalytic system can be seen in IR 2.13. As in the allyl alcohol case the infrared spectra are important as the reaction does not suffer from gas starvation or liquid / gas interface problems.

At 25 °C, the IR spectrum is very similar to that when there is no substrate present. The rhodium dimer complex species, **46**, exhibits  $\nu_{\text{CO}}$  absorption bands at 1980  $\text{cm}^{-1}$  and 1747  $\text{cm}^{-1}$  and the rhodium hydride complex species exhibits an absorption at 1946  $\text{cm}^{-1}$ . The band at 1639  $\text{cm}^{-1}$  arises from the substrate 1-hexene, as 1-hexene gives a band at 1640  $\text{cm}^{-1}$  in the IR spectrum of a 1:9 solution in toluene.

On heating to 30 °C, the  $\nu_{\text{CO}}$  bands from the rhodium hydride complex species increase in intensity with respect to the  $\nu_{\text{CO}}$  bands from the rhodium dimer complex. This is analogous to the case where there is no substrate present, see section 2.3.1.2. It also fits with the HP NMR results of the hydroformylation reaction of 1-hexene.

With further heating to 40 °C, this same pattern continues, with one change. A new band at 1727  $\text{cm}^{-1}$ , thought to be from the products of reaction, is observed.

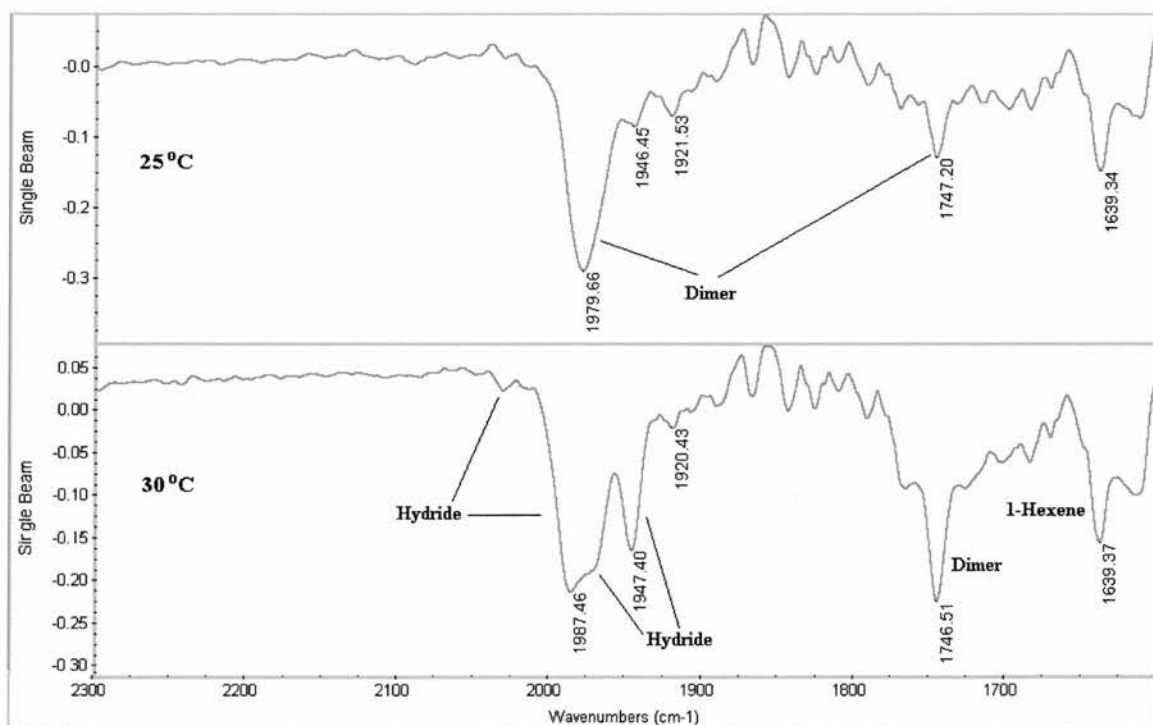
On further heating to 50 °C, the  $\nu_{\text{CO}}$  bands due to the hydride are greatly reduced in intensity. The product band at 1727  $\text{cm}^{-1}$  becomes more intense and a new band at 1984  $\text{cm}^{-1}$  is observed. At 80 °C, the spectrum shows the rhodium hydride bands have disappeared completely, and the product band at 1727  $\text{cm}^{-1}$  has increased further in intensity, and there are two bands in the 1900  $\text{cm}^{-1}$  to 2000  $\text{cm}^{-1}$  range, one at 1983  $\text{cm}^{-1}$

and one at  $1959\text{ cm}^{-1}$ . This is analogous to the allyl alcohol case. The broad  $\nu_{\text{CO}}$  band at  $1983\text{ cm}^{-1}$  is speculated to belong to the new complex species present under hydroformylation conditions in the *in situ*  $^{31}\text{P}\{^1\text{H}\}$  NMR spectrum under hydroformylation conditions at  $8.4\text{ ppm}$   $^1J_{\text{PRh}} = 109\text{ Hz}$ . Again, it is also speculated that the band of low intensity at  $1950\text{ cm}^{-1}$  is a  $\nu_{\text{RhH}}$  band.

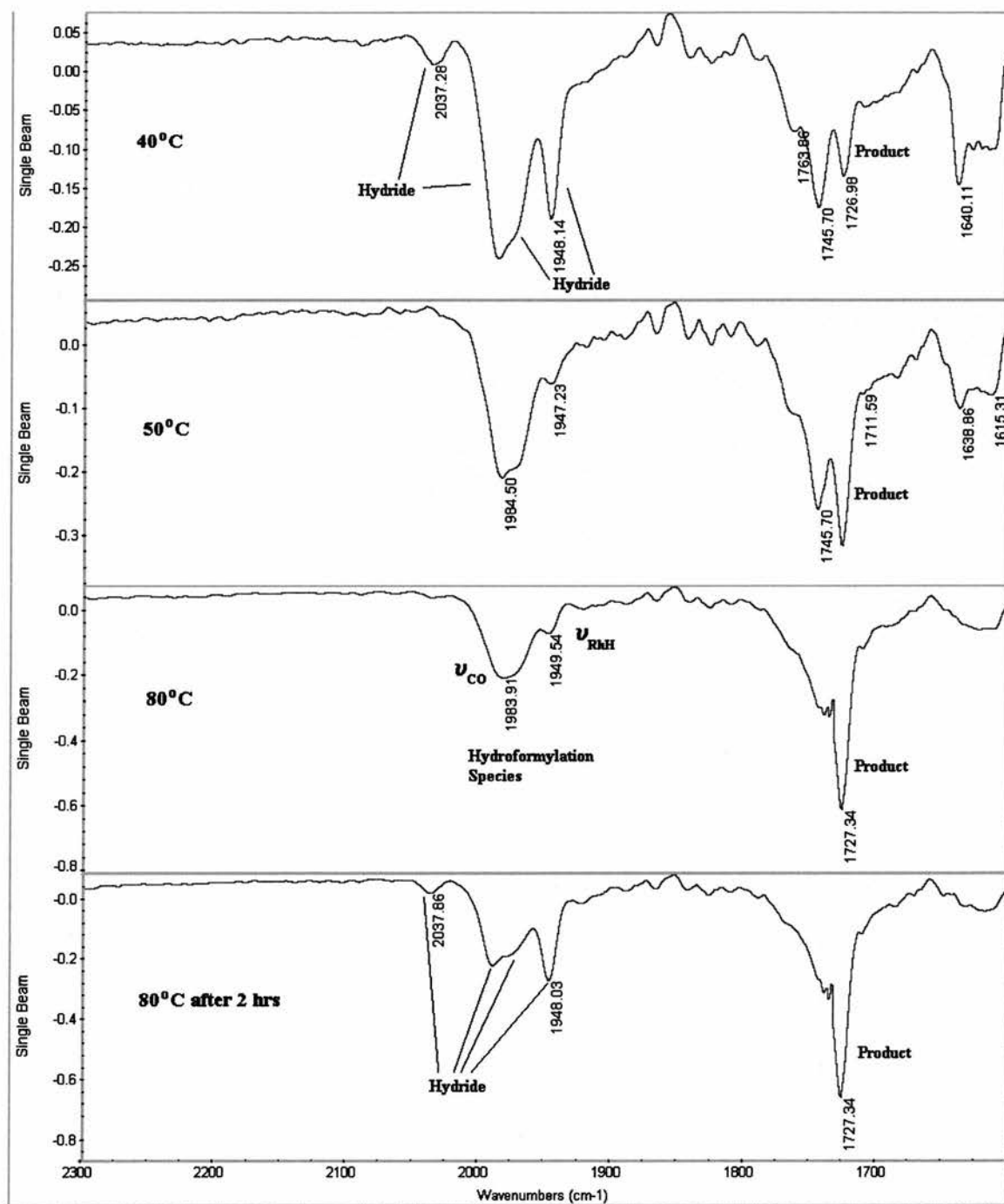
It was suggested in section 2.5 that the doublet resonance observed at  $8.4\text{ ppm}$  in the *in situ* HP NMR study of the hydroformylation of allyl alcohol, and the doublet resonance at  $8.5\text{ ppm}$  in the *in situ* HP NMR study of the hydroformylation of 1-hexene are the same complex species. The band positions in the IR spectra of the two systems are different however. It is suggested that the reason for this is the different nature of the solvent systems, because of the polar nature of allyl alcohol and the non-polar nature of 1-hexene.

## IR 2.13

*In-situ infrared spectra of the hydroformylation of 1-hexene.*



IR 2.13 continued.



### 2.6.3 Kinetic Studies of the Hydroformylation of 1-Hexene.

The hydroformylation of 1-hexene with the rhodium-DIOP catalytic system was carried out at 70 °C, under a constant pressure of 8 bar synthesis gas (CO/H<sub>2</sub> 1:1), and the gas uptake from a ballast vessel was monitored over the reaction period. The rate profiles of the reaction can be seen in Graph 2.3.

The rate profile shows zero order kinetics with respect to substrate over the first half of the reaction, after which the curvature of the profile indicates > zero order in the later half of the reaction.

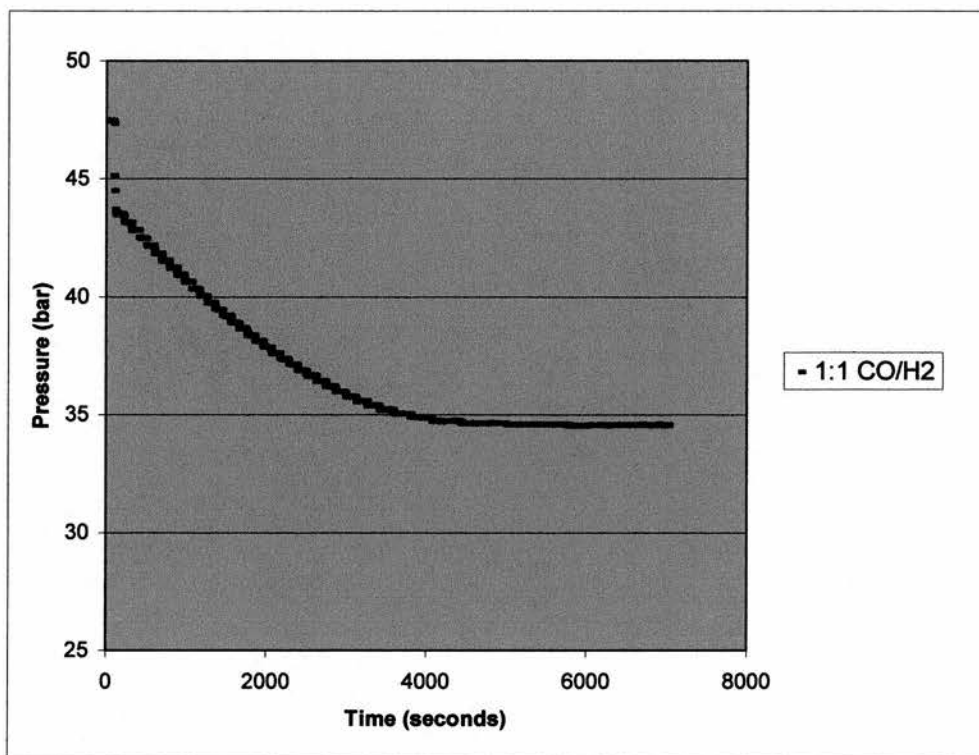
At high alkene concentration, the equilibrium between [HRh(DIOP)CO] and [HRh(DIOP)(alkene)CO] lies totally to the right hand side. Thus, as all the rhodium is available to the reaction, it is zero order in alkene concentration. As the 1-hexene concentration drops, the equilibrium shifts to the left, and the reaction becomes dependant on the alkene concentration, consistent with saturation kinetics. Saturation kinetics have been previously reported for the hydroformylation of 1-hexene using the rhodium TPP catalytic system.<sup>60</sup>

The product distribution was analysed by g.l.c. it showed 0.4 % of unreacted substrate 1-hexene, trace amounts of isomerised substrate 2-hexene and 3-hexene, 3.9 % of the hydrogenated product hexane, 19.9 % of the branched hydroformylation product 2-methyl-1-hexanal, and 75.8 % of the linear hydroformylation product heptanal, therefore having a l:b ratio of 3.8:1

It would be interesting to study the rate of reaction with respect to the partial pressures of carbon monoxide and hydrogen in the same way as suggested for the hydroformylation of allyl alcohol. In this way, it will be possible to determine how the rate is effected by CO and H<sub>2</sub> concentration and especially, whether the reaction follows type I or II kinetics, see Equation 2.1 and Equation 2.2 on page 119.

**Graph 2.3**

*The rate profile of the hydroformylation reaction of 1-hexene under synthesis gas*



## 2.7 References for Chapter Two.

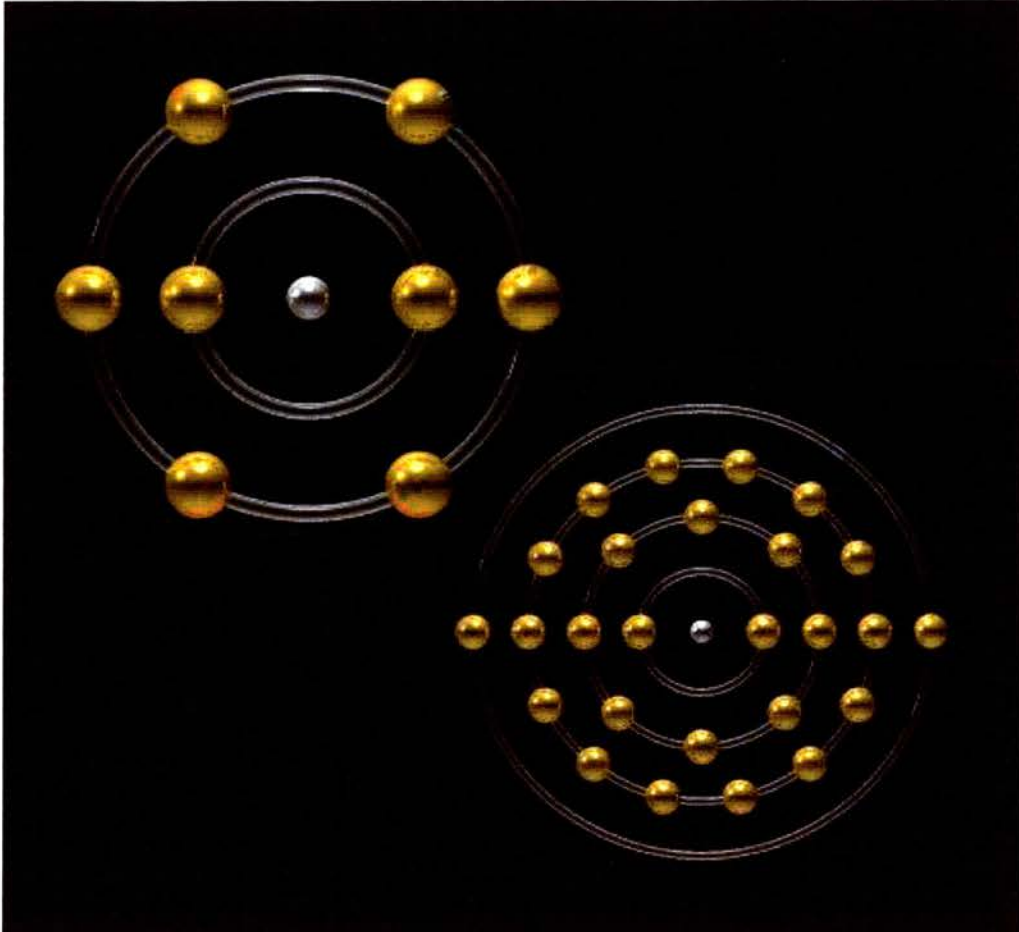
- 1 T. P. Dang and H. B. Kagan, *J. Chem. Soc., Chem. Commun.*, 1971, 481.
- 2 H. B. Kagan and T. Dang, *J. Am. Chem. Soc.*, 1972, **94**, 6429.
- 3 J. Poulin, T. Dang, and H. B. Kagan, *J. Organomet. Chem.*, 1975, **84**, 87.
- 4 J. M. Townsend, J. F. Blount, R. C. Sun, S. Zawoiski, and J. D. Valentine, *J. Org. Chem.*, 1980, **45**, 2995.
- 5 W. Levason and C. A. McAuliffe, *Inorg. Synth.*, 1976, **16**, 188.
- 6 B. A. Murrer, J. M. Brown, P. A. Chaloner, P. N. Nicholson, and D. Parker, *Synthesis*, 1979, 350.
- 7 E. I. Klabunovski and E. S. Levitina, *Russ. Chem. Rev.*, 1970, **39**, 1035.
- 8 Y. Izumi, *Bull. Chem. Soc. Jap.*, 1963, **36**, 155.
- 9 F. H. Jardine, J. A. Osborn, G. Wilkinson, and J. F. Young, *Chem. Ind.*, 1965, 560.
- 10 J. F. Young, J. A. Osborn, F. H. Jardine, and G. Wilkinson, *J. Chem. Soc., Chem. Commun.*, 1965, 131.
- 11 C. O'Connor and G. Wilkinson, *Tetrahedron Lett.*, 1969, **18**, 1375.
- 12 L. Horner, H. Siegel, and H. Buthe, *Angew. Chem. Int. Ed. Engl.*, 1968, **7**, 232.
- 13 W. S. Knowles and M. J. Sabacky, *J. Chem. Soc., Chem. Commun.*, 1968, 1445.
- 14 J. D. Morrison, R. E. Burnett, A. M. Agniar, C. J. Morrow, and C. Phillips, *J. Am. Chem. Soc.*, 1971, **93**, 1301.
- 15 M. van der Berg, A. J. Minnaard, E. P. Schdde, J. van Esch, J. G. de Vries, and B. L. Feringa, *J. Am. Chem. Soc.*, 2000, **122**, 11539.
- 16 B. D. Vineyard, W. S. Knowles, M. J. Sabacky, G. L. Bachman, and D. J. Weinkauff, *J. Am. Chem. Soc.*, 1977, **99**, 5946.
- 17 T. Morimoto, M. Chiba, and Achiwa, *Tetrahedron Lett.*, 1989, **30**, 735.
- 18 H. Abe, H. Amii, and K. Uneyama, *Org. Lett.*, 2001, **3**, 313.
- 19 J. Madec, X. Pfister, P. Phansavath, V. Ratovelomanana-Vidal, and J. P. Genet, *Tetrahedron*, 2001, **57**, 2563.

- 20 P. Pino, G. Consiglio, L. I. Flowers, and J. C. U. Pittman, *J. Chem. Soc., Chem Commun.*, 1983, 612.
- 21 S. Gladiali and L. Pinna, *Tetrahedron: Asymmetry*, 1990, **1**, 693.
- 22 C. F. Hobbs and W. S. Knowles, *J. Org. Chem.*, 1981, **46**, 4422.
- 23 Y. Watanabe, T. Mitsudo, Y. Yasunori, J. Kikuchi, and Y. Takegami, *Bull. Chem. Soc. Jap.*, 1979, **52**, 2735.
- 24 G. Consiglio, S. C. A. Nefkens, and A. Borer, *Organometalics*, 1991, **10**, 2046.
- 25 A. Serivanti, S. Paganelli, and U. Matteoli, *J. Organomet. Chem.*, 1990, **397**, 119.
- 26 P. W. N. M. van Leeuwen, P. C. J. Kamer, J. N. H. Reek, and P. Dierkes, *Chem. Rev.*, 2000, **100**, 2741.
- 27 C. P. Casey, G. T. Whiteker, M. G. Melville, L. M. Petrovich, J. A. J. Gavney Jr, and D. R. Powell, *J. Am. Chem. Soc.*, 1992, **114**, 5535.
- 28 P. W. N. M. van Leeuwen, M. Kranenburg, Y. E. M. van der Burgt, and P. C. J. Kamer, *Organometalics*, 1995, **14**, 3081.
- 29 K. Maki, T. Kujuta, and K. Marumo, *Chem. Abstr.*, **118**, 6622f.
- 30 W. S. Dubner and W. P. Shum, , US 6,225,509, 2001, .
- 31 J. C. U. Pittman and W. D. Honnick, *J. Org. Chem.*, 1980, **45**, 2132.
- 32 L. Ballard, C. Reiner, and J. Jonas, *J. Magn. Reson. Ser. a*, 1996, **123**, 81.
- 33 P. Koziol, C. Reiner, and J. Jonas, *Appl. Magn. Res.*, 1996, **11**, 19.
- 34 S. Gaemers, H. Luyten, J. M. Ernsting, and C. J. Elsevier, *Magn. Res. Chem.*, 1999, **37**, 25.
- 35 W. R. Moser, B. J. Marshik-Guerts, and S. J. Okrasinski, *J. Mol. Catal. A*, 1999, **143**, 57.
- 36 W. R. Moser, J. E. Cnossen, A. W. Wang, and S. A. Krouse, *J. Catal.*, 1985, **95**, 21.
- 37 <http://ch-www.st-andrews.ac.uk/cats/>, 06/05/2000.
- 38 A. M. Trzeciak and J. J. Ziolkowski, *Inorg. Chim. Acta.*, 1982, **64**, L267.
- 39 P. W. N. M. van Leeuwen, G. J. H. Buisman, E. J. Vos, and P. C. J. Kamer, *J. Chem. Soc., Dalton Trans.*, 1995, 409.

- 40 A. van Rooy, P. C. J. Kamer, P. W. N. M. van Leeuwen, K. Goubitz, J. Fraanje, N. Veldman, and A. L. Spek, *Organometallics*, 1996, **15**, 835.
- 41 W. Simanko, K. Mereiter, R. Schmid, K. Kirchner, A. M. Trzeciak, and J. J. Ziolkowski, *J. Organomet. Chem.*, 2000, **602**, 59.
- 42 J. G. Leipoldt, G. J. Lamprecht, and G. J. van Zyl, *Inorg. Chim. Acta*, 1985, **96**, L31.
- 43 M. A. Esteruelas, F. J. Lahoz, E. Onate, L. A. Oro, L. Rodriguez, P. Steinert, and H. Werner, *Organometallics*, 1996, **15**, 3436.
- 44 K. Angermund, A. Baumann, E. Dinjus, R. Fornika, H. Gorls, M. Kessler, M. Kruger, and W. Leitner, *Chem. Eur. J.*, 1997, **3**, 755.
- 45 R. Fornika, H. Gorls, B. Seemann, and W. Leitner, *J. Chem. Soc., Chem. Commun.*, 1995, **18**, 1929.
- 46 T. Jongsma, G. Challa, and P. W. N. M. van Leeuwen, *J. Organomet. Chem.*, 1991, **121**, 421.
- 47 E. A. V. Ebsworth, D. W. H. Rankin, and S. Craddock, 'Structural Methods in Inorganic Chemistry', Oxford, 1987.
- 48 B. R. James, D. Mahajan, S. J. Rettig, and G. A. Williams, *Organometallics*, 1983, **2**, 1452.
- 49 C. Claver, A. Castellanos-Paez, S. Castillon, P. W. N. M. v. Leewen, and W. G. J. der Lange, *Organometallics*, 1998, **17**, 2543.
- 50 O. R. Hughes and D. A. Young, *J. Am. Chem. Soc.*, 1981, **103**, 6636.
- 51 P. Meakin, E. L. Muetterties, and J. P. Jesson, *J. Mol. Catal.*, 1972, **19**, 41.
- 52 P. W. N. M. van Leewen, L. A. v. d. Veen, M. D. K. Boele, F. R. Breman, P. C. J. Kamer, K. Goubitz, J. Fraanje, H. Schenk, and C. Bo, *J. Am. Chem. Soc.*, 1998, **120**, 11616.
- 53 J. M. Brown and A. G. Kent, *J. Chem. Soc. Perkin Trans II*, 1987, 1597.
- 54 D. H. Williams and I. Fleming, 'Spectroscopic Methods in Organic Chemistry', McGraw Hill, London, 1980.
- 55 A. M. Trzeciak and J. J. Ziolkowski, *J. Mol. Catal.*, 1983, **19**, 41.
- 56 C. P. Casey and L. M. Petrovich, *J. Am. Chem. Soc.*, 1995, **117**, 6007.

- 57 C. P. Casey, E. L. Paulsen, E. W. Beuttenmueller, B. R. Proft, L. M. Petrovich, B. A. Matter, and D. R. Powell, *J. Am. Chem. Soc.*, 1997, **119**, 11817.
- 58 P. W. N. M. v. Leeuwen and C. Claver, 'Rhodium Catalysed Hydroformylation', ed. B. R. James and R. Ugo, Kluwer Academic Publishers, Dordrecht, 2000.
- 59 W. Shum, Unpublished Results.
- 60 I. T. Horvath, G. Kiss, R. A. Cook, J. E. Bond, P. A. Stevens, J. Rabai, and E. J. Mozeleski, *J. Am. Chem. Soc.*, 1998, **120**, 3133.

*CHAPTER THREE: CATALYST POISONING*



### 3 CHAPTER THREE: CATALYST POISONING.

#### 3.1 A Study of The Oxidation Properties of DIOP and DPPB.

The rhodium DIOP catalytic system produces high linear to branched ratios in the hydroformylation of allyl alcohol compared with previous catalytic systems,<sup>1</sup> see section 2.4.4.1. This is of industrial interest as the linear product of reaction, 4-hydroxybutanal which is further hydrogenated with the Raney nickel catalyst to 1,4-butanediol is more commercially desirable than the hydrogenated branched product 2-methyl-1,3-propanediol, see section 1.2.

The interest behind the study into the rhodium DIOP catalytic system stems from this and from the desire to turn the reaction from a laboratory scale into an industrial process. One problem with changing from the laboratory environment to an industrial one is catalyst poisoning, from oxidation for example.<sup>2</sup> The catalytic systems under investigation are all oxygen sensitive, and the chiral DIOP ligand is expensive. If the rhodium DIOP catalytic system is to provide a viable industrial process for the hydroformylation of allyl alcohol, DIOP and the rhodium DIOP complex species present during the reaction must have a certain degree of stability towards oxidation. To study this, it is proposed to study the oxide species formed in several catalytic systems containing rhodium in combination with DIOP and / or dppb and / or TPP, see table 4.1, in oxygen free and oxygenated atmospheres. The idea is to evaluate the stability of the DIOP ligand towards oxidation with respect to the stability of dppb which is already used in the industrial process,<sup>2</sup> see section 1.2.5. Experiments one to seven were, therefore, designed to accomplish this.

Experiment one studies the catalytic system we have been working with so far, see chapter two. Experiment two studies a possible industrial catalytic system. Experiment three compares the rhodium DIOP catalytic system with the similar rhodium DPPB catalytic system. Experiments four and five have been devised to test interpretations made from the initial three experiments. Experiments six and seven are of the rhodium DIOP and rhodium dppb catalytic systems in the presence of allyl alcohol.

The complex solutions (Experiment one to Experiment five) were studied by high pressure  $^{31}\text{P}\{^1\text{H}\}$  NMR spectroscopy. The NMR spectra was recorded at 25 °C for one

hour, the complex solution was then heated to 70 °C over half an hour, and the NMR spectrum recorded every hour for the next five hours.

The *in-situ* studies (Experiment six and Experiment seven) were also carried out by high pressure  $^{31}\text{P}\{^1\text{H}\}$  NMR spectroscopy. The NMR spectrum was recorded at 25 °C for one hour, the complex solution heated to 70 °C over half an hour, and the NMR spectrum recorded every hour for the next two hours (as the reaction is over within 5 minutes). The solution was then cooled to 25 °C over half an hour, and the NMR spectrum taken at 25 °C over the next hour.

The complex species present are discussed in section 4.2, and are listed in table 4.2, at the end of this chapter. The concentration of each complex in solution was worked out by dividing the integral of the area of each resonance by the number of phosphine atoms in the complex and expressing it as a percentage of the total integral of all the resonances present.

**Table 3.1**

*Catalytic systems under study.*

Experiment One	Compound	Rh(CO) <sub>2</sub> (acac)	DIOP	
	Ratio	1.0	1.5	
Experiment Two	Compound	Rh(CO) <sub>2</sub> (acac)	DIOP	TPP
	Ratio	1.0	2	3
Experiment Three	Compound	Rh(CO) <sub>2</sub> (acac)	DPPB	TPP
	Ratio	1.0	2	3
Experiment Four	Compound	Rh(CO) <sub>2</sub> (acac)	DIOP	
	Ratio	1.0	1.0	
Experiment Five	Compound	Rh(CO) <sub>2</sub> (acac)	DPPB	
	Ratio	1.0	1.0	
Experiment Six	Compound	Rh(CO) <sub>2</sub> (acac)	DIOP	Allyl Alcohol
	Ratio	1.0	1.0	0.5 cm <sup>3</sup>
Experiment Seven	Compound	Rh(CO) <sub>2</sub> (acac)	DPPB	Allyl Alcohol
	Ratio	1.0	1.0	0.5 cm <sup>3</sup>

### 3.1.1 Experiment One: Results For the Rhodium DIOP Ratio 1:1.5 Catalytic Solution.

Graph 3.1 to Graph 3.3 show the concentrations of the phosphorus species present in solution with a  $[\text{Rh}(\text{CO})_2(\text{acac})]$  / DIOP ratio of 1:1.5, under 20 bar synthesis gas at 25 °C (at 0 hrs), and at 70 °C for 5 hours (1-6 hrs). Graph 3.4 to Graph 3.6 show the same situation under 99 % synthesis gas and 1 % air (0.2 % oxygen).

Graph 3.1 and Graph 3.4 show the relative concentrations of all the phosphorus species present. Graph 3.2 and Graph 3.5 show the concentrations of the rhodium complexes present. Graph 3.3 and Graph 3.6 show the concentrations of the uncomplexed phosphorous species present.

On heating the sample with no oxygen present the concentration of the dimer  $[\text{Rh}(\text{DIOP})(\text{CO})_2]_2$  drops and the concentration of the hydride  $[\text{HRh}(\text{DIOP})(\text{CO})_2]$  increases, this is as we would expect from section 2.3.1.1. However, the rise in concentration of the hydride is not as great as the drop on concentration of the dimer.

We also see a drop in the concentration of DIOP, but no great change in the concentration of the oxide species. It is, therefore, possible that there are trace amounts of  $[\text{Rh}(\text{CO})_2(\text{acac})]$  present in the solution to begin with, and this takes up the DIOP to form the hydride.

When the sample is spiked with oxygen, again we see the drop in concentration of the dimer and the rise in concentration of the hydride. The difference in the rise and fall of the two species is much greater this time, this is due to the initial presence of substantial amounts of  $[\text{Rh}(\text{DIOP})(\text{acac})]$  and the  $[\text{Rh}(\text{P})_3]$  species which are also converted to the hydride species over the first three hours of study.

There is also a rise in the concentration of DIOP over the first three hours of study. This is due to the continued conversion of the  $[\text{Rh}(\text{P})_3]$  species 15 to the hydride species 9 and 10 with the release of one equivalent of DIOP.

As we would expect, there is a small amount of oxidation in this system, however, it is important to note there is a much greater rise in the concentration of the mono-oxidised DIOP ligand  $\text{DIOP}(\text{O})$  than the dioxide  $\text{DIOP}(\text{O})_2$ .

It is also noted that this increase in the concentration of  $\text{DIOP}(\text{O})$  occurs over the first three hours, the period where we see the decrease in concentration of the  $[\text{Rh}(\text{P})_3]$

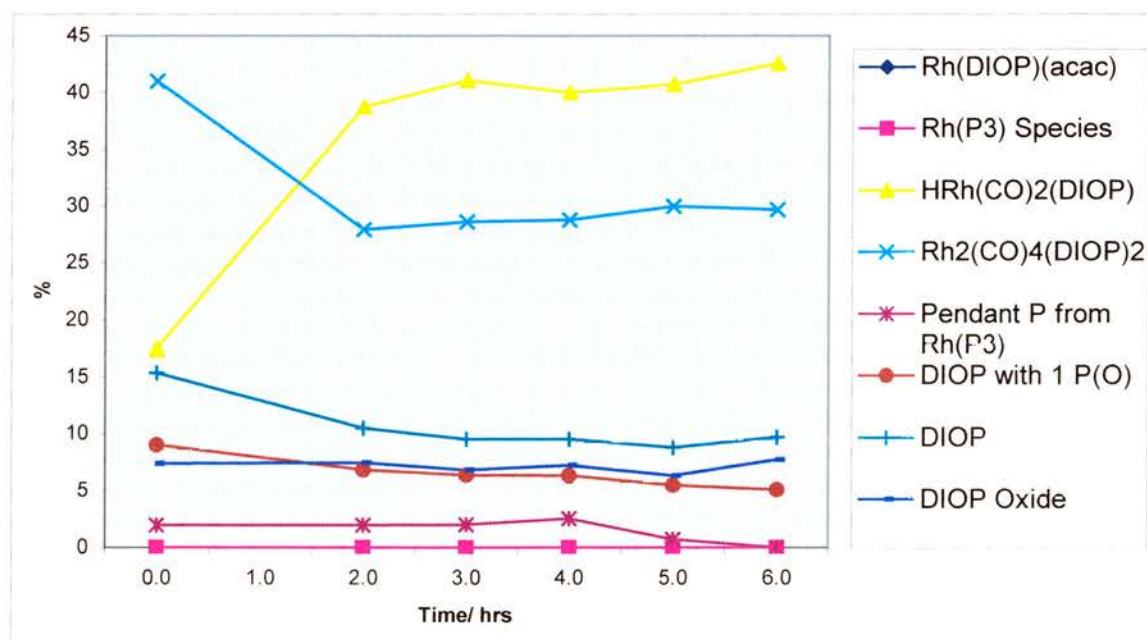
species. There is three times the amount of oxygen present required to oxidise all the DIOP so it is not possible that the oxygen runs out after this amount of time.

It is also possible that the gas exchange over the first three hours of study, involved in the interchange of species resulting in the rise in concentration of the hydride species encourages oxidation. Or that the  $[\text{Rh}(\text{P})_3]$  species catalyses the oxidation of DIOP, and that with its decrease in concentration the oxidation stops. This could also explain why the oxidation only occurs at one of the phosphorus atoms.

To test these possibilities the system was studied with a  $\text{Rh}(\text{CO})_2(\text{acac}) / \text{DIOP}$  ratio of 1:1. The solution was pressurised for 10 hours under 20 bar synthesis gas before study. It was our hope to convert fully the  $[\text{Rh}(\text{CO})_2(\text{acac})]$ ,  $[\text{Rh}(\text{DIOP})(\text{acac})]$  and  $[\text{Rh}(\text{P})_3]$  complex species to the dimer and hydride before we began studying the system. For the oxygen spiked system, a mixture of 98 % and 2 % air was added after this time.

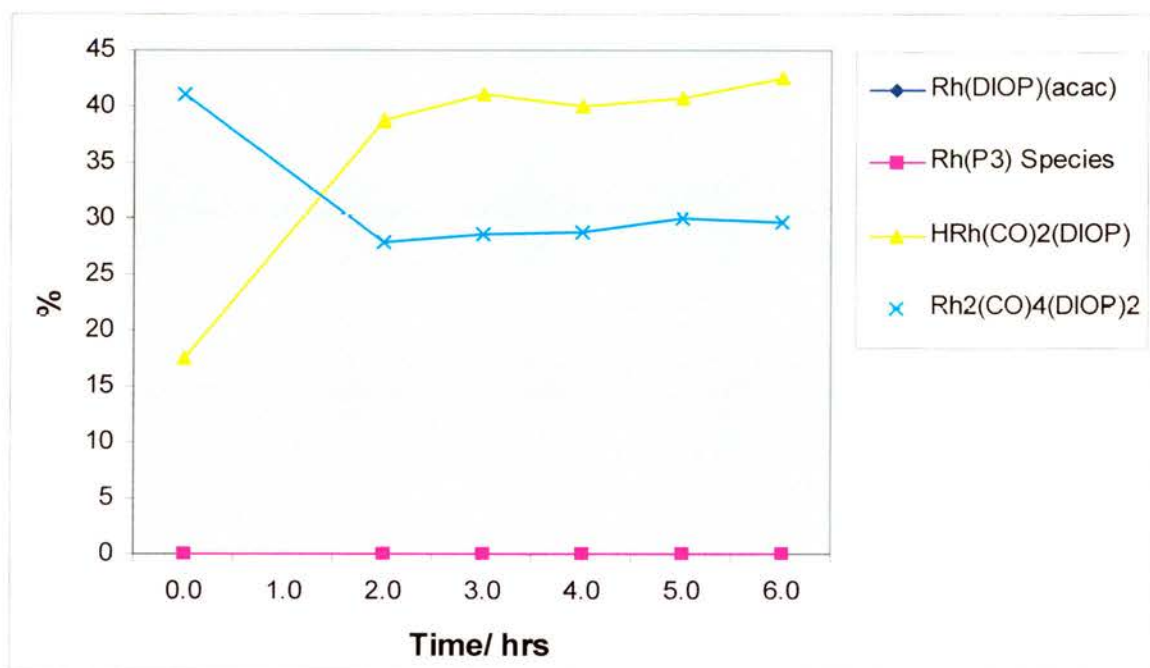
**Graph 3.1**

*$\text{Rh}(\text{CO})_2(\text{acac}) / \text{DIOP}$  1:1.5, 20 bar synthesis gas, all phosphorous species.*



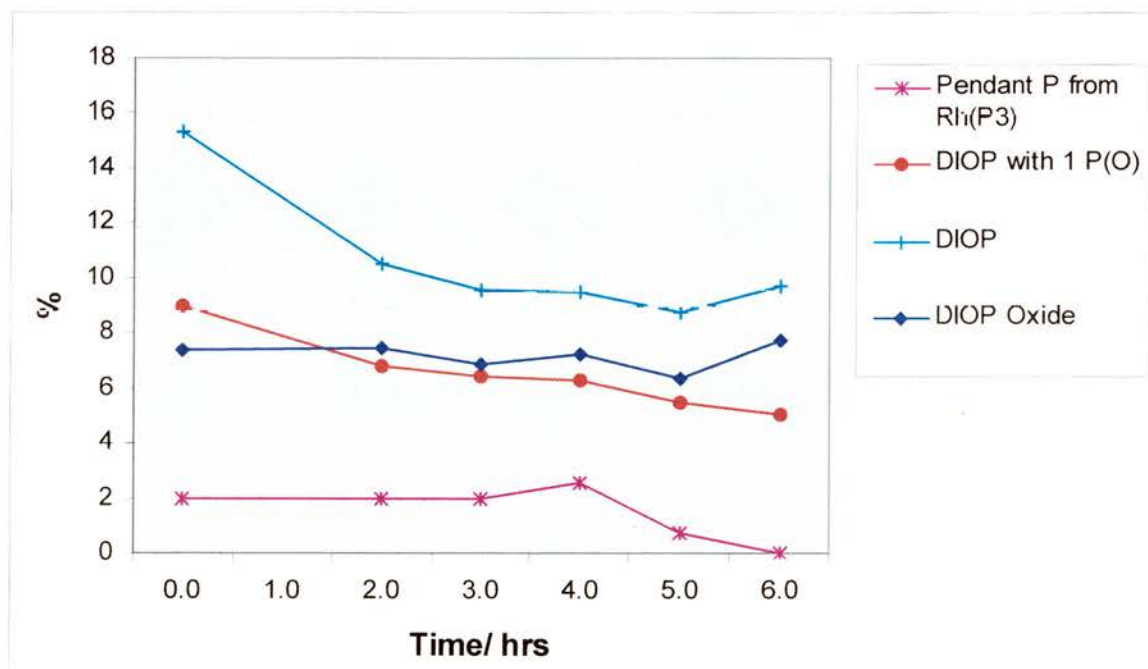
**Graph 3.2**

*Rh(CO)<sub>2</sub>(acac) / DIOP 1:1.5, 20 bar synthesis gas, complex species.*



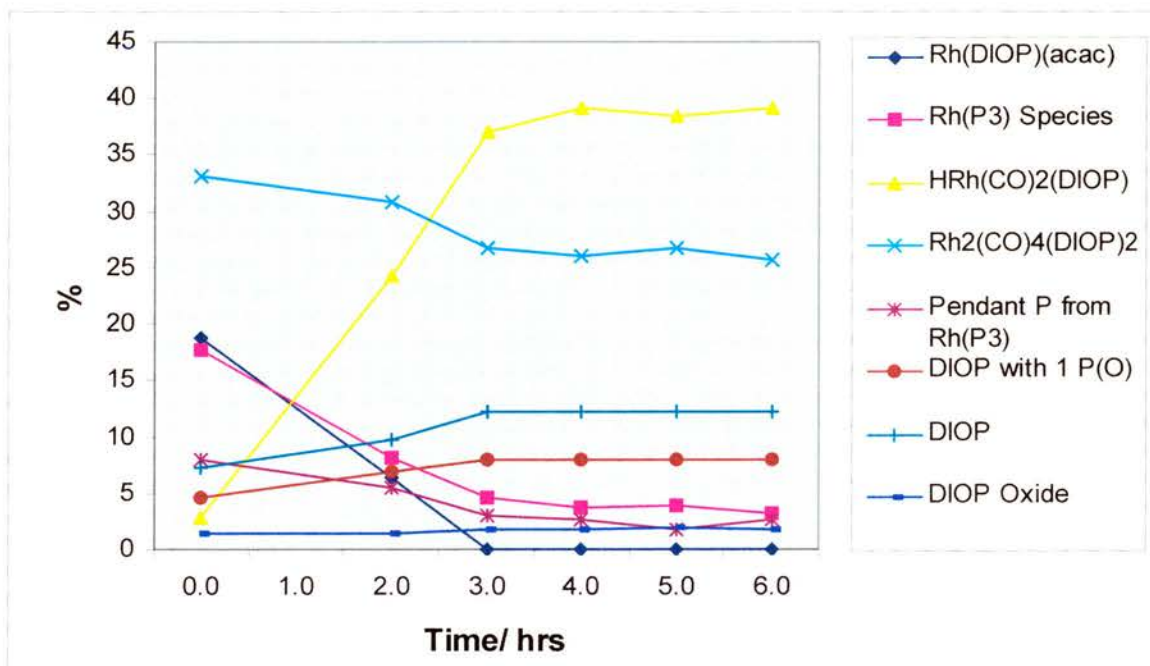
**Graph 3.3**

*Rh(CO)<sub>2</sub>(acac) / DIOP 1:1.5, 20 bar synthesis gas, uncomplexed species.*



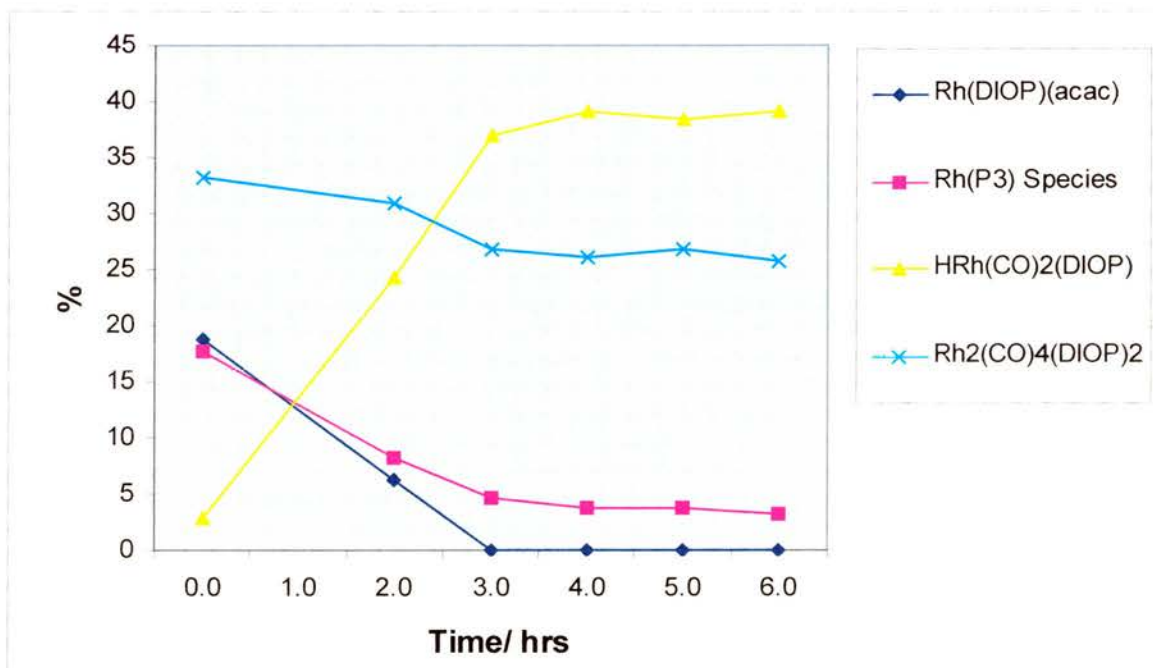
**Graph 3.4**

*Rh(CO)<sub>2</sub>(acac) / DIOP 1:1.5, 20 bar synthesis gas 99 % & air 1 %, all phosphorous species.*



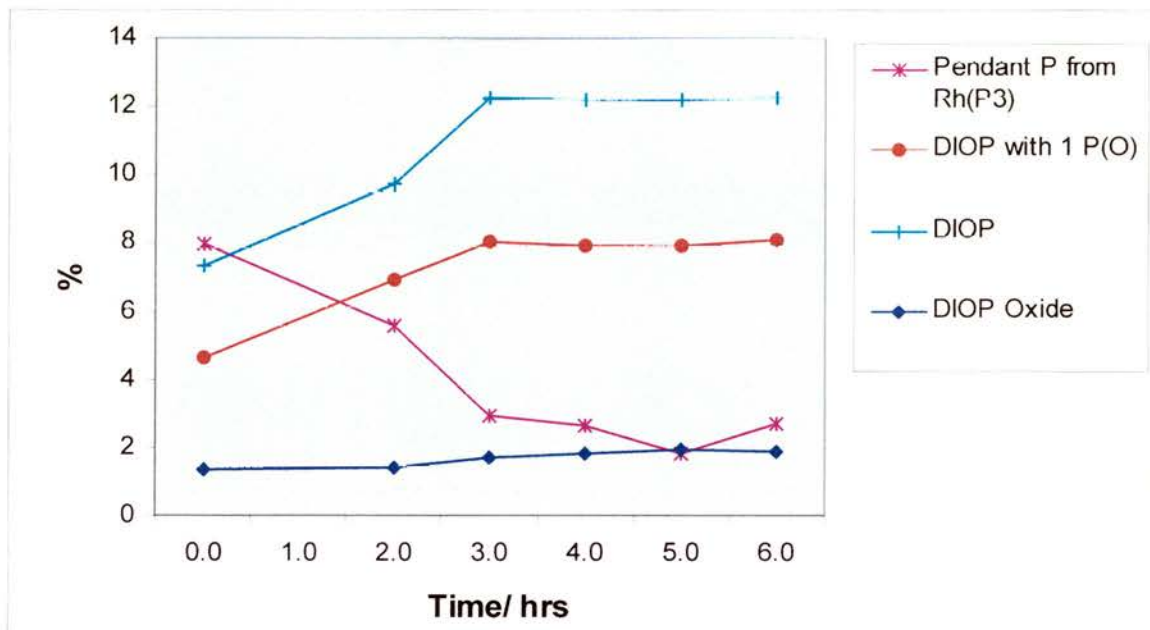
**Graph 3.5**

*Rh(CO)<sub>2</sub>(acac) / DIOP 1:1.5, 20 bar synthesis gas 99 % & air 1 %, complex species.*



**Graph 3.6**

*Rh(CO)<sub>2</sub>(acac) / DIOP 1:1.5, 20 bar synthesis gas 99 % & air 1 %, uncomplexed species.*



### 3.1.2 Experiment Two: Results For the Rhodium: DIOP: TPP Ratio 1:2:3 Catalytic Solution.

Graph 3.7 to Graph 3.12 show the concentrations of the phosphorus species present in solution with a  $[\text{Rh}(\text{CO})_2(\text{acac})] / \text{DIOP} / \text{TPP}$  ratio of 1:2:3, under 20 bar synthesis at 25 °C (at 0 hrs), and at 70 °C for 5 hours (1-6 hrs). Graph 3.10 Graph 3.12 show the same situation under 99 % synthesis gas and 1 % air (0.2 % oxygen).

Graph 3.7 and Graph 3.10 show the relative concentrations of all the phosphorus species present. Graph 3.8 and Graph 3.11 show the concentrations of the rhodium complexes present. Graph 3.9 and Graph 3.12 show the concentrations of the uncomplexed phosphorus species present.

Over the first two hours there is a decrease in the concentration of the dimer species  $[\text{Rh}_2(\text{DIOP})_2(\text{CO})_4]$  and an increase in the concentration of the  $[\text{Rh}(\text{P})_3]$  species. At this time there is no hydride present. After two hours the concentration of the  $[\text{Rh}(\text{P})_3]$  species decreases and the concentration of the hydride increases. There is a small increase in the concentration of the oxide species over the first two hours, but none after

this time. There is also a decrease in concentration of TPP although no TPP oxide was observed. It is possible that this is forming  $[\text{HRh}(\text{CO})(\text{DIOP})(\text{TPP})]$ , a  $[\text{Rh}(\text{P})_3]$  complex where TPP has displaced the unidentate DIOP ligand

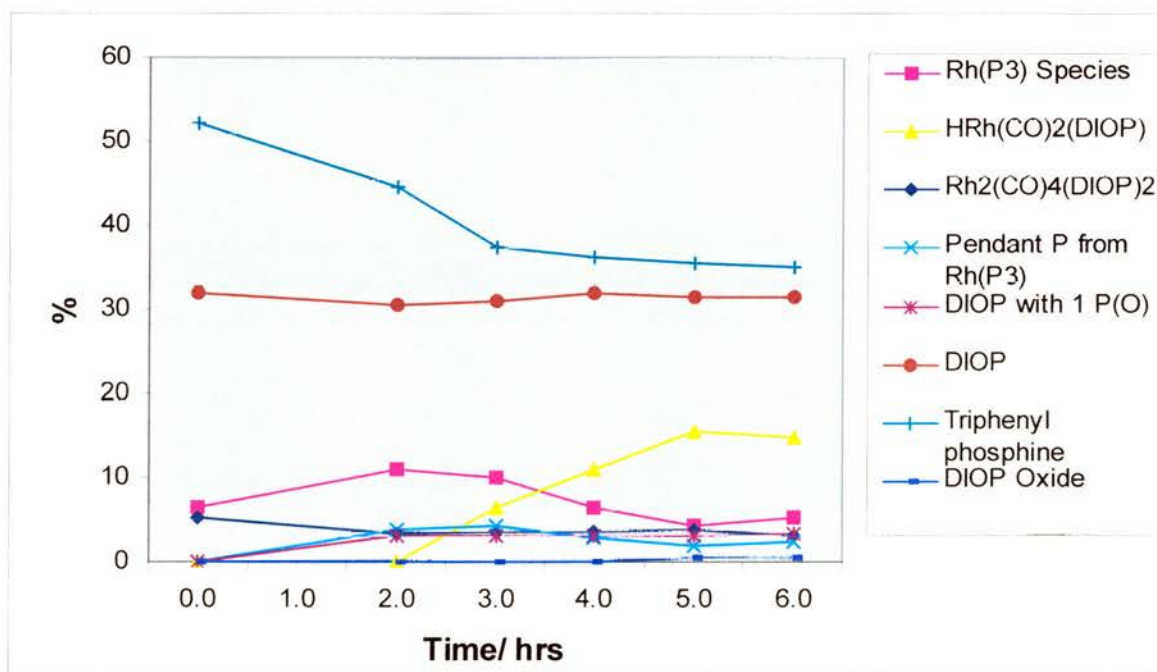
In the oxygen spiked case, there is a rise in the hydride concentration over the first two hours matched by a fall in the dimer concentration. What is surprising is that there is a rise in the  $[\text{Rh}(\text{P})_3]$  species over the full six hours, especially as there is no drop in the DIOP concentration or rise in the DIOP oxide concentration. Again, there is a drop in the TPP concentration.

It could be that the TPP is acting as the third phosphorous atom in the  $\text{Rh}(\text{P})_3$  species, which is preventing it acting as a catalyst for DIOP oxidation.

The small amount of oxidation which does occur is over the first two hours, the same time as the dimer / hydride exchange and the monoxide and the dioxide are formed in equal measure.

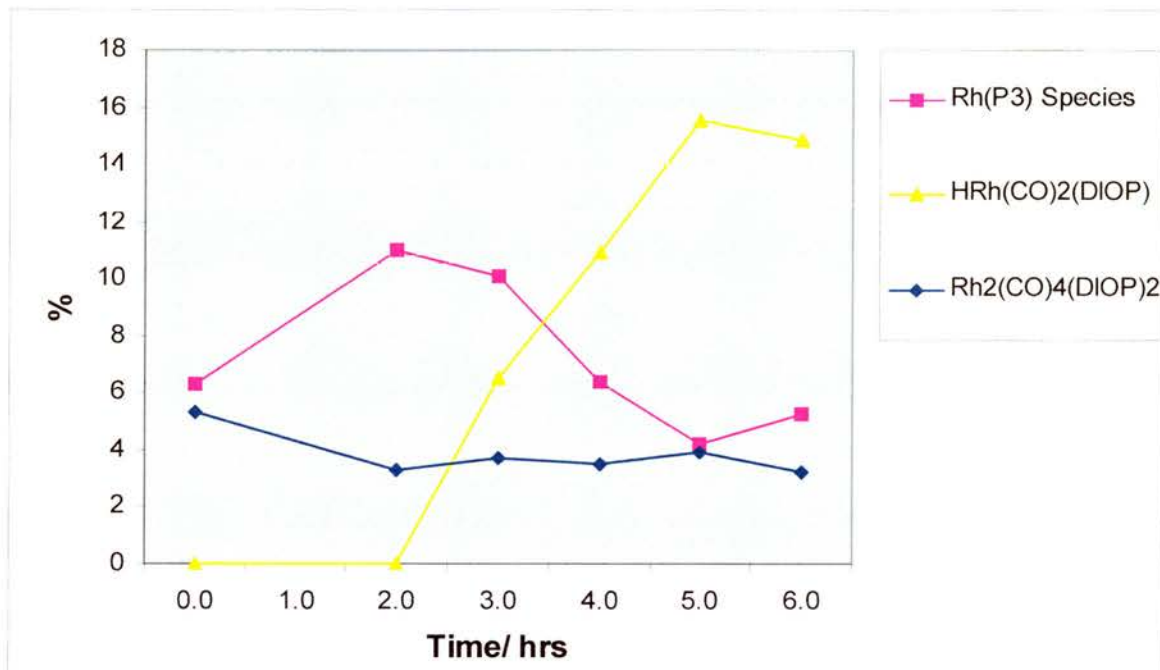
**Graph 3.7**

*$\text{Rh}(\text{CO})_2(\text{acac}) / \text{DIOP} / \text{TPP} 1:2:3$ , 20 bar synthesis gas, all phosphorous species.*

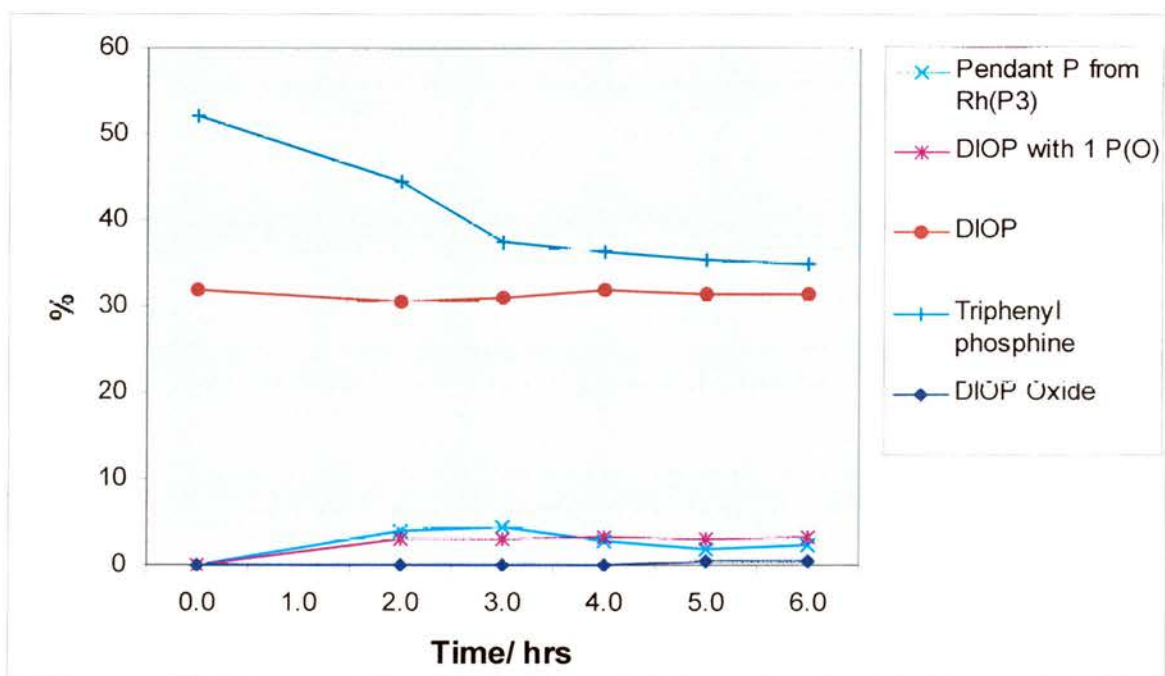


**Graph 3.8**

*Rh(CO)<sub>2</sub>(acac) / DIOP / TPP 1:2:3, 20 bar synthesis gas, complex species.*

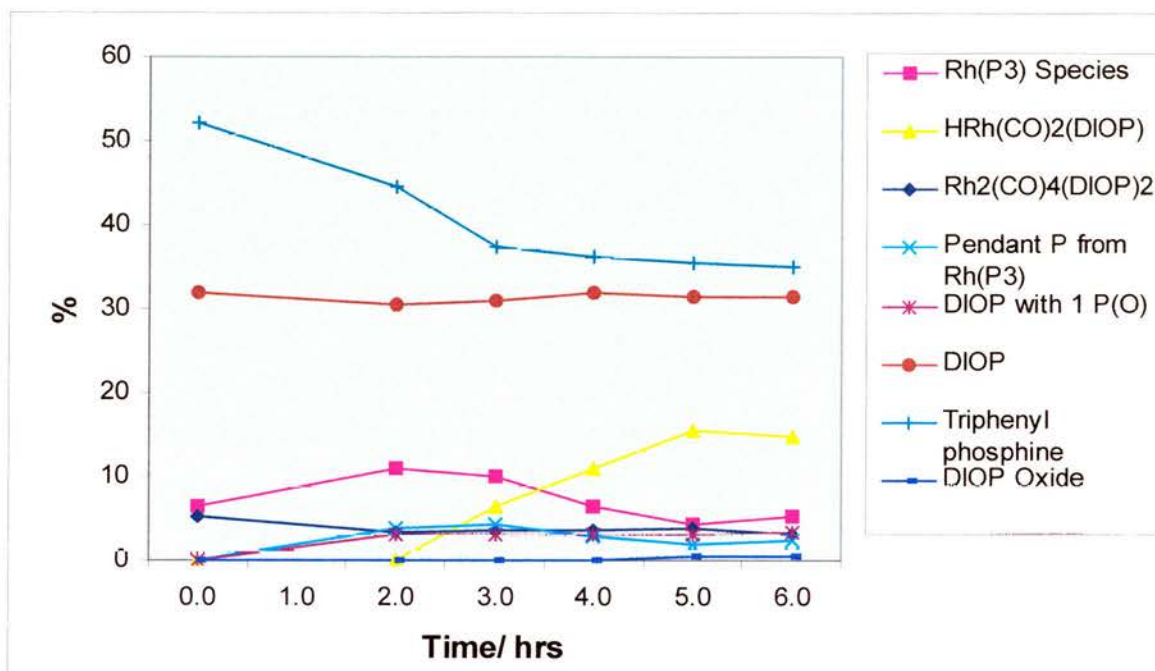
**Graph 3.9**

*Rh(CO)<sub>2</sub>(acac) / DIOP / TPP 1:2:3, 20 bar synthesis gas, uncomplexed species.*



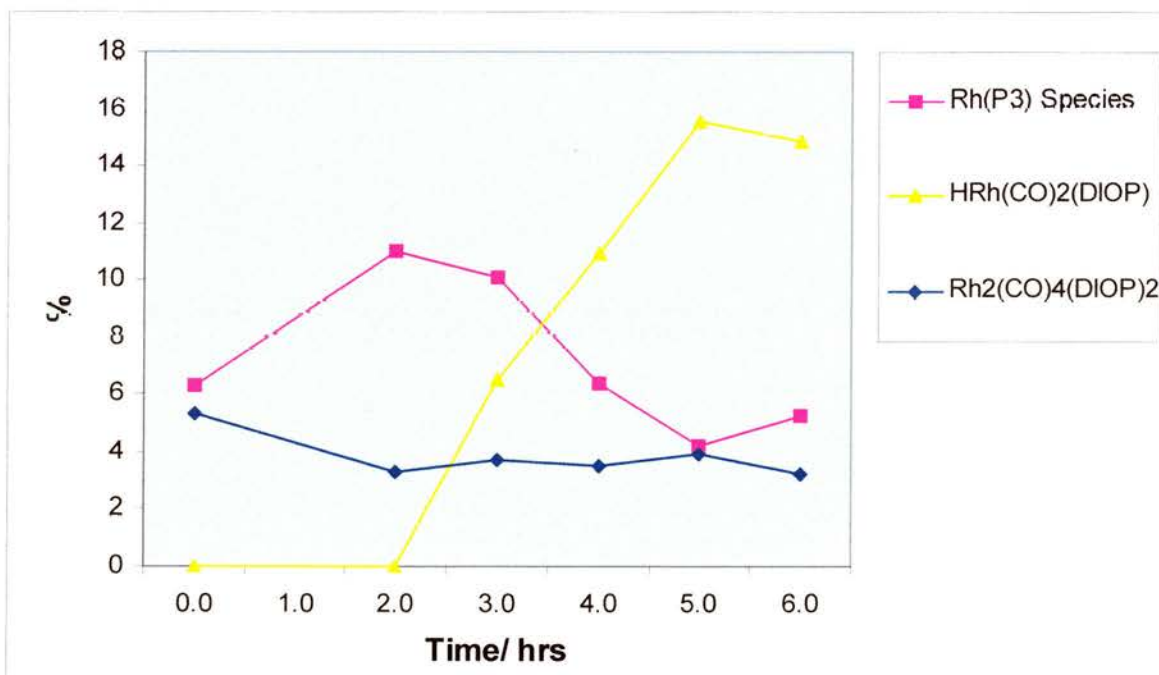
**Graph 3.10**

*Rh(CO)<sub>2</sub>(acac) / DIOP / TPP 1:2:3, 20 bar synthesis gas 99 % & air 1 %, all phosphorous species.*



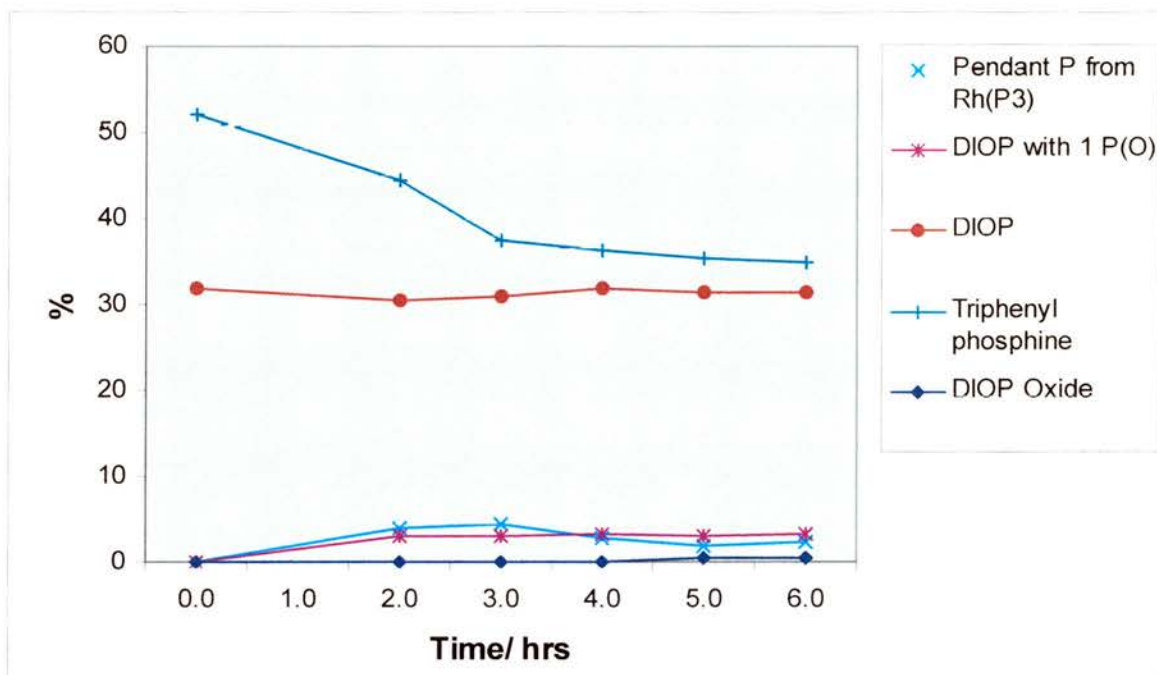
**Graph 3.11**

*Rh(CO)<sub>2</sub>(acac) / DIOP / TPP 1:2:3, 20 bar synthesis gas 99 % & air 1 %, complex species.*



**Graph 3.12**

*Rh(CO)<sub>2</sub>(acac) / DIOP / TPP 1:2:3, 20 bar synthesis gas 99 % & air 1 %, uncomplexed species.*



### 3.1.3 Experiment Three: Results For the Rhodium: dppb: TPP Ratio 1:2:3 Catalytic Solution.

Graph 3.13 to Graph 3.15 show the concentrations of the phosphorus species present in solution with a  $[Rh(CO)_2(acac)] / dppb / TPP$  ratio of 1:2:3, under 20 bar synthesis at 25 °C (at 0 hrs), and at 70 °C for 5 hours (1-6 hrs). Graph 3.16 to Graph 3.18 show the same situation under 99 % synthesis gas and 1 % air, (0.2 % oxygen).

Graph 3.13 and Graph 3.16 show the relative concentrations of all the phosphorus species present. Graph 3.14 and Graph 3.17 show the concentrations of the rhodium complexes present. Graph 3.15 and Graph 3.18 show the concentrations of the uncomplexed phosphorous species present.

Initially, in some previous experiments, there is a high concentration of  $[Rh(DIOP)(acac)]$ , which decreases over the first two hours. The concentration of the

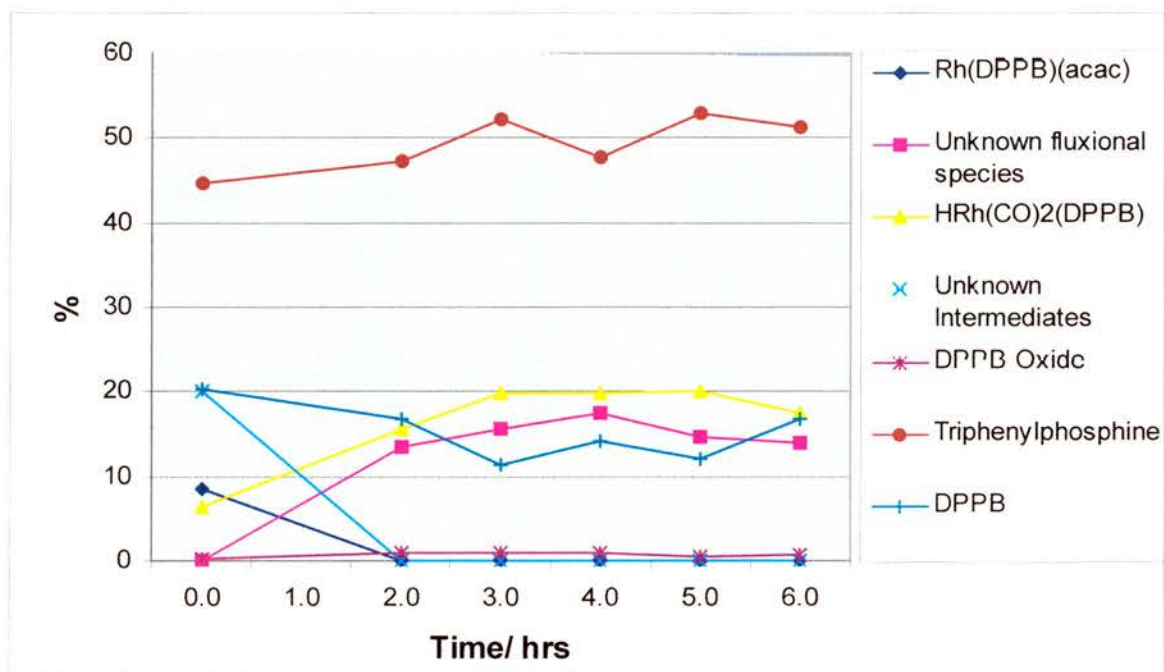
hydride increases over this time, as does the concentration of an unknown fluxional species. There is no evidence of a rhodium dimer complex species.

The concentration of the hydride and the unknown species increases further over the next hour, this is matched by a decrease in the dppb concentration. It is possible that there is some unreacted  $[\text{Rh}(\text{CO})_2(\text{acac})]$  in solution to begin with, which reacts with dppb to form the hydride. There is no  $[\text{Rh}(\text{P})_3]$  species present, and the TPP concentration does not go down, in fact it goes up. It also goes up by the same amount as [dppb] goes down. Rather than their being some  $[\text{Rh}(\text{CO})_2(\text{acac})]$  present, there is a Rh / TPP complex present, which is converted to the Rh / dppb hydride over the first three hours. The Rh / TPP complex species could be the unknown intermediate complex species, however, the concentration of this complex species fall to zero after two hours while the concentration of the TPP carries on increasing over the full six hours. There are small amounts of dppb oxide formed initially but after the first two hours this was stable.

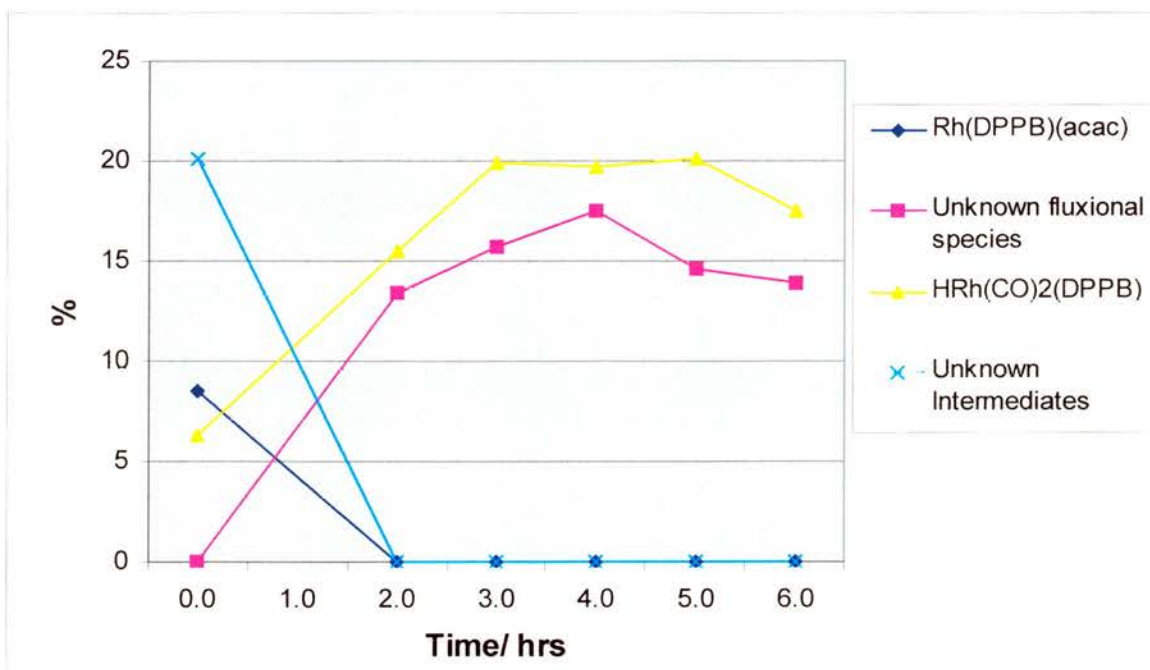
In the oxygen spiked experiment there is an initial high concentration of  $[\text{Rh}(\text{DIOP})(\text{acac})]$ , which decreases over the first two hours, as in the non-oxygen spiked experiment. The concentration of the unknown intermediate complex species also decreases to zero over the first two hours. The concentration of the rhodium hydride complex species increases over this time, as does the concentration of an unknown fluxional species. There is no evidence of a rhodium dimer complex species. The concentration of the rhodium hydride complex species and the unknown species increases further over the next hour, this is matched by a decrease in the dppb concentration. In the last hour, the concentration of the rhodium hydride complex species and the unknown species decreases slightly. This is matched by a slight increase in the dppb concentration. The concentration of the TPP goes up over the experiment as in the non-oxidised experiment; the same assumptions for this are made as for the non-oxidised experiment. Again, as in the non-oxidised experiment, there are small amounts of dppb oxide formed initially but after the first two hours this was stable.

**Graph 3.13**

$Rh(CO)_2(acac) / DPPB / TPP$  1:2:3, 20 bar synthesis gas, all phosphorous species.

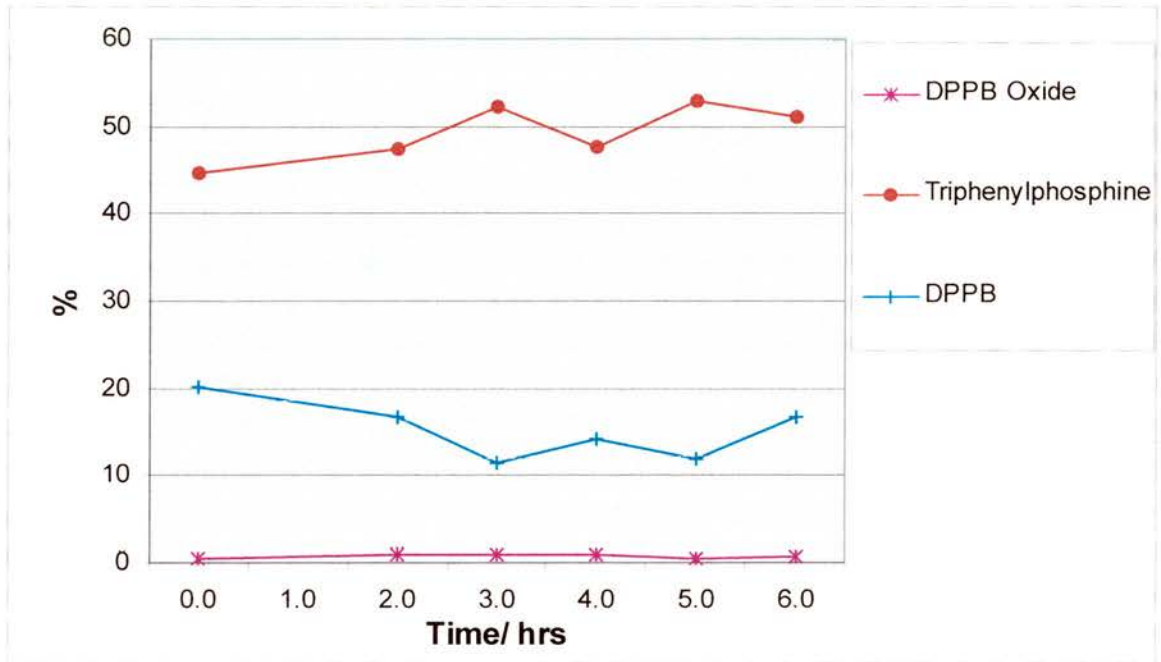
**Graph 3.14**

$Rh(CO)_2(acac) / DPPB / TPP$  1:2:3, 20 bar synthesis gas, complex species.



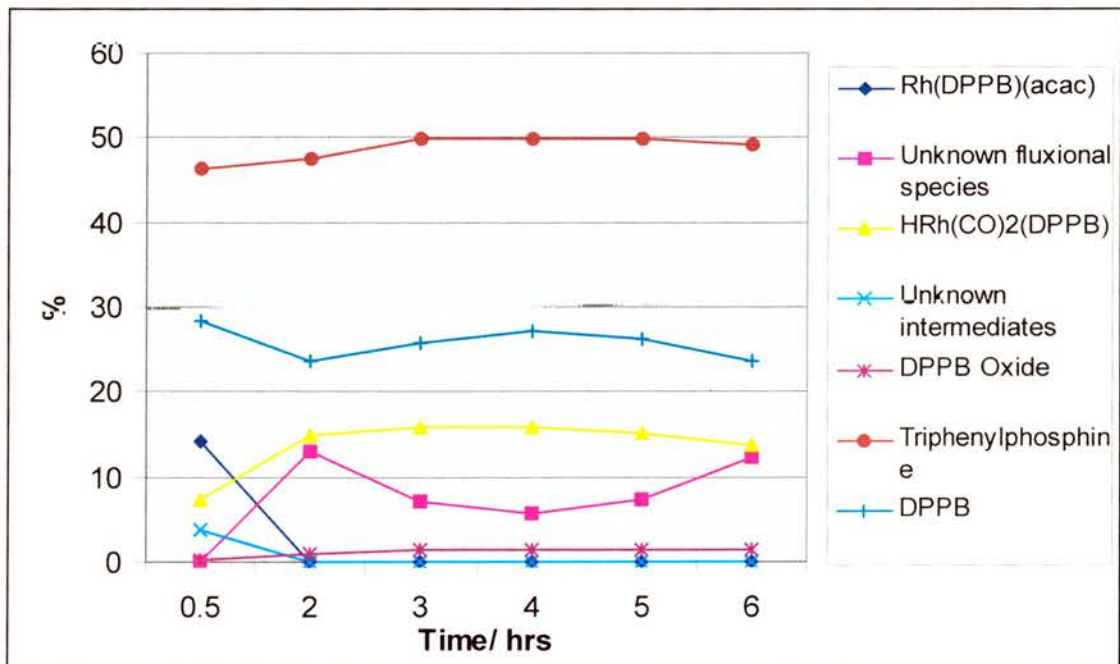
**Graph 3.15**

*Rh(CO)<sub>2</sub>(acac) / DPPB / TPP 1:2:3, 20 bar synthesis gas, uncomplexed species.*



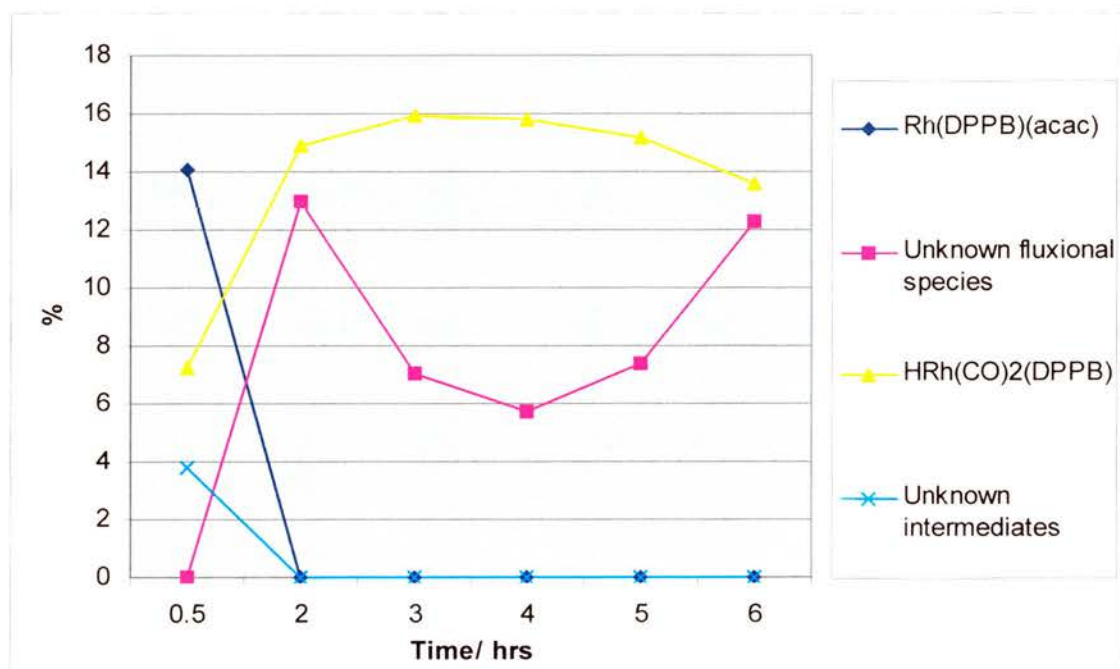
**Graph 3.16**

*Rh(CO)<sub>2</sub>(acac) / DPPB / TPP 1:2:3, 20 bar synthesis gas 99 % & air 1 %, all phosphorous species.*

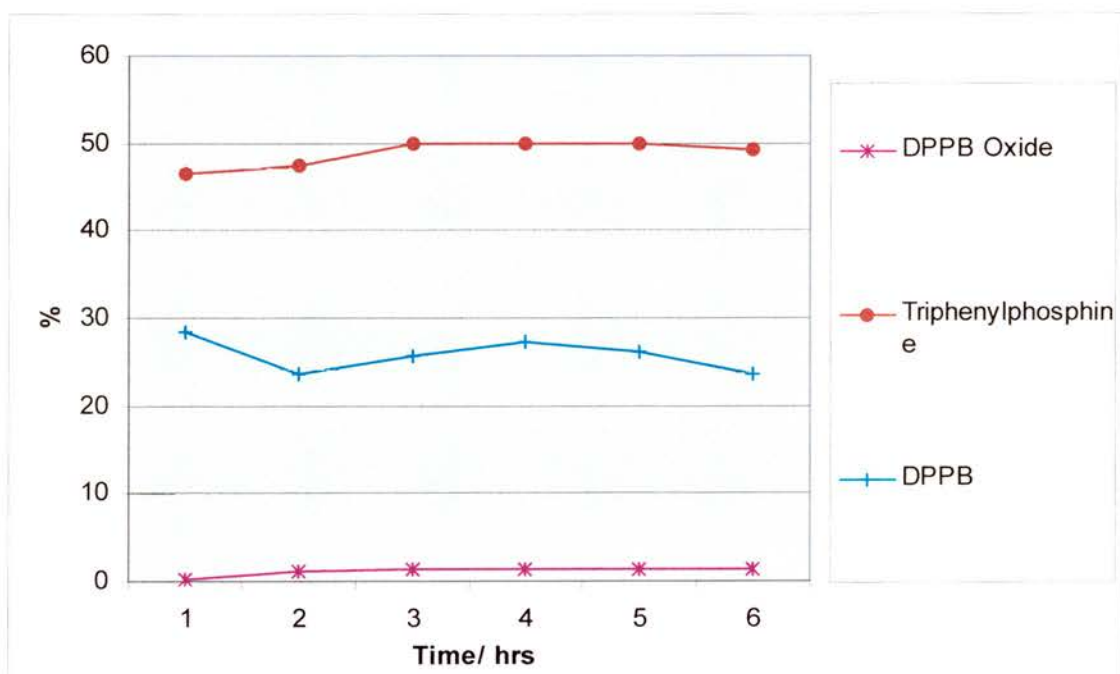


**Graph 3.17**

$Rh(CO)_2(acac) / DPPB / TPP$  1:2:3, 20 bar synthesis gas 99 % & air 1 %, complex species.

**Graph 3.18**

$Rh(CO)_2(acac) / DPPB / TPP$  1:2:3, 20 bar synthesis gas 99 % & air 1 %, uncomplexed species.



### 3.1.4 Experiment Four: Results For the Rhodium: DIOP Ratio 1:1 Catalytic Solution.

Graph 3.19 and Graph 3.20 show the concentrations of the phosphorus species present in solution with a  $[\text{Rh}(\text{CO})_2(\text{acac})]$  / DIOP ratio of 1:1, under 20 bar synthesis at 25 °C (at 0 hrs), and at 70 °C for 5 hours (1-6 hrs). Graph 3.21 and Graph 3.22 show the same situation under 98 % synthesis gas and 2 % air (0.4 % oxygen).

Graph 3.19 and Graph 3.21 show the relative concentrations of all the phosphorus species present. Graph 3.20 and Graph 3.22 show the concentrations of only the uncomplexed phosphorus species present.

In both cases, there is no initial presence of  $[\text{Rh}(\text{DIOP})(\text{acac})]$  or the  $[\text{Rh}(\text{P})_3]$  species. In both cases, there is a low concentration of DIOP present (even though it was added in a 1:1 ratio). In the non oxygen spiked study, this is about 3 % of the total DIOP concentration whereas in the oxygen spiked study this is about 10 % of the total DIOP concentration.

In the non oxygen spiked study, when there is 3 % free DIOP, there is also an unknown complex at 8 ppm in the  $^{31}\text{P}\{^1\text{H}\}$  NMR spectrum, which is not observed at higher concentration of DIOP.

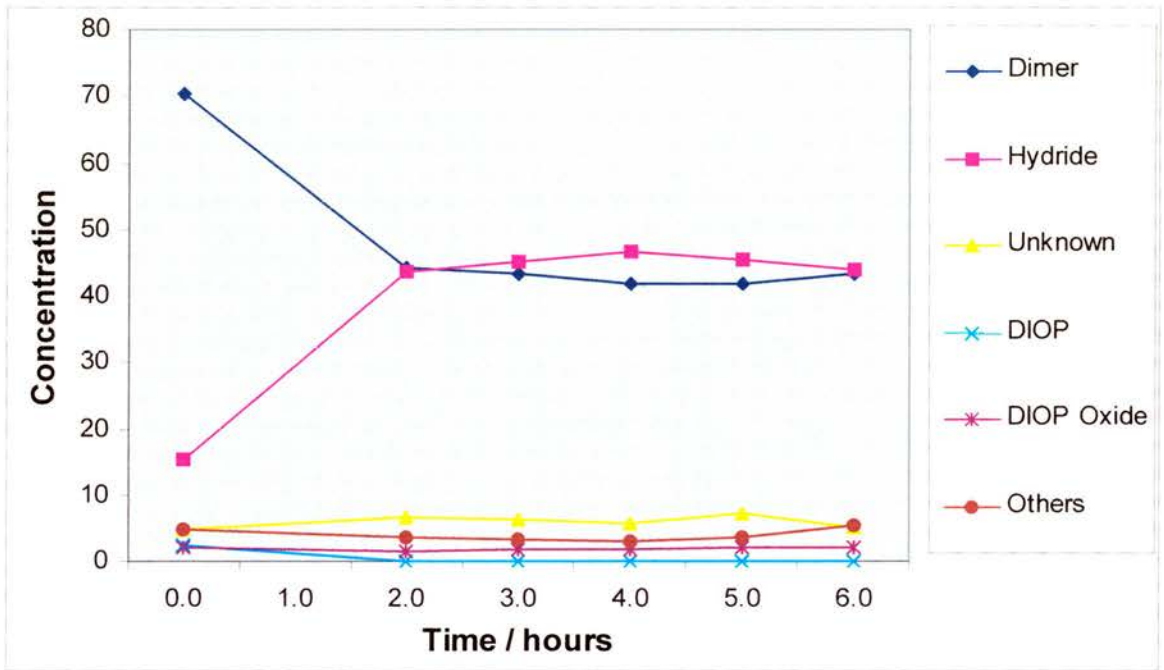
Over the first 2 hours, there is a drop in the dimer concentration and a rise in the hydride concentration. Both the drop and rise are approximately 15 %. When there is no oxygen present the DIOP concentration drops to zero, but the oxide concentration stays about the same. In the oxygen spiked case, there is a small amount of oxidation over the first two hours, after which the DIOP and DIOP oxide concentrations stay constant. There is no DIOP monoxide present in either case.

### 3.1.5 Experiment Five: Results For the Rhodium dppb Ratio 1:1 Catalytic Solution.

Initially, there are many different rhodium complex species present, even when kept under pressure for ten hours, and further studies into the system are required to assign these species. Over the first two hours (on heating), all these are converted to what is believed to be the rhodium dppb hydride complex. There was no oxidation observed in either the non-oxygen spiked or oxygen spiked systems.

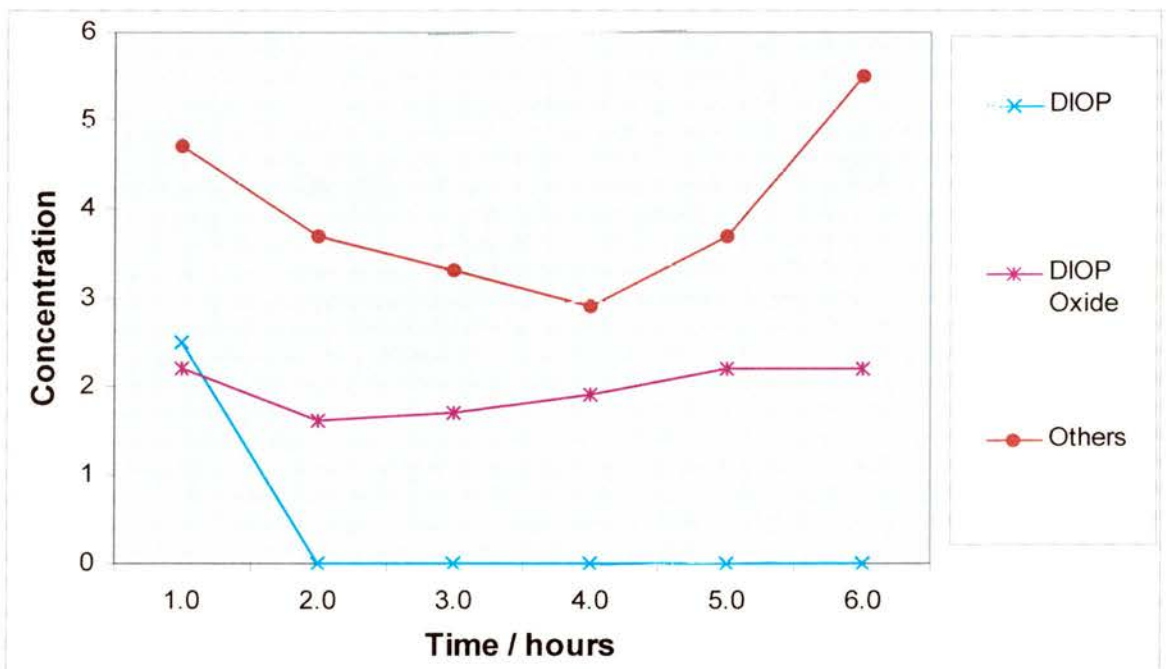
**Graph 3.19**

*Rh(CO)<sub>2</sub>(acac) / DIOP 1:1, 20 bar synthesis gas, all phosphorous species.*



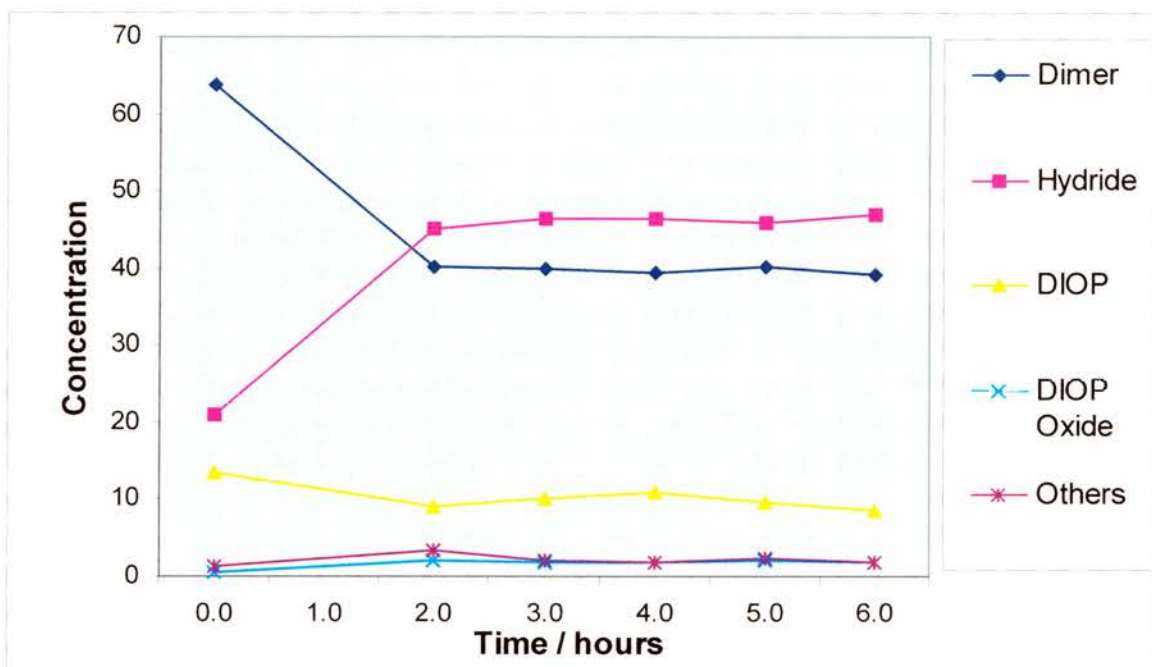
**Graph 3.20**

*Rh(CO)<sub>2</sub>(acac) / DIOP 1:1, 20 bar synthesis gas, uncomplexed species.*



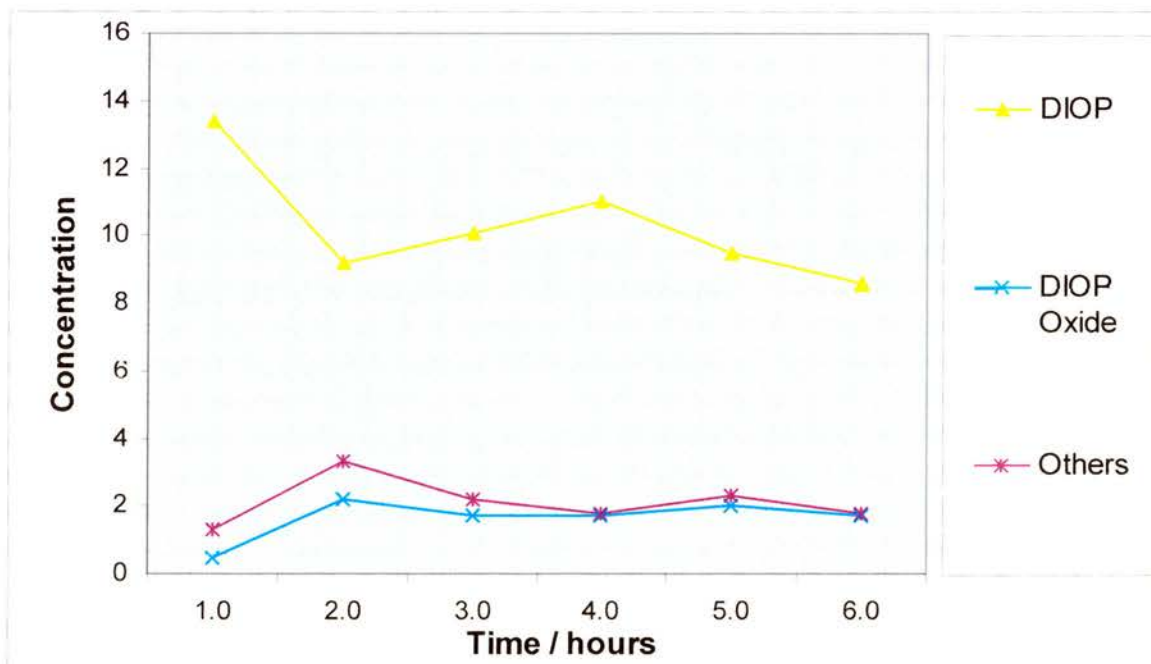
**Graph 3.21**

*Rh(CO)<sub>2</sub>(acac) / DIOP 1:1, 20 bar synthesis gas 98 % & air 2 %, all phosphorous species.*



**Graph 3.22**

*Rh(CO)<sub>2</sub>(acac) / DIOP 1:1, 20 bar synthesis gas 98 % & air 2 %, uncomplexed species.*



### 3.1.6 Experiment Six: Results For the Rhodium: DIOP Ratio 1:1 Catalytic Solution in the Presence of Allyl Alcohol.

We have already studied the rhodium DIOP complex species present during the hydroformylation reaction by *in-situ* high pressure NMR spectroscopy. At 25 °C, the  $^{31}\text{P}\{^1\text{H}\}$  NMR spectrum has two singlets at 31.1 and 31.0 ppm which are the protonated  $\text{DIOP}(\text{O})_2$  and  $\text{DIOP}(\text{O})$  respectively. It also has two sets of two double doublet resonances at 15.25 and 4.5 ppm and at 13.75 and 4.5 ppm which correspond to the acyl rhodium complex species **49** and **51**. Initially, at 70 °C, the major complex species present is an uncharacterised one at 8.4 ppm ( $^1J_{\text{P-Rh}} = 110$  Hz) this is speculated to be the dominant, if not only species present during the hydroformylation reaction itself. After a short period, there is the re-emergence of the acyl rhodium complex species **49** and **51**, and the emergence of the rhodium dimer complex species **46** at 5.3 ppm ( $^1J_{\text{P-Rh}} = 150$  Hz). By the end of the first hour of study, the  $^{31}\text{P}\{^1\text{H}\}$  NMR spectrum at 70 °C shows no evidence of the uncharacterised species at 8.4 ppm, only the acyl rhodium complex species **49** and **51**, the rhodium dimer complex species **46**, the rhodium hydride species **24** and **25**, the complex species present under an inert atmosphere **41** at 38.76 ppm ( $^1J_{\text{P-Rh}} = 190$  Hz), and the triphosphorus complex species  $[\text{RhP}_3]$ . This is consistent with what we have already observed for this system, see section 2.5. The presence of the last complex species  $[\text{RhP}_3]$  is very important. As speculated earlier, this is either a rival complex species in the formation of the rhodium dimer species from the species present under an inert atmosphere, or an intermediate in the formation of the dimer complex species **46**. It is, therefore, not surprising that it is present considering the presence of the species **41** and **46**.

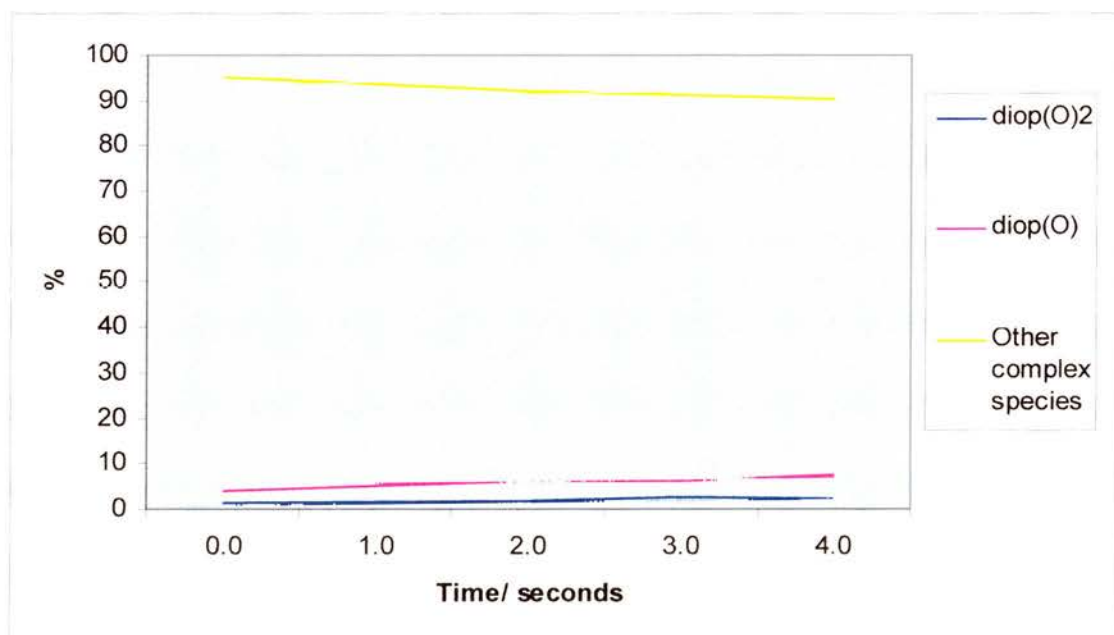
Graph 3.23 and Graph 3.24 show the concentrations of the phosphorus species present in solution with a  $[\text{Rh}(\text{CO})_2(\text{acac})]$  / DIOP ratio of 1:1, under 20 bar synthesis in the presence of excess allyl alcohol at 25 °C (at 0 hrs), at 70 °C for 2 hours (1-3 hrs), and at 25 °C (4 hrs). Graph 3.25 and Graph 3.26 show the same situation under 98 % synthesis gas and 2 % air, or 0.4 % oxygen.

For the sake of simplicity the rhodium complex species of DIOP are grouped together in Graph 3.23 and Graph 3.25 which shows the concentration of the complex species and of  $\text{DIOP}(\text{O})$  and  $\text{DIOP}(\text{O})_2$  during the experiments. Graph 3.24 and Graph 3.26 shows the concentration of  $\text{DIOP}(\text{O})$  and  $\text{DIOP}(\text{O})_2$  during the experiments.

In both the oxygen free and oxygen spiked experiments the samples show oxidation at the beginning of the reaction. This is consistent with small quantities of oxygen being present during the pressurising stage of the reaction which have not been purged from the system. In both experiments there is an increase in the level of oxide species though out the experiment. The concentration of the  $\text{DIOP}(\text{O})_2$  species levels out towards the end of both experiments. The concentration of the  $\text{DIOP}(\text{O})$  species does not level out but continues to rise for the full four hours of both experiments. It is noted, however, that the rise in the oxygen spiked case is 1.5 times that of the non-oxygen spiked case.

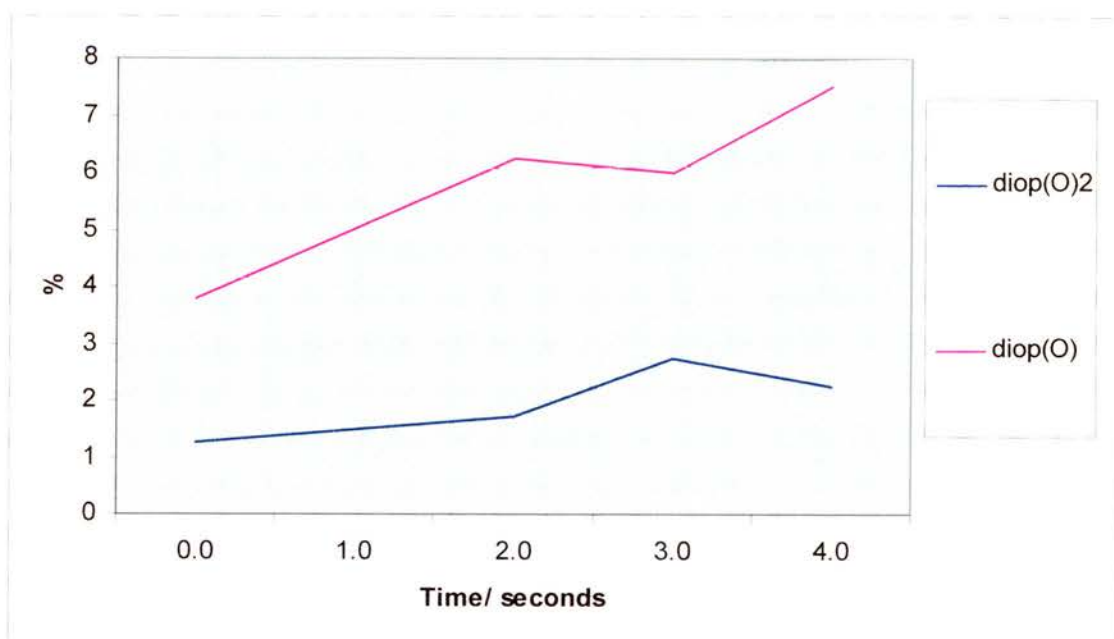
### Graph 3.23

*$\text{Rh}(\text{CO})_2(\text{acac}) / \text{DIOP} 1:1$ , 20 bar synthesis gas, in the presence of excess allyl alcohol, all phosphorus species.*

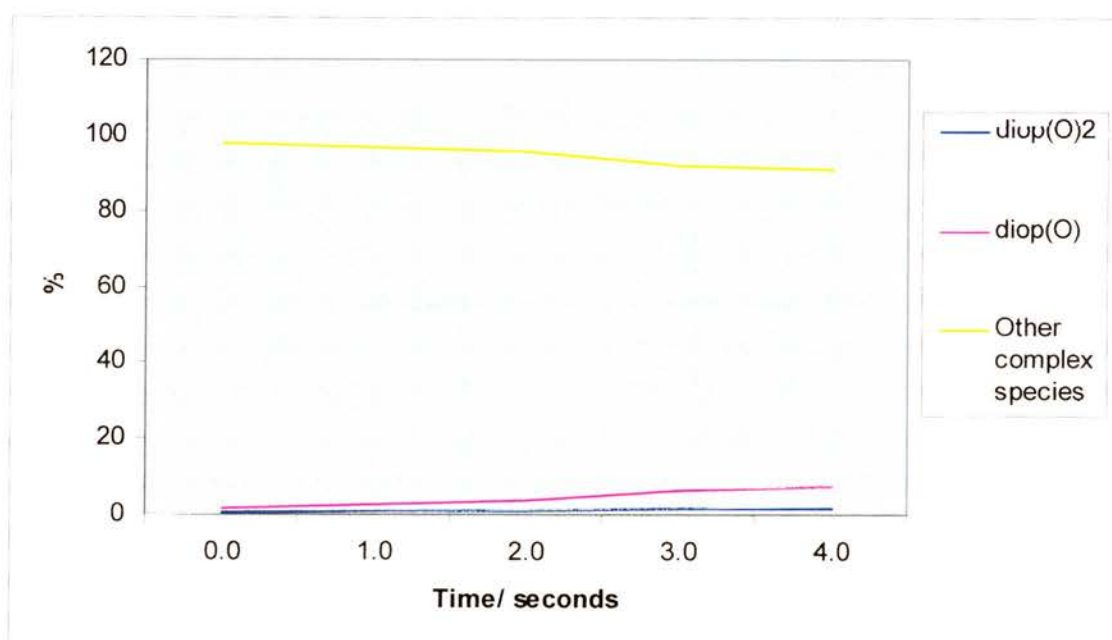


**Graph 3.24**

*Rh(CO)<sub>2</sub>(acac) / DIOP 1:1, 20 bar synthesis gas, in the presence of excess allyl alcohol, DIOP(O) & DIOP(O)<sub>2</sub>.*

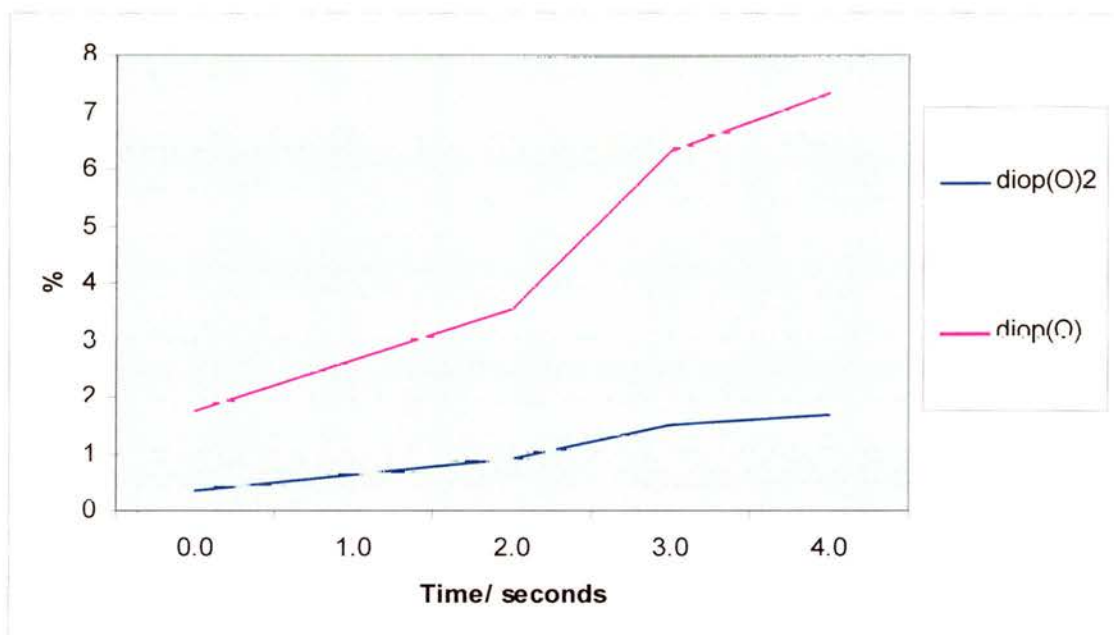
**Graph 3.25**

*Rh(CO)<sub>2</sub>(acac) / DIOP 1:1, 20 bar synthesis gas 98 % & air 2 %, in the presence of excess allyl alcohol, all phosphorus species.*



**Graph 3.26**

*Rh(CO)<sub>2</sub>(acac) / DIOP 1:1, 20 bar synthesis gas 98 % & air 2 %, in the presence of excess allyl alcohol, DIOP(O) & DIOP(O)<sub>2</sub>.*



### 3.1.7 Experiment Seven: Results For the Rhodium: dppb Ratio 1:1 Catalytic Solution in the Presence of Allyl Alcohol.

We have not previously studied the rhodium dppb complex species present during the hydroformylation of allyl alcohol so we must first define them, as they can give very important insights into how the system might behave differently from the rhodium DIOP system.

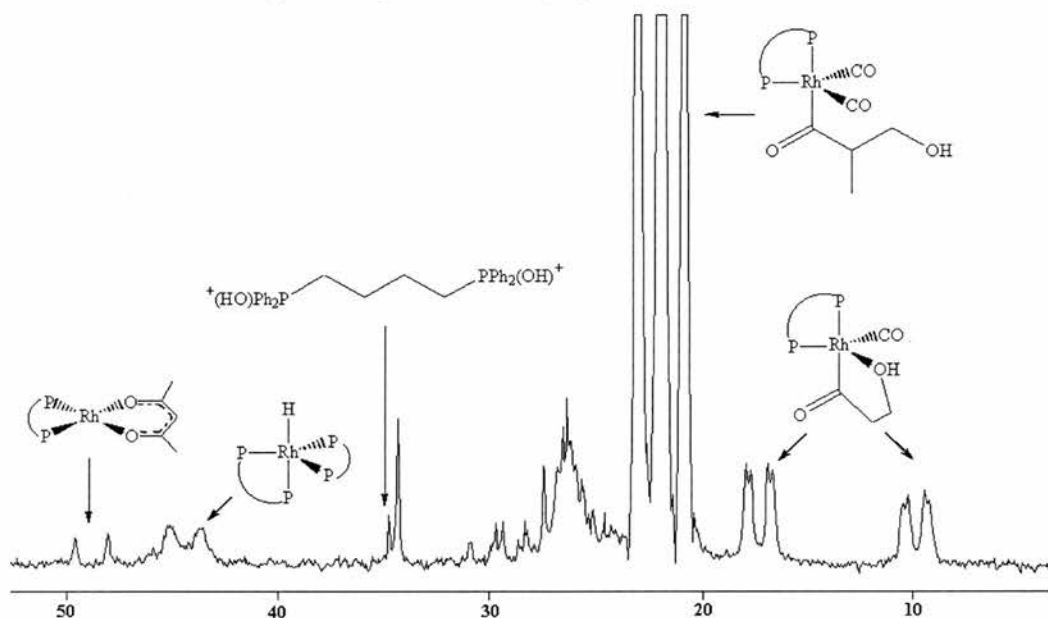
The complex species present during the hydroformylation of allyl alcohol have been studied by *in situ* high pressure  $^{31}\text{P}\{^1\text{H}\}$  NMR spectroscopy.

At 25 °C, the  $^{31}\text{P}\{^1\text{H}\}$  NMR spectrum shows a sharp doublet resonance at 48.77 ppm ( $^1J_{\text{PRh}} = 183$  Hz), a broad doublet resonance at 44.43 ppm ( $^1J_{\text{PRh}} = 189$  Hz), singlet resonances at 34.76 ppm, and at 34.31 ppm, a multiplet at 30 ppm to 24 ppm, two double doublet resonances of high intensity at 22.49 ppm and 21.29 ppm ( $^1J_{\text{PRh}} = 128$  Hz and  $^1J_{\text{PP}} = 24$  Hz, it is noted that the neighbouring peaks of the two doublet doublets have the same chemical shift which forms a pseudo triplet), and two double doublets of

low intensity at 17.35 ppm and 9.87 ppm ( $^1J_{\text{PRh}} = 128$  Hz and  $^1J_{\text{PP}} = 24$  Hz), see NMR 3.1 and NMR 3.2.

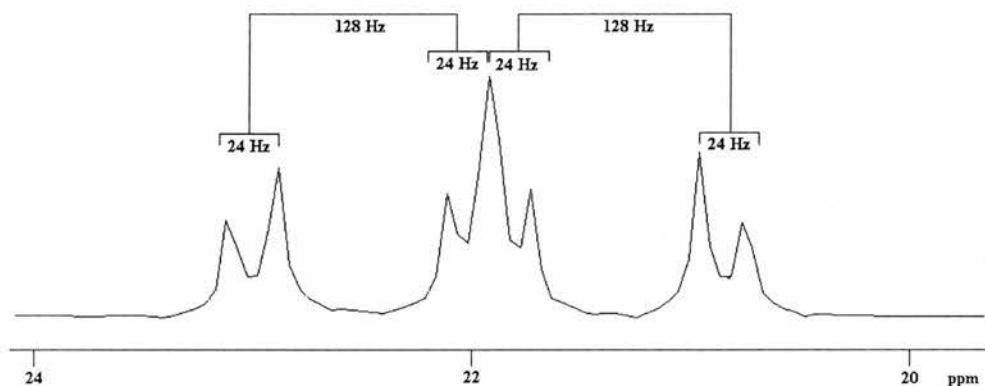
### NMR 3.1

*Expansion of the  $^{31}\text{P}\{^1\text{H}\}$  NMR spectrum of the rhodium dppb allyl alcohol complex species of low intensity, present at 25 °C.*



### NMR 3.2

*The  $^{31}\text{P}\{^1\text{H}\}$  NMR spectrum of the double doublets of high intensity in NMR 3.1.*



It is suggested that the doublet at 48.77 ppm arises from  $[\text{Rh}(\text{dppb})(\text{acac})]$ , the doublet at 44.43 ppm  $[\text{HRh}(\text{dppb})_2]$ ,<sup>3</sup> the singlet at 34.76 ppm from the protonated form of dppb dioxo  $[(\text{dppb})(\text{OH})_2^{2+}]$ , the singlet at 34.31 ppm from the protonated form of dppb monooxo  $[(\text{dppb})(\text{OH})^{2+}]$  (note there is no singlet for the non-oxidised phosphorus of the dppb monooxo, it is suggested that it is complexed to rhodium and resonates as part

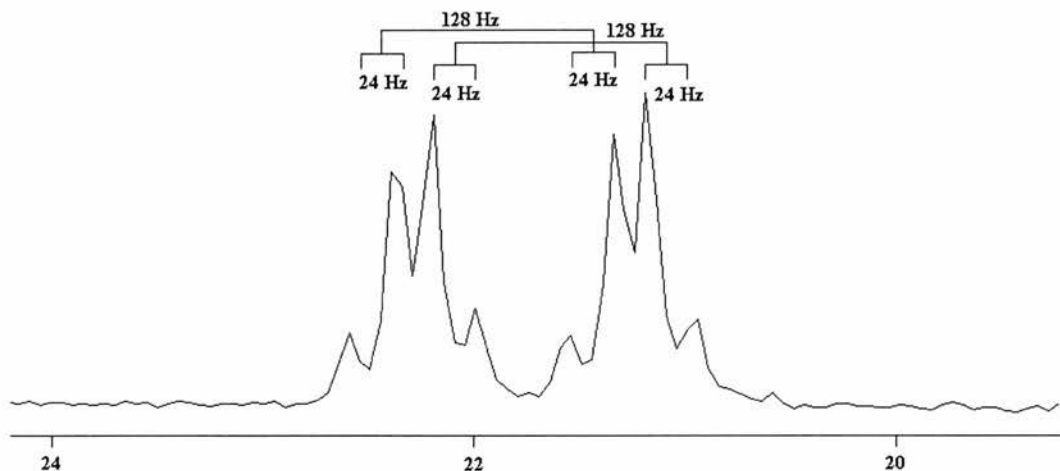
of the multiplet resonance). The two double doublet resonances of high intensity at 22.49 ppm and 21.29 ppm are proposed to be the linear acyl rhodium complex species, analogous to the rhodium DIOP complex species, **49**. The two double doublet resonances of low intensity at 17.35 ppm and 9.87 ppm are proposed to be the branched acyl rhodium complex species, analogous to the rhodium DIOP complex species, **51**. It is proposed the double doublets of low intensity arise from the branched isomer because of the difference in the chemical shifts between the two resonances. One is near the double doublets of the proposed linear isomer, 5 ppm downfield, while the other is much further away, 12 ppm downfield. It is speculated that the reason for this arises from the formation of a chelate, analogous to that formed in the DIOP case. It is interesting that the linear isomer is by far the most abundant isomer; in section 2.5 it was suggested that the increased l:b ratio in the hydroformylation of allyl alcohol with the rhodium DIOP catalytic system could stem from the branched acyl rhodium complex species being stabilised by the chelate effect, so the linear form is more reactive. For the rhodium dppb catalytic system, even though we observe a similar chelate effect in the branched isomer, the linear one is by far the most abundant, thus more stable. So, even though the DIOP and dppb ligands are quite similar, the greater rigidity of the DIOP ligand and the remote electronic effects have a great effect on the stabilities of the catalytic intermediates.

At 60 °C, the only observed species are the dppb oxides and the two major double doublet resonances with slightly shifted chemical shifts of 22.31 ppm and 21.28 ppm ( $^1J_{\text{PRh}} = 128$  Hz and  $^1J_{\text{PP}} = 24$  Hz, see NMR 3.3).

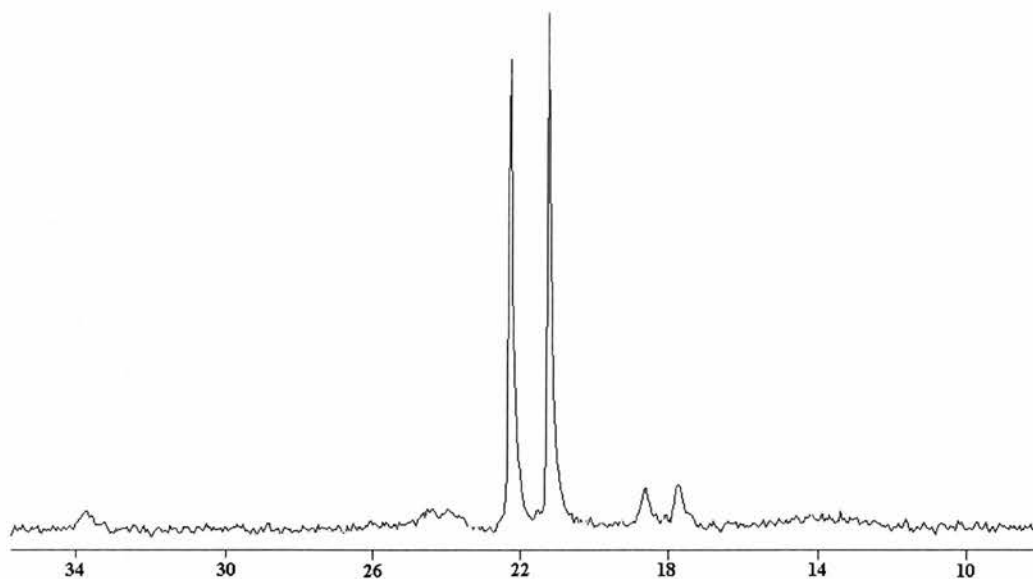
At 65 °C, the  $^{31}\text{P}\{^1\text{H}\}$  NMR spectrum shows a doublet at 21.78 ppm ( $^1J_{\text{PRh}} = 128$  Hz). Initially, at 70 °C, the  $^{31}\text{P}\{^1\text{H}\}$  NMR spectrum also shows the presence of the doublet only. After one hour at 70 °C, the  $^{31}\text{P}\{^1\text{H}\}$  NMR spectrum shows the presence of DIOP oxides, a broad resonance at 24.20 ppm, the intense doublet at 21.78 ppm ( $^1J_{\text{PRh}} = 128$  Hz), and a new doublet at 18.19 ppm ( $^1J_{\text{PRh}} = 104$  Hz), and broad resonance at 14.20 ppm, see NMR 3.4.

**NMR 3.3**

$^{31}\text{P}\{^1\text{H}\}$  NMR spectrum of the rhodium dppb allyl alcohol complex present at 60 °C.

**NMR 3.4**

$^{31}\text{P}\{^1\text{H}\}$  NMR spectrum of the rhodium dppb allyl alcohol complex present after one hour at 70 °C.



After two hours at 70 °C, the  $^{31}\text{P}\{^1\text{H}\}$  NMR spectrum shows the presence of DIOP oxides, the broad resonance at 24.20 ppm, the intense doublet at 21.78 ppm ( $^1J_{\text{PRh}} = 128$  Hz), and the broad resonance at 24.20 ppm. After the cell has been cooled to room temperature, the  $^{31}\text{P}\{^1\text{H}\}$  NMR spectrum shows the presence of DIOP oxides, the broad resonance at 24.20 ppm, the two double doublet resonances of high intensity at 22.49 ppm and 21.29 ppm ( $^1J_{\text{PRh}} = 128$  Hz and  $^1J_{\text{PP}} = 24$  Hz), the doublet at 18.19 ppm

which is now broad, and the broad resonance at 14.20 ppm. Note that at 25 °C, initially, the double doublets overlap such that the resonance looks like a triplet and two doublets.

It is proposed that the doublet at 21.78 ppm ( $^1J_{\text{PRh}} = 128$  Hz) at 70 °C is the same complex species that gives rise to the double doublet resonances at 22.49 ppm and 21.29 ppm ( $^1J_{\text{PRh}} = 128$  Hz and  $^1J_{\text{PP}} = 24$  Hz at 25 °C). It has already been speculated that this is the linear acyl rhodium complex.

Graph 3.27 and Graph 3.28 show the concentrations of the phosphorus species present in solution with a  $\text{Rh}(\text{CO})_2(\text{acac}) / \text{dppb}$  ratio of 1:1, under 20 bar synthesis in the presence of excess allyl alcohol at 25 °C (at 0 hrs), at 70 °C for 2 hours (1-3 hrs), and at 25 °C (4 hrs). Graph 3.29 and Graph 3.30 show the same situation under 98 % synthesis gas and 2 % air, or 0.4 % oxygen.

For the sake of simplicity, the rhodium complex species of dppb are grouped together in Graph 3.27 and Graph 3.29 which shows the concentration of the complex species and of  $\text{dppb}(\text{OH})^+$  and  $\text{dppb}(\text{OH})_2^{2+}$  during the experiments. Graph 3.28 and Graph 3.30 shows the concentration of  $\text{dppb}(\text{OH})^+$  and  $\text{dppb}(\text{OH})_2^{2+}$  during the experiments.

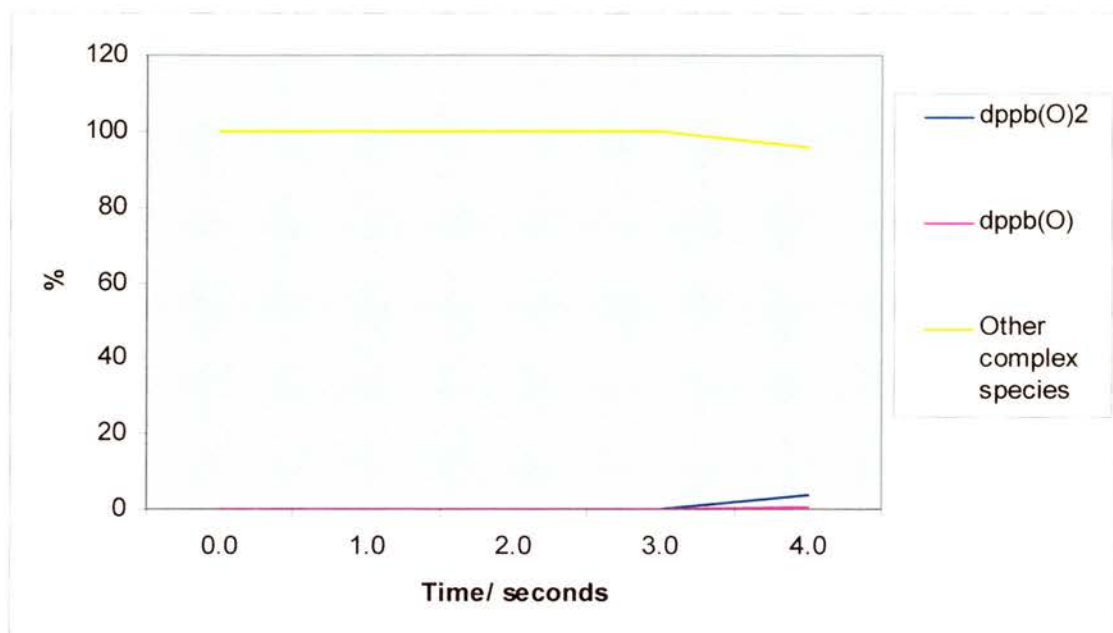
The rhodium / dppb / allyl alcohol experiments are very interesting as there is no oxidation in the non-oxygen spiked experiment over the first 3 hours. However, a small amount of oxidation is observed towards the end of the experiment. It is, therefore, concluded that the catalytic precursors are stable towards oxidation, which confirms what is observed in section 4.2.5. The oxidation at the end of the experiment, however, suggests the catalytic species are not as stable when cooling the reaction.

In the oxygen spiked experiment there are small levels of dppb mono-oxide and dppb-dioxide over the whole reaction period. The oxidation of dppb is put down to the greater susceptibility towards oxidation of the new complex species observed as double doublet resonances in the  $^31\text{P} \{^1\text{H}\}$  NMR, 22.49 ppm and 21.29 ppm ( $^1J_{\text{PRh}} = 128$  Hz and  $^1J_{\text{PP}} = 24$  Hz). Unlike with DIOP, this is the species we see during the hydroformylation reaction, rather than the complex species observed after the hydroformylation reaction if gas starvation has occurred.

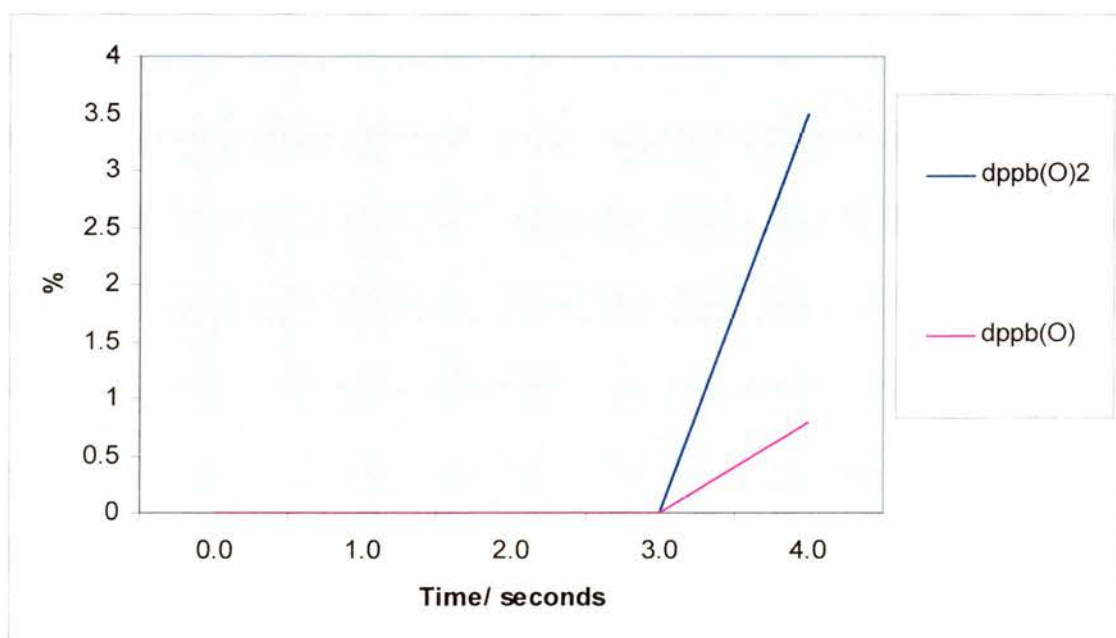
It is concluded that while the rhodium dppb catalytic precursors are slightly more stable than the rhodium DIOP catalyst precursors, the active catalytic complex species are comparable.

**Graph 3.27**

*Rh(CO)<sub>2</sub>(acac) / dppb 1:1, 20 bar synthesis gas, in the presence of excess allyl alcohol, all phosphorus species.*

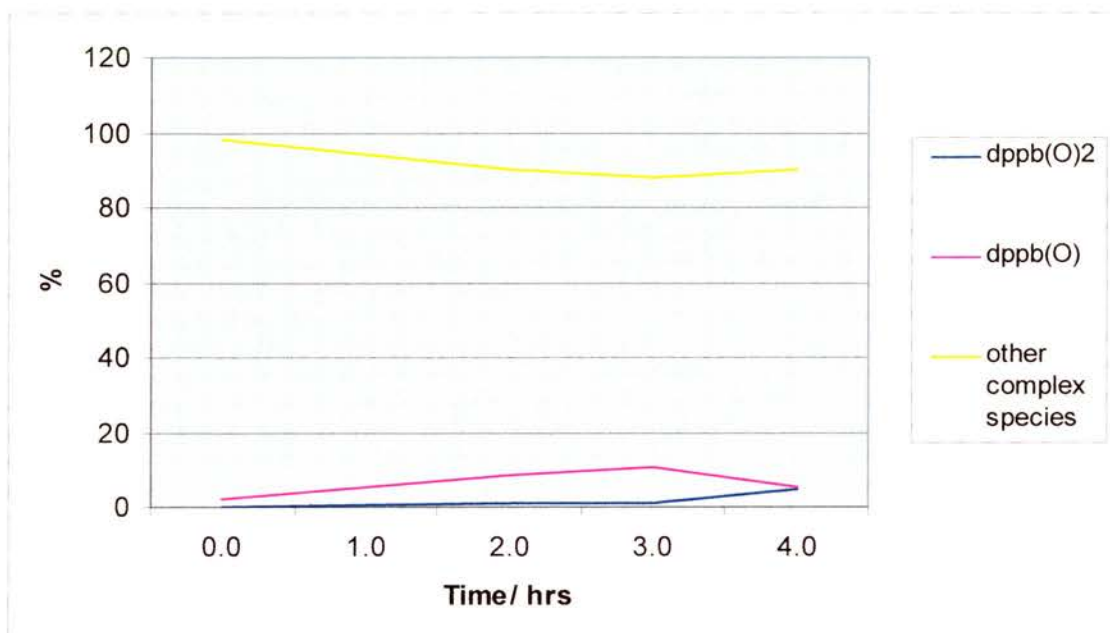
**Graph 3.28**

*Rh(CO)<sub>2</sub>(acac) / dppb 1:1, 20 bar synthesis gas, in the presence of excess allyl alcohol, DIOP(O) & DIOP(O)<sub>2</sub>.*

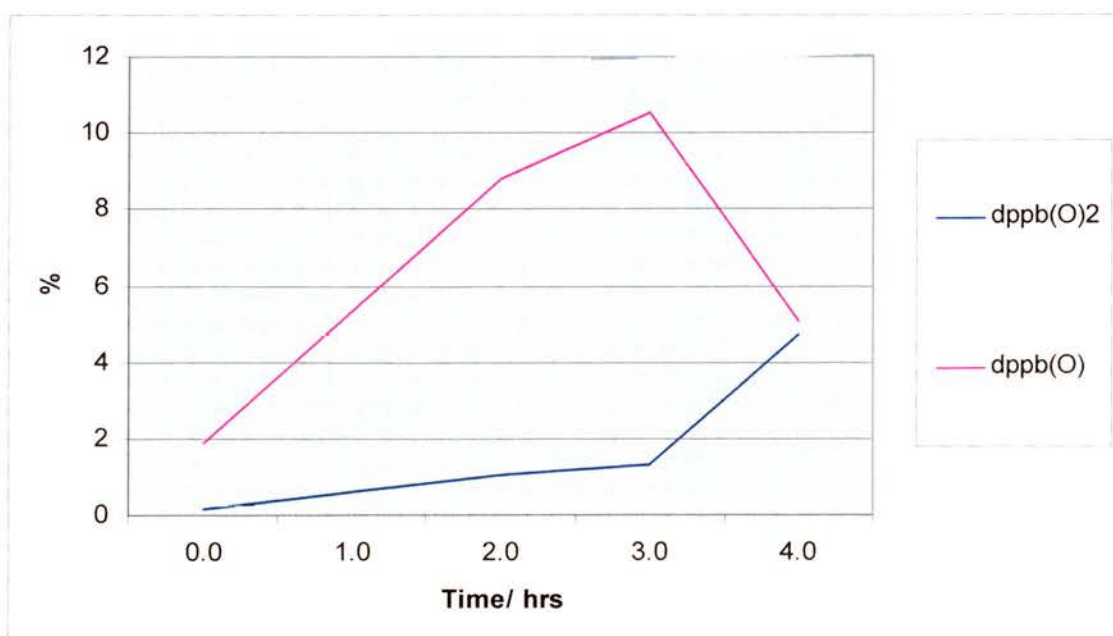


**Graph 3.29**

*Rh(CO)<sub>2</sub>(acac) / dppb 1:1, 20 bar synthesis gas 98 % & air 2 %, in the presence of excess allyl alcohol, all phosphorus species.*

**Graph 3.30**

*Rh(CO)<sub>2</sub>(acac) / dppb 1:1, 20 bar synthesis gas 98 % & air 2 %, in the presence of excess allyl alcohol, DIOP(O) & DIOP(O)<sub>2</sub>.*



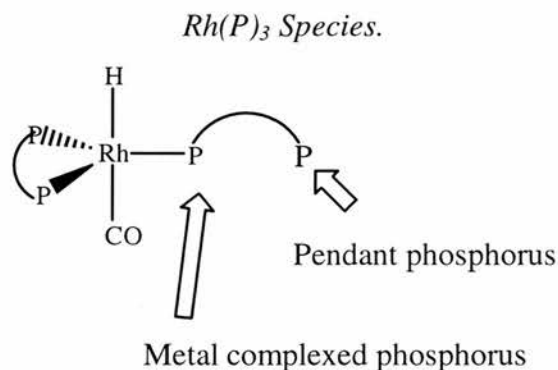
### 3.1.8 Conclusions.

Our results show that oxidation can occur to DIOP and DPPB, and that this oxidation follows two patterns.

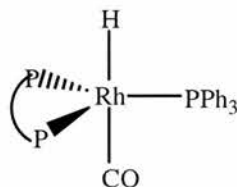
Firstly, there seems to be a small amount of oxidation of DIOP over the first two hours of study, when the complex species are reaching a new equilibrium after the sample has been heated up. This produces both the monoxide and the dioxide in approximately equal measure. There does not seem to be any oxidation of DPPB under the same circumstances.

However, there seems to be a greater amount of oxidation of DIOP occurring when the  $[\text{Rh}(\text{P})_3]$  species is present which results in the monoxide DIOP(O). It is, therefore, hypothesised that the  $\text{R}(\text{P})_3$  species, see fig 4.1, catalyses the oxidation of the unidentate DIOP ligand at either pendant phosphorus atom or at the metal complexed phosphorus atom, resulting in high levels of DIOP(O).

**Figure 3.1**



The presence of triphenylphosphine reduced the amount of monoxide formed in the presence of the  $[\text{Rh}(\text{P})_3]$  species. It is hypothesised that this is due to the triphenylphosphine replacing the unidentate DIOP, see figure 4.2. This complex has no pendant phosphorous atom to be oxidised. As there is no TPP oxide, it is probable that it is the pendant phosphorus atom of the unidentate complexed DIOP which is being oxidised. So we hypothesis further that the  $[\text{Rh}(\text{P})_3]$  complex catalyses the oxidation of the pendant DIOP phosphorous atom, when it is bound unidentate. Possibly because of a proximity effect or a remote electronic one, although this is not likely over so many bonds.

**Figure 3.2**

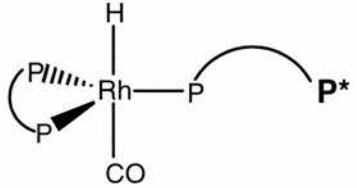
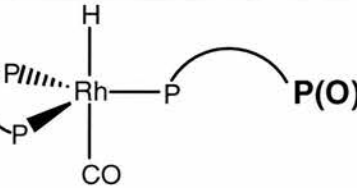
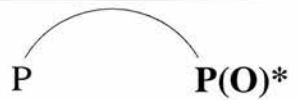
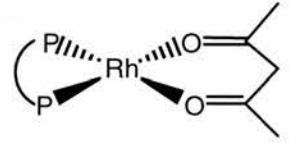
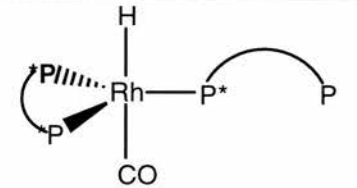
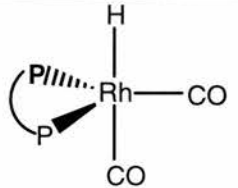
It is also interesting to note that there is no oxidation of DPPB observed in the Rh / DPPB 1:1 and 0.4 % oxygen study. However, oxidation was observed in the Rh / DPPB / TPP 1:2:3 study when the rhodium DPPB  $[\text{Rh}(\text{P})_3]$  complex species was present. It is further hypothesised that the rhodium DPPB  $[\text{Rh}(\text{P})_3]$  complex species also catalyses the mono-oxidation of DPPB, as the rhodium DIOP  $[\text{Rh}(\text{P})_3]$  complex species catalyses the mono-oxidation of DIOP, and that the oxide species formed in the Rh / DPPB / TPP 1:2:3 study was, therefore, DPPB(O) not DPPB(O)<sub>2</sub>.

It was also noted in the *in situ* hydroformylation studies that, while the DIOP catalytic precursors are slightly more stable than the dppb catalytic precursors to the active hydroformylation rhodium complex species, the active hydroformylation complex species are comparable in stability towards oxidation.

**Table 3.2**

*The species involved in the oxidation studies and there chemical shifts.*

Phosphorus Species	Chemical Shift (C <sub>7</sub> D <sub>8</sub> , 121.4 MHz) $\delta$ / ppm
 DIOP	-22.24 Singlet
 "P"-DIOP monoxide	-21.02 Singlet

 <p>"Pendant P"-P<sub>3</sub> complex</p>	<p>-20.47</p> <p>Singlet</p>
 <p>"Pendant P(O)"-P<sub>3</sub> complex</p>	<p>25.13</p> <p>Singlet</p>
 <p>"P(O)"-DIOP monoxide</p>	<p>25.61</p> <p>Singlet</p>
 <p>DIOP oxide</p>	<p>26.18</p> <p>Singlet</p>
 <p>Rh(acac)(DIOP)</p>	<p>38.67</p> <p>Doublet</p>
 <p>P<sub>3</sub> complex</p>	<p>34-29 &amp; 23-20</p> <p>16 Line multiplet</p>
 <p>Rhodium DIOP hydride.</p>	<p>17.7</p> <p>doublet</p>

### 3.2 Effect of $\text{Fe}(\text{CO})_5$ on the Oxidation Properties of DIOP.

As mentioned in section 1.2.5, the hydroformylation of allyl alcohol with the rhodium TPP catalyst system is carried out in the presence of iron.<sup>2</sup>

It is well documented that iron can form complexes with phosphines<sup>4,5</sup> and with rhodium.<sup>6</sup> Several experiments were therefore developed to investigate the complex species present in the rhodium DIOP catalytic system when in the presence of an iron precursor  $[\text{Fe}(\text{CO})_5]$ . We have also studied how the presence of  $[\text{Fe}(\text{CO})_5]$  effects the stability of DIOP towards oxidation.

Experiment one is a study of the iron / DIOP (ratio 1:1) complex species that form in an argon atmosphere. Experiment two is a study of the iron / DIOP (ratio 1:1) complex species that form under a pressure of 20 bar synthesis gas. Experiment three is a study of the iron / DIOP / allyl alcohol complex species that form under a pressure of 20 bar synthesis gas. Experiment four is a study of the rhodium / iron / DIOP / allyl alcohol complex species under a pressure of 20 bar synthesis gas 98 % and air 2 %.

#### 3.2.1 Experiment One: $\text{Fe}(\text{CO})_5$ / DIOP.

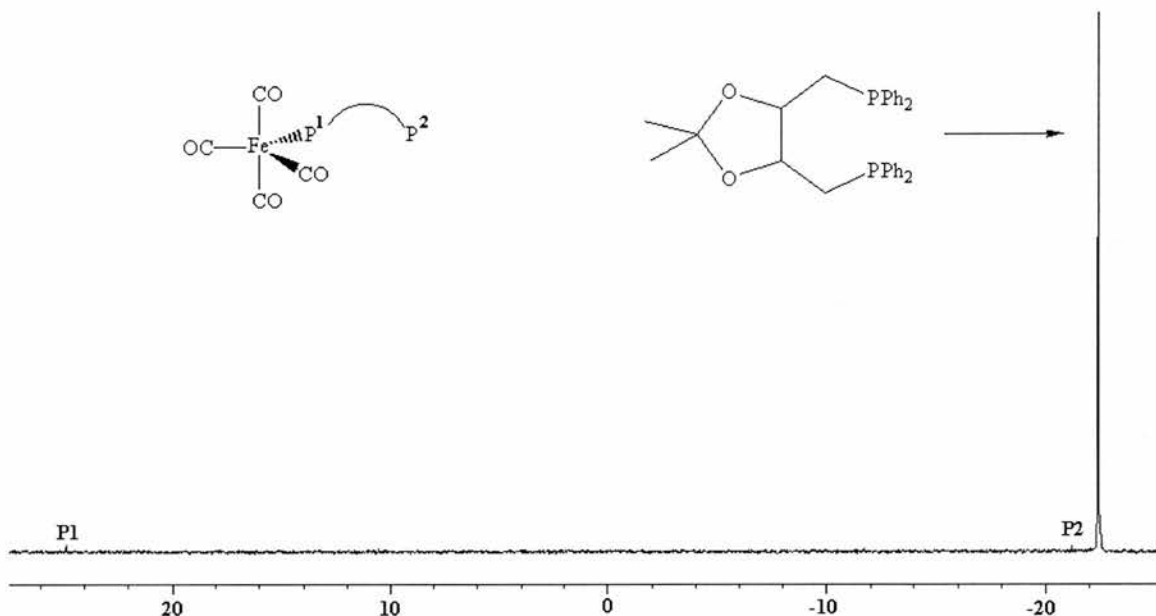
The  $^{31}\text{P}$   $\{^1\text{H}\}$  NMR spectrum of the  $[\text{Fe}(\text{CO})_5]$  / DIOP (ratio 1:1) solution can be seen in NMR 3.5. It shows that under these conditions there is very little reaction between  $[\text{Fe}(\text{CO})_5]$  and DIOP. There are three resonances. Most of the DIOP is uncomplexed and can be observed as free DIOP at  $-22.23$  ppm. The other two resonances are at  $24.83$  ppm, and  $-21.13$  ppm. It is suggested that the peaks at  $24.83$  ppm and  $-21.13$  ppm are from a single iron DIOP complex  $[\text{Fe}(\text{CO})_4(\text{DIOP})]$  where the DIOP is bound unidentate, see NMR 3.5. The resonance at  $24.83$  ppm is the complexed phosphorus resonance and the resonance at  $-21.13$  ppm is the pendant phosphorus resonance.

The  $^{13}\text{C}$  NMR spectrum of the  $[\text{Fe}(\text{CO})_5]$  / DIOP (ratio 1:1) solution can be seen in NMR 3.6. The spectrum clearly shows the carbonyl resonance from  $[\text{Fe}(\text{CO})_5]$  at  $210.80$  ppm; the rest of the spectrum can be assigned to DIOP,  $137.35$ - $127.41$  ppm ( $-\text{PPh}_2$ , m),  $108.00$  ppm ( $((\text{CH}_3)_2\text{C}(\text{O})_2$ , s),  $78.00$  ppm ( $-\text{OCH}-$ , t),  $32.91$  ppm

(-CHCH<sub>2</sub>P-, t), 26.90 ppm (CH<sub>3</sub>C-, s), and d<sup>8</sup>-toluene, 137.85 ppm (s), 129.23 ppm (t), 128.32 ppm (t), 125 ppm (t), 20.40 ppm (hept)

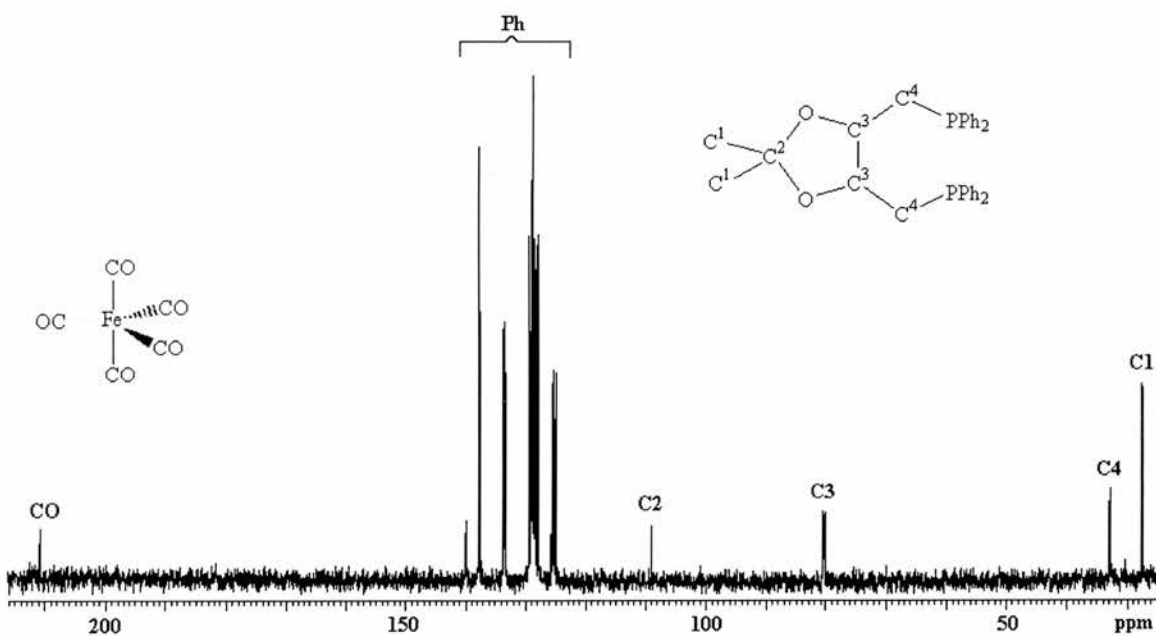
### NMR 3.5

<sup>31</sup>P{<sup>1</sup>H} NMR spectrum of Fe(CO)<sub>5</sub> / DIOP 1:1 under an argon atmosphere at 25 °C.



### NMR 3.6

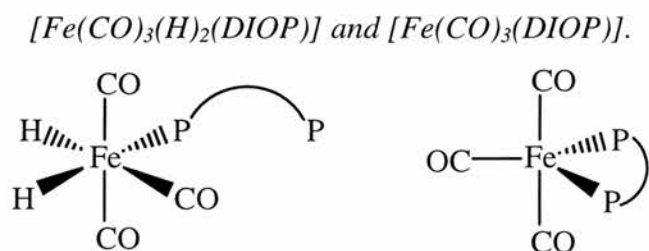
<sup>13</sup>C NMR spectrum of Fe(CO)<sub>5</sub> / DIOP 1:1 under an argon atmosphere at 25 °C.



### 3.2.2 Experiment Two: $\text{Fe}(\text{CO})_5$ / DIOP under Synthesis gas 20 bar.

The  $^{31}\text{P}$   $\{^1\text{H}\}$  NMR spectrum of the  $[\text{Fe}(\text{CO})_5]$  / DIOP (ratio 1:1) solution under an atmosphere of 20 bar synthesis gas at 25 °C can be seen in NMR 3.7. It shows that, as under argon, there is very little reaction between  $[\text{Fe}(\text{CO})_5]$  and DIOP as most of the DIOP is uncomplexed at  $-22.56$  ppm. An expansion of the peaks of low intensity can be seen in NMR 3.8. It shows there are five resonances of low intensity at 25.87 ppm, 24.87 ppm, 24.11 ppm,  $-22.50$  ppm, and  $-21.30$  ppm. The resonances at 24.87 ppm and  $-21.30$  ppm are a single iron DIOP complex  $[\text{Fe}(\text{CO})_4(\text{DIOP})]$  where the DIOP is bound unidentate which was observed in section 3.2.1. The resonance at 24.87 ppm is the complexed phosphorus resonance and the resonance at  $-21.30$  ppm is the pendant phosphorus resonance. It is suggested that the two resonances at 25.87 ppm and  $-20.50$  ppm are from a similar complex species, possibly a hydride, for example  $[\text{Fe}(\text{CO})_3(\text{H})_2(\text{DIOP})]$ , where the DIOP is bound unidentate, see Figure 3.3. The resonance at 25.87 ppm is from the complexed phosphorus resonance and the resonance at  $-20.50$  ppm is from the pendant phosphorus resonance. The resonance at 24.11 ppm has no corresponding resonance in the free DIOP region, it is suggested therefore that this arises from a complex where the DIOP is chelated to the iron,  $[\text{Fe}(\text{CO})_3(\text{DIOP})]$ , see Figure 3.3.

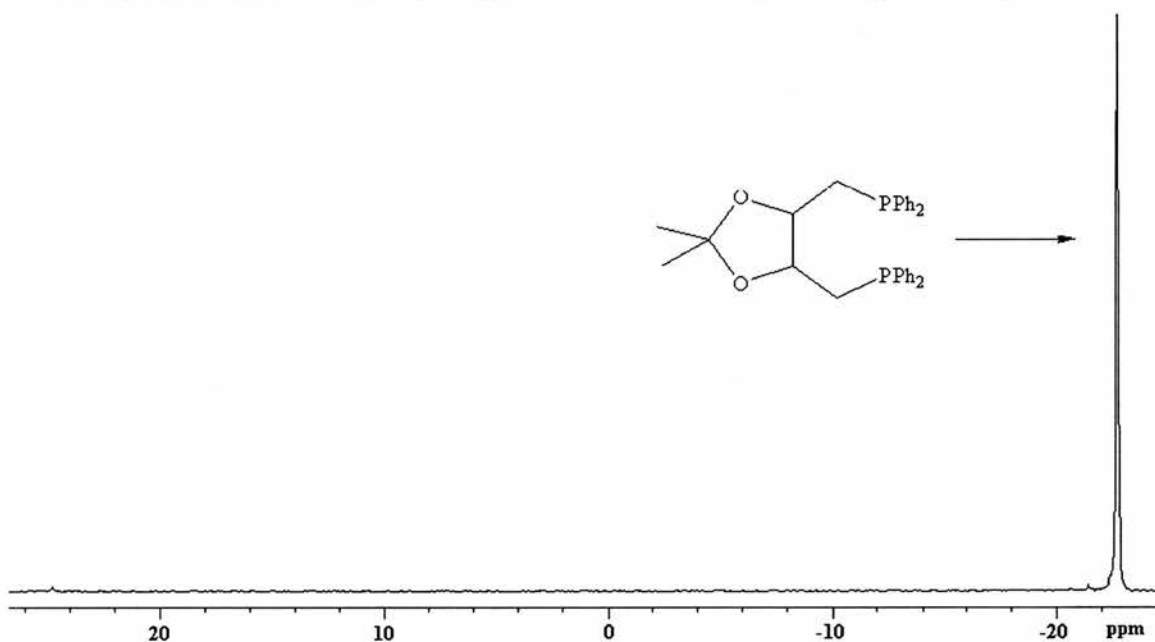
**Figure 3.3**



The  $^{31}\text{P}$   $\{^1\text{H}\}$  NMR spectrum of the  $[\text{Fe}(\text{CO})_5]$  / DIOP (ratio 1:1) solution under an atmosphere of 20 bar synthesis gas at 80 °C can be seen in NMR 3.9. It shows the presence of all the complex species observed previously at 25 °C; their intensity relative to that of DIOP, and therefore their concentration has grown. Also, it is noted that the intensity of the chelated DIOP complex  $[\text{Fe}(\text{CO})_3(\text{DIOP})]$  at 24.11 ppm has grown in intensity with respect to that of the unidentate DIOP complex  $[\text{Fe}(\text{CO})_4(\text{DIOP})]$ .

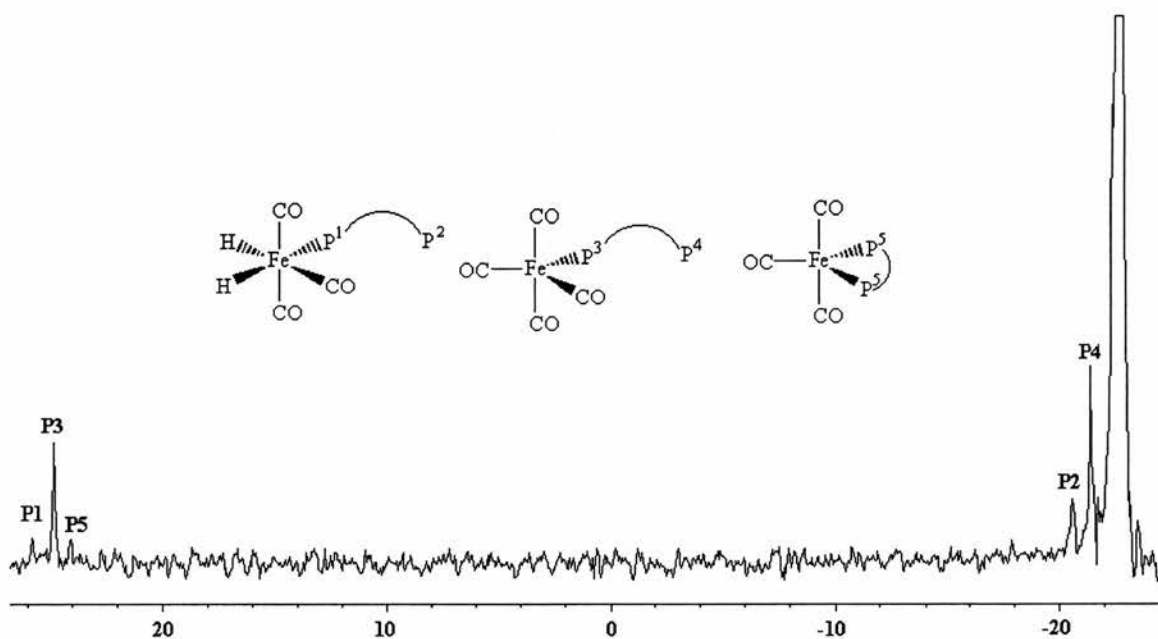
## NMR 3.7

$^{31}\text{P}\{^1\text{H}\}$  NMR spectrum of  $\text{Fe}(\text{CO})_5$  / DIOP 1:1 under synthesis gas 20 bar, at 25 °C.



## NMR 3.8

Expansion of the low intensity resonances in the  $^{31}\text{P}\{^1\text{H}\}$  NMR spectrum of  $\text{Fe}(\text{CO})_5$  / DIOP 1:1 under synthesis gas 20 bar, at 25 °C.



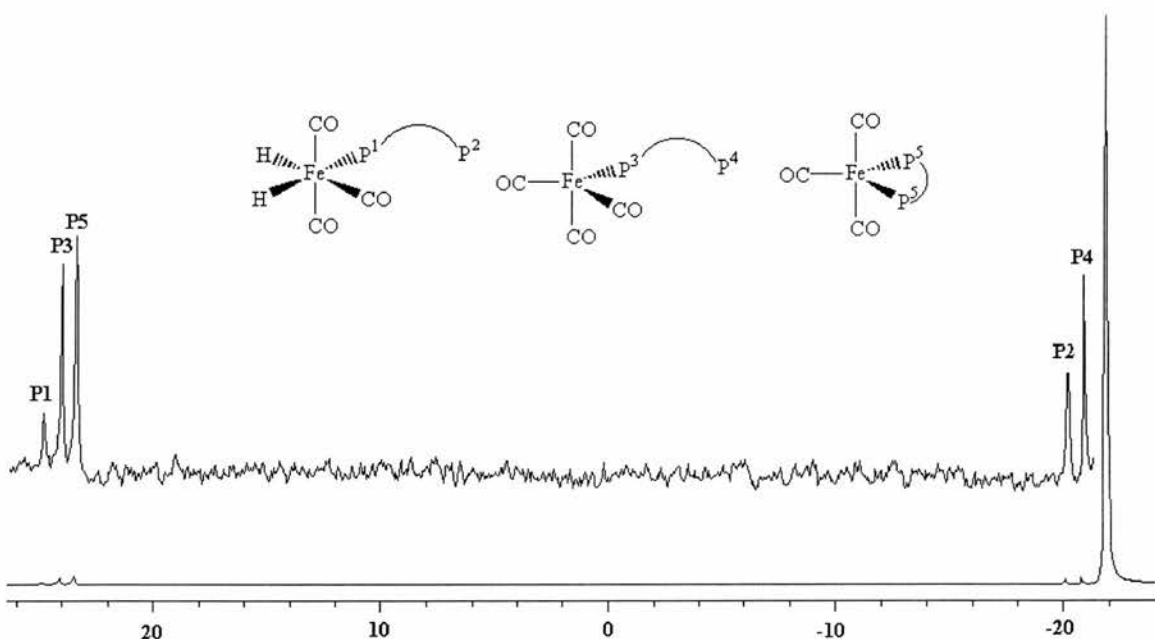
The  $^{31}\text{P}\{^1\text{H}\}$  NMR spectrum after one hour at  $80^\circ\text{C}$  can be seen in NMR 3.10. It is observed that the concentrations of the iron complexes have grown with respect to the free DIOP, however, the concentration of the chelated DIOP complex  $[\text{Fe}(\text{CO})_3(\text{DIOP})]$  at 24.11 ppm is now decreasing with respect to that of the unidentate DIOP complex  $[\text{Fe}(\text{CO})_4(\text{DIOP})]$ .

The  $^{31}\text{P}\{^1\text{H}\}$  NMR spectrum after one hour at  $80^\circ\text{C}$  can be seen in NMR 3.11. It is observed that the concentration of the iron complexes has grown even further and that the concentration of the chelated DIOP complex  $[\text{Fe}(\text{CO})_3(\text{DIOP})]$  at 24.11 ppm has decreased even further with respect to that of the unidentate DIOP complex  $[\text{Fe}(\text{CO})_4(\text{DIOP})]$ .

The  $^{31}\text{P}\{^1\text{H}\}$  NMR spectrum after the experiment has been cooled to  $25^\circ\text{C}$  can be seen in NMR 3.12. It is observed that the concentration of the chelated DIOP complex  $[\text{Fe}(\text{CO})_3(\text{DIOP})]$  at 24.11 ppm and the speculated hydride complex  $[\text{Fe}(\text{CO})_3(\text{H})_2(\text{DIOP})]$ , have decreased to the level observed originally at  $25^\circ\text{C}$ . The concentration of the unidentate DIOP complex  $[\text{Fe}(\text{CO})_4(\text{DIOP})]$ , however, is still quite high.

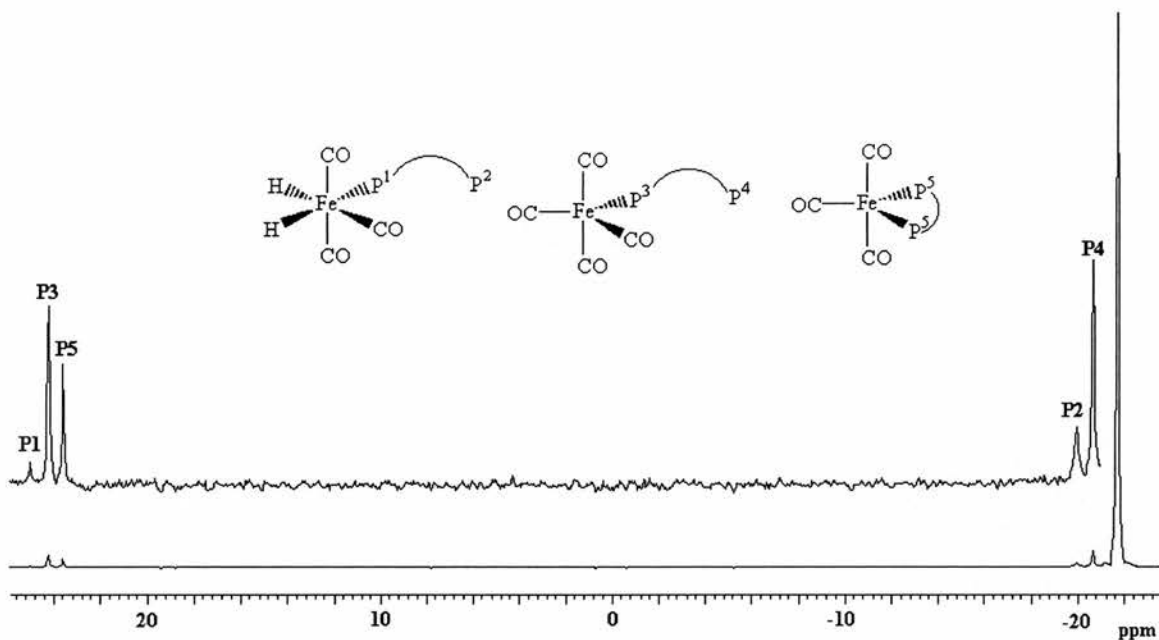
### NMR 3.9

$^{31}\text{P}\{^1\text{H}\}$  NMR spectrum of  $\text{Fe}(\text{CO})_5 / \text{DIOP}$  1:1 under synthesis gas 20 bar, at  $80^\circ\text{C}$ .

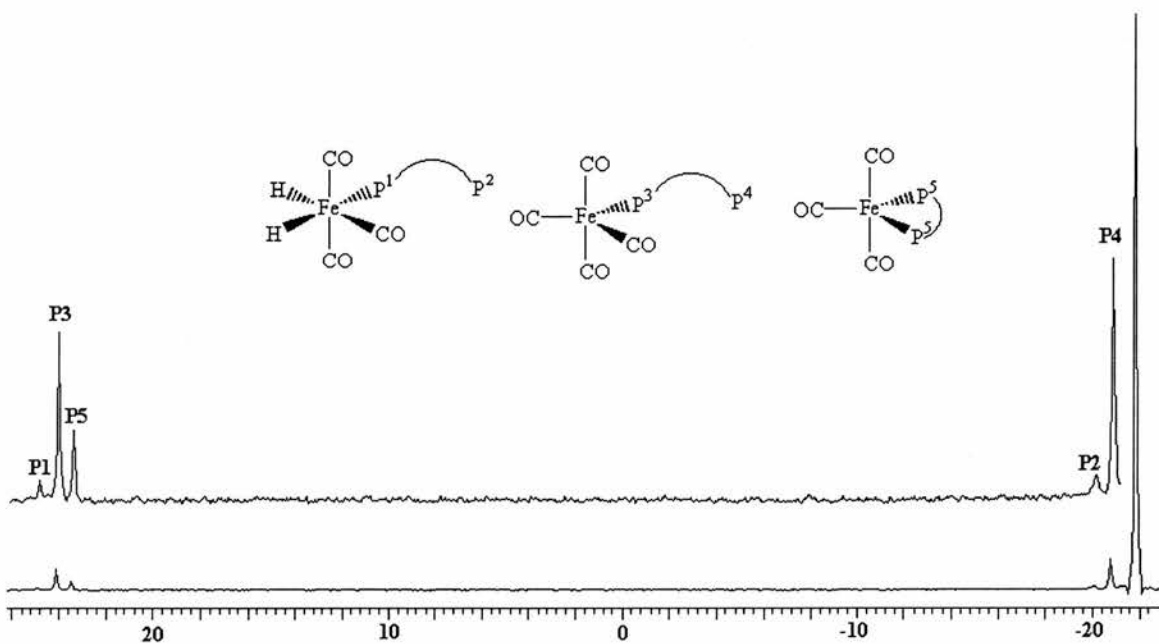


**NMR 3.10**

$^{31}\text{P}\{^1\text{H}\}$  NMR spectrum of  $\text{Fe}(\text{CO})_5$  / DIOP 1:1 under synthesis gas 20 bar, at 80 °C for one hour.

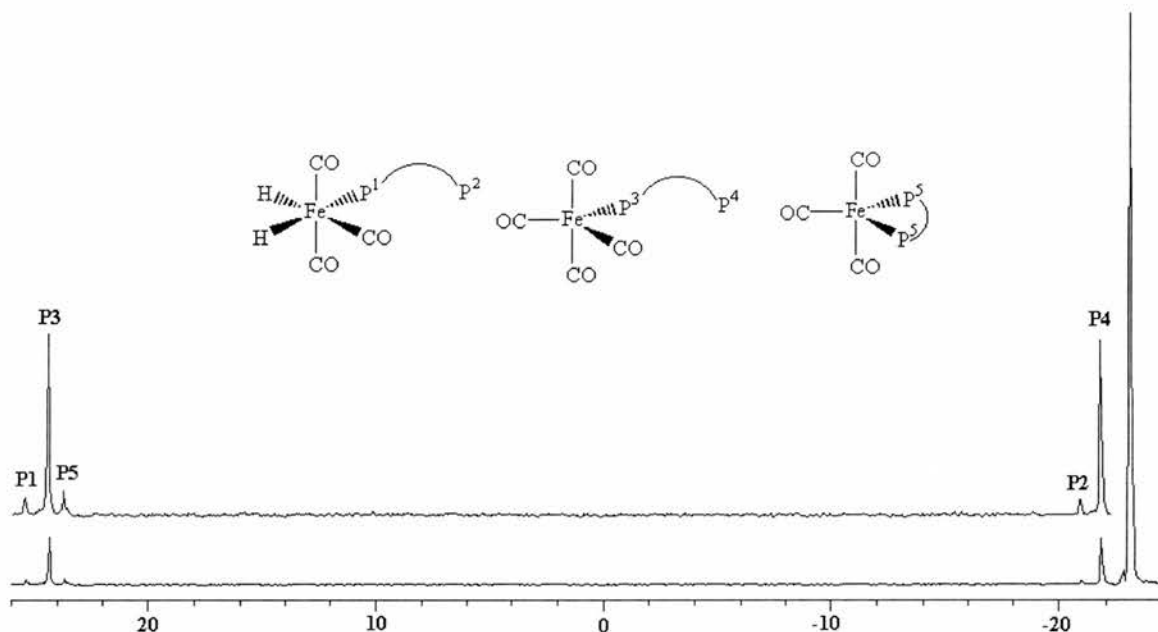
**NMR 3.11**

$^{31}\text{P}\{^1\text{H}\}$  NMR spectrum of  $\text{Fe}(\text{CO})_5$  / DIOP 1:1 under synthesis gas 20 bar, at 80 °C for two hours.



**NMR 3.12**

$^{31}\text{P}\{^1\text{H}\}$  NMR spectrum of  $\text{Fe}(\text{CO})_5$  / DIOP 1:1 under synthesis gas 20 bar, cooled to 25 °C.



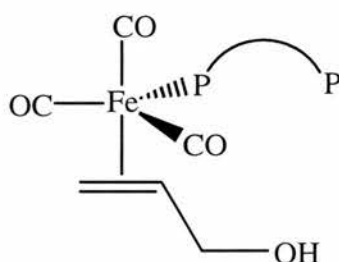
### 3.2.3 Experiment Three: $\text{Fe}(\text{CO})_5$ / DIOP / Allyl Alcohol Under Synthesis Gas 20 bar.

The  $^{31}\text{P}\{^1\text{H}\}$  NMR spectrum of the  $[\text{Fe}(\text{CO})_5]$  / DIOP / (ratio 1:1) catalyst solution in the presence of allyl alcohol under an atmosphere of 20 bar synthesis gas at 25 °C can be seen in NMR 3.13. It shows that, as under argon, there is very little reaction between  $[\text{Fe}(\text{CO})_5]$  and DIOP as most of the DIOP is uncomplexed at -23.03 ppm. There are also five resonances of low intensity at 25.45 ppm, 24.44 ppm, 23.69 ppm, -20.95 ppm, and -21.80 ppm. These resonances have already been assigned to the iron DIOP complexes,  $[\text{Fe}(\text{CO})_4(\text{DIOP})]$  at 22.44 ppm and -21.80 ppm,  $[\text{Fe}(\text{CO})_3(\text{H})_2(\text{DIOP})]$  at 25.45 ppm and -20.95 ppm, and  $[\text{Fe}(\text{CO})_3(\text{DIOP})]$  at 23.69 ppm. The spectrum looks the same as when there is no allyl alcohol present, there has been no reaction between the iron DIOP complexes and allyl alcohol.

The  $^{31}\text{P}\{^1\text{H}\}$  NMR spectrum of the  $[\text{Fe}(\text{CO})_5]$  / DIOP / (ratio 1:1) catalyst solution in the presence of allyl alcohol under an atmosphere of 20 bar synthesis gas at 80 °C can be seen in NMR 3.14. It is noted that the complex species present began to form at 60 °C. The spectrum shows the presence of free DIOP at -23.03 ppm,

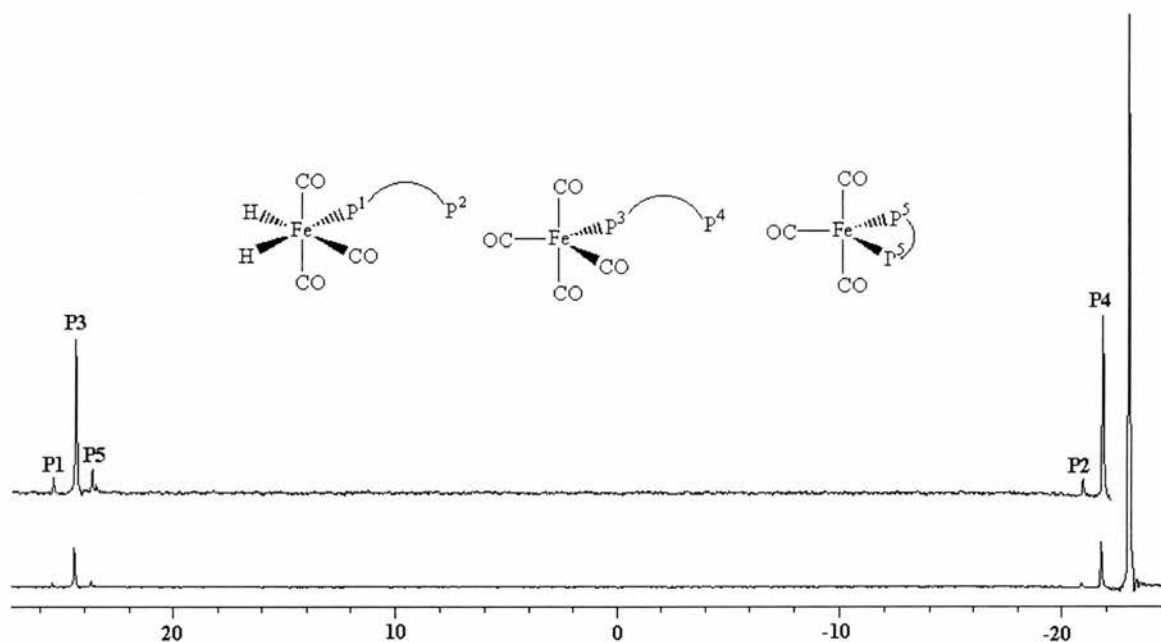
$[\text{Fe}(\text{CO})_3(\text{DIOP})]$  at 24.44 ppm. It also shows the presence of a two previously unobserved resonances, a broad resonance at 24.54 ppm and a resonance at -20.82 ppm. It is proposed that the two resonances are from one iron DIOP allyl alcohol complex species where the DIOP ligand is bound to the iron unidentate for example  $[\text{Fe}(\text{CO})_3(\text{DIOP})(\text{allyl alcohol})]$ , see Figure 3.4, although there is no further evidence that this is the complexes exact structure. The broad resonance at 24.54 ppm is the resonance from bound phosphorus and the resonance at -20.82 ppm is the resonance from the pendant phosphorus.

**Figure 3.4**



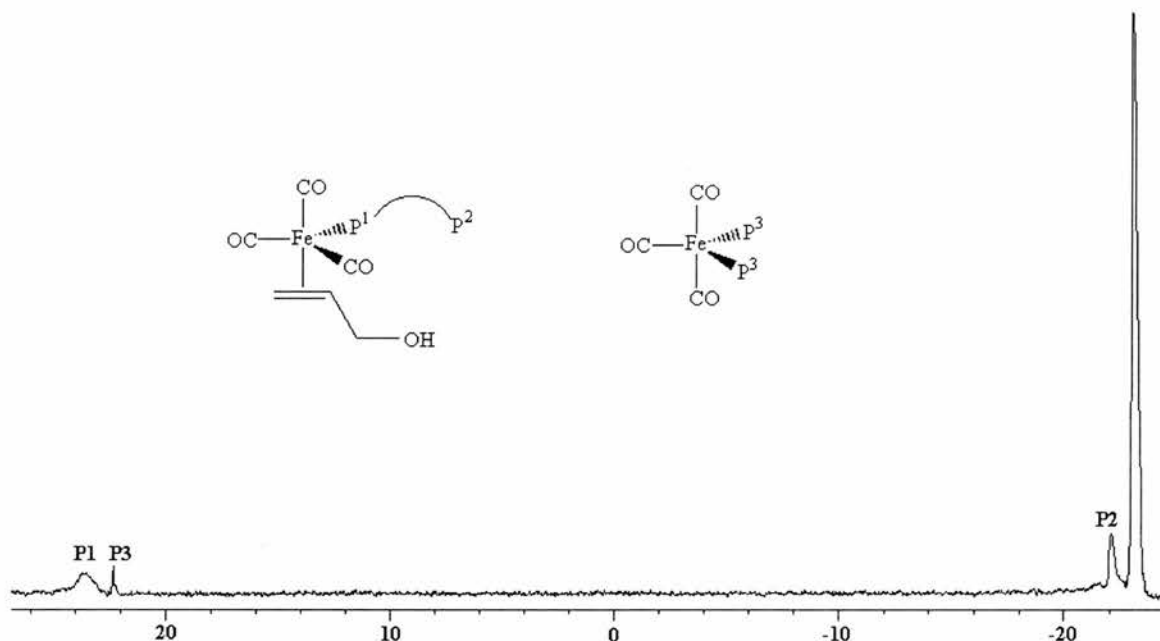
### NMR 3.13

$^{31}\text{P}\{^1\text{H}\}$  NMR spectrum of  $\text{Fe}(\text{CO})_5$  / DIOP 1:1 in the presence of allyl alcohol under synthesis gas 20 bar, at 25 °C.



**NMR 3.14**

$^{31}\text{P}\{^1\text{H}\}$  NMR spectrum of  $\text{Fe}(\text{CO})_5$  / DIOP 1:1 in the presence of allyl alcohol under synthesis gas 20 bar, at 80 °C.

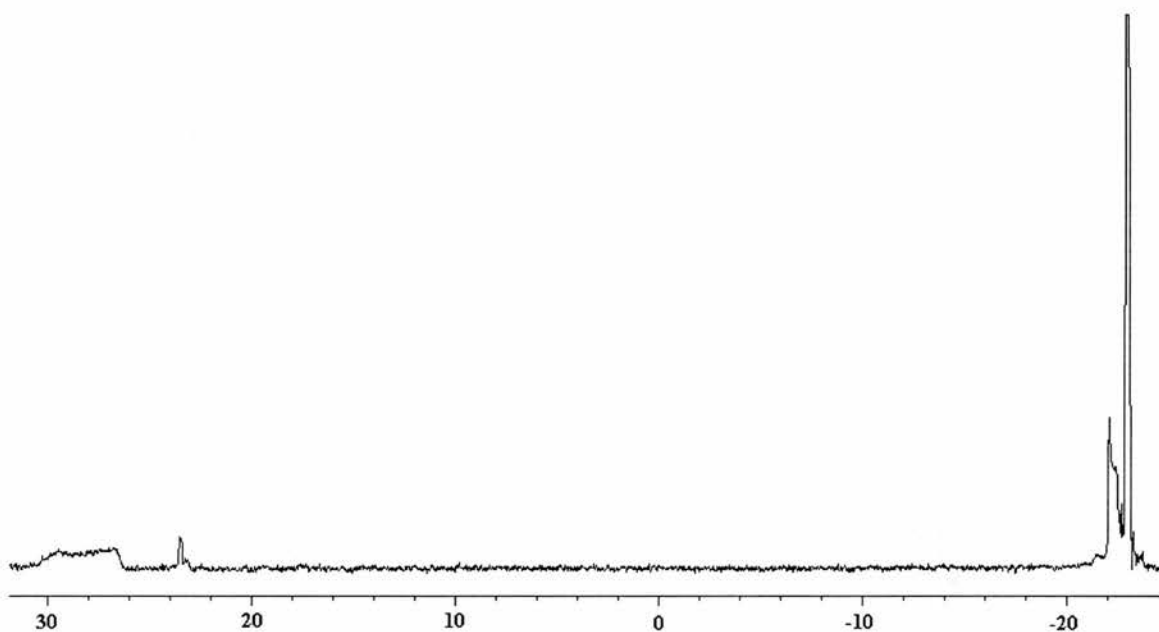


The  $^{31}\text{P}\{^1\text{H}\}$  NMR spectrum of the  $[\text{Fe}(\text{CO})_5]$  / DIOP / (ratio 1:1) catalyst solution in the presence of allyl alcohol under an atmosphere of 20 bar synthesis gas at 80 °C after one hour and two hours was recorded. It showed no change to that of the initial spectrum at 80 °C. As there were no products detected it is suggested that the allyl alcohol is fluxional in the complex which explains why the resonance is broad, but it does not insert (note there is no hydrogen in the proposed complex but it could be  $[\text{Fe}(\text{CO})_2(\text{H})_2(\text{DIOP})(\text{allyl alcohol})]$  and if so, insertion into the iron hydride bond would be possible).

When the experiment is cooled to 25 °C, the  $^{31}\text{P}\{^1\text{H}\}$  NMR spectrum shows (NMR 3.15) the presence of the broad resonance at 30.0 ppm to 26.6 ppm and singlets at 23.51 ppm, -22.10 ppm, signifying the presence of the iron DIOP complexes  $[\text{Fe}(\text{CO})_3(\text{DIOP})]$  and  $[\text{Fe}(\text{CO})_3(\text{DIOP})(\text{allyl alcohol})]$ .

**NMR 3.15**

*<sup>31</sup>P{<sup>1</sup>H} NMR spectrum of Fe(CO)<sub>5</sub> / DIOP 1:1 in the presence of allyl alcohol under synthesis gas 20 bar, cooled to 25 °C.*



**3.2.4 Experiment Four: Rh(CO)<sub>2</sub>(acac) / Fe(CO)<sub>5</sub> / DIOP / Allyl Alcohol Under 98 % Synthesis Gas & 2 % Air at 20 bar.**

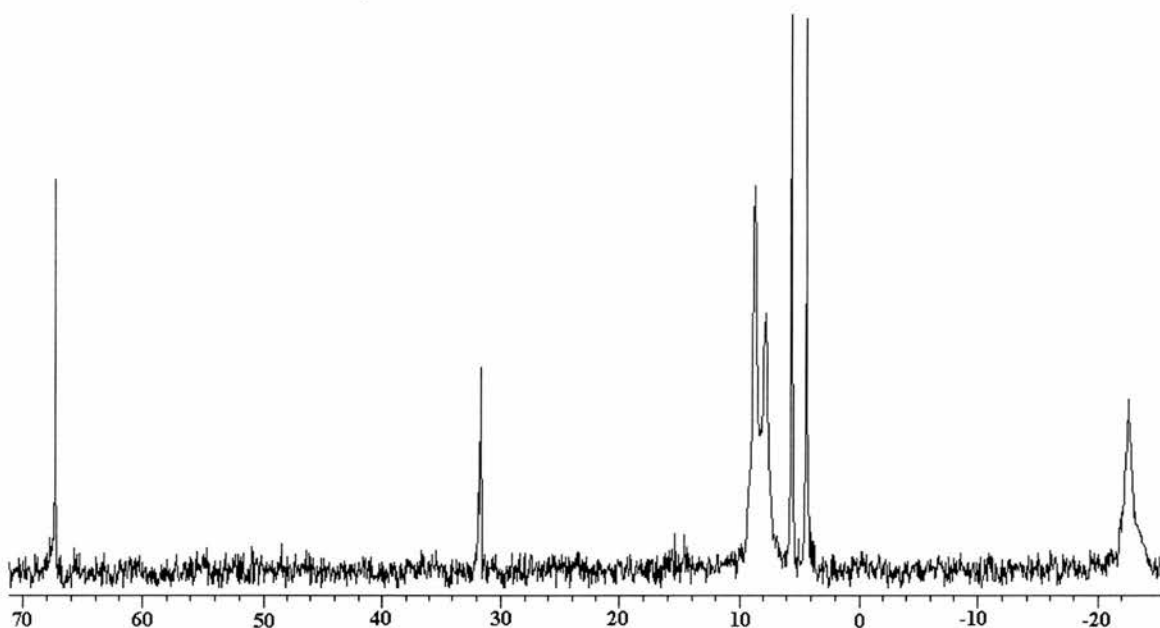
The <sup>31</sup>P {<sup>1</sup>H} NMR spectrum of the [Rh(CO)<sub>2</sub>(acac)] / [Fe(CO)<sub>5</sub>] / DIOP / (ratio 1:1:1) catalyst solution in the presence of allyl alcohol under an atmosphere of 20 bar synthesis gas 98 % and 2 % air at 25 °C can be seen in NMR 3.16. The complex species present are surprising. In section 2.5 we saw that in the absence of iron pentacarbonyl we would expect to observe the presence of the acyl rhodium complex species, 49 and 50, which have double doublet resonances at 15.25 ppm, 13.75 ppm, 9.5 ppm and 4.5 ppm. However, although our previous studies have suggested there is very little interaction between the iron pentacarbonyl and DIOP we see a very different situation in the rhodium / DIOP / allyl alcohol catalytic system in the presence of iron pentacarbonyl.

In NMR 3.16 there are singlet resonances observed at 67.31 ppm, 31.69 ppm, and -22.56 ppm, doublet resonances observed at 8.23 ppm <sup>1</sup>J<sub>PRh</sub> = 110 Hz, and 4.97 ppm <sup>1</sup>J<sub>PRh</sub> = 159 Hz. The singlet at 67.31 ppm is unknown, it is noted that this has not been observed in the absence of iron pentacarbonyl. The singlet at 31.69 ppm is from the

protonated form of DIOP dioxide  $[\text{DIOP}(\text{OH})^{2+}]$ , and the singlet at  $-22.56$  ppm is DIOP. The doublet at  $8.23$  ppm has been observed before in the rhodium / DIOP / allyl alcohol system, however, only at higher temperatures. The complex species was identified as the only rhodium complex species present in solution during the hydroformylation reaction itself when allyl alcohol and gases were readily available. The doublet resonance at  $4.97$  ppm is in fact a second order pattern which has also been previously identified as the rhodium dimer complex species, **46**.

### NMR 3.16

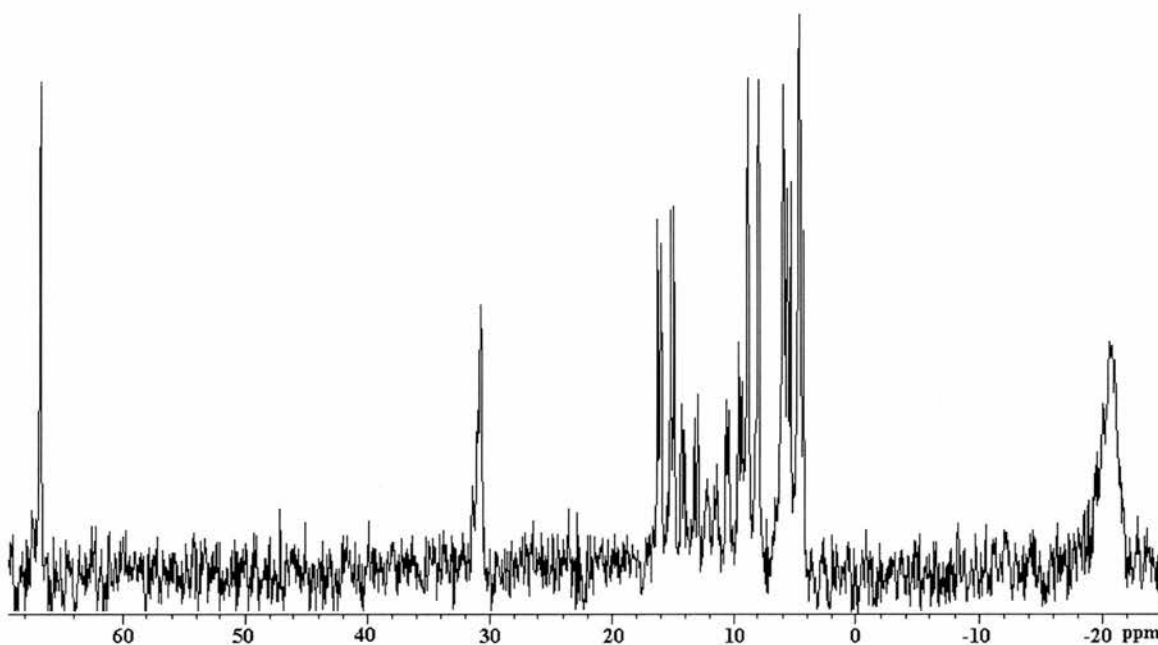
*$^{31}\text{P}\{^1\text{H}\}$  NMR spectrum of  $\text{Rh}(\text{CO})_2(\text{acac}) / \text{Fe}(\text{CO})_5 / \text{DIOP}$  1:1 under 98 % synthesis gas & 2 % air at 20 bar and  $25^\circ\text{C}$ .*



The  $^{31}\text{P}\{^1\text{H}\}$  NMR spectrum of the  $[\text{Rh}(\text{CO})_2(\text{acac})] / [\text{Fe}(\text{CO})_5] / \text{DIOP}$  / (ratio 1:1:1) catalyst solution in the presence of allyl alcohol under an atmosphere of 20 bar synthesis gas 98 % and 2 % air after one hour at  $80^\circ\text{C}$  can be seen in NMR 3.17. In the spectrum the unidentified singlet is observed at  $67.31$  ppm, as is DIOP dioxide at  $31.69$  ppm, and DIOP at  $-22.56$  ppm. There are also four double doublet resonances at  $15.25$  ppm,  $13.75$  ppm,  $9.5$  ppm and  $4.5$  ppm which correspond to the presence of the acyl rhodium complex species, **49** and **51**. The dimer complex species is also observed at  $4.97$  ppm.

**NMR 3.17**

*<sup>31</sup>P{<sup>1</sup>H} NMR spectrum of Rh(CO)<sub>2</sub>(acac) / Fe(CO)<sub>5</sub> / DIOP 1:1 under 98 % synthesis gas & 2 % air at 20 bar after one hour at 80 °C.*



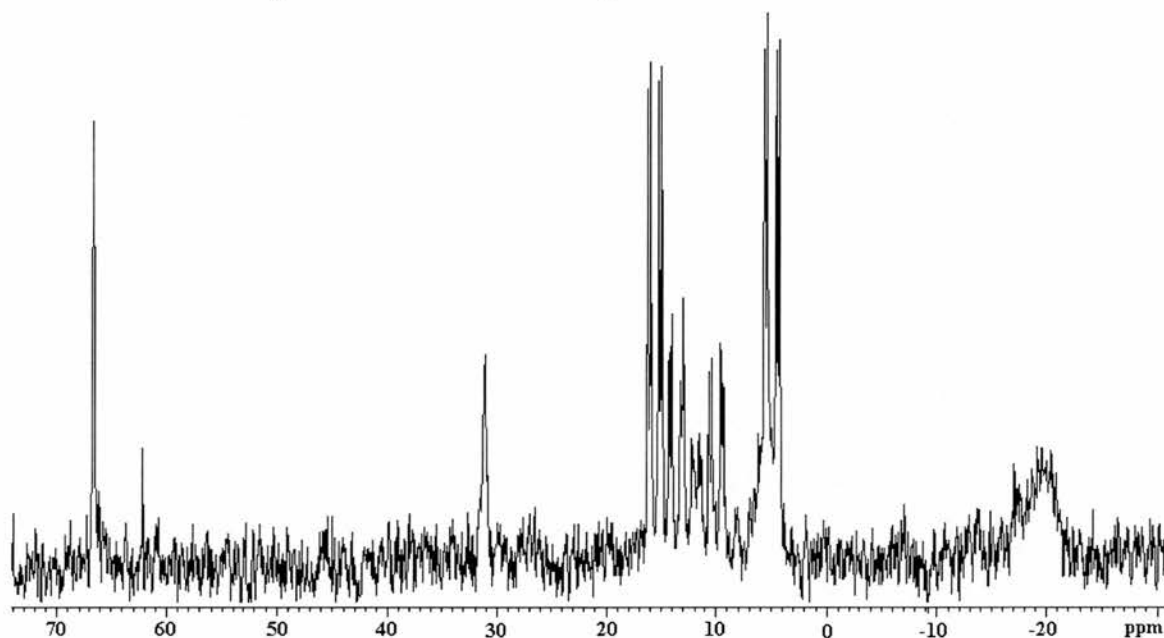
The <sup>31</sup>P {<sup>1</sup>H} NMR spectrum of the [Rh(CO)<sub>2</sub>(acac)] / [Fe(CO)<sub>5</sub>] / DIOP / (ratio 1:1:1) catalyst solution in the presence of allyl alcohol under an atmosphere of 20 bar synthesis gas 98 % and 2 % air after two hour at 80 °C can be seen in NMR 3.18. In the spectrum, the unidentified singlet is observed at 67.31 ppm, as is DIOP dioxide at 31.69 ppm, and DIOP at -22.56 ppm. There are also four double doublet resonances at 15.25 ppm, 13.75 ppm, 9.5 ppm and 4.5 ppm which correspond to the presence of the acyl rhodium complex species, **49** and **51**. The dimer complex species is not observed at 4.97 ppm in this spectrum.

The <sup>31</sup>P {<sup>1</sup>H} NMR spectrum of the [Rh(CO)<sub>2</sub>(acac)] / [Fe(CO)<sub>5</sub>] / DIOP / (ratio 1:1:1) catalyst solution in the presence of allyl alcohol under an atmosphere of 20 bar synthesis gas 98 % and 2 % air after the cell has been cooled to 25 °C can be seen in NMR 3.19. All the same complex species are observed as in the last spectrum at 80 °C. The last two spectra are also contrary to what was expected. In the experiment without iron pentacarbonyl, the doublet at 8.2 ppm was a transient and after the reaction was over the emergence of several complex species was observed. These were the rhodium dimer complex species, the rhodium hydride complex species, the tri phosphorus rhodium complex species, and the rhodium acac complex species. This is an important

factor as the presence of the tri phosphorus rhodium complex species was observed to catalyse the oxidation of DIOP.

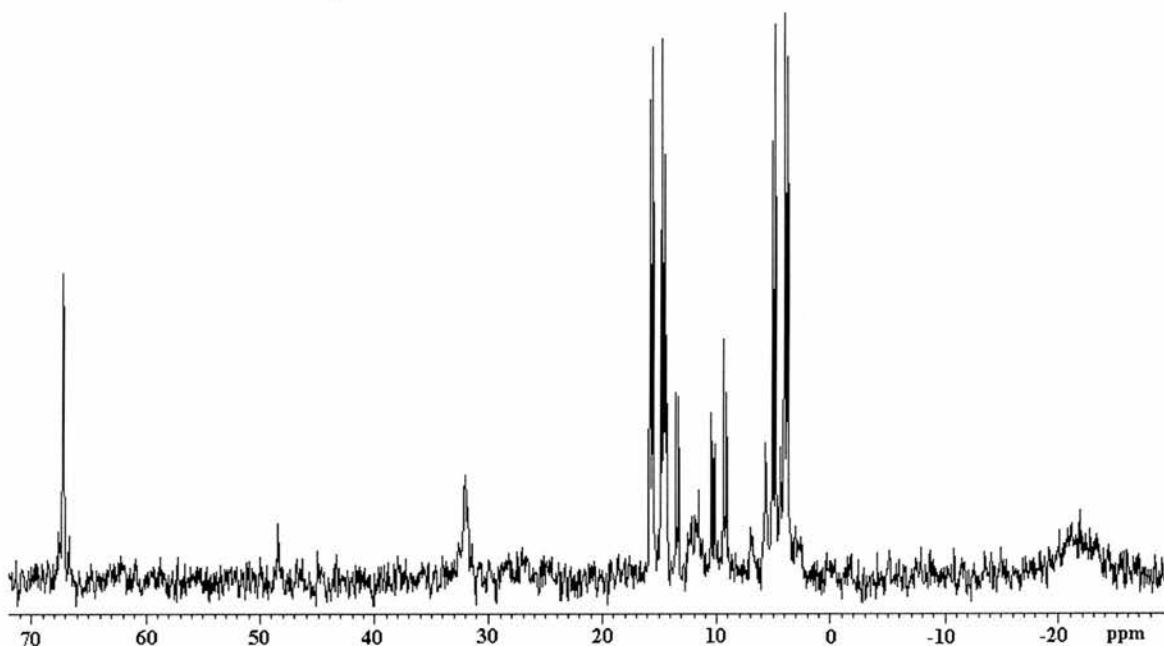
### NMR 3.18

*$^{31}\text{P}\{^1\text{H}\}$  NMR spectrum of  $\text{Rh}(\text{CO})_2(\text{acac}) / \text{Fe}(\text{CO})_5 / \text{DIOP}$  1:1 under 98 % synthesis gas & 2 % air at 20 bar after one hour at 80 °C.*



### NMR 3.19

*$^{31}\text{P}\{^1\text{H}\}$  NMR spectrum of  $\text{Rh}(\text{CO})_2(\text{acac}) / \text{Fe}(\text{CO})_5 / \text{DIOP}$  1:1 under 98 % synthesis gas & 2 % air at 20 bar cooled to 25 °C.*

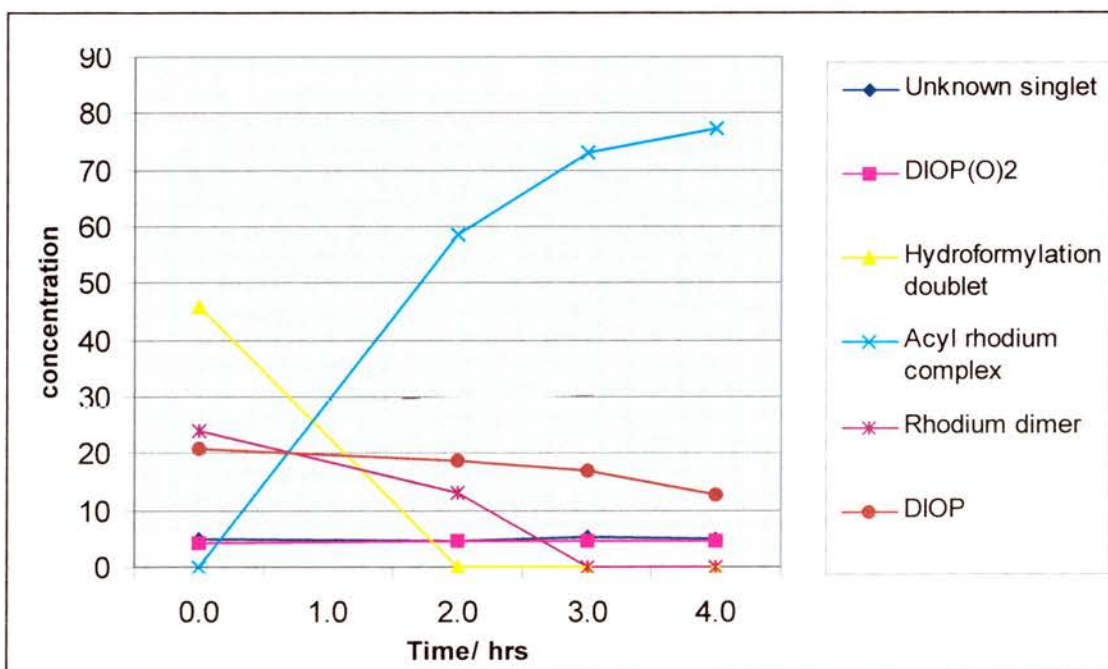


Graph 3.31 shows the concentrations of the phosphorus species present in solution with a  $[\text{Rh}(\text{CO})_2(\text{acac})] / [\text{Fe}(\text{CO})_5] / \text{DIOP}$  ratio of 1:1:1, under 98 % synthesis gas and 2 % air, (0.4 % oxygen) in the presence of excess allyl alcohol at 25 °C (at 0 hrs), at 70 °C for 2 hours (1-3 hrs), and when cooled to 25 °C (4 hrs).

The graph shows that after two hours the hydroformylation complex species has disappeared, and after three hours the rhodium dimer complex species has disappeared. The concentration of the acyl rhodium complex species rises throughout the experiment. It is interesting to note that the concentration of DIOP decreases throughout the experiment. This could have something to do with the acyl rhodium complex species rising throughout the experiment, or an inaccuracy due to the increased broadness of the DIOP resonance as the experiment progresses.

The DIOP dioxide resonance, although quite large at the start of the experiment at 4.4 %, probably caused during the preparation, stays stable throughout the experiment. This is as expected due to the non-appearance of the tri phosphorus rhodium complex species.

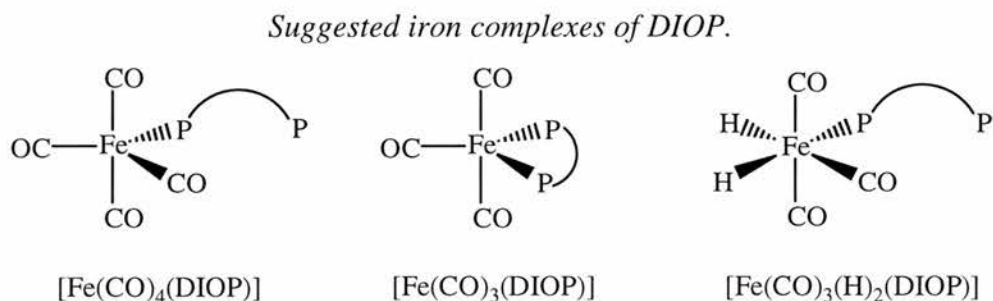
**Graph 3.31**



### 3.2.5 Conclusions.

We have identified that DIOP will form complexes with  $\text{Fe}(\text{CO})_5$ , we have also identified that when in a ratio of 1:1 most of the DIOP will be free in solution. However, in the industrial process, iron will be added in a much lower ratio, so all the iron may be complexed. We have also speculated what these complexes may be. The structures suggested can be seen in Figure 3.5.

**Figure 3.5**



We have also identified that the iron DIOP complex does indeed react with allyl alcohol under high CO and  $\text{H}_2$  pressures. However, it is noted that there was gas left in the HP NMR cell after the experiment and there were no detectable product of, hydrogenation, isomerisation or hydroformylation.

The most important observation though is that there was no excess oxidation of the ligand under an oxygen spiked atmosphere. There is another important observation that can be made from experiment 4, however. It is observed that the presence of the  $[\text{Fe}(\text{CO})_5]$  has a large influence on the complex species present at different stages of the reaction.

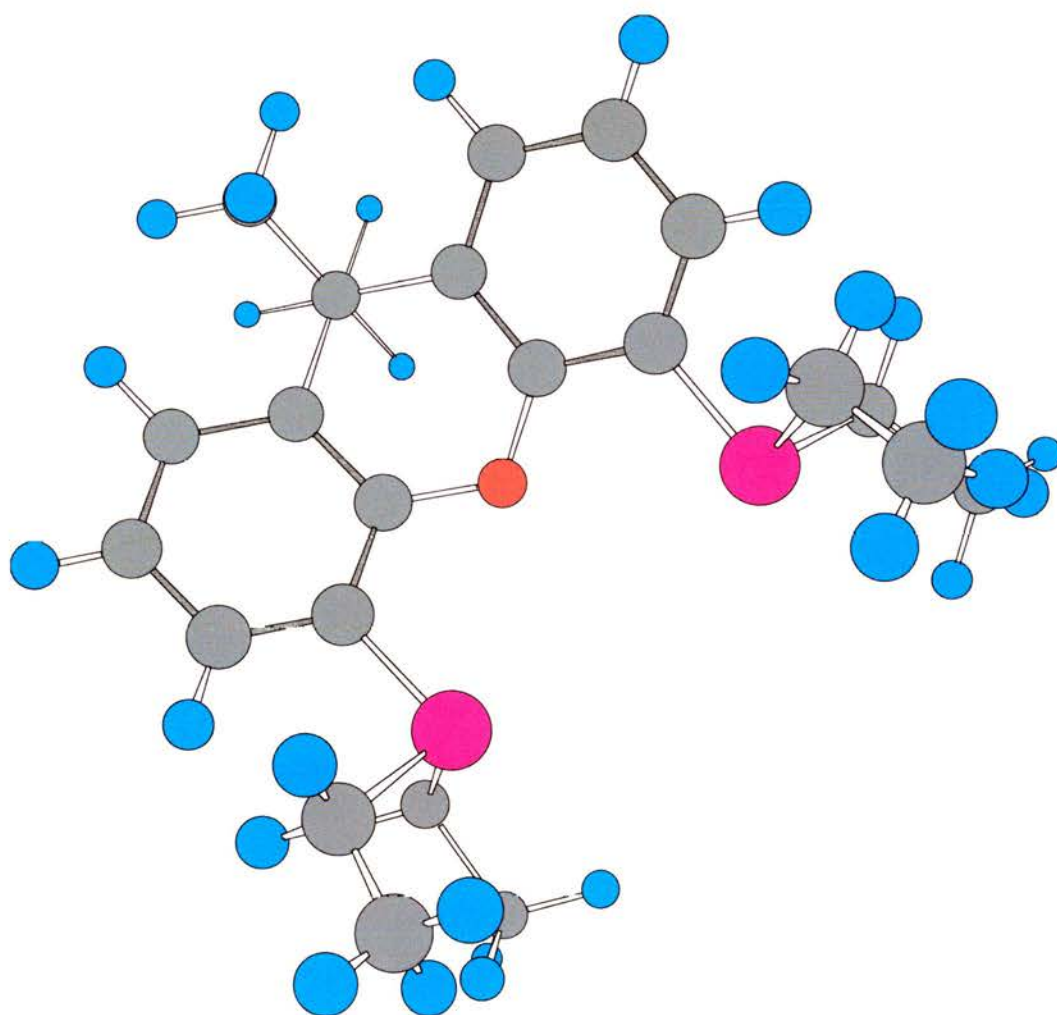
The experiment was carried out in the presence of excess allyl alcohol. In Chapter 2 we saw how at 25 °C the  $^{31}\text{P}\{^1\text{H}\}$  NMR spectrum shows the two sets of double doublets at 15.25 ppm, 13.75 ppm and 9.5 ppm, 4.5 ppm corresponding to species **49** and species **51**. In the presence of iron pentacarbonyl this was not the case. In fact, a complex species was observed that had only previously been observed during the hydroformylation reaction itself. It was also noticed that after hydroformylation was finished, the complex species present were the expected acyl rhodium complex species, containing substrate. Previously, the complex species present at this stage of reaction did not contain substrate. In fact, the system was so reactive in the presence of excess

substrate, it would utilise as much gas as possible such that the complex species present included those observed under an inert atmosphere. This is interesting as the prevention of the formation of the complex species present under inert conditions also prevents the formation of the tri phosphorus rhodium complex species which is an intermediate between this complex and the rhodium dimer complex species. The tri phosphorus complex species has previously been shown to catalyse the oxidation of DIOP. It is observed that there is no additional oxidation of the DIOP ligand over the course of experiment 4. Although the iron pentacarbonyl was added in a concentration that is much higher than would be present on an industrial scale, it can be concluded that the presence of iron pentacarbonyl in the catalytic solution did not have a detrimental effect of the oxidation properties of DIOP. If anything, at high concentrations, it had a beneficial inhibitory effect.

### 3.3 References for Chapter Three.

- 1 J. C. U. Pittman and W. D. Honnick, *J. Org. Chem.*, 1980, **45**, 2132.
- 2 P. W. N. M. v. Leeuwen and C. Claver, in 'Rhodium Catalysed Hydroformylation', ed. B. R. James and R. Ugo, Kluwer Academic Publishers, Dordrecht, 2000.
- 3 I. del Rio, W. G. J. de Lange, P. W. N. M. van Leeuwen, and C. Claver, *J. Chem. Soc., Dalton Trans.*, 2001, 1293.
- 4 J. J. Brunet, G. Commenges, F. B. Kindela, and D. Neibecker, *Organometallics*, 1992, **11**, 1343.
- 5 R. Glaser, P. E. Haney, and C. L. Barnes, *Inorg. Chem.*, 1996, **35**, 1758.
- 6 M. L. Buhl, G. J. Long, and J. F. O'Brien, *Organometallics*, 1993, **12**, 1902.

*CHAPTER FOUR: NEW LIGANDS FOR THE HYDROFORMYLATION REACTION.*



## 4 CHAPTER FOUR: NEW LIGANDS FOR THE HYDROFORMYLATION REACTION.

In section 1.2.5 it was reported that the interest behind our research into the hydroformylation of allyl alcohol was as a potential route to the production of 1,4-butanediol (BDO). At the moment the industrial process hydroformylates allyl alcohol with a rhodium TPP catalyst to the hydroxyaldehyde products, 4-hydroxybutanal and 3-hydroxy-2-methylpropanal.<sup>1</sup> The hydroxyaldehydes are subsequently hydrogenated with a Raney nickel catalyst to the diol products, BDO and 2-methyl-1,3-propanediol (MPD).<sup>2</sup>

Our interest in the rhodium DIOP catalytic system originates from the enhanced linear to branched ratio, l:b, obtainable over that of rhodium TPP catalytic system, as BDO is by far the more commercially desirable product.<sup>3</sup> Another way it may be possible to make the reaction more desirable would be if we could hydroformylate allyl alcohol directly to the diol products in a single pot reaction. This would be attractive as it would be economically more efficient than the present two step process. This chapter details attempts to develop a catalyst, which will produce the diol products as the primary products of reaction, such that the hydroxyaldehydes are not observed as intermediates in the reaction. This approach is particularly interesting as the hydroxyaldehydes have the potential to undergo several side reactions such as aldol condensation, inter or intramolecular acetal formation, and polymerisation through aldol condensation.

It is possible to hydroformylate alkenes directly to alcohols by using cobalt catalysts,<sup>4</sup> however, these will not be suitable as they are less reactive and less selective than rhodium catalysts, see section 1.1.1.

In section 1.1.3 it was reported that rhodium complexes of electron rich alkyl phosphines such as triethyl phosphine (PEt<sub>3</sub>) rhodium catalysts can be used to hydroformylate allyl alcohol to the diols under mild conditions when in protic solvents.<sup>5</sup> The process relies upon the electron donating trialkylphosphines increasing the electron density on the metal and therefore on the acyl oxygen formed by the insertion of CO into the rhodium-alkyl intermediate. This is then protonated by the protic solvent (ethanol) or by the allyl alcohol itself. Subsequent hydrogen transfer then

leads to the alcohol (butanediol in the linear case), as the primary product of reaction, therefore 4-hydroxybutanal is not an intermediate of the reaction. The branched product of reaction requires further explanation however. Following the same mechanism as for the production of 1,4-butanediol the branched product of reaction would be 2-methyl-1,3-propanediol rather than the observed 2-methylpropan-1-ol. Formally, the later product arises from the addition of methane across the carbon-carbon double bond of allyl alcohol. The production of 2-methylpropan-1-ol must therefore involve the dehydration of the branched hydroxyaldehyde product, 2-methyl-3-hydroxypropanal at some point. It is possible that this could occur in several ways. Analysis of the products showed that 2-methylpropan-1-ol was not the primary product of reaction but that it is formed *via* 2-methylpropanal, which is hydrogenated to 2-methylpropan-1-ol by the catalytic system.

The production of 2-methylpropan-1-ol is a problem, however, as markets are being developed for MPD. The other drawback with the rhodium  $\text{PEt}_3$  catalytic system is the l:b ratio, which is very low at 2:1; for a possible industrial application the l:b ratio would have to be above 6:1. To overcome this problem with the l:b ratio it was proposed to develop some electron rich bidentate ligands with bite angles near  $120^\circ$ . It has been shown that by, using bidentate diphosphine ligands with bite angles near  $120^\circ$  as ligands of rhodium in the hydroformylation reaction, particularly high l:b ratios can be achieved,<sup>6,7</sup> see section 1.1.3. It is postulated therefore, that the development of electron rich analogous of these may hydrocarboxylate alkenes, including allyl alcohol directly to the alcohol products of reaction, producing high l:b ratios.

#### **4.1 9,9-Dimethyl-4,6-bis(diethylphosphino)xanthene [Et-Xantphos].**

Dimethyl-4,6-bis(diethylphosphino) xanthene, [Et-Xantphos] was chosen as a possible alkyl diphosphine for the direct hydroformylation of allyl alcohol to 1,4-butanediol and 2-methyl-1,3-propanediol for several reasons. Xantphos, the diphenylphosphine analogue has been shown to give high l:b ratios for the rhodium catalysed hydroformylation of several substrates.<sup>1,7</sup> Because of the ligand's rigid nature there are lower levels of reaction by-products for the rhodium catalysed hydroformylation reaction than for other ligands, which also give high l:b ratios but are more flexible.

This is more pronounced at high temperatures which is even more important considering the higher temperatures of reaction required for the direct hydroformylation to alcohols. Lastly, it was hoped that the ethyl groups on the phosphine will make a rhodium phosphine catalytic system with enough electron density on the rhodium to promote the direct hydrocarboxylation to alcohols.

#### 4.1.1 Synthesis.

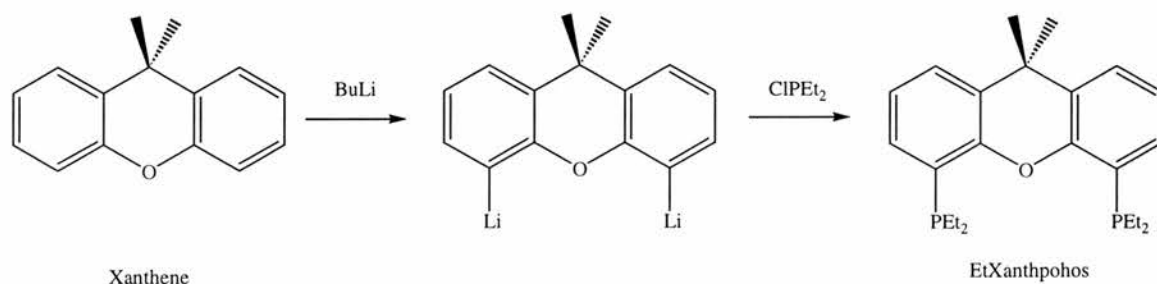
9,9-Dimethyl-4,6-bis(diethylphosphino)xanthene, Et-Xantphos an alkyl analogue of Xantphos, was prepared from xanthene and chlorodiethylphosphine, see section 6.2.3. Addition of secondary butyl lithium to a solution containing xanthene results in proton abstraction from xanthene and the formation of a lithium xanthene salt. Addition of chlorodiethylphosphine to the salt results in the formation of Et-Xantphos and lithium chloride.<sup>8</sup>

The  $^{31}\text{P}\{^1\text{H}\}$ ,  $^{13}\text{C}$  and  $^1\text{H}$  NMR spectra of Et-Xantphos can be seen in NMR 4.1, NMR 4.3, and NMR 4.4 respectively.

The  $^{31}\text{P}\{^1\text{H}\}$  NMR spectrum of Et-Xantphos shows that that the sample contains almost 100 % Et-Xantphos at  $-27.0$  ppm. The small peak at  $39.1$  ppm arises from the dioxide of Et-Xantphos  $[\text{Et-Xantphos}(\text{O})_2]$ . The  $^{31}\text{P}\{^1\text{H}\}$  NMR spectrum of the impurities of the reaction, which were insoluble in hexane can be see in NMR 4.2. The peak at  $-27$  ppm is from Et-Xantphos (**24**) the peak at  $39$  ppm is from the dioxide of Et-Xantphos  $[\text{Et-Xantphos}(\text{O})_2]$  and the peaks at  $38.64$  and  $-32.95$  ppm are from the oxidised and non-oxidised phosphorous atoms of the mono-oxidised Et-Xantphos  $[\text{Et-Xantphos}(\text{O})]$ .

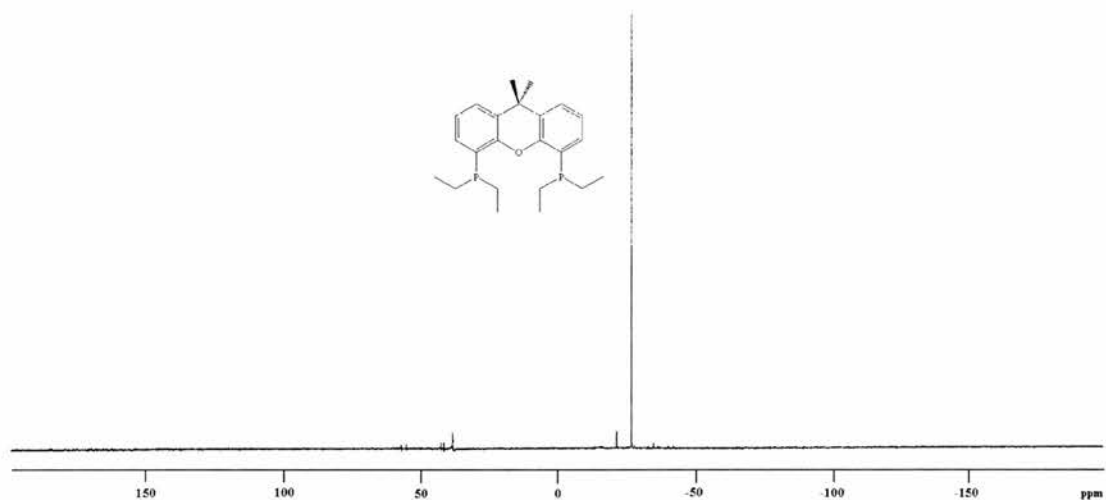
#### Scheme 4.1

*Synthesis of 9,9-dimethyl-4,6-bis(diethylphosphino)xanthene.*

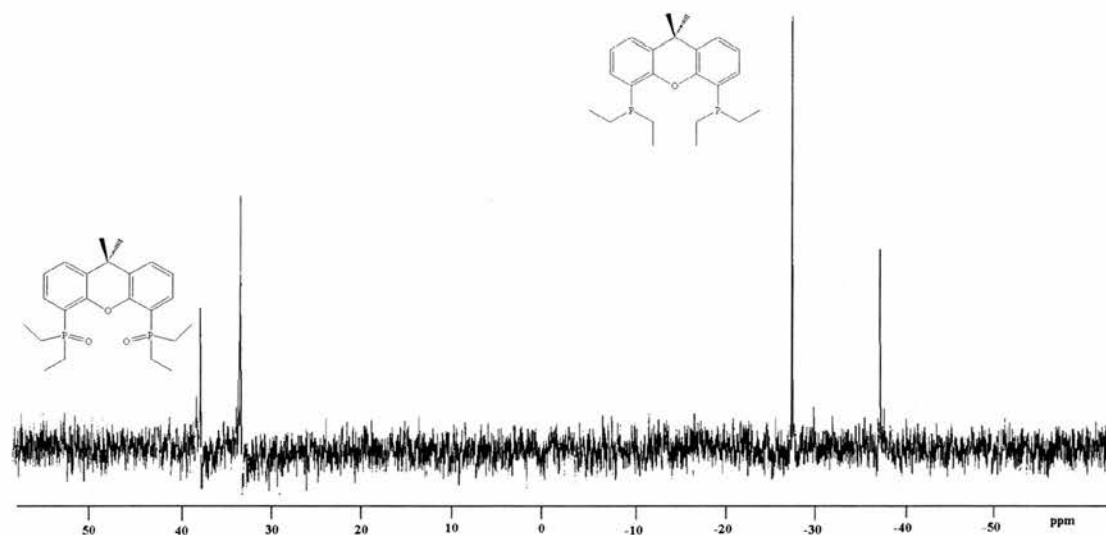


**NMR 4.1**

$^{31}\text{P}\{^1\text{H}\}$  NMR Spectra of 9,9-Dimethyl-4,6-bis(diethylphosphino)xanthene  
[Et-Xantphos].

**NMR 4.2**

$^{31}\text{P}\{^1\text{H}\}$  NMR Spectra of Et-Xantphos by-products.

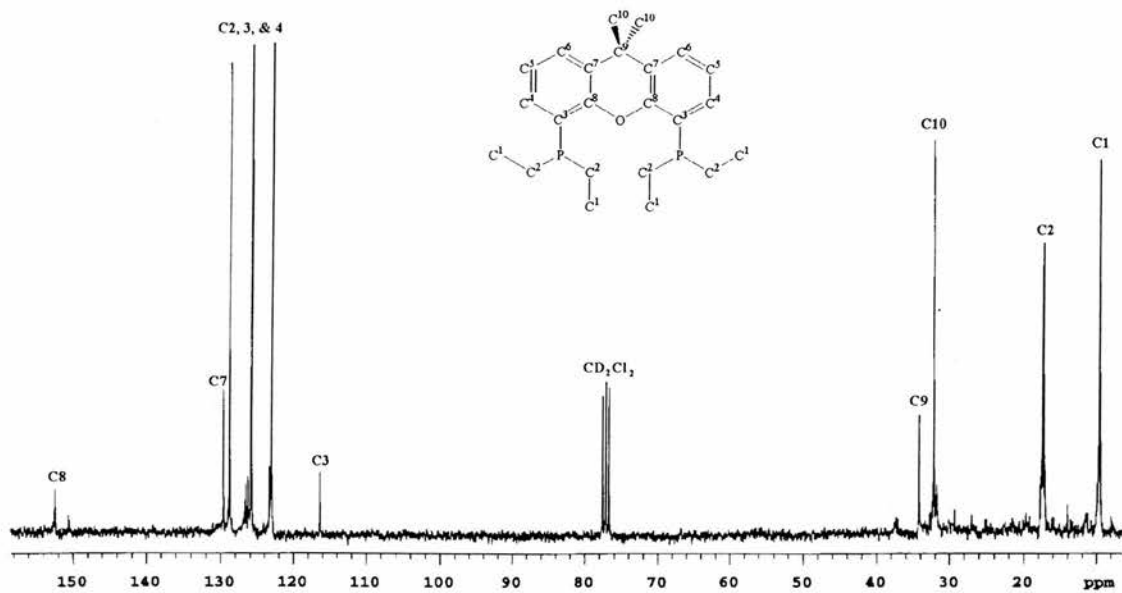


The  $^{13}\text{C}$  NMR and  $^1\text{H}$  NMR spectra of Et-Xantphos agree with the reported  $^{13}\text{C}$  NMR and  $^1\text{H}$  NMR spectra of Xantphos, the phenyl analogue of Et-Xantphos, see Table 4.1. One difference in the  $^1\text{H}$  NMR spectrum is that a double doublet in the spectrum for Xantphos appears as a double double doublet, or pseudo double quartet at 7.2 ppm for Et-Xantphos. This resonance is due to the hydrogen para to the phosphorus atom in

Et-Xantphos coupling to the phosphorous  $^5J_{H-P} = 7.7$  Hz, and to its ortho and meta hydrogen's  $^3J_{H-H} = 1.7$  Hz, and  $^4J_{H-H} = 3.0$  Hz.

### NMR 4.3

$^{13}C$  NMR Spectra of 9,9-Dimethyl-4,6-bis(diethylphosphino)xanthene [Et-Xantphos].



### NMR 4.4

$^1H$  NMR Spectra of 9,9-Dimethyl-4,6-bis(diethylphosphino)xanthene [Et-Xantphos].

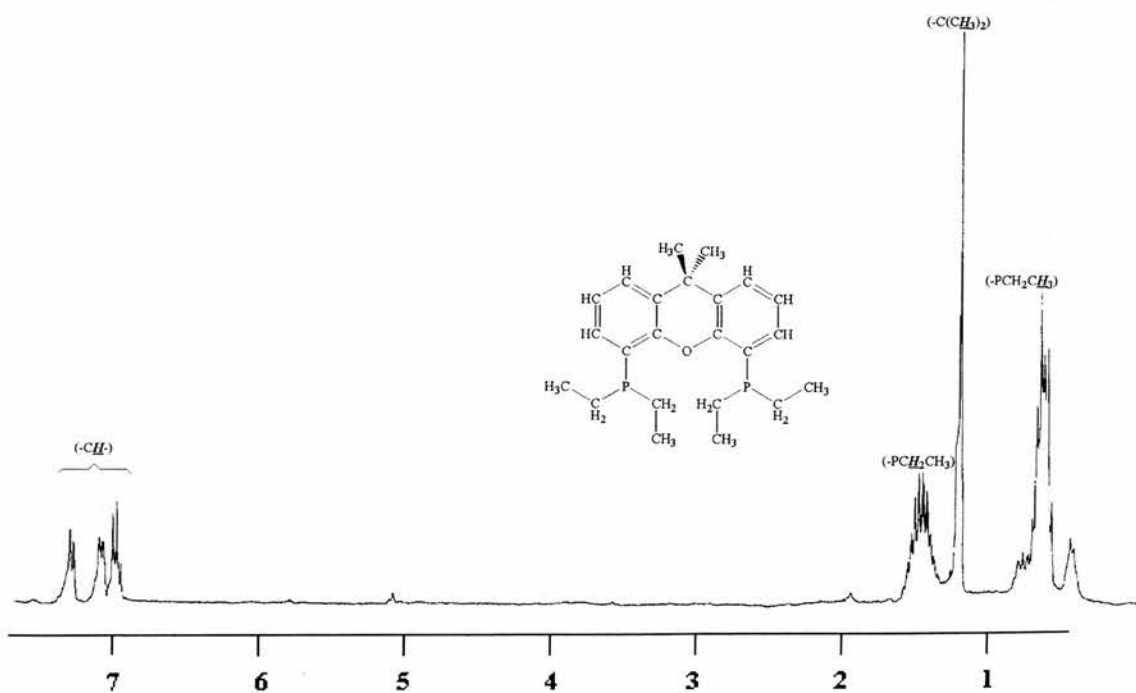


**Table 4.1***<sup>13</sup>C and <sup>1</sup>H NMR data for Et-Xantphos and Xantphos.*

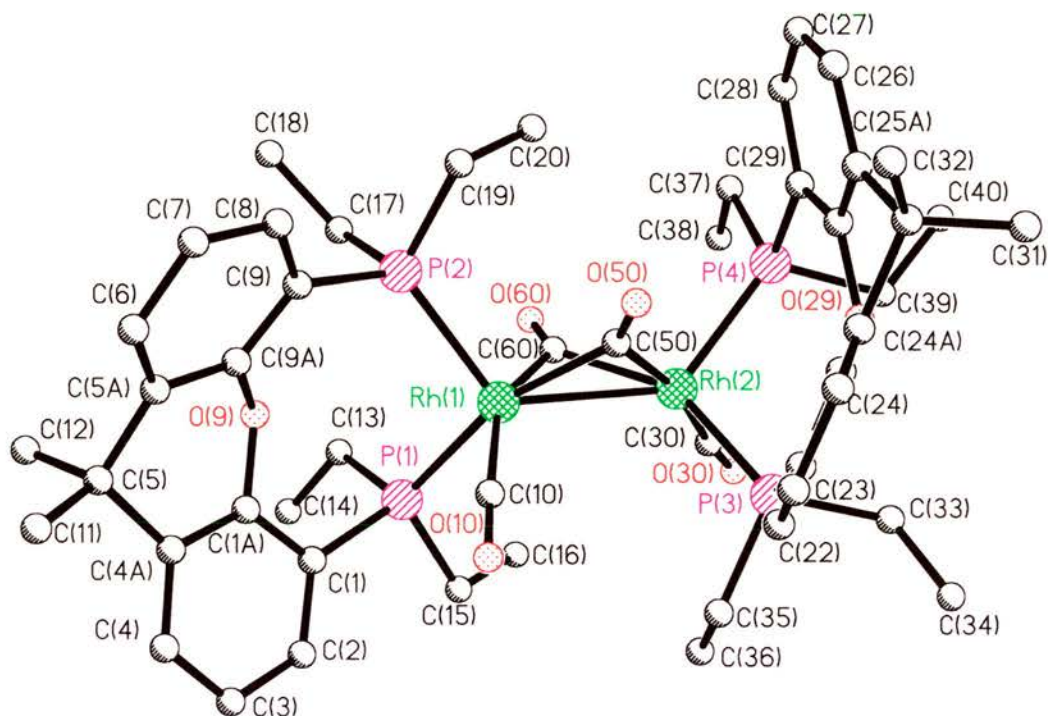
Ligand	<sup>13</sup> C { <sup>1</sup> H} NMR δ / ppm	<sup>1</sup> H NMR δ / ppm	<sup>31</sup> P NMR / ppm
Xantphos	137.2, 133.7, 131.9, 129.7, 128.0, 126.1, 125.7, 31.6.	7.8, 7.3, 7.2, 7.0, 6.5, 1.7.	-17.5
Et-Xantphos	152.5, 129.7, 128.8, 125.9, 123.1, 116.4, 34.2, 32.1, 17.41, 9.6.	7.3, 7.2, 7.1, 1.9, 1.6, 1.1.	-27.02

#### 4.1.2 Rhodium Et-Xantphos complexes.

Similarly to DIOP, the ligand Et-Xantphos reacts with [Rh(CO)<sub>2</sub>(acac)], CO and H<sub>2</sub> to form the rhodium dimer complex, [Rh<sub>2</sub>(CO)<sub>4</sub>(Et-Xantphos)<sub>2</sub>]. The <sup>31</sup>P {<sup>1</sup>H} spectra of the dimer consists of a resonance at 1.8 ppm with a second order AA'XX'X''X''' spin pattern with <sup>1</sup>J<sub>RhP</sub> = 118 Hz, <sup>3</sup>J<sub>RhP</sub> = 12 Hz, and <sup>4</sup>J<sub>PP</sub> = 12 Hz. The <sup>1</sup>H NMR consists of the Et-Xantphos protons only; there is no hydride resonance associated with the hydridorhodiumcarbonyl complexes.

Crystals suitable for single crystal X-ray crystallography were obtained from methanol. The X-ray crystal structure of [Rh<sub>2</sub>(CO)<sub>4</sub>(Et-Xantphos)<sub>2</sub>] can be seen in Figure 4.1. Selected bond angles and bond lengths can be seen in Table 4.2, and the full crystallography data can be seen in Appendix 2, Table 1 to Table 5.

Similar rhodium dimer complexes of dppe, dppp, and DIOP have been reported in the literature, including the X-ray crystal structure of [Rh<sub>2</sub>(CO)<sub>4</sub>(dppp)<sub>2</sub>].<sup>9</sup> The reported Rh-C-Rh bond angles, where C is the carbon from the bridging carbonyl group for [Rh<sub>2</sub>(CO)<sub>4</sub>(dppp)<sub>2</sub>] are 83.2 ° (4) and 83.5 °(4). The observed Rh(1)-C(50)-Rh(2) and Rh(1)-C(60)-Rh(2) bond angles for [Rh<sub>2</sub>(CO)<sub>4</sub>(Et-Xantphos)<sub>2</sub>] are 84.2 ° (4) and 83.1 °(5), which are in good agreement. The reported Rh-Rh bond distance for [Rh<sub>2</sub>(CO)<sub>4</sub>(dppp)<sub>2</sub>] is 2.725 Å (2), the observed Rh(1)-Rh(2) bond distance is 2.7388 Å (12), also in good agreement.

**Figure 4.1***X-Ray crystal structure of  $[Rh_2(CO)_4(Et-Xantphos)_2]$ .***Table 4.2***Selected bond lengths (Å) and bond angles (°) for  $[Rh_2(CO)_4(Et-Xantphos)_2]$ .*

Bond lengths (Å).			
Rh(1)-Rh(2)	2.7388(12)	Rh(1)-C(2)	2.057(10)
Rh(1)-P(1)	2.405(3)	Rh(1)-C(10)	1.916(13)
Rh(1)-P(2)	2.385(3)	Rh(2)-C(30)	1.920(2)
Rh(2)-P(3)	2.410(3)	C(10)-O(10)	1.140(13)
Rh(2)-P(4)	2.354(3)	C(30)-O(30)	1.130(2)
Rh(1)-C(1)	2.036(9)	Rh(1)-C(50)	2.042 (11)
		Rh(1)-C60)	2.047 (13)

Bond angles ( $^{\circ}$ ).			
Rh(1)-C(60)-Rh(2)	83.1(5)	Rh(1)-C(2)-O(2)	136.3(8)
Rh(1)-C(50)-Rh(2)	84.2(4)	Rh(1)-C(10)-O(10)	174.0(11)
Rh(1)-C(1)-O(1)	140.2(8)	Rh(1)-C(30)-O(30)	173.7(12)
Rh(1)-C(50)-O(50)	134.8 (9)	Rh(1)-C(60)-O(60)	140.3 (9)
		Rh(2)-C(30)-O(30)	175.7 (12)

In this geometry one of the phosphines occupies an "apical" position the other a "basal" position. The Rh-P bond lengths of the apical phosphines are reported to be shorter in  $[\text{Rh}_2(\text{CO})_4(\text{dppp})_2]$  than the Rh-P bond lengths of the basal phosphines, 2.329 Å (3) and 2.340 Å (3) for the apical and 2.368 Å (3) and 2.399 Å (3) for the basal phosphines. The observed Rh-P bond lengths in  $[\text{Rh}_2(\text{CO})_4(\text{Et-Xantphos})_2]$  are in agreement with this with bond lengths of Rh(1)-P(2) = 2.385 Å (3), Rh(2)-P(4) = 2.354 Å (3) for the apical phosphines and bond lengths of Rh(1)-P(1) = 2.405 Å (3), Rh(2)-P(3) = 2.410 Å (3) for the basal phosphines.

For  $[\text{Rh}_2(\text{CO})_4(\text{dppp})_2]$  the carbonyl bridges show a degree of asymmetry, the Rh-C bond length of the C which is trans to P is greater than the Rh-C bond which is trans to CO. The reported Rh-C bond lengths for the bridging carbonyls of  $[\text{Rh}_2(\text{CO})_4(\text{dppp})_2]$  are 2.036 Å (9) and 2.057 Å (10), which are associated with Rh-C-O bond angles of 140.2 $^{\circ}$  (8) and 136.3 $^{\circ}$  (8) respectively.

The observed bond lengths in  $[\text{Rh}_2(\text{CO})_4(\text{Et-Xantphos})_2]$  are Rh(1)-C(50) = 2.042 Å (11) and Rh(1)-C(60) = 2.047 Å (13) associated with bond angles of Rh(1)-C(50)-O(50) = 134.8 $^{\circ}$  (9) and Rh(1)-C(60)-O(60) = 140.3 $^{\circ}$  (9). C(50) is trans to the carbonyl C(30)O(30), and C(60) is trans to P(1). The Rh(1)-C(50) bond length which is trans to CO is indeed the shorter bond, whereas the Rh(1)-C(60) bond length which is trans to P is the longer.

The unsymmetrical bridging of the rhodium atoms by the carbonyls is ascribed to steric effects.<sup>9</sup> The reported Rh-C bond lengths for the terminal carbonyls in  $[\text{Rh}_2(\text{CO})_4(\text{dppp})_2]$  were 1.944 Å (11) and 1.929 Å (11), the C-O bond lengths for the terminal carbonyls are 1.115 Å (11) and 1.128 Å (11), and the Rh-C-O bond angles of the terminal carbonyls are 174.7 $^{\circ}$  (12) and 175 $^{\circ}$  (10). The observed Rh-C bond lengths for the terminal carbonyls in  $[\text{Rh}_2(\text{CO})_4(\text{Et-Xantphos})_2]$  were Rh(1)-C(10) = 1.916 Å (13) and Rh(2)-C(30) = 1.920 Å (2), the C-O bond lengths for the terminal carbonyls

are C(10)-O(10) = 1.140 Å (13) and C(30)-O(30) = 1.30 Å (2), , and the Rh-C-O bond angles of the terminal carbonyls are Rh(1)-C(10)-O(10) = 174.0° (11) and Rh(2)-C(30)-O(30) = 173.7°(12), all of which are in good agreement.

The rhodium / Et-Xantphos (ratio 1:1.5) complex species present in solution under high temperature and pressures, were studied by high pressure NMR. The  $^{31}\text{P}\{^1\text{H}\}$  NMR spectra can be seen in NMR 4.5 to NMR 4.8, they show the complex species present with a rhodium Et-Xantphos ratio of 1:1.5, under 20 bar synthesis gas at 25-95 °C.

NMR 4.5 shows the complex species present at 25 °C. There are resonances at 38.7 ppm, 8.7 ppm, 8.1 ppm, 7.5 ppm, 7.0 ppm, 1.6 ppm, and -26.9 ppm. The resonance at 38.7 ppm is a doublet with  $^1J_{\text{RhP}} = 110$  Hz. This is possibly [Rh(acac)(Et-Xantphos)], analogous to [Rh(acac)(DIOP)], the rhodium DIOP complex species present under an inert gas, seen in Chapter 2.

The resonance at 1.6 ppm has a  $^1J_{\text{RhP}} = 119$  Hz, which fits for the rhodium dimer complex species  $[\text{Rh}_2(\text{CO})_4(\text{Et-Xantphos})_2]$ .

The resonances at 8.7 ppm, 8.1 ppm, 7.5 ppm, and 7.0 ppm are of low intensity and could be from an intermediate complex species of [Rh(acac)(Et-Xantphos)] and  $[\text{Rh}_2(\text{CO})_4(\text{Et-Xantphos})_2]$ .

The resonance at -26.9 ppm is the un-complexed ligand Et-Xantphos.

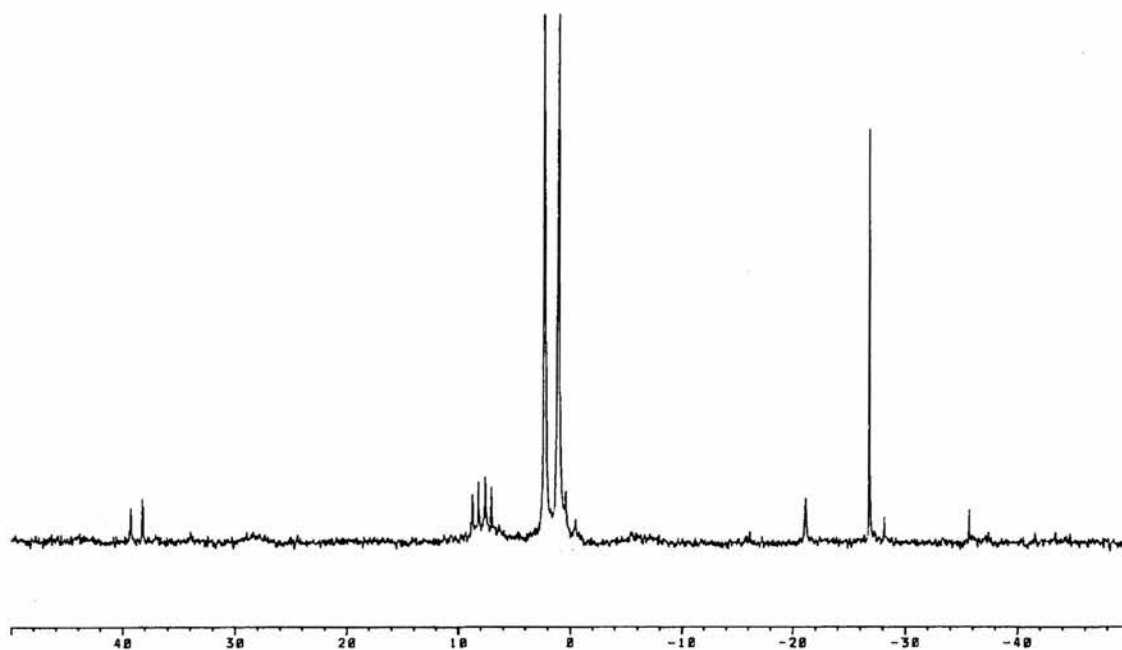
On heating, the doublet at 39 ppm and the singlets at 8 ppm disappear leaving the dimer and Et-Xantphos. See NMR 4.6 and NMR 4.7, the  $^{31}\text{P}\{^1\text{H}\}$  NMR spectrum at 60 °C and 95 °C respectively.

After cooling, the  $^{31}\text{P}\{^1\text{H}\}$  NMR spectrum has the previously assigned doublet of weak intensity at 39 ppm, strong doublet at 1.6 ppm, two singlets of weak intensity at -21 ppm and -36 ppm, and a singlet of high intensity at -26 ppm. It also has a singlet at 34 ppm which is from the Et-Xantphos oxide, see NMR 4.8.

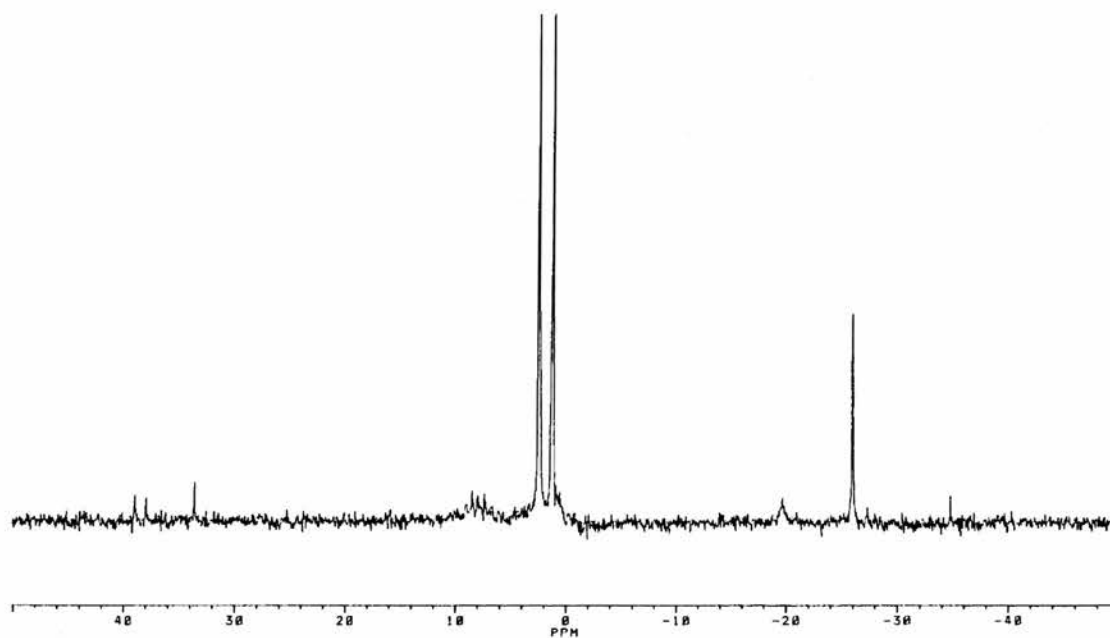
Under these conditions of study we do not see the formation of the rhodium hydride species  $[\text{RhH}(\text{CO})_2(\text{Et-Xantphos})]$  analogous to the rhodium DIOP complex species **24** and **25**. It is believed that these kind of species are in equilibrium with the dimeric species of the type  $[\text{Rh}(\text{CO})_4(\text{Et-Xantphos})_2]$ . It is a worry that if the hydride is not formed, the system will not catalyse the hydroformylation reaction.

**NMR 4.5**

*$^{31}\text{P}\{^1\text{H}\}$  NMR spectrum of  $\text{Rh}(\text{CO})_2(\text{acac}) / \text{Et-Xantphos}$  1:1.5 under 20 bar synthesis gas at 25 °C.*

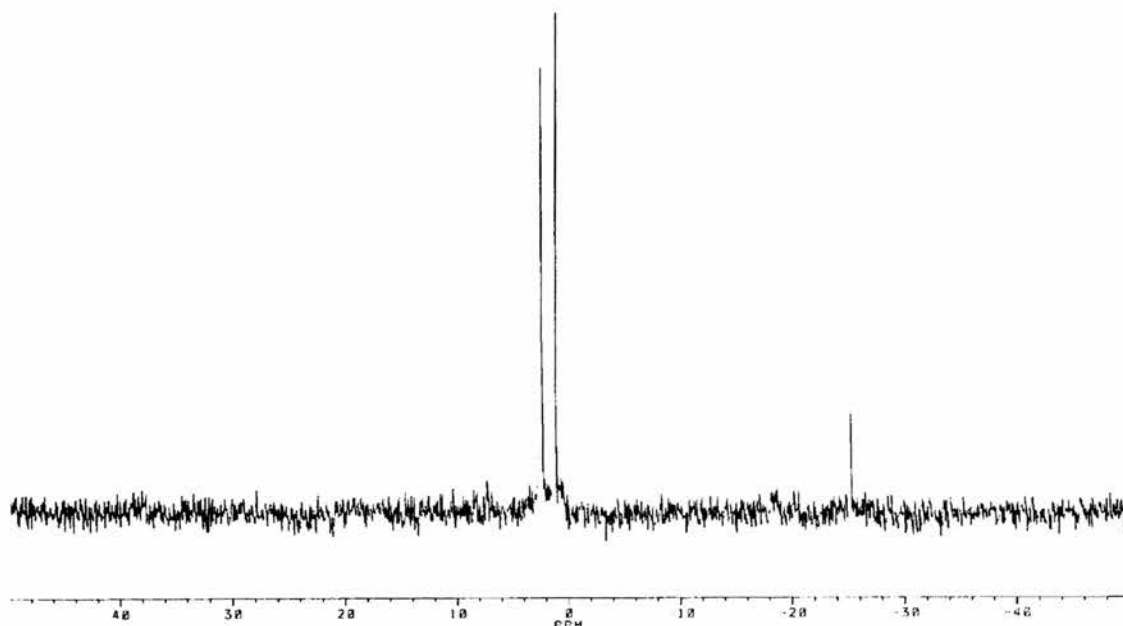
**NMR 4.6**

*$^{31}\text{P}\{^1\text{H}\}$  NMR spectrum of  $\text{Rh}(\text{CO})_2(\text{acac}) / \text{Et-Xantphos}$  1:1.5 under 20 bar synthesis gas at 60 °C.*

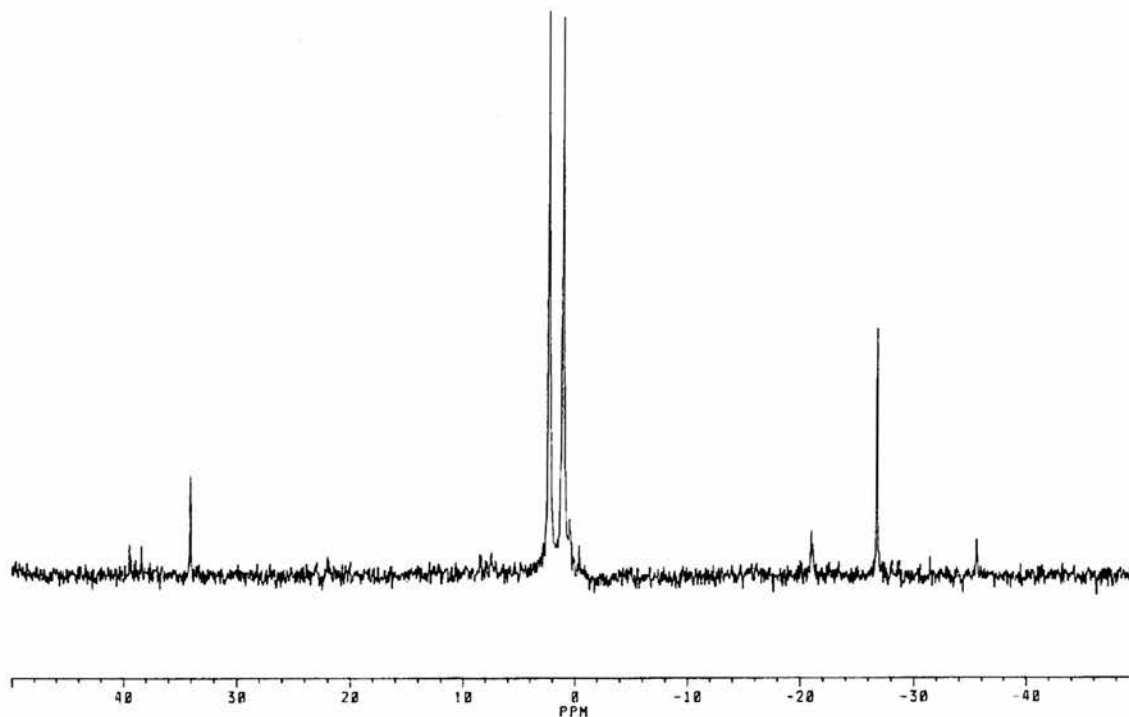


**NMR 4.7**

$^{31}\text{P}\{^1\text{H}\}$  NMR spectrum of  $\text{Rh}(\text{CO})_2(\text{acac}) / \text{Et-Xantphos } 1:1.5$  under 20 bar synthesis gas at 95 °C.

**NMR 4.8**

$^{31}\text{P}\{^1\text{H}\}$  NMR spectrum of  $\text{Rh}(\text{CO})_2(\text{acac}) / \text{Et-Xantphos } 1:1.5$  under 20 bar synthesis gas cooled to 25 °C.



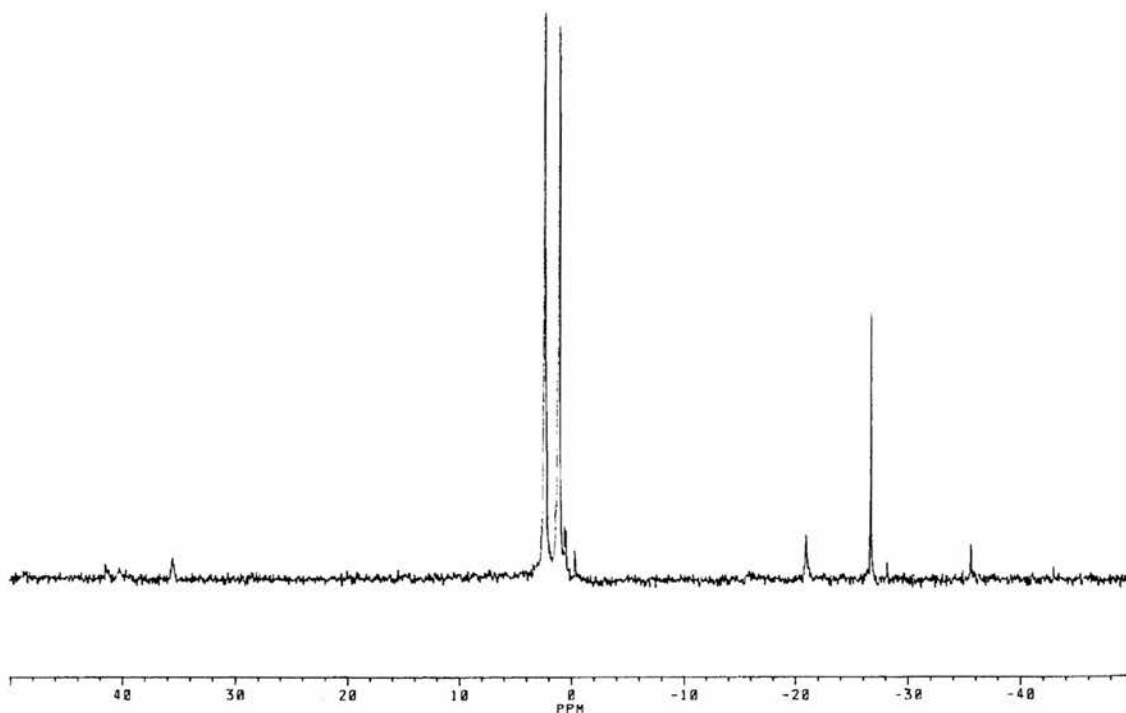
Therefore, the complex species present in solution in the presence of substrate, allyl alcohol, were also studied. The  $^{31}\text{P}\{^1\text{H}\}$  NMR spectra NMR 4.9 to NMR 4.13 show the complex species present with a rhodium Et-Xantphos ratio of 1:1.5, under 20 bar synthesis gas in the presence of allyl alcohol.

NMR 4.9 shows the complex species present at 25 °C, before the complex solution is heated. The spectrum shows there is no change in the complex species present from when there was no substrate present. NMR 4.10 shows that even after the solution has been heated to 90 °C there is no change in the spectrum.

After cooling, the  $^{31}\text{P}\{^1\text{H}\}$  NMR spectrum contains several new resonances, a doublet at 9 ppm several peaks between 2 and -2 ppm, and two broad peaks at -4 and -20 ppm, see NMR 4.11.

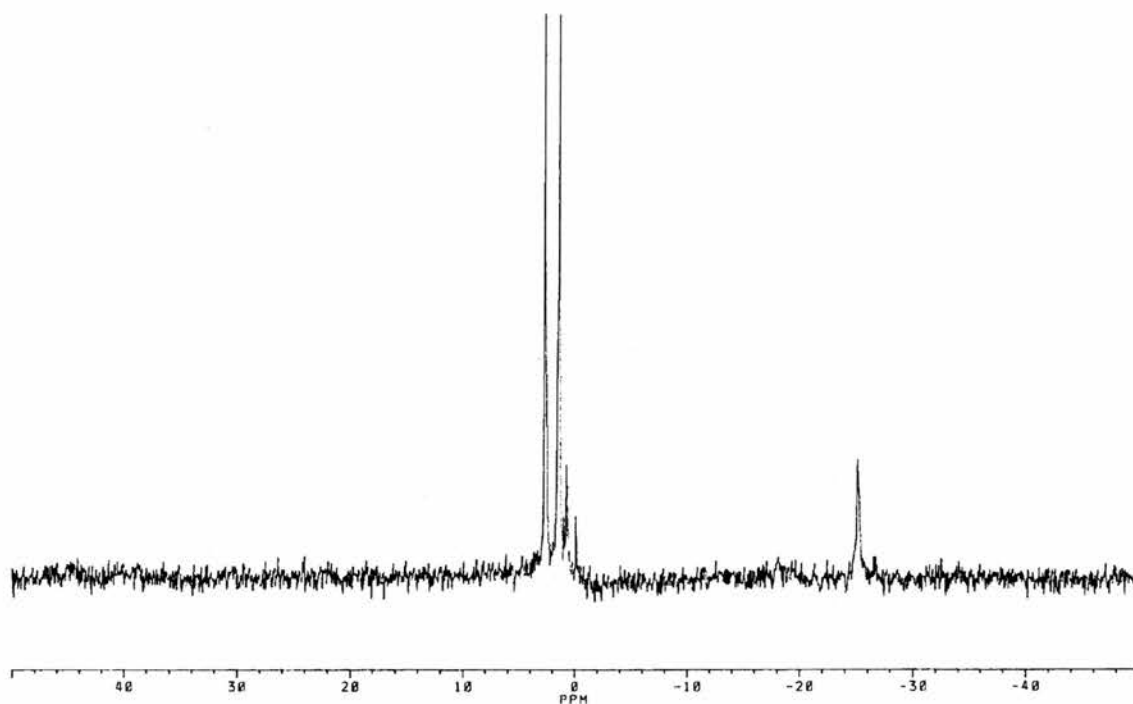
#### NMR 4.9

*$^{31}\text{P}\{^1\text{H}\}$  NMR spectrum of  $\text{Rh}(\text{CO})_2(\text{acac}) / \text{Et-Xantphos } 1:1.5$  & allyl alcohol under 20 bar synthesis gas at 25 °C.*

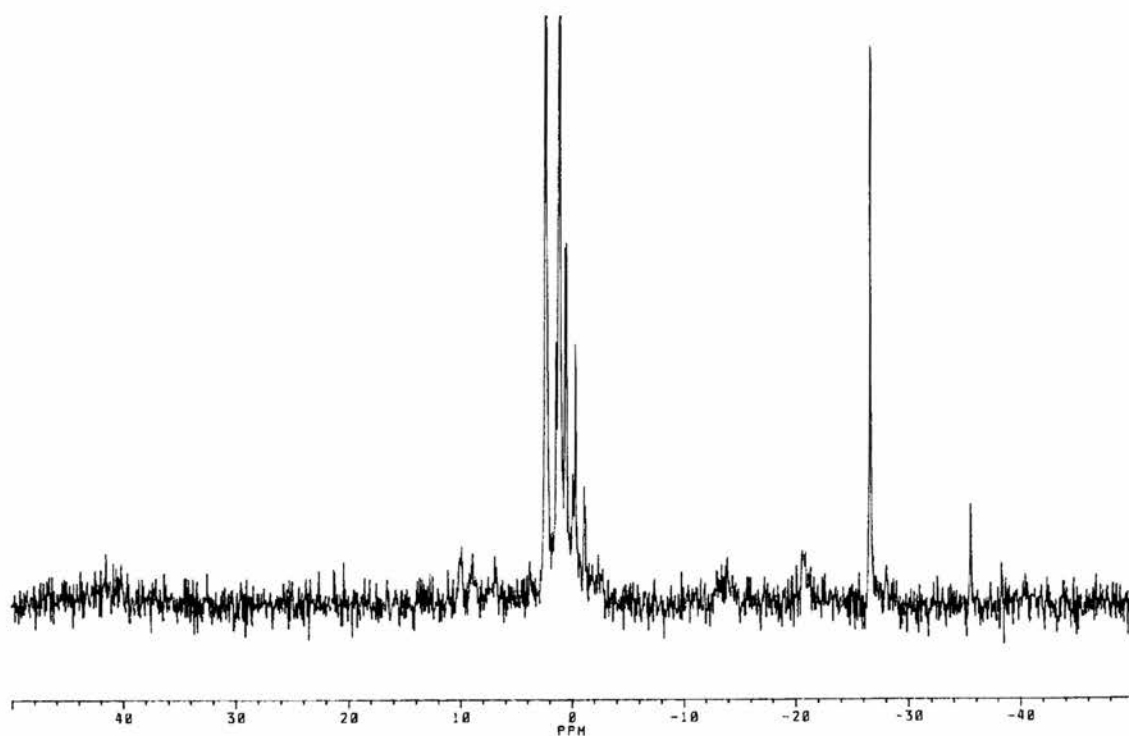


**NMR 4.10**

*<sup>31</sup>P{<sup>1</sup>H} NMR spectrum of Rh(CO)<sub>2</sub>(acac) / Et-Xantphos 1:1.5 & allyl alcohol under 20 bar synthesis gas at 90 °C.*

**NMR 4.11**

*<sup>31</sup>P{<sup>1</sup>H} NMR spectrum of Rh(CO)<sub>2</sub>(acac) / Et-Xantphos 1:1.5 & allyl alcohol under 20 bar synthesis gas cooled to 25 °C.*

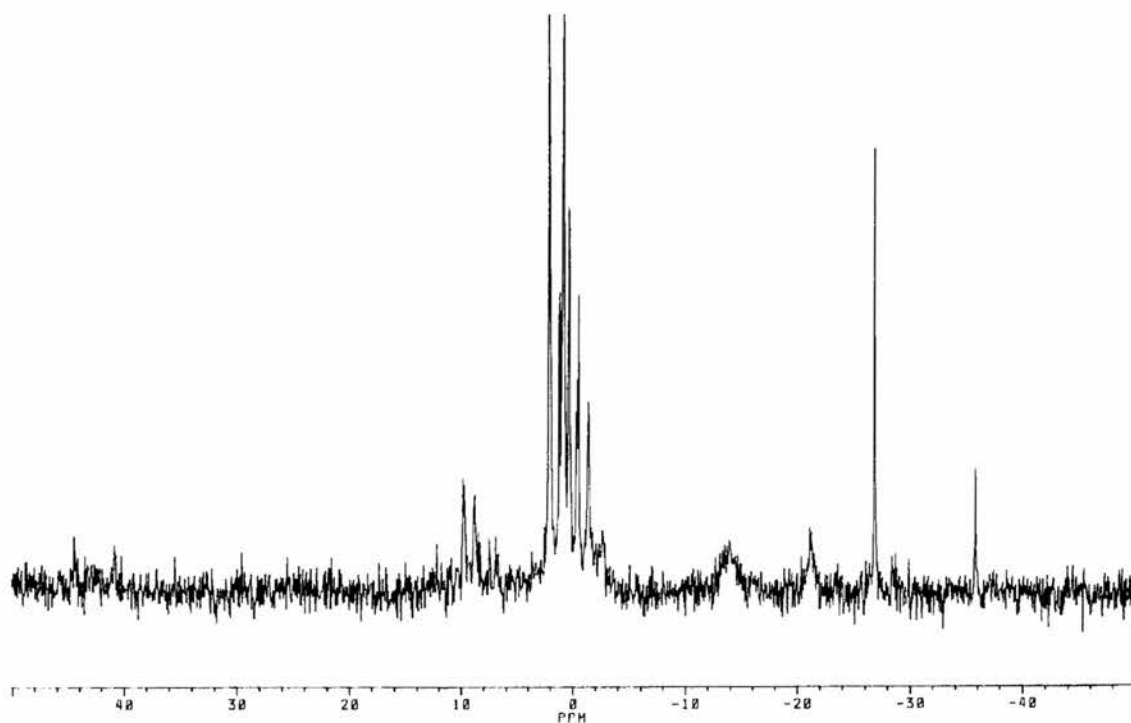


The complex solution is reheated to 80 °C and we see an increase in the intensity of the doublet at 9 ppm and in the intensity of the peaks between 2 and -2 ppm was observed, see NMR 4.12. The free diphosphine also became very broad, indicating it is exchanging with one or more of the new species at high temperature.

When the complex solution was cooled for the second time, the peaks at 9, 2, -2, -4, and -10 were more intense than after the solution was initially cooled. The free diphosphine gave a sharp singlet once more.

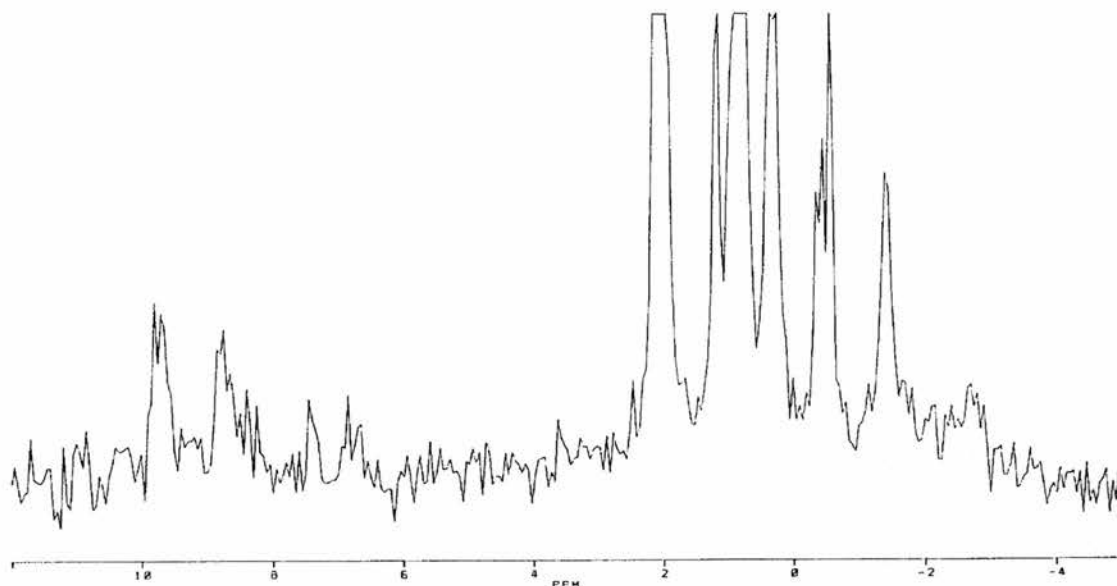
#### NMR 4.12

*<sup>31</sup>P{<sup>1</sup>H} NMR spectrum of Rh(CO)<sub>2</sub>(acac) / Et-Xantphos 1:1.5 & allyl alcohol under 20 bar synthesis gas cooled to 25 °C and reheated to 80 °C.*



An expanded view of the peaks at 2 ppm to -2 ppm can be seen in NMR 4.13, it is difficult to say what type of resonances they represent as they are obscured by the dimer species. The peak at 9 ppm is interesting, however, it could possibly be split into a double doublet. No evidence of a hydride species was available in the <sup>1</sup>H NMR spectrum.

For a better understanding of this system it will be necessary to study the sample in the 10 mm HP NMR cell, with greater gas / liquid interface and volume. This will also allow analysis of the reaction products, which is not possible for the 5 mm cell, (the product percentage is too small).

**NMR 4.13***Expansion of new peaks in NMR 4.14.***4.1.3 Catalytic Results.**

The selectivity of the diphosphine ligand Et-Xantphos was tested in the rhodium catalysed hydroformylation of allyl alcohol and 1-octene. The reactions were carried out with the CATS service at St. Andrews University.<sup>10</sup> The CATS kinetic autoclave enables the recording of the gas consumed by the reaction which then allows for the calculation of the rates of reaction, see section 2.2.3.

The volume of catalyst solution used was 4 cm<sup>3</sup> and the volume of substrate used was 1 cm<sup>3</sup> in both cases, this equates to 1.5 x 10<sup>-2</sup> mol of allyl alcohol and 8.0 x 10<sup>-3</sup> mol of 1-octene used. The rhodium concentration was 2.0 x 10<sup>-3</sup> mol dm<sup>-3</sup> or 200 ppm. The rhodium source was [Rh(CO)<sub>2</sub>(acac)], 0.00258 g or 1 x 10<sup>-5</sup> mol. For accuracy, 40 cm<sup>3</sup> batch solutions of the catalyst were made. The Et-Xantphos to rhodium ratio was 2:1 in all cases.

Work by Cole-Hamilton and coworkers<sup>5, 11</sup> on the effect of the solvent to the catalytic system has shown it to be very important. It has been reported that only by using protic solvents such as ethanol can the direct formation of alcohol products be achieved, and that the use of polar aprotic solvents allows the formation of alcohols, but via a two step

process. However, when protic solvents such as ethanol are used for the hydroformylation of allyl alcohol the branched product of reaction is 2-methylpropanol rather than 2-methyl-1,3-propanediol, which is undesirable. Studies at the Lyondell Chemical Company have shown that the branched product of reaction can be 2-methyl-1,3-propanediol if tertiary alcohols such as 1,1-dimethylpropanol (amyl alcohol) are used. For this reason, we wished to study the effect of a range of solvents and mixed solvents, which are both protic and aprotic. The solvents investigated were toluene, ethanol, tetrahydrofuran (THF), methyl-*tert*-butyl ether (MTBE), amyl alcohol, THF / H<sub>2</sub>O, and toluene / acetic acid.

The catalyst solutions were prepared under argon using Schlenk techniques, the rhodium complex species present at this stage was presumably [Rh(acac)(Et-Xantphos)] or [Rh(acac)(CO)(Et-Xantphos)],<sup>12</sup> see section 2.3.1. The catalyst solution was injected into the CATS kinetic autoclave where it was pressurised under an atmosphere of CO and H<sub>2</sub> with stirring. The catalyst solution was left under CO and H<sub>2</sub> pressure for half to one hour to form the active catalyst precursor, presumably [HRh(CO)<sub>2</sub>(Et-Xantphos)].<sup>1</sup> The substrate, allyl alcohol or 1-octene, was injected at the reaction temperature and pressure and the gas uptake of the hydroformylation reaction studied. When the reaction was complete, shown by zero gas uptake, the reaction solution was cooled and depressurised, and the reaction products analysed by GC-FID and GCMS, see Chapter 6.

As mentioned earlier, the rates of reaction are calculated from the gas uptake of the reaction, see section 2.2.3. The kinetics autoclave measures the gas uptake from the ballast vessel with time. The reactions were first order with respect to substrate except if mass transport limited. For a first order reaction, the plot of  $[\ln(1-\text{conversion}/100)]$  versus time is linear over two or more half lives,  $\geq 75\%$  of the reaction.<sup>13</sup> In practice, this value is the natural logarithm of the total amount of gas in bar consumed by the reaction, minus the amount of gas in bar consumed at time  $t$ , divided by the total amount of gas in bar consumed by the reaction, see Equation 4.1.

#### Equation 4.1

$$k = \ln(P_t/P_{t=0})$$

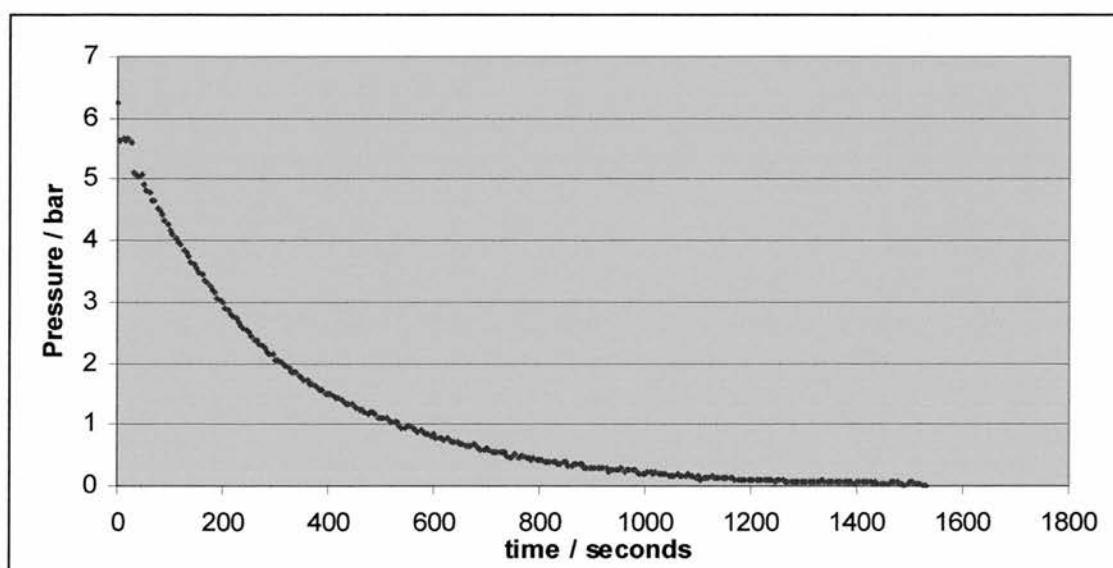
$P_t$  = Ballast vessel pressure, assuming  $P_{\text{final}} = 0$ .

$P_{t=0}$  = Total pressure of gas consumed by the reaction.

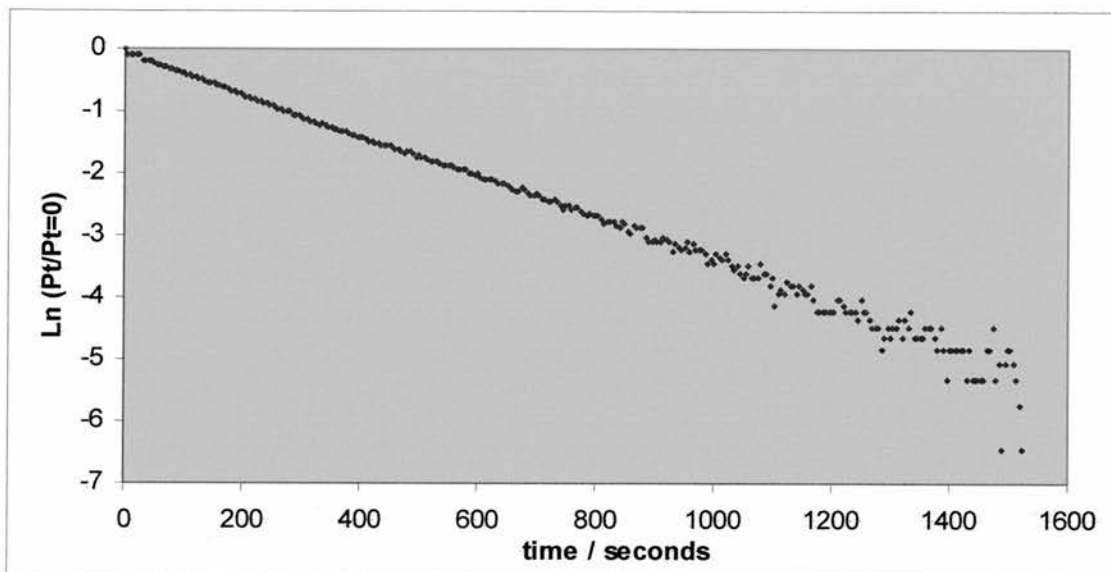
An example of this can be seen in Graph 4.1 and Graph 4.2. Graph 4.1 is a plot of the gas uptake from the ballast vessel of the CATS kinetic autoclave, against time in seconds. The gas uptake represents the gas consumption of the hydroformylation of allyl alcohol with the Rh / Et-Xantphos catalytic system, rhodium / diphosphine ratio 1:2, rhodium concentration  $2 \times 10^{-2} \text{ mol dm}^{-1}$ , in toluene, at  $80^\circ\text{C}$  and under 10 bar synthesis gas.

#### Graph 4.1

*Gas consumption of the hydroformylation of allyl alcohol with the Rh / Et-Xantphos catalytic system, rhodium / diphosphine ratio 1:2, rhodium concentration  $2 \times 10^{-2} \text{ M}$ , in toluene, at  $80^\circ\text{C}$  and under 10 bar synthesis gas.*



Graph 4.2 is a plot of  $\ln(P_t/P_{t=0})$  versus time, the linear nature of Graph 4.2 over the first two half lives (75 %), or when  $0 \geq \ln(P_t/P_{t=0}) \geq -1.4$ , of the reaction, demonstrates a first order reaction with respect to substrate concentration. It is the gradient of that line 0.0032, which represents the rate constant of the reaction in  $\text{s}^{-1}$ . The initial rate of reaction in  $\text{s}^{-1} \text{ mol dm}^{-1}$  can therefore be calculated by multiplying the rate constant by the concentration of allyl alcohol at the start of the reaction, which is  $2.94 \text{ mol dm}^{-1}$ . In this case that gives a rate of  $0.01 \text{ mol dm}^{-1} \text{ s}^{-1}$ .

**Graph 4.2***Logarithmic rate Profile of the reaction.*

This initial rate is dependent upon the concentration of rhodium and the initial concentration of substrate. The initial rate of reaction can therefore be expressed as the initial turn over frequency ( $\text{TOF}_{\text{init}}$ ), which represents the number of moles of substrate one mole of catalyst (or rhodium) hydrocarboxylates in a second or an hour, in  $\text{s}^{-1}$  or  $\text{h}^{-1}$  respectively.

**Equation 4.2**

$$\text{TOF} = \frac{k [\text{substrate}]}{[\text{Rh}]}$$

It is the initial TOF, ( $\text{TOF}_{\text{init}}$ ) which is quoted in the catalytic results below, this is the rate constant multiplied by the initial substrate concentration, divided by the rhodium concentration. In the given example this is  $0.5 \text{ s}^{-1}$ , or  $1800 \text{ h}^{-1}$ .

In some reactions, the rate of reaction is not stated. In the early stages of these studies a block stirrer was employed in the autoclave, which did not give adequate gas mixing at higher rates of reaction; the rate of reaction in these cases was therefore mass transport limited. This is when the rate of gas transfer from the gaseous phase to the liquid phase limits the rate of the reaction. The rate of reaction is given as mass transport limited if this was the case.

The effect of the conditions of the reaction was also studied. The reaction was carried out under synthesis (CO/H<sub>2</sub> ratio 1:1) gas pressures of 10 bar to 40 bar, and at temperatures of 60 °C to 140 °C. The results of the hydroformylation of allyl alcohol are summarised in Table 4.3 and the results of the hydroformylation of 1-octene are summarised in Table 4.4.

The column indicating other products in Table 4.3, represents 2-methylpropanal, 2-methylprop-2-enal (methacrolein), 2-methylpropanol, 2-methylprop-2-enol, *iso*-butanol,  $\gamma$ -butyrolactone, 1,2-dihydrofuran, and 2-ethoxytetrahydrofuran. These could be degradation products of the hydroxyaldehydes, for example methacrolein is a known degradation product of 2-methyl-3-hydroxypropanal, and 1,2-dihydrofuran can come from the dehydration of 2-hydroxytetrahydrofuran, a known degradation product of 4-hydroxybutanal. When the reaction is carried out in ethanol 1,2-dihydrofuran can react with ethanol to form 2-ethoxytetrahydrofuran. For this reason the amount of other products must be considered in conjunction with the l:b ratio, which is the ratio of 4-hydroxybutanal and 2-methyl-3-hydroxypropanal, and when necessary 1,4-butanediol and 2-methyl-1,3-propandiol.

The other cyclic products are unknown and could be degradation products of both 2-methylpropanal and 4-hydroxybutanal. The branched aldehyde product, 2-methyl-3-hydroxypropanal can dehydrate at higher temperatures to give 2-methylprop-2-enal which can oligomerise or polymerise. The linear aldehyde product, 4-hydroxybutanal, can undergo ring closure to form the hemiacetal 2-hydroxytetrahydrofuran, which is thermally unstable and degraded to new products.

In some reactions iridium was present as well as rhodium, and the monophosphine PPhEt<sub>2</sub> was present as well as Et-Xantphos, see section 4.1.3.13. The results of the hydroformylation of allyl alcohol with Rh(CO)<sub>2</sub>(acac), Ir(CO)<sub>2</sub>(acac), Et-Xantphos, and PPhEt<sub>2</sub> can be seen in Table 4.3. The concentration of Ir(CO)<sub>2</sub>(acac) in the reaction represented in run 22 was  $8 \times 10^{-4}$  mol dm<sup>-3</sup> or 80 ppm. The Rh / Ir / Et-Xantphos was 1:0.4:2. The concentration of Ir(CO)<sub>2</sub>(acac), and PPhEt<sub>2</sub> in the reaction represented in run 23 was  $8 \times 10^{-4}$  mol dm<sup>-3</sup> or 80 ppm. The Rh / Ir / Et-Xantphos / PPhEt<sub>2</sub> was 1:0.4:2:20.

**Table 4.3**

Results for the hydroformylation of allyl alcohol with the Rhodium / Et-Xantphos catalytic system in the given solvent. [Rh] 200 ppm, Rh:Et-Xantphos ratio 1:2. Row 22 is a di-catalyst system containing Rh / Ir / Et-Xantphos, [Rh] 200 ppm, [Ir] 80 ppm, Rh:Ir:Et-Xantphos ratio 1:0.4:2. Row 23 is a di-catalyst system containing Rh / Ir / Et-Xantphos / PPhEt<sub>2</sub> [Rh] 200 ppm, [Ir] 80 ppm, Rh: Ir: Et-Xantphos: PPhEt<sub>2</sub> ratio 1:0.4:2:20.

Key: AA = allyl alcohol; HBA = 4-hydroxybutanal; MHPA = 2-methylpropanal; BDO = 1,4-butanediol.

## Toluene

Run	T/ °C	P/ bar	TOF h <sup>-1</sup>	AA	HBA	MHPA	BDO	MPD	propanal	Propanol	Other products	L:b <sup>a</sup> ratio
1	80	10	1690	2.46	86.28	7.17	0.29	0.0	0.64	0.38	2.78	12.0
2	100	10	Mt	2.19	73.81	9.89	0.18	0.0	9.59	2.81	1.53	7.5
3	120	10	Mt	1.73	43.58	11.06	0.14	0.0	36.12	4.92	2.45	3.9
4	80	30	1270	0.42	73.55	20.31	0.25	0.0	1.49	0.95	3.03	3.6
5	100	30	Mt	0.59	87.06	7.54	0.49	0.0	1.24	0.69	2.39	11.6
6	120	30	Mt	1.34	75.76	10.74	0.23	0.0	7.96	2.13	1.84	7.1

## Ethanol

Run	T/ °C	P/ bar	TOF h <sup>-1</sup>	AA	HBA	MHPA	BDO	MPD	propanal	Propanol	Other products	L:b <sup>a</sup> ratio
7	80	10	800	0.77	75.23	15.04	0.29	0.0	0.83	0.89	6.88	5.0
8	90	10	2860	0.50	78.74	13.99	0.29	0.0	0.78	0.99	4.71	5.6
9	100	10	7410	0.49	74.45	15.57	0.25	0.0	3.31	0.99	4.94	4.77
10 <sup>b</sup>	120	40	52920	0.60	76.99	14.92	0.27	0.0	1.14	1.47	4.61	5.2
11 <sup>c</sup>	120	40	28050	0.09	40.42	0.55	5.96	0.75	0.52	1.42	50.29	73.2 ald 8.0 alc

## THF

Run	T/ °C	P/ bar	TOF h <sup>-1</sup>	AA	HBA	MHPA	BDO	MPD	propanal	Propanol	Other products	L:b <sup>a</sup> ratio
12	80	10	2010	1.52	86.60	7.95	0.13	0.0	1.04	1.04	4.71	10.9
13 <sup>d</sup>	100/ 120	10/ 40	MT	0.12	81.23	7.36	0.24	0.0	6.28	0.15	4.62	11.0

## MTBE

Run	T/ °C	P/ bar	TOF h <sup>-1</sup>	AA	HBA	MHPA	BDO	MPD	propanal	propanol	Other products	L:b <sup>a</sup> ratio
14	80	10	3070	0.38	87.57	8.92	0.23	0.0	0.91	0.74	1.25	9.8
15	100	30	Mt	0.35	63.84	14.79	0.07	0.0	17.98	1.04	1.93	4.3

## Amyl alcohol

Run	T/ °C	P/ bar	TOF h <sup>-1</sup>	AA	HBA	MHPA	BDO	MPD	propanal	propanol	Other products	L:b <sup>a</sup> ratio
16	80	10	1110	0.32	85.37	11.65	0.08	0.0	0.69	0.32	1.57	7.3
17	100/ 150	10/ 40	Mt	0	77.21	6.39	1.80	0	6.49	1.93	6.18	12.1

THF / H<sub>2</sub>O

Run	T/ °C	P/ bar	TOF h <sup>-1</sup>	AA	HBA	MHPA	BDO	MPD	propanal	propanol	Other products	L:b <sup>a</sup> ratio
18	100/ 120/ 140	10/ 40/ 60	Mt	0.08	54.79	3.85	0.62	0.0	8.39	1.08	31.19	14.22

## Toluene / AcOH

Run	T/ °C	P/ bar	TOF h <sup>-1</sup>	AA	HBA	MHPA	BDO	MPD	propanal	propanol	Other products	L:b <sup>a</sup> ratio
19	80	10	530	0.26	79.00	7.28	0.11	0.0	0.36	1.02	11.97	10.8

## MTBE / EtOH

Run	T/ °C	P/ bar	TOF h <sup>-1</sup>	AA	HBA	MHPA	BDO	MPD	propanal	propanol	Other products	L:b <sup>a</sup> ratio
20	80	10	2910	0.22	84.94	9.29	0.25	0.0	0.83	1.14	3.33	9.1
21	100	10	Mt	0.0	52.67	8.77	0.0	0.0	32.68	5.88	0.0	6.00

## Toluene / Iridium

Run	T/ °C	P/ bar	TOF h <sup>-1</sup>	AA	HBA	MHPA	BDO	MPD	propanal	propanol	Other products	L:b <sup>a</sup> ratio
22	80	10	1850	0.26	76.84	15.79	0.29	0.0	2.53	1.03	3.26	4.9
23	80	10	1910	2.03	74.37	0.0	0.59	0.0	0.32	2.77	19.92 <sup>e</sup>	N/A

a) The l:b ratio is the ratio of 4-hydroxybutanal : 2-methyl-3-hydroxypropanal. At higher temperatures the l:b ratio can be seriously distorted by the formation of by-products from these products. The percentage of the reaction products that these products account for is listed under other by-products in Appendix 4, which is especially important in row 23 where the l:b ratio of is N/A as all MHPA has further reacted to other products.

- b) Reaction repeated at 2000 ppm Rh concentration under these conditions. GC data N/A but observed about 30 % conversion to the diol products of reaction. L:b ratios were very poor however.
- c) Reaction left for an extended period of time, 18 hours.
- d) At 10 bar 100 °C for 2 hours then 40 bar 120 °C for a further 2 hours.
- e) Although the cyclic product of this reaction are reported as 0 %, they in fact make up to 50 % of the products. This value is estimated from the GC MS spectrum. The cyclic products of this reaction were different from all previous reactions, and although they are observed in the GC MS they are not observed in the GC FID, so accurate deduction of their percentage proved impossible.

**Table 4.4**

Results for the hydroformylation of 1-octene with the Rhodium / Et-Xantphos catalytic system in the given solvent. [Rh] 200 ppm, Rh:Et-Xantphos ratio 1:2.

Key: NA = Nonanal; MOA = 2-methyloctanal; NOL = nonanol; MOO = 2-methyloctanol; OE = octenes (1-octene, 2-octene, 3-octene, 4-octene); Oct = octane; EHA = 2-ethylheptanal; PHA = 2-propylhexanal; DEN = diethoxynonane.

Toluene													
Run	T / °C	P / bar	TOF <sub>int</sub> h <sup>-1</sup>	NA	MOA	NOL	MOO	OE <sup>a</sup>	Oct	EHA & PHA	DEN	Unknown	L:b <sup>b</sup>
1	80	10	161	85.17	5.48	0.12	0.00	7.78	0.99	5.63	0.00	0.32	15.5
2	120	40	9790	81.75	3.20	0.14	0.00	12.72	1.91	3.27	0.00	0.20	25.5

## EtOH

Run	T / °C	P / Bar	TOF <sub>int</sub> h <sup>-1</sup>	NA	MOA	NOL	MOO	OE <sup>a</sup>	Non	EHA & PHA	DEN	Unknown	L:b <sup>b</sup>
3	40	120	1580	84.38	4.08	1.35	0.00	8.35	1.40	4.08	0.22	0.23	20.7
4 <sup>c</sup>	40	120	1610	75.03	4.55	8.34	0.26	7.03	1.41	4.82	2.25	0.86	16.5 ald 32.1 alc
5 <sup>d</sup>	40	120	1440	39.34	6.01	41.49	1.84	5.00	1.53	7.11	0.21	3.31	6.5 ald 22.5 alc

a) OE represents all octenes; however, 1-octene was 0 % in all reactions, it therefore represents all internal octenes.

b) The l:b ratio is representative of the NA:MOA ratio. When necessary a second l:b ratio will be added for NOL and MOO in which case they will be labeled **ald** for the aldehyde ratio and **alc** for the alcohol ratio. It can also be said that the true l:b ratio should be representative of all products, including the internal octenes, EHA and PHA as branched products. For this reason it is important to consider the selectivity to NA also.

c) Reaction 3 left for an extended time, 17 hours.

d) 2000 ppm rhodium concentration.

#### 4.1.3.1 *Hydroformylation of Allyl Alcohol with the Rh/ Et-Xantphos Catalytic System in Toluene.*

The results of the hydroformylation of allyl alcohol with the Rh/ Et-Xantphos catalytic system in toluene can be seen in Table 4.3 runs 1 to 6.

Run 1, at 80 °C and 10 bar synthesis gas the  $\text{TOF}_{\text{init}}$  was  $1700 \text{ h}^{-1}$ , the l:b ratio<sup>†</sup> was 12.0, and the selectivity to the aldehyde products, 4-hydroxybutanal and 2-methyl-3-hydroxypropan-1-al, was 93.4 %. The selectivity to the linear aldehyde product is therefore 86.3% %. Unreacted allyl alcohol accounted for 2.4 % of the reaction products, the isomerisation product propanal 0.6 % and the hydrogenation product 0.4 %. The reaction produced a very small amount of BDO, 0.3 %, and no MPD, as expected for the non-polar / non protic solvent. Other products of reaction account for 2.9 % of the reaction products.

The high l:b ratio of this experiment is significant as it is the first time a high l:b ratio has been obtained for the hydroformylation of allyl alcohol catalysed by a rhodium complex of a phosphine containing two small alkyl substituents.

The results for the hydroformylation of allyl alcohol with  $[\text{Rh}(\text{CO})_2(\text{acac})]$  and Et-Xantphos under varying conditions are compared in Graph 4.3 to Graph 4.5.

At 10 bar synthesis gas the l:b ratio decreases with increasing temperature, as does the HBA selectivity, the selectivity to propanal increases, and the selectivity to other products remains low. The rate of reaction is increases with temperature as it is mass transport limited, Graph 4.3.

The significantly lower HBA selectivity, and higher propanal selectivity at higher temperature, can be explained by considering the different activation energies of  $\beta$ -hydride elimination, and CO addition. If the activation energy of  $\beta$ -hydride elimination is higher than that of CO addition, at lower temperature the equilibrium between the two will lie heavily on the side of CO addition. Thus, you observe low propanal levels, as propanal is the eventual product of allyl isomerisation to propan-2-enol, via  $\beta$ -

---

<sup>†</sup> The l:b ratio is the ratio of 4-hydroxybutanal : 2-methyl-3-hydroxypropanal. At higher temperatures the l:b ratio can be seriously distorted by the formation of by-products from these products. The percentage of the reaction products that these products account for is listed under other by-products in table 4.3. A full account of the products of reaction and their abundance can be seen in Appendix 4.

hydride elimination of the branched rhodium alkyl species, see Figure 4.2. However, at higher temperature, the equilibrium will lie more towards  $\beta$ -hydride elimination and the levels of propanal will be higher. The regioselectivity of Rh-H addition across the double bond must therefore be even lower at higher temperatures than represented by the l:b ratio alone, as propanal is a product of the branched rhodium alkyl complex species.

### Graph 4.3

Results for the hydroformylation of allyl alcohol with  $[Rh(CO)_2(acac)]$  & *Et-Xantphos*, at 10 bar synthesis gas & varying temperature.  $[Rh] = 200$  ppm, diphosphine:Rh = 2.

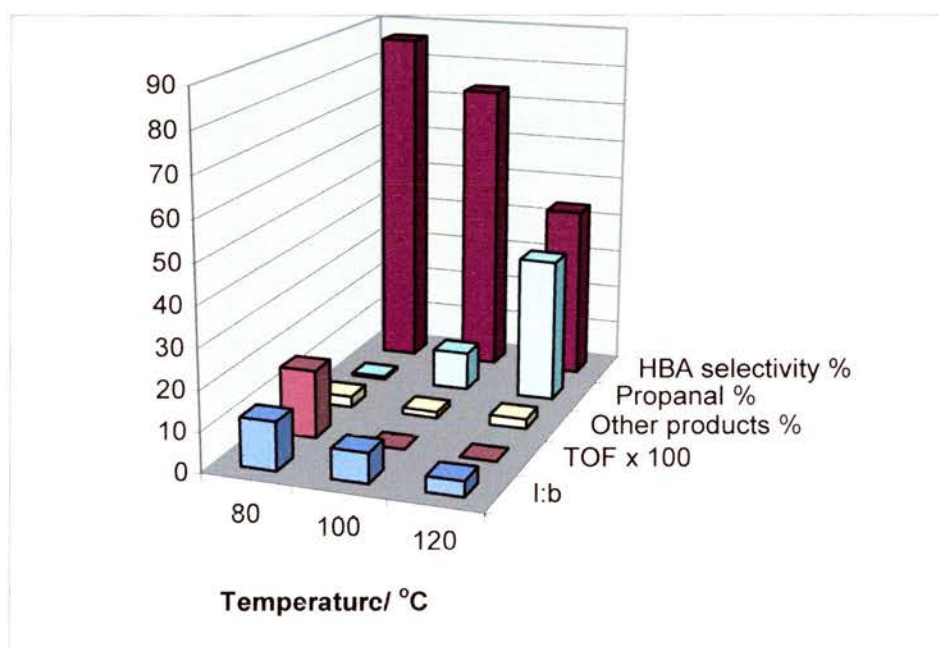
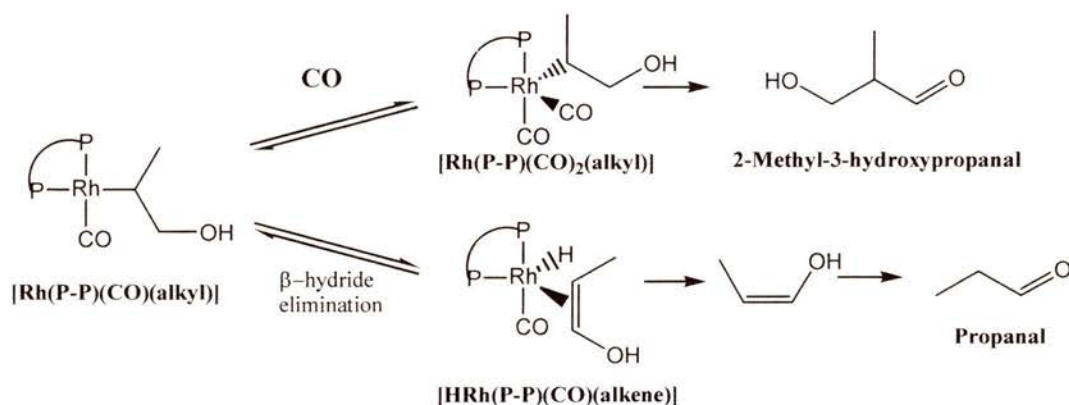


Figure 4.2

$\beta$ -Hydride elimination from  $[Rh(\text{diphosphine})(CO)(\text{alkyl})]$  to form propanal.



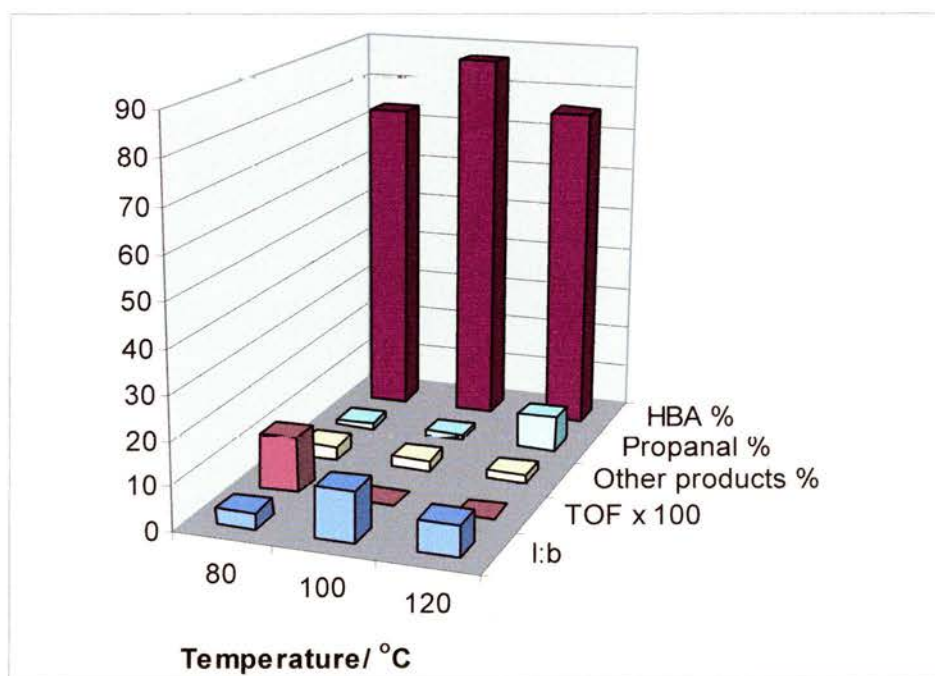
At 30 bar synthesis gas the patterns are more complicated, see Graph 4.4. At 80 °C the l:b ratio is low, and increases as the temperature is increased to 100 °C, however, when the temperature is increased further to 120 °C the l:b ratio decreases, in line with what we observed at 10 bar. The HBA selectivity also follows this same pattern. The selectivity to other products remains low for all three reactions, the selectivity to propanal is low at 80 °C and 100 °C, but increases at 120 °C. As the rate of reaction is mass transported limited at higher temperatures, the rate of reaction can be said to have increased, although it is not known by how much.

The result at 80 °C and 30 bar synthesis gas can be said to be a true one as it was repeated with near identical selectivities. As the selectivity to both propanal and other products is low the l:b ratio can be said to be a truly representative.

The same pattern was found in ethanol at 10 bar and 80 °C, see section 4.1.3.2. It is noted that both reactions have the lowest  $TOF_{init}$  for their respective solvents. It is suggested that the low  $TOF_{init}$  may be a factor in the poor catalytic results.

#### Graph 4.4

*Results for the hydroformylation of allyl alcohol with  $[Rh(CO)_2(acac)]$  & *Et-Xantphos*, at 30 bar synthesis gas & varying temperature.  $[Rh] = 200$  ppm, diphosphine:Rh = 2.*

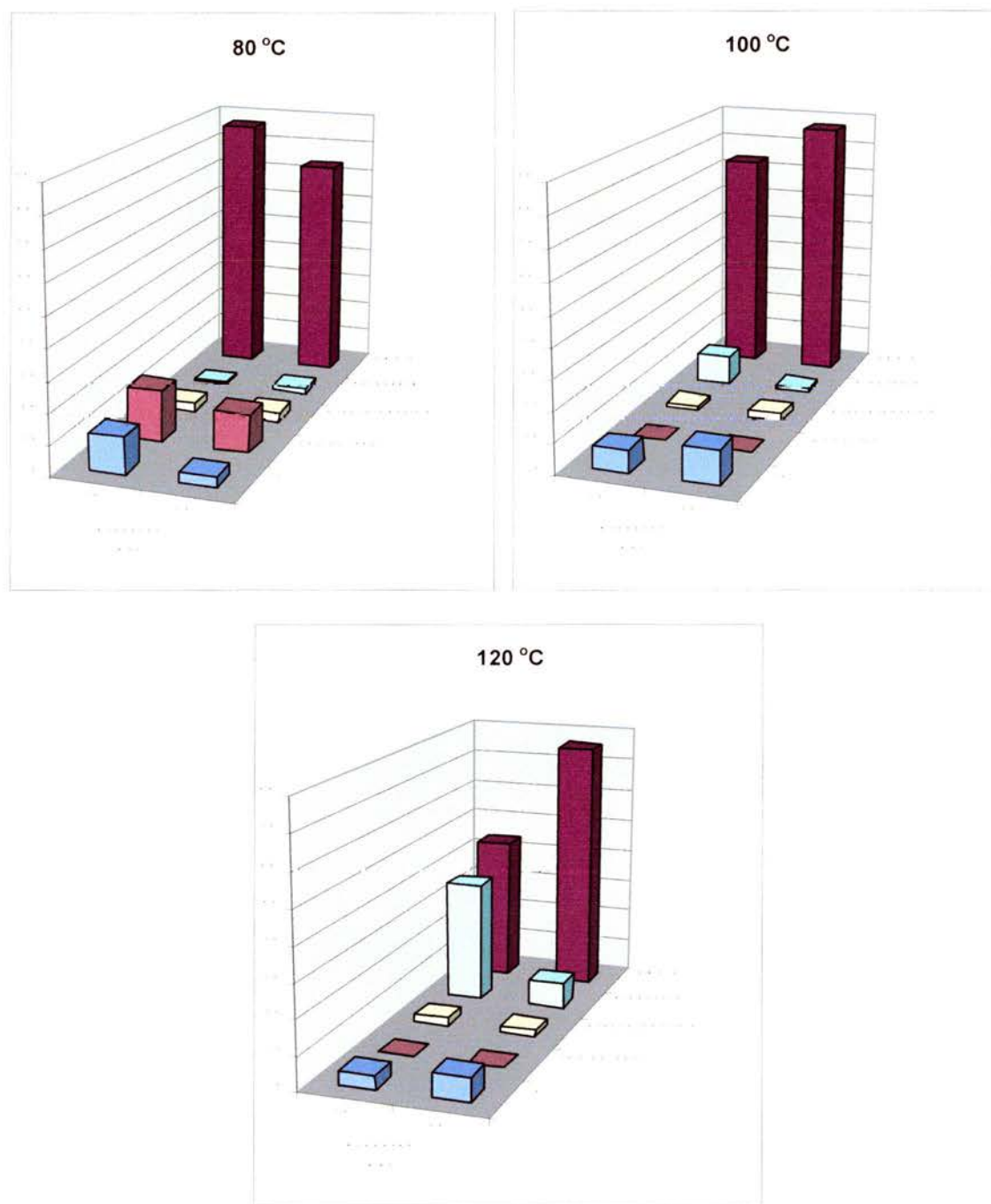


Graph 4.5 shows how the results change with increasing pressure, from 10 bar to 30 bar, at 80 °C, 100 °C and 120 °C. At 80 °C the l:b ratio decreases with increasing pressure, as does the selectivity to HBA. The selectivity to propanal and other products remains

low, and the  $\text{TOF}_{\text{init}}$  decreases. At 100 °C and 120 °C, the 1:b ratio increases with increasing pressure, as does the HBA selectivity. The selectivity to propanal decreases and the selectivity to other products remains low.

### Graph 4.5

*Results for the hydroformylation of allyl alcohol with  $[\text{Rh}(\text{CO})_2(\text{acac})]$  & Et-Xantphos, at 80 °C, 100 °C and 120 °C and varying pressure.  $[\text{Rh}] = 200 \text{ ppm}$ , diphosphine:Rh = 2.*



#### ***4.1.3.2 Hydroformylation of Allyl Alcohol with the Rh/ Et-Xantphos Catalytic System in Ethanol.***

The results of the hydroformylation of allyl alcohol with the Rh/ Et-Xantphos catalytic system in ethanol can be in Table 4.3 runs 7 to 11.

For run 7, at 80 °C and 10 bar synthesis gas, the  $\text{TOF}_{\text{init}}$  was  $800 \text{ h}^{-1}$ , the l:b ratio was 5.0, and the selectivity to the aldehyde products, 4-hydroxybutanal and 2-methyl-3-hydroxypropan-1-al, was 90.3 %. The selectivity to the linear aldehyde product is therefore 75.2 %. Unreacted allyl alcohol accounted for 0.77 % of the reaction products, the isomerisation product propanal, 0.8 %, and the hydrogenation product propanol 0.9 %. The reaction produced a very small amount of BDO, 0.3 %, and no MPD. Other products of reaction account for 6.9 % of the reaction products.

The l:b ratio increases going from 80 °C to 90 °C at 10 bar synthesis gas, as does the HBA selectivity. The level of propanal stays low, and the level of other products stays constant, although higher than when the reaction is carried out in toluene. The main reason for this being increased levels of 2-methylpropanal and 1,2-dihydrofuran. 2-Methylpropanal can come from the dehydration of 2-methyl-3-hydroxypropanal to 2-methylprop-2-enal, followed by hydrogenation to 2-methylpropanal. 1,2-Dihydrofuran can come from the dehydration of 4-hydroxybutanal. The  $\text{TOF}_{\text{init}}$  of the reaction increases 3.5 times on increasing the temperature 10 °C.

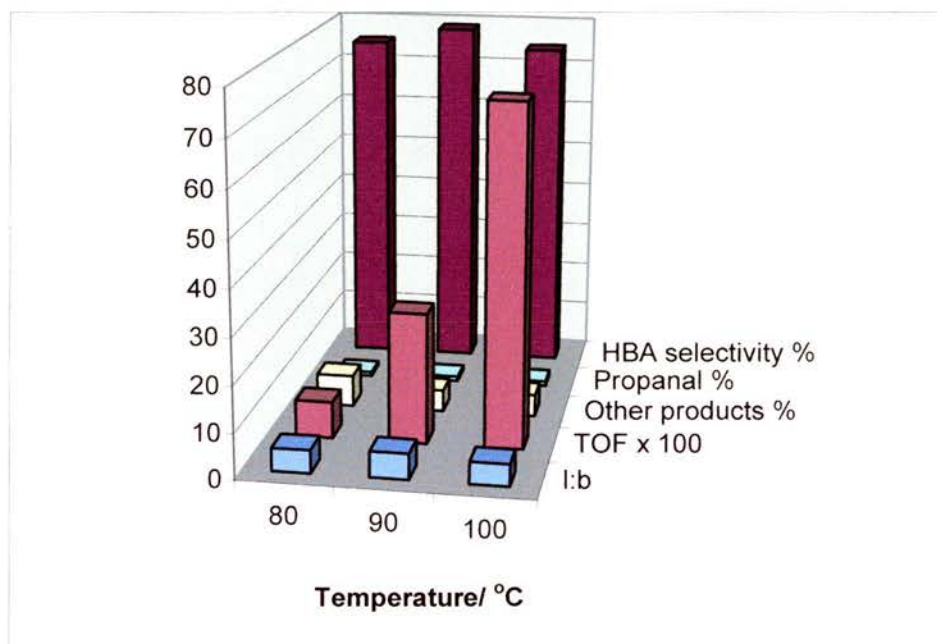
When further increasing the temperature to 100 °C the l:b ratio decreases as does the HBA selectivity. The selectivity to other products stays constant, and the selectivity to propanal remains low. The  $\text{TOF}_{\text{init}}$  of the reaction increases a further 2.6 times on increasing the temperature a further 10 °C.

The low l:b ratio and HBA selectivity observed at 80 °C and 10 bar synthesis gas, was observed at 80 °C and 30 bar synthesis gas in toluene also, see section 4.1.3.1. Both reactions were repeated and gave near identical results. It is also observed that the  $\text{TOF}_{\text{init}}$  of reaction is lower in ethanol than in toluene. The  $\text{TOF}_{\text{init}}$  of the reaction in toluene at 80 °C and 30 bar synthesis gas is therefore similar to the  $\text{TOF}_{\text{init}}$  of reaction in ethanol at 80 °C and 10 bar synthesis gas. It is therefore suggested, as in section 4.1.3.1, that the low l:b ratios observed could be linked to the low  $\text{TOF}_{\text{init}}$  observed in these reactions.

As the pressure and temperature is increased from 90 °C and 10 bar to 120 °C and 40 bar, the l:b ratio decreases slightly as does the HBA selectivity. The selectivity to propanal and the other products stays constant. The  $TOF_{init}$  of the reaction increases by 18.5 times.

#### Graph 4.6

*Results for the hydroformylation of allyl alcohol with  $[Rh(CO)_2(acac)]$  & *Et-Xantphos*, at 10 bar synthesis gas & varying temperature.  $[Rh] = 200$  ppm, diphosphine:Rh = 2.*

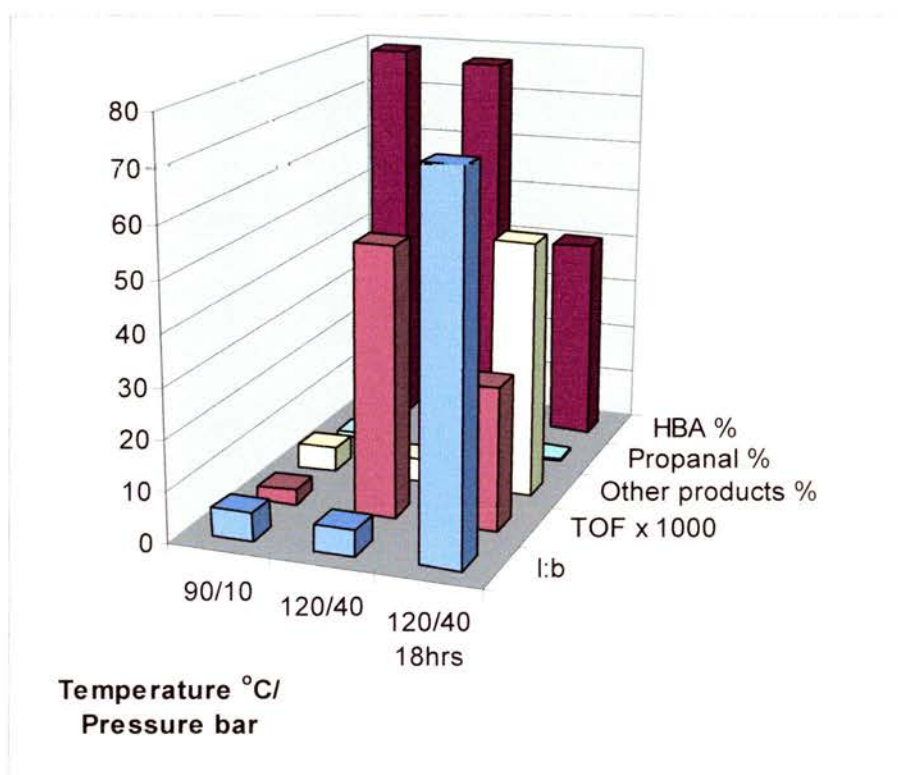


When the reaction is left at 120 °C and 40 bar synthesis gas for an extended period of time the l:b ratio of the hydroxyaldehydes increases dramatically, the HBA selectivity decreases dramatically however. The selectivity to propanal remains low but the selectivity to the other products increases dramatically. The reason for this is an increase in the level of ethoxytetrahydrofuran, (EOF), and 2-methylpropanal, (MPA), degradation products of the linear hydroxyaldehyde and the branched hydroxyaldehyde respectively. It is also observed that there was partial conversion of the hydroxyaldehydes to the diol products. The l:b ratio of the diol products was 8.0, the selectivity to BDO was 6.0 % and to MPD it was 0.8 %, see Graph 4.7.

The difference in the l:b ratio under these conditions can be explained by the increase in the degradation products, and the increase in the diol products. If you class HBA, EOF, and BDO as linear products, and HPA, MPA, and MPD as branched products their respective selectivities stay the same as to when the reaction is not left for an extended period of time, see Graph 4.8.

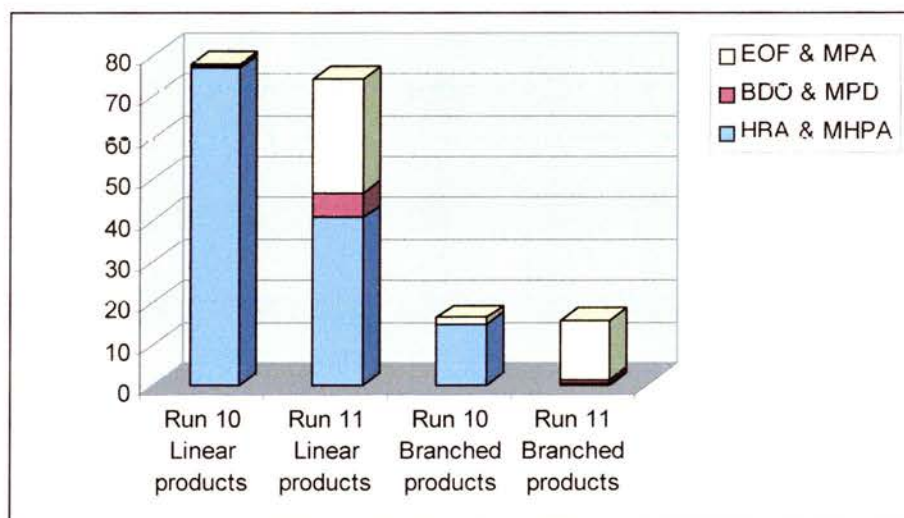
**Graph 4.7**

Results for the hydroformylation of allyl alcohol with  $[Rh(CO)_2(acac)]$  & *Et-Xantphos*, at 90 °C and 10 bar synthesis gas & at 120 °C and 40 bar synthesis gas.  $[Rh] = 200$  ppm, diphosphine:Rh = 2.



**Graph 4.8**

Selectivities to all the linear and branched products of run 10 and run 11, at 120 °C and 40 bar synthesis gas, where run 10 is stopped at the end of the reaction and run 11 is left under those conditions for 18 hours.



Because the Rh / Et-Xantphos catalytic system failed to hydroformylate allyl alcohol to the alcohol products of reaction in a one step process, or even hydrogenate the aldehyde hydroformylation products in a two step process, it was decided to repeat the reaction with a rhodium concentration an order of magnitude higher in order to force the formation of the diol products.

The rhodium concentration was 2000 ppm, the Rh / Et-Xantphos ratio was 1:2, and the conditions were 120 °C and 40 bar synthesis gas. The GC data for the reaction is not available, however, over short reaction periods, a normal product distribution of hydroxyaldehydes, propanal and other products, but with a poor l:b ratio, 1.7 was observed. Over longer reaction periods the formation of the diols was observed, however, this was associated with this was the break up of the reaction products and the formation of large amounts of by-products. After 12.5 hours there was approximately 30 % conversion to the diol products, with an l:b ratio of 2.4. However, the level of the by-products accounted for approximately 30 % of the reaction products.

#### ***4.1.3.3 Hydroformylation of Allyl Alcohol with the Rh/ Et-Xantphos Catalytic System in THF.***

The results of the hydroformylation of allyl alcohol with the Rh/ Et-Xantphos catalytic system in THF can be in Table 4.3 runs 12 and 13.

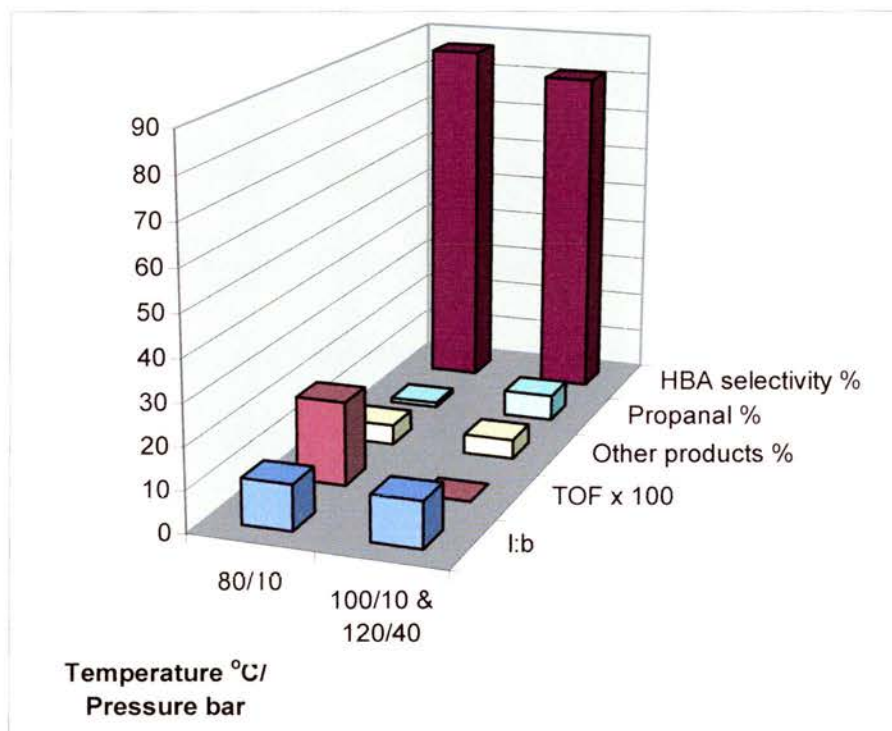
For run 12, at 80 °C and 10 bar synthesis gas the  $TOF_{init}$  was  $2010\text{ h}^{-1}$ , the l:b ratio was 10.9, and the selectivity to the aldehyde products, 4-hydroxybutanal and 2-methyl-3-hydroxypropan-1-al, was 94.6 %. The selectivity to the linear aldehyde product is therefore 86.6 %. Unreacted allyl alcohol accounted for 1.5 % of the reaction products, the isomerisation product propanal 1.04 % and the hydrogenation product propanol 1.04 %. The reaction produced a very small amount of BDO, 0.1 %, and no MPD. Other products of reaction account for 4.7 % of the total.

The results of Run 12 and 13 are summarised in Graph 4.9. Run 13 was carried out at 100 °C and 10 bar synthesis gas for 2 hours, and then at 120 °C and 40 bar for 2 hours. The conditions were ramped to try to hydrogenate the hydroxyaldehydes to the diols. This did not occur however, not was there an increase in the level of other products. For this reason the distribution can be said to be as it was at the original conditions of 100 °C and 10 bar synthesis gas.

With increasing temperature the l:b ratio stays the same, the selectivity to HBA decreases slightly however. The selectivity to propanal goes up and the selectivity to other products stays at the same level. The  $\text{TOF}_{\text{init}}$  goes up with increasing temperature as the experiment at 100 °C and 10 bar synthesis gas in mass transport limited

#### Graph 4.9

Results for the hydroformylation of allyl alcohol with  $[\text{Rh}(\text{CO})_2(\text{acac})]$  & *Et-Xantphos*, at 80 °C and 10 bar synthesis gas & at 100 °C and 10 bar synthesis gas ramped to 100 °C and 40 bar synthesis gas.  $[\text{Rh}] = 200 \text{ ppm}$ , diphosphine:Rh = 2.



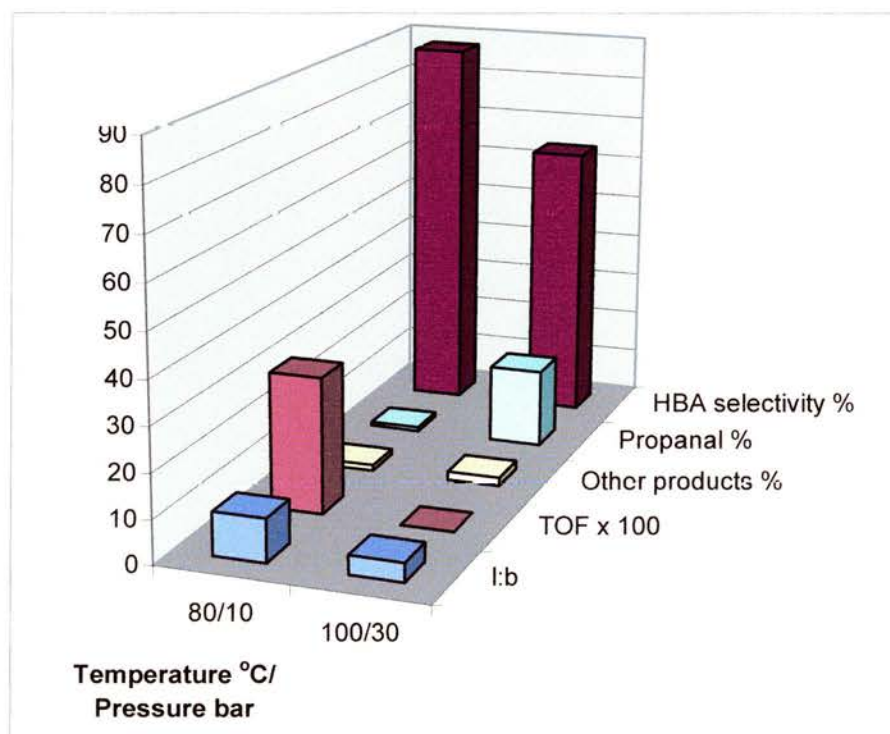
#### 4.1.3.4 Hydroformylation of Allyl Alcohol with the Rh/ Et-Xantphos Catalytic System in MTBE.

The results of the hydroformylation of allyl alcohol with the Rh/ Et-Xantphos catalytic system in MTBE can be seen in Table 4.3 runs 14 and 15.

For run 14, at 80 °C and 10 bar synthesis gas the  $TOF_{init}$  was  $3070\text{ h}^{-1}$ , the l:b ratio was 9.8, and the selectivity to the aldehyde products, 4-hydroxybutanal and 2-methyl-3-hydroxypropan-1-al, was 96.5 %. The selectivity to the linear aldehyde product is therefore 87.6 %. Unreacted allyl alcohol accounted for 0.4 % of the reaction products, the isomerisation product propanal 1.3 % and the hydrogenation product propanol 0.7 %. The reaction produced a very small amount of BDO, 0.1 %, and no MPD. Other products of reaction account for 4.7 % of the reaction products.

#### Graph 4.10

Results for the hydroformylation of allyl alcohol with  $[Rh(CO)_2(acac)]$  & Et-Xantphos, at 80 °C and 10 bar synthesis gas & at 100 °C and 30 bar synthesis gas.  $[Rh] = 200$  ppm, diphosphine:Rh = 2.



The results of run 14 and 15 are summarised in Graph 4.10. With increasing temperature and pressure there is a decrease in the l:b ratio and in the HBA

selectivity. The selectivity to propanal goes up and the selectivity to other products stays low. Only trace amounts of BDO and in MPD were observed.

#### ***4.1.3.5 Hydroformylation of Allyl Alcohol with the Rh/ Et-Xantphos Catalytic System in Amyl Alcohol.***

The results of the hydroformylation of allyl alcohol with the Rh/ Et-Xantphos catalytic system in amyl alcohol can be in Table 4.3 runs 16 and 17.

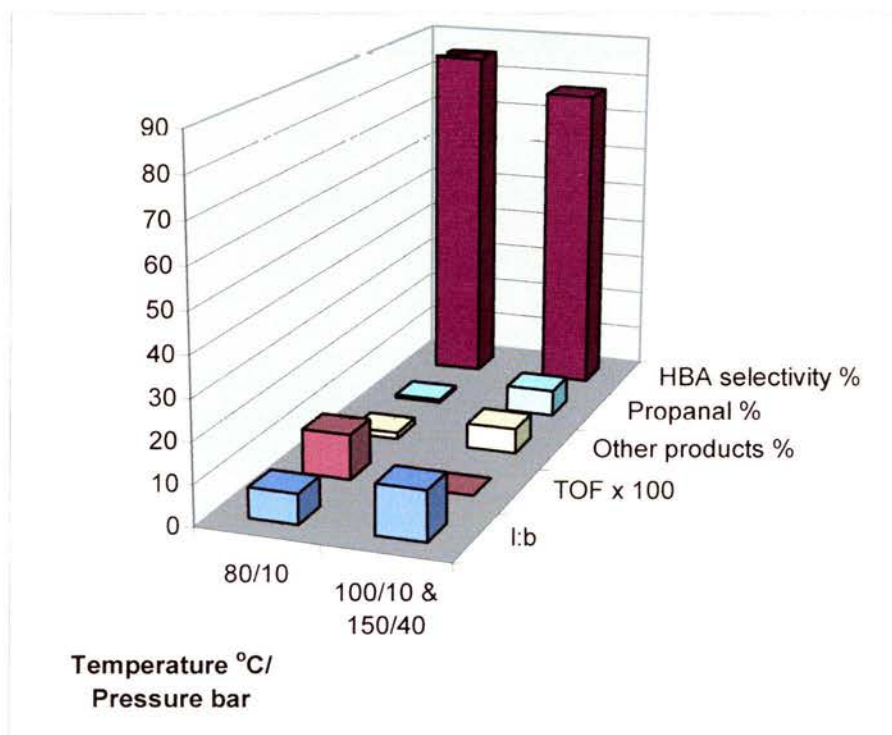
For run 16, at 80 °C and 10 bar synthesis gas the  $TOF_{init}$  was  $1110\text{ h}^{-1}$ , the l:b ratio was 7.3, and the selectivity to the aldehyde products, 4-hydroxybutanal and 2-methyl-3-hydroxypropan-1-al, was 97.0 %. The selectivity to the linear aldehyde product is therefore 85.4 %. Unreacted allyl alcohol accounted for 0.3 % of the reaction products, the isomerisation product propanal 0.7 % and the hydrogenation product propanol 0.3 %. The reaction produced a very small amount of BDO, 0.1 %, and no MPD. Other products of reaction account for 1.6 % of the reaction products.

Run 17 was carried out at 100 °C and 10 bar synthesis gas for 2 hours, and then at 150 °C and 40 bar for 2 hours. The conditions were ramped to try to hydrogenate the hydroxyaldehydes to the diols. There was a small increase in the level of BDO present although this was not appreciable, and there was no MPD present. However, there was an increase in the level of other products, mainly MPA, see Appendix 4, which could have occurred when the more forcing conditions were used. For this reason the distribution can not be said to be as at 100 °C and 10 bar.

On increasing the temperature and pressure there was an increase in the l:b ratio, but a decrease in the HBA selectivity. This is largely due to an increase in the selectivity to propanal and other products, mainly MPA. If HBA and BDO are classed as linear products, and MHPA, propanal, and MPA are classed as branched products, the l:b ratio for run 16 and 17 are 6.6 and 4.9 respectively, see Graph 4.12.

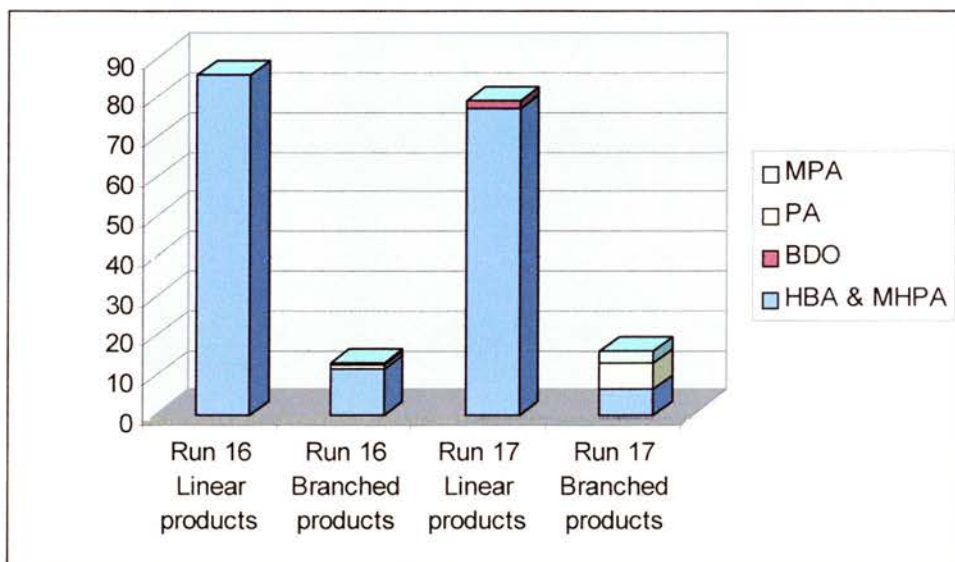
**Graph 4.11**

Results for the hydroformylation of allyl alcohol with  $[Rh(CO)_2(acac)]$  & *Et-Xantphos*, at 80 °C and 10 bar synthesis gas & at 100 °C and 10 bar synthesis gas ramped to 150 °C and 40 bar synthesis gas.  $[Rh] = 200$  ppm, diphosphine:Rh = 2.



**Graph 4.12**

Selectivities to all the linear and branched products of run 16 and run 17.



#### ***4.1.3.6 Hydroformylation of Allyl Alcohol with the Rh/ Et-Xantphos Catalytic System in THF/H<sub>2</sub>O.***

The results of the hydroformylation of allyl alcohol with the Rh/ Et-Xantphos catalytic system in THF / H<sub>2</sub>O can be in Table 4.3 run 18.

Run 18 was conducted at 100 °C and 10 bar synthesis gas, followed by 120 °C and 40 bar synthesis gas, followed by 140 °C and 60 bar synthesis gas. The rate of reaction was mass transport limited, the l:b ratio was 14.22, and the selectivity to the aldehyde products, 4-hydroxybutanal and 2-methyl-3-hydroxypropan-1-al, was 58.6 %. The selectivity to the linear aldehyde product is therefore 54.8 %. Unreacted allyl alcohol accounted for 0.1 % of the reaction products, the isomerisation product propanal 8.4 % and the hydrogenation product propanol 1.1 %. The reaction produced a very small amount of BDO, 0.6 %, and no MPD. Other products of reaction account for 31.2 % of the reaction products.

Similarly to the reaction in amyl alcohol at 100 °C and 10 bar synthesis gas, followed by 150 °C and 40 bar synthesis gas the reaction has a high l:b ratio of 14.2 but a low HBA selectivity of 54.79 %. This is accounted for by the high levels of other products observed, however, they are mainly the unknown cyclics. In section 4.1.3 it was explained how these can come from either the linear or branched hydroxyaldehydes so we can not give an estimated l:b ratio from including these. The level of propanal produced is higher but comparable with the reaction in THF at 100 °C and 10 bar synthesis gas, 8.39 % with respect to 6.28 %, an indication that the initial l:b ratio may also have been similar, therefore not far below 11.

#### ***4.1.3.7 Hydroformylation of Allyl Alcohol with the Rh/ Et-Xantphos Catalytic System in Toluene/ Acetic Acid.***

The results of the hydroformylation of allyl alcohol with the Rh/ Et-Xantphos catalytic system in toluene / acetic acid can be in Table 4.3 run 19.

For run 19, at 80 °C and 10 bar synthesis gas the TOF<sub>init</sub> was 530 h<sup>-1</sup>, the l:b ratio was 10.8, and the selectivity to the aldehyde products, 4-hydroxybutanal and 2-methyl-3-hydroxypropan-1-al, was 86.3 %. The selectivity to the linear aldehyde product is therefore 79.0 %. Unreacted allyl alcohol accounted for 0.3 % of the reaction products,

the isomerisation product propanal 0.4 % and the hydrogenation product propanol 1.0 %. The reaction produced a very small amount of BDO, 0.1 %, and no MPD. Other products of reaction account for 12.0 % of the reaction products.

It is observed that the l:b ratio is lower than under the same conditions in toluene alone, 10.8 with respect to 12.0, as is the selectivity to HBA, 79.0 % with respect to 86.3 %. The levels of propanal and propanol are similar, however, the level of other products was much greater at 11.97 % with respect to 2.78 % in toluene alone. There was no hydrogenation of HBA to BDO either as the level of BDO is in fact slightly lower at 0.1 % with respect to 0.3 %.

It is also observed that the  $\text{TOF}_{\text{init}}$  is 3.4 times lower at  $503 \text{ h}^{-1}$  than when in toluene alone when it is  $1690 \text{ h}^{-1}$ .

#### ***4.1.3.8 Hydroformylation of Allyl Alcohol with the Rh/ Et-Xantphos Catalytic System in MTBE / EtOH.***

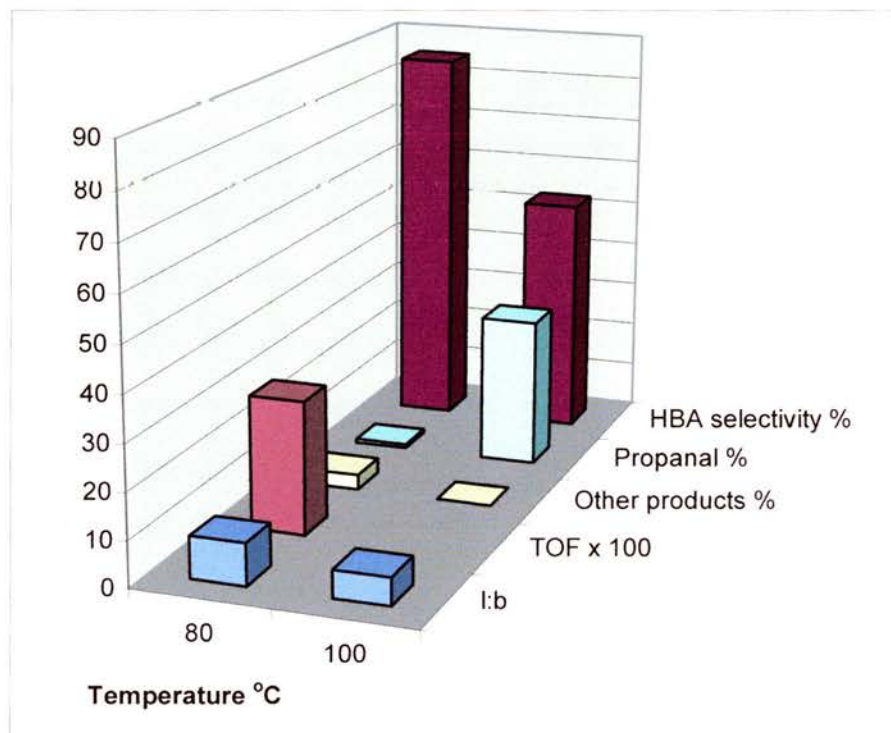
The results of the hydroformylation of allyl alcohol with the Rh/ Et-Xantphos catalytic system in toluene / acetic acid can be seen in Table 4.3 runs 20 and 21.

For run 20, at  $80 \text{ }^\circ\text{C}$  and 10 bar synthesis gas the  $\text{TOF}_{\text{init}}$  was  $2910 \text{ h}^{-1}$ , the l:b ratio was 9.1, and the selectivity to the aldehyde products, 4-hydroxybutanal and 2-methyl-3-hydroxypropan-1-al, was 94.2 %. The selectivity to the linear aldehyde product is therefore 84.9 %. Unreacted allyl alcohol accounted for 0.2 % of the reaction products, the isomerisation product propanal 0.8 % and the hydrogenation product propanol 1.1 %. The reaction produced a very small amount of BDO, 0.3 %, and no MPD. Other products of reaction account for 3.3 % of the reaction products.

When the temperature of the reaction was increased to  $100 \text{ }^\circ\text{C}$  the l:b ratio decreased, as does the selectivity to HBA. The selectivity to propanal increases significantly, while the selectivity to other products stays low. The  $\text{TOF}_{\text{init}}$  increases as it is mass transport limited at  $100 \text{ }^\circ\text{C}$ .

**Graph 4.13**

Results for the hydroformylation of allyl alcohol with  $[Rh(CO)_2(acac)]$  & *Et-Xantphos*, at 10 bar synthesis gas & varying temperature.  $[Rh] = 200$  ppm, diphosphine:Rh = 2.



#### 4.1.3.9 Hydroformylation of 1-Octene with the Rh/ *Et-Xantphos* Catalytic System in Toluene.

The results of the hydroformylation of 1-octene with the Rh/ *Et-Xantphos* catalytic system in toluene can be in Table 4.4 runs 22 and 23.

Run 1, at 80 °C and 10 bar synthesis gas the  $TOF_{init}$  was  $161\text{ h}^{-1}$ , the l:b ratio was 15.5, and the selectivity to the aldehyde products, nonanal and 2-methyloctanal, was 90.65 %. The selectivity to the linear aldehyde product is therefore 85.17 %. The alcohol products nonanol and 2-methyloctanol account for 0.1 % and 0.0 % of the reaction products, internal octenes, 7.8 %, nonane, 1.0 %, EHA and PHA, 5.6 %, and unknowns 0.3 %.

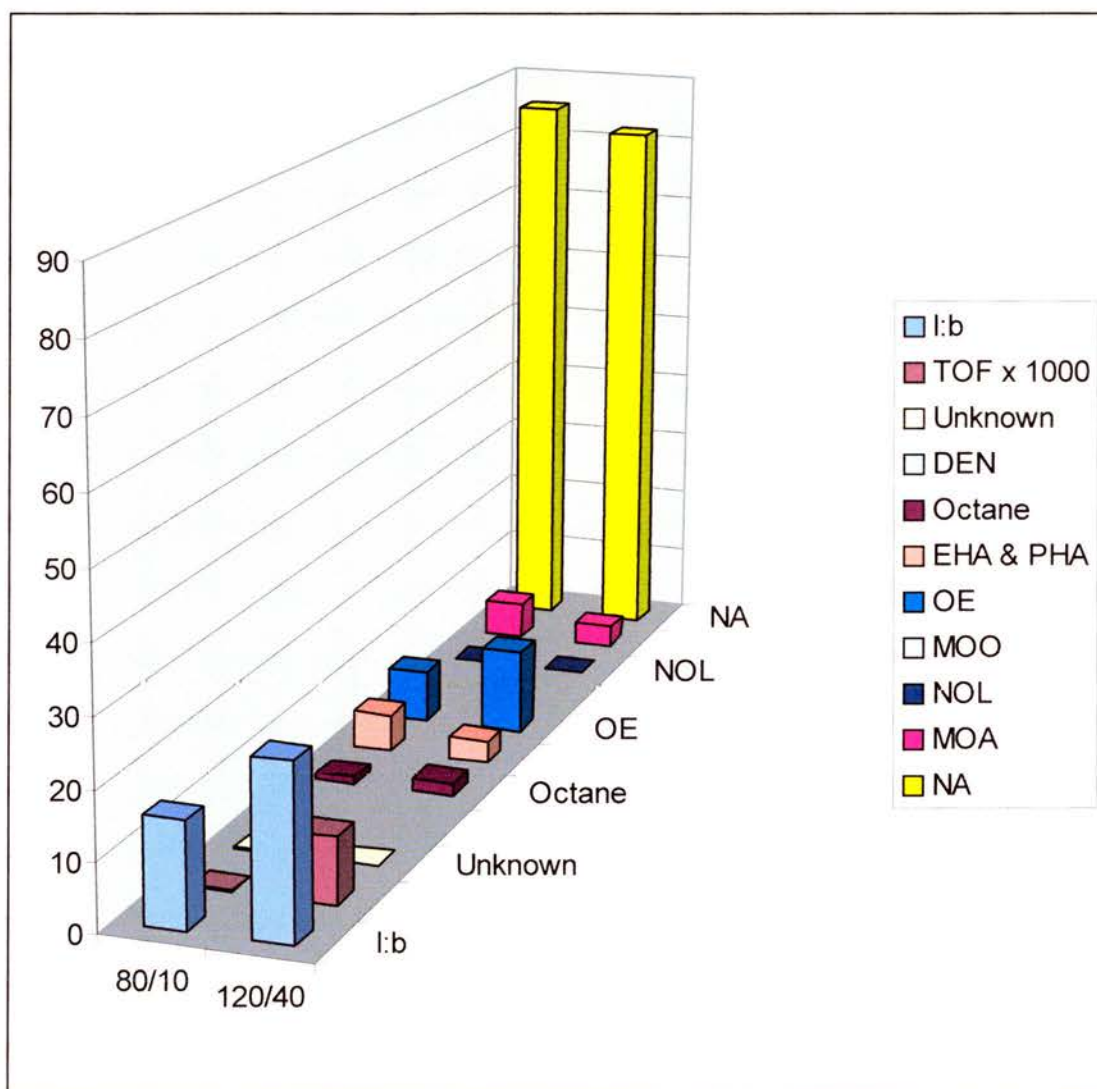
The results of the hydroformylation of 1-octene in toluene at 80 °C and 10 bar and at 120 °C and 40 bar synthesis gas are compared in Graph 4.14.

The reaction at 120 °C and 40 bar has a higher l:b ratio but a lower selectivity to nonanal. The reason for this is that greater levels of internal alkenes are present as

reaction products. These trends fit with what we have already observed for the hydroformylation of allyl alcohol.

#### Graph 4.14

*Results for the hydroformylation of 1-octene with  $[Rh(CO)_2(acac)]$  & Et-Xantphos, at 80 °C and 10 bar & 120 °C and 40 bar synthesis gas.  $[Rh] = 200$  ppm, diphosphine:Rh = 2.*



The  $TOF_{init}$  is 60 times faster at 120 °C and 40 bar than at 80 °C and 10 bar synthesis gas. Although we do not have the  $TOF_{init}$  for all the allyl alcohol hydroformylation reactions in toluene using Et-Xantphos as ligand, this increase is comparable to the increase in  $TOF_{init}$  for the hydroformylation of allyl alcohol in ethanol, which is 65 times greater at 120 °C and 40 bar than at 80 °C and 10 bar synthesis gas. It is also observed that at 80 °C and 10 bar synthesis gas, in toluene, the  $TOF_{init}$  is 10 times

slower for the hydroformylation of 1-octene than for the hydroformylation of allyl alcohol.

#### ***4.1.3.10 Hydroformylation of 1-Octene with the Rh/ Et-Xantphos Catalytic System in Ethanol.***

The results of the hydroformylation of 1-octene with the Rh/ Et-Xantphos catalytic system in ethanol can be seen in Table 4.4 runs 3 to 5.

For run 3, at 120 °C and 40 bar synthesis gas the  $\text{TOF}_{\text{init}}$  was  $1580 \text{ h}^{-1}$ . The l:b ratio of the aldehyde product was 20.7, and the selectivity to nonanal and 2-methyloctanal, was 88.5 %. The selectivity to the linear aldehyde product is therefore 84.4 %. The alcohol products; NOL and MOO, account for 1.35 % and 0.00% of the reaction products respectively. Internal octenes account for 8.35 % of the reaction products, nonane, 1.4 %, EHA and PHA, 4.1 %, DEN, 0.2 %, and unknowns 0.2 %.

Run 2 was left at 120 °C and 40 bar synthesis gas for an extended period of time. Run 3 was carried out with a rhodium concentration 10 times that of run 1 and 2. The results of runs 1, 2, and 3 are compared in Graph 4.15. The l:b ratio is of the aldehyde and alcohol products. The l:b ratio is slightly lower in run 1 than in 2, when left for 2 hours and 17 hours respectively. This can be explained by the increased levels of DEN, a by-product formed from nonanal and ethanol, observed in Run 2. There was partial conversion to the alcohol products and the l:b ratio of the alcohols was higher than that of the l:b ratio of the aldehydes. Because of this it can be said that the linear aldehyde was hydrogenated faster than the branched one.

At a higher rhodium concentration the l:b ratio of the combined aldehydes and alcohols decreases. There is no significant increase in the selectivity to any of the other branched products. There is a decrease in the level of the internal octenes, however this is matched by an increase in the level of EHA and PHA, formed from their hydroformylation. The level of DEN also decreases, but is matched by an increase in the level of the unknowns. The lower combined l:b ratio is therefore a feature of increasing the rhodium concentration.

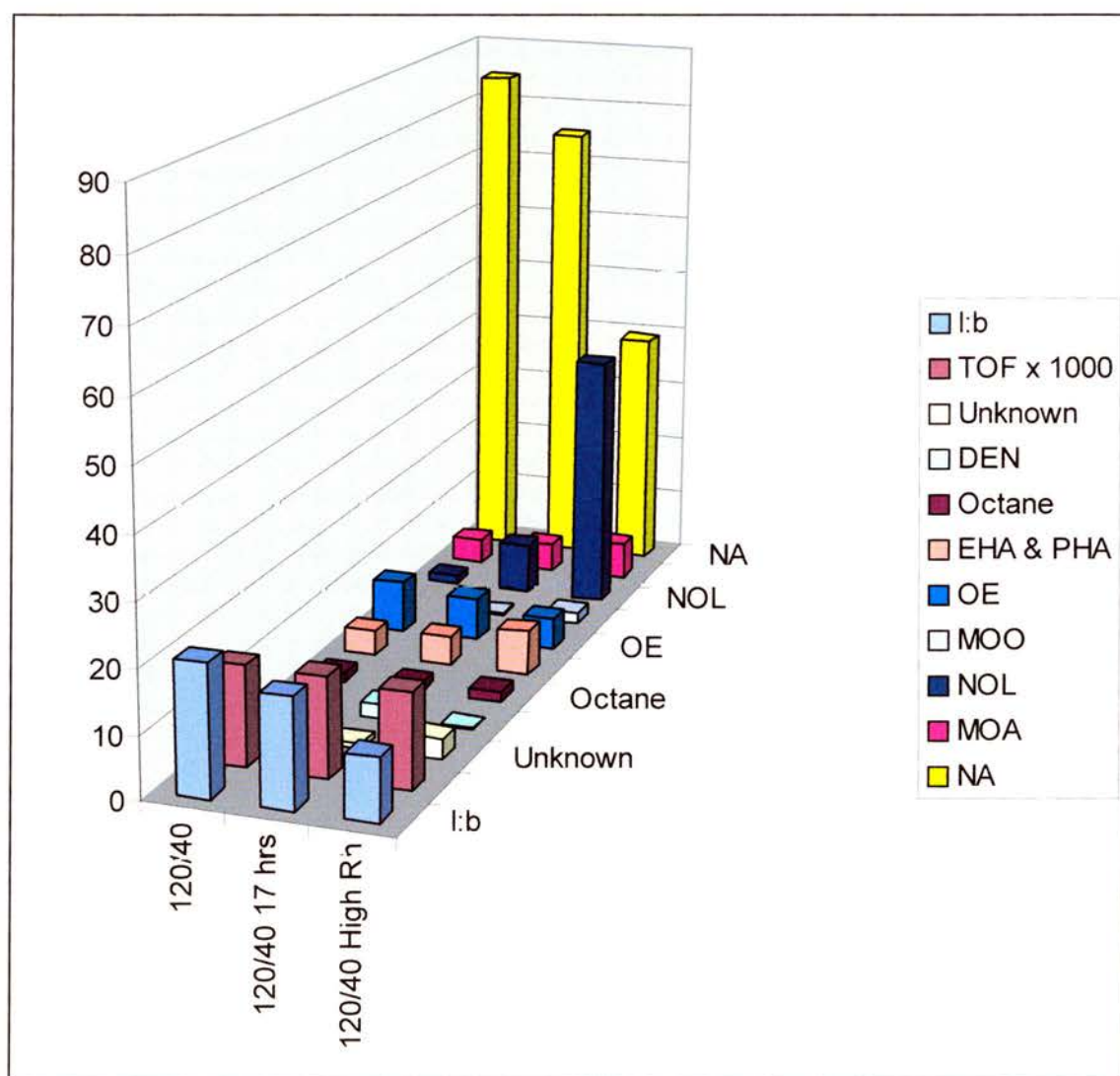
It is also observed that as in Run 2, the l:b ratio of the alcohols is greater than the l:b ratio of the aldehydes. This is because, as in run 2, the linear hydroxyaldehyde is being

hydrogenated preferentially to the branched hydroxyaldehyde, 50 % of HBA is hydrogenated to BDO while only 23 % of MHPA is being hydrogenated to MPD.

The  $TOF_{init}$  the same in all three experiments, and is 6 times less that observed under the same conditions in toluene, and 33 times less than observed with the same catalytic system, in the same solvent, and under the same conditions, but with allyl alcohol as substrate.

### Graph 4.15

Results for the hydroformylation of 1-octene with  $[Rh(CO)_2(acac)]$  & *Et-Xantphos*, at 120 °C and 40 bar synthesis gas.  $[Rh] = 200$  ppm, and 2000 ppm, diphosphine:Rh = 2.

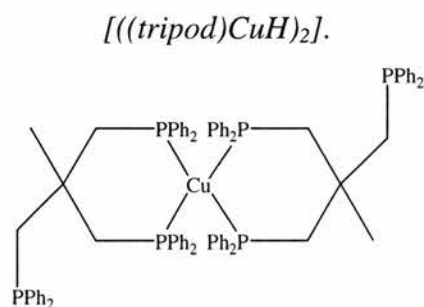


#### 4.1.3.11 Iridium Et-Xantphos Hydrogenation Catalysts?

Because of the failure of the rhodium Et-Xantphos catalytic system to hydrogenate the hydroxyaldehyde products of the hydroformylation of allyl alcohol, a second catalyst could be introduced to the catalytic system to accomplish this step. For this reason a homogeneous catalyst that will selectively hydrogenate an aldehyde over an alkene was selected. In a one pot reaction this should avoid the hydrogenation of allyl alcohol.

There are some reports of such catalysts. Rhodium catalysts have been reported for the selective hydrogenation of carbonyls in the presence of alkenes.<sup>18</sup> Selectivities of 98 % were obtained; however, the catalyst contains of a 2,2'-bipyridine ligand and the reaction is carried out in a basic methanol/ NaOH solvent. It is believed that this could effect the hydroformylation step of our reaction. Copper(I) hydride complexes have also been reported for the chemoselective hydrogenation of unsaturated ketones and aldehydes to unsaturated alcohols.<sup>19</sup> The catalytic system is interesting as it is comprised of a binuclear copper complex with a bidentate phosphine,  $[\{(tripod)CuH\}_2]$ , (tripod = 1,1,1-tris(diphenylphosphinomethyl) ethane)), see Figure 4.3, with excess tripod (2 to 3 equivalents) in THF and pressurised with hydrogen. This is similar to the way in which our experiments are conducted. However, the introduction of a second phosphine so dissimilar to Et-Xantphos is undesirable. More recently, there has been a major break though in this area of chemistry with a catalyst comprised of  $[trans-RuCl_2(phosphine)_2(1,2-diamine)]$  in an alkaline medium.<sup>20</sup> It is reported that the hydrogenation of the aldehyde is 1500 times faster than the hydrogenation of the alkene. However, this is dependent on the presence of both the diamine and the base KOH, without them present, the ruthenium complex hydrogenates the alkenes 250 times faster than the aldehyde. The presence of the diamine and KOH are considered too unfavourable so this system was also discounted.

**Figure 4.3**



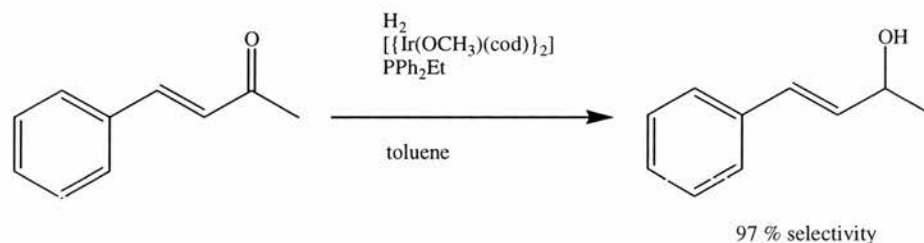
There was one reported system that was of interest however, this was the “selective hydrogenation of the carbonyl group of  $\alpha,\beta$ -unsaturated aldehydes to alcohols with iridium(I) complexes”.<sup>21-23</sup> It reported that by using phosphines with the correct cone angle, and by using the correct iridium to phosphine ratio it is possible to favour the triphosphine iridium complex  $[\text{Ir}(\text{P})_3]$ , over that of the diphosphine complex  $[\text{Ir}(\text{P})_2]$ . The triphosphine complex  $[\text{Ir}(\text{P})_3]$  is reported to be chemoselective for the hydrogenation of the carbonyl group of unsaturated aldehydes and ketones, where the diphosphine complex  $[\text{Ir}(\text{P})_2]$  hydrogenates the alkene group.

The best results were obtained with the ligands  $\text{PPh}_2\text{Et}$  and  $\text{PPhEt}_2$ . An iridium to phosphine ratio of 1:10 was used, with an iridium concentration of  $4 \times 10^{-4} \text{ mol dm}^{-3}$ , under 30 bar  $\text{H}_2$  and at  $100^\circ\text{C}$  in toluene. The conversions were 99 % after 10 hours, and 96 % after 28 hours, the selectivities to the unsaturated alcohol were 97 % and 94 % respectively, see Scheme 4.2.

What is of interest to us is the similarity of the catalytic system to the rhodium Et-Xantphos one. Both use a phosphine containing phenyl and ethyl groups, both use excess phosphine, and both reactions can be carried out in toluene. The differences between the systems is that we carried out reactions under synthesis gas, where these reactions were carried out under hydrogen and we use a chelating diphosphine not a monophosphine.

#### Scheme 4.2

*Carbonyl selective hydrogenation of the unsaturated ketone benzalacetone with iridium phosphine complexes.*



It was, therefore, decided to add an iridium source to our catalytic system.  $[\text{Ir}(\text{CO})_2(\text{acac})]$ , would be expected to form the complexes  $[\text{HIr}(\text{CO})_2(\text{Et-Xantphos})]$  or  $[\text{HIr}(\text{CO})(\text{Et-Xantphos})_2]$  where Et-Xantphos would be bound both bidentate and unidentate in the later complex. It was hoped that the formation of the latter complex might be favoured by using a ligand to iridium ratio of 5:1. It was hoped that this would catalyse the hydrogenation of the aldehyde products of the hydroformylation reaction,

while neither effecting the hydroformylation reaction nor hydrogenating allyl alcohol to propanol.

One problem we foresaw was that because we were using a chelating diphosphine the formation of the triphosphine complex would be unfavourable as the monodentate Et-Xantphos ligand would chelate displacing another CO group to form  $[\text{HIr}(\text{Et-Xantphos})_2]$ . It was therefore also proposed to add the monophosphine ligand  $\text{PPhEt}_2$  to the catalytic system to act as the third phosphine ligand to iridium to form the complex  $[\text{HIr}(\text{CO})(\text{Et-Xantphos})(\text{PPhEt}_2)]$ . There is some concern on how this might effect the hydroformylation step as rhodium complexes containing the monophosphine ligand would have decreased selectivity to the linear product of reaction, see Chapter 1. However, it was hoped that the chelating diphosphine Et-Xantphos will preferentially chelate to rhodium. This is feasible as much higher P:Rh ratios are required to form the diphosphine rhodium complex when using monophosphines (up to 100:1)<sup>1</sup> than when using diphosphines (~2:1),<sup>8</sup> thus suggesting the chelate effect of the diphosphine would be favourable and the hydroformylation catalyst would remain unaffected.

The results of the hydroformylation of allyl alcohol with the Rh/ Ir/ Et-Xantphos catalytic system in toluene can be in Table 4.3 run 22.

Run 22, was conducted at 80 °C and 10 bar synthesis gas, with a rhodium / iridium / Et-Xantphos ratio of 1:0.4:2, a rhodium concentration of 200 ppm, and an iridium concentration of 80 ppm. The  $\text{TOF}_{\text{init}}$  was  $1850 \text{ h}^{-1}$ , the l:b ratio was 4.9, and the selectivity to the aldehyde products, 4-hydroxybutanal and 2-methyl-3-hydroxypropan-1-al, was 92.6 %. The selectivity to the linear aldehyde product was therefore 76.8 %. Unreacted allyl alcohol accounted for 0.3 % of the reaction products, the isomerisation product propanal 2.5 % and the hydrogenation product 1.0 %. The reaction produced a very small amount of BDO, 0.3 %, and no MPD. Other products of reaction account for 3.26 % of the reaction products.

The results of the hydroformylation of allyl alcohol with the Rh/ Ir/ Et-Xantphos/  $\text{PPhEt}_2$  catalytic system in toluene can be in Table 4.3 run 23.

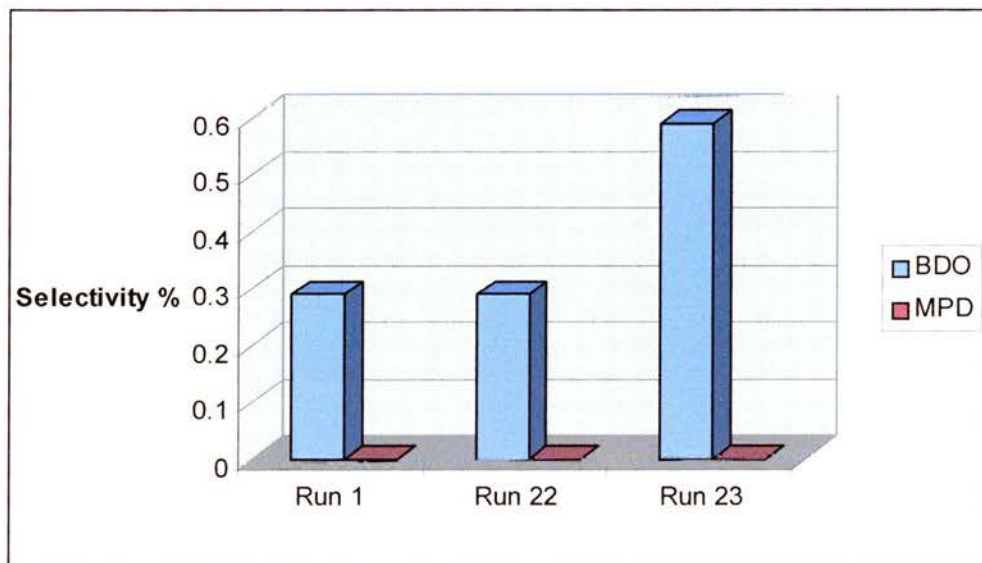
Run 23, was conducted at 100 °C and 10 bar synthesis gas, with a rhodium / iridium / Et-Xantphos /  $\text{PPhEt}_2$  ratio of 1:0.4:2:20, a rhodium concentration of 200 ppm, and an iridium concentration of 80 ppm. The  $\text{TOF}_{\text{init}}$  was  $1910 \text{ h}^{-1}$ , there was no l:b ratio as the selectivity to MHPA was 0.0, the selectivity to 4-hydroxybutanal was 74.4 %. Allyl alcohol accounted for 2.0 % of the reaction products, propanal, 0.3 %, propanol, 2.8 %, and

BDO 0.6 % and MPD 0 %. Other products of reaction account for 19.9 % of the reaction products.

The selectivities to BDO and MPD for the two runs containing iridium are compared in Graph 4.16, they are also compared to the selectivities obtained with the rhodium Et-Xantphos catalytic system in toluene under the same conditions with no iridium present, run 1. It is observed that there is no improvement in the selectivity to the diols in run 22, with the addition of iridium alone. There is only a slight improvement in the selectivity to BDO in run 23, with the addition of iridium and PPhEt<sub>2</sub>, although the selectivity is still below 1 %. We can say, therefore, that the iridium complex is failing to hydrogenate the aldehydes. This may be because the hydroformylation conditions are unfavourable for the hydrogenation catalyst, 80 °C and 10 bar synthesis gas with respect to 100 °C and 30 bar hydrogen. It could also be because the iridium complexes obtained under synthesis gas instead of hydrogen alone do not hydrogenate the aldehydes. It could also be that the effect of the chelating diphosphine Et-Xantphos needs investigation.

**Graph 4.16**

*Selectivity to BDO & MPD for runs 1, 22, and 23.*

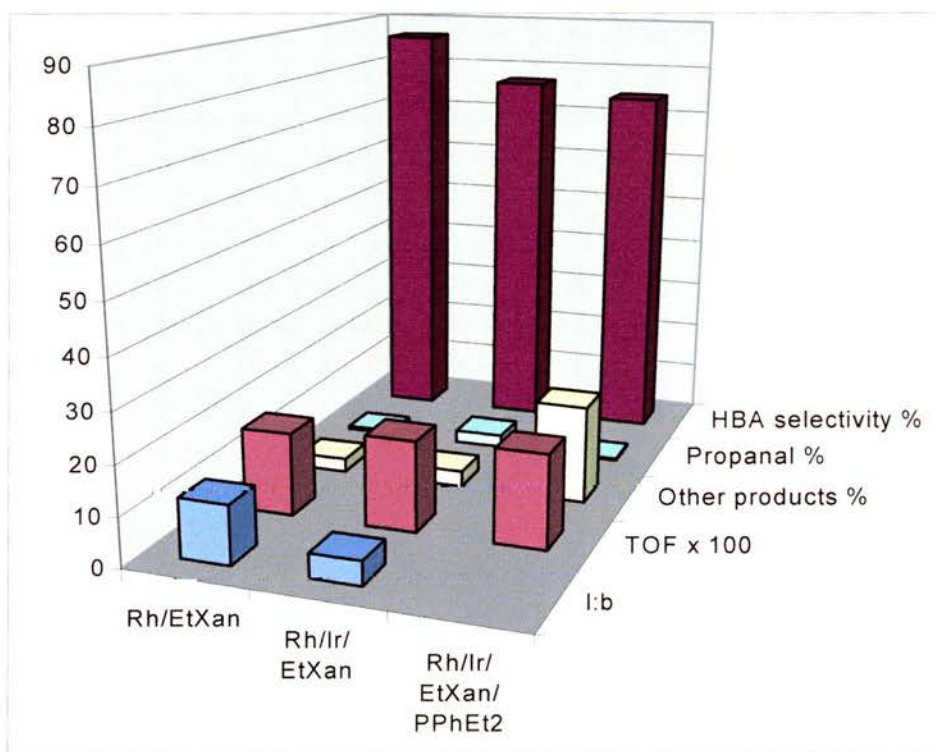


Graph 4.17 compares the results of the hydroformylation of allyl alcohol, run 1 with the rhodium Et-Xantphos catalytic system, run 22 with added iridium, and run 23 with added iridium and PPhEt<sub>2</sub>. The I:b ratio decreases with addition of iridium, as does the HBA selectivity. The selectivity to propanal and other products remains low. The TOF<sub>init</sub> of the reaction stays the same.

With the addition of iridium and  $\text{PPhEt}_2$  there is no 1:b ratio as there is no MHPA produced. The selectivity to HBA decreases further, however, and the level of other products goes up, mainly due to an increase in the selectivity to 2-methylprop-2-enal, a degradation product of MHPA. The selectivity to propanal is still low and the  $\text{TOF}_{\text{init}}$  is the same as before.

#### Graph 4.17

Results for the hydroformylation of allyl alcohol with  $[\text{Rh}(\text{CO})_2(\text{acac})]$  & Et-Xantphos,  $[\text{Rh}(\text{CO})_2(\text{acac})]$ ,  $[\text{Ir}(\text{CO})_2(\text{acac})]$  & Et-Xantphos, and  $[\text{Rh}(\text{CO})_2(\text{acac})]$ ,  $[\text{Ir}(\text{CO})_2(\text{acac})]$ , Et-Xantphos, &  $\text{PPhEt}_2$  at 10 bar synthesis gas  $80^\circ\text{C}$ .  
 $[\text{Rh}] = 200 \text{ ppm}$ , diphosphine:Rh = 2.



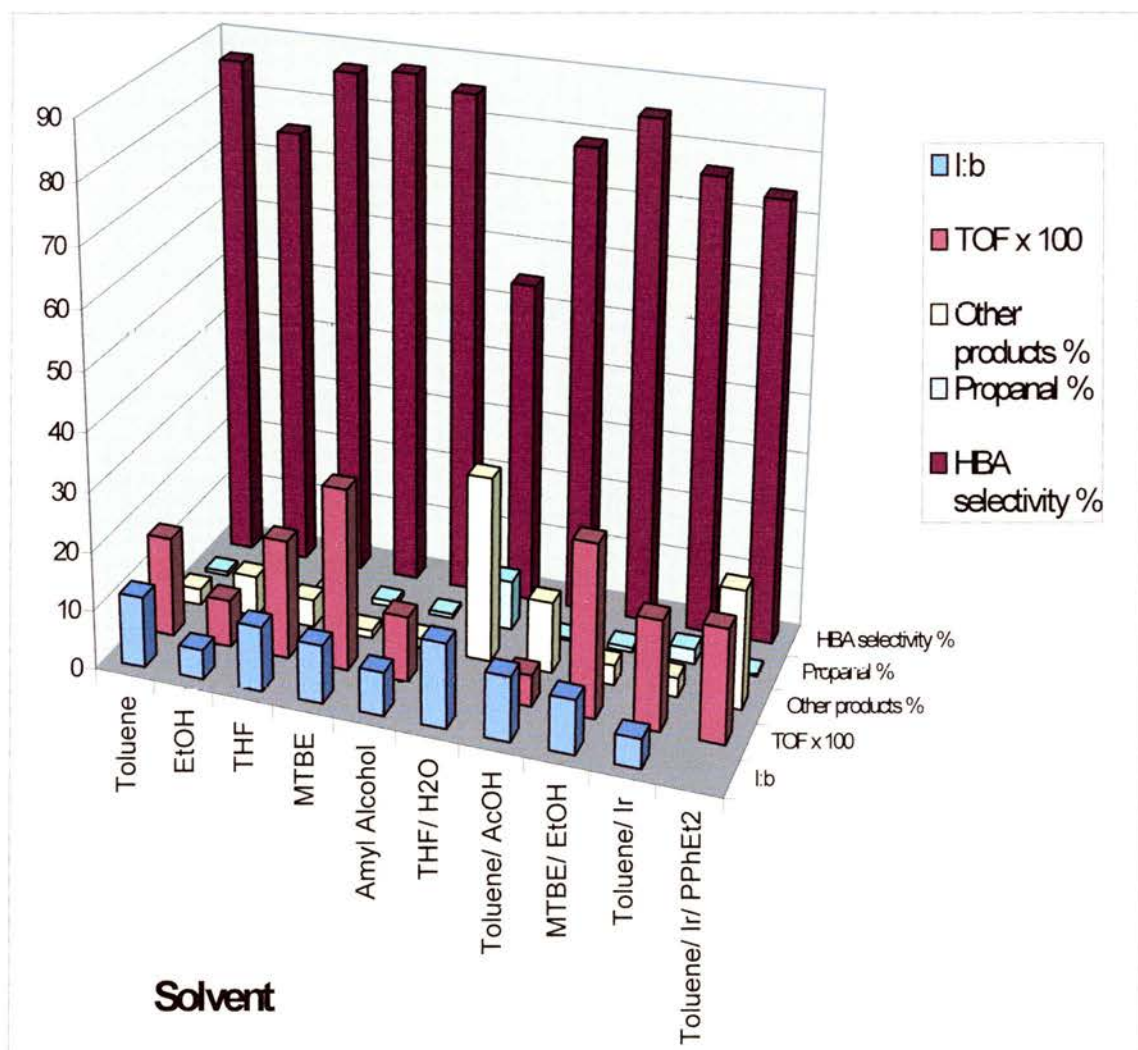
It is also observed that the level of the unknown cyclic products is quoted as zero in the reaction. In fact this is not the case, however, the cyclic products for this reaction only is different than those observed in all the other reactions and is not observed in the GC FID. Instead they are only observed in the GC MS, so accurate calculation of their percentage proved impossible, although they did account for approximately 50 % of the products, however.

#### 4.1.3.12 Comparison of the Results of the Hydroformylation of Allyl Alcohol in Different Solvents.

The results for the hydroformylation of allyl alcohol at 80 °C and 10 bar synthesis gas in the different solvents can be seen in Graph 4.18. It is observed that the HBA selectivity is highest in MTBE, toluene, THF, Amyl alcohol, and MTBE/ EtOH respectively. The highest TOF<sub>init</sub> is observed in MTBE, MTBE/ EtOH, THF and toluene respectively. The highest selectivity to other products is in THF/ H<sub>2</sub>O, toluene/ Ir/ PPhEt<sub>2</sub>, toluene/ AcOH, and ethanol respectively.

**Graph 4.18**

Results for the hydroformylation of allyl alcohol with  $[Rh(CO)_2(acac)]$  & *Et-Xantphos*, at 80 °C and 10 bar synthesis gas & varying solvent.  $[Rh] = 200$  ppm, diphosphine:Rh = 2.



## 4.2 9,9-Dimethyl-4,6-bis(di-*tert*-butylphosphino)xanthene [<sup>t</sup>Bu-Xantphos].

One of the reasons considered for the failure of Et-Xantphos to hydroformylate allyl alcohol to the diol products was that the diphosphine is not electron donating enough because of the electron withdrawing nature of the aryl backbone. For this reason it was proposed to synthesise some more electron rich analogous of Xantphos. The first of these was 9,9-dimethyl-4,6-bis(di-*tert*-butylphosphino)xanthene (<sup>t</sup>Bu-Xantphos). It was proposed that the increased electron donation from the *tert*-butyl groups to the phosphine with respect to ethyl groups would overcome this problem.

### 4.2.1 Synthesis.

9,9-Dimethyl-4,6-bis(di-*tert*-butylphosphino)xanthene, <sup>t</sup>Bu-Xantphos, was prepared from xanthene and di-*tert*-butylchlorophosphine, see section 6.2.4. Addition of secondary butyl lithium to a solution containing xanthene results in proton abstraction from xanthene and the formation of a lithium xanthene salt. Addition of chlorodiethylphosphine to the salt results in the formation of <sup>t</sup>Bu-Xantphos and lithium chloride.<sup>8</sup>

<sup>t</sup>Bu-Xantphos has a resonance at 11.71 ppm in the <sup>31</sup>P {<sup>1</sup>H} NMR spectrum, resonances at 7.9 ppm, 7.4 ppm, 7.2 ppm, (6H, ar); 1.5 ppm (6H, CCH<sub>3</sub>, s); 1.4 ppm (36H, PC(CH<sub>3</sub>)<sub>3</sub>, d <sup>3</sup>J<sub>HP</sub> = 64 Hz) in the <sup>1</sup>H NMR spectrum, and at 137.5 ppm (ar, PCCOC); 134.0 ppm (ar, CH); 131.1 ppm (ar, CHCC); 126.3 ppm (ar, CH); 122.0 (ar, CH); 117.2 ppm (ar, CHCPC); 33.1 ((CH<sub>3</sub>)<sub>3</sub>CP); 32.9 (C(CH<sub>3</sub>)<sub>2</sub>); 31.1 (C(CH<sub>3</sub>)<sub>2</sub>); 31.0 (C(CH<sub>3</sub>)<sub>3</sub>); in the <sup>13</sup>C NMR spectrum.

## 4.2.2 Catalytic Results.

The selectivity of the diphosphine ligand <sup>t</sup>Bu-Xantphos was tested in the rhodium catalysed hydroformylation of allyl alcohol and 1-octene. The reactions were carried out under identical conditions to when testing Et-Xantphos.

### 4.2.2.1 *Hydroformylation of Allyl Alcohol with the Rh/ <sup>t</sup>Bu-Xantphos Catalytic System in Toluene.*

The hydroformylation of allyl alcohol with the Rh/ <sup>t</sup>Bu-Xantphos catalytic system was very slow, showing only partial conversion after 18 hours. The GC FID of the reaction solution showed there to be many products, most uncharacterised by GC MS.

The reason for this became clear when a <sup>31</sup>P {<sup>1</sup>H} NMR spectrum was recorded of the ligand mixed with [Rh(CO)<sub>2</sub>(acac)] ratio 1:1. It is clear that although some of the ligand is complexed to the rhodium it is only a very small proportion. In other words, most of the rhodium in solution is unmodified.

A reason for why the ligand is not chelating to rhodium is suggested after by some simple molecular modelling with Chem 3D. It is proposed that if the ligand <sup>t</sup>Bu-Xantphos were to chelate to the rhodium the steric hindrance of the <sup>t</sup>Bu groups on the ligand result in chelation being unfavourable. In fact, the molecular model, shown in Figure 4.4, shows many of the H's of the <sup>t</sup>Bu groups occupying the same space.

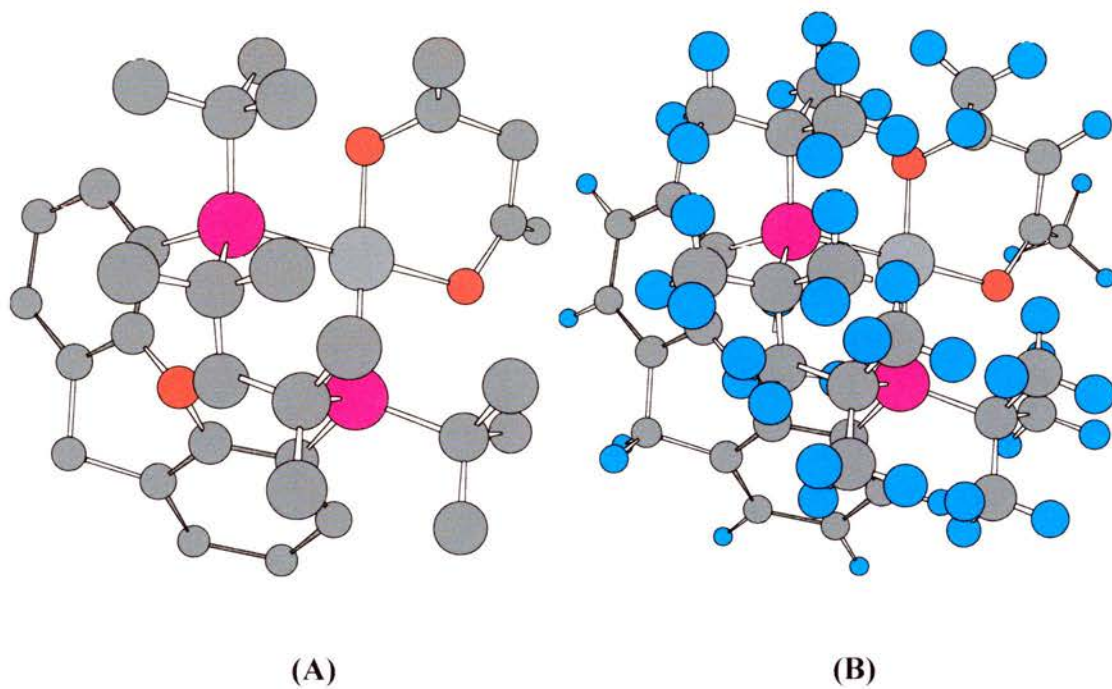
The poor results of the catalytic system can therefore be put down to the catalyst actually being unmodified rhodium rather than a phosphine modified rhodium system.

### 4.2.2.2 *Hydroformylation of Allyl Alcohol with the Rh/ <sup>t</sup>Bu-Xantphos Catalytic System in Ethanol.*

As for to the reaction in toluene, the results of the hydroformylation of allyl alcohol with the Rh/ <sup>t</sup>Bu-Xantphos catalytic system in toluene was very slow, showing only partial conversion after 18 hours. The GC FID of the reaction solution showed there to be many products, most uncharacterised by GC MS.

## Figure 4.4

*Chem 3D drawing of  $[Rh(^tBu\text{-}Xantphos)(acac)]$ , (A) with out H atoms and (B) with H atoms.*



### 4.3 9,9-Dimethyl-2,7-di-*t*-butyl--4,5-bis(diethylphosphino)xanthene [Et-<sup>t</sup>BuXantphos].

Another way in which to make a more electron rich xanthene analogue was to make 9,9-dimethyl-2,7-di-*t*-butyl-4,5-bis(diethylphosphino)xanthene or Et-<sup>t</sup>BuXantphos. This ligand has *t*-butyl groups in the meta position relative to the phosphines on the aryl xanthene backbone. They should add electron density to the aryl rings thus reducing the electron withdrawing nature of the aryl rings with respect to the phosphine groups.

#### 4.3.1 Synthesis.

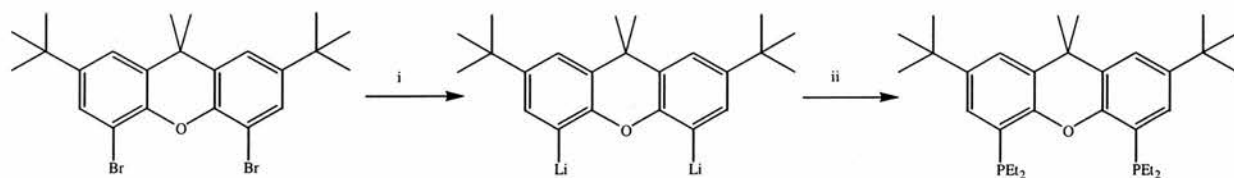
9,9-Dimethyl-2,7-di-*t*-butyl-4,5-bis(diethylphosphino)xanthene, Et-<sup>t</sup>BuXantphos, was prepared from 4,5-dibromo-2,7-di-*t*-butyl-9,9-xanthene and chlorodiethylphosphine, see section 6.2.5 and Scheme 4.3.

Addition of *n*-butyl lithium to a solution containing 4,5-dibromo-2,7-di-*t*-butyl-9,9-xanthene results in bromine substitution and the formation of a lithium xanthene salt. Addition of chlorodiethylphosphine to the salt results in the formation of Et-<sup>t</sup>BuXantphos and lithium chloride.<sup>8</sup>

Et-<sup>t</sup>BuXantphos has a resonance at -23.6 ppm ppm in the <sup>31</sup>P {<sup>1</sup>H} NMR spectrum, resonances at 145.1 ppm (ar PCCOC); 130.0 ppm (ar CHCC); 128.8 ppm, 125.2 ppm, 122.7 ppm (ar CH), 116.8 ppm (ar CHCPC); 34.9 ppm (CCCH<sub>3</sub>); 34.8 ppm (C(CH<sub>3</sub>)<sub>3</sub>); 32.7 ppm (C(CH<sub>3</sub>)<sub>2</sub>); 31.7 ppm (C(CH<sub>3</sub>)<sub>3</sub>); 17.9 ppm (CH<sub>3</sub>CH<sub>2</sub>P); 10.1 ppm (CH<sub>3</sub>CH<sub>2</sub>P) in the <sup>1</sup>C NMR spectrum, and at 7.5 ppm-7.1 ppm (6H, ar, m); 2.0 ppm (8H, CH<sub>3</sub>CH<sub>2</sub>P, m); 1.6 ppm (6H, C(CH<sub>3</sub>)<sub>2</sub>, s); 1.4 ppm (18H, C(CH<sub>3</sub>)<sub>3</sub>, s); 1.2 ppm (12H, CH<sub>3</sub>CH<sub>2</sub>P, m) in the <sup>1</sup>H NMR spectrum.

**Scheme 4.3**

*Synthesis of 9,9-Dimethyl-2,7-di-*t*-butyl-4,5-bis(diethylphosphino)xanthene, Et-<sup>t</sup>BuXantphos.*



(i) *n*-BuLi, THF, -60 °C 1 hr, 0 °C; (ii) ClPEt<sub>2</sub>, THF, -60 °C 1 hr, 25 °C 18 hr.

**4.3.2 Catalytic Results.**

The selectivity of the diphosphine ligand Et-<sup>t</sup>BuXantphos was tested in the rhodium catalysed hydroformylation of allyl alcohol and 1-octene. The reactions were carried out under identical conditions to when testing Et-Xantphos.

**Table 4.5**

Results for the hydroformylation of allyl alcohol with the Rhodium / Et-BuXantphos catalytic system in the given solvent. [Rh] 200 ppm, Rh: Et-BuXantphos ratio 1:2.

Key: AA = allyl alcohol; HBA = 4-hydroxybutanal; MHPA = 2-methylpropanal; BDO = 1,4-butanediol.

Run	T/ °C	P/ bar	TOF h <sup>-1</sup>	AA	HBA	MHPA	BDO	MPD	propanal	propanol	Other products	L:b <sup>a</sup> ratio
1	80	10	790	5.03	71.91	11.01	0.25	0.0	0.76	0.82	10.22	6.5
2	100	10	3230	0.60	56.22	6.31	0.24	0.0	1.80	0.81	34.02	8.9
3	120	40	14820	0.04	43.06	2.38	2.10	0.38	0.41	1.42	50.21	18.1 ald 5.5 alc

a) The l:b ratio is the ratio of 4-hydroxybutanal : 2-methyl-3-hydroxypropanal. At higher temperatures the l:b ratio can be seriously distorted by the formation of by-products form these products. A full list of the reaction can be seen in Appendix 4.

Ald aldehyde ratio  
Alc lcohol ratio

**Table 4.6**

Results for the hydroformylation of 1-octene with the Rhodium / Et<sup>-1</sup>BuXantphos catalytic system in the given solvent. [Rh] 200 ppm, Rh: Et<sup>-1</sup>BuXantphos ratio 1:2.

Key: NA = Nonanal; MOA = 2-methyloctanal; NOL = nonanol; MOO = 2-methyloctanol; OE = octenes (1-octene, 2-octene, 3-octene, 4-octene); Oct = octane; EHA = 2-ethylheptanal; PHA = 2-propylhexanal; DEN = diethoxynonane.

Run	T/ °C	P/ Bar	TOF <sub>int</sub> h <sup>-1</sup>	NA	MOA	NOL	MOO	OE <sup>a</sup>	Oct	EHA & PHA	DEN	Unknown	L:b <sup>b</sup>
1 <sup>c</sup>	40	120	1640	77.37	8.04	1.26	0.0	8.78	1.31	0.24	2.64	0.35	9.62
2 <sup>d</sup>	40	120	1640	50.77	7.70	10.75	0.71	0.95	2.18	2.97	22.96	1.96	6.6 ald 15.1 alc

a) OE represents all octenes; however, 1-octene was 0 % in all reactions, it therefore represents all internal octenes.

b) The l:b ratio is representative of the NA:MOA ratio. When necessary a second l:b ratio will be added for NOL and MOO in which case they will be labeled **ald** for the aldehyde ratio and **alc** for the alcohol ratio. It can also be said that the true l:b ratio should be representative of all products, including the internal octenes, EHA and PHA as branched products. For this reason it is important to consider the selectivity to NA also.

c) Reaction left for 2 hours.

d) Reaction left for 20 hours.

#### 4.3.2.1 *Hydroformylation of Allyl Alcohol with the Rh/ Et<sup>t</sup>BuXantphos Catalytic System in Ethanol*

The results of the hydroformylation of allyl alcohol with the Rh/ Et<sup>t</sup>BuXantphos catalytic system and are presented in ethanol in Table 4.5 runs 1 to 3.

Run 1, was conducted at 80 °C and 10 bar synthesis gas the TOF<sub>init</sub> was 790 h<sup>-1</sup>, the l:b ratio was 6.2, and the selectivity to the aldehyde products, 4-hydroxybutanal and 2-methyl-3-hydroxypropan-1-al, was 82.9 %. The selectivity to the linear aldehyde product is therefore 71.0 %. Unreacted allyl alcohol accounted for 5.0 % of the reaction products, the isomerisation product propanal 0.8 % and the hydrogenation product propanol, 0.8 %. The reaction produced a very small amount of BDO, 0.3 %, and no MPD. Other products of reaction account for 10.2 % of the reaction products.

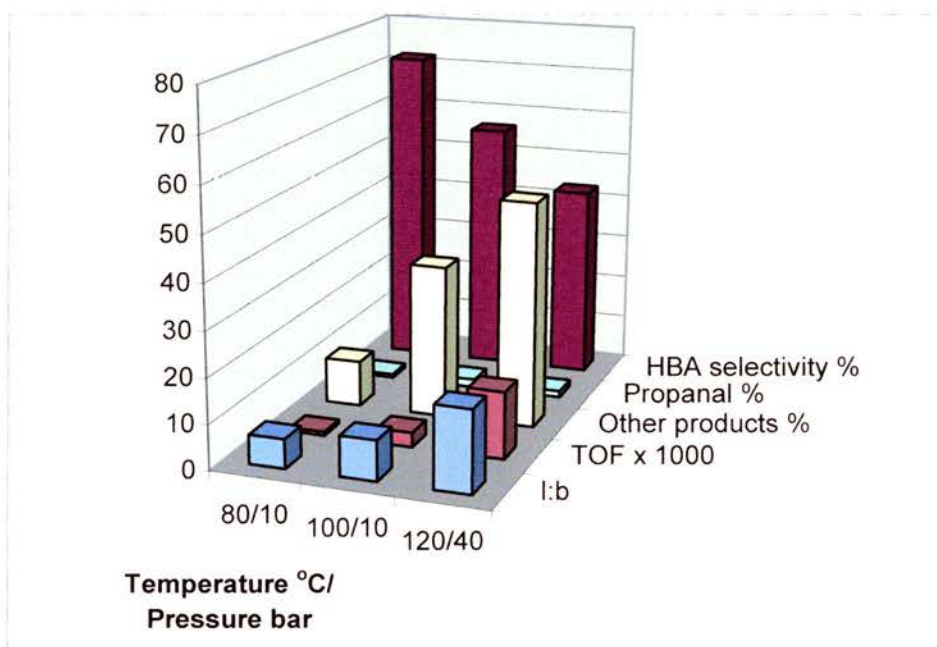
At 10 bar synthesis gas pressure, the l:b ratio increases as the temperature of reaction is increased from 80 °C to 100 °C, the selectivity to HBA, however decreases. The propanal and propanol levels remain comparable, however. The reason for the increased l:b ratio is due to the greater degradation of the branched product of reaction, the level of other products increases. Increasing the temperature and pressure to 100 °C and 40 bar synthesis gas results in an increased l:b ratio for the aldehyde products of reaction. Again, the levels of propanal and propanol are comparable to those previously observed. As before, the reason for the increased l:b ratio of aldehyde products is due to the greater degradation of the branched aldehyde product. There is also a slight increase in the diol products BDO and MPD.

The main degradation products are EOF a degradation product 4-hydroxybutanal, and MPA a degradation product of 2-methyl-3-hydroxypropanal. The levels of the linear product HBA, BDO and EOF, and the branched products MHPA, MPD, and MPA are compared in Graph 4.20. It is noticed that although lower in runs 2 and 3 they are in fact comparable.

At 10 bar synthesis gas pressure the TOF<sub>init</sub> of the reaction increases with increasing temperature, from 790 h<sup>-1</sup> to 3230 h<sup>-1</sup>. When the temperature and the pressure of the reaction is increased the TOF<sub>int</sub> increases to 14820 h<sup>-1</sup>.

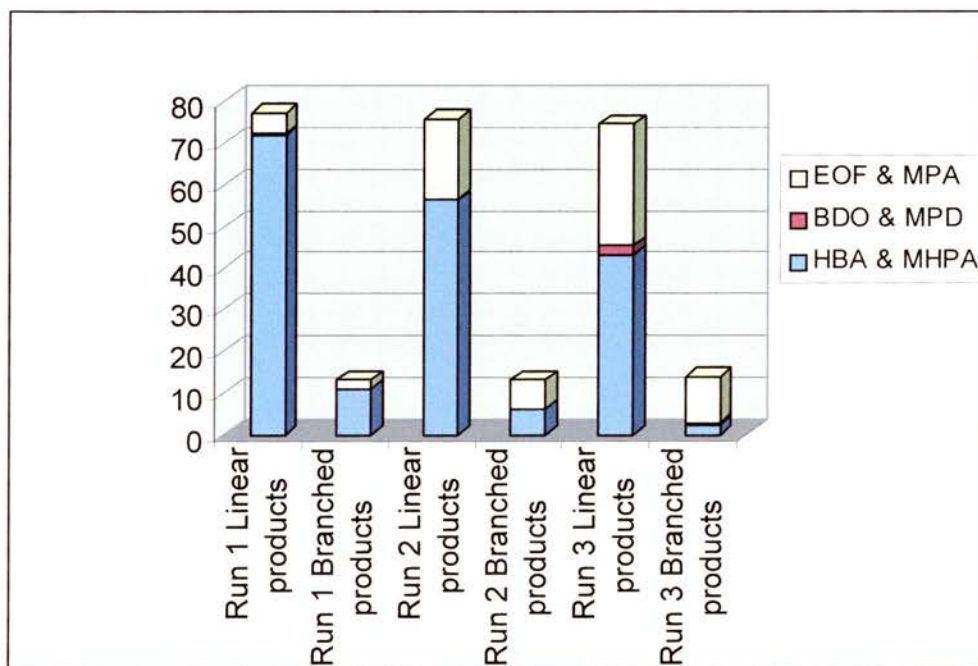
**Graph 4.19**

Results for the hydroformylation of allyl alcohol with  $[Rh(CO)_2(acac)]$  &  $Et^tBuXantphos$ , at 80 °C and 10 bar, 100 °C and 10 bar, and at 120 °C and 40 bar synthesis gas.  $[Rh] = 200$  ppm, diphosphine:Rh = 2.



**Graph 4.20**

Selectivities to the linear products HBA, BDO, and EOF, and the branched products MHPA, MPD, and MPA for runs 1, 2, & 3.



#### 4.3.2.2 *Hydroformylation of 1-Octene with the Rh/ Et-<sup>t</sup>BuXantphos Catalytic System in Ethanol*

The results of the hydroformylation of 1-octene with the Rh/ Et-<sup>t</sup>BuXantphos catalytic system in ethanol can be seen in Table 4.6, run 1.

The results of the hydroformylation of 1-octene with the Rh/ Et-Xantphos catalytic system in ethanol can be seen in Table 4.4 runs 3 to 5.

Run 1, was conducted at 120 °C and 40 bar synthesis gas and the TOF<sub>init</sub> was 1640 h<sup>-1</sup>. The l:b ratio of the aldehyde product was 9.62, and the selectivity to nonanal and 2-methyloctanal, was 85.41 %, the selectivity to the linear aldehyde product is therefore 77.4 %. The alcohol products NO and MOO account for 1.26 % and 0.00% of the reaction products respectively. Internal octenes account for 8.8 % of the reaction products, nonane, 1.3 %, EHA and PHA, 0.2 %, DEN, 2.6 %, and unknowns 0.4 %.

The results of the hydroformylation of 1-octene with rhodium and Rh/ Et-<sup>t</sup>BuXantphos are compared to the results with rhodium and Rh/ Et-Xantphos.

At 120 °C and 40 bar synthesis gas with Et-<sup>t</sup>BuXantphos as ligand, run 1, shows a similar distribution in for the alcohol products, internal octenes, octane, and the unknowns as with Et-Xantphos as ligand. The level of EHA and PHA was slightly decreased and the level of DEN was slightly increased. The l:b ratio was decreased, as was the selectivity to NA.

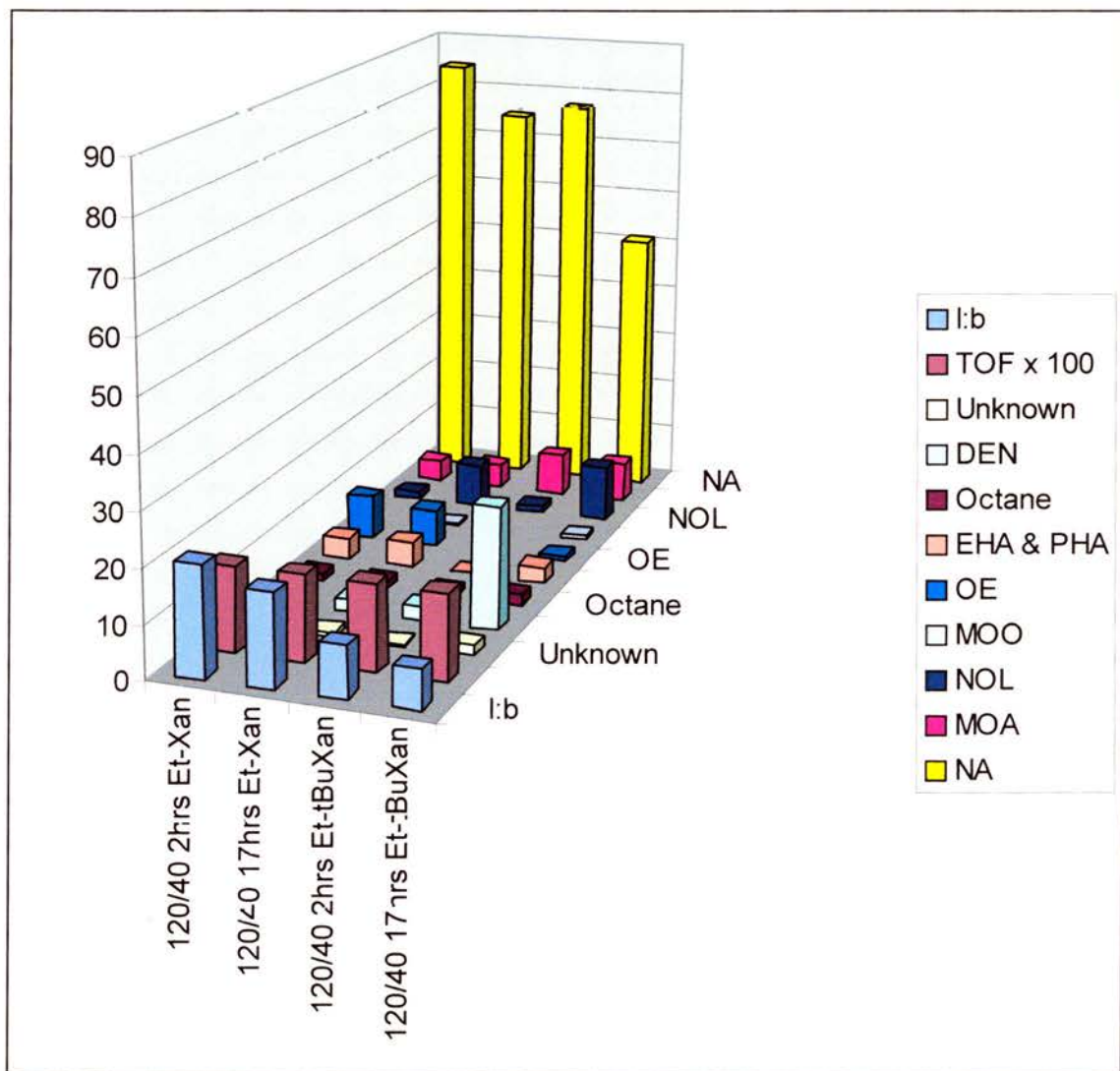
When the reaction is left for an extended period of time (run 2) there is partial conversion of the aldehydes to the alcohols. As before, the l:b ratio is greater for the alcohol products, suggesting the catalytic system preferentially hydrogenated the linear product. It is also observed that there is a greater proportion of the alcohol products produced.

It is also observed that the drop in the selectivity to HBA can not be fully explained by the increase in the selectivity to BDO. The reason for this drop is the large increase in the level of DEN produced.

The TOF<sub>init</sub> of the reactions using Et-<sup>t</sup>BuXantphos are comparable to when using Et-Xantphos as ligand.

**Graph 4.21**

Results for the hydroformylation of 1-octene with  $[Rh(CO)_2(acac)]$  & Et-Xantphos and with  $[Rh(CO)_2(acac)]$  & Et<sup>t</sup>BuXantphos, at 120 °C and 40 bar synthesis gas for 2 hours and 17 hours.  $[Rh] = 200$  ppm, diphosphine:Rh = 2.



## 4.4 2,2'-Bis di-*iso*-propylphosphanyl biphenol [<sup>i</sup>Pr-Bisbite].

The ligand <sup>i</sup>Pr-Bisbite was originally prepared to compare with the ligand Et-BISBI, which was never isolated. However, the effect of the *iso*-propyl groups on the phosphine was interesting.

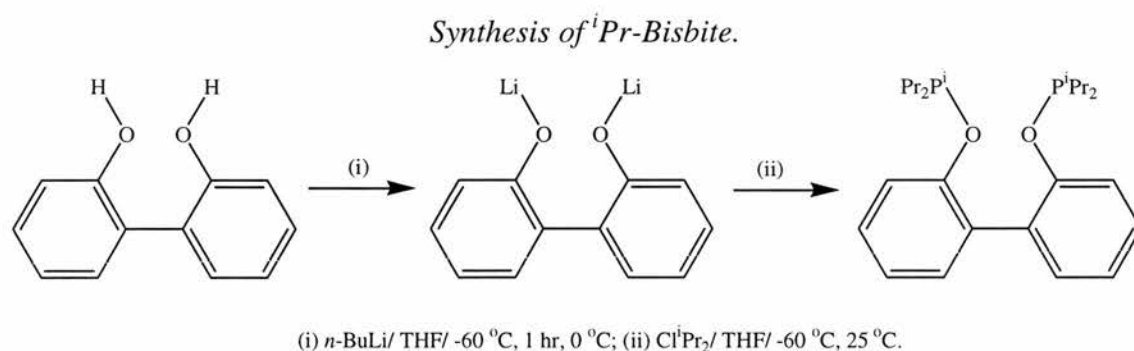
### 4.4.1 Synthesis.

<sup>i</sup>Pr-Bisbite was prepared from 2,2'-biphenol and di-*iso*-propylchlorophosphine, see section 6.2.6 and Scheme 4.4.

Addition of *n*-butyl lithium to a solution 2,2'-biphenol results in proton abstraction and the formation of a lithium salt. Addition of di-*iso*-propylchlorophosphine to the salt results in the formation of <sup>i</sup>Pr-Bisbite and lithium chloride.<sup>8</sup>

<sup>i</sup>Pr-Bisbite has a resonance at 148.31 ppm in the <sup>31</sup>P {<sup>1</sup>H} NMR spectrum, and resonances at 7.5-6.9 ppm (8H, **ar**, m); 1.7 ppm (2H, **CH**(CH<sub>3</sub>), m); 0.9 ppm (m, 24H, **CH**(CH<sub>3</sub>)) in the <sup>1</sup>H NMR spectrum, and at 157.1 ppm (**COP**); 137.4 ppm (**CH**); 130.1 ppm (**C**); 121.0 ppm, 117.9 ppm, 117.6 ppm (**CH**); 28.4 ppm (**CH**(CH<sub>3</sub>)<sub>2</sub>); 17.7 ppm (**CH**(CH<sub>3</sub>)<sub>2</sub>) in the <sup>13</sup>C NMR spectrum.

### Scheme 4.4



### 4.4.2 Catalytic Results.

The selectivity of the diphosphine ligand, <sup>i</sup>Pr-Bisbite, was tested in the rhodium catalysed hydroformylation of allyl alcohol and 1-octene. The reactions were carried out under identical conditions to those used when testing Et-Xantphos.

**Table 4.7**

Results for the hydroformylation of allyl alcohol with the Rhodium / <sup>i</sup>Pr-Bisbite catalytic system in the given solvent. [Rh] 200 ppm, Rh: <sup>i</sup>Pr-Bisbite ratio 1:2.

Key: AA = allyl alcohol; HBA = 4-hydroxybutanal; MHPA = 2-methylpropanal; BDO = 1,4-butanediol.

Toluene												
Run	T/ °C	P/ bar	Rate	AA	HBA	MHPA	BDO	MPD	propanal	propanol	Other <sup>a</sup> products	L:b ratio
1	120	10	Mt	0.55	47.99	24.01	0	0	23.56	0.58	3.31	2.0

A full list of the products of reaction can be seen in Appendix 4.

#### ***4.4.2.1 Hydroformylation of Allyl Alcohol with the Rh/<sup>i</sup>Pr-Bisbite Catalytic System in Toluene.***

The results of the hydroformylation of allyl alcohol with the Rh/ <sup>i</sup>Pr-Bisbite catalytic system in toluene can be seen in Table 4.7, run 1.

Run 1, at 120 °C and 10 bar synthesis gas the of reaction was mass transport limited, the l:b ratio was 2.0, and the selectivity to the aldehyde products, 4-hydroxybutanal and 2-methyl-3-hydroxypropan-1-al, was 72.0 %. The selectivity to the linear aldehyde product is therefore 48.0 %. Unreacted allyl alcohol accounted for 0.6 % of the reaction products, the isomerisation product propanal 23.56 % and the hydrogenation product propanol 0.6 %. Only trace amounts of BDO and MPD were produced. Other products of reaction account for 3.3 % of the total.

Because of the low selectivity of the reaction studies with this ligand in toluene were terminated. The ligand was used in ethanol to see if any interesting results would be observed.

#### ***4.4.2.2 Hydroformylation of Allyl Alcohol with the Rh/<sup>i</sup>Pr-Bisbite Catalytic System in Ethanol.***

The hydroformylation of allyl alcohol with the Rh/ <sup>i</sup>Pr-Bisbite catalytic system in ethanol showed only 2 bar of gas uptake (approx. 1/8<sup>th</sup> of the reaction) at which point the reaction ceased. The GC FID showed a forest of products, most of which were uncharacterised by GC MS.

## 4.5 DIOP.

The hydroformylation of allyl alcohol and 1-octene with the rhodium DIOP catalytic system was carried out to compare with the results obtained from the other catalytic systems. The reactions were carried out under identical conditions to when testing Et-Xantphos.

### 4.5.1 Catalytic Results.

The selectivity of the diphosphine ligand DIOP was tested in the rhodium catalysed hydroformylation of allyl alcohol and 1-octene. The reactions were carried out under identical conditions to those used when testing Et-Xantphos.

**Table 4.8**

Results for the hydroformylation of allyl alcohol with the Rhodium / DIOP catalytic system in the given solvent. [Rh] 200 ppm, Rh: DIOP ratio 1:2.

Key: AA = allyl alcohol; HBA = 4-hydroxybutanal; MHPA = 2-methylpropanal; BDO = 1,4-butanediol.

Run	T/ °C	P/ bar	TOF h <sup>-1</sup>	AA	HBA	MHPA	BDO	MPD	propanal	propanol	Other products	L:b <sup>a</sup> ratio
1	80	10	4390	0.0	80.80	12.57	0.10	0.0	1.61	0.09	4.83	6.4
2	80	10	4450	1.01	78.42	11.80	0.0	0.0	0.35	0.21	8.21	6.6

a) The l:b ratio is the ratio of 4-hydroxybutanal : 2-methyl-3-hydroxypropanal. At higher temperatures the l:b ratio can be seriously distorted by the formation of by-products form these products. The percentage of the reaction products that these products account for is listed under other by-products in Appendix 4.

**Table 4.9**

Results for the hydroformylation of 1-octene with the Rhodium / DIOP catalytic system in the given solvent. [Rh] 200 ppm, Rh: DIOP ratio 1:2.

Key: NA = Nonanal; MOA = 2-methyloctanal; NOL = nonanol; MOO = 2-methyloctanol; OE = octenes (1-octene, 2-octene, 3-octene, 4-octene); Oct = octane; EHA = 2-ethylheptanal; PHA = 2-propylhexanal; DEN = diethoxynonane.

Run	T/ °C	P/ Bar	TOF <sub>int</sub> h <sup>-1</sup>	NA	MOA	NOL	MOO	OE <sup>†</sup>	Oct	EHA & PHA	DEN	Unknown	L:b <sup>a</sup> ratio
1	80	10	980	86.33	12.01	0.00	0.00	0.90	0.62	0.00	0.00	0.15	7.2

a) The l:b ratio is the ratio of 4-hydroxybutanal : 2-methyl-3-hydroxypropanal. At higher temperatures the l:b ratio can be seriously distorted by the formation of by-products form these products. The percentage of the reaction products that these products account for is listed under other by-products in Appendix 4.

#### ***4.5.1.1 Hydroformylation of Allyl Alcohol with the Rh/DIOP Catalytic System in Toluene.***

The results of the hydroformylation of allyl alcohol with the Rh/ DIOP catalytic system in toluene can be in Table 4.8 run 1.

For run 1, at 80 °C and 10 bar synthesis gas, the  $\text{TOF}_{\text{init}}$  was  $4450 \text{ h}^{-1}$ , the l:b ratio was 6.6, and the selectivity to the aldehyde products, 4-hydroxybutanal and 2-methyl-3-hydroxypropan-1-al, was 93.4 %. The selectivity to the linear aldehyde product is therefore 80.8 %. There was no unreacted allyl alcohol, the isomerisation product propanal accounted for 1.6 % of the reaction products, and the hydrogenation product propanol, 0.1 %. The reaction produced only trace amounts of BDO and MPD. Other products of reaction account for 4.8 % of the reaction products.

Compared to the results from the hydroformylation of allyl alcohol with the rhodium / Et-Xantphos catalyst system in toluene under the same conditions of 80 °C and 10 bar synthesis gas, the l:b ratio is lower at 6.6 with respect to 12.0. The selectivity to HBA is also lower at 78.42 % with respect to 86.28 %. The selectivity to both the hydroxyaldehydes is the same, at 93.37 % when using DIOP and 93.45 % when using Et-Xantphos.

The  $\text{TOF}_{\text{init}}$  is 2.6 times greater when using DIOP at 4390 than when using Et-Xantphos at  $1690 \text{ h}^{-1}$ .

#### ***4.5.1.2 Hydroformylation of 1-Octene with the Rh/DIOP Catalytic System in Toluene.***

The results of the hydroformylation of allyl alcohol with the Rh/ DIOP catalytic system in toluene can be in Table 4.9 runs 1 and 2.

For run 1, at 80 °C and 10 bar synthesis gas, the  $\text{TOF}_{\text{init}}$  was  $980 \text{ h}^{-1}$ , the l:b ratio was 7.2, and the selectivity to the aldehyde products, nonanal and 2-methyloctanal, was 98.34 %. The selectivity to the linear aldehyde product is therefore 86.33 %. The reaction produced none of the alcohol products nonanol and 2-methyloctanol. Internal octenes account for 0.9 % of the reaction products, octane, 0.6 %, EHA and PHA, 0.0 %, and unknowns 0.2 %.

The results are compared to the results from the hydroformylation of 1-octene with the rhodium Et-Xantphos catalytic system under the same conditions of 80 °C and 10 bar synthesis gas. The l:b ratio is lower, 7.2, than when using Et-Xantphos as ligand, 15.5, however, the selectivity to NA is higher at 86.3 % with respect to 85.2 %. The reason for is being the lower levels of internal alkenes when using DIOP, 0.90 % with respect to 7.78 % when using Et-Xantphos, and of EHA & PHA, 0.0 %, with respect to 5.63 %. The levels of octane and unknowns are also slightly higher for the Et-Xantphos case. It is also observed that the  $TOF_{init}$  for the hydroformylation of 1-octene with the DIOP ligand is 6 times higher than with the Et-Xantphos ligand.

## 4.6 Xantphos.

The hydroformylation of allyl alcohol and 1-octene with the rhodium Xantphos catalytic system was carried out to compare with the results obtained from the other catalytic systems.

### 4.6.1 Catalytic Results.

The selectivity of the diphosphine ligand Xantphos was tested in the rhodium catalysed hydroformylation of allyl alcohol and 1-octene. The reactions were carried out under identical conditions to when testing Et-Xantphos.

**Table 4.10**

Results for the hydroformylation of allyl alcohol with the Rhodium / Xantphos catalytic system in the given solvent.  $[Rh]$  200 ppm, Rh: Xantphos ratio 1:2.

Key: AA = allyl alcohol; HBA = 4-hydroxybutanal; MHPA = 2-methylpropanal; BDO = 1,4-butanediol.

Toluene												
Run	T/ °C	P/ bar	TOF h <sup>-1</sup>	AA	HBA	MHPA	BDO	MPD	propanal	propanol	Other products	L:b <sup>a</sup> ratio
1	80	10	9530	0.16	82.89	9.13	0.10	0.0	3.12	1.70	2.89	9.1

EtOH												
Run	T/ °C	P/ bar	TOF h <sup>-1</sup>	AA	HBA	MHPA	BDO	MPD	propanal	propanol	Other products	L:b <sup>a</sup> ratio
2	40	120	116420	0.17	75.18	9.78	0.21	0.0	4.09	2.84	7.73	7.7
3 <sup>b</sup>	40	120	58210	1.83	42.69	0.73	4.06	0.49	2.58	3.63	43.99	58.5 ald 8.3 alc

a) The l:b ratio can be seriously distorted, especially at higher temperatures by the formation of by products. A full account of the products of the reaction can be seen in Appendix 4.

b) Reaction left for an extended period of time, 22 hours.

**Table 4.11**

*Results for the hydroformylation of 1-octene with the Rhodium / Xantphos catalytic system in the given solvent. [Rh] 200 ppm, Rh: Xantphos ratio 1:2.*

**Key:** NA = Nonanal; MOA = 2-methyloctanal; NOL = nonanol; MOO = 2-methyloctanol; OE = octenes (1-octene, 2-octene, 3-octene, 4-octene); Oct = octane; EHA = 2-ethylhexanal; PHA = 2-propylhexanal; DEN = diethoxynonane.

Run	T / °C	P / Bar	TOF <sub>int</sub> h <sup>-1</sup>	NA	MOA	NOL	MOO	OE	Oct	EHA & PHA	DEN	Unknown	L:b
1	80	10	550	90.32	1.88	0.28	0.00	4.59	2.71	1.88	0.00	0.21	48.0
2	100	10	2850	87.88	2.00	0.66	0.00	6.61	2.52	2.00	0.00	0.32	43.9
3	120	40	12670	83.66	2.16	1.09	0.00	10.17	2.58	2.16	0.00	0.33	38.7

#### 4.6.1.1 *Hydroformylation of Allyl Alcohol with the Rh/Xantphos Catalytic System in Toluene.*

The results of the hydroformylation of allyl alcohol with the Rh/ Xantphos catalytic system in toluene can be in Table 4.11, run 1.

For run 1, at 80 °C and 10 bar synthesis gas, the  $\text{TOF}_{\text{init}}$  was  $9530 \text{ h}^{-1}$ , the l:b ratio was 9.1, and the selectivity to the aldehyde products, 4-hydroxybutanal and 2-methyl-3-hydroxypropan-1-al, was 92.0 %. The selectivity to the linear aldehyde product is therefore 82.9 %. Unreacted allyl alcohol accounted for 0.2 % of the reaction products, the isomerisation product propanal 3.1 % and the hydrogenation product propanol 1.7 %. The reaction produced a very small amount of BDO, 0.1 %, and MPD, 0.0 %. Other products of reaction account for 2.9 % of the reaction products.

Compared to the results from the hydroformylation of allyl alcohol with the rhodium / Et-Xantphos catalyst system in toluene under the same conditions of 80 °C and 10 bar synthesis gas, the l:b ratio is lower at 9.1 with respect to 12.0. The selectivity to HBA is also lower at 82.9 % with respect to 86.3 %. The selectivity to both the hydroxyaldehydes is also lower at 92.0 % when using Xantphos and 93.45 % when using Et-Xantphos.

The  $\text{TOF}_{\text{init}}$  is 5.6 times greater when using Xantphos at  $9530 \text{ h}^{-1}$  than when using Et-Xantphos at  $1690 \text{ h}^{-1}$ .

Compared to the results from the hydroformylation of allyl alcohol with the rhodium / DIOP catalyst system in toluene under the same conditions of 80 °C and 10 bar synthesis gas, the l:b ratio is higher at 9.1 with respect to 6.6. The selectivity to HBA is also higher at 82.9 % with respect to 80.8 %. The selectivity to both the hydroxyaldehydes, however, is lower at 92.0 % when using Xantphos and 93.4 % when using DIOP.

The  $\text{TOF}_{\text{int}}$  is 2.1 times greater when using Xantphos at  $9530 \text{ h}^{-1}$  than when using DIOP at  $4450 \text{ h}^{-1}$ .

#### ***4.6.1.2 Hydroformylation of Allyl Alcohol with the Rh/Xantphos Catalytic System in Ethanol.***

The results of the hydroformylation of allyl alcohol with the Rh/ DIOP catalytic system in ethanol can be in Table 4.11, run 2.

For run 1, at 120 °C and 40 bar synthesis gas, the  $\text{TOF}_{\text{init}}$  was  $116420 \text{ h}^{-1}$ , the l:b ratio was 7.7, and the selectivity to the aldehyde products, 4-hydroxybutanal and 2-methyl-3-hydroxypropan-1-al, was 85.0 %. The selectivity to the linear aldehyde product is therefore 75.2 %. Unreacted allyl alcohol accounted for 0.2 % of the reaction products, the isomerisation product propanal 4.1 % and the hydrogenation product propanol 2.8 %. The reaction produced a very small amount of BDO, 0.2 %, and MPD, 0.0 %. Other products of reaction account for 7.7 % of the reaction products.

The reaction represented in run 2 is compared to that when using Et-Xantphos under the same conditions, see run 11 in Table 4.3. The l:b ratio is 7.7 using Xantphos and 5.2 when using Et-Xantphos, the selectivity to HBA, however, is 75.2 % when using Xantphos and 77.0 % when using Et-Xantphos. The reason for this is the greater amounts of propanal, propanol and other products when using Xantphos, at 4.1 %, 2.8 %, and 7.7 % respectively, to 1.1 %, 1.5, and 4.6 % when using Et-Xantphos.

When the reaction is left for an extended period of time at 120 °C and 40 bar you see partial hydrogenation to the diol products BDO and MDD. The level of other products increases seriously to 44.0 % however. This is due to the degradation of the hydroxyaldehyde products HBA and MHPA, see the full product distribution in Appendix 4. The l:b ratio of the aldehyde products HBA and MHPA is 58.5, the reason for this being that the branched product of reaction degrades faster.

#### ***4.6.1.3 Hydroformylation of 1-Octene with the Rh/Xantphos Catalytic System in Toluene.***

The results of the hydroformylation of allyl alcohol with the Rh/ DIOP catalytic system in toluene can be in Table 4.11, runs 1 to 3.

For run 1, at 80 °C and 10 bar synthesis gas, the  $\text{TOF}_{\text{init}}$  was  $550 \text{ h}^{-1}$ , the l:b ratio was 48.0, and the selectivity to the aldehyde products, nonanal and 2-methyloctanal, was 92.2 %. The selectivity to the linear aldehyde product is therefore 90.3 %. The alcohol

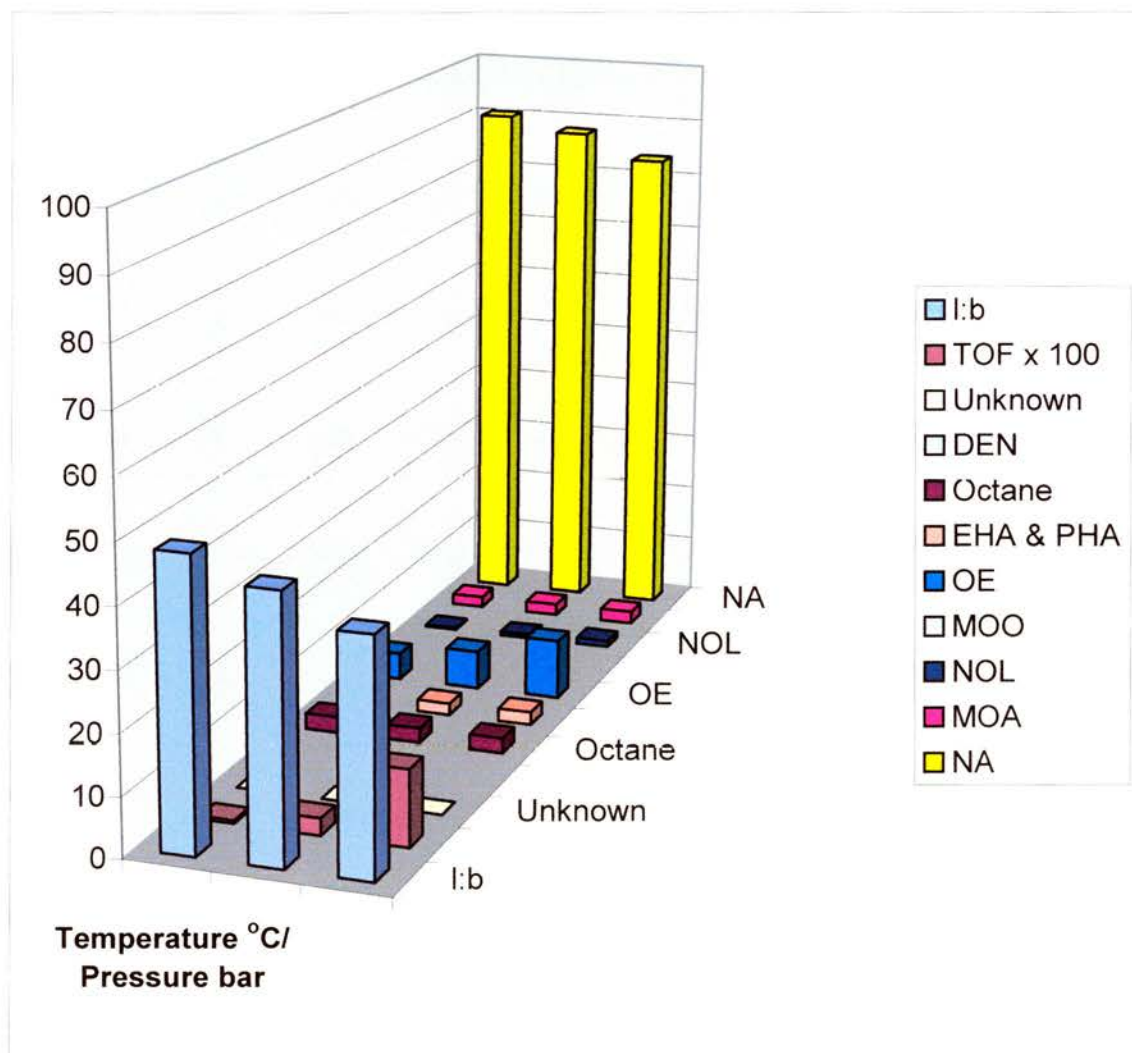
products nonanol and 2-methyloctanol account for 0.3 % and 0.0 % of the reaction products, internal octenes, 4.6 %, nonane, 2.7 %, EHA and PHA, 1.9 %, and unknowns 0.2 %.

It is observed in runs 1 and 2 that the I:b ratio decreases with increasing temperature, as does the selectivity to NA. It is also observed that the level of internal octenes goes up from 4.6 % at 80 °C and 10 bar to 6.6 % at 100 °C and 10 bar synthesis gas. The levels of NO, MOO, octane, EHA & PHA, DEN and the unknowns remain similar. The  $TOF_{int}$  increases 5 times on increasing the temperature.

### Graph 4.22

*Results for the hydroformylation of 1-octene with  $[Rh(CO)_2(acac)]$  & Xantphos, at 80 °C and 100 °C at 10 bar synthesis gas for and at 120 °C and 40 bar synthesis gas.*

*$[Rh] = 200$  ppm, diphosphine:Rh = 2.*



On increasing the temperature and pressure to 120 °C and 40 bar synthesis gas the l:b ratio is even lower at 38.7, as is the selectivity to NA which is 83.7 % with respect to 87.9 %. Again the levels of the internal octenes goes up to 10.2 %.

The results are compared with the results for the hydroformylation of 1-octene with the rhodium Et-Xantphos catalytic system. At 80 °C and 10 bar synthesis gas the l:b ratio is at 48.0 for Xantphos and 15.5 for Et-Xantphos. The selectivity to NA is 90.32 % for Xantphos and 85.17 % for Et-Xantphos. The levels of OE are higher for Et-Xantphos at 7.78 % with respect to 4.59 % for Et-Xantphos, as is the level of EHA and PHA which are 1.88 for Xantphos and 5.63 % for Et-Xantphos. The level of octane is slightly higher for Xantphos at 2.71 % with respect to 0.99 % for Et-Xantphos. The levels of NOL, MOO, DEN, and unknowns are effectively the same.

The  $TOF_{init}$  is 3.4 times greater when using Et-Xantphos as ligand than when using Xantphos as ligand.

At 120 °C and 40 bar synthesis gas the l:b ratio is still higher as is the selectivity to NA, however, the difference is not so great, the difference is that although the level of internal alkenes present is still greater when using Et-Xantphos as ligand, the increase in their levels was not so great when increasing temperature and pressure as when using Xantphos as ligand. The  $TOF_{init}$  is 1.2 times greater when using Et-Xantphos as ligand than when using Xantphos as ligand.

The results are compared with the results for the hydroformylation of 1-octene with the rhodium DIOP catalytic system.

At 80 °C and 10 bar synthesis gas the l:b ratio is much greater when using Xantphos as ligand rather than DIOP. The selectivity to NA is also greater, however the selectivity to NA and MOA is lower at 92.2 % with respect to 98.3 % when using DIOP as ligand. The main reason for this is the increased levels of internal octenes, 4.6 % with respect to 0.9 %, nonane, 2.7 % with respect to 0.6 %, and EHA & PHA, 1.9 % with respect to 0.0 % when using DIOP as ligand.

The  $TOF_{int}$  is also 1.8 times greater when using DIOP as ligand than when using Xantphos as ligand

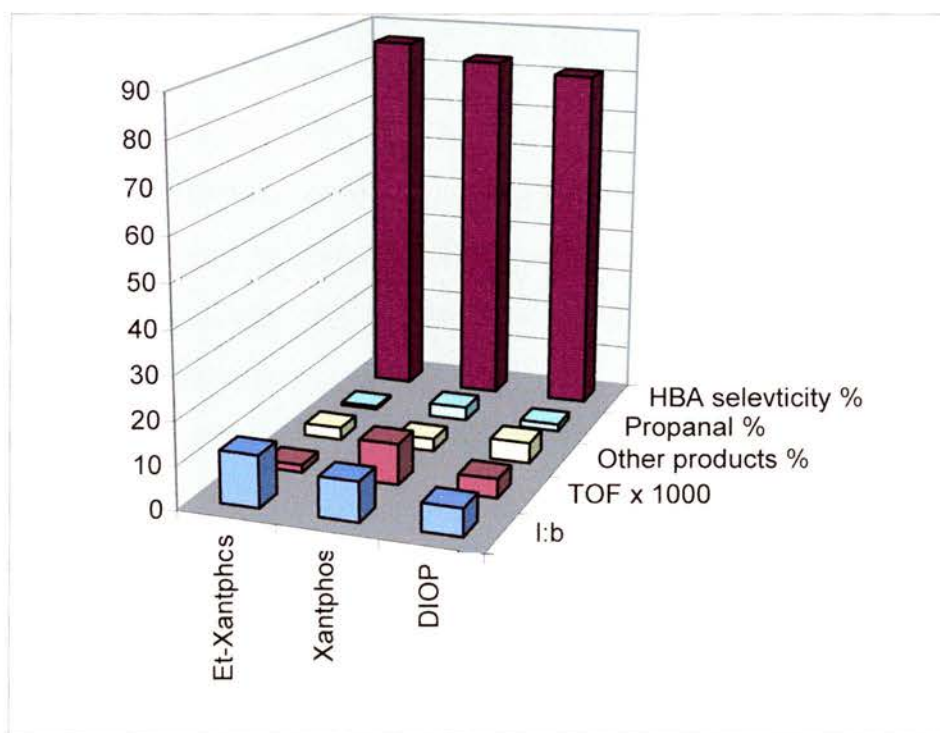
## 4.7 Comparison of the Ligands.

### 4.7.1 Hydroformylation of Allyl alcohol.

Comparison of Et-Xantphos, Xantphos, and DIOP as ligand for the rhodium catalysed hydroformylation of allyl alcohol in toluene at 80 °C and 10 bar synthesis gas can be seen in Graph 4.23. Going from Et-Xantphos to Xantphos to DIOP as ligand of rhodium, the l:b ratio of the reaction decreases, as does the HBA selectivity. The level of other products was higher for Xantphos, as was the level of propanal. The  $TOF_{init}$  was greatest for Xantphos, lower for DIOP, and lowest for Et-Xantphos.

#### Graph 4.23

*Results for the hydroformylation of allyl alcohol with  $[Rh(CO)_2(acac)]$  & Et-Xantphos, Xantphos, or DIOP, at 80 °C and 10 bar synthesis gas.  $[Rh] = 200$  ppm, diphosphine:Rh = 2.*

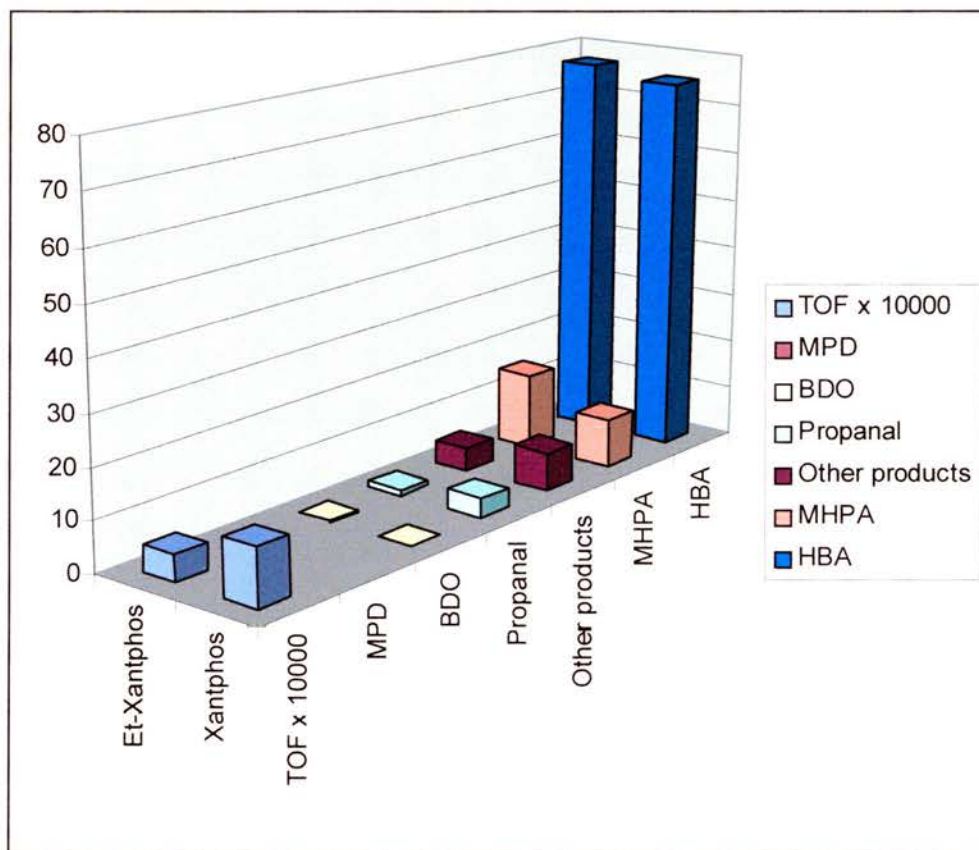


Comparison of Et-Xantphos, and Xantphos as ligand for the rhodium catalysed hydroformylation of allyl alcohol in ethanol at 120 °C and 40 bar synthesis gas can be seen in Graph 4.24. There is very little BDO observed in both reactions. There was a higher level of other products and propanal when using Xantphos as ligand compared

with when using Et-Xantphos as ligand. The selectivity to MHPA is decreased and the selectivity to HBA was slightly decreased when using Xantphos as ligand. The  $TOF_{init}$  is higher when using Xantphos as ligand compared to when using Et-Xantphos as ligand.

#### Graph 4.24

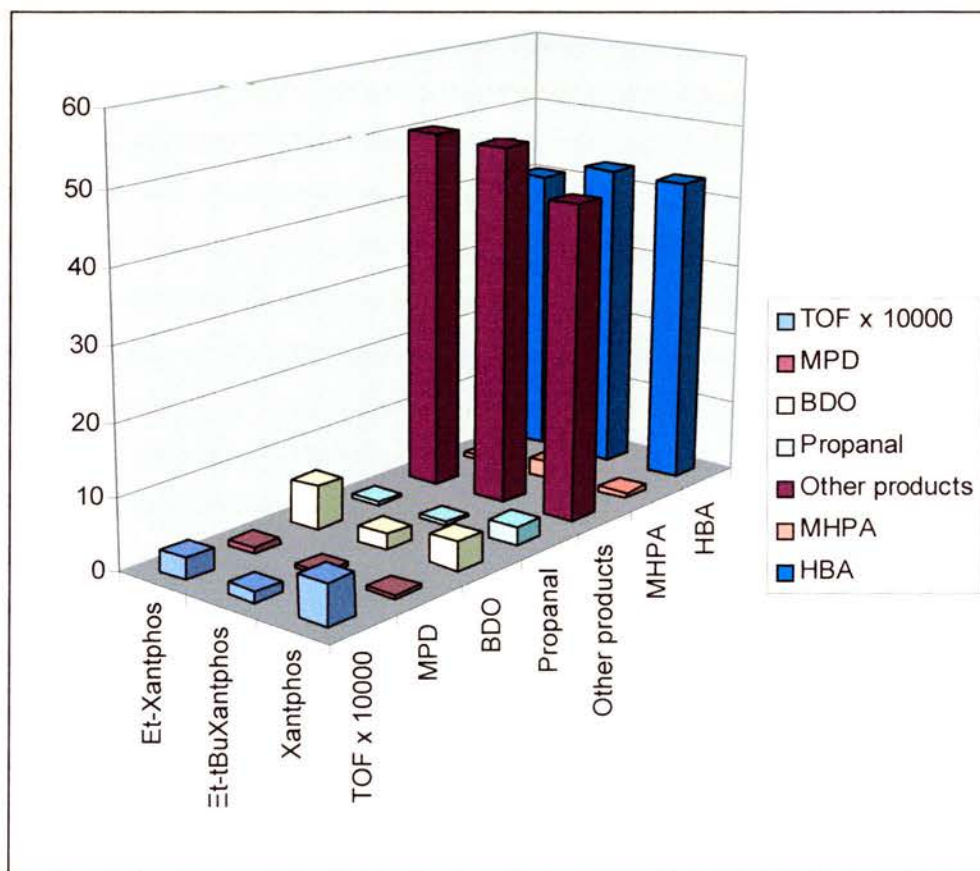
Results for the hydroformylation of allyl alcohol with  $[Rh(CO)_2(acac)]$  & Et-Xantphos, or Xantphos, at 120 °C and 40 bar synthesis gas.  $[Rh] = 200$  ppm, diphosphine:Rh = 2.



Comparison of Et-Xantphos, Et-Xantphos, and Xantphos as ligand for the rhodium catalysed hydroformylation of allyl alcohol in ethanol at 120 °C and 40 bar synthesis gas for an extended period of time can be seen in Graph 4.25. The selectivity to MPD was low when using all three ligands. The selectivity to BDO was lowest when using Et-tBuXantphos as ligand, then Xantphos, and highest when using Et-Xantphos as ligand. The level of propanal was highest when using Xantphos as ligand. The level of other products was high for all three ligands, and lowest when using Xantphos. The selectivity to HBA was lowest when using Et-Xantphos, but similar for all three ligands. The  $TOF_{init}$  was lowest for Et-tBuXantphos, higher for Et-Xantphos, and highest for Xantphos.

**Graph 4.25**

Results for the hydroformylation of allyl alcohol with  $[Rh(CO)_2(acac)]$  & Et-Xantphos, or Xantphos, at 120 °C and 40 bar synthesis gas for an extended period of time.  $[Rh] = 200$  ppm, diphosphine:Rh = 2.

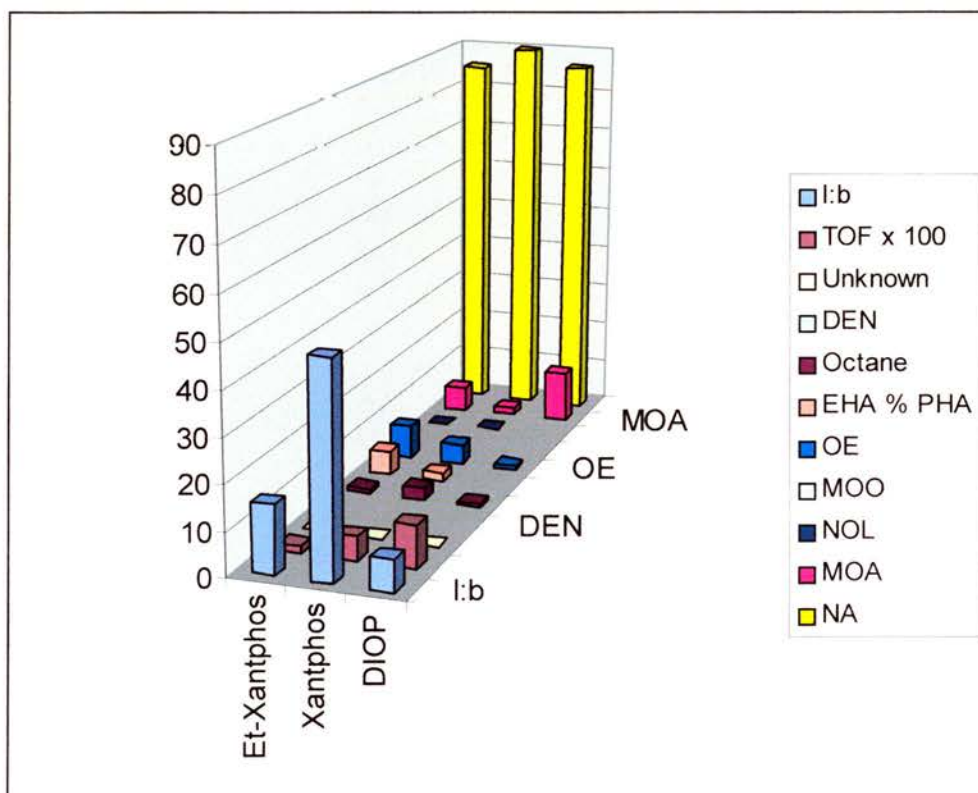
**4.7.2 Hydroformylation of 1-Octene.**

Comparison of Et-Xantphos, Xantphos, and DIOP as ligand for the rhodium catalysed hydroformylation of allyl alcohol in toluene at 80 °C and 10 bar synthesis gas can be seen in Graph 4.26.

The l:b ratio increases when you use Xantphos instead of Et-Xantphos as ligand. The level of DEN observed was highest when using Xantphos as ligand, and similar when using Et-Xantphos and DIOP. The level of OE and EHA & PHA was higher when using Xantphos as ligand instead of DIOP, and highest when using Et-Xantphos as ligand. The selectivity to NA was best for Xantphos, then for DIOP then for Et-Xantphos.

**Graph 4.26**

Results for the hydroformylation of allyl alcohol with  $[Rh(CO)_2(acac)]$  & Et-Xantphos, Xantphos, or DIOP, at 80 °C and 10 bar synthesis gas.  $[Rh] = 200$  ppm, diphosphine:Rh = 2

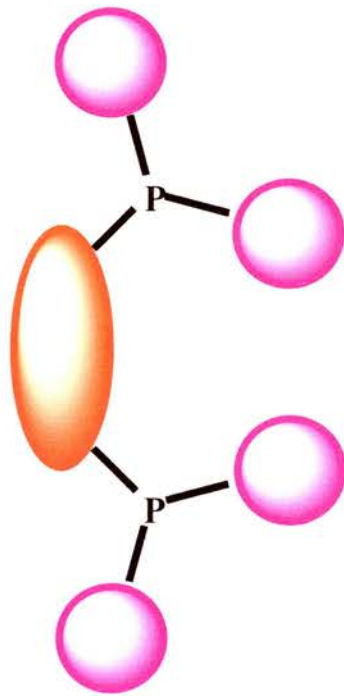


## 4.8 References for Chapter Four

- 1 P. W. N. M. v. Leeuwen and C. Claver, in 'Rhodium Catalysed Hydroformylation', ed. B. R. James and R. Ugo, Kluwer Academic Publishers, Dordrecht, 2000.
- 2 Y. Harano, in 'Process for obtaining butanediols', 1984.
- 3 W. Shum, 'Unpublished Results'.
- 4 B. Cornils, 'New Synthesis with Carbon Monoxide', ed. J. Falbe, Springer Verlag, 1980.
- 5 D. J. Cole-Hamilton, M. C. Simpson, A. W. S. Currie, and J. M. Anderson, *J Chem. Soc., Dalton Trans*, 1996, 1793.
- 6 C. P. Casey, G. T. Whiteker, M. G. Melville, L. M. Petrovich, J. A. G. Jr., and D. R. Powell, *J. Am. Chem. Soc.*, 1992, **114**, 5535.
- 7 P. W. N. M. van Leeuwen, P. C. J. Kamer, and J. N. H. Reek, *Pure Appl. Chem.*, 1999, **71**, 1443.
- 8 P. W. N. M. van Leewen, L. A. v. d. Veen, M. D. K. Boele, F. R. Breman, P. C. J. Kamer, K. Goubitz, J. Fraanje, H. Schenk, and C. Bo, *J. Am. Chem. Soc.*, 1998, **120**, 11616.
- 9 B. R. James, D. Mahajan, S. J. Rettig, and G. A. Williams, *Organometallics*, 1983, **2**, 1452.
- 10 in '<http://ch-www.st-andrews.ac.uk/cats/>'.
- 11 D. J. Cole-Hamilton, J. K. MacDougall, M. C. Simpson, and M. J. Green, *J. Chem. Soc., Dalton Trans.*, 1996, 1161.
- 12 W. Simanko, K. Mereiter, R. Schmid, K. Kirchner, A. M. Trzeciak, and J. J. Ziolkowski, *J. Organomet. Chem.*, 2000, **602**, 59.
- 13 I. T. Horvath, G. Kiss, R. A. Cook, J. E. Bond, P. A. Stevens, J. Rabai, and E. J. Mozeleski, *J. Am. Chem. Soc.*, 1998, **120**, 3133.
- 14 M. J. Palmer and M. Willis, *Tetrahedron: Asymmetry*, 1999, **10**, 2045.
- 15 R. Noyori and S. Hashiguchi, *Acc. Chem. Res.*, 1997, **30**, 97.

- 16 P. A. Chaloner, M. A. Esteruelas, F. Joo, and A. Oro, 'Homogeneous Hydrogenation', Kluwer Academic Publishers, Dordrecht, 1994.
- 17 P. N. Rylander, 'Hydrogenation Methods', Academic Press, 1985.
- 18 G. Mestroni, R. Spogliarich, A. Camus, F. Martinelli, and G. Zassinovich, *J. Organomet. Chem.*, 1978, **157**, 345.
- 19 J. Chen, J. F. Daeuble, D. M. Brestensky, and J. M. Stryker, *Tetrahedron*, 2000, **56**, 2153.
- 20 R. Noyori and T. Ohkuma, *Angew. Chem. Int. Ed.*, 2001, **40**, 40.
- 21 C. S. Chin, B. Lee, and S. C. Park, *J. Organomet. Chem.*, 1990, **393**, 131.
- 22 K. Mashima, S. Akutagawa, X. Zhang, H. Takaya, T. Taketomi, H. Kumobayashi, and S. AKutagawa, *J. Organomet. Chem.*, 1992, **428**, 213.
- 23 E. Farnetti, J. Kaspar, R. Spongliarich, and M. Graziani, *J. Chem. Soc., Dalton Trans.*, 1988, 947.

*CHAPTER FIVE: FURTHER WORK.*



## 5 CHAPTER FIVE: FURTHER WORK.

The main aim of the work presented in this thesis has been to gain a mechanistic understanding as to why the rhodium DIOP catalytic system works so well for the hydroformylation of allyl alcohol. Continuing work can be carried out in the field of the design of new bidentate ligands for the reaction. The aim behind the design of these ligands will be two fold, firstly to increase the l:b ratio further, and secondly to produce alcohols as the primary products of the reaction. The eventual aim will be to design a ligand which will do both. The ligand design process can be helped by mechanistic studies of the new ligands, to compare how they behave relative to the rhodium DIOP catalytic system.

Another of the aims in this thesis has been to test the stability of the rhodium DIOP catalytic system towards oxidation. One problem with the design of electron rich phosphines is that they have an increased sensitivity towards oxidation. Continuing work therefore must also evaluate how stable the new ligands are towards oxidation compared with their phenyl analogues and ligands such as dppb and DIOP.

It has also been observed in this work that the electron rich alkyl diphosphines can have another benefit over their phenyl analogous. Thus, we observe lower levels of isomerisation products in the rhodium catalysed hydroformylation reaction when using the electron rich ligands as opposed to their phenyl analogous. It would be interesting to find if there is any mechanistic reason for this.

Our work has indicated that only certain types of compound are suitable as ligands for rhodium in the direct formation of alcohol products from the hydroformylation reaction. Continuing work will require the design of new bidentate ligand analogues with bite angles near  $120^\circ$ . The ligands will also be required to be electron rich at the phosphine, but must contain primary alkyl groups on the phosphorus as our work has indicated that secondary and tertiary alkyl groups in this position fail to give good catalysts.

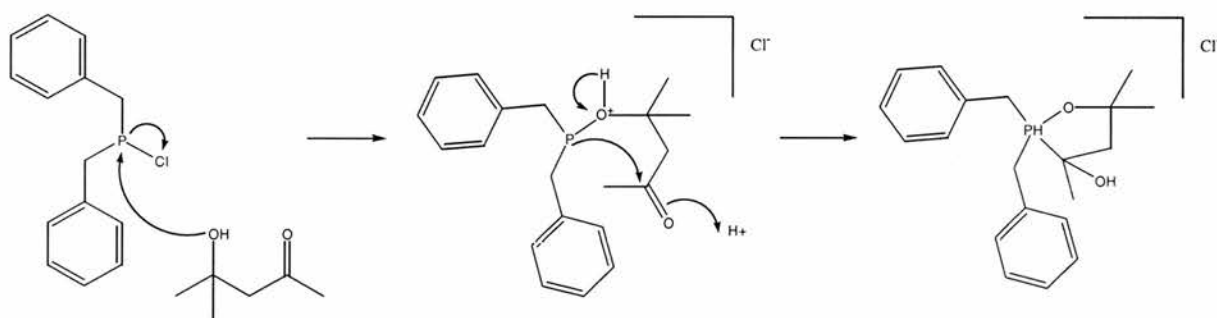
One of the considerations when designing the new ligands will be the substituents on the phosphorus. One way of increasing the l:b ratio is to increase the steric hindrance around the phosphine, as this destabilises the branched alkyl groups on the metal in crucial 5-coordinate TBP catalytic intermediates to a greater extent than the linear alkyl groups. We have already considered ethyl substituents on the phosphorus, and another option is methyl groups. While these retain the properties desired for the direct

formation of alcohol products, they are relatively small substituents, and are unlikely to improve the l:b ratio. Larger alkyl groups are also an option, from propyl to octyl, these will have the added benefit of being more insoluble in water which will be a consideration for the extraction stage. Another option will be benzyl groups, as these will be both electron donating and sterically demanding. Work has already begun on the synthesis of the benzyl analogous, see the synthesis of ClPBz<sub>2</sub> in Chapter 6. This was achieved by the reaction of two equivalents of the Grignard reagent BzMgCl with Et<sub>2</sub>NPCl<sub>2</sub>, effectively PCl<sub>3</sub> with a protected PCl site. Anhydrous HCl was then bubbled through the resulting solution of Et<sub>2</sub>NPBz<sub>2</sub> to form a solution of Et<sub>2</sub>NH and ClPBz<sub>2</sub>. Dibenzylchlorophosphine gives a resonance at 106.7 ppm in the <sup>31</sup>P NMR {<sup>1</sup>H} spectrum, and resonances at 7.4-7.2 ppm (10 H, ar), and 3.3 ppm (4 H, CH<sub>2</sub>, d, <sup>2</sup>J<sub>HP</sub> = 8 Hz) in the <sup>1</sup>H spectrum. The GC MS of dibenzylchlorophosphine can be seen in Figure 6.2 in Chapter 6.

When recrystallised from acetone Bz<sub>2</sub>PCl reacted with its aldol product CH<sub>3</sub>COCH<sub>2</sub>C(OH)(CH<sub>3</sub>)<sub>2</sub>, which was present in small quantities, to form crystals of the phosphonium salt, [Bz<sub>2</sub>P(C(OH)(CH<sub>3</sub>)CH<sub>2</sub>C(CH<sub>3</sub>)<sub>2</sub>O)]Cl, see Figure 5.1. Unfortunately, crystals of Bz<sub>2</sub>PCl of high enough quality for X-ray crystallography were not obtained from any other solvent.

**Figure 5.1**

*Reaction of Bz<sub>2</sub>PCl with CH<sub>3</sub>COCH<sub>2</sub>C(OH)(CH<sub>3</sub>)<sub>2</sub>.*

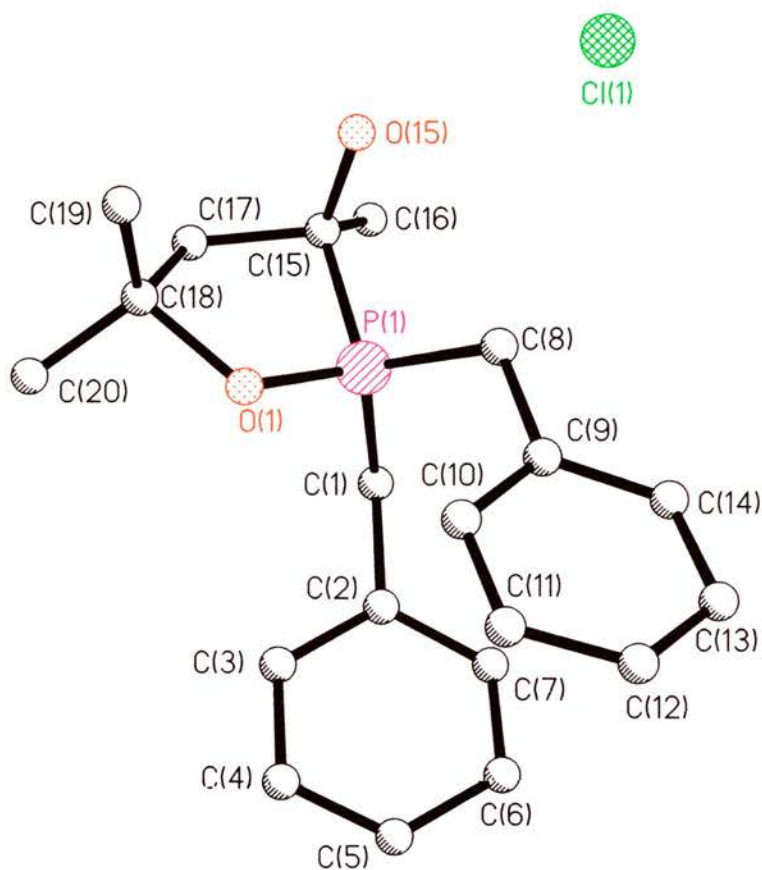


The X-ray crystal structure of [Bz<sub>2</sub>P(C(OH)(CH<sub>3</sub>)CH<sub>2</sub>C(CH<sub>3</sub>)<sub>2</sub>O)]Cl can be seen in Figure 5.2, selected bond lengths and angles can be seen in Table 5.1, a full set of crystallography data can be seen in Appendix 3, Table 1 to Table 5. There were no X-ray crystal structures of molecules with the form A or B, seen in Figure 5.3 found in the

literature. However, the phosphonium salts **C**<sup>1</sup> and **D**<sup>2</sup> were found in the literature and compared with  $[\text{Bz}_2\text{P}(\text{C}(\text{OH})(\text{CH}_3)\text{CH}_2\text{C}(\text{CH}_3)_2\text{O})]\text{Cl}$ .

**Figure 5.2**

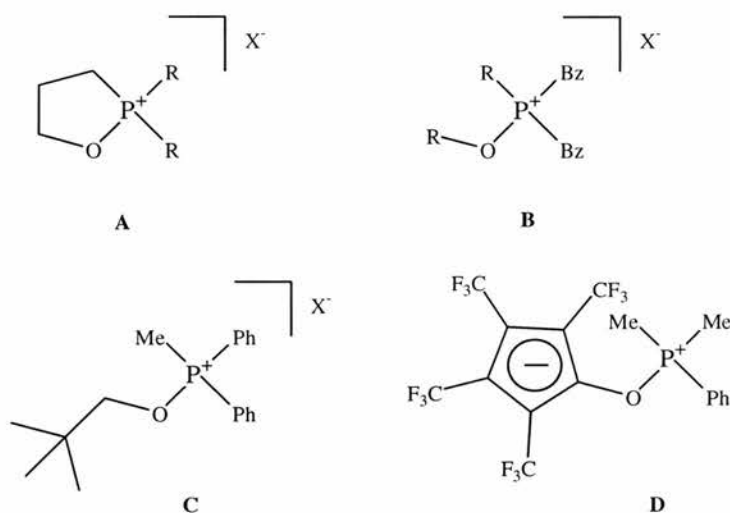
*X-Ray crystal structure of  $\text{Bz}_2\text{P}(\text{C}(\text{OH})(\text{CH}_3)\text{CH}_2\text{C}(\text{CH}_3)_2\text{O})\text{Cl}$*



The X-ray crystal structure of the phosphonium salt  $[\text{Bz}_2\text{P}(\text{C}(\text{OH})(\text{CH}_3)\text{CH}_2\text{C}(\text{CH}_3)_2\text{O})]\text{Cl}$  has a slightly distorted tetrahedral cation about the phosphorus. The bond lengths to the phosphorus atom are, P(1)-O(1) 1.563 Å (5), P(1)-C(15) 1.842 Å (7), P(1)-C(8) 1.789 Å (8), and P(1)-C(1) 1.779 Å (8). Compared to P(1)-O(1) 1.568 Å (4), P(1)-C(3) 1.779 Å (7), P(1)-C(2) 1.790 Å (6), and P(1)-C(1) 1.785 Å (6) in **C**, and to P(1)-O(1) 1.584 Å (2), P(1)-C(17) 1.771 Å (4), P(1)-C(16) 1.760 Å (4), and P(1)-C(10) 1.770 Å (3) in **D**. The P-O bond length, and the P-C bond lengths to the  $\text{CH}_2$  of the benzyl groups are in agreement with those observed in **C** and

**D.** The P-C bond length to the five membered ring is slightly longer than those previously reported to non-ring systems.

**Figure 5.3**



The bond angles around the phosphorus atom are C(1)-P(1)-C(8) 114.2 °(4), O(1)-P(1)-C(15) 98.9 °(3), O(1)-P(1)-C(1) 109.6 °(3), O(1)-P(1)-C(8) 110.2 ° (3), C(15)-P(1)-C(8) 110.6 ° (3), C(15)-P(1)-C(1) 112.3 ° (4), the mean angle is 109.3 °. The mean angles of **C** and **D** are 109.4 ° and 109.5 ° respectively. The individual angles are in agreement with **C**, the structure of which is closest to [Bz<sub>2</sub>P(C(OH)(CH<sub>3</sub>)CH<sub>2</sub>C(CH<sub>3</sub>)<sub>2</sub>O)]Cl with two phenyls and one methyl on the phosphorus. The angle between C(1)-P(1)-C(2) in **C** is 111.9 ° (3), compared with 114.2 ° (4), the angle between C(1)-P(1)-C(8) in [Bz<sub>2</sub>P(C(OH)(CH<sub>3</sub>)CH<sub>2</sub>C(CH<sub>3</sub>)<sub>2</sub>O)]Cl. This is slightly larger than the tetrahedral 109.5 °. The angle between O(1)-P(1)-C(3) in **C** is 104.2 ° (3), compared with 98.9 ° (3), the angle between O(1)-P(1)-C(15) in [Bz<sub>2</sub>P(C(OH)(CH<sub>3</sub>)CH<sub>2</sub>C(CH<sub>3</sub>)<sub>2</sub>O)]Cl, which is slightly below the tetrahedral 109.5 °.

**Table 5.1***Selected bond lengths and bond angles for [Bz<sub>2</sub>P(C(OH)(CH<sub>3</sub>)CH<sub>2</sub>C(CH<sub>3</sub>)<sub>2</sub>O)]Cl.*

Bond lengths (Å)			
C(1)-P(1)	1.779(8)	C(17)-C(15)	1.503(10)
C(8)-P(1)	1.789(8)	C(15)-P(1)	1.842(7)
P(1)-O(1)	1.563(5)	C(15)-O(15)	1.421(9)
P(1)-C(15)	1.842(7)	C(15)-C(16)	1.513(10)
O(1)-C(18)	1.546(8)	C(18)-C(19)	1.512(12)
C(18)-C(17)	1.543(10)	C(18)-C(20)	1.500(11)

Bond angles (°)			
C(1)-P(1)-C(8)	114.2(4)	C(18)-C(17)-C(15)	111.8(7)
C(1)-P(1)-O(1)	109.6(3)	C(17)-C(15)-P(1)	98.8(5)
C(8)-P(1)-C(15)	110.6(3)	O(15)-C(15)-P(1)	106.7(5)
O(1)-P(1)-C(15)	98.9(3)	O(15)-C(15)-C(16)	112.5(6)
C(15)-P(1)-C(1)	112.3(4)	O(15)-C(15)-C(17)	108.4(6)
O(1)-P(1)-C(8)	110.2(3)	O(1)-C(18)-C(17)	103.2(5)
P(1)-O(1)-C(18)	114.0(4)	C(20)-C(18)-C(19)	112.4(7)
O(1)-C(18)-C(17)	103.2(5)		

Another consideration is the backbone. In general ligands containing five or six atoms between the two phosphorus atoms seem to give the best l:b ratios as they have the desired bite angle. The rigidity of the backbone must also be considered for the ligand to benefit from the chelate effect and to minimise the amount of side products produced. The most successful bidentate ligands of this kind are BISBI and Xantphos (Figure 5.4), DIOP (Figure 5.4), has also shown benefits as a ligand for the hydroformylation of allyl alcohol.

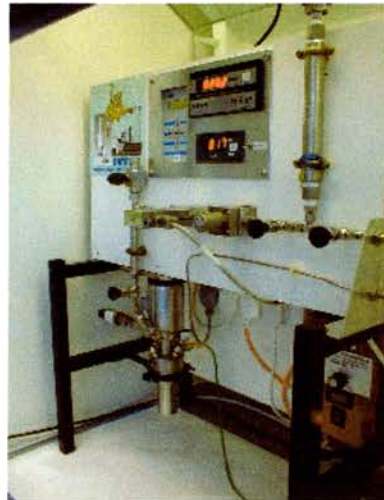
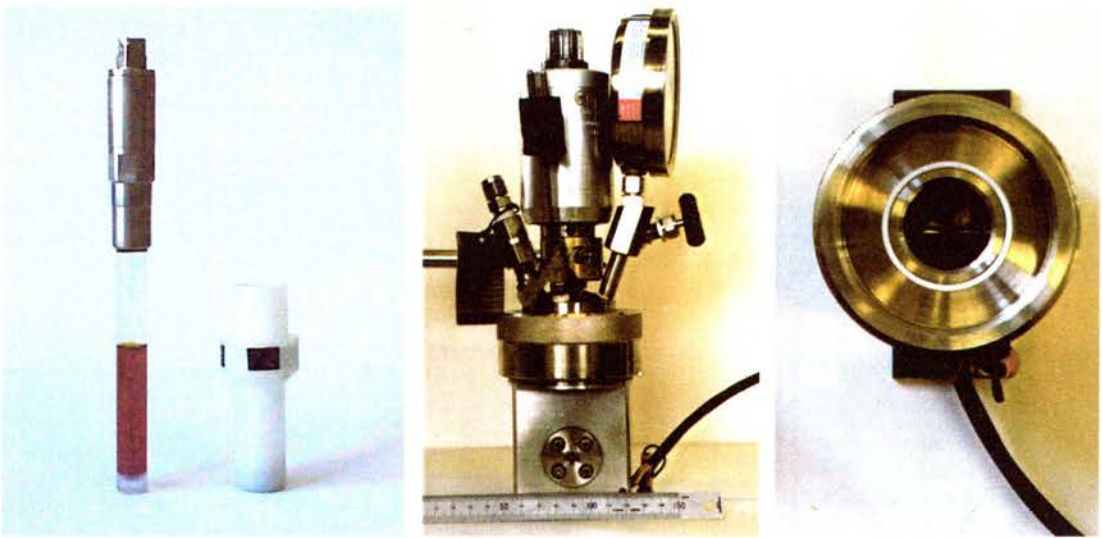
Further the work can therefore be on the development of analogues of BISBI, Xantphos and DIOP. The ethyl version of Xantphos has already been synthesised and the results are promising. The ethyl versions of BISBI and DIOP could be even more interesting for the one step process as the backbone possesses primary alkyl groups on the phosphorus, not aryl groups as does Xantphos.



## 5.1 References for Chapter Five

- 1 K. Henrick, H. R. Hudson and A. Kow, *J. Chem. Soc., Chem. Commun.*, 1980, 226.
- 2 M. J. Burk, J. C. Calabrese, F. Davidson, R. L. Harlow and D. C. Roe, *J. Am. Chem. Soc.*, 1993, **113**, 2209.

*CHAPTER SIX: EXPERIMENTAL.*



## 6 CHAPTER SIX: EXPERIMENTAL.

### 6.1 General Procedure.

#### 6.1.1 Laboratory Reagents.

All experiments under a dry nitrogen / argon atmosphere were carried out on vacuum lines. Nitrogen / argon was dried through a Cr (II) / silica packed glass column. Liquids were transferred under inert atmosphere by syringe or canular through suba seals. Solids were transferred directly from one Schlenk tube to another or weighed out in a glove box under argon.

All gases was purchased from BOC gases. Ethanol and methanol were distilled over magnesium alkoxide under nitrogen and stored under nitrogen / argon over molecular sieves. Cyclohexane and hexane were stored over sodium.

Water was distilled and stored under nitrogen / argon. Petroleum ether (boiling range 40-60 °C) and diethyl ether were distilled over sodium diphenylketyl. Dichloromethane was distilled over calcium hydride. Toluene was distilled over sodium.

Deuteriated solvents were purchased from Cambridge Isotope Laboratories, degassed by repeated freeze-pump-thaw cycles under high vacuum and stored under nitrogen / argon over molecular sieves.

The metal complexes  $[\text{RhCl}_3 \cdot 3\text{H}_2\text{O}]$ ,  $[\text{Rh}(\text{CO})_2(\text{acac})]$  and  $[\text{Ir}(\text{CO})_2(\text{acac})]$  were purchased from Strem. The phosphine ligands 4,5-bis(diphenylphosphinomethyl)-2,2-dimethyl-1,3-dioxolan (DIOP), triphenylphosphine (TPP) and 1,4-bis(diphenylphosphino)butane (dppb) were purchased from Aldrich. The phosphine precursors 9,9-dimethylxanthene, chlorodiethylphosphine, diethylphosphine, (+)-trans-4,5-bis[hydroxymethyl]-2,2-dimethyl-1,3-dioxolan, 2,2'-bis(bromomethyl)-1,1'-biphenyl, 4-bromo-2,6-dimethylanisole, p-toluenesulfonylchloride, *sec*-butyllithium, and diethylphosphite were purchase from Aldrich. The substrates allyl alcohol and 1-hexene were purchased from Aldrich, prop-2-enol was dried with  $\text{CaSO}_4$ , refluxed with magnesium, and fractionally distilled, allyl alcohol was stored under argon / nitrogen over molecular sieves in the dark.

### 6.1.2 Analytical Techniques.

Infrared spectra were obtained using a Nicolet Protege 460 Fourier Transform Spectrometer with CsI optics. The infrared spectrometer was interfaced to a personal computer via the OMNIC operating system.

G.C. analyses were carried out using a Phillips PU 4000 fitted with a NEW column.

G.C. M.S. were carried out using a Hewlett Packard 5890 G.C. with an Incos quadrupole mass spectrometer fitted with a SGE BP1 column and a Hewlett Packard HP6890 G.C. with a 5973 mass selective detector fitted with a 5 % phenyl methyl siloxane capillary column.

Carbon, proton and phosphorous NMR spectra were recorded on a Bruker AM 300 NMR spectrometer or a Varian 300 NMR spectrometer. Broad band decoupling was used for  $^{13}\text{C}$  spectra and  $^{31}\text{P}$  spectra.  $^1\text{H}$  and  $^{13}\text{C}$  NMR spectra were referenced internally to deuterated solvents, which were referenced relative to TMS at  $\delta=0$ :  $\text{CD}_2\text{Cl}_2$ :  $^1\text{H}$ ,  $\delta$ , 5.35 ppm,  $^{13}\text{C}$ ,  $\delta$ , 53.8 ppm;  $\text{CD}_3\text{OD}$ :  $^1\text{H}$ ,  $\delta$ , 3.35 ppm,  $^{13}\text{C}$ ,  $\delta$ , 49.0 ppm;  $\text{C}_6\text{D}_6$ :  $^1\text{H}$ ,  $\delta$ , 7.16 ppm,  $^{13}\text{C}$ ,  $\delta$ , 128.39 ppm;  $\text{C}_7\text{H}_8$ :  $^1\text{H}$ ,  $\delta$ , 2.09 ppm,  $^{13}\text{C}$ ,  $\delta$ , 20.4 ppm;  $\text{CDCl}_3$ :  $^1\text{H}$ ,  $\delta$ , 7.27 ppm,  $^{13}\text{C}$ ,  $\delta$ , 77.23 ppm.  $^{31}\text{P}$  NMR spectra were referenced externally to phosphoric 85 %  $\text{H}_3\text{PO}_4$ . Coupling constants are given in Hz.

## 6.2 Synthesis.

### 6.2.1 (Acetylacetonato) (dicarbonyl) rhodium(I) $[\text{Rh}(\text{CO})_2(\text{acac})]^{1,2}$ .

A solution of rhodium chloride  $[\text{RhCl}_3 \cdot 3\text{H}_2\text{O}]$  (1 eq, 0.5g,  $2.2 \times 10^{-3}$  mol) in dimethylformamide ( $50 \text{ cm}^3$ ) was heated at reflux under nitrogen for 30 minutes, to yield a pale yellow solution of  $[\text{Rh}_2\text{Cl}_2(\text{CO})_4]$ . 2,4-Pentanedione (1.1 eq, 0.242 g,  $2.4 \times 10^{-3}$  mol) was added and the solution stirred under nitrogen for 18 hours. The resulting green solution was diluted with water ( $25 \text{ cm}^3$ ), filtered and the precipitate washed with petroleum ether ( $3 \times 5 \text{ cm}^3$ ) to give dicarbonyl acetylacetonato rhodium(I)  $[\text{Rh}(\text{CO})_2(\text{acac})]$  as red-green crystals (0.32 g,  $1.2 \times 10^{-3}$  mol, 58 %).

$^{13}\text{C}$  NMR ( $\text{CDCl}_3$ , 75.4 MHz)  $\delta$ : 187.5 ( $\text{CH}_3\text{COCH}_2^-$ , s), 183.9 ( $\text{OCRh}$ , d,  $^1J_{\text{C-Rh}} = 72.5$  Hz); 101.7 ( $-\text{COCH}_2\text{CO}-$ , s); 26.9 ( $\text{CH}_3\text{CO}-$ , s) ppm.

$^1\text{H}$  NMR ( $\text{CDCl}_3$ , 300.0 MHz)  $\delta$ : 5.61 (1H, s); 2.06 (6 H, s) ppm.

IR (nujol mull): 2011, 1980  $\text{cm}^{-1}$  ( $\text{C}=\text{O}$ ).

Literature values<sup>1,2</sup>:  $^1\text{H}$  NMR ( $\text{CDCl}_3$ , 300.0 MHz)  $\delta$ : 5.59, 2.05 ppm: IR (hexane): 2014, 1984  $\text{cm}^{-1}$  ( $\text{C}=\text{O}$ ).

### 6.2.2 $[\text{Rh}(\text{acac})(\text{DIOP})]$ .

A solution of 4,5-Bis(diphenylphosphinomethyl)-2,2-dimethyl-1,3-dioxolan (DIOP) (1.5 eq, 0.072 g,  $1.5 \times 10^{-4}$  mol) in dry / degassed toluene under argon was added to  $[\text{Rh}(\text{CO})_2(\text{acac})]$  (1.0 eq, 0.025 g,  $9.7 \times 10^{-5}$  mol) under a stream of argon and stirred for 1 hour. Carbon monoxide was evolved resulting in a red solution of  $[\text{Rh}(\text{acac})(\text{DIOP})]$ . Crystals suitable for X-ray crystallography were obtained from hot acetone.

$^{31}\text{P}$  NMR ( $\text{C}_7\text{D}_8$ , 121.4 MHz)  $\delta$ : 4.155 (d,  $^1J_{\text{P-Rh}} = 186.8$ ) ppm.

$^{13}\text{C}$  NMR ( $\text{C}_7\text{D}_8$ , 75.4 MHz)  $\delta$ : 184.14 ( $\text{CH}_3\text{COCH}_2^-$ , s); 137.35-127.41 ( $-\text{PPh}_2$ , m); 108.00 ( $(\text{CH}_3)_2\text{C}(\text{O})_2$ , s); 99.38 ( $-\text{COCH}_2\text{CO}-$ , s); 78.00 ( $-\text{OCH}-$ , t); 32.91 ( $-\text{CHCH}_2\text{P}-$ , t); 26.90 ( $\text{CH}_3\text{C}-$ , s), 26.70 ( $-\text{COCH}_3$ , s) ppm.

$^1\text{H}$  NMR ( $\text{C}_7\text{D}_8$ , 300.0 MHz)  $\delta$ : 8.1-7.7, 7.3-7.1 (20 H,  $-\text{PPh}$ , m); 5.3 (2 H,  $-\text{COCH}_2\text{CO}-$ , s); 4.2 (2 H,  $\text{CH}$ , m); 3.1-2.6 (4H,  $-\text{CHCH}_2\text{P}-$ , m); 1.6 (6 H,  $-\text{COCH}_3$ , s); 1.4 (6 H,  $-\text{CCH}_3$ , s) ppm.

The preparation was repeated with  $[\text{Rh}(\text{CO})_2(\text{acac})]$  / DIOP ratios of 1:1 and 1:2.

### 6.2.3 $[\text{Rh}_2(\text{CO})_4(\text{DIOP})_2]$ .

Carbon monoxide or synthesis gas was bubbled through a red solution of  $[\text{Rh}(\text{DIOP})(\text{acac})]$ , in toluene for 3 hours, resulting in a pale yellow solution of  $[\text{Rh}_2(\text{CO})_4(\text{DIOP})]$ . The complex was detected by NMR and IR but not isolated.

Alternatively, [Rh(acac)(DIOP)] was prepared from [Rh(CO)<sub>2</sub>(acac)] as described in section 6.2.2. The resulting solution was then transferred to a high pressure cell (NMR or IR), which was then pressurised to 20 bar with synthesis gas. The resulting solution contained [Rh<sub>2</sub>(DIOP)<sub>2</sub>(CO)<sub>4</sub>] as the major complex species present, in equilibrium with [HRh(CO)<sub>2</sub>(DIOP)]. The complex was detected by NMR and IR but not isolated.

<sup>31</sup>P {<sup>1</sup>H} NMR (C<sub>7</sub>D<sub>8</sub>, 121.4 MHz) δ: 5.22 ppm (2<sup>nd</sup> order AA'XX'X''X''' spin system).

<sup>13</sup>C NMR (C<sub>7</sub>D<sub>8</sub>, 75.4 MHz) δ: 222.00 ppm (-CO); 133.36-127.98 ppm (-PPh<sub>2</sub>, m); 107.54 ppm ((CH<sub>3</sub>)<sub>2</sub>C(O)<sub>2</sub>); 78.23 ppm (-OCHCH<sub>2</sub>-); 33.96 ppm (-CHCH<sub>2</sub>(O)<sub>2</sub>-); 26.67 ppm (CH<sub>3</sub>C-).

<sup>1</sup>H NMR (C<sub>7</sub>D<sub>8</sub>, 300.0 MHz) δ: 7.64-7.53 ppm, 7.30-7.01 ppm (40H, -PPh, m); 4.16 ppm (4H, -OCHCH<sub>2</sub>-, m); 3.2-3.18 ppm (8H, -CHCH<sub>2</sub>P-, m); 1.46 ppm (12H, CH<sub>3</sub>C-, s).

IR (C<sub>7</sub>H<sub>8</sub>) ν<sub>max</sub> (CO): 1985.00, 1723.93 cm<sup>-1</sup>.

Literature values<sup>3</sup>: <sup>31</sup>P {<sup>1</sup>H} NMR (C<sub>7</sub>D<sub>8</sub>, 121.4 MHz) δ: 3.7 ppm: IR (C<sub>7</sub>H<sub>8</sub>) ν<sub>max</sub> (CO): 1960, 1740 cm<sup>-1</sup>.

#### 6.2.4 [HRh(CO)<sub>2</sub>(DIOP)].

Carbon monoxide / hydrogen 1:2, or hydrogen was bubbled through a pale yellow solution of [Rh<sub>2</sub>(CO)<sub>4</sub>(DIOP)] to yield low levels of Rh(CO)<sub>2</sub>H(DIOP). The complex was detected by NMR and IR but not isolated.

Alternatively [Rh(acac)(DIOP)] was prepared from [Rh(CO)<sub>2</sub>(acac)] as described in section 6.2.2. The resulting solution was then transferred to a high pressure cell (NMR or IR), which was then pressurised to 20 bar with synthesis gas, the resulting solution contained [HRh(CO)<sub>2</sub>(DIOP)] as the minor complex species present in equilibrium with [Rh<sub>2</sub>(DIOP)<sub>2</sub>(CO)<sub>4</sub>], see section 6.2.3, heating the sample resulted in a shift in the equilibrium towards [HRh(CO)<sub>2</sub>(DIOP)]. The complex was detected by NMR and IR but not isolated.

<sup>31</sup>P {<sup>1</sup>H} NMR (C<sub>7</sub>D<sub>8</sub>, 121.4 MHz) δ: 17.5 ppm (d, <sup>1</sup>J<sub>P-Rh</sub> = 120 Hz).

$^1\text{H}$  NMR ( $\text{C}_7\text{D}_8$ , 300.0 MHz)  $\delta$ : 7.73-6.91 ppm (20H, **Ph**, m); 4.49 ppm (2H, **CHCH**<sub>2</sub>, m); 2.64 ppm (4H, **CHCH**<sub>2</sub>**P**, m); 1.17 ppm (6H, **CH**<sub>3</sub>**C**, s); -9.17 ppm (1H, **RhH**, td,  $^1J_{\text{H-Rh}} = 8.3$  Hz,  $^2J_{\text{H-P}} = 35.5$  Hz).

IR ( $\text{C}_7\text{H}_8$ )  $\nu_{\text{max}}$  (CO): 2040.07(ee), 1990.36(ea), 1977.89(ee), 1947.3(ea)  $\text{cm}^{-1}$ .

### 6.2.5 $[\text{Rh}(\text{COCH}_2\text{CH}_2\text{CH}_2\text{OH})(\text{CO})_2(\text{DIOP})]$ & $[\text{Rh}(\text{COCHCH}_3\text{CH}_2\text{OH})(\text{CO})(\text{DIOP})]$ , Complex Species **49** and **50**.

$[\text{Rh}(\text{acac})(\text{DIOP})]$  was prepared from  $[\text{Rh}(\text{CO})_2(\text{acac})]$  as described in section 6.2.2, allyl alcohol (0.3  $\text{cm}^3$ , 0.26 g,  $4.4 \times 10^{-3}$  mol) was then added. Synthesis gas was bubbled through the solution for 1 hour. The resulting solution contained  $[\text{Rh}(\text{COCH}_2\text{CH}_2\text{CH}_2\text{OH})(\text{CO})_2(\text{DIOP})]$  &  $[\text{Rh}(\text{COCHCH}_3\text{CH}_2\text{OH})(\text{CO})(\text{DIOP})]$ , or complex species **49** and **50**. The complex was detected by NMR and IR but not isolated. Alternatively  $[\text{Rh}(\text{acac})(\text{DIOP})]$  was prepared from  $[\text{Rh}(\text{CO})_2(\text{acac})]$  as described in section 6.2.2, allyl alcohol (0.3  $\text{cm}^3$ , 0.26 g,  $4.4 \times 10^{-3}$  mol) was then added. The resulting solution was transferred to a high pressure cell (NMR or IR), which was then pressurised to 20 bar with synthesis gas, the resulting solution contained  $[\text{Rh}(\text{COCH}_2\text{CH}_2\text{CH}_2\text{OH})(\text{CO})_2(\text{DIOP})]$  and  $[\text{Rh}(\text{COCHCH}_3\text{CH}_2\text{OH})(\text{CO})(\text{DIOP})]$ , or complex species **49** and **50**. The complex was detected by NMR and IR but not isolated. Attempts were made to isolate the complex. If a solution containing the complex was put under reduced pressure, a colour change was observed.  $^{31}\text{P}$   $\{^1\text{H}\}$  NMR showed that the complexes rhodium acyl complexes had reverted back to  $[\text{Rh}(\text{CO})_2(\text{acac})]$ . Attempts were also made to recrystallise the complexes from diethyl ether. Small yellow particles did begin to form which could have been crystals of the rhodium acyl complexes, however, they were unstable and turned red after 24 hrs.

$^{31}\text{P}\{^1\text{H}\}$  NMR ( $\text{CD}_2\text{Cl}_2$ , 121.4 MHz)  $\delta$ : 15.13 ppm ( $^1J_{\text{PRh}} = 125$  Hz,  $^2J_{\text{PP}} = 33$  Hz); 13.72 ppm ( $^1J_{\text{PRh}} = 128$  Hz,  $^2J_{\text{PP}} = 33$  Hz); 9.45 ppm ( $^1J_{\text{PRh}} = 128$  Hz,  $^2J_{\text{PP}} = 33$  Hz); 4.84 ppm ( $^1J_{\text{PRh}} = 125$  Hz,  $^2J_{\text{PP}} = 33$  Hz).

$^1\text{H}$  NMR ( $\text{C}_7\text{D}_8$ , 300.0 MHz)  $\delta$ : 7.68-6.86 ppm (20H, **Ph**, m); 4.40 ppm (2H, **CHCH**<sub>2</sub>, m); 2.63 ppm (4H, **CHCH**<sub>2</sub>**P**, m); 1.17 ppm (6H, **CH**<sub>3</sub>**C**, s).

IR ( $\text{C}_7\text{H}_8$ )  $\nu_{\text{max}}$  (CO): 1986, 1948  $\text{cm}^{-1}$ .

**6.2.6 9,9-Dimethyl-4,6-bis(diethylphosphino)xanthene, [Et-Xantphos].**

At room temperature under argon a solution of *sec*-BuLi (22 cm<sup>3</sup>, 1.3 mol dm<sup>-3</sup>, 0.029 mol, 3 eq) in hexane was added dropwise to a stirred solution of 9,9-dimethylxanthene (2 g, 9.5 x 10<sup>-3</sup> mol, 1 eq) and TMEDA (3.41 g, 0.029 mol, 3 eq) in dry / degassed diethyl ether. After addition the solution was stirred for 16 hours. A solution of chlorodiethylphosphine (3.5 cm<sup>3</sup>, 0.029 mol, 3 eq) in hexane was added dropwise, and the reaction mixture stirred for a further 16 hours. The solvent was removed under reduced pressure, and the resulting oil dissolved in CH<sub>2</sub>Cl<sub>2</sub>, washed with water and dried with MgSO<sub>4</sub>. The solvent was removed under reduced pressure to leave a yellow crystalline product. Hexane was added and the solution stirred and decanted from the insoluble orange paste. The solvent was removed under reduced pressure to give 9,9-dimethyl-4,6-bis(diethylphosphino)xanthene [Et-Xantphos] (1.1g, 29.9 % yield).

<sup>31</sup>P{<sup>1</sup>H} NMR (CD<sub>2</sub>Cl<sub>2</sub>, 121.4 MHz) δ: -21.59 ppm.

<sup>13</sup>C NMR (CD<sub>2</sub>Cl<sub>2</sub>, 75.4 MHz) δ: 152.46 ppm (ar PCCOC); 129.65 ppm (ar CHCC); 128.80 ppm, 125.86 ppm, 123.10 ppm (ar CH); 116.41 ppm (ar CHCPC); 34.20 ppm (CCCH<sub>3</sub>); 32.15 ppm (C(CH<sub>3</sub>)<sub>2</sub>); 17.41 ppm (CH<sub>3</sub>CH<sub>2</sub>P); 9.59 ppm (CH<sub>3</sub>CH<sub>2</sub>P).

<sup>1</sup>H NMR (C<sub>2</sub>Cl<sub>2</sub>, 300.0 MHz) δ: 7.34 ppm (2H, CPCHCH, dd, J = 7.7, 1.7 Hz); 7.17 ppm (2H, CIICHCH, ddd, J = 7.7, 3.0, 1.7 Hz); 7.06 ppm (2H, CHCHCH, t, J = 7.6 Hz); 1.87 ppm (8H, CH<sub>3</sub>CH<sub>2</sub>P, m); 1.59 ppm (6H CCH<sub>3</sub>, s); 1.05 ppm (12H, CH<sub>3</sub>CH<sub>2</sub>, m).

**6.2.7 [Rh<sub>2</sub>(CO)<sub>4</sub>(Et-Xantphos)<sub>2</sub>].**

A solution of 9,9-dimethyl-4,6-bis(diethylphosphino)xanthene (Et-Xantphos) (1.5 eq, 0.072 g, 1.5 x 10<sup>-4</sup> mol) in dry / degassed toluene under argon was added to [Rh(CO)<sub>2</sub>(acac)] (1.0 eq, 0.025 g, 9.7 x 10<sup>-5</sup> mol) under a stream of argon and stirred. Synthesis gas was bubbled through the resulting red solution for 3 hours, resulting in a pale yellow solution of [Rh<sub>2</sub>(CO)<sub>4</sub>(Et-Xantphos)<sub>2</sub>]. The solvent was removed under vacuum and crystals suitable for X-ray crystallography were obtained from hot ethanol.

$^{31}\text{P} \{^1\text{H}\}$  NMR ( $\text{C}_7\text{D}_8$ , 121.4 MHz)  $\delta$ : 1.8 ppm ( $2^{\text{nd}}$  order AA'XX'X''X''' spin system).

$^1\text{H}$  NMR ( $\text{C}_2\text{Cl}_2$ , 300.0 MHz)  $\delta$ : 7.19-6.88 ppm (6H, **ar**, m); 1.87 (8H,  $\text{CH}_3\text{CH}_2\text{P}$ , m); 1.42 (6H  $\text{CCH}_3$ , s); 1.03 (12H,  $\text{CH}_3\text{CH}_2\text{P}$ ).

### 6.2.8 9,9-Dimethyl-4,6-bis(di-*tert*-butylphosphino)xanthene [ $^t\text{Bu-Xantphos}$ ].

At room temperature under argon a solution of 1.3 M *sec*-BuLi ( $22 \text{ cm}^3$ ,  $1.3 \text{ mol dm}^{-3}$ , 0.029 mol, 3 eq) in hexane was added dropwise to a stirred solution of 9,9-dimethylxanthene (2 g,  $9.5 \times 10^{-3}$  mol, 1 eq) and TMEDA (3.41 g, 0.029 mol, 3 eq) in dry / degassed diethylether. After addition the solution was stirred for 16 hours. A solution of chlorodi-*tert*-butylphosphine ( $5.5 \text{ cm}^3$ , 5.2 g, 0.029 mol) in hexane was added dropwise, and the reaction mixture stirred for a further 16 hours. The solvent was removed under reduced pressure, and the resulting oil dissolved in  $\text{CH}_2\text{Cl}_2$ , washed with water and dried with  $\text{MgSO}_4$ . The solvent was removed under reduced pressure to leave a yellow crystalline product. Hexane was added and the solution stirred and decanted from the insoluble orange paste. The solvent was removed under reduced pressure to give 9,9-dimethyl-4,6-bis(diethylphosphino)xanthene [ $^t\text{Bu-Xantphos}$ ] (1.6195 g,  $3.2 \times 10^{-3}$  mol, 34 % yield).

$^{31}\text{P} \{^1\text{H}\}$  NMR ( $\text{C}_2\text{Cl}_2$ , 121.4 MHz)  $\delta$ : 11.71 ppm.

$^{13}\text{C}$  NMR ( $\text{CD}_2\text{Cl}_2$ , 75.4 MHz)  $\delta$ : 137.46 ppm (ar, PCCOC); 133.97 ppm (ar, CH); 131.09 ppm (ar, CHCC); 126.13 ppm, 121.97 (ar, CH); 117.15 ppm (ar, CHCPC); 33.09 ppm ( $(\text{CH}_3)_3\text{CP}$ , d,  $^1J_{\text{CP}} = 28 \text{ Hz}$ ); 32.91 ppm ( $\text{C}(\text{CH}_3)_2$ ); 31.05 ppm ( $\text{C}(\text{CH}_3)_2$ , s); 30.99 ppm ( $\text{C}(\text{CH}_3)_3$ ,  $^2J_{\text{CP}} = 18 \text{ Hz}$ ).

$^1\text{H}$  NMR ( $\text{CD}_2\text{Cl}_2$ , 300.0 MHz)  $\delta$ : 7.89 ppm, 7.41 ppm, 7.17 ppm, (6H, **ar**); 1.55 ppm (6H,  $\text{CCH}_3$ , s); 1.41 ppm (36H,  $\text{PC}(\text{CH}_3)_3$ , d  $^3J_{\text{HP}} = 64 \text{ Hz}$ ).

### 6.2.9 2,7-Di-*tert*-butyl-9,9-dimethyl-4,6-bis(diethylphosphino)xanthene, [Et-<sup>t</sup>BuXantphos].

At  $-60\text{ }^{\circ}\text{C}$  a solution of *n*-BuLi in hexane ( $5.8\text{ cm}^3$ ,  $1.6\text{ mol dm}^{-3}$ ,  $9.2 \times 10^{-3}\text{ mol}$ , 2.2 eq) was added dropwise under argon to a solution of 4,5-dibromo-2,7-di-*tert*-butyl-9,9-dimethylxanthene (2 g,  $4.2 \times 10^{-3}\text{ mol}$ , 1 eq) in THF ( $50\text{ cm}^3$ ). The suspension was stirred for 1 hour at  $-60\text{ }^{\circ}\text{C}$ . The reaction mixture was slowly warmed to  $0\text{ }^{\circ}\text{C}$ , then cooled to  $-60\text{ }^{\circ}\text{C}$  again. A solution of chlorodiethylphosphine ( $1.12\text{ cm}^3$ , 1.14 g,  $9.2 \times 10^{-3}\text{ mol}$ , 2.2 eq) in THF ( $10\text{ cm}^3$ ) was added dropwise under argon, the reaction mixture was then warmed to room temperature. The solvent was removed under reduced pressure and the resulting white residue dissolved in  $\text{CH}_2\text{Cl}_2$ , washed with water and dried with  $\text{MgSO}_4$ . The solvent was removed under reduced pressure to give [Et-<sup>t</sup>BuXantphos] (1.3395 g,  $2.7 \times 10^{-3}$ , 64 % yield) as a white solid.

$^{31}\text{P}\{^1\text{H}\}$  NMR ( $\text{CD}_2\text{Cl}_2$ , 121.4 MHz)  $\delta$ : -23.58 ppm (s).

$^{13}\text{C}$  NMR ( $\text{CD}_2\text{Cl}_2$ , 75.4 MHz)  $\delta$ : 145.07 ppm (ar PCCOC); 130.01 ppm (ar CHCC); 128.80 ppm, 125.16 ppm, 122.69 ppm (ar CH), 116.79 ppm (ar CHCPC); 34.94 ppm (CCCH<sub>3</sub>); 34.78 ppm (C(CH<sub>3</sub>)<sub>3</sub>); 32.71 ppm (C(CH<sub>3</sub>)<sub>2</sub>); 31.68 ppm (C(CH<sub>3</sub>)<sub>3</sub>); 17.87 ppm (CH<sub>3</sub>CH<sub>2</sub>P); 10.09 ppm (CH<sub>3</sub>CH<sub>2</sub>P).

$^1\text{H}$  NMR ( $\text{CD}_2\text{Cl}_2$ , 300.0 MHz)  $\delta$ : 7.46 ppm-7.11 ppm (6H, ar, m); 1.97 ppm (8H, CH<sub>3</sub>CH<sub>2</sub>P, m); 1.59 ppm (6H, C(CH<sub>3</sub>)<sub>2</sub>, s); 1.35 ppm (18H, C(CH<sub>3</sub>)<sub>3</sub>, s); 1.16 ppm (12H, CH<sub>3</sub>CH<sub>2</sub>P, m).

### 6.2.10 2,2'-Bis di-*iso*-propylphosphanyl biphenyl, [<sup>i</sup>Pr-Bisbite].

At  $-60\text{ }^{\circ}\text{C}$  a solution of *n*-BuLi in hexene ( $15\text{ cm}^3$ ,  $1.6\text{ mol dm}^{-3}$ ,  $2.4 \times 10^{-2}\text{ mol}$ , 2.2 eq) was added dropwise under argon to a solution of 1,4-biphenol (2 g,  $1.1 \times 10^{-2}\text{ mol}$ , 1 eq), in THF ( $60\text{ cm}^3$ ). The suspension was stirred for 1 hour at  $-60\text{ }^{\circ}\text{C}$ . The reaction mixture was slowly warmed to  $0\text{ }^{\circ}\text{C}$ , then cooled to  $-60\text{ }^{\circ}\text{C}$  again. A solution of chlorodi-*iso*-propylphosphine ( $3.8\text{ cm}^3$ , 3.61 g,  $2.4 \times 10^{-2}\text{ mol}$ ) in THF ( $10\text{ cm}^3$ ) was added dropwise under argon, the reaction mixture was then warmed to room temperature. The solvent was removed under reduced pressure and the residue dissolved

in  $\text{CH}_2\text{Cl}_2$  washed with water and dried with  $\text{MgSO}_4$ . The solvent was removed under reduced pressure to give [ $^1\text{Pr-Bisbite}$ ] (3.13 g,  $7.5 \times 10^{-3}$ , 68 %) as a red oil.

$^{31}\text{P}\{^1\text{H}\}$  NMR ( $\text{C}_7\text{D}_8$ , 121.4 MHz)  $\delta$ : 148.31 ppm.

$^{13}\text{C}$  NMR ( $\text{C}_7\text{D}_8$ , 75.4 MHz)  $\delta$ : 157.11 ppm (COP); 137.41 ppm (CH); 130.13 ppm (C); 120.95 ppm, 117.90 ppm, 117.64 ppm (CH); 28.40 ppm ( $\text{CH}(\text{CH}_3)_2$ ); 17.67 ppm ( $\text{CH}(\text{CH}_3)_2$ ).

$^1\text{H}$  NMR ( $\text{C}_7\text{D}_8$ , 300.0 MHz)  $\delta$ : 7.51-6.86 ppm (8H, **ar**, m); 1.67 ppm-1.57 ppm (2H,  $\text{CH}(\text{CH}_3)$ , m); 0.99 ppm-0.85 ppm (m, 24H,  $\text{CH}(\text{CH}_3)$ ).

### 6.2.11 Chlorodibenzylphosphine, [ $\text{Bz}_2\text{PCI}$ ].

A solution of  $\text{BzMgCl}$  ( $30.3 \text{ cm}^3$ ,  $1.6 \text{ mol dm}^{-3}$ ,  $6.1 \times 10^{-2} \text{ mol}$ , 2.2 eq) in THF was added dropwise with stirring to a solution of (N,N-diethylamino)dichlorophosphine ( $4.0 \text{ cm}^3$ , 4.8 g,  $2.8 \times 10^{-2} \text{ mol}$ , 1 eq) in dry degassed THF ( $150 \text{ cm}^3$ ) under argon at  $0^\circ\text{C}$ . The solution was allowed to warm to room temperature, then heated at reflux for 6 hours and allowed to cool. The solvent was removed under vacuum and the resulting brown solid slurried with petrol. Anhydrous HCl was then bubbled through the mixture and a white precipitate formed. When no more precipitate formed, the HCl addition was stopped. The supernatant solution was then decanted from the mixture of brown and white solid. The solvent was removed under vacuum to give chlorodibenzylphosphine [ $\text{Bz}_2\text{PCI}$ ] (3.1229 g,  $1.4 \times 10^{-2} \text{ mol}$ , 51 %) as a white crystalline solid.

m.p.  $80\text{-}82^\circ\text{C}$ .

$^{31}\text{P}\{^1\text{H}\}$  NMR ( $\text{CD}_2\text{Cl}_2$ , 121.4 MHz)  $\delta$ : 106.69 ppm.

$^{13}\text{C}$  NMR ( $\text{CD}_2\text{Cl}_2$ , 75.4 MHz)  $\delta$ : 135.82 ppm ( $\text{CCH}_2$ , d,  $^2J_{\text{CP}} = 6.9 \text{ Hz}$ ); 130.12 ppm ( $\text{CHC}$ , d,  $^3J_{\text{CP}} = 5.3 \text{ Hz}$ ); 129.80 ppm ( $\text{CHCHC}$ , s); 127.44 ppm ( $\text{CHCHCHC}$ , d,  $^5J_{\text{CP}} = 1.6 \text{ Hz}$ ); 42.86 ppm ( $\text{CH}_2$ , d,  $^1J_{\text{CP}} = 34 \text{ Hz}$ ).

$^1\text{H}$  NMR ( $\text{CD}_2\text{Cl}_2$ , 300.0 MHz)  $\delta$ : 7.37 ppm-7.24 ppm (10H, **ar**); 3.28 ppm (4H,  $\text{BzCH}_2\text{P}$ , d,  $^2J_{\text{HP}} = 8 \text{ Hz}$ ).

The GC of a solution of  $\text{Bz}_2\text{PCl}$  in methylene chloride can be seen in Figure 6.1.

The MS of  $\text{Bz}_2\text{PCl}$  can be seen in Figure 6.2.

#### 6.2.12 $[\text{Bz}_2\text{P}(\text{COH})(\text{CH}_3)\text{CH}_2\text{C}(\text{CH}_3)_2\text{O}]\text{Cl}$

$\text{Bz}_2\text{PCl}$  was recrystallised from acetone, in which the aldol product  $\text{CH}_3\text{COCH}_2\text{C}(\text{OH})(\text{CH}_3)_2$  was present. This reacted with  $\text{Bz}_2\text{PCl}$  to form  $[\text{Bz}_2\text{P}(\text{C}(\text{OH})(\text{CH}_3)\text{CH}_2\text{C}(\text{CH}_3)_2\text{O})]\text{Cl}$ , see Fig 5.1 in Chapter 5. The X-ray crystal structure of  $[\text{Bz}_2\text{P}(\text{C}(\text{OH})(\text{CH}_3)\text{CH}_2\text{C}(\text{CH}_3)_2\text{O})]\text{Cl}$  can be seen in Fig 5.2, Chapter 5, and Figure 1, Appendix 3. The X-ray crystallography data can be seen in Appendix 3, Table 1 to Table 5.

Figure 6.1

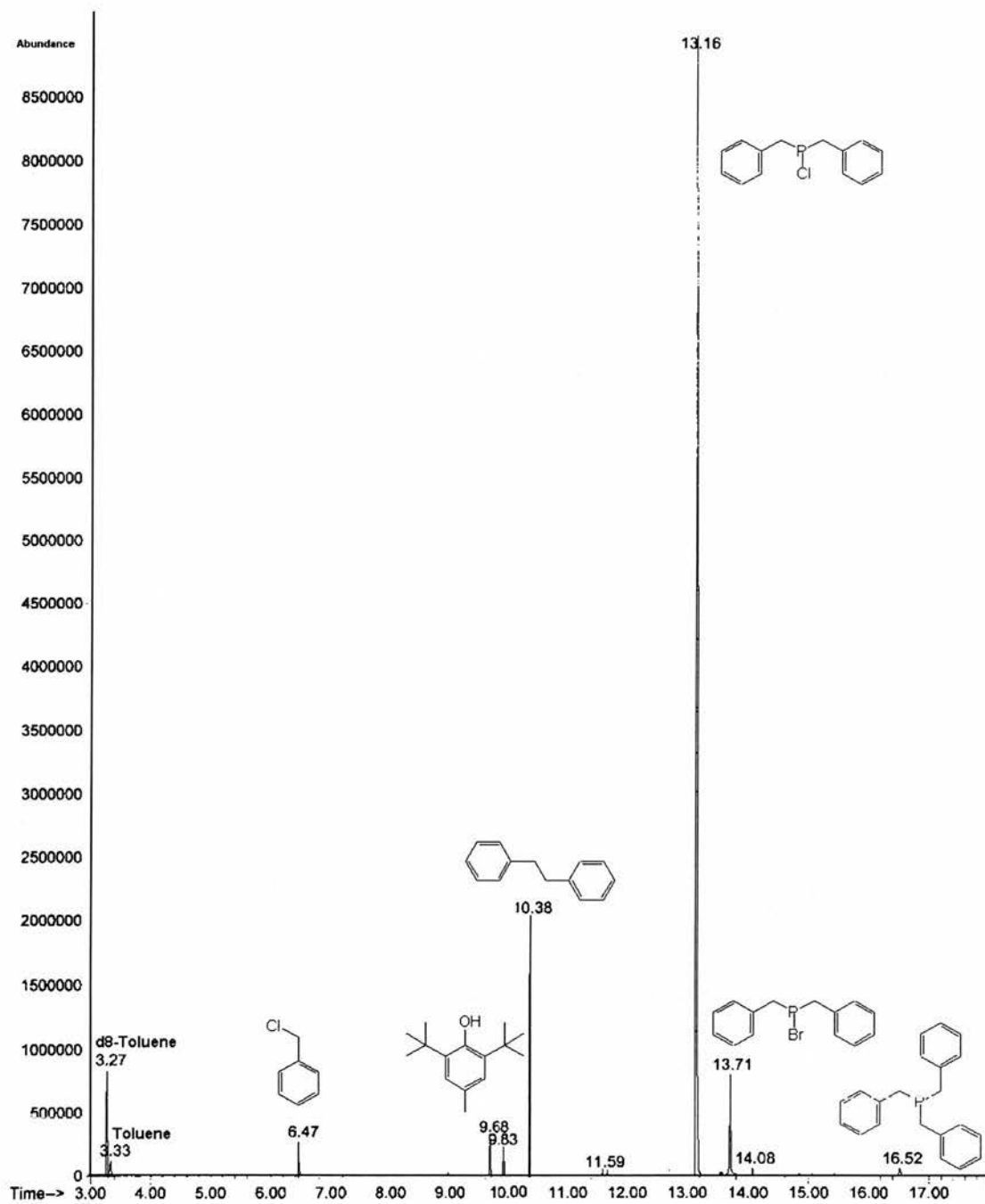
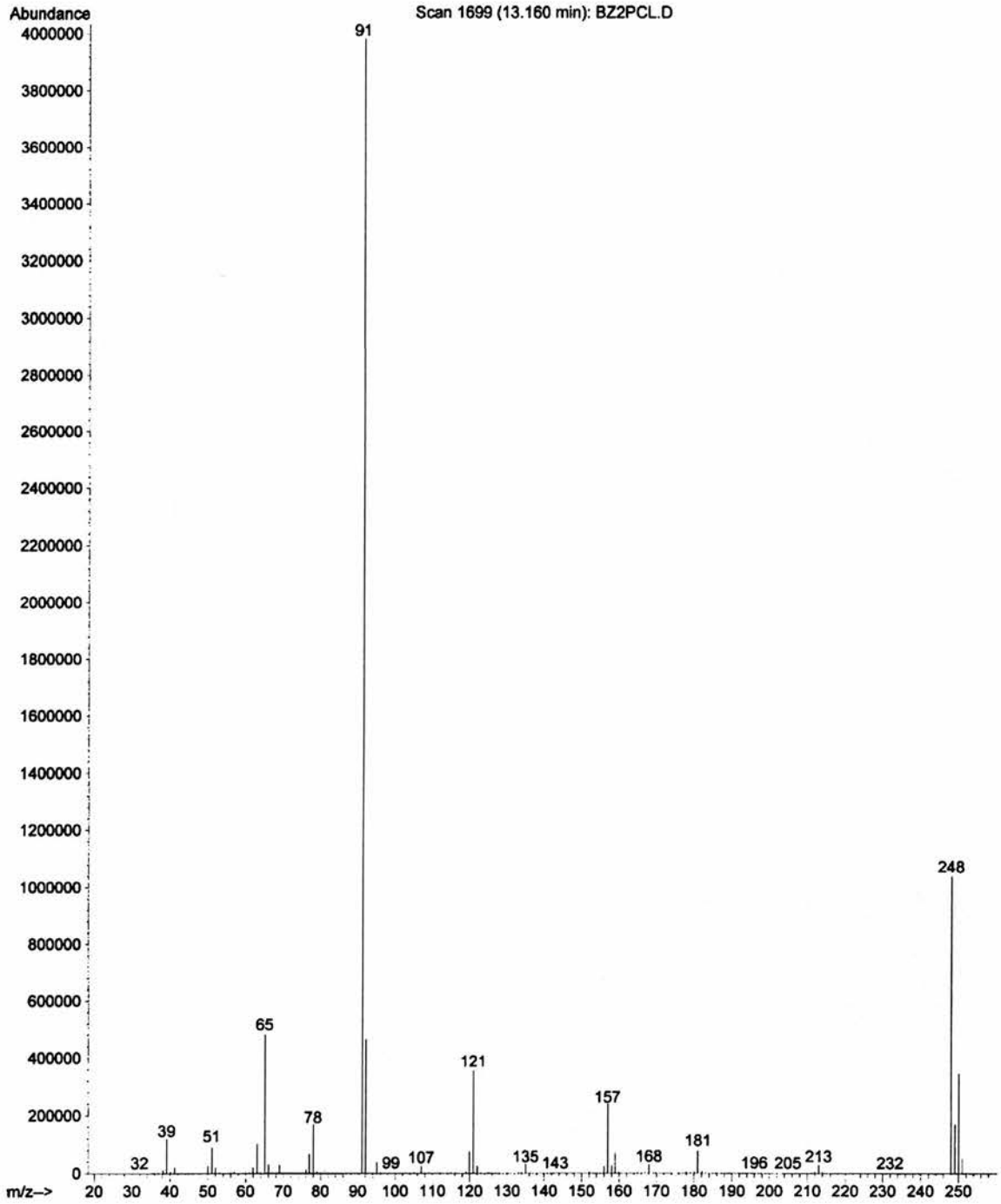
*GC of Bz<sub>2</sub>PCl in methylene chloride.*

Figure 6.2

*MS of Bz<sub>2</sub>PCL.*

## 6.3 High Pressure Nuclear Magnetic Resonance Studies.

### 6.3.1 Apparatus.

The NMR equipment is detailed in section 2.2.1 on page 63. The high pressure NMR equipment consists of a sapphire and titanium cell, a brass and aluminium housing, two brass fittings, an NMR spinner, a spiral hose, and an extendable clamp. The sapphire titanium cell has been pressure tested to 100 bar and 100 °C, although the specifications are greater than that. The brass / aluminium housing allows the cell to be pressurised, depressurised, and stored under pressure safely. The brass fittings for the housing allow the cell to be pressurised / depressurised, they can be removed so that the cell can be placed in its spinner, the spiral hose connects the cell to a conventional high pressure head / gas cylinder, and the extendable clamp allows the cell to be removed and placed in the cell safely, as well as placed in the NMR magnet.

**Figure 6.3**

*Brass and aluminium NMR tube protective case, 10 mm high pressure NMR cell and spinner.*



**Table 6.1***The properties of the sapphire tubes.*

<b>Tube</b>	<b>OD / cm</b>	<b>ID / cm</b>	<b>Bursting Pressure / bar</b>	<b>Safe Working Pressure / bar</b>
<b>5 mm</b>	0.7	0.4	621	207
<b>10 mm</b>	1.1	0.9	434	145

**6.3.2 General Procedure.**

Solutions containing the complex species (for example  $[\text{Rh}_2(\text{DIOP})_2(\text{CO})_4]$  and  $[\text{HRh}(\text{CO})_2(\text{DIOP})]$ ) to be studied were prepared as described above in section 6.2. The solutions were prepared in  $d^6$ -benzene, or  $d^8$ -toluene. The high pressure NMR cell was degassed by removing the screw top and placing in a Shlenk tube, which was then degassed in the normal manner. The solutions containing the rhodium complexes were then transferred to the NMR cell under a stream of argon. The cell was then removed under an umbrella of argon and sealed by screwing on the screw top fully.

The cell was placed in the brass aluminium housing with a brass pressurising / depressurising attachment fitted. The spiral hose was attached to the cell via the screw top, and at the other end to a cylinder or autoclave containing the desired gas mixture. The hose was then degassed three times with the gas mixture, the hose was left under a low pressure atmosphere of the desired gas mixture. The cell was then opened to the gas mixture by turning the screw top a  $\frac{3}{4}$  turn anticlockwise. The cell was then pressurised to the desired pressure. The cell was left under pressure for 1 to 12 hours. The cell was sealed by turning the screw top a  $\frac{3}{4}$  turn clockwise. The pressure in the hose was then released and the spiral hose detached from the cell. The cell was removed from its housing with the extendable clamp, this was used to remove the cell from the housing at all times when under pressure as the cell is kept behind a wall of brass within the clamp. The brass fitting which allowed pressurising and depressurising was then removed from the housing and replaced with the NMR spinner. The cell was then placed in the spinner with the clamp, and pushed down firmly to ensure the cell is tightly held in the spinner. The cell was then released from the clamp and was ready to be placed in the Bruker AM 300 NMR spectrometer.

The spin air and the gas uplift for the NMR spectrometer were turned off. The cell was removed from its housing with the extendable clamp. The bottom of the clamp was fitted to the top of the NMR spectrometer such that the cell was kept vertical. The cell was then lowered to the correct height in the NMR magnet with the extendable clamp. The cell was then released from the clamp and the clamp removed from the spectrometer. The NMR spin air was then put back on, and adjusted to spin the heavy cell. The NMR spectrum of the solution was then acquired.

### 6.3.3 High Pressure NMR Conditions.

The rhodium concentrations varied from  $0.002 \text{ mol dm}^{-3}$  (200 ppm) to  $0.04 \text{ mol dm}^{-3}$  (4000 ppm) in the 10 mm cell, and as high as  $0.2 \text{ mol dm}^{-3}$  (20000 ppm) in the 5 mm cell. The rhodium to phosphorus ratio varied from 1:1 to 1:7. The pressure in the cell varied from 20 bar to 60 bar, and the temperature varied from  $-80 \text{ }^{\circ}\text{C}$  to  $95 \text{ }^{\circ}\text{C}$ .

## 6.4 High Pressure Infrared Experiments.

The CIR FT IR equipment is detailed in section 2.2.2 on page 65. The high pressure infrared autoclave consists of a Parr high pressure vessel with a single crystal silicon rod passing through it. The autoclave allows *in situ* pressure and temperature readings, catalyst injection and pressurising / depressurising through a tap. The autoclave was stirred mechanically from above. The silicon rod bathes in the reaction solution. The apparatus lies in the infrared beam with the laser beam focussed on the pointed end of the silicon rod which protrudes out of the vessel. The optics are optimised by making small adjustments to the autoclave position relative to the beam. The infrared spectrometer is set for ATR correction. Once optimised, the beam will pass into the rod, reflect along the inside of the crystal and pass out of the other end in to the infrared detector. At the surface of the rod the solution absorbs energy from the beam and the resultant beam which emerges is deficient in the specific frequencies absorbed by the species in solution. Heating is effected by heating rods which pass into holes in the base of the Parr vessel.

### 6.4.1 General Procedure.

Solutions containing the complex species (for example  $[\text{Rh}_2(\text{DIOP})_2(\text{CO})_4]$  and  $[\text{HRh}(\text{CO})_2(\text{DIOP})]$ ) to be studied were prepared as described above in section 6.2. The autoclave was degassed by pressurising to 10 bar with argon or nitrogen, then releasing the pressure three times. Argon or nitrogen was then allowed to flow into the gassing / degassing side arm and out of the open injection port. The reaction solution was then injected into the vessel through the injection port; substrate could be injected at this point in the same manner or later when the cell was at temperature and pressure by isolating the cell from the injection port before injecting the substrate. The autoclave was then sealed. The autoclave was then pressurised to the required pressure with the required gas and tested for leaks. The autoclave was fixed into the infrared beam and the optics were optimised. The autoclave was fitted with a mechanical stirrer, and heating rods. The cell was heated to the required temperature. If required the substrate can be injected at this point by opening the valve between the injection port and the autoclave. To ensure that all the substrate was injected, the port was pressurised to a higher pressure than the autoclave. The FT IR spectrum of the solution could then be measured and saved to the hard disk of a PC. The background spectrum of the catalytic solutions under atmospheres of the same gases at identical pressures and temperatures had been previously taken in the same manner. Background spectra were then subtracted manually using the OMNIC package.

### 6.4.2 High Pressure IR Experiments.

The rhodium concentrations varied from  $0.01 \text{ mol dm}^{-3}$  (1000 ppm) to  $0.04 \text{ mol dm}^{-3}$  (4000 ppm). The rhodium to phosphorus ratio varied from 1:2 to 1:4. The pressure in the cell varied from 20 bar to 60 bar, and the temperature varied from  $25 \text{ }^\circ\text{C}$  to  $95 \text{ }^\circ\text{C}$ . The experiments were carried out in dry degassed toluene,  $10 \text{ cm}^3$  in the absence of substrate,  $9 \text{ cm}^3$  in the presence of substrate,  $1 \text{ cm}^3$ .

## 6.5 Hydroformylation with the CATS Catalyst Testing Unit

### 6.5.1 Apparatus.

A schematic of the CATS kinetic autoclave can be seen in Figure 6.4. The set-up includes an autoclave (A), an injection arm (B), a pressure controller and transducer (C), a ballast vessel (D), and a control panel (E). Each section can be isolated from the others with valves. The autoclave parts were supplied by Baskerville and assembled by the University of St. Andrews, School of Chemistry Workshop.

The reaction took place in the autoclave, which is flushed with CO and H<sub>2</sub>. The catalyst solution was injected with a gas tight syringe. The autoclave was then heated to the reaction temperature and pressurised to just below the reaction pressure. The substrate was then injected with a stream of synthesis gas which brought the autoclave to the reaction pressure. As the reaction proceeded the synthesis gas was consumed. The pressure in the autoclave, however, was kept constant by the pressure controller, the gas stream was fed by the ballast vessel which was pressurised to a value such that when the reaction was over it would still be higher than the pressure in the reaction vessel. There are gas inlets to the autoclave and ballast vessel, which allows for them to be filled with gas independently of each other. The pressures of the autoclave, ballast vessel, and injection port were monitored by pressure transducers, which were in turn controlled from the control panel.

The gas consumed by the reaction was monitored by recording the drop in pressure in the ballast vessel during the reaction period. Data were collected via a link from data logging hardware (Pico Monitor, model ADC16) which was fitted to a PC though a COM port. The computer used data logging software (PicoLog for Windows, version 5.04.2) to monitor and record the pressures. The data collected then allowed for the calculation of the rates of reaction, see Chapter 4.

**Figure 6.4**

*Schematic of the CATS kinetic autoclave.*

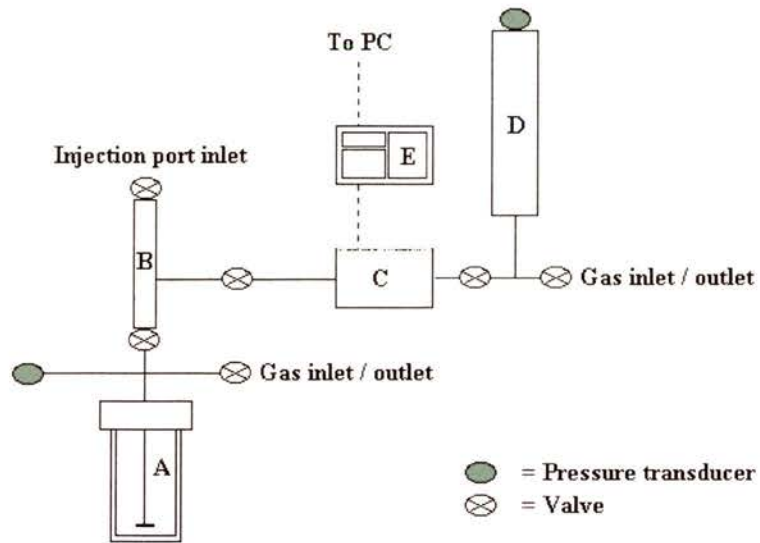
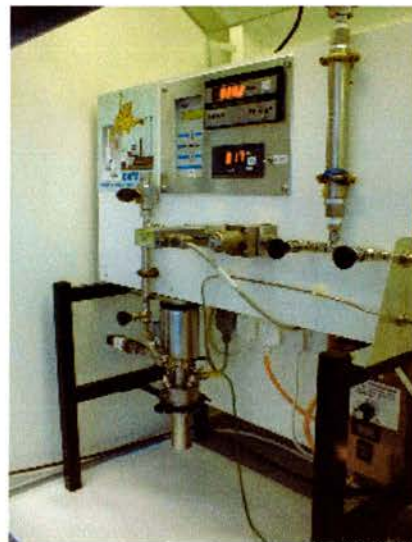


**Figure 6.5**

*A) Photograph of the CATS kinetic autoclave. B) Full set up for measuring kinetics at constant pressure.*



**(A)**



**(B)**

### 6.5.2 General Procedure.

In a typical reaction a solution of the desired phosphine ( $2 \times 10^{-5}$  mol) in dry degassed solvent, for example toluene ( $4 \text{ cm}^3$ ), was added under a stream of argon or nitrogen to  $[\text{Rh}(\text{CO})_2(\text{acac})]$  (0.0258 g,  $1 \times 10^{-5}$  mol) under an argon or nitrogen atmosphere. The resulting solution was then transferred to the CATS kinetic autoclave in a gastight syringe under a nitrogen or argon atmosphere.

The solution was flushed with two cycles of  $\text{CO} / \text{H}_2$  (1:1) and pressurized to 5 bar with synthesis gas. The autoclave was then heated to  $80^\circ\text{C}$  with stirring. Once the temperature had stabilized the pressure was increased to 9 bar. Allyl alcohol ( $1 \text{ cm}^3$ ) was then injected and the autoclave pressurized to 10 bar, the gas uptake from the ballast vessel was then monitored.

After there was no more gas uptake the autoclave was cooled and the autoclave depressurized. The resulting solution was analysed by G.C. and G.C. M.S. to determine the products of the reaction.

### 6.5.3 Reaction Conditions.

Typically  $[\text{Rh}(\text{CO})_2(\text{acac})]$ , (0.00258 g,  $1 \times 10^{-5}$  mol) was used in  $5 \text{ cm}^3$  of catalyst solution. This makes a solution of  $2 \times 10^{-3} \text{ mol dm}^{-3}$  or 200 ppm rhodium concentration. One and a half or two equivalents of DIOP (0.007478 g,  $1.5 \times 10^{-5}$  mol, and, 0.009971 g,  $2 \times 10^{-5}$  mol) were used in the experiments. Two equivalents of Et-Xantphos, <sup>t</sup>Bu-Xantphos, Et-<sup>t</sup>BuXantphos, and <sup>i</sup>Pr-Bisbite were used. This equates to  $2 \times 10^{-5}$  mol, or 0.007729 g, 0.009973 g, 0.009973 g, 0.008370 g, of each respectively. Experiments were also carried out with 0.0258 g,  $1 \times 10^{-4}$  mol of  $[\text{Rh}(\text{CO})_2(\text{acac})]$ , which makes a solution of  $2 \times 10^{-2} \text{ M}$  or 2000 ppm rhodium concentration. 2 equivalents or  $2 \times 10^{-4}$  mol, 0.07729 g of Et-Xantphos was used as ligand in the said experiments.  $2 \times 10^{-3} \text{ M}$  or 2000 ppm rhodium concentration.

The solvent used was  $4 \text{ cm}^3$  of either dry degassed toluene, ethanol, THF, MTBE, amyl alcohol, THF /  $\text{H}_2\text{O}$  (in a ratio of 7:1), or toluene / acetic acid (in a ratio of 7:1).

The gas composition was either  $\text{CO} / \text{H}_2$ , 1:1, 2:3, or 3:2. The gas pressure ranged from 10 bar to 40 bar, and the temperature ranged from  $70^\circ\text{C}$  to  $140^\circ\text{C}$ .

The substrate used was of either allyl alcohol, 1-hexene, or 1-octene ( $1 \text{ cm}^3$ ).

## 6.6 References for Chapter Six

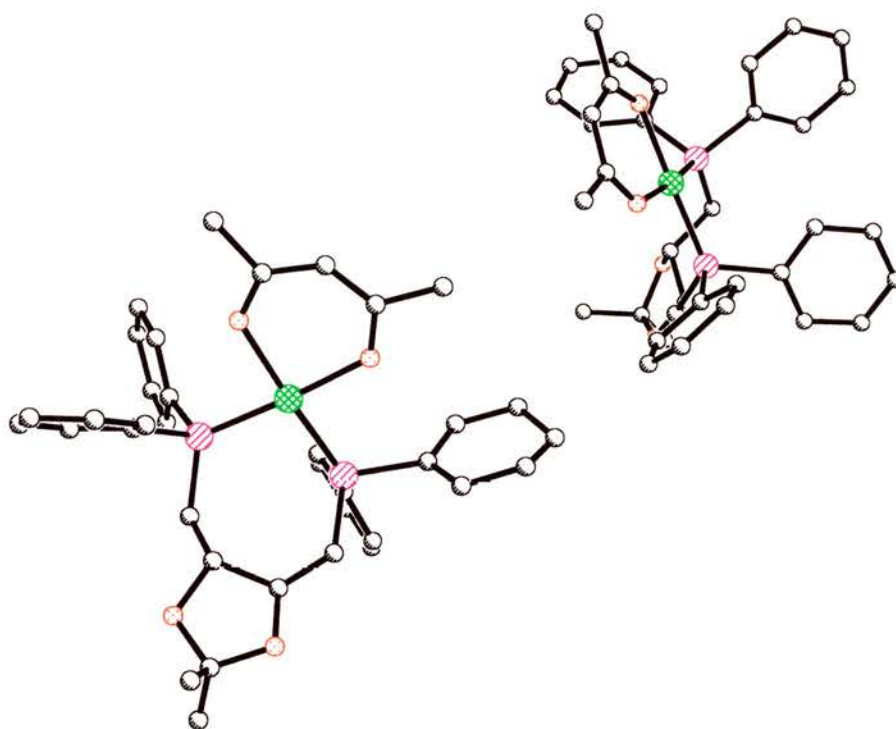
- 1 F. Bontati and G. Wilkinson, *J. Chem. Soc.*, 1964, 3156.
- 2 J. G. Leipoldt, L. D. C. Bok, S. S. Basson, J. S. van Vollenhoven, T. L. A. Gerber, *Inorg. Chim. Acta*, 1977, **25**, L63.
- 3 B. R. James, D. Mahajan, S. J. Rettig and G. M. Williams, *Organometallics*, 1983, **2**, 1452.

**APPENDIX ONE: X-RAY CRYSTALLOGRAPHY DATA FOR THE COMPLEX  
SPECIES [Rh(acac)(DIOP)].**

It can be noticed from the crystal data that the complex [Rh(acac)(DIOP)] crystallised as a pair of molecules. The X-ray crystal structure of the two molecules of [Rh(acac)(DIOP)] can be seen in Figure 1.

**Figure 1**

*X-ray crystal structure of two molecules of [Rh(acac)(DIOP)].*



The atoms of one molecule of [Rh(acac)(DIOP)] are numbered Rh(1), P(1) & P(6), O(3)-(4), & O(35)-O(37), C(2)-C(5), C(7)-C(9), and C(11)-C(39). The corresponding atoms of the second molecule of [Rh(acac)(DIOP)] are numbered in the same manner, plus 40.

It has been previously noted that the empirical formula of the complex is given as  $C_{37.5}H_{42}O_{4.5}P_2Rh$ , but the molecular formula of the given complex is  $C_{36}H_{39}O_4P_2Rh$ . The reason for this is that half a molecule of acetone co-crystallises with every molecule of [Rh(acac)(DIOP)].

Table 1.  
Crystal data and structure refinement for [Rh(acac)(DIOP)].

Identification code	dwdch2
Empirical formula	$C_{37.5}H_{42}O_{4.5}P_2Rh$
Formula weight	729.56
Temperature	293(2) K
Wavelength	0.71073 Å
Crystal system	Monoclinic
Space group	$P2_1$
Unit cell dimensions	a = 10.6780(7) Å    alpha = 90 ° b = 17.6957(10) Å    beta = 92.2980(10) ° c = 20.2971(12) Å    gamma = 90 °
Volume, z	3832.1(4) Å <sup>3</sup> , 4
Density (calculated)	1.265 Mg/m <sup>3</sup>
Absorption coefficient	0.565 mm <sup>-1</sup>
F (000)	1512
Crystal size	0.14 x 0.1 x .1 mm
θ range for data collection	1.91 to 23.19 °
Limiting indices	-11 ≤ h ≤ 10, -19 ≤ k ≤ 14, -22 ≤ l ≤ 22
Reflections collected	19222
Independent reflections	9540 (R <sub>int</sub> = 0.0595)
Absorption correction	Sadabs
Max. and mm. Transmission	1.000000 and 0.605382
Refinement method	Full-matrix least-squares on F <sup>2</sup>
Data / restraints / parameters	9487 / 1 / 828
Goodness-of-fit on F <sup>2</sup>	0.938
Final R indices [I > 2σ (I)]	R1 = 0.0564, wR2 = 0.1273
R indices (all data)	R1 = 0.0823, wR2 = 0.1530
Absolute structure parameter	-0.01(4)
Extinction coefficient	0.0000(2)
Largest diff. peak and hole	0.826 and -0.869 eÅ <sup>-3</sup>

Table 2.

Atomic coordinates [  $\times 10^4$  ] and equivalent isotropic displacement parameters [ $\text{\AA}^2 \times 10^3$ ] for 1.  $U(\text{eq})$  is defined as one third of the trace of the orthogonalized  $U_{ij}$  tensor.

	x	y	z	$U(\text{eq})$
Rh(1)	6769(1)	11489(1)	9958(1)	44(1)
P(1)	4926(3)	10967 (2)	10011(1)	55(1)
C(2)	3544(8)	11466(8)	9637(4)	60(3)
C(3)	3371(8)	11426(7)	8920(4)	52(2)
O(3)	2321(6)	11895(5)	8718(3)	77(2)
C(4)	4408(9)	11752(6)	8498(4)	54(3)
O(4)	3727(6)	11931(5)	7897(3)	66(2)
C(5)	5479(8)	11214(6)	8350(4)	51(3)
P(6)	6864(2)	11397(2)	8883 (1)	41(1)
C(7)	2476(10)	12150(8)	8061(5)	67(3)
C(8)	1606(11)	11773 (9)	7592 (5)	97 (6)
C(9)	2400(16)	12981(10)	8052(8)	133(7)
C(11)	4470(12)	10867 (10)	10875(6)	86(4)
C(12)	4979(18)	10247(10)	11231(7)	129(7)
C(13)	4761(25)	10202(14)	11915(8)	183(13)
C(14)	3834(42)	10822(28)	12197 (11)	286(27)
C(15)	3527(26)	11225(27)	11836(8)	257 (25)
C(16)	3707(13)	11399(14)	11165(7)	141(7)
C(17)	4698(11)	9994(7)	9735(5)	63 (3)
C(18)	3505(14)	9612(10)	9694(6)	102(5)
C(19)	3410(19)	8888(11)	9502(7)	108(6)
C(20)	4432(19)	8466(10)	9365(8)	109(5)
C(21)	5575(18)	8819(9)	9387(8)	115(5)
C(22)	5704(14)	9566(7)	9570(6)	79(4)
C(23)	7442(9)	12261(6)	8506(5)	55(3)
C(24)	7973 (11)	12254(7)	7892 (6)	72(4)
C(25)	8353(13)	12924(13)	7635(8)	101(5)
C(26)	8229(15)	13605(12)	7963 (10)	107 (6)
C(27)	7658(15)	13621(9)	8550(9)	96(5)
C(28)	7270(10)	12964(7)	8819(6)	67(3)
C(29)	7991(9)	10683 (6)	8609 (5)	45(3)
C(30)	7639(12)	10041(7)	8292(6)	78(4)
C(31)	8515(17)	9472(8)	8164 (8)	104(5)
C(32)	9754(17)	9579(10)	8334 (8)	102 (5)
C(33)	10095(12)	10237(9)	8646(7)	89(4)
C(34)	9220(11)	10778(8)	8797 (6)	80(4)
O(35)	6792(6)	11631(4)	10961(3)	61(2)
C(35)	7655(11)	11960(7)	11326(5)	63(3)
C(36)	8730(12)	12265(7)	11093 (6)	72(4)
O(37)	8539(7)	11993 (5)	9965(3)	69(2)
C(37)	9138(11)	12256(7)	10465(7)	70(4)
C(38)	7397(14)	11981(10)	12039(5)	113 (5)
C(39)	10391(12)	12598(11)	10324(7)	125(6)
Rh(41)	8184(1)	7054(1)	14348(1)	38(1)

## APPENDIX ONE

P(41)	6150(2)	6867(1)	14249(1)	37 (1)
C(42)	5512(9)	6233(5)	13618(5)	41(3)
C(43)	5723(8)	5380(6)	13731(5)	47(2)
0(43)	5303 (6)	4988(4)	13163 (3)	57(2)
C(44)	7034(8)	5106(5)	13852(5)	44(2)
0(44)	6922(6)	4340(4)	13645(4)	59(2)
C(45)	7535(8)	5130(5)	14564 (5)	48(3)
P(46)	8644(2)	5920(1)	14708(1)	39(1)
C(47)	6006(11)	4313(6)	13103(6)	60(3)
C(48)	5245(13)	3623(7)	13167 (8)	106(5)
C(49)	6675(13)	4362(9)	12462(6)	99(5)
C(51)	5378(8)	7760(5)	14046(5)	40(2)
C(52)	5353(9)	8320(6)	14530(5)	50(3)
C(53)	4962(9)	9035(6)	14345(6)	62(3)
C(54)	4560(10)	9209(7)	13711(7)	67 (3)
C(55)	4545 (10)	8648(7)	13254(7)	70(3)
C(56)	4977(10)	7952(6)	13404(5)	55(3)
C(57)	5314(8)	6596(5)	14990(4)	38(2)
C(58)	4094(9)	6310(6)	14955(5)	53(3)
C(59)	3513(11)	6129(6)	15543(6)	70(3)
C(60)	4092(12)	6259(7)	16139(6)	77(4)
C(61)	5287(12)	6574(8)	16170(5)	73(3)
C(62)	5914(10)	6730(6)	15595(4)	57(3)
C(63)	10074(9)	5541(5)	14353(4)	38(2)
C(64)	10784(9)	4997 (7)	14688(5)	60(3)
C(65)	11856(11)	4695(8)	14411(7)	78(4)
C(66)	12192(11)	4956(8)	13816(8)	72(4)
C(67)	11544(13)	5470(8)	13489(7)	85(4)
C(68)	10459(10)	5783 (6)	13770(5)	61(3)
C(69)	9039 (9)	5868(5)	15588(5)	47(3)
C(70)	8365(10)	5446(6)	16037(5)	59(3)
C(71)	8722(14)	5492(8)	16720(6)	79(4)
C(72)	9736(15)	5947 (10)	16931(6)	85(4)
C(73)	10380(11)	6327 (7)	16479(5)	66(3)
C(74)	10044(10)	6299(6)	15816(5)	54(3)
0(75)	7907(6)	8105(4)	13948(3)	57(2)
C(75)	8731(10)	8608(6)	13832(5)	52(3)
C(76)	10038(9)	8517 (6)	13992(5)	52(3)
0(77)	10085(6)	7309(4)	14468(3)	54(2)
C(77)	10594 (10)	7925(7)	14302 (5)	53(3)
C(78)	8239(11)	9330(6)	13518(6)	72(3)
C(79)	12007(9)	7951(7)	14469(6)	78(4)
C(81)	10314(18)	8365(11)	16375(13)	133(10)
C(82)	9461(17)	8067 (8)	16846(9)	68(5)
0(82)	9756(16)	7950(8)	17410(7)	136(6)
C(83)	8254(15)	7866(9)	16557(9)	81(5)
C(91)	10468 (51)	10318(30)	10659(24)	83 (15)
C(92)	9651(30)	10142(18)	11109(15)	23(7)
0(92)	9281(44)	10003 (25)	11535(23)	124(14)
C(93)	8644(60)	9644(34)	10544(28)	104(19)

Table 3.  
Bond lengths [Å] and angles [°] for [Rh(acac)(DIOP)].

Rh(1) -O(35)	2.051(7)	Rh(1) -O(37)	2.090(7)
Rh(1) -P(1)	2.181(3)	Rh(1) -P(6)	2.195(2)
P(1) -C(17)	1.824(13)	P(1) -C(11)	1.847(12)
P(1) -C(2)	1.855(10)	C(2) -C(3)	1.463(11)
C(3) -O(3)	1.441(11)	C(3) -C(4)	1.538(13)
O(3) -C(7)	1.423(12)	C(4) -O(4)	1.432(10)
C(4) -C(5)	1.528(13)	O(4) -C(7)	1.442(12)
C(5) -P(6)	1.826(9)	P(6) -C(23)	1.827(11)
P(6) -C(29)	1.847(10)	C(7) -C(8)	1.46(2)
C(7) -C(9)	1.47(2)	C(11) -C(16)	1.39(2)
C(11) -C(12)	1.41(2)	C(12) -C(13)	1.42(2)
C(13) -C(14)	1.60(6)	C(14) -C(15)	1.07(7)
C(15) -C(16)	1.42(2)	C(17) -C(22)	1.37(2)
C(17) -C(18)	1.44(2)	C(18) -C(19)	1.34(2)
C(19) -C(20)	1.36(2)	C(20) -C(21)	1.37(2)
C(21) -C(22)	1.38(2)	C(23) -C(24)	1.391(14)
C(23) -C(28)	1.41(2)	C(24) -C(25)	1.36(2)
C(25) -C(26)	1.38(2)	C(26) -C(27)	1.36(2)
C(27) -C(28)	1.36(2)	C(29) -C(30)	1.35(2)
C(29) -C(34)	1.362(14)	C(30) -C(31)	1.41(2)
C(31) -C(32)	1.37(2)	C(32) -C(33)	1.37(2)
C(33) -C(34)	1.38(2)	O(35) -C(35)	1.298(12)
C(35) -C(36)	1.37(2)	C(35) -C(38)	1.483(14)
C(36) -C(37)	1.36(2)	O(37) -C(37)	1.266(12)
C(37) -C(39)	1.51(2)	Rh(41) -O(75)	2.047(7)
Rh(41) -O(77)	2.084(7)	Rh(41) -P(46)	2.185(3)
Rh(41) -P(41)	2.197(3)	P(41) -C(42)	1.815(9)
P(41) -C(51)	1.821(10)	P(41) -C(57)	1.844(8)
C(42) -C(43)	1.542(13)	C(43) -O(43)	1.402(10)
C(43) -C(44)	1.492(12)	O(43) -C(47)	1.418(12)
C(44) -O(44)	1.423(11)	C(44) -C(45)	1.521(13)
O(44) -C(47)	1.443(12)	C(45) -P(46)	1.847(9)
P(46) -C(69)	1.821(9)	P(46) -C(63)	1.841(10)
C(47) -C(48)	1.47(2)	C(47) -C(49)	1.51(2)
C(51) -C(52)	1.397(13)	C(51) -C(56)	1.398(13)
C(52) -C(53)	1.379(14)	C(53) -C(54)	1.375(14)
C(54) -C(55)	1.36(2)	C(55) -C(56)	1.35(2)
C(57) -C(62)	1.382(12)	C(57) -C(58)	1.396(12)
C(58) -C(59)	1.404(13)	C(59) -C(60)	1.36(2)
C(60) -C(61)	1.39(2)	C(61) -C(62)	1.397(13)
C(63) -C(68)	1.338(13)	C(63) -C(64)	1.386(14)
C(64) -C(65)	1.40(2)	C(65) -C(66)	1.35(2)
C(66) -C(67)	1.31(2)	C(67) -C(68)	1.42(2)
C(69) -C(74)	1.381(14)	C(69) -C(70)	1.401(13)
C(70) -C(71)	1.42(2)	C(71) -C(72)	1.40(2)
C(72) -C(73)	1.35(2)	C(73) -C(74)	1.380(13)
O(75) -C(75)	1.279(11)	C(75) -C(76)	1.430(14)

## APPENDIX ONE

C(75) -C (78)	1.514(14)	C(76) -C(77)	1.347(14)
0(77)-C (77)	1.270(11)	C(77) -C (79)	1.533(14)
C(81) -C(82)	1.45(3)	C(82) -0(82)	1.19(2)
C(82) -C(83)	1.44(2)	C(91) -C(92)	1.33(6)
C(92) -0(92)	1.00(5)	C(92) -C(93)	1.77(7)
0(35) -Rh(1) -0(37)	88.1(3)	0(35) -Rh(1) -P(1)	88.7(2)
0(37) -Rh(1) -P(1)	176.8(2)	0(35) -Rh(1) -P(6)	175.6(2)
0(37) -Rh(1) -P (6)	87.7(2)	P(1) -Rh(1) -P(6)	95.50(10)
C(17) -P(1) -C(11)	99.5(6)	C(17) -P(1) -C(2)	103.3(6)
C(11) -P(1) -C(2)	101.4(6)	C(17) -P(1) -Rh(1)	119.6(4)
C(11) -P (1) -Rh(1)	111.1(4)	C(2) -P(1) -Rh(1)	118.9(4)
C(3) -C(2) -P (1)	116.8(7)	0(3) -Co) -C(2)	108.8(8)
0(3) -C(3) -C (4)	101.2(8)	0(2) -C(3) -C (4)	118.0(8)
C(7) -0(3) -C(3)	109.3(7)	0(4)-C (4) -C(S)	109.1(7)
0(4)-C (4) -C(3)	101.8(7)	C(6) -C (4) -0(3)	115.9(9)
C(4) -0(4)-C (7)	107.8(7)	C(4) -C(6)-P(S)	111.6(7)
C(23) -P(6)-C(6)	100.3(5)	C(23) -P(6) -0(29)	102.2(5)
C(5)-P(6) -C(29)	102.8(5)	C(23) -P(6) -Rh(1)	112.6(4)
C(5)-P(6) -Rh(1)	122.2(3)	C(29) -P(6) -Rh(1)	114.0(3)
0(3)-C (7) -0(4)	106.0(8)	0(3) -0(7)-C(6)	111.8(11)
0(4) -C(7) -C(8)	107.3(10)	0(3)-C (7) -C(9)	108.6(11)
0(4) -C(7) -C(9)	108.4(11)	C(S) -0(7) -0(9)	114.4(12)
C(16) -C(11) -C(12)	121.9(14)	0(16) -C(11) -P(1)	121.2(13)
C(12) -C(11) -P (1)	116.8(13)	0(11) -C(12) -0(13)	118(2)
0(12) -0(13) -C(14)	116(2)	C(15) -0(14) -C(13)	113(3)
0(14) -0(15) -C(16)	139(5)	C(11) -0(16) -0(15)	111(2)
C(22) -C(17) -C(18)	115.4(13)	0(22) -C(17) -P(1)	120.1(9)
C(18) -C(17) -P(1)	124.5(12)	0(19) -C(18) -C(17)	121(2)
0(18) -C(19) -C (20)	122(2)	0(19) -C(20) -C(21)	118(2)
C(22) -0(21) -C(20)	122(2)	C(17) -C(22) -C (21)	121.7(14)
C(24) -C(23) -C(28)	118.4(10)	0(24)-C (23) -P(6)	121.6(9)
0(28) -C(23) -P(6)	119.8(8)	C(25) -C(24) -0(23)	118.3(13)
C(24) -C(25) -C(26)	122(2)	C(27) -0(26) -C (25)	120(2)
C(28) -C (27) -C (26)	119(2)	C(27) -0 (28) -0(23)	121.9(13)
0(30) -C(29) -C(34)	119.0(11)	C(30) -C(29) -P(6)	123.1(8)
C(34) -C(29) -P(6)	117.5(9)	C(29) -C(30) -0(31)	121.0(13)
C(32) -0(31) -0(30)	119.9(14)	0(33) -0(32) -0(31)	118.2(13)
0(32) -C(33) -C(34)	121.5(14)	0(29) -C(34) 0(33)	120.3(13)
C(35) -0(35) -Rh(1)	127.0(7)	0(35) -C(35) -0(36)	124.4(9)
0(35) -C(35) -C(38)	114.4(11)	C(36) -C(35) -C(38)	121.2(11)
0(37) -C(35) -C(35)	128.5(11)	C(37) -0(37) -Rh(1)	126.2(7)
0(37) -C(37) -0(36)	125.7(11)	0(37) -C(37) -C(39)	114.9(11)
0(36) -C(37) -0(39)	119.4(11)	0(75) -Rh(41) -0(77)	88.5(3)
0(75) -Rh(41) -P (46)	174.0(2)	0(77) -Rh(41) -P (46)	87.4(2)
0(75) -Rh(41) -P (41)	88.5(2)	0(77) -Rh(41) -P (41)	175.8(2)
P(46) -Rh(41) -P (41)	95.80(9)	0(42)-P (41) -0(51)	102.9(4)
C(42) -P (41) -0(57)	103.6(4)	0(51)-P (41) -0(57)	100.4(4)
C(42) -P (41) -Rh (41)	119.9(3)	0(51)-P (41) -Rh(41)	109.1(3)
0(57)-P (41) -Rh(41)	118.3(3)	0(43)-C (42) -P (41)	116.9(7)

## APPENDIX ONE

0(43)-C (43) -0(44)	104.0(7)	0(43) -0(43) -0(42)	108.9(8)
C(44) -C (43) -C (42)	118.2(8)	0(43) -0(43)-C (47)	109.6(8)
0(44)-C (44) -C (43)	101.2(7)	0(44)-C (44) -C (45)	109.3(8)
0(43)-C (44) -C (45)	116.1(8)	0(44) -0(44)-C (47)	107.6(7)
C(44) -C(45) -P (46)	111.8(5)	0(69)-P (46) -0(63)	101.7(4)
0(69)-P (46) -C (45)	103.9(5)	0(63)-P (46) -0(45)	101.5(4)
C(69) -P (46) -Rh(41)	114.4(3)	0(63)-P (46) -Rh(41)	112.5(3)
C(45) -P (46) -Rh(41)	120.5(3)	0(43) -0(47) -0(44)	104.5(7)
0(43)-C (47) -C (48)	113.2(10)	0(44) -0(47) -0(48)	108.6(10)
0(43)-C (47) -C (49)	107.2(10)	0(44)-C (47) -0 (49)	108.9(9)
C(48) -C (47) -0(49)	113.9(11)	0(52) -0(51) -0(56)	118.0(9)
C(52) -0(51)-P (41)	118.5(7)	0(56) -0(51)-P (41)	122.7(8)
C(53) -C(52) -C(51)	118.2(10)	0(54)0(53) -0(52)	122.8(11)
C(55) -C(54) -C(53)	118.0(11)	0(56) -0(55) -0(54)	121.3(12)
C(55) -0(56) -C(51)	121.5(11)	0(62) -0(57)0(58)	120.4(8)
C(52) -C(57) -P (41)	117.2(7)	0(58) -0(57)-P (41)	122.3(7)
0(57) -C(58) -0(59)	118.9(9)	0(60) -0(59) -0(58)	121.2(11)
C(59) -0(60) -C(S1)	119.5(10)	0(60) -0(61) -0(62)	120.7(10)
C(57) -C(62) -C(S1)	119.2(10)	0(68) -0(63) -0(64)	118.4(10)
C(58) -C(53) -P(45)	121.2(8)	0(64) -0(63)-P (46)	120.5(7)
C(53) -0(64) -C(55)	120.5(11)	0(66) -0(65) -0(64)	118.5(12)
0(67) -C(66) -0(65)	122.4(12)	0(66) -0(67) -0(68)	119.4(11)
C(53) -0(68) -C(57)	120.9(11)	0(74) -0(69) -0(70)	119.3(9)
C(74) -C(59) -P (46)	116.6(8)	0(70) -0(69)-P (46)	124.1(8)
C(59) -C (70) -C (71)	118.6(11)	0(72) -0(71) -0(70)	120.3(12)
C(73) -0 (72) -0(71)	119.1(12)	0(72) -0(73)-C (74)	121.8(12)
0(69)-C (74) -0(73)	121.0(11)	0(75) -0(75) -Rh(41)	128.0(7)
0(75)-C (75) -C (76)	123.5(9)	0(75) -0(75)-C (78)	115.8(9)
0(76) -0(75) -0(78)	120.7(9)	0(77) -0(76)-C (75)	127.0(10)
0(77) -0(77) -Rh(41)	125.5(6)	0(77)-C (77) -0(76)	127.3(10)
0(77)-C (77) -0(79)	113.3(10)	0(76) -0(77) -0(79)	119.4(10)
0(82) -0(82) -0(83)	123(2)	0(82) -0(82) -0(81)	123(2)
0(83) -0(82) -0(81)	114(2)	0(92) -0(92) -0(91)	162(5)
0(92) -0(92) -0(93)	101(4)	0(91) -0(92) -0(93)	94(3)

Symmetry transformations used to generate equivalent atoms.

Table 4.

Anisotropic displacement parameters [  $\text{\AA}^2 \times 10^3$  ] for [Rh(acac)(DIOP)]. The anisotropic displacement factor exponent takes the form:  $-2\pi^2 [(ha^*)^2 U_{11} + \dots + hka^*b^*U_{12}]$ .

	U11	U22	U33	U23	U13	U12
Rh(1)	37 (1)	53(1)	43 (1)	0(1)	-2 (1)	-6(1)
P(1)	50(2)	77(2)	38(1)	2 (1)	4(1)	-17(2)
C(2)	35(6)	99(8)	46(5)	-4(6)	17 (4)	-1(6)
C(3)	40(6)	79(7)	36(5)	7(6)	1(4)	2 (6)
O(3)	34(4)	129(8)	67 (5)	7 (5)	6(3)	18(4)
C(4)	42(7)	81(9)	39(5)	-10(5)	0(5)	0(5)
O(4)	43(4)	111(6)	45(4)	14(4)	4(3)	8(4)
C(5)	29(6)	76(8)	48(6)	2 (5)	5(5)	-3 (5)
P(6)	32 (1)	50(2)	42(1)	-1(1)	7 (1)	-2(1)
C(7)	47(7)	90(10)	64(7)	12(7)	3 (5)	17(7)
C(S)	44(8)	177(18)	69(8)	-7 (8)	-5(6)	16(7)
C(9)	129(16)	126(16)	147 (15)	36(12)	53(12)	50(12)
C(11)	63 (9)	130(13)	65(8)	10(9)	5(7)	-50(9)
C(12)	188(20)	119(15)	78(10)	39(10)	3 (10)	-40(13)
C(13)	267 (31)	217(25)	59(11)	78(13)	-51(14)	-150(22)
C(14)	326(42)	475 (56)	66(16)	-95(27)	114(24)	-298(41)
C(15)	138(19)	597 (75)	39(11)	-100(23)	52(13)	-123(32)
C(16)	53 (9)	282(23)	89(11)	-60(14)	9(8)	18(13)
C(17)	56(8)	83(9)	50(6)	21(6)	-9(6)	-23 (7)
C(18)	85(11)	133 (15)	86(9)	37 (9)	-16(8)	-58(10)
C(19)	134(17)	87(13)	101(12)	5(9)	-21(11)	-75(12)
C(20)	112(15)	76(12)	141(15)	-15(10)	6(12)	-37 (11)
C(21)	140(17)	66(12)	139(14)	20(10)	16(12)	4(11)
C(22)	86(11)	57(9)	96(10)	-2(7)	2 (8)	-24(7)
C(23)	31(6)	74(10)	60(6)	12(6)	7 (5)	-2 (5)
C(24)	60(8)	88(11)	70(7)	26(7)	24(6)	3 (6)
C(25)	55(9)	161(17)	87(11)	54(12)	11(7)	7 (10)
C(26)	71(11)	127(17)	120(15)	46(12)	-20(10)	-32 (11)
C(27)	94(12)	77 (11)	114(12)	9(9)	-24(10)	-24(9)
C(28)	52(8)	55(8)	93(9)	14(7)	1(6)	-8(6)
C(29)	27 (6)	58(8)	51(6)	-2(5)	5(5)	10(5)
C(30)	50(8)	75(10)	109(10)	-26(8)	17(7)	13(7)
C(31)	104(14)	80(11)	131(13)	-28(9)	41(11)	7(10)
C(32)	85(13)	94(13)	129(13)	-8(10)	33(10)	35(10)
C(33)	55(9)	86(11)	124(11)	0(9)	11(8)	18(8)
C(34)	53(9)	100(11)	88(9)	-21(8)	9(7)	3(7)
O(35)	48(4)	72(6)	61(4)	-4(4)	-11(4)	-6(4)
C(35)	61(8)	79(9)	47(6)	0(6)	-17 (6)	18(7)
C(36)	58(8)	85(11)	69(8)	-4(7)	-30(7)	-2 (6)
O(37)	48(4)	91(6)	68(4)	-17 (5)	1(4)	-26(5)
C(37)	57 (8)	70(10)	83(9)	-5(7)	-13(7)	-9(6)
C(38)	126(13)	152(14)	59(8)	-29(9)	-8(7)	-1(12)
C(39)	44(9)	215(19)	117 (12)	-33(12)	13(8)	-51(10)
Rh(41)	23 (1)	38(1)	55(1)	5(1)	2 (1)	-2 (1)

## APPENDIX ONE

P(41)	28(1)	40(2)	44(1)	1(1)	3 (1)	-2 (1)
C(42)	35(6)	38(7)	51(6)	1(4)	11(5)	-3(4)
C(43)	29(6)	53(7)	58(6)	-11(5)	6(5)	-9(5)
0(43)	37(4)	58(5)	75(5)	-24(4)	-6(4)	-6(4)
C(44)	19(5)	50(7)	63(6)	-8(5)	13(5)	-2(4)
0(44)	41(4)	36(4)	101(6 )	-19(4)	10(4)	7(3)
C(45)	23 (5)	43(6)	78(7)	10(5)	12(5)	-6(4)
P(46)	25(1)	42(2)	50(1)	6(1)	4 (1)	2 (1)
C(47)	56(8)	37(7)	87 (8)	-22(6)	7(7)	-5(6)
C(48)	73 (10)	51(9)	193(16)	-22(9)	-6(10)	0(7)
C(49)	81(11)	132(13)	85(9)	-28(8)	26(8)	7 (9)
C(51)	18(5)	49(7)	53(6)	4(5)	7(4)	-7(4)
C(52)	39(6)	38(7)	72(7)	-4(6)	3 (5)	6(5)
C(53)	32(7)	60(9)	96(10)	-9(7)	11(6)	3 (5)
C(54)	35(7)	48(8)	120(11)	18(8)	15(7)	7 (5)
C(55)	53 (8)	56(9)	101(10)	34(8)	-3(7)	4(6)
c(56)	50(7)	45(7)	72(8)	10(6)	14(6)	-9(5)
C(57)	18(5)	44(6)	54(6)	-1(5)	13 (4)	-6(4)
c(58)	36(6)	73 (8)	51(6)	-8(5)	11(5)	-5(5)
C(59)	43(7)	72(9)	96(9)	-5(7)	24(7)	-9(5)
C(60)	60(9)	104(11)	70(8)	19(7)	29(7)	4(7)
C(61)	77(9)	94(10)	48(6)	-4(7)	4(6)	15(8)
C(62)	34(6)	94(10)	45(6)	-12 (5)	10(5)	-11(5)
C(63)	31(6)	46(6)	38(5)	0(5)	6(4)	-8(5)
C(64)	33(7)	83(9)	63(7)	-15(6)	2 (5)	11(6)
C(65)	36(8)	91(10)	106(11)	-19(8)	-15(7)	3(6)
C(66)	34(7)	71(9)	111(11)	-27 (8)	17(7)	-4(6)
C(67)	79(10)	82(10)	99(10)	0(8)	67 (8)	-8(8)
C(68)	49(7)	64(8)	72(7)	6(6)	17(6)	3 (6)
C(69)	49(7)	34(6)	60(6)	0(5)	9(5)	24 (5)
C(70)	37(7)	80(8)	61(7)	14(6)	13(5)	8(6)
C(71)	98(12)	91(11)	49(8)	32(7)	20(7)	41(9)
C(72)	91(12)	116(12)	48(7)	1(8)	-1(8)	54(10)
C(73)	76(9)	73(9)	47(6)	-13(6)	-13 (6)	14(7)
C(74)	58(7)	50(8)	54(6)	-6(5)	0(5)	7(6)
0(75)	34(4)	53 (5)	84(5)	6(4)	-5(4)	-8(4)
C(75)	59(8)	41(7)	57(6)	-2(5)	-1(5)	-12 (6)
C(76)	30(6)	52(7)	76(8)	8(6)	23(6)	-2 (5)
0(77)	24(4)	53(6)	86(5)	5(4)	0(3)	-3(3)
C(77)	42(7)	50(7)	68(7)	2(6)	24(6)	-2(6)
C(78)	65(8)	40(7)	112(10)	25(6)	4(7)	-20(6)
C(79)	20(6)	79(9)	134(11)	21(8)	-3 (6)	-6(5)
C(81)	65(14)	80(15)	251(28)	60(17)	-26(16)	-26(11)
C(82)	87(14)	30(9)	83(12)	7 (8)	-37 (10)	21(8)
0(82)	201(17)	99(11)	104(10)	-33(8)	-52(11)	69(11)
C(83)	48(11)	68(12)	128(15)	20(10)	17(10)	11(8)

Table 5.  
Hydrogen coordinates ( $\times 10^4$ ) and isotropic displacement parameters ( $\text{Å}^2 \times 10^3$ ) for  
[Rh(acac)(DIOP)].

	x	y	z	U(eq)
H(2A)	2799(8)	11263(8)	9830(4)	72
H(2B)	3603(8)	11994(8)	9762(4)	72
H(3A)	3200(8)	10902(7)	8787(4)	62
H(4A)	4745(9)	12216(6)	8702(4)	65
H(5A)	5694 (8)	11272(6)	7893(4)	61
H(5B)	5206(8)	10697(6)	8412(4)	61
H(8A)	1736(11)	11958(9)	7155(5)	145
H(83)	760(11)	11877 (9)	7707 (5)	145
H(8C)	1750(11)	11238(9)	7605(5)	145
H(9A)	2503(16)	13160(10)	7611(8)	199
H(9B)	3050(16)	13187(10)	8339(8)	199
H(9C)	1598(16)	13137(10)	8199(8)	199
H(12A)	5444(18)	9879(10)	11024(7)	154
H(13A)	5136(25)	9833(14)	12184(8)	219
H(14A)	3589(42)	10829(28)	12632 (11)	344
H(15A)	2974(26)	11566(27)	12016(8)	308
H(16A)	3359(13)	11816(14)	10947(7)	170
H(18A)	2786(14)	9873(10)	9803 (6)	122
H(19A)	2620(19)	8668(11)	9462(7)	130
H(20A)	4358(19)	7956(10)	9260(8)	131
H(21A)	6282 (18)	8548(9)	9275(8)	138
H(22A)	6497 (14)	9785(7)	9581(6)	95
H(24A)	8068(11)	11804(7)	7663(6)	87
H(25A)	8707(13)	12924(13)	7224(8)	121
H(26A)	8535(15)	14048(12)	7783 (10)	128
H(27A)	7536(15)	14078(9)	8765(9)	115
H(28A)	6879(10)	12977(7)	9220(6)	80
H(30A)	6804(12)	9975(7)	8156(6)	93
H(31A)	8252(17)	9024(8)	7964(8)	125
H(32A)	10348(17)	9214(10)	8240(8)	122
H(33A)	10936(12)	10321(9)	8759(7)	106
H(34A)	9471(11)	11210(8)	9028(6)	96
H(36A)	9250(12)	12511(7)	11403(6)	86
H(38A)	6607(14)	11743 (10)	12109(5)	169
H(38B)	7369(14)	12497 (10)	12184 (5)	169
H(38C)	8050(14)	11718(10)	12284(5)	169
H(39A)	10544(12)	12548(11)	9864(7)	188
H(39B)	11038(12)	12341(11)	10579(7)	188
H(39C)	10391(12)	13124(11)	10442(7)	188
H(42A)	4617(9)	6321(5)	13571(5)	50
H(42B)	5871(9)	6368(5)	13203 (5)	50
H(43A)	5222(8)	5219(6)	14099(5)	56
H(44A)	7602(8)	5378(5)	13568(5)	53
H(45A)	7955(8)	4657 (5)	14670(5)	58

## APPENDIX ONE

H(45B)	6840(8)	5185(5)	14853(5)	58
H(48A)	5769(13)	3186(7)	13122(8)	159
H(48B)	4591(13)	3617(7)	12829(8)	159
H(48C)	4882(13)	3616(7)	13592(8)	159
H(49A)	7163(13)	3913(9)	12405(6)	148
H(49B)	7218(13)	4795(9)	12473(6)	148
H(49C)	6070(13)	4410(9)	12102(6)	148
H(52A)	5593 (9)	8214(6)	14966(5)	59
H(53A)	4971(9)	9414(6)	14662(6)	75
H(54A)	4307 (10)	9697(7)	13599(7)	81
H(55A)	4228(10)	8746(7)	12829(7)	84
H(56A)	5010(10)	7590(6)	13072 (5)	66
H(58A)	3674(9)	6241(6)	14550(5)	64
H(59A)	2717(11)	5916(6)	15523(6)	84
H(60A)	3694(12)	6139(7)	16525(6)	93
H(61A)	5672(12)	6682(8)	16578(5)	87
H(62A)	6726 (10)	6921(6)	15618(4)	69
H(64A)	10548(9)	4832(7)	15100(5)	71
H(65A)	12326(11)	4323 (8)	14630(7)	93
H(66A)	12910(11)	4763(8)	13633 (8)	86
H(67A)	11789(13)	5630(8)	13078(7)	102
H(68A)	10011(10)	6161(6)	13546(5)	74
H(70A)	7698(10)	5142(6)	15893 (5)	71
H(71A)	8282(14)	5220(8)	17026(6)	95
H(72A)	9961(15)	5987(10)	17377(6)	102
H(73A)	11070 (11)	6615(7)	16618(5)	79
H(74A)	10502(10)	6575(6)	15518(5)	65
H(76A)	10561(9)	8908(6)	13869(5)	63
H(78A)	7347 (11)	9293(6)	13445(6)	108
H(78B)	8626(11)	9407(6)	13104(6)	108
H(78C)	8432 (11)	9749(6)	13805(6)	108
H(79A)	12261(9)	7492(7)	14687(6)	116
H(793)	12191(9)	8373(7)	14754(6)	116
H (79C)	12452(9)	8006(7)	14070(6)	116
H(81A)	11099(18)	8486(11)	16597(13)	199
H(81B)	9961(18)	8812(11)	16175(13)	199
H(81C)	10448(18)	7993(11)	16041(13)	199
H(83A)	7733(15)	7673(9)	16893 (9)	122
II(83B)	8356(15)	7487(9)	16225(9)	122
H(83C)	7868(15)	8306(9)	16360(9)	122

**APPENDIX TWO: X-RAY CRYSTALLOGRAPHY DATA FOR THE COMPLEX  
SPECIES  $[\text{Rh}_2(\text{CO})_4(\text{Et-Xantphos})_2]$ .**

The X-ray crystal structure of  $[\text{Rh}_2(\text{CO})_4(\text{Et-Xantphos})_2]$  can be seen in Figure 1. The Crystallography data for the molecule can be seen in Table 1 to Table 5, Appendix 2.

**Figure 1**

*X-ray crystal structure of  $[\text{Rh}_2(\text{CO})_4(\text{Et-Xantphos})_2]$ .*

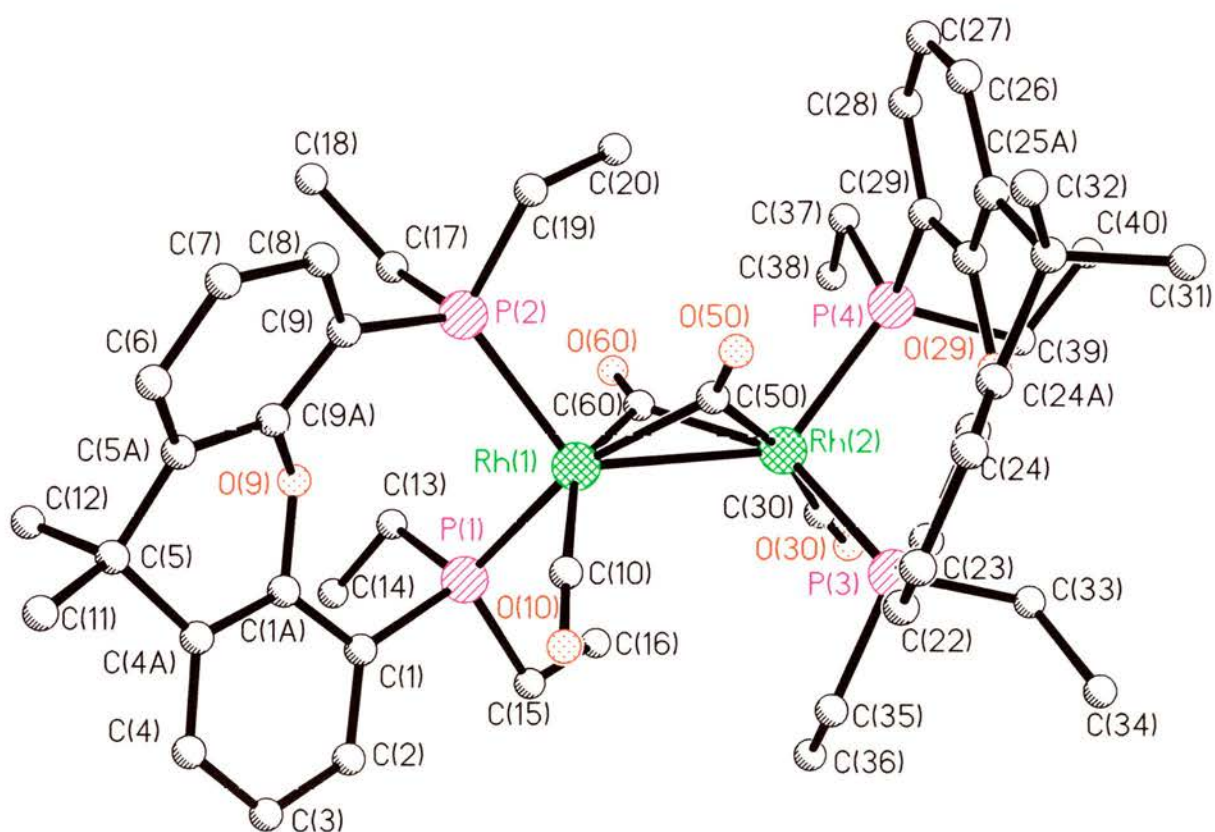


Table 1. Crystal data and structure refinement for  $[\text{Rh}_2(\text{CO})_4(\text{Et-Xantphos})_2]$ .

Identification code	Dwdchl
Empirical formula	$\text{C}_{50}\text{H}_{64}\text{O}_6\text{P}_4\text{Rh}_2$
Formula weight	1090.71
Temperature	293(2) K
Wavelength	0.71073 Å
Crystal system	Triclinic
Space group	P1
Unit cell dimensions	$a = 10.8013(5)$ Å $\alpha = 76.881(2)^\circ$ $b = 12.7324(6)$ Å $\beta = 85.5740(10)^\circ$ $c = 19.367$ Å $\gamma = 78.238(3)^\circ$
Volume, Z	2538.1 (2) Å <sup>3</sup> , 2
Density (calculated)	1.427 Mg/m <sup>3</sup>
Absorption coefficient	0.822 mm <sup>-1</sup>
F(000)	1124
Crystal size	0.16 x 0.1 x 0.1 mm
8 range for data collection	1.67 to 23.32°
Limiting indices	$-12 \leq h \leq 11$ , $-13 \leq k \leq 14$ , $-21 \leq l \leq 20$
Reflections collected	14466
Independent reflections	7229 ( $R_{\text{int}} = 0.0623$ )
Absorption correction	Sadabs
Max. and mm. Transmission	1.00000 and 0.570100
Refinement method	Full-matrix least-squares on $F^2$
Data I restraints I parameters	7179 / 0 / 560
Goodness-of-fit on $F^2$	0.844
Final R indices [ $I > 2\sigma(I)$ ]	$R1 = 0.0689$ , $wR2 = 0.1749$
R indices (all data)	$R1 = 0.1242$ , $wR2 = 0.2599$
Extinction coefficient	0.0004(4)
Largest diff. peak and hole	1.627 and $-0.722$ e Å <sup>-3</sup>

Table 2. Atomic coordinates [ $\times 10^4$ ] and equivalent isotropic displacement parameters [ $\text{\AA}^2 \times 10^3$ ] for 1.  $U(\text{eq})$  is defined as one third of the trace of the orthogonalized  $U_{ij}$  tensor.

	x	y	z	U(eq)
Rh(1)	6336(1)	-2258(1)	2895(1)	38(1)
P(1)	4824(3)	-591(2)	2913(2)	43 (1)
P(2)	7168(3)	-2766(2)	4055(2)	42 (1)
C(1)	3368(10)	-828(8)	3416(6)	40(3)
C(2)	2168(11)	-567 (9)	3156(7)	51(3)
C(3)	1101(11)	-814(11)	3552(8)	67 (4)
C(4)	1258(12)	-1373 (10)	4250(8)	62 (4)
C(4A)	2414(10)	-1708(11)	4555(6)	54(3)
C(6)	2679(11)	-2275(10)	5317(7)	54(3)
C(5A)	3970(13)	-2990(11)	5335(6)	58(3)
C(6)	4291(14)	-4002 (12)	5791(7)	68(4)
C(7)	5508(16)	-4647 (13)	5774(8)	88(5)
C(8)	6392(13)	-4302(11)	5263(7)	68(4)
C(9)	6110(11)	-3273(9)	4788(6)	51(3)
C(9A)	4907(10)	-2690(9)	4854(6)	45(3)
O(9)	4643(7)	-1649(6)	4398(4)	43(2)
C(1A)	3453(10)	-1373(9)	4123 (6)	42(3)
C(10)	4920(11)	-2941(10)	2867 (6)	51(3)
O(10)	4052(10)	-3282(8)	2795(6)	87(3)
C(11)	1642(14)	-2944(12)	5652 (8)	80(4)
C(12)	2724(14)	-1399(12)	5751(7)	76(4)
C(13)	5264 (11)	473(10)	3289(7)	57(3)
C(14)	4304(13)	1502(10)	3269(8)	73(4)
C(15)	4220(12)	201(11)	2052(7)	65(4)
C(16)	5241(14)	750(12)	1586(8)	86(5)
C(17)	7649(11)	-1669(10)	4395(7)	56(3)
C(18)	8055(14)	-1950(15)	5161(7)	90(5)
C(19)	8582 (11)	-3857 (11)	4192 (6)	57(3)
C(20)	9723(12)	-3560(12)	3741(7)	71(4)
C(50)	7525(10)	-3518(10)	2555(6)	46(3)
O(50)	7809(7)	-4488(7)	2778(4)	52(2)
C(60)	7724(12)	-1411(9)	2452 (6)	51(3)
O(60)	8217(8)	-712(7)	2542 (5)	64(2)
Rh(2)	7799(1)	-2330(1)	1681(1)	39(1)
P(3)	6764(3)	-3244(2)	998(2)	45(1)
P(4)	9980(3)	-2983(3)	1521(2)	47(1)
C(21)	6821(11)	-4707(9)	1334(6)	49(3)
C(22)	5796(13)	-5223(11)	1515(8)	70(4)
C(23)	5934(16)	-6288(13)	1842(10)	98(6)
C(24)	7138(14)	-6952(12)	1993(8)	74(4)
C(24A)	8191(12)	-6482(10)	1832 (6)	52(3)
C(25)	9553(12)	-7109(9)	1966(6)	54(3)
C(25A)	10283 (11)	-6323(10)	2163(6)	55(3)
C(26)	11244(14)	-6623(12)	2650(8)	79(4)

## APPENDIX TWO

C(27)	11882(14)	-5849(15)	2745(9)	90(5)
C(28)	11608(11)	-4763(12)	2406(7)	67 (4)
C(29)	10606(11)	-4417 (10)	1937(6)	55(3)
C(29A)	9993 (11)	-5214(10)	1815(6)	50(3)
O(29)	9043(7)	-4878(6)	1328(4)	43(2)
C(21A)	8011(10)	-5396(9)	1504(6)	47(3)
O(30)	7780(11)	-354(9)	448(6)	104(4)
C(30)	7750(11)	-1045(11)	927(8)	61(3)
C(31)	10143 (15)	-7424(13)	1283 (8)	87 (5)
O(32)	9575(14)	-8154(11)	2539(8)	78(4)
O(33)	7318(12)	-3195(10)	66(6)	55(3)
C(34)	6587(15)	-3680(13)	-379(7)	85(5)
C(35)	5051(11)	-2710(11)	917(7)	60(3)
O(36)	4742(13)	-1494(11)	574(8)	80(4)
O(37)	11076(12)	-2228(11)	1815(7)	62(4)
O(38)	10824(14)	-1006(12)	1418(8)	80(4)
O(39)	10468(11)	-2928(11)	588(6)	55(3)
O(40)	11896(13)	-3198(18)	424 (9)	112(7)

Table 3. Bond lengths [ $\text{\AA}$ ] and angles [ $^\circ$ ] for  $[\text{Rh}_2(\text{CO})_4(\text{Et-Xantphos})_2]$ .

Rh(1) -C(10)	1.916(13)	Rh(1) -C(60)	2.047(13)
Rh(1) -C(50)	2.042 (11)	Rh(1) -P (2)	2.385(3)
Rh(1) -P(1)	2.405(3)	Rh(1) -Rh(2)	2.7388(12)
P(1) -C(13)	1.831(12)	P(1) -C(15)	1.834(12)
P(1) -C(1)	1.827(11)	P(2) -C(9)	1.836(12)
P(2) -C(19)	1.834(11)	P(2) -C(17)	1.851(12)
C(1) -C(2)	1.38(2)	C(1) -C(1A)	1.39(2)
C(2) -C(3)	1.39(2)	C(3) -C (4)	1.38(2)
C(4) -C(4A)	1.37(2)	C(4A) -C(1A)	1.42(2)
C(4A) -C(5)	1.51(2)	C(6) -C(5A)	1.50(2)
C(5) -C(12)	1.55(2)	C(6) -C(11)	1.56(2)
C(5A) -C(9A)	1.37(2)	C(6A) -C(6)	1.38(2)
C(6) -C(7)	1.40(2)	C(7) -C(S)	1.38(2)
C(6) -C(9)	1.41(2)	C(9) -C(9A)	1.37(2)
C(9A) -O(9)	1.404(13)	O(9) -C(1A)	1.378(12)
C(10) -O(10)	1.140(13)	C(13) -C(14)	1.49(2)
C(15) -C(16)	1.55(2)	C(17) -C(18)	1.52(2)
C(19) -C (20)	1.52(2)	C(50) -O(50)	1.195(13)
C(50) -Rh(2)	2.045(12)	C(60) -O(60)	1.177(13)
C(60) -Rh(2)	2.084(11)	Rh(2) -C(30)	1.92(2)
Rh(2) -P (4)	2.354(3)	Rh(2) -P(3)	2.410(3)
P(3) -C(21)	1.819(11)	P(3) -C(35)	1.842(12)
P(3) -C (33)	1.849(12)	P(4) -C(29)	1.831(12)
P(4) -C(39)	1.832(11)	P(4) -C(37)	1.862(12)
C(21) -C(22)	1.38(2)	C(21) -C(21A)	1.42(2)
C(22) -C(23)	1.34(2)	C(23) -C(24)	1.41(2)
C(24) -C(24A)	1.37(2)	C(24A) -C(21A)	1.37(2)
C(24A) -C(25)	1.53(2)	C(25) -C(31)	1.52(2)
C(25) -C(32)	1.52(2)	C(25) -C(25A)	1.52(2)
C(25A) -C(29A)	1.40(2)	C(25A) -C(26)	1.39(2)
C(26) -C(27)	1.36(2)	C(27) -C(28)	1.37(2)
C(28) -C(29)	1.40(2)	C(29) -C(29A)	1.39(2)
C(29A) -O(29)	1.383(13)	O(29) -C(21A)	1.389(13)
O(30) -C(30)	1.13(2)	C(33) -C(34)	1.51(2)
C(35) -C(36)	1.52(2)	C(37) -C(38)	1.55(2)
C(39) -C (40)	1.54(2)		
C(10) -Rh(1) -C(60)	154.3(5)	C(10) -Rh(1) -C(50)	90.6(5)
C(60) -Rh(1) -C(50)	82.5(4)	C(10) -Rh(1) -P (2)	110.5(4)
C(60) -Rh(1) -P (2)	94.7(4)	C(50) -Rh(1) -P(2)	93.5(3)
C(10) -Rh(1) -P(1)	86.9(3)	C(60) -Rh(1) -P (1)	92.2(3)
C(50) -Rh(1) -P (1)	162.4(3)	P(2) -Rh(1) -P(1)	103.72(11)
C(10) -Rh(1) -Rh(2)	109.2(4)	C(60) -Rh(1) -Rh(2)	49.0(3)
C(50) -Rh(1) -Rh(2)	48.0(3)	P(2) -Rh(1) -Rh(2)	123.63(8)
P(1) -Rh(1) -Rh(2)	116.86(8)	C(13) -P(1) -C(15)	101.8(6)

## APPENDIX TWO

C(13) -P(1) -C(1)	102.3(5)	C(15) -P(1) -C(1)	102.0(5)
C(13) -P(1) -Rh(1)	119.2(4)	C(15) -P(1) -Rh(1)	116.1(4)
C(1) -P(1) -Rh(1)	113.1(3)	C(9) -P (2) -C(19)	101.9(5)
C(9) -P (2) -C(17)	100.2(6)	C(19) -P (2) -C(17)	102.2(6)
C(9) -P (2) -Rh(1)	116.8(4)	C(19) -P(2) -Rh(1)	116.4(4)
C(17) -P (2) -Rh(1)	116.7(4)	C(2) -C(1) -C(1A)	115.1(10)
C(2) -C(1) -P (1)	126.4(9)	C(1A) -C(1) -P(1)	118.5(8)
C(1) -C(2) -C(3)	124.1(12)	C(4) -C(3) -C(2)	117.7(12)
C(3) -C (4) -C(4A)	123.0(12)	C(4) -C(4A) -C(1A)	115.6(10)
C(4) -C(4A) -C(5)	127.0(11)	C(1A) -C(4A) -C(5)	116.9(10)
C(4A) -C(5) -C(5A)	108.0(10)	C(4A) -C(5) -C(12)	109.2(11)
C(5A) -C(5) -C(12)	107.1(10)	C(4A) -C(5) -C(11)	111.5(10)
C(5A) -C(5) -C(11)	111.9(11)	C(12) -C(5) -C(11)	109.1(11)
C(9A) -C(5A) -C(6)	115.2(12)	C(9A) -C(5A) -C(5)	120.6(11)
C(6) -C(5A) -C(6)	124.1(12)	C(7) -C(6) -C(5A)	121.6(12)
C(8) -C (7) -C(6)	119.7(13)	C(7) -C(8) -C(9)	120.6(13)
C(9A) -C(9) -C(8)	115.4(11)	C(9A) -C(9) -P (2)	119.9(8)
C(8) -C(9) -P(2)	124.4(9)	C(5A) -C(9A) -C(9)	127.3(11)
C(5A) -C(9A) -O(9)	117.3(10)	C(9) -C(9A) -O(9)	115.3(10)
C(1A) -O(9) -C(9A)	114.6(8)	O(9) -C(1A) -C(1)	116.4(10)
O(9) -C(1A) -C(4A)	119.2(9)	C(1) -C(1A) -C(4A)	124.3(10)
O(10) -C(10) -Rh(1)	174.0(11)	C(14) -C(13) -P(1)	117.0(9)
C(16) -C(15) -P(1)	111.8(9)	C(18) -C(17) -P(2)	117.2(10)
C(20) -C(19) -P(2)	113.6(9)	O(50) -C(50) -Rh(1)	134.8(9)
O(50) -C(50) -Rh(2)	140.9(9)	Rh(1) -C(50) -Rh(2)	84.2(4)
O(60) -C(60) -Rh(1)	140.3(9)	O(60) -C(60) -Rh(2)	136.6(10)
Rh(1) -C(60) -Rh(2)	83.1(5)	C(30) -Rh(2) -C(50)	168.5(5)
C(30) -Rh(2) -C(60)	91.9(5)	C(50) -Rh (2) -C(60)	81.6(5)
C(30) -Rh(2) -P (4)	94.3(4)	C(50) -Rh(2) -P (4)	96.4(3)
C(60) -Rh(2) -P (4)	103.4(4)	C(30) -Rh(2) -P(3)	93.1(4)
C(50) -Rh(2) -P (3)	88.2(3)	C(60) -Rh(2) -P(3)	150.2(4)
P(4) -Rh(2) -P (3)	105.42(11)	C(30) -Rh(2) -Rh(1)	121.0(4)
C(50) -Rh(2) -Rh(1)	47.9(3)	C(60) -Rh(2) -Rh(1)	47.9(3)
P(4) -Rh (2) -Rh(1)	130.65(9)	P(3) -Rh(2) -Rh(1)	105.70(8)
C(21) -P (3) -C(35)	102.1(6)	C(21) -P (3) -C(33)	101.8(6)
C(35) -P (3) -C(33)	102.7(6)	C(21) -P(3) -Rh(2)	116.7(4)
C(35) -P(3) -Rh (2)	114.0(4)	C(33) -P(3) -Rh(2)	117.3(4)
C(29) -P (4) -C(39)	102.3(6)	C(29) -P (4) -C(37)	102.9(6)
C(39) -P (4) -C(37)	102.6(6)	C(29) -P (4) -Rh(2)	117.3(4)
C(39) -P (4) -Rh(2)	113.0(4)	C(37) -P (4) -Rh(2)	116.8(4)
C(22) -C (21) -C(21A)	114.8(11)	C(22) -C(21) -P (3)	126.5(10)
C(21A) -C(21) -P(3)	118.4(9)	C(23) -C(22) -C(21)	121.8(13)
C(22) -C (23) -C (24)	121.7(14)	C(24A) -C(24) -C(23)	119.0(13)
C(24) -C(24A) -C(21A)	117.5(12)	C(24) -C(24A) -C(25)	124.3(11)
C(21A) -C(24A) -C(25)	118.2(11)	C(31) -C(25) -C(32)	108.6(11)
C(31) -C(25) -C(25A)	108.5(11)	C(32) -C(25) -C(25A)	112.7(11)
C(31) -C(25) -C(24A)	109.2(11)	C(32) -C(25) -C(24A)	110.8(10)
C(25A) -C(25) -C(24A)	106.9(9)	C(29A) -C(25A) -C(26)	117.2(13)
C(29A) -C(25A) -C(25)	117.7(11)	C(26) -C(25A) -C(25)	125.1(12)

## APPENDIX TWO

C(27) -C(26) -C(25A)	119.3(14)	C(26) -C(27) -C(28)	124.0(14)
C(29) -C(28) -C(27)	118.5(14)	C(29A) -C(29) -C(28)	117.5(12)
C(29A) -C(29) -P (4)	117.7(9)	C(28) -C(29)-P (4)	124.7(11)
O(29) -C(29A) -C(25A)	123.4(11)	C(29) -C(29A) -O(29)	117.3(10)
C(25A) -C(29A) -O(29)	119.2(11)	C(21A) -O(29) -C(29A)	115.0(9)
C(24A) -C(21A) -O(29)	120.0(10)	C(24A) -C(21A) -C(21)	125.1(11)
O(29) -C(21A) -C(21)	114.9(10)	O(30) -C(30) -Rh(2)	173.7(12)
C(34) -O(33)-P (3)	117.0(10)	C(36) -C(35)-P (3)	112.9(9)
C(38) -O(37)-P (4)	110.5(9)	C(40) -C(39)-P (4)	116.5(10)

Symmetry transformations used to generate equivalent atoms.

Table 4. Anisotropic displacement parameters [ $\text{\AA}^2 \times 10^3$ ] for  $[\text{Rh}_2(\text{CO})_4(\text{Et-Xantphos})_2]$ .  
 The anisotropic displacement factor exponent takes the form:  $-2\pi^2 [(ha^*)^2 U_{11} + \dots + 2hka^*b^*U_{12}]$ .

	U11	U22	U33	U23	U13	U12
Rh(1)	39(1)	36 (1)	38(1)	-9(1)	-2(1)	-4(1)
P(1)	42(2)	42(2)	44(2)	-6(1)	-2(1)	-6(1)
P(2)	41(2)	41(2)	43(2)	-9(1)	-6(1)	-3(1)
C(1)	41(7)	39(6)	38(7)	-11(5)	-2(5)	0(5)
C(2)	46(7)	44(7)	61(8)	-7(6)	0(6)	-10(6)
C(3)	35(7)	74(9)	82(11)	-9(8)	13(7)	3 (6)
C(4)	47(8)	60(8)	78(10)	-16(8)	4(7)	-11(6)
C(4A)	34(7)	88(9)	28(6)	2(6)	3(5)	2 (6)
C(5)	43(7)	56(8)	62(8)	-14(6)	-1(6)	-10(6)
C(5A)	74(9)	65(8)	38(7)	2(6)	-8(7)	-29(7)
C(6)	67 (9)	87(10)	51(8)	4(8)	3(7)	-42 (8)
C(7)	94(12)	92(12)	60(10)	33(8)	-2(9)	-34(10)
C(8)	58(8)	68(9)	66(9)	3(7)	-8(7)	2(7)
C(9)	47(7)	44(7)	56(8)	1(6)	-11(6)	-8(6)
C(9A)	44(7)	56(7)	34(6)	-1(6)	-8(5)	-14 (6)
0(9)	48(5)	40(4)	44 (5)	-8(4)	-4(4)	-11(3)
C(1A)	46(7)	39(6)	48(7)	-16(6)	-12(6)	-11(5)
C(10)	44(7)	50(7)	53(8)	-7 (6)	-9(6)	3 (6)
0(10)	84(7)	87 (7)	100(8)	-6(6)	12 (6)	-52 (6)
C(11)	83 (11)	90(11)	74(10)	-5(8)	0(8)	-48(9)
C(12)	89(11)	89(11)	65(9)	-29(8)	9(8)	-42 (9)
C(13)	47(7)	56(8)	67(9)	-13(7)	-2 (6)	-6(6)
C(14)	72 (9)	47(8)	99(12)	-27(8)	13 (8)	-2(7)
C(15)	58(8)	71(9)	52 (8)	1(7)	-1(7)	2(7)
C(16)	97(12)	79(10)	64(10)	11(8)	4(9)	-8(9)
C(17)	44(7)	69(8)	65(9)	-29(7)	1(6)	-16(6)
C(18)	74(10)	159(16)	54(9)	-32 (10)	11(8)	-57(11)
C(19)	45(7)	70(9)	49(8)	-14(7)	-6(6)	10(6)
C(20)	56(8)	84(10)	73(10)	-27(8)	-18(7)	2(7)
C(50)	34(6)	47(8)	58(8)	-18(6)	-6(6)	2(5)
0(50)	64(5)	45(5)	46(5)	-14(4)	0(4)	-3(4)
C(60)	70(8)	33(6)	50(7)	-18(6)	3 (6)	-3(6)
0(60)	64(6)	57(6)	84(7)	-28(5)	2(5)	-27(5)
Rh(2)	37 (1)	40(1)	39(1)	-8(1)	-1(1)	-3(1)
P(3)	41(2)	49(2)	44(2)	-9(1)	-7 (1)	-2(1)
P(4)	40(2)	52 (2)	51(2)	-18(2)	0(1)	-9(1)
C(21)	51(7)	43 (7)	54(8)	-5(6)	-9(6)	-12(6)
C(22)	59(9)	59(9)	93(11)	-2(8)	-20(8)	-24(7)
C(23)	81(12)	80(12)	129(15)	13 (11)	-15(10)	-42(10)
C(24)	82(11)	58(9)	83(11)	-16(8)	-13 (9)	-12(8)
C(24A)	67(8)	46(7)	41(7)	-7(6)	-1(6)	-11(6)
C(25)	9(8)	41(7)	41(7)	-9(6)	8(6)	12(6)

## APPENDIX TWO

C(25A)	53(8)	58(8)	47(7)	-21(6)	1(6)	15(6)
C(26)	67 (10)	55(9)	100(12)	-15(8)	-26(9)	25(8)
C(27)	55(9)	96(13)	104(13)	-19(11)	-24(9)	24(9)
C(28)	37(7)	78(10)	81(10)	-25(8)	-20(7)	13(7)
C(29)	42(7)	63(8)	53(8)	-22(6)	-8(6)	15(6)
C(29A)	42(7)	63(8)	42(7)	-19(6)	1(6)	2(6)
C(29)	50(5)	39(4)	36(4)	-6(3)	-3(4)	-1(4)
C(21A)	42(7)	52(7)	48(7)	-15(6)	-4(6)	-8(6)
O(30)	117(9)	91(8)	77(8)	43(7)	-1(7)	-23(7)
C(30)	46(7)	63(9)	69(10)	-15(8)	4(7)	-1(6)
C(31)	106(12)	84(11)	70(10)	-38(9)	25(9)	0(9)
C(32)	80(10)	56(8)	82 (11)	0(8)	12 (8)	3(7)
C(33)	61(8)	55(7)	47(7)	-17 (6)	-10(6)	2 (6)
C(34)	108(12)	99(12)	55(9)	-30(8)	-17 (8)	-17(10)
C(35)	48(7)	77 (9)	49(8)	-10(7)	-8(6)	1(6)
C(36)	62(9)	77 (10)	89(11)	-14(8)	-24(8)	21(7)
C(37)	54(8)	76 (9)	65(9)	-20(7)	-8(7)	-24(7)
C(38)	78(10)	91(11)	82(11)	-17(9)	2(8)	-44(9)
C(39)	50(8)	71(9)	49(8)	-18(6)	11(6)	-21(6)
C(40)	50(9)	13(22)	93(13)	-85(14)	27(9)	-19(11)

Table 5. Hydrogen coordinates ( $\times 10^4$ ) and isotropic displacement parameters ( $\text{\AA}^2 \times 10^3$ ) for  $[\text{Rh}_2(\text{CO})_4(\text{Et-Xantphos})_2]$ .

	x	y	z	U(eq)
H(2A)	2068(11)	-200(9)	2684(7)	61
H(3A)	306(11)	-612(11)	3355(8)	80
H(4A)	546(12)	-1528(10)	4525(8)	74
H(6A)	3686(14)	-4261(12)	6117(7)	81
H(7A)	5719(16)	-5304(13)	6105(8)	105
H(8A)	7179(13)	-4753(11)	5232 (7)	82
H(11A)	1828(14)	-3283(12)	6138(8)	120
H(11B)	1627 (14)	-3502(12)	5394(8)	120
H(11C)	831(14)	-2461(12)	5630(8)	120
H (12A)	2886(14)	-1756(12)	6237(7)	114
H(12B)	1928(14)	-895(12)	5725(7)	114
H(12C)	3387(14)	-1006(12)	5560(7)	114
H(13A)	5475(11)	155(10)	3780(7)	68
H(13B)	6025(11)	670(10)	3039(7)	68
H(14A)	4640(13)	1997 (10)	3476(8)	110
H(14B)	3553(13)	1329(10)	3531(8)	110
H(14C)	4099(13)	1843 (10)	2785(8)	110
H(15A)	3933(12)	-284(11)	1804(7)	78
H(15B)	3500(12)	763(11)	2127(7)	78
H(16A)	4889(14)	1162(12)	1143 (8)	129
H(16B)	5945(14)	194(12)	1500(8)	129
H (16C)	5523(14)	1234(12)	1828(8)	129
H (17A)	8344(11)	-1429(10)	4095(7)	68
H(17B)	6947(11)	-1048(10)	4343(7)	68
H(18A)	8281(14)	-1320(15)	5274(7)	135
H(18B)	8771(14)	-2546(15)	5221(7)	135
H(18C)	7369(14)	-2163(15)	5470(7)	135
H(19A)	8794(11)	-4027 (11)	4688(6)	69
H(19B)	8390(11)	-4514(11)	4084(6)	69
H(20A)	10426(12)	-4164(12)	3835(7)	106
H(20B)	9937(12)	-2924(12)	3854(7)	106
H(20C)	9528(12)	3402(12)	3248(7)	106
H(22A)	4987(13)	-4821(11)	1408(8)	84
H(23A)	5218(16)	-6596(13)	1972(10)	118
H(24A)	7218(14)	-7696(12)	2198(8)	88
H(26A)	11449(14)	-7343(12)	2907(8)	95
H(27A)	12543(14)	-6071(15)	3058(9)	108
H(28A)	12076(11)	-4267(12)	2486(7)	80
H(31A)	10126(15)	-6772(13)	917(8)	131
H(31B)	9671(15)	-7898(13)	1142(8)	131
H(31C)	11003 (15)	-7799(13)	1361(8)	131
H(32A)	9195(14)	-7968(11)	2971(8)	117
H(32B)	10435(14)	-8529(11)	2619(8)	117

## APPENDIX TWO

H(32C)	9111(14)	-8625(11)	2388(8)	117
H(33A)	7305(12)	-2433(10)	-165(6)	66
H(33B)	8193 (12)	-3577 (10)	66(6)	66
H(34A)	6958(15)	-3606(13)	-850(7)	127
H(34B)	5723(15)	-3297(13)	-400(7)	127
H(34C)	6616(15)	-4444(13)	-170(7)	127
H (35A)	4707 (11)	-3117 (11)	636(7)	72
H (35B)	4646(11)	-2830(11)	1385(7)	72
H(36A)	3841(13)	-1258(11)	546(8)	121
H(36B)	5122(13)	-1372(11)	105(8)	121
H(36C)	5067(13)	-1084 (11)	853 (8)	121
H(37A)	10959(12)	-2273 (11)	2322(7)	74
H(37B)	11944(12)	-2565(11)	1721(7)	74
H(38A)	11397(14)	-629(12)	1574(8)	120
H(38B)	9969(14)	-671(12)	1516(8)	120
H(38C)	10951(14)	-963(12)	917(8)	120
H(39A)	10071(11)	-3435(11)	418(6)	66
H(39B)	10140(11)	-2195(11)	319(6)	66
H(40A)	12043(13)	-3138(18)	-77 (9)	168
H(40B)	12234(13)	-3934(18)	670(9)	168
H(40C)	12305(13)	-2691(18)	577(9)	168

**APPENDIX THREE: X-RAY CRYSTALLOGRAPHY DATA**  
**[Bz<sub>2</sub>P(C(OH)(CH<sub>3</sub>)CH<sub>2</sub>C(CH<sub>3</sub>)<sub>2</sub>O)]Cl.**

The X-ray crystal structure of [Bz<sub>2</sub>P(C(OH)(CH<sub>3</sub>)CH<sub>2</sub>C(CH<sub>3</sub>)<sub>2</sub>O)]Cl can be seen in Figure 1. The Crystallography data for the molecule can be seen in Table 1 to Table 5, Appendix 3.

**Figure 1**

*The X-ray crystal structure of Bz<sub>2</sub>P(C(OH)(CH<sub>3</sub>)CH<sub>2</sub>C(CH<sub>3</sub>)<sub>2</sub>O)Cl.*

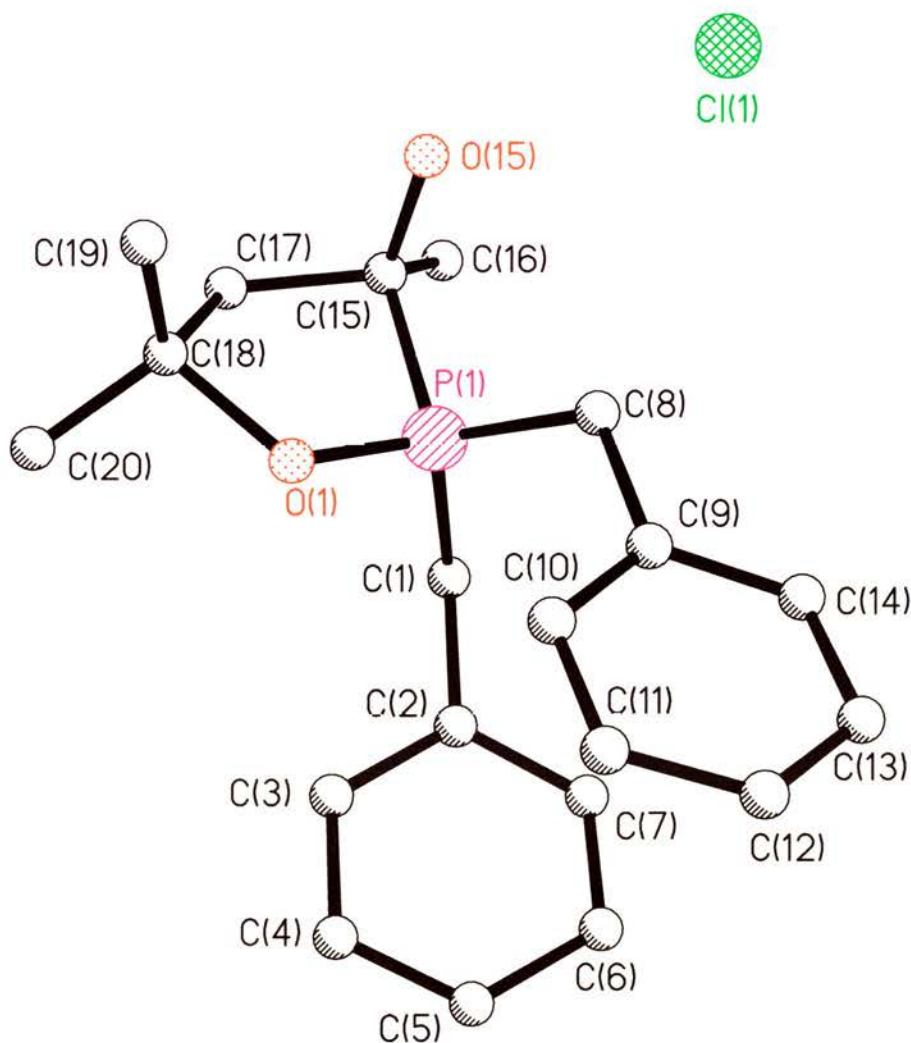


Table 1. Crystal data and structure refinement for [Bz<sub>2</sub>P(C(OH)(CH<sub>3</sub>)CH<sub>2</sub>C(CH<sub>3</sub>)<sub>2</sub>O)]Cl.

Identification code	dwdch6	
Empirical formula	C <sub>20</sub> H <sub>26</sub> ClO <sub>2</sub> P	
Formula weight	364.83	
Temperature	293(2) K	
Wavelength	0.71073 Å	
Crystal system	Monoclinic	
Space group	C2/c	
Unit cell dimensions	a = 29.059(10) Å	alpha = 90°
	b = 10.250(3) Å	beta = 115.068(5)°
	c = 14.801(5) Å	gamma = 90°
Volume, Z	3993(2) Å <sup>3</sup> , 8	
Density (calculated)	1.214 Mg/m <sup>3</sup>	
Absorption coefficient	0.280 mm <sup>-1</sup>	
F(000)	1552	
Crystal size	0.04 x 0.05 x 0.11 mm	
θ range for data collection	1.55 to 23.36°	
Limiting indices	-32 ≤ h ≤ 32, -11 ≤ k ≤ 11, -16 ≤ l ≤ 16	
Reflections collected	9942	
Independent reflections	2905 (R <sub>int</sub> = 0.4433)	
Absorption correction	Sadabs	
Max and min transmission	1.00000 and 0.492473	
Refinement method	Full-matrix least-squares on F <sup>2</sup>	
Data / restraints / parameters	2855 / 1 / 246	
Goodness-of-fit on F <sup>2</sup>	0.698	
Final a indices [I > 2σ(I)]	R1 = 0.0878, wR2 = 0.1712	
R indices (all data)	R1 = 0.2250, wR2 = 0.4416	
Extinction coefficient	0.010(2)	
Largest diff. peak and hole	0.355 and -0.513 eÅ <sup>-3</sup>	

Table 2. Atomic coordinates [ $\times 10^4$ ] and equivalent isotropic displacement parameters [ $\text{\AA}^2 \times 10^3$ ] for  $[\text{Bz}_2\text{P}(\text{C}(\text{OH})(\text{CH}_3)\text{CH}_2\text{C}(\text{CH}_3)_2\text{O})]\text{Cl}$ .  $U(\text{eq})$  is defined as one third of the trace of the orthogonalized  $U_{ij}$  tensor.

	x	y	z	U(eq)
Cl(1)	7611(1)	1140(2)	-1159(2)	83(1)
P(1)	6692(1)	247(2)	637(2)	46(1)
O(1)	6318(2)	-906(4)	505(4)	56(2)
C(1)	6817(3)	1085(7)	1771(6)	54(2)
C(2)	6335(3)	1614(8)	1827(6)	58(2)
C(3)	6009(3)	795(8)	2031(7)	69(3)
C(4)	5572(4)	1259(13)	2061(9)	101(4)
C(5)	5465(5)	2554(17)	1872(11)	144(6)
C(6)	5788(5)	3407(11)	1652(11)	128(5)
C(7)	6205(4)	2925(9)	1642(8)	84(3)
C(8)	6453(3)	1267(7)	-446(6)	55(2)
C(9)	5957(3)	1983(7)	-679(7)	64(2)
C(10)	5515(3)	1345(8)	-784(8)	76(3)
C(11)	5083(4)	2016(11)	-999(10)	105(4)
C(12)	5064(4)	3304(13)	-1206(12)	146(6)
C(13)	5485(4)	3982(10)	-1102(11)	140(6)
C(14)	5934(4)	3327(8)	-841(9)	98(4)
C(15)	7244(3)	-697(7)	701(6)	49(2)
O(15)	7172(2)	-913(5)	-298(4)	63(2)
C(16)	7759(3)	-113(8)	1338(7)	71(3)
C(17)	7140(3)	-1953(7)	1106(7)	64(3)
C(18)	6568(3)	-2269(7)	660(7)	57(2)
C(20)	6401(4)	-2956(8)	1365(9)	101(4)
C(19)	6362(3)	-2907(8)	-356(8)	84(3)

Table 3. Bond lengths [ $\text{\AA}$ ] and angles [ $^\circ$ ] for  $[\text{Bz}_2\text{P}(\text{C}(\text{OH})(\text{CH}_3)\text{CH}_2\text{C}(\text{CH}_3)_2\text{O})]\text{Cl}$ .

P(1)–O(1)	1.563(5)	P(1)–C(1)	1.779(8)
P(1)–C(8)	1.789(8)	P(1)–C(15)	1.842(7)
O(1)–C(18)	1.546(8)	C(1)–C(2)	1.538(9)
C(2)–C(3)	1.39	C(2)–C(7)	1.392(10)
C(3)–C(4)	1.376(12)	C(4)–C(5)	1.37(2)
C(S)–C(6)	1.42(2)	C(6)–C(7)	1.313(11)
C(8)–C(9)	1.521(9)	C(9)–C(10)	1.39
C(9)–C(14)	1.395(10)	C(10)–C(11)	1.347(10)
C(11)–C(12)	1.351(14)	C(12)–C(13)	1.359(13)
C(13)–C(14)	1.368(11)	C(15)–O(15)	1.421(9)
C(15)–C(17)	1.503(10)	C(15)–C(16)	1.513(10)
C(17)–C(18)	1.543(10)	C(18)–C(20)	1.500(11)
C(18)–C(19)	1.512(12)		
O(1)–P(1)–C(1)	109.6(3)	O(1)–P(1)–C(8)	110.2(3)
C(1)–P(1)–C(8)	114.2(4)	O(1)–P(1)–C(15)	98.9(3)
C(1)–P(1)–O(15)	112.3(4)	C(8)–P(1)–C(15)	110.6(3)
C(18)–O(1)–P(1)	114.0(4)	C(2)–C(1)–P(1)	113.2(5)
C(3)–C(2)–C(7)	118.2(7)	C(3)–C(2)–C(1)	121.3(7)
C(7)–C(2)–C(1)	120.5(7)	C(2)–C(3)–C(4)	121.4(8)
C(5)–C(4)–C(3)	117.6(10)	C(6)–C(5)–C(4)	122.1(10)
C(5)–C(6)–C(7)	118.3(10)	C(6)–C(7)–C(2)	122.4(10)
C(9)–C(8)–P(1)	117.1(6)	C(10)–C(9)–C(14)	118.0(8)
C(10)–C(9)–C(8)	122.7(6)	C(14)–C(9)–C(8)	119.2(7)
C(9)–C(10)–C(11)	120.8(8)	C(12)–C(11)–C(10)	119.7(10)
C(11)–C(12)–C(13)	121.7(10)	C(14)–C(13)–C(12)	119.1(9)
C(13)–C(14)–C(9)	120.3(9)	O(15)–C(15)–C(17)	108.4(6)
O(15)–C(15)–C(16)	112.5(6)	C(17)–C(15)–C(16)	113.8(7)
O(15)–C(15)–P(1)	106.7(5)	C(17)–C(15)–P(1)	98.8(5)
C(16)–C(15)–P(1)	115.7(5)	C(15)–C(17)–C(18)	111.8(7)
C(20)–C(18)–C(19)	112.4(7)	C(20)–C(18)–O(1)	104.9(6)
C(19)–C(18)–O(1)	106.3(6)	C(20)–C(18)–C(17)	114.2(8)
C(19)–C(18)–C(17)	114.6(7)	O(1)–C(18)–C(17)	103.2(5)

Symmetry transformations used to generate equivalent atoms.

Table 4. Anisotropic displacement parameters [ $\text{\AA}^2 \times 10^3$ ] for  $[\text{Bz}_2\text{P}(\text{C}(\text{OH})(\text{CH}_3)\text{CH}_2\text{C}(\text{CH}_3)_2\text{O})\text{Cl}]$ . The anisotropic displacement factor exponent takes the form:  $-2\pi^2 [(\text{ha}^*)^2 U_{11} + \dots + 2\text{hka}^*\text{b}^*U_{12}]$ .

	U11	U22	U33	U23	U13	U12
Cl (1)	117(2)	73(2)	78(2)	-10(1)	58(2)	-36(2)
P(1)	54(1)	36(1)	53(2)	1(1)	28(1)	3(1)
O(1)	48(3)	42(3)	83(5)	-4(3)	32(3)	1(3)
C(1)	65(5)	34(4)	54(6)	-6(4)	17(4)	-4(4)
C(2)	69(5)	58(6)	62(7)	-8(5)	43(5)	7(5)
C(3)	85(6)	68(6)	66(7)	-8(5)	43(6)	-1(6)
C(4)	98(7)	123(10)	123(11)	-31(8)	86(8)	-10(8)
C(5)	110(9)	168(15)	185(17)	-44(12)	91(10)	48(11)
C(6)	132(9)	85(8)	204(16)	-11(9)	107(11)	26(9)
C(7)	95(7)	58(7)	124(10)	-9(6)	71(7)	15(6)
C(8)	64(5)	48(5)	51(6)	2(4)	24(5)	8(4)
C(9)	79(6)	40(5)	54(7)	3(4)	10(5)	-10(5)
C(10)	72(6)	44(5)	106(10)	-11(6)	31(6)	-12(6)
C(11)	64(6)	71(8)	167(13)	6(7)	37(7)	22(6)
C(12)	91(8)	74(8)	250(20)	45(10)	49(10)	47(8)
C(13)	83(7)	41(6)	277(19)	19(8)	58(9)	19(7)
C(14)	87(7)	41(6)	137(12)	25(6)	18(7)	-2(6)
C(15)	77(5)	43(5)	31(5)	3(4)	28(5)	2(4)
O(15)	87(4)	53(3)	71(5)	2(3)	52(3)	11(3)
C(16)	73(5)	75(6)	76(8)	1(5)	42(5)	-7(5)
C(17)	85(6)	38(5)	85(8)	13(5)	54(6)	26(5)
C(18)	76(6)	26(4)	74(7)	3(4)	36(5)	4(4)
C(20)	146(8)	64(6)	145(12)	32(7)	112(9)	12(7)
C(19)	119(7)	48(6)	88(9)	-28(5)	45(7)	-19(6)

Table 5. Hydrogen coordinates ( $\times 10^4$ ) and isotropic displacement parameters ( $\text{\AA}^2 \times 10^3$ ) for  $[\text{Bz}_2\text{P}(\text{C}(\text{OH})(\text{CH}_3)\text{CH}_2\text{C}(\text{CH}_3)_2\text{O})]\text{Cl}$ .

	x	y	z	U(eq)
H(1A)	6988(3)	495(7)	2325(6)	65
H(1B)	7046(3)	1806(7)	1840(6)	65
H(3A)	6089(14)	-86(24)	2150(61)	83
H(4A)	5357(4)	711(13)	2206(9)	121
H(5A)	5170(5)	2887(17)	1887(11)	173
H(6A)	5707(5)	4285(11)	1518(11)	153
H(7A)	6421(4)	3481(9)	1508(8)	101
H(8A)	6711(3)	1912(7)	-372(6)	66
H(8B)	6408(3)	732(7)	-1018(6)	66
H(10A)	5518(6)	445(29)	-705(56)	91
H(11A)	4798(4)	1594(11)	-1005(10)	126
H(12A)	4754(4)	3738(13)	-1425(12)	176
H(13A)	5469(4)	4879(10)	-1206(11)	168
H(14A)	6224(4)	3780(8)	-772(9)	118
H(150)	7339(20)	-208(39)	-494(50)	50(21)
H(16A)	7801(3)	682(8)	1039(7)	107
H(16B)	8021(3)	-719(8)	1388(7)	107
H(16C)	7782(3)	68(8)	1992(7)	107
H(17A)	7270(3)	-1889(7)	1825(7)	76
H(17B)	7319(3)	-2659(7)	954(7)	76
H(20A)	6541(4)	-2520(8)	1999(9)	152
H(20B)	6517(4)	-3843(8)	1449(9)	152
H(20C)	6036(4)	-2944(8)	1098(9)	152
H(19A)	6475(3)	-2431(8)	-783(8)	127
H(19B)	5997(3)	-2907(8)	-640(8)	127
H(19C)	6483(3)	-3790(8)	-291(8)	127

## APPENDIX FOUR: PRODUCT DISTRIBUTION OF THE HYDROFORMYLATION REACTIONS IN CHAPTER FOUR.

Table 1. Hydroformylation of allyl alcohol with  $[\text{Rh}(\text{CO})_2(\text{acac})]$  and Et-Xantphos.

Key: PA = Propanal; MPA = 2-methylpropanal; DHF = dihydrofutan; MPEA = 2-methylprop-2-enal; POL = propanol; IBO = isobutanol; EOF = ethoxyfuran; AA = allyl alcohol; MAA = methyl allyl alcohol;  $\gamma$ BA =  $\gamma$ -butyrolactone; HBA = 4-hydroxybutanal; MHPA = 2-methyl-3-hydroxypropanal; BDO = butanediol; MPD = 2-methyl-1,3-propanediol; CY = cyclics.

Run No.	PA	MPA	DHF	MPEA	POL	IBO	EOF	AA	MAA	$\gamma$ BA	HBA	MHPA	MPD	BDO	CY
1	0.54	0.05	0.56	0.64	0.38	0.00	0.00	2.46	0.00	0.92	86.28	7.17	0.00	0.29	0.52
2	9.59	0.20	0.24	0.43	2.8	0.00	0.00	2.19	0.00	0.60	73.81	9.89	0.00	0.18	0.08
3	36.12	0.52	0.20	0.34	4.92	0.00	0.00	1.73	0.00	0.74	43.58	11.06	0.00	0.14	0.54
4	1.49	0.07	0.64	0.65	0.95	0.00	0.00	0.42	0.00	0.91	73.54	20.31	0.00	0.25	0.76
5	1.24	0.06	0.26	0.59	0.69	0.00	0.00	0.59	0.00	1.12	87.06	7.54	0.00	0.49	0.36
6	7.96	0.15	0.26	0.48	2.13	0.00	0.00	1.34	0.00	0.75	75.76	10.74	0.00	0.23	0.18
7	0.83	4.09	1.51	0.29	0.89	0.00	0.77	0.23	0.05	0.57	75.23	15.03	0.00	0.29	0.21
8	0.78	2.56	0.73	0.38	0.99	0.00	0.50	0.24	0.03	0.47	78.74	13.99	0.00	0.29	0.30
9	3.31	2.02	1.68	0.35	0.99	0.00	0.49	0.00	0.00	0.74	74.45	15.58	0.00	0.25	0.15
10	1.14	1.35	1.78	0.31	1.47	0.00	0.60	0.44	0.00	0.53	76.99	14.92	0.00	0.27	0.18
11	0.52	14.18	1.31	0.00	1.42	0.00	27.93	0.09	0.00	0.63	40.42	0.55	0.75	5.96	6.23
12	1.04	0.06	0.82	0.14	1.04	0.00	0.00	1.52	0.00	0.38	86.60	7.95	0.00	0.13	0.33
13	1.04	0.06	0.82	0.14	1.04	0.00	0.00	1.52	0.00	0.38	86.60	7.95	0.00	0.13	0.33
14	0.91	0.07	0.34	0.23	0.74	0.00	0.00	0.38	0.00	0.50	87.57	8.92	0.00	0.23	0.11
15	17.98	0.26	0.61	0.36	1.04	0.00	0.00	0.35	0.00	0.32	63.84	14.79	0.00	0.07	0.39
16	0.59	0.53	0.40	0.31	0.32	0.00	0.00	0.32	0.00	0.23	85.37	11.65	0.00	0.08	0.10
17	6.49	3.09	0.41	0.23	1.93	0.00	0.00	0.00	0.00	0.75	77.21	6.39	0.00	1.80	1.70
18	8.39	4.48	1.33	0.14	1.08	0.00	0.00	0.08	0.00	0.69	54.79	3.85	0.00	0.62	24.56
19	0.36	1.93	0.89	0.24	1.03	0.00	0.00	0.26	0.00	0.17	79.00	7.28	0.00	0.11	8.71

20	0.83	0.93	0.97	0.45	1.14	0.00	0.22	0.07	0.00	0.21	84.94	9.29	0.00	0.25	0.59
21	32.68	0.00	0.00	0.00	5.88	0.00	0.00	0.00	0.00	0.00	52.67	8.77	0.00	0.00	0.00
22	2.53	0.14	0.83	0.67	1.03	0.00	0.00	0.26	0.00	1.03	76.84	15.79	0.00	0.29	0.59
23	0.32	1.53	0.92	14.62	2.77	0.00	0.00	2.03	0.00	2.76	74.47	0.00	0.00	0.59	0.00

**Table 2.** Hydroformylation of allyl alcohol with  $[\text{Rh}(\text{CO})_2(\text{acac})]$  and Et-BuXantphos.

Run No.	PA	MPA	DHF	MPEA	POL	IBO	EOF	AA	MAA	$\gamma$ BA	HBA	MHPA	MPD	BDO	CY
1	0.76	2.12	2.05	0.24	0.82	0.00	5.03	3.22	0.23	0.56	71.91	11.01	0.00	0.25	1.80
2	1.80	6.82	1.68	0.20	0.81	0.00	19.27	0.60	0.28	0.51	56.22	6.31	0.00	0.24	5.24
3	0.41	11.02	1.38	0.07	1.42	0.00	29.43	0.00	0.04	0.45	43.06	2.38	0.38	2.10	7.84

**Table 3.** Hydroformylation of allyl alcohol with  $[\text{Rh}(\text{CO})_2(\text{acac})]$  and Pr-Bisbite.

Run No.	PA	MPA	DHF	MPEA	POL	IBO	EOF	AA	MAA	$\gamma$ BA	HBA	MHPA	MPD	BDO	CY
1	23.56	0.58	0.19	0.76	0.43	0.00	0.00	0.55	0.00	0.61	47.99	24.01	0.00	0.00	1.32

**Table 4.** Hydroformylation of allyl alcohol with  $[\text{Rh}(\text{CO})_2(\text{acac})]$  and DIOP.

Run No.	PA	MPA	DHF	MPEA	POL	IBO	EOF	AA	MAA	$\gamma$ BA	HBA	MHPA	MPD	BDO	CY
1	1.61	0.07	0.30	0.32	0.14	0.09	0.00	0.00	0.00	0.43	80.80	12.57	0.00	0.10	3.57
2	0.35	0.03	0.39	0.20	0.21	0.21	0.00	1.01	0.00	0.83	78.42	11.80	0.00	0.00	6.55

**Table 5.** Hydroformylation of allyl alcohol with  $[\text{Rh}(\text{CO})_2(\text{acac})]$  and Xantphos.

Run No.	PA	MPA	DHF	MPEA	POL	IBO	EOF	AA	MAA	$\gamma$ BA	HBA	MHPA	MPD	BDO	CY
1	3.12	0.03	1.77	0.15	1.70	0.00	0.00	0.16	0.00	0.54	82.89	9.13	0.00	0.10	0.41
2	4.09	0.40	2.30	0.33	2.84	0.00	2.80	0.17	0.00	0.81	75.19	9.78	0.00	0.22	1.07
3	2.58	7.21	1.31	0.00	3.63	0.00	27.58	1.83	0.00	0.74	42.69	0.73	0.49	4.06	7.15

**Table 6.** Hydroformylation of 1-octene with  $[\text{Rh}(\text{CO})_2(\text{acac})]$  and Et-Xantphos.

Key: O = octane; 1OE = 1-octene; 2OE = 2-octene; 3OE = 3-octene; 4OE = 4-octene; PHA = 2-propylhexanal; EHA = 2-ethylheptanal; MOA = 2-methyloctanal; NA = nonanal; MOO = 2-methyloctanol; NOL = nonanol; DEN = diethoxynonane; UN = unknowns.

Run No.	O	1OE	2OE	3OE & 4OE	PHA	EHA	MOA	NA	MOO	NOL	DEN	UN
1	0.99	0.00	7.51	0.27	Trace	0.15	5.48	85.17	0.00	0.12	0.00	0.32
2	1.91	0.00	12.34	0.38	Trace	0.07	3.20	81.75	0.00	0.14	0.00	0.20
3	1.40	0.00	8.11	0.24	0.00	Trace	4.08	84.38	0.00	1.35	0.22	0.23
4	1.41	0.00	6.23	0.80	0.00	0.27	4.55	75.03	0.26	8.34	2.25	0.86
5	1.53	0.00	2.47	2.53	0.17	1.10	6.01	39.34	1.84	41.49	0.21	3.31

**Table 7.** Hydroformylation of 1-octene with  $[\text{Rh}(\text{CO})_2(\text{acac})]$  and Et-<sup>t</sup>BuXantphos.

Run No.	O	1OE	2OE	3OE & 4OE	PHA	EHA	MOA	NA	MOO	NOL	DEN	UN
1	1.31	0.00	8.42	0.36	0.00	0.24	8.04	77.37	Trace	1.26	2.64	0.35
2	1.23	0.00	0.32	0.63	0.93	2.04	7.70	50.77	0.71	10.75	22.96	1.96

**Table 8.** Hydroformylation of 1-octene with  $[\text{Rh}(\text{CO})_2(\text{acac})]$  and DIOP.

Run No.	O	1OE	2OE	3OE & 4OE	PHA	EHA	MOA	NA	MOO	NOL	DEN	UN
1	0.62	0.00	0.67	0.23	0.00	0.00	12.01	86.33	0.00	0.00	0.00	0.15

**Table 9.** Hydroformylation of 1-octene with  $[\text{Rh}(\text{CO})_2(\text{acac})]$  and Xantphos.

Run No.	O	1OE	2OE	3OE & 4OE	PHA	EHA	MOA	NA	MOO	NOL	DEN	UN
1	2.71	0.00	4.38	0.21	0.00	Trace	1.88	90.32	0.00	0.28	0.00	0.21
2	2.52	0.00	6.42	0.19	0.00	Trace	2.00	87.88	0.00	0.66	0.00	0.32
3	2.58	0.00	9.94	0.23	0.00	Trace	2.16	83.66	0.00	1.09	0.00	0.33